Mucin-like glycocalyx modules for creating complex artificial glycocalyxes

Laia Saltor Núñez

Submitted in accordance with the requirements for the degree of Doctor of Philosophy

The University of Leeds

School of Chemistry

February 2023

Per a tu Papa, espero que estigui orgullós des d'on m'estiguis observant.

Per a mi sempre serà un orgull ser la teva filla.

Aprendimos a mirar con la duda entre los dedos

Vetusta Morla

Acknowledgments

I would like to start giving my (huge) gratitude to Prof. Bruce Turnbull and Dr. Ralf Richter, which decided four years ago to give a change that I could have never imagined. Thank you so much for putting your trust and faith of this project in me, for teaching and helping me to learn about field far away from my "chemist background" and making the scientist I am today. Last but not least, thank you for trying to give to my project a positive sight when I could not find it and for always understanding my personal situation and giving me the chance to make this path easier.

This project could not be carried with all the help and support from 1.49 and Ralf's labs. Thank you to everyone who have been there to share good and bad results and give a hand when needed. Thanks to Charlie, Chloe, Eva, Jonny and the rest of the 1.49 lab for making everyday a nice work environment. On Ralf's lab thanks to all to welcome to this amazing family and make me feel like home! In the lab I really appreciate the guidance from Abigail, Itzel, Sumitra and Xiaoli when I was on the Bragg building and for giving me the inductions in techniques news for me. I would like to thank specially Chunyue for all the time shared in our parallel projects, for all the help provided on the QCM-D and SE and for our trips to Manchester. Finally, thank you Darshita for all the chemistry discussions and help about sugars and the chatting after, it was always a delight.

Huge gratitude to Kristian for so many things! First of all, for being my first friend in Leeds and have the patience to repeat each conversation twice as my English was not good enough. Thank you, thank you so much for our friendship translated in lunches in benches, hiking on the hills and support when most needed. Second, for being my Jedi in the biolab and help me to become an enzymatic queen now, thank you so much to teach me and help me to turn into the scientist I am today. Another person really important for me during this journey has been Jack, my "husband". Jaaaaack, massive thank you for all the time shared, for all the support in the lab and in my life, for making things always easy for me and for all the good food we've eaten together. Last but not least, thanks to you my Twin sister Alexandra! I cannot tell how amazing has been sharing these years with you being twins, thank you so much for the help in the lab but, more important, for all the support in my life, for always being there and for understanding me by sharing a glance.

I would also like to express my gratefulness to Pablo and Tam: thank you so much for being my main support Tam when you were in Leeds, for all the time and feelings shared, the songs sang together late in the lab and for our adventures to visit UK. I miss you so much girl! Meloooon! Muchisimas gracias por ser mi pequeña spanish familia en Inglaterra, por ayudarme con todo lo

que has podido y más y por ofrecer always risas con tu dramatismo, no sé qué habría hecho sin tu ayuda. ¡Es un placer tenerte en mi vida!

Moltíssimes gràcies a tota la xarxa de Barcelona que han vetllat i aconseguit que em senti sempre com una més quan estic per casa. Voldria en especial agrair a les "Chicas Malas": l'Anna, la Clara, l'Ada i la Marta. Moltes moltes gràcies pels sopars quan he estat per Barcelona, per sempre incloure'm tot i la distància i per tot el suport que he rebut per part vostre durant aquests anys. Irina, moltíssimes gràcies per ser-hi aquests quatre anys, per ser la primera a venir a Leeds i ajudar-me a gestionar l'enyorança i per deixar-me desprotricar de la feina però oferint-me sempre un cop de mà. També li voldria agrair a l'Eli i la Laia tota l'ajuda i comprensió rebuda per part vostra i sempre confiar que tiraria endavant aquest projecte. Moltíssimes gràcies boniques per ensenyar-me en molts moments a prioritzar-me i a oferir-me un espai de confort on expressar el que sentia, us estimo un munt!

També voldria agrair a l'Anna, la meva primera mentora, tots els consells que m'ha donat des de l'experiència i tota l'ajuda que m'ha ofert per a que les coses m'anessin el millor possible. També voldria agrair-li totes les quedades que hem fet per posar-nos al dia, tots els llibres regalats i la seva preocupació genuïna per mi. Moltíssimes gràcies Anna, significa moltíssim la nostra amistat! Un altre persona molt important en aquest viatge ha estat en Cristian: infinites gràcies per escoltar-me i fer l'esforç de comprendre'm aquests quatre anys, per evadir-nos junts dels nostres doctorats anant de concert i per compartir mateixos sentiment d'estres i dubtes aquests últims mesos de tancament d'etapa. Gràcies per tenir sempre la certesa que hi seràs per mi, de veritat.

Elisa i Júlia, no tinc paraules per agrair tot el que heu fet per mi aquests quatre anys. Moltíssimes gràcies per tantíssimes coses! Gràcies per escoltar-me sempre, per preocupar-vos pel meu benestar, per encarregar-te Júlia que no em senti mai fora de lloc a Barcelona, per no deixar-me sola a Leeds quan tornava de Barcelona Elisa. Sou les millors, i no puc arribar a expressar com d'important us heu tornat a la meva vida però si he pogut treure aquesta tesis endavant és gran part al vostre suport. Us estimo moltíssim boniques i heu aconseguit que no em senti mai sola tot i la distància.

Moltíssimes gràcies a tu Jordi. Sabem els dos que podria escriure pagines senceres perquè és moltíssim el que has fet per mi i les mils maneres que m'has ajudat durant aquests anys però sí vull agrair-te que hagis confiat sempre en mi, fins i tot quan jo no donava ni dos duros per mi mateixa, i que mai dubtessis ni de mi ni de les meves capacitats per tirar endavant. També vull que quedi constància que estic aquí en gran part per tu, perquè tu vas ajudar-me a posar el fonaments de la química que soc ara i perquè tu has estat en els meus pitjors i millors moments

d'aquests doctorat. Bonic, t'estimo moltíssim, però molt molt, i només puc donar-te les gràcies per la manera que estàs a la meva vida i esperar que sigui així sempre.

Per últim i no menys important, jo he arribat tant lluny gràcies a la meva família: la Illa por todo los jerseis que me han mantenido calentita en invierno), la iaia Susana, la Prima Georgina (que guay descobrir-nos a Leeds!), l'Abel, la Laura i en Sergio. Però sobretot i en especial a vosaltres Sergi i Mama. Hermano, si tu no t'haguessis quedat a casa i haguessis ajudat a la mama com ho has fet, jo mai hauria estat tranquil·la així que infinites gràcies per donar aquest pas endavant, donar-li companyia a la mama i cuidar al papa en els seus últims anys com ho has fet. També voldria agrair-te totes les "risas" i temps que hem compartit quan he estat per Barcelona, tinc moltíssimes ganes de seguir-ho fent d'ara en endavant.

Per tu Mama, no saps com d'agraïda que t'estic i t'estaré sempre. Moltíssimes gràcies per fer el cor fort ara fa quatre anys i encoratjar-me a marxar de casa tot i la situació familiar, moltíssimes gràcies per estar per mi des de la distància i tenir-te sempre present en el meu dia a dia, infinites gràcies per atrevir-te a portar el papa en el seu últim viatge i que pogués veure com de lluny havia arribat. Gràcies per escoltar-me quan t'explicava el meus problemes de la feina, tot i que no entenguessis res, i que no passessin a segon terme tot i la situació familiar. Gràcies per preocupar-te per mi als estius i intentar fer-me més fàcil les visites a la residencia. Gràcies per cuidar al papa com ho has fet i aconseguir alhora que jo estigues tranquil·la. Gràcies per tot i més, nena, perquè cada vegada tinc més clar que sense tu, jo mai hagués acabat vivint a Leeds i defensant aquesta tesis. Si estic aquí, és per tot el que has fet tu, així que moltes gràcies.

Abstract

The glycocalyx on the outer surface of cells is made of glycoproteins, glycolipids, and proteoglycans (along with hyaluronan), and accomplishes many crucial functions in the communication of the cell with its environment. Mucins are one major class of glycoproteins in the glycocalyx; they are highly glycosylated (with sugars typically representing around 80% of the molecular mass) and accomplish important functions in the defence against pathogens. Other important glycocalyx elements are Lewis carbohydrate antigens, a group of oligosaccharides which contain Fucose. Two of them, Lewis^y and Lewis^x, are also targets for cholera toxin (CT), a lectin secreted by *Vibrio cholerae* that causes life-threating diarrhoea. Finally, on the cell membrane there is also the presence of the Gb_3 glycosphingolipid, which its overexpression leads to Fabry's disease. This glycolipid is also the target for shiga toxin (STx), a lectin secreted by *Shigella dysenteriae* type 1 (*S. dysenteriae*) and some strains of *Escherichia coli*, and it causes abdominal pain, watery diarrhoea, haemorrhagic colitis (HC) and hemolytic uremic syndrome (HUS).

Even though the general mechanism of infection for both cholera toxin and shiga toxin are well known, how these proteins interact with the glycocalyx toward infecting its host cell remains poorly understood. Recent discoveries have shown the need of fucosylated structures to perform a first binding between the cell surface and cholera toxin, while for shiga toxin is well known the need of high concentration of Gb_3 on the cell membrane but it is unknown the interactions between the protein and the glycocalyx. The complexity of the glycocalyx, and the scarcity of tools to control and analyse glycocalyx composition and organisation, make mechanistic studies *in vivo* and *in vitro* challenging.

Our work aims to generate well-defined glycocalyx models to understand how cholera and shiga toxins interact with the cell surface. To synthesize a well-defined structure suitable to perform binding studies with these lectins, we are building mucin-like structures that have hyaluronic acid as a backbone and present a single type of pendant oligosaccharide, Lewis^x for cholera toxin and Gb_3 for shiga toxin, at defined densities along the hyaluronic acid contour.

To this end, hyaluronic acid and oligosaccharides were prepared with appropriate bio-orthogonal reactive groups to allow their conjugation. This was followed by the incorporation of a biotin (or His-tag) on the reducing end of hyaluronic acid to build a well-defined molecular structure suitable for anchorage to cell membrane models, and to perform quantitative binding studies using quartz crystal microbalance (QCM-D) or spectroscopic ellipsometry (SE). The data obtained with the mucin-like structures offered a better understanding about how the glycocalyx interacts with cholera toxin and shiga toxin.

Acronyms

AC	Alternating current
AcOH	Acetic acid
ADP	Adenosine diphosphate
Ala	Alanine
Asn	Asparagine
Asp	Aspartic acid
ATP	Adenosine triphosphate
Boc	*tert*-Butyloxycarbonyl
BSA	Bovine serum albumin
BTTES	3-(4-((*bis*((1-(*tert*-butyl)-1*H*-1,2,3-Triazol-4-yl)methyl)amino)methyl)-1*H*-1,2,3-triazol-1-yl)propane-1-sulfonic acid
cCTB	Classic cholera toxin B-subunit
CDMT	2-Chloro-4,6,-dimethoxy-1,3,5-triazine
COSY	Homonuclear correlation spectroscopy
CSA	Camphorsulfonic acid
CT	Cholera Toxin
CTA1	Catalytic part 1
CuAAC	Copper(I) catalysed azide-alkyne cycloaddition
Cys	Cysteine
DA	Diels-Alder
DCE	1,2-Dichloroethane
DIC	*N,N'*-Diisopropylcarbodiimide
DMF	*N,N*-Dimethylformamide
DMTMM	4-(4,6-dimethoxy-1,3,5-triazin-2-yl)-4-methyl-morpholinium chloride
DNA	Deoxyribonucleic acid
DODA	Dioctadecylamine
DOPC	1,2-Dioleoyl-sn-glycero-3-phosphocholine
DOPE-CAP-B	1,2-Dioleoyl-sn-glycero-3-phosphoethanolamine-*N*-cocamidopropyl-biotin
DTT	Dithiothreitol
EDC	1-Ethyl-3-(3-dimethylaminopropyl)carbodiimide
EDG	Electron-donating group

EDTA	Ethylenediaminetetraacetic acid
ER	Endoplasmic Reticulum
ESI-HRMS	Eletrospray ionization high resolution mass spectrometry
ET-CTB	El Tor cholera toxin B-subunit
EtOAc	Ethyl acetate
EWG	Electron-withdrawing group
FKP	GDP-fucose pyrophosphorylase
Fmoc	Fluorenylmethyloxycarbonyl
Fuc	Fucose
GAGs	Glycosaminoglycans
Gal	Galactose
GalNAc	*N*-Acetyl galactosamine
Gb_3	Globotriaosylceramide
GBP	Glycan binding proteins
Glc	Glucose
$Glc(4)_{ep}$	UDP-Glc-4-epimerase
GlcA	Glucuronic acid
GlcNAc	*N*-Acetlglucosamine
Glu	Glutamic acid
GMP	Guanosine monophosphate
GTP	Guanosine triphosphate
GUV	Giant unilamellar vesicles
HA	Hyaluronan
HA_{ss}	Small size hyaluronic acid
HBS	Hepes buffered saline
HC	Heamorrhagic Colitis
HCTU	O-(1*H*-6-Chlorobenzotriazole-1-yl)-1,1,3,3-tetramethyluronium hexafluorophosphate
HEPES	4-(2-Hydroxyethyl)-1-piperazineethanesulfonic acid
HOMO	Highest occupied molecular orbital
HPLC	High performance liquid cromatography
HS	Heparan Sulfate
HSQC	Heteronuclear single quantum coherence spectroscopy

HUS	Hemolytic Uremic Syndrome
IdoA	Iduronic Acid
IEDDA	Inverse electron demand Diels-Alder
IPTG	Isopropyl β-D-1-thiogalactopyranoside
Itag	Imidazolium-based molecular tag
ITC	Isothermal titration calorimetry
Lac	Lactose
LacNAc	*N*-Acetyllactosamine
LC-MS	Liquid chromatography mass spectroscopy
Leu	Leucine
LgtC	α-1,4-Galactosyltransferase
LT	Heat-labile enterotoxins
LUMO	Lowest unoccupied molecular orbital
Lys	Lysine
Man	Mannose
MBHA	Methylbenzhydryl amine
MeCN	Acetonitrile
MeOH	Methanol
MeONa	Sodium methoxide
MES	2-(*N*-Morpholino)ethanesulfonic acid
Mw	Molecular weight
NAD	Nicotinamide adenine dinucleotide
Neu5Ac	*N*-Acetylneuraminic acid
NHS	*N*-Hydroxysuccinimide
NMM	*N*-Methylmorpholine
NMR	Nuclear magnetic resonance
NTA	Nitrilotriacetic acid
OD	Optical density
PAGE	Polyacrylamide gel electrophoresis
PBS	Phosphate-buffered saline
PC	Partition Coeffficient
PDI	Protein disulfide isomerase
PEG	Polyethylene glycol

Đ	Dispersity
Pro	Proline
PT	Pertussis toxin
QCM-D	Quartz Crystal Microbalance and Dissipation
RBF	Round bottomed flask
RNA	Ribonucleic acid
ROS	Reactive oxygen species
SAv	Streptavidin
SDS	Sodium dodecyl sulfate
SE	Spectroscopic Ellipsometry
SEC-MALS	Size exclusion column with multi-angle scattering light detector
Ser	Serine
SLB	Supported lipid bilayer
SPAAC	Strain-promoted azide-alkyne cycloaddition
SPPS	Solid phase peptide synthesis
STx	Shiga Toxin
SUV	Small unilamellar vesicles
TBA	Tetrabutylammonium
TBTA	*tris*(Benzyltriazolylmethyl)amine
TCO	*trans*-Cyclooctene
TEA	Triethylamine
TEMED	*N,N,N′,N′*-Tetramethyl ethylenediamine
TFA	Trifluoroacetic acid
THPTA	*tris*(3-Hydroxypropyltriazolylmethyl)amine
Thr	Threonine
TIS	Triisopropylsilane
TLC	Thin layer chromatography
TMS	Tetramethylsilane
TMSOTf	Trimethylsilyl trifluoromethanesulfonate
TRIS	*tris*(Hydroxymethyl)aminomethane
Trp	Tryptophan
Tyr	Tyrosine
UDP	Uridine diphosphate

VNTR	Variable number of tandem repeats
vWF	von-Willebrand-factor
WHO	World Heath Organization
Xyl	Xylose
α(1-2)FucT	α-1,2-fucosalytransferase
α(1-3)FucT	α-1,3-fucosalytransferase
β(1-4)GalT1	*β*-1,4-Galactosyltransferase 1
Γ	Molar surface density

Index

CHAPTER 1: INTRODUCTION

1.1 The glycocalyx

The glycocalyx is a group of glycoproteins, glycolipids, proteoglycans and glycosaminoglycans presented on the cell membrane of mammalian cells.[1,2] This biological interface performs several functions including protecting the cell from external agents, regulation of the immune response and mediation of cellular communication.[3–5] The glycocalyx can extend from ten to hundreds of nanometres producing a dynamic layer with a high level of complexity.[6,7] Glycan structures can be recognized by glycan binding proteins (GBPs), which includes lectins and antibodies of the immune system, as well as neighbouring cells or extracellular matrix molecules (Figure 1.1).[8]

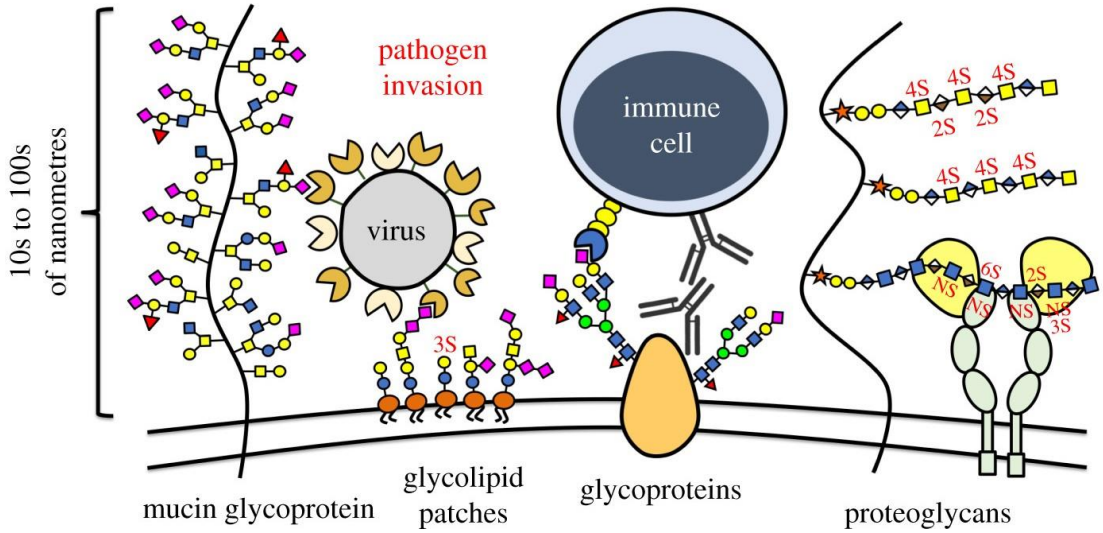

Figure 1.1: Glycocalyx cartoon reproduced from Purcell *et al.*[3] The coloured symbols are part of the now widely accepted symbolic nomenclature for glycans.[9] This figure is reproduced from reference 3 under the licence 1319367-1 provided by Copyright Clearance Center, Inc.

1.1.1 Composition of the glycocalyx

1.1.1.1 Glycoproteins

Glycoproteins are proteins which contain short chains of oligosaccharides (between 2 and 15 residues) that are typically branched. These oligosaccharides have been studied extensively because of their biological importance. Glycoproteins have an important role in cell-cell interactions, both in cell signalling and in cell adhesion molecules.[1] Different types of glycoproteins are classified according to the linkage between the carbohydrate and protein layers, but the two principal ones are *O*-linked glycoproteins and *N*-linked glycoproteins.[7]

O-Linked glycoproteins are the proteins which have an oligosaccharide linked to an oxygen atom of an amino acid residue. The amino acids used to perform this linkage are usually serine (Ser) or threonine (Thr) but it also can be seen on tyrosine (Tyr) (Figure 1.2).[10] The glycosylation in these proteins is a post-translational modification which takes place in endoplasmic reticulum

(ER) and Golgi apparatus by different glycosyltransferases. However, sometimes it also takes place in the cytoplasm. Some carbohydrate chains contain a sialic acid linked to a galactose (Gal) or *N*-acetyl galactosamine (GalNAc) in the membrane glycoproteins. *O*-linked glycoproteins provide antibody recognition as well as cell adhesion, including P- and L-selectins,[10] or microorganism binding like *Helicobacter pylori* and *Clostridium difficile* toxin A which are the suggested causative agents of gastric ulcers and pseudomembranous colitis, respectively .[11]

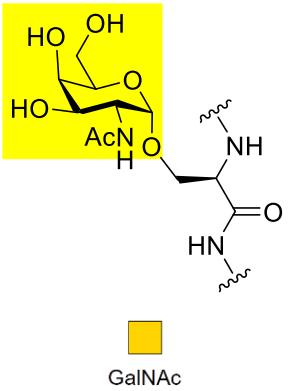

Figure 1.2: α Linkage between Ser and GalNAc presents in the majority of *O*-linked glycoprotein structure.

N-Linked glycoproteins form a group of proteins which contain a carbohydrate chain attached to asparagine (Asn) residues.[12] This linkage is also a post-translational modification and it is performed by three different steps in ER lumen and Golgi apparatus.[13] These proteins are easier to predict from genome data than *O*-linked ones because only specific sequences (Asn-Xaa-Thr preferred to Asn-Xaa-Ser) situated at the protein surface can be glycosylated (Figure 3).[14,15] The principal functions of *N*-linked glycosylation are as cell-surface receptors, cell-adhesion molecules and, sometimes, the control of the protein conformation.[16]

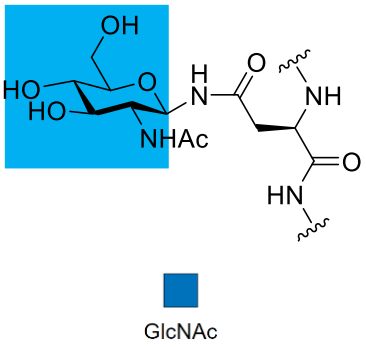

Figure 1.3: β Linkage between Asn and a GlcNAc presents in the *N*-linked glycoprotein structure.

There are some others types of glycoproteins which contain different linkages from those described thus far. As an example, it has been reported the post translational modification S-glycosylation using cysteine (Cys) as a residue in the protein moiety (Figure 1.4, a).[17,18] Moreover,

there are also C-linked glycoproteins using tryptophan (Trp) to attach the carbohydrate chain after protein expression (Figure 1.4, b).[19]

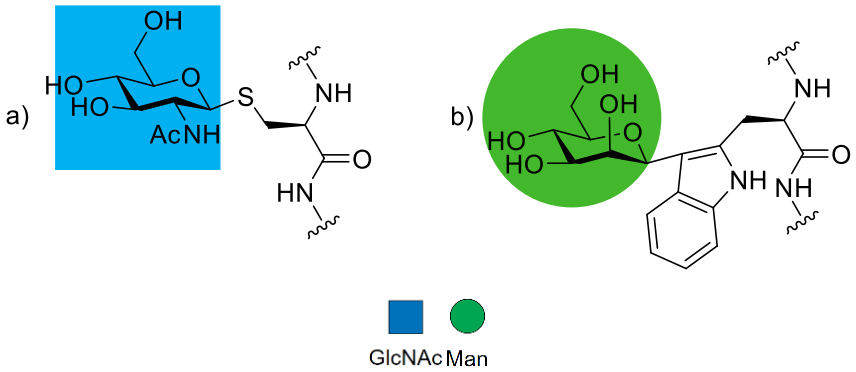

Figure 1.4: a) Example of a β linkage between Cys and GlcNAc in a *S*-linked glycoprotein. b) Example of a β linkage between Trp and mannose (Man) in a *C*-linked glycoprotein.

1.1.1.2 Glycolipids

Glycolipids are lipids which have an oligosaccharide chain linked covalently by a glyosidic bond. The lipid molecules in cell membranes include two different parts: a polar moiety attached to a fatty acid and it is normally known as sphingolipids.[20,21] Different structures formed the sphingolipids family including ganglosides, which contains at least one sialic acid residue, glycophosphosphingolipids or globosides.[22] The fatty structure of this last one is called ceramide (Figure 1.5).

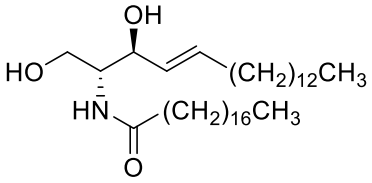

Figure 1.5: Structure of ceramide.

One of the glycosphingolipids present in the cell membrane is Gb_3. The trisaccharide attached to the lipid, comprising a glucose (Glc) and two galactose (Gal) residues (Figure 1.6), is the core structure belonging to the globoside family.[23] Gb_3, also known as CD77 or P^k blood group antigen, is synthesised in cells by α-1,4-galactosyltransferases.[24] The overexpression of this glycosphingolipid leads to Fabry's disease, which affect the kidneys, heart and skin, and it can also be associated with different types of cancers including lymphatic (Burkitt Lymphoma), pancreas and colon.[25–27] Gb_3 is also the cell surface ligand recognized by Shiga Toxin, a protein belonging to the AB_5 toxin group which is secreted by *Shigella dysenteriae* type 1 (*S. dysenteriae*) and some strain of *Escherichia coli*.[28]

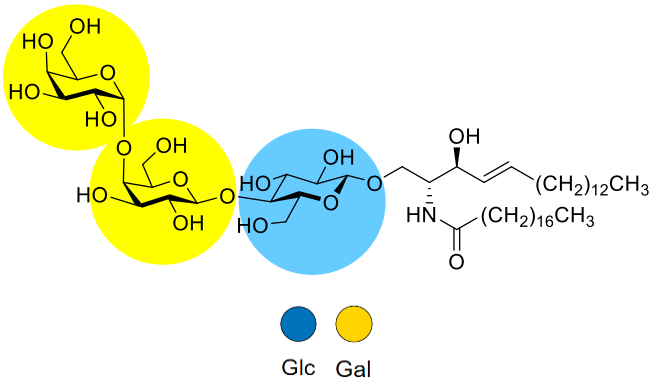

Figure 1.6: Gb_3 structure.

Glycosphingolipids can be divided in two groups according the type of oligosaccharide attached to the ceramide moiety: neutral glycolipids or gangliosides. The main difference between these two groups is that gangliosides contain at least one sialic residue in their carbohydrate chain. Gangliosides are some of the more prevalent components in the nervous system,[29,30] however, they have also an important role in endothelial cells. Gangliosides can create lipid raft microdomains with low concentrations of cholesterol which have important roles in adhesion, growth and motility in cells.[31]

Gangliosides are classified in different groups according the number of sialic residues present in the oligosaccharide chain. In this way, four categories have been found reported: G_M family (one sialic acid residue), G_D family (two sialic acid residues), G_T (three sialic acid residues) and G_Q (four sialic acid residues). All the gangliosides are synthesized from lactosylceramide in the ER and Golgi apparatus, except GM_4, which is derived from galactosyl ceramide.[32]

G_{M1} is a ganglioside present in neuron cells and it has important protective roles for the stability and regeneration of axons.[33] Moreover, G_{M1} in cell membrane in endothelial cells interacts strongly with Cholera Toxin (CT), a protein secreted by *Vibrio cholerae* belonging to AB_5 toxin group.[34] The ceramide moiety is responsible to anchor GM_1 in the cell membrane while the pentasaccharide belongs to the cell glycocalyx. The oligosaccharide is formed by four different types of residues: two galactoses, a *N*-acetyl galactosamine, a glucose (Glc) and an *N*-acetylneuraminic acid (Neu5Ac), the sialic acid residue (Figure 1.7).

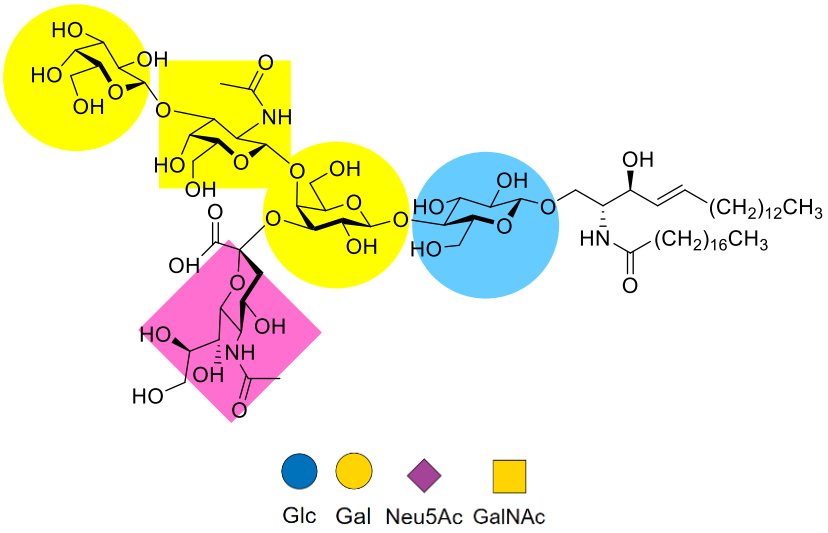

Figure 1.7: GM_1 ganglioside structure.

1.1.1.3 Proteoglycans and glycosaminoglycans

Proteoglycans are heavily glycosylated proteins that are formed by a core protein linked covalently to at least one, but usually many glycosaminoglycan polysaccharide chains (Figure 1.8, a).[1] These structures are considered among the most important backbone components of the glycocalyx. The glycans are linked from a Ser residue through a tetrasaccharide bridge present on the glycosaminoglycan (GAGs) (Figure 1.8, b).[35]

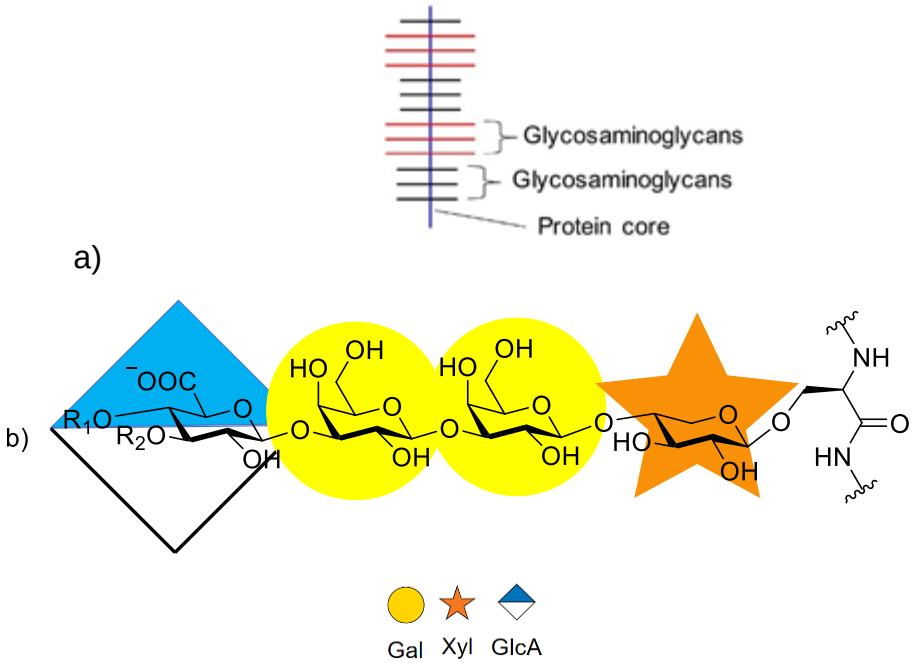

Figure 1.8: a) Scheme of glycosaminoglycans attached to the protein core to form proteoglycans The protein core is represented by the blue line and the glycosaminoglycans are represented by black and red lines attached to the protein core. b) Structure of tetrasaccharide bridge between GAGs and Ser. The different GAGs are attached in R_1 or R_2.

There is a wide variety of protein cores in proteoglycans with a large variation in the size of proteins in this family. Besides, the same protein core can contain different types of glycosaminoglycan chains, which is regulated by the different stimuli experienced by the cells. Their principal function is to participate in transport process (internalization and release of components into the cell) as well as the movement of molecules across the glycocalyx.[2] In addition they are one of the principal component playing structural roles as lubricating joints, repairing wounds or acting as shock absorbers.[36]

There are five common types of glycosaminoglycan chains: heparin/heparan sulfate (Figure 1.9 a), chondroitin sulfate (Figure 1.9, b), dermatan sulfate (Figure 1.9, c), keratan sulfate (Figure 1.9, d) and hyaluronan (Figure 1.9, e).[35] All of them are linear polymers of variable lengths formed by repeating disaccharides comprising a hexauronic acid and a hexosamine with different modifications that can include the sulfation or the (de)acetylation of some residues.[2]

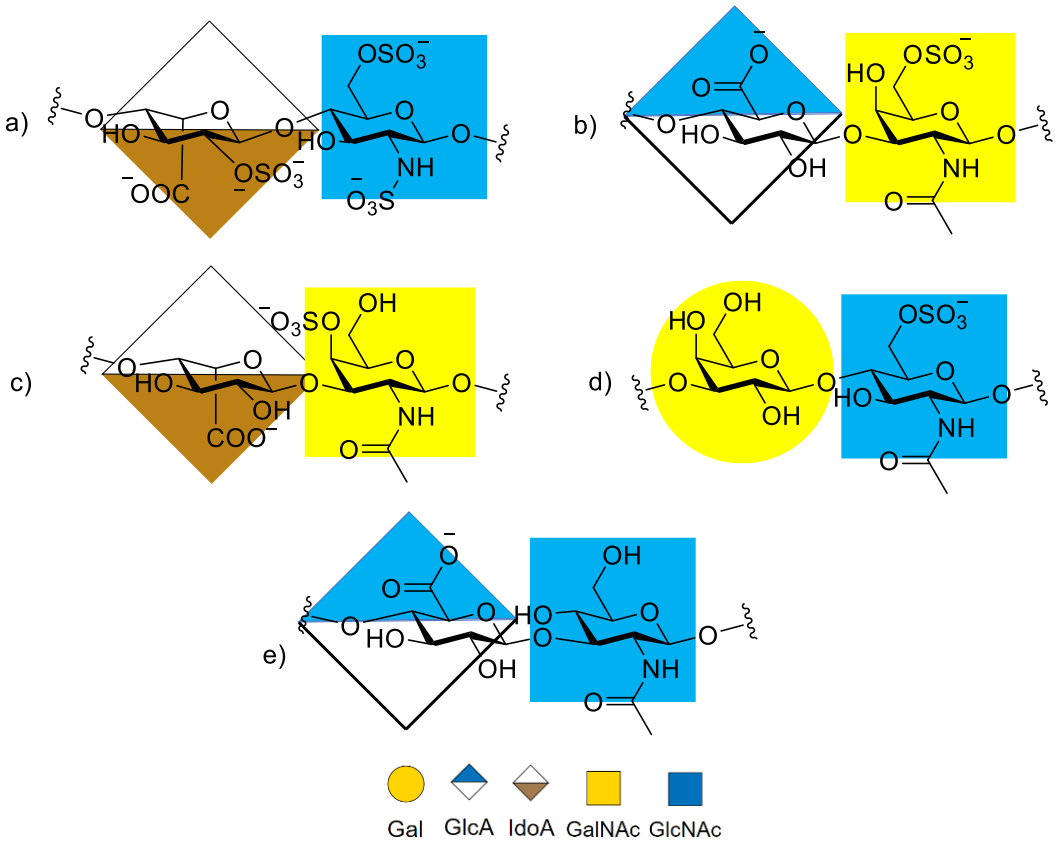

Figure 1.9: Representative structures of glycosaminoglycan repeating units. Only one example of the possible sulfation patterns is shown in each case: a) Heparin; b) Chondroitin sulfate; c) Dermatan sulfate; d) Keratan sulfate; e) Hyaluronan.

There are many possible sulfation modification patterns that arise depending on expression levels of different sulfotransferases. The resulting diversity of glycosaminoglycan modifications provides an heterogenous surface which can affect protein binding as well as the modulation of

protein functions,[1] for example, anticoagulant regulation by antithrombin III which binds to specific regions in heparan sulfate,[35,37] or modulation of ligand-receptor encounters on the cell membrane by immobilizing the ligand performed by heparan sulfate.[38]

Hyaluronan is the only member of the GAG family that does not contain any sulfate groups. Its structure consist of a long polysaccharide chain in which glucuronic acid (GlcA) and GlcNAc are linked via alternating β(1-4) and β(1-3) glycosidic bonds (Figure 1.10).[39] It is the principal component of synovial tissue and fluid and soft connective tissues.[40] Moreover, as a member of the GAG family, it is found in the cell glycocalyx, where hyaluronan plays different roles in helping the diffusion of molecules through the extracellular matrix, like lymphocytes during inflammation once HA is bound to CD44, maintaining tissues hydration due to its viscoelastic properties.[39]

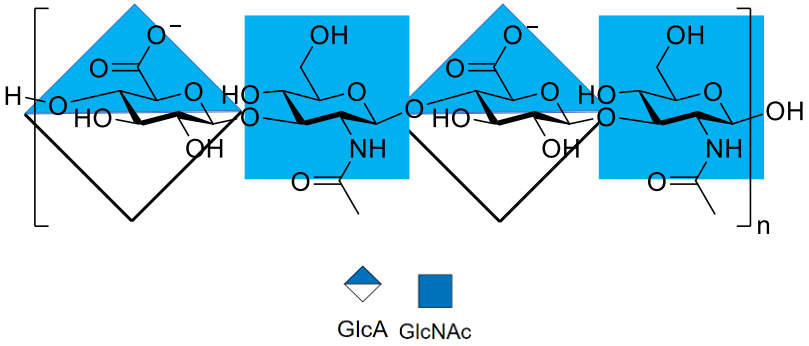

Figure 1.10: Hyaluronan structure.

1.1.2 Mucin glycoproteins

Mucins are large *O*-linked glycoproteins present on the cell membrane as a part of the glycocalyx. They are also part of mucus present on epithelia that helps to protect all organs providing viscous and elastic gel-like properties. This group of proteins is highly glycosylated (from 50% to 80% of the protein mass). Oligosaccharide chains contain between 2 and 20 monosaccharide residues linked to the backbone of the protein.[41,42] The principal residues present in these carbohydrates are GalNAc, GlcNAc, fucose (Fuc), Gal and sialic acid (Neu5Ac). Finally, mucins are characterized by a variable number of tandem repeats (VNTR) forming domains inside the glycoprotein (Figure 1.11) which are rich in Tyr, Ser or Pro and also known as PTS domainse.[42,43]

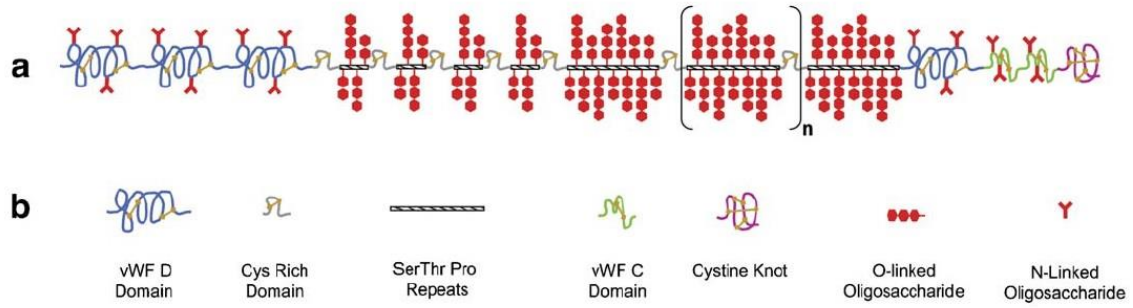

Figure 1.11: a) A schematic representation of mucin structure containing different domains with variable numbers of tandem repeats. The oligosaccharide structures are only an example. b) Key defining the symbols for different domains shown in panel a). This figure is reproduced from reference 41 under the licence 5481270992845 provided by Elsevier and Copyright Clearance Center, Inc.

There are two different subfamilies of mucins according to their location relative to the cell surface: gel forming (secreted) and cell-surface (transmembrane, membrane-tethered) mucins.[44] Mucins from the first group are entirely located in the extracellular matrix and there is no linkage to the cell. Moreover, glycoproteins that are part of this group contribute to achieving the gel texture of the mucus presented on the respiratory tract, gastrointestinal tract, reproductive tract and oculo-rhino-ottolaryngeal tract.[45] Mucins included in the secreted group are MUC2, MUC5AC, MUC5B, MUC6-9 and MUC19 which are characterized for containing von-Willebrand-factor (vWF) domains (C and D types).[42] The second group is formed of the mucins that are presented on the cell-membrane and they have a single transmembrane domain which links a short cytoplasmic tail and an extensive extracellular domain. Mucins belonging this group are MUC1, MUC3A, MUC3B, MUC4, MUC11-18, MUC20 and MUC21.[43]

1.1.2.1 Structure and properties of mucins

A common feature observed in mucins is the high concentration of Thr and Ser residues present in the backbone because they offer the possibility for glycosylation of their hydroxyl groups. Around 50-90% of the mass of mucins is provided by the oligosaccharide and moieties there is a high concentration of sialyl groups found in this layer. Another characteristic of mucins is the repeated presence of proline (Pro) in its backbone structure. The combination of the large carbohydrate structures with the variable size of the tandem repeats forms branched structures that can be up to 1500 nm long from the cell-surface.[45]

Cell-surface mucins are formed of three different regions: an *N*-terminal extracellular domain that is highly glycosylated, a transmembrane domain, and a *C*-terminal cytoplasmic tail (Figure 1.12). This type of mucin is responsible for interacting with different proteins present inside or

outside the cell using both termini. In the case of the cytoplasmic tail, it interacts with several kinases,[46] while the extracellular domain interacts with lectins localized outside the cell, for example galectins, lectins responsible of the mediation of cell–cell interactions or the cell–matrix adhesion.[47] Moreover, there are some proteins that can also interact with the transmembrane domain for example ErbB /HER family of protein-tyrosine kinases, closely related to the cell growth.[47]

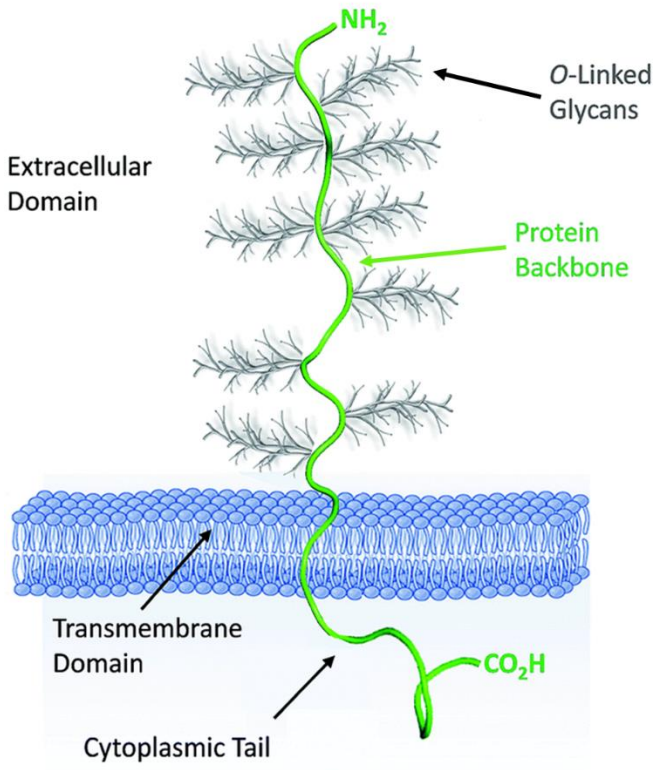

Figure 1.12: Transmembrane mucin structure. This figure is reproduced from reference 48 under the licence 1357312-1 provided by Copyright Clearance Center, Inc.

The structure of mucins backbone is typically a random coil but occasionally it can form short α-helices or β-sheets. In addition, the conformation of mucins can be influenced a lot by different factors such as pH or ionic strength.[48] As mucins tend to form coils, they exhibit a predisposition to aggregate and form gels because of the interpenetration of the carbohydrate side chains which leads to adhesive properties in solution. The relation between gelation and pH has been studied: at low pH (around 4) the hydrophobicity of the protein core increases forming aggregates and gels. Also, it has been observed the interaction between oligosaccharides with side chains of amino acids with pK_as around 4.[41]

Finally, diffusion of macromolecules and particles through these glycoproteins has been studied.[48] Small molecules can diffuse quickly in the mucin layer while diffusion of large particles depends both on size and muco-adhesive interactions. In cases where liquids need to cross the

mucin layer, like hydrochloric acid in the stomach, channels form through the mucin layer by a process of viscous fingering.

1.1.2.2 Functions of mucin

The principal function of mucins in humans is to cover several tracts and organs as a protection against bacterial and fungal infections. However, as a mucus layer, they are associated to more functions such as hydration, lubrication and protection from the degradation caused by proteases.[45]

The large number of oligosaccharide chains provides a hydrophilic environment which hydrates and lubricates epithelial cells. These structures also are an impediment for any pathogen to enter the epithelial cell and they present this resistance far away from the cell because of their large size. As an example, mucin glycans presented on the lungs are involved in host-microbial interactions leading to colonisation of *Pseudomonas aeruginosa* and viral infection in the lungs. Besides, mucins also have an important role offering a matrix to link cells

Several studies have also indicated that cancer cells overexpress large amounts of mucins because these proteins contain a wide range of oligosaccharides that are potential ligands for interaction with other receptors at the cell surface. Mucins in cancer cells are known to promote tumorigenesis or metastasis.[45,47,49,50]

1.1.3 Lewis carbohydrates antigens

The Lewis carbohydrate antigens name makes reference to a family which presented incompatibility on the red blood cells. This family of carbohydrates includes two subtypes: Lewis type I (Lewis^a and Lewis^b), which have a Gal residue attached by β(1-3) to GlcNAc and a Fuc residue attached to position 4 on GlcNAc, and Lewis type II (Lewis^x and Lewis^y) are the ones with Gal β(1-4)GlcNAc and Fuc linked by α(1-3) to position 3 on GlcNAc.[51–53]

These oligosaccharides are presented on red blood cells and epithelial. There are three Lewis type II carbohydrates associated to histo-blood antigens: A-Lewis^y pentasaccharide (A-Le^y), B-Lewis^y pentasaccharide (B-Le^y) and an H-Lewis^y tetrasaccharide (H-Le^y) (Figure 1.13). The last one corresponds to the O blood group but is called the H-antigen. Lewis^x trisaccharide also belongs to Lewis type II (Figure 1.13).[53] These group of oligosaccharides are synthesized by the enzymes FUT1 and/or FUT2, which are α(1-2) fucosyltransferase, and FUTs3-7 and/or FUT9, which are the α(1-3) fucosyltransferase.[52]

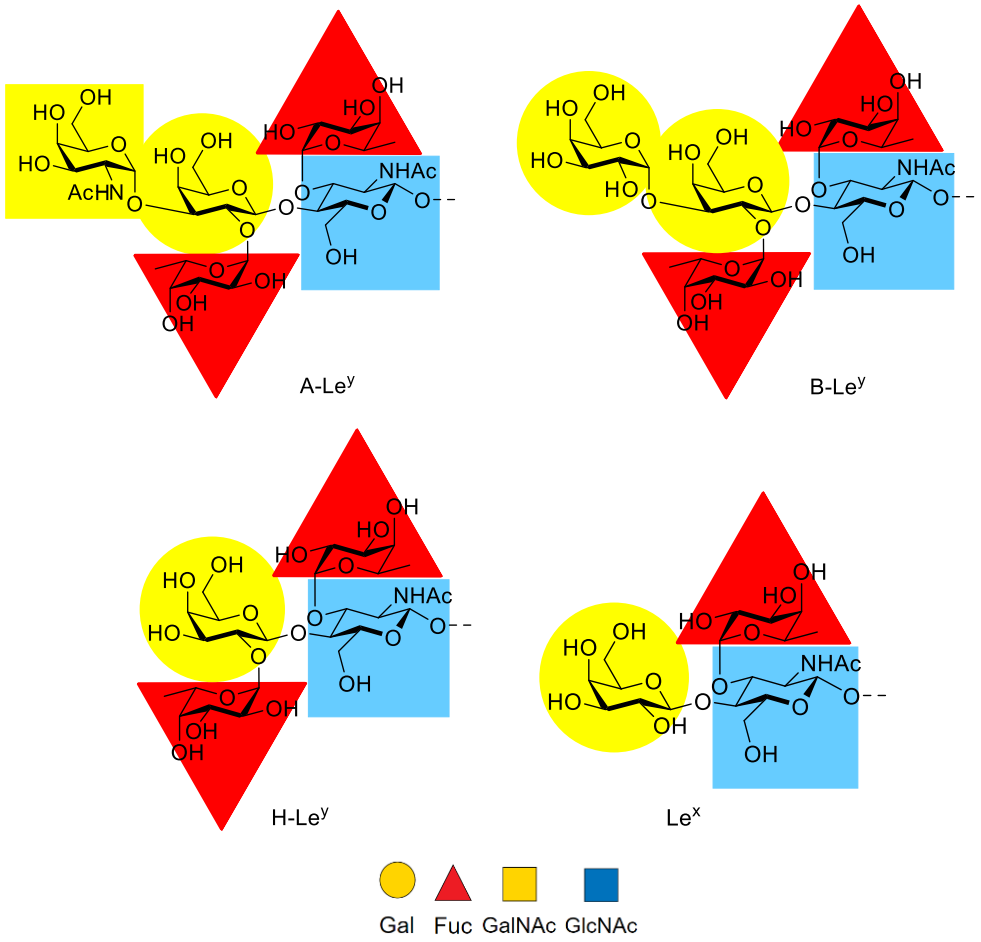

Figure 1.13: Lewis^y blood groups antigens and Lewis^x structures.

The over expression of Lewis^y tetrasaccharide on epithelial cells is a signal of human carcinomas in cancers as ovary, breast, colon or prostate,[52,54–57] however, the reason for this fact it is not clear yet. As an example, in the case of ovarian cancer it has been shown there is 75% more expression of various type-II structures in ovarian cancer cells.[55] In the case of the breast cancer, it has been reported that there is a significant increase of H-Le^y.[52,57]

Lewis^x antigen, on the other hand, is the main fucosylated antigen expressed in brain tissues facilitating cell-cell interaction in neuronal development.[52] The overexpression of this antigen is also related to different types of cancer because it mediates the adhesion between tumor cells and endothelium by its interaction with their selectin ligands.[58,59] In addition, the increased expression of FUT enzymes giving as a result a high-density expression of fucosylated antigens in carcinomas, like colorectal cancer, indicates low possibilities of survival to its patients.[52,60] Apart from the previously mentioned, several types of cancer are related to the increase of Le^x including head and neck, breast, kidney, lung and pancreas.[59]

1.2 AB_5 toxins

AB_5 toxins are a class of protein toxins that are secreted by various bacteria.[61,62] They are responsible of several diseases including cholera, dysentery and haemolytic uremic syndrome. There are four families distinguished by the differences in the cytotoxin and the catalytic part: cholera toxin (CT), heat-labile enterotoxins (LT), Shiga toxin (STx) and pertussis toxin (PT).[63]

CT and LT are secreted by *Vibrio cholerae* and *Escherichia coli*, respectively. Both proteins belong to the cholera toxin family responsible of causing strong diarrhoea. There are several different types of LTs toxins: *Escherichia coli* heat-labile enterotoxin (LT-I) and type II heat-labile enterotoxin (LT-II which includes LT-IIa and LT-IIb).[64,65] The Shiga toxin (STx) family causes homolytic uremic syndrome. There are several similarities between STx and CT families in their structures such as the same overall protein fold and AB_5 architecture even though they share very little sequence similarity.[63] Nevertheless, in Shiga toxins the structure of B is smaller than cholera toxins and the A-subunit only shares a 15-20% of amino acid sequence with LT group.[62] Finally, there is another family in AB_5 toxins called pertussis toxin (PT), secreted by *Bordetella pertussis*, which causes whooping cough.[66] Although it belongs to the AB_5 toxin family, its amino acid sequence is not similar to the other toxins previously mentioned but the structure of the protein (the A and B-subunits) maintains structural homology.[62] There is only 15% of similarity between cholera toxins and PT.[63]

1.2.1 Structure and functions of A and B-subunits

All the members of the AB_5 toxins family have structural homology in that they have a pentameric B_5 subunit and an A-subunit formed by two different parts: An A1 domain that contains the cytotoxic moiety and a peptide A2 that is responsible to link the A- and B-subunits as a non-covalent complex (Figure 1.14).

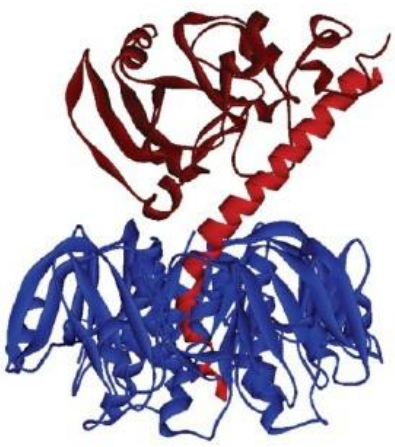

Cholera Toxin

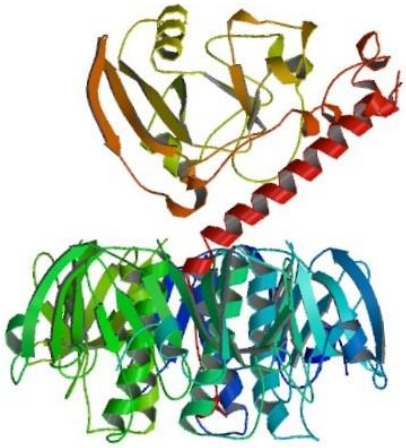

Escherichia coli heat-labile enterotoxin

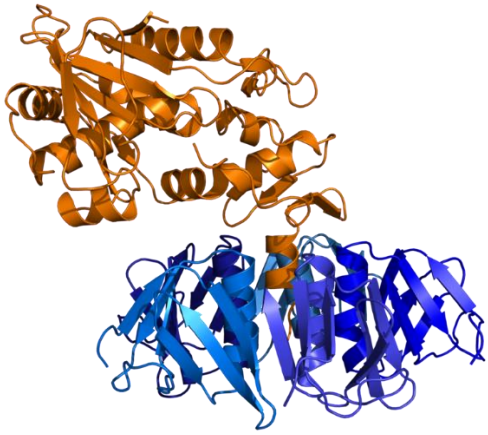

Shiga Toxin

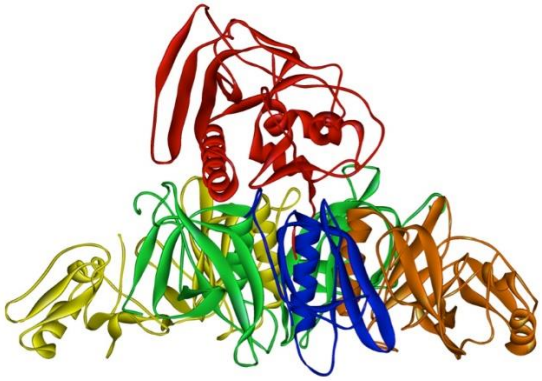

Pertussis toxin

Figure 1.14: Structures of the different AB_5 family toxins.

The B-subunit is, as in all the AB_5 toxins, a lectin which interacts with different and specific glycans present at the cell surface. In both the CT and STx families, the B_5 subunit is formed by five identical subunits creating a homo-pentameric ring. However, pertussis toxin does not share this same structure; in its case the B_5 subunit is constituted by four different subunits forming a hetero-pentameric ring. Even though CT, LT and STx share the same fold, each toxin has different numbers of binding sites and interacts with different glycan receptors at the cell membrane.

CT and LT-I toxins contain five principal binding sites, one per monomer, which interact with ganglioside GM_1. LT-II has the same number of principal binding sites but they preferentially interact with GD_1 (Figure 1.15). On the other hand, Shiga toxins' B-subunit contains 15 binding sites, three per monomer, with different levels of affinity for the Gb_3 glycosphingolipid.[62,63,67–69] Finally, PT contains two different binding domains with different specifies on subunits S2 and S3 (S2-S4 binging site and S3-S4 binding site) and they interact only with a glycoprotein.[66,70]

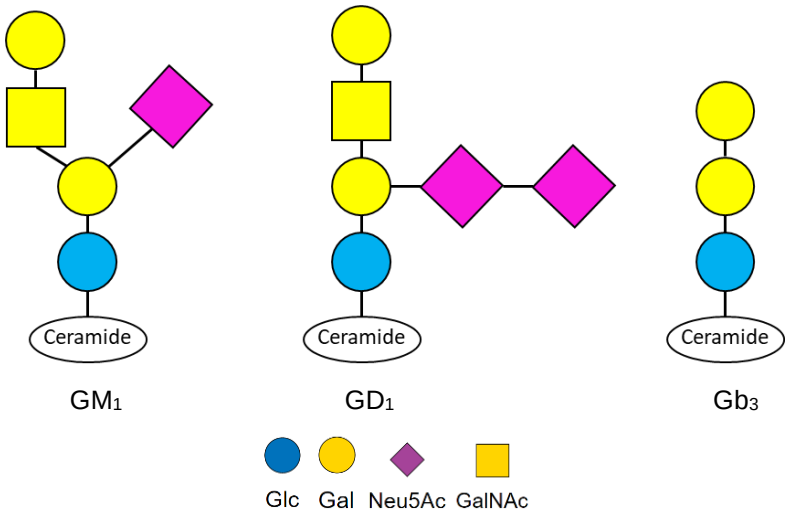

Figure 1.15: Structures of the ligands.

1.2.2 The cholera toxin

Cholera toxin is the archetypal AB_5 toxin in the cholera toxin family. The bacterium responsible for secreting this toxin is *Vibrio cholerae* (*V. cholerae*), which causes life-threating diarrhoea, can principally be found in water but also in food products. Cholera is endemic in the Ganges Delta and since the 19th century it has become pandemic from India to the rest of the world. Moreover the number of affected people has increased dramatically since 2005, becoming the world's longest pandemic according to World Health Organization (WHO).[71,72]

Two different biotypes of *V. cholerae* have been discovered: the classical one and El Tor.[73] Both of them secrete CT with only a small variation in sequence (they differ by only two residues in the B-subunit). This variation causes the El Tor biotype (ET-CTB) to have a stronger interaction with blood group carbohydrates than the classical one (cCTB).[74] However, a curious fact has been observed: people with blood group O have a higher risk to suffer severe symptoms than individuals with other blood groups but, contradictorily, people from the first group do not have a greater predisposition to cholera infection.[75,76]

1.2.2.1 Cholera toxin structure and binding sites

The A1 moiety is an ADP-ribosyltransferase that transfers an ADP-ribose group from NAD to a regulatory G-protein. The first 132 amino acids form a compact globular unit containing the enzyme active site responsible far away from the linkage between A1 and A2, or A- and B-subunits.[77] A2 is a relatively short α-helix that is responsible to link A1 by a disulfide bond, and CTB by non-polar interactions across their interface. However, as the project will focus on the binding properties of the B-subunit, no further discussion of the A-subunit is presented here.

The CTB unit is formed of five equal monomers and each of them consist of a short helix α1 at the N-terminus, a long helix α2 and two 3-stranded antiparallel β-sheets. The β-sheets of the different monomers are combined making an interface formed by 6-stranded antiparallel sheet which link the monomers. The five α2 helices are situated inside the pentamer forming a pore whose diameter is 12 Å.[77,78] The principal binding sites located on the base of the protein and interacts with the ganglioside GM_1 (Figure 1.16).[34] Moreover, there are another five pockets located on the lateral side of the CTB. These correspond to the secondary binding sites, and they present some difference according to the biotype, but both of them interact with Lewis^y carbohydrate, one of the histo-blood group antigens, or Lewis^x trisaccharide (Figure 1.16).[75]

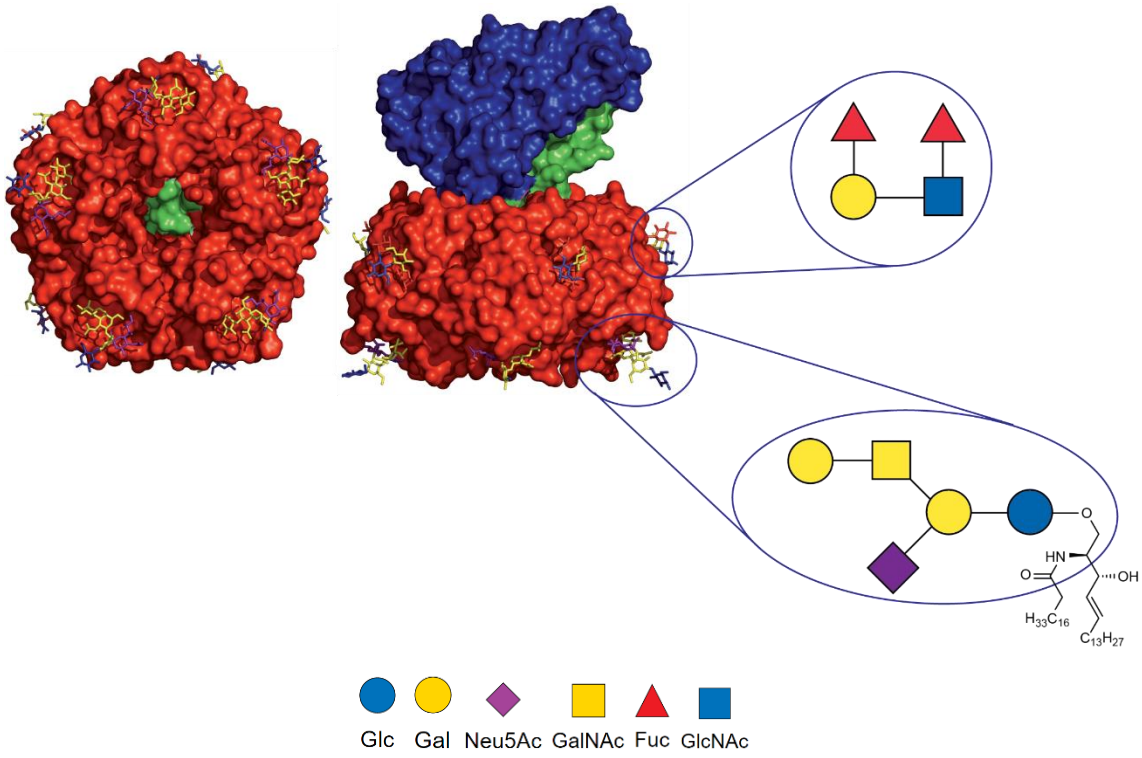

Figure 1.16: CT and its binding sites. The principal binding site, on the down, interacting with GM_1 and the second binding site, on the lateral, interacting with Lewis^y tetrasaccharide.

As mentioned above, GM_1 is a ganglioside presented on the cell membrane which interacts strongly with CTB. The selectivity of this binding site relies on the arrangement of the terminal Gal and the Neu5Ac.[79] The amino acids involved in this recognition process are part of a flexible loop that becomes more ordered upon binding making effective hydrogen bonds including through bound water molecules to stabilize the toxin-GM_1 complex. After isothermal titration calorimetry studies, it was concluded that the dissociation constant is 40 nM resulting to a strong non-covalent interaction.[80]

On the other hand, it has been observed that CTB also interacts with some other oligosaccharides such as Lewis^y or Lewis^x carbohydrates. Interaction with Lewis glycans and the lateral pocket of CTB were first reported by Holmner *et al.* in 2004.[81] Krengel and co-workers noted that the two biotypes of CTB differ in the residues involved in the interaction with Lewis oligosaccharides.[75] El Tor biotype contains a tyrosine (residue 18) and an isoleucine (residue 47) instead of histidine and threonine residues, respectively, in the classical biotype (Figure 1.18).

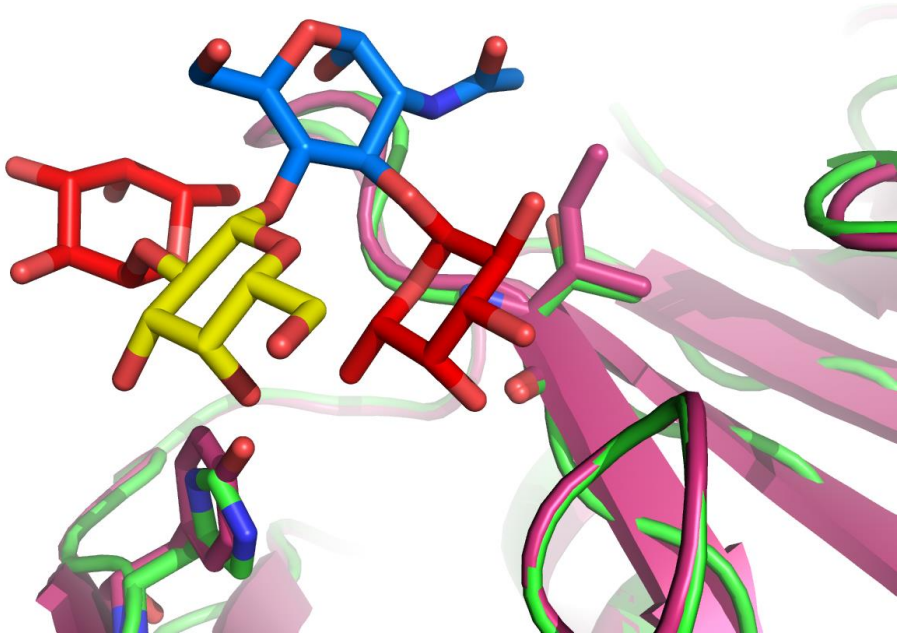

Figure 1.18: Difference between El Tor biotype and the classical biotype. El Tor biotype is in pink (Tyr20 bottom left and Ile47 top right) and the classical biotype is in green (His20 bottom left and Thr47 top right). The yellow, blue and red structure is the Lewis^y tetrasaccharide.

All histo-blood Lewis oligosaccharides (A-Le^y, B-Le^y and H-Le^y) were studied by surface plasmon resonance (SPR) experiments to define which interacts with CTB and which do not.[75] The A-Le^y pentasaccharide had an extremely weak interaction with ET-CTB (K_d over than 30 mM) while cCTB interacted more strongly (K_d = 2.19 mM).[74,75] Secondly, in the case of B-Le^y both proteins had high K_d values (over 30 mM) indicating there was no significant interaction between either CTB and this pentasaccharide. The difference between antigen A and B is the presence of GalNAc instead of Gal, meaning that the *N*-acetyl group helps A-Le^y to interact with cCTB. Finally, in the case of H-Le^y, both CTBs interact with the same strength (their K_d values are 1.05 and 1.48 mM for cCTB and ET-CTB, respectively).[75] However, X-ray crystallography revealed that the orientation of the tetrasaccharide differs in each biotype. The results of these studies concluded that ET-CTB can effectively distinguish the different antigens, while the classic biotype shows a reduced ability to distinguish between blood groups.

Isothermal titration calorimetry (ITC) studies provided complementary data after ensuring that the different histo-blood oligosaccharides were not interacting with the principal GM_1 binding site.[82] Dissociation constants calculated were very similar to the SPR data: the K_d for H-Le^y–ET-CTB interaction was 1.8 mM while interaction B-Le^y–ET-CTB was not measurable. These results concluded that El Tor CTB is prevented from binding to B-antigen.

This combined binding data has led to the hypothesis that the additional GalNAc or Gal residues in blood group A and B, respectively, produce more steric interferences avoiding strong interaction with ET-CTB but not for cCTB.[75] In contrast, H-Le^y antigen has pseudo-C2 symmetry with respect to the two fucose residues so it has two alternative orientations to bind with cholera toxin. The differential recognition may help to protect epithelial cells which contains A, B or AB antigens from the endocytosis of CT because there is low affinity with the glycocalyx, while epithelial cells with H antigen present have higher affinity with the toxin.[75] Probably for this reason individuals with blood group O suffer more severe symptoms than other people with different blood groups.

Lewis^x (Le^x) is also a binder for CTB in human epithelial cells.[34] This trisaccharide interacts only with the secondary binding site, as it was found by Heim *at al.*,[73] and its affinity is lower (K_d = 10 ± 3 mM) than the histo-blood antigens A-Le^y and H-Le^y because they contain an extra fucose residue increasing its affinity to the binding site. Although this oligosaccharide is smaller, the binding mode is very similar to H-Le^y.[73] Cervin *et al.* also showed that CT can recognize fucosylated structures including histo-blood antigens and Le^x and that the protein could be partially inhibited from binding to human enteroids by fucose and galactose derivatized polymer.[83] They suggested that CT binds weakly to any fucosylated structure from the glycocalyx and once this first binding has been achieved, the protein could go through the glycocalyx to arrive to the cell membrane.[34]

1.2.2.2 Mechanism of toxicity

The mechanism of action for cytotoxicity has several different stages: receptor binding, toxin endocytosis, A1 translocation and, finally, the catalysis of ADP-ribosylation (Figure 1.19).

The first step, once the toxin has been released in the intestine, is binding to sugars in the glycocalyx. While the traditional view of cell entry by CTB has assumed binding to GM_1 on the cell membrane, recent studies by Cervin *et al.* have suggested that binding to fucosylated structures through the secondary binding site can be sufficient to mediate cell entry.[34] Nevertheless, GM_1 ganglioside is believed to associate with lipid rafts forming membrane microdomains which help to achieve endocytosis. The lipid rafts also contain cholesterol and it is known that the endocytosis stage depends on the presence of cholesterol present on the cell membrane, as sterol-binding

agents immobilize the toxin and disrupt vesicle entry into the cell. These clusters also associate with caveolin proteins that can help CT to enter into the cell by endocytosis.

Following endocytosis, the vesicle containing the GM_1-CT complex is trafficked to the endoplasmic reticulum (ER).[84,85] Vesicles containing only the CTB-pentamer go through the Golgi apparatus but, curiously, this is not the case of CT holotoxin-vesicles, which are redirected to the ER. To enter the ER, the vesicle needs a COPI coat, a group of proteins around the vesicle membrane. By this way, the vesicle can be recognized by ARF receptors in ER and enters into this organelle. Normally, a protein also needs to be tagged with a KDEL motif located in the C-terminal position for ER trafficking. The A-subunit contains a KDEL motif in the C-terminal position but, in the case of CT, it seems that it is not essential to enter on ER.[84]

Once cholerae toxin is inside the ER, the A1 moiety needs to separate from the protein complex to access to the cytosol and catalyse the ADP-ribosylation. Protein disulfide isomerase (PDI) present in this organelle is responsible for catalysing the cleavage of the disulfide bond that links A1 and A2-B_5. After dissociation, the catalytic part (CTA1) adopts an unfolded state and it is identified as a misfolded protein triggering its translocation to the cytosol mediated by the Sec61p complex and ATP.[85]

Finally, when CTA1 is present in the cytosol, it is stabilised and activated by the formation of a complex with ARF-6 which activates it to transfer an ADP-ribose moiety from NAD to Arg201 in $G_s\alpha$. Irreversible ADP-ribosylation inhibits the GTPase activity of $G_s\alpha$ causing the activation of adenylate cyclase which is a key enzyme which transforms ATP to cAMP and pyrophosphate. The resulting increase of cAMP levels is involved in several processes such as the stimulation of Cl^- secretion, the opening of potassium channels and secretion of Na^+ and K^+ to balance the Cl^- secretion and, also, the activation of phospholipase A2 (an enzyme which cleaves fatty acids).[84] All of these effects causes the loss of liquid to try to compensate the extracellular high concentration of ions, and results in diarrhoea.

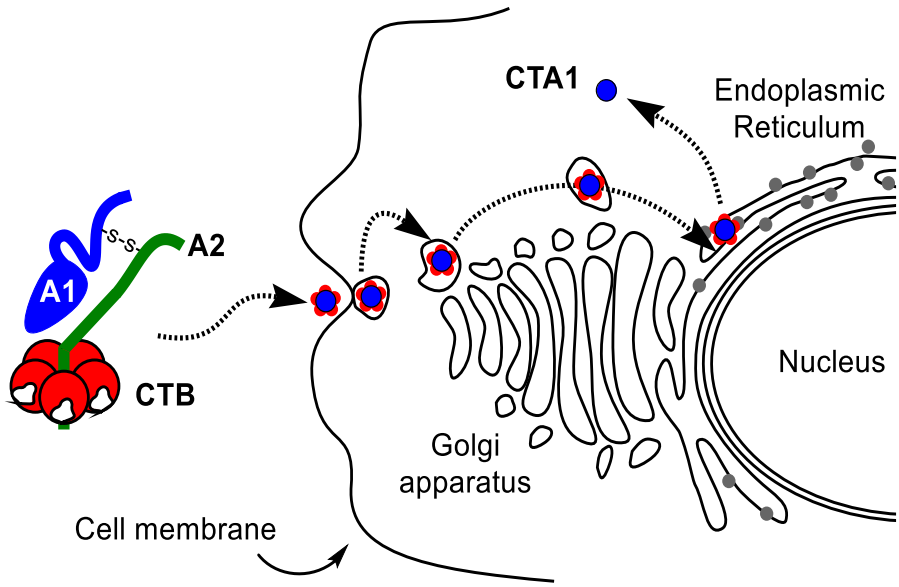

Figure 1.19: Mechanism of toxicity performed by CT. This figure is reproduced from reference 85 under a Creative Commons CCBY4.0 licence.

1.2.3 Shiga Toxin

Shiga Toxin is also a protein belonging to the AB_5 toxin family, and is secreted by two different bacteria: *Shigella dysenteriae* type 1 (*S. dysenteriae*) and some strain of *Escherichia coli* such as O157:H7.[28,86] Both bacteria cause food poisoning resulting of abdominal pain, watery diarrhoea, haemorrhagic colitis (HC) and hemolytic uremic syndrome (HUS).[87–90]

Shiga Toxins are classified into two main subtypes according to the immunological responses: Shiga Toxin (STx) and Shiga Toxin type one (STx1) on one side, secreted by *S. dysenteriae* type 1 and *E.coli*, respectively; and Shiga Toxin type 2 (STx2) produced by *E.coli*.[86] The difference between these two subtypes relates to both parts of the protein complex: the A-subunit of STx/STx1 is four amino acids shorter than STx2 and only 55% of both sequences are identical. In addition, in STx2 the last two amino acids from C-terminal of peptide A2 subunit partially blocked one of the binding sites as the peptide protrudes through the pore and interacting with a binding site on the opposite face of the B-subunit.[28,91] The B-subunits of both subtypes are formed by 5 identical monomers but again the amino acids sequence is slightly shorter for STx/STx1 than for STx2, in this case by 2 amino acids. Nevertheless, both B-pentamers are able to recognize Gb_3 in the cell membrane.[28,86]

1.2.3.1 Structure and binding sites

The A-subunit is formed of two domains: A1 (27.5 kDa) which is the cytotoxic agent, and A2 (4.5 kDa), which links A1 with the B-subunit. The A1-subunit, which is formed mainly of β-sheets, has ribonuclease activity responsible for removing a specific adenine base from RNA of the 60S

ribosomal subunit in the infected cell. Once that happens, the host cell is unable to express any protein due to the failing of the ribosomes[91–94] The A1-subunit is attached to A2 by a disulfide bond between cysteines, Cys-A241 and Cys-A260 for STx2 and Cys-A242 and Cys-A261 for STx/STx1. Finally, the A2-subunit is basically an α-helix of which the C-terminal residues interact with Shiga Toxin B subunit (STxB).[91,95]

The B-subunit for Shiga Toxin is, as a member of the AB_5 toxin, a pentamer formed by five equal monomers (69 amino acids for STx/STx1 and 71 residues for STx2). Each of these monomers are folded into one α-helix and six β-sheets forming a pore of 11 Å for the diameter. Facing the inside of the pentamer, there are the five α-helix while the β-sheets cover the outside of the protein.[95] Both types of Shiga Toxin proteins have three binding sites per monomer, meaning 15 binding sites in total, that recognize Gb_3 ceramide and, in some subtypes, Gb_4 ceramide too. However, there are differences between STx/STx1 and STx2 regarding how the binding sites work due to the amino acids sequence differs from one type to another giving as a result different affinities for the Gb_3.[28,91]

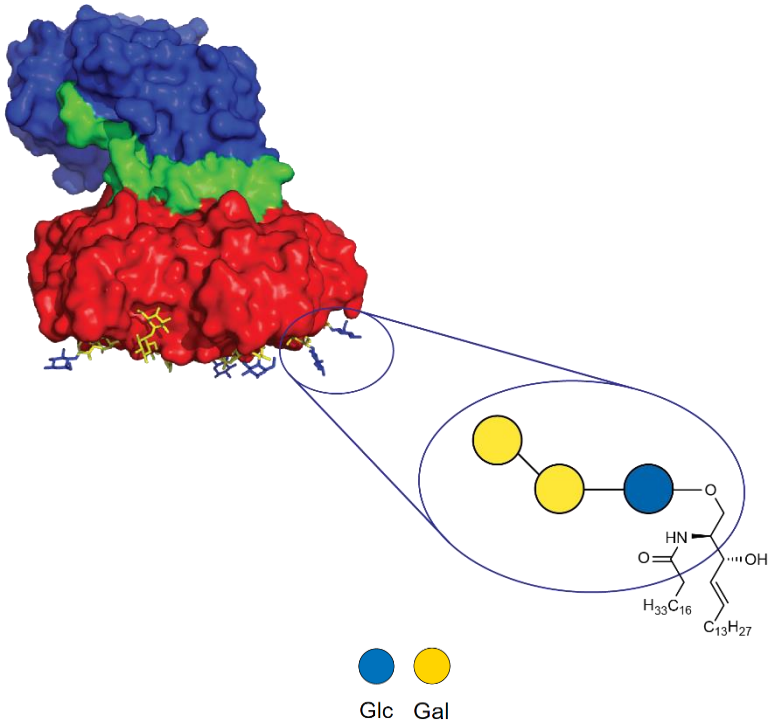

Figure 1.20: STx/STx1 and STx2 and its binding sites. The principal binding sites, on the down, interacting with Gb_3 ceramide.

The three binding sites per monomer of the Shiga Toxin B-subunit are identified as binding site 1, binding site 2 and binding site 3 (Figure 1.21). Site one is a pocket found between B monomers where a groove is created between two β-sheets when two subunits interact.[91] This binding site is formed by Phe30 and Asp17/18: Asp17 for STx/STx1, and by Asp18 for STx2 form hydrogen bonds

with the polar groups of the carbohydrate providing binding specificity, while the aromatic ring from the phenylalanine stacks against the beta Gal ring.[96,97] In the case of type STx2e, a protein which is associated with pig disease and only interacts with Gb_4 ceramide, binding site 1 also has a Gln64 and Lys66 to interact with *N*-acetyl-galactosamine.[28,96] Binding with Gb_3 in binding site 1 occurred once binding site 2 is saturated with the oligosaccharide.[98]

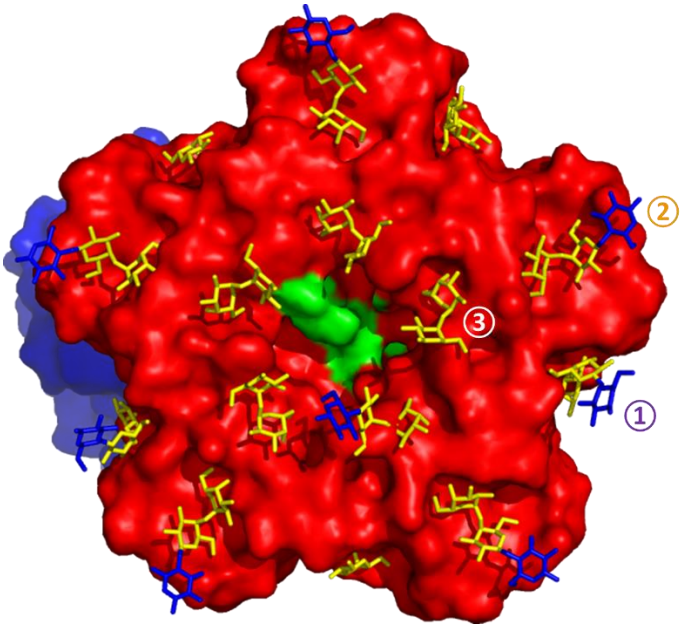

Figure 1.21: STx/STx1 and STx2 and its binding sites. Binding Site 1 is marked in purple, Binding Site 2 marked in orange and Binding Site 3 in white.

The second binding site is located, as it can be seen in Figure 1.21, on the bottom face of the protein. For binding site 2, there are differences between the conformation of STx/STx1 and STx2 giving rise to differences in the affinity for Gb_3 ceramide. In the case of STx2, the first amino acid of the sequence (Ala-B1) forms a hydrogen bond with Ser-B53, while for STx and STx1, the second amino acid of the sequence (Pro-B2) is responsible for making a hydrogen bond with Ser-B53. The switch from alanine to proline in the binding site leads to a change in the conformation in the loop and, hence, to different affinities with the same oligosaccharide. In addition, there are differences in the conformation due to the disulfide bond between Cys-B3 and Cys-B56 for STx2, and between Cys-B4 and Cys-B57 for STx/STx1, that lead to different binding interactions with Gb_3 in the binding pocket.[91,95,96]

Finally, binding site 3 is found in the base of the protein, close to the pore formed by the five monomers. The last two residues from the A2 tail in Stx2 block the tryptophan crucial for the binding of Gb_3 in one of the binding sites, decreasing dramatically the binding with the carbohydrate for this subtype.[28,91] On the other hand, STx1 show the same and common conformation for Trp leading

to easier binding to Gb_3 ceramide.[91] This binding site has the lowest affinity for the oligosaccharide for all Shiga Toxins.[96]

It is difficult to quantify in K_d for binding between Shiga Toxins and Gb_3 oligosaccharide because all binding sites showed different affinities with the same ligand. However, Shimizu *et al.*[99] were able to provide some light on this aspect.[99] According to their study, a 1.9 mM solution of STx/STx1 with an equimolar amount of Gb_3 oligosaccharide, less than 15% of binding site 1 is occupied relative to binding site 2, and no evidence could be found for interaction with binding site 3.[99] Combining microcalorimentry experiments performed by St Hilaire, *et al.*,[67] and the data achieved by NMR,[99] it seems plausible to conclude that the K_d is 2 mM for binding site 2, and 6 mM for binding site 1. Furthermore, mutation of binding site 1 led to a decrease in the affinity of the StxB protein to cells by a factor of about three, while mutation in binding site 3 did not change the lectin affinity with cells.[100]

1.2.3.2 Mechanism of toxicity

Shiga Toxin has a similar mechanism of toxicity to Cholera Toxin that shares the same steps: interaction with the receptor, endocytosis of the protein, release of A1 into the cytosol. (Figure 1.22).

The individual affinity of Gb_3 oligosaccharide for each STx binding site are low, but multivalent presentation of the Gb_3 glycolipid in the cell membrane allows multiple STx binding sites to be bound simultaneously, enhancing the affinity substantially. It seems likely that binding sites 1 and 2 are the ones that bind first followed by the recognition of binding site 3 in the presence of sufficient Gb_3 glycolipid.[101]

Once the lectin has bound to the receptor, it is endocytosed by different pathways. One of these endocytosis paths involves activating the kinase Syk followed by clathrin-dependent endocytosis and the other is dynamin-dependent tubular endocytosis.[101,102] For the first path, it is reported that it involves formation of a clathrin-coated basket containing the toxin which is internalized by the cell.[103] However, inhibition of clathrin-dependent uptake did not lead to absence of STx inside the cell meaning that there is another pathway for the toxin to be internalized. For this pathway, Shiga Toxin binding leads to rearrangement of the lipids, inducing tubular intermediate formation that leads to its internalization.[102] It is not possible to ensure the importance of this pathway because, while tubule formation happens in giant unilamellar vesicles it is not clear that this effect also occurs in the cell membrane due to the differences between the cell membrane and the lipid bilayer models.[100,101]

Sorting Shiga Toxin from the endosome to the Golgi apparatus is one of the most important steps for the cell's intoxication because the cleavage of the A-subunit into its A1 and A2 chains

(which are still disulfide-linked) takes place in the Golgi.[96,104] Its cleavage is performed by a Furin enzyme, which is a calcium-sensitive serine protease that recognizes Arg-X-Arg or Arg-X-Lys motifs, present in the A-subunit. Once in the Golgi, different paths can lead STx to ER including COPI-dependent (proteins which induce functional transport of vesicles), and independent transport routes.[105] Either way, Shiga Toxin controls the signalling of the vesicle to ensure its path to the ER.[101]

Finally, once in the ER, the disulfide bond is reduced, releasing A1 from A2 and thus the dissociation of the A- and B-subunits of Shiga Toxin. Then A1 is associates with ER intraluminal chaperones, that are responsible for the folding and unfolding of big proteins, and the toxin is translocated to the cytosol, where it re-folds into its active conformation which it acts as an enzyme removing of a base from the 60S ribosomal subunit, inhibiting protein expression in eukaryote cells which lead to cell death.[28,96]

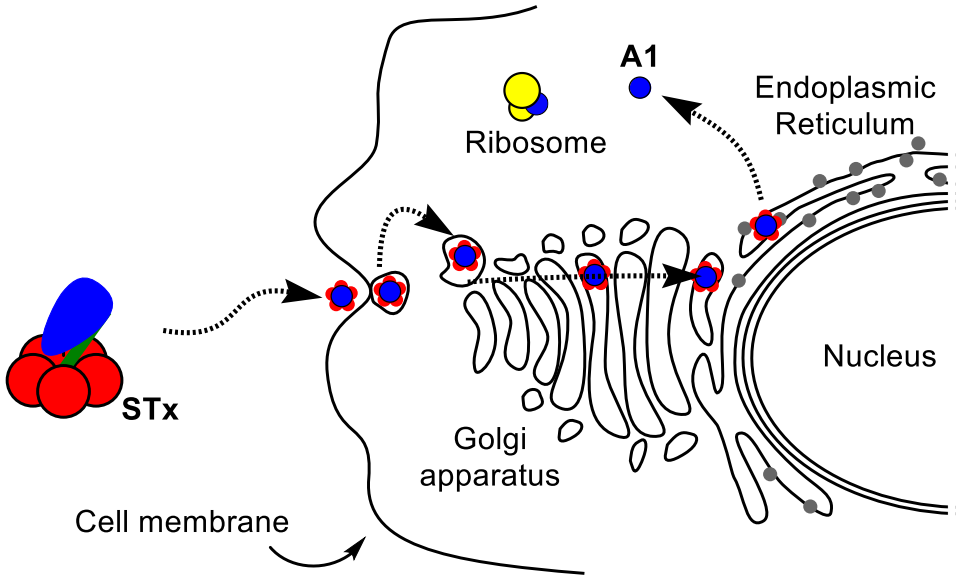

Figure 1.22: Mechanism of toxicity performed by STx.[28,96,101]

1.3 Bioorthogonal reactivity

Conjugation of proteins, DNA, RNA or carbohydrates with molecules which offer new functionality, such as drugs or reporter groups (like fluorophores or radiolabels), in a specific way is an important and widely researched topic in chemical biology.

Not all the reactions available in chemistry are useful for this purpose as reagents have to be chemoselective over other reactive functional groups present in biomolecules. They also need to be compatible with aqueous conditions at physiological pH and the reaction rate must be reasonable at 37 °C while using low concentrations of reactants to be suitable for reaction *in vitro*

and *in vivo*.[106] When these requirements are applied to a range of reactions, only a few could be useful as bioorthogonal reactions. For all the discoveries in this field, M. Meldal and B. Sharpless won the Nobel Prize in 2022 for the discovery of copper-catalysed azide-alkyne (CuAAC) as well as C. Bertozzi due to her discoveries applying click chemistry in living organism and establishing the strain-promoted [3+2] azide alkyne cycloaddition (SPAAC).[107]

The most used and common reaction to synthesize conjugates is copper-catalysed azide-alkyne (CuAAC) cycloadditions between an azide and alkyne (Figure 1.23, a).[108] This reaction offers all the conditions previously mentioned but the use of copper (Cu(I)) as a catalyst presents a significant challenge: its toxicity. Different strategies have been developed to make CuAAC more biocompatible as, for example, water-soluble Cu(I) ligands that stabilize the metal oxidation state. Consequently, this reaction has been commonly used in protein labelling.[109,110] CuAAC will be described in more detail in section 1.3.1.

Other reactions are also useful for bioconjugation and less toxic, for example, strain-promoted [3+2] azide alkyne cycloaddition (SPAAC) (Figure 1.23, b).[111] The principal advantage of this reaction is the absence of a metal catalyst and its compatibility in physiological conditions. While these reactions are relatively slow, using different cyclooctyne analogues has been shown to improve the reaction's rate.[112]

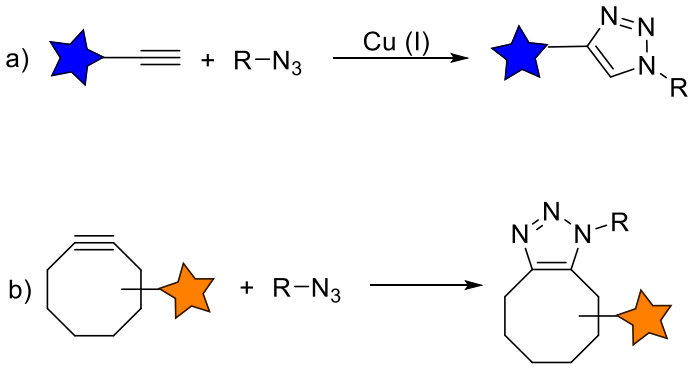

Figure 1.23: a) CuAAC reaction, b) SPAAC reaction.

Maleimides are also frequently used for bioconjugation because they offer two different reactivities useful in biochemistry: the Michael-type reaction with a thiol and the Diels-Alder cycloaddition with a diene (Figure 1.24). The first reaction is useful to link different moieties, such as a reporter group or a drug, to a cysteine residue in a protein. Nevertheless, a problem has been reported for Michael-type reactions: thiol-exchange (Figure 1.24, a).[113,114] On the other hand, maleimides can react with a conjugated diene by the Diels-Alder reaction. This type of reaction does not produce side products and it can be done under physiological conditions but, in some

cases, the resulting cycloadducts can be reversible in mild condition (retro-Diels-Alder reaction) (Figure 1.24, b).[115]

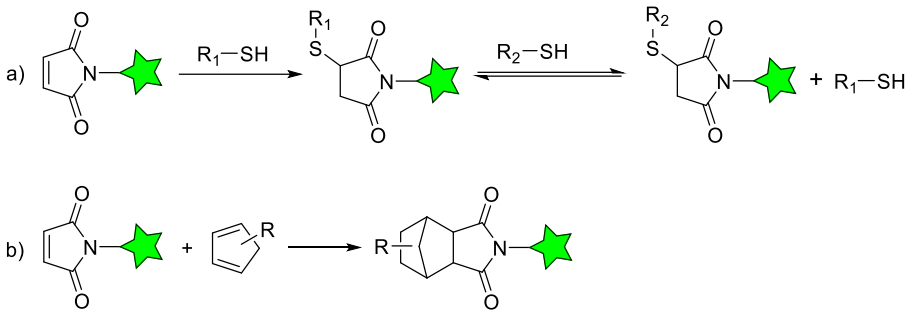

Figure 1.24: a) The two side reactions taking place on maleimide-thiol Michael-type adducts. b) Diels-Alder reaction between maleimides and dienes.

Finally, there is a bioorthogonal reaction which almost accomplishes all the requirements: the [4+2] cycloaddition between 1,2,4,5-tetrazines and different dienophiles, for example, norbornene, cyclopropene or *trans*-cyclooctene.[116] Inverse electron demand Diels-Alder (IEDDA) cycloaddition is fast, very chemoselective, without the need for a catalyst and biocompatible. Furthermore, its kinetics depend directly on the reagents. For all these reasons, IEDDA is one of the best "click" reactions that can be used nowadays (Figure 1.25).[116] IEDDA will be described in depth in section 1.3.2.

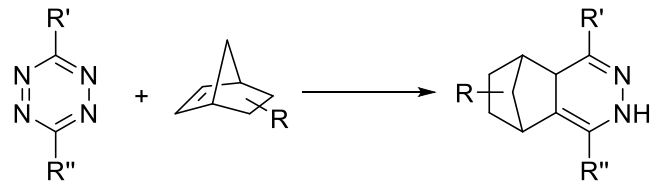

Figure 1.25: IEDDA reaction between a tetrazine and norbornene.

1.3.1 Copper (I)-catalysed azide-alkyne cycloaddition (CuAAC)

Copper (I)-catalysed azide-alkyne cycloaddition (CuAAC), a version of Huisgen 1,3-dipolar cycloaddition or click-reaction, is a reaction that takes place between organic azides and alkynes to give triazoles as a product.[117,118] This reaction gained importance in 2001, when the research groups of Meldal and Sharpless, independently, introduced copper (I) as a catalyst improving the regioselectivity and speed of the reaction.[119,120]

Among the benefits of CuAAC reactions are high yields, very strong regio-selectivity and suitability for both biomolecular ligation and tagging. In addition, the triazole formed is chemically inert to many reaction conditions such as oxidations, reductions and hydrolysis.[119] For all these

reasons, CuAAC cycloadditions offer a range of applications in several fields including material science, polymer chemistry or conjugation of biomolecules.[108,119,121]

The first reaction mechanism was suggested by Sharpless and co-workers,[120] but recent studies seem to indicate that it was more complicated than it was suggested initially involving copper binuclear complexes. The alkyne molecule is complexed with one of the atoms of copper. Then, this formed the Cu(I) acetylide complexes with another copper center *via* the acetylide π-orbitals. This resulting complex reacts with the azide to generate a bis(copper)triazole. Finally, protonation from the acetylide takes place to give the final triazole product and regenerate the active catalyst as shown in Figure 1.26.[119]

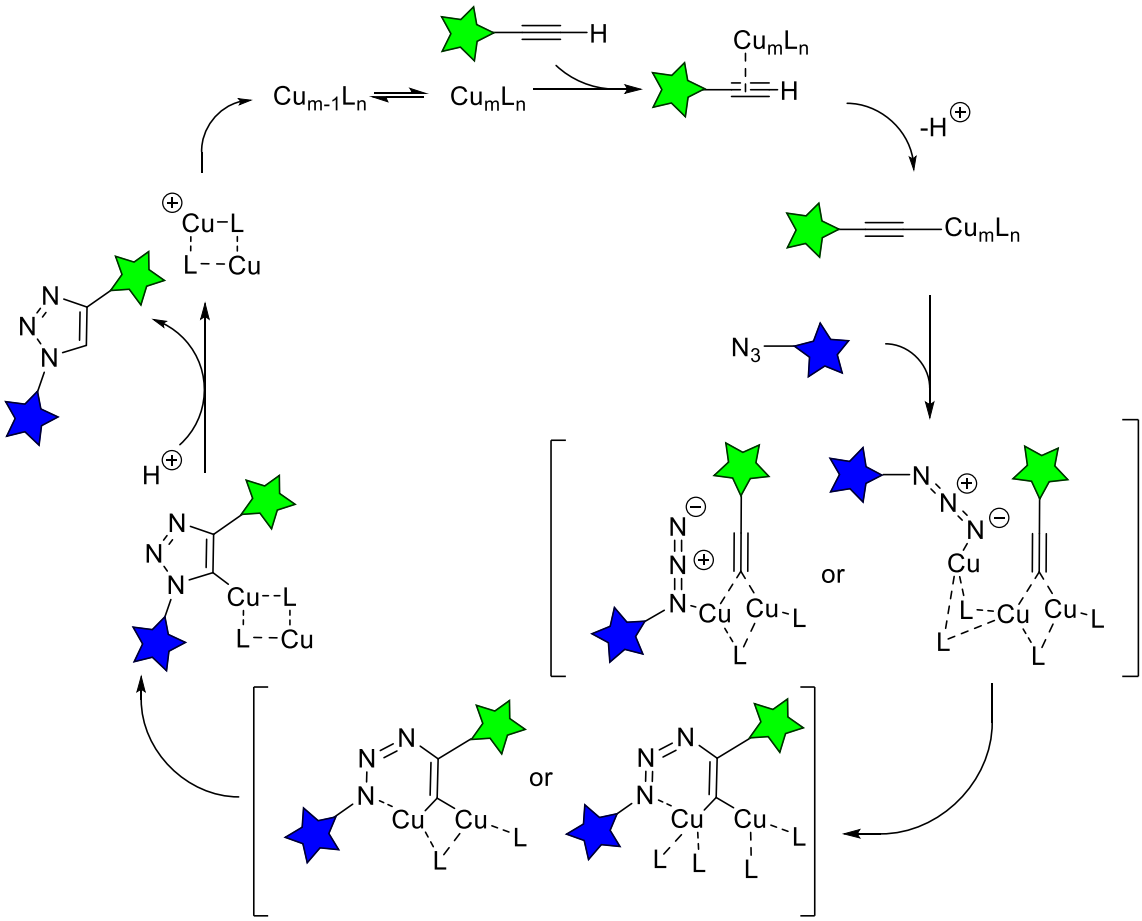

Figure 1.26: Mechanism of Copper(I) catalysed between an alkyne and azide. “m” refers to the oxidative state of Cu and “n” refers to the number of ligands complexed to the ion metal.

Formation of triazoles from azides and terminal alkynes under catalysis by Cu(I) can be performed under a wide variety of conditions as long as the reagents are maintained in solution and the Cu(I) is not removed by oxidation to Cu(II). Nevertheless, the most important factor seems to be the maintaining of high concentrations of Cu(I) at all times during the reaction. For this reason, other reagents are added during CuAAC reactions, like sodium ascorbate, to reduce Cu(II) to Cu(I).

Despite the broad applicability of CuAAC cycloaddition in synthetic modification, this reactivity cannot be used in living organism or with its components, like proteins, due to the toxicity of copper which can lead to the formation of reactive oxygen species (ROS), like superoxide and peroxides, which are able to oxidase amino acids such as cysteines, tryptophans or serins.[122] These species are highly reactive and they continue to be generated in the presence of molecular oxygen until the reducing agent is consumed. To reduce this effect, ligands such as tris((1-benzyl-4-triazolyl)methyl)amine (TBTA) (Figure 1.27, a) or 3-(4-((bis((1-(*tert*-butyl)-1H-1,2,3-triazol-4-yl)methyl)amino)methyl)-1H-1,2,3-triazol-1-yl)propane-1-sulfonic acid (BTTES) (Figure 1.27, b) have been used to improve catalytic activity, stabilize the Cu(I) oxidation state and try to prevent oxidation of amino acid residues like cysteines and histidines in proteins.[123,124] For this reason, even though it has great advantages, the CuAAC chemistry has been gradually set aside in biological applications in favour of alternative biorthogonal reactions such as SPAAC or IEDDA.

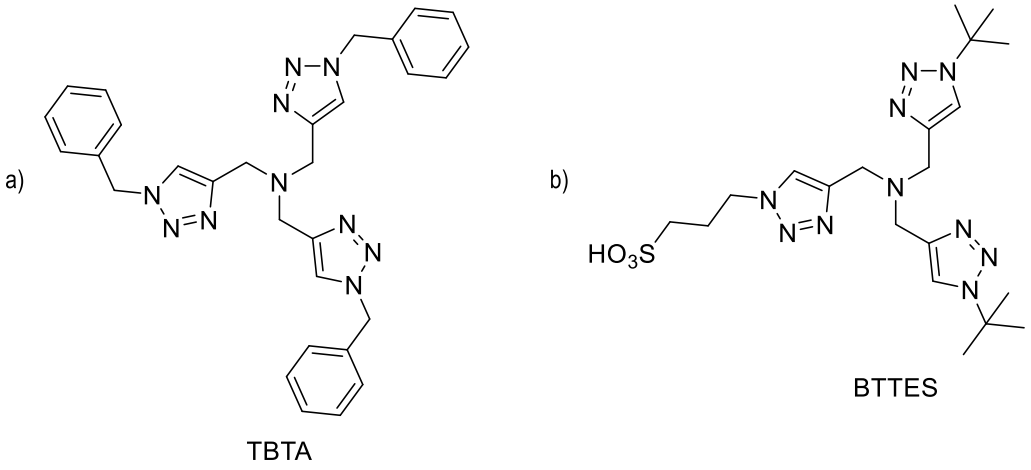

Figure 1.27: Chemical structure for a) TBTA and b) BTTES useful to improve CuAAC side effects in presence of proteins.

1.3.2 Inverse Electron Demand Diels-Alder Reaction (IEDDA)

The Diels-Alder reaction (DA) is a pericyclic [4+2] cycloaddition reaction between a dienophile and a diene that produces a cyclohexene product. The inverse electron demand Diels-Alder (IEDDA) reaction has been reported to be one of the most optimal bioorthogonal reactions because it presents several advantages which include; high selectivity; fast rates at low concentration; no requirement for metal catalysis; and compatibility with physiological conditions to perform the cycloaddition. Moreover, it offers the possibility to perform other orthogonal click reactions without influencing the formation of its product.[125] For these reasons, it has been really useful for the study of different biological process or for the synthesis of bioconjugates.[126–128]

The different substituents on the diene and dienophile establish the electronic effects that allows the classification of DA cycloadditions into “normal” electron demand and “Inverse” Electron Demand Diels-Alder reaction. According to molecular orbital theory, normal DA reactions between electron-rich dienes and electron-deficient dienophiles are controlled by diene HOMO and dienophile LUMO interactions. Different electron-withdrawing groups (EWG) or electron-donating groups (EDG) inserted in the dienes or dienophiles can help the kinetics of DA reactions. Dienophiles with EWG and dienes with EDG decrease the energy gap between the frontier orbitals allowing greater reaction rates in DA cycloadditions. IEDDA reactions take place between electron-poor dienes and electron-rich dienophiles. In this case, EDG in the dienophile raise the energy of HOMO whereas EWG in dienes reduce the LUMO energy, so these groups contribute to increase the kinetics of IEDDA (Table 1.1).

Table 1.1: Optimal combinations of dienes and dienophiles for “normal” DA cycloaddition and IEDDA reaction.

Normal DA reaction	**IEDDA**
	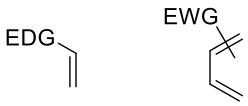
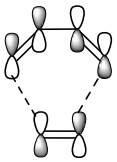 $HOMO_{Diene}$ $LUMO_{Dienophile}$	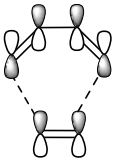 $LUMO_{Diene}$ $HOMO_{Dienophile}$

IEDDA reactions are used for biorthogonal ligation usually take place in one step but while using norbornenes as dienophiles, there is an extra step: firstly, the diene, normally a tetrazine, reacts with an alkene or alkyne in a [4+2] cycloaddition forming a bicyclic intermediate. Then, a retro-DA reaction takes place releasing nitrogen and generating a dihydropyridazine (Figure 1.28).

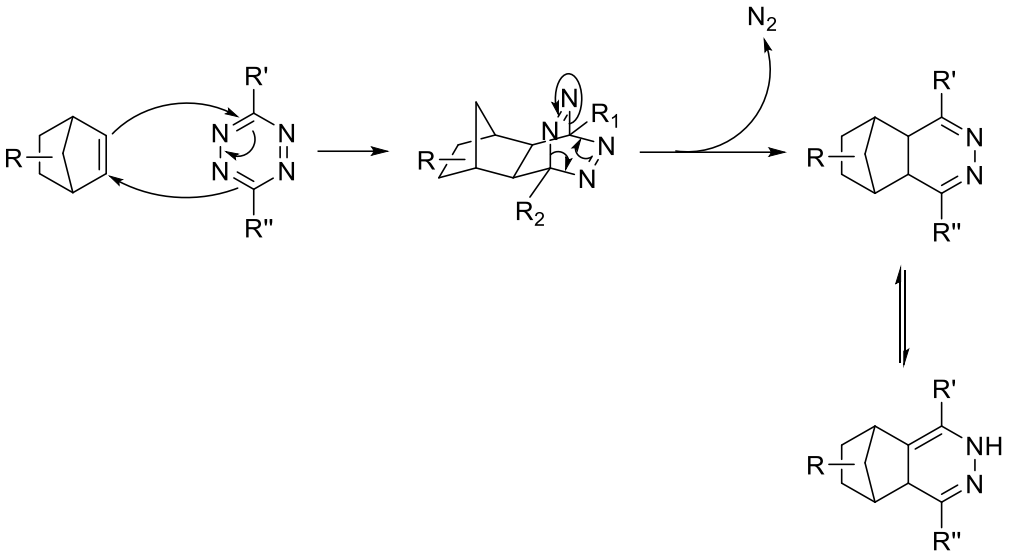

Figure 1.28: Mechanism of IEDDA reaction between a tetrazine and a norbornene.

Moreover, other factors can influence to the speed of the reaction, and changes in each reagent can improve the rate of the reaction. In the case of the dienophiles, there is a relationship between the IEDDA kinetics and the degree of strain of the dienophile so, for this reason, strained rings react faster than non-tensioned alkenes. For example, *trans*-cyclooctene (TCO) is the fastest dienophile because of its "crown" conformation, followed by cyclopropene, which is the most strained ring containing a cis-double bond (Figure 1.29).[116]

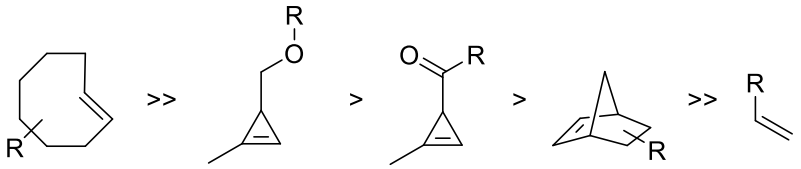

Figure 1.29: Different dienophiles ordered by their reactivity in IEDDA cycloaddition.

Two different factors influence kinetics of tetrazines in IEDDA reaction.[116] The most important effect reported for these dienophiles is steric hindrance, consequently, if the tetrazine is monosubstituted the reaction rates are higher than for disubstituted tetrazines (Figure 1.30). The use of small substituents such as methyl groups substantially decrease the kinetics of the cycloaddition reaction: for a tetrazine, which contains the same substituent, the addition of a methyl group decreases the rate by factor 30.[129] The incorporation of other substituents in a tetrazine, even if it is a strong EWG, does not fully compensate for the impeding steric effect. However, substituents such as 2-pyrimidinyl does not reduce the speed of the reaction significantly because of its high electron-withdrawing properties.[130]

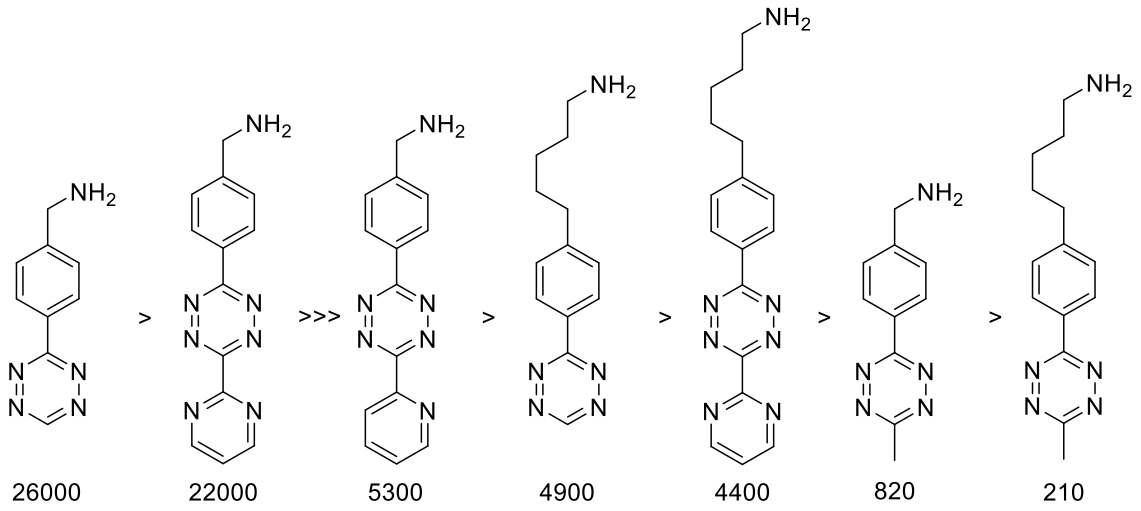

Figure 1.30: Different tetrazine derivatives ordered by their reactivity with TCO in PBS at 37 °C. The numbers provided correspond to the second order rate (M^{-1} s^{-1}) constant of these reactions.[129]

1.4 Aims and objectives

The aim of this project was to build mucin-like glycopolymers with well-defined structures and composition, to study the interactions with B-subunits of the AB_5 toxins: CTB and STxB. The complexity of the glycocalyx containing hundreds of different oligosaccharides makes difficult to know exactly how these proteins interact with this layer, therefore, the creation of a glycocalyx model using the mucin-like glycopolymers with well-defined structures provides a tool to study these first interactions and achieve a better understanding about this process impossible to perform in cell membrane.

As explained in the introduction, CTB can recognize Le^x in its secondary binding site but it is unknown how interactions of this protein with the glycocalyx affects its biological function. For this reason, to understand better how CTB interacts with a glycocalyx model enriched with fucosylated structures and the role of its secondary binding site, a mucin-like structure containing Le^x was to be synthesized and the interaction with different glycocalyx model and CTB studied.

On the other hand, STxB shows affinity to Gb_3 ceramide in the cell membranes, but similar oligosaccharides can also be found in glycoproteins higher in the glycocalyx. It is unknown how this protein behaves in a film enriched with Gb_3 oligosaccharide so, for this reason, a mucin-like structure containing a high percentage of this trisaccharide was to be prepared. Then, using it as a building block to construct different glycocalyx models, it would allow the interaction between these models and STxB to be studied providing new insight into how this protein may behave within the glycocalyx.

The requirements for these mucin-like glycopolymer structures include having a backbone that is soluble in physiological conditions and suitable to perform derivatization; the attachment of oligosaccharides to the backbone while controlling degree of derivatization; and, finally, a method suitable to anchor the structure from a single site on the glycopolymer to a surface to mimic the mucin's structure (Figure 1.31).

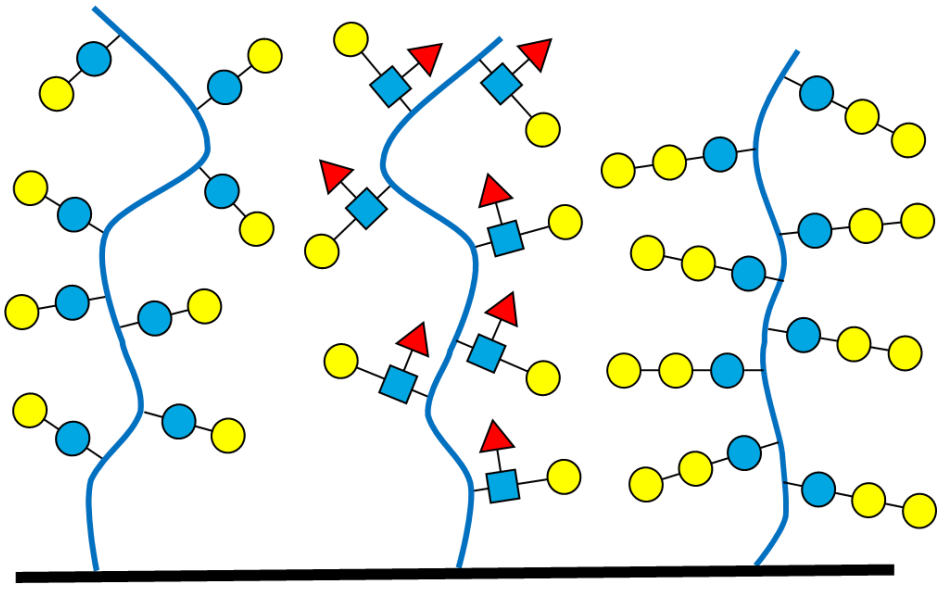

Figure 1.31: Scheme of the mucin-like structures to be built as the aim of this project.

The first objective of this project was to construct these complex structures; for this reason, different reactive functional groups were introduced onto hyaluronic acid (HA) which was chosen as the backbone of the glycopolymer structures. Then various oligosaccharides including, lactose, Le^x and Gb_3 oligosaccharides were prepared with functional groups complementary to those introduced into HA. These mucin-like structures were then prepared and evaluated as building blocks for the creation of glycocalyx models, followed by their exposure to CTB or STxB to have better understanding how these proteins interact with the glycocalyx models. The various processes that were performed to achieve the main goal of the project are outlined in the following paragraphs.

Chapter 2 describes the first plan to build the mucin-like structures, which was to incorporate of tetrazines on the HA backbone while norbornene would be incorporated in the anomeric position of the oligosaccharides. Due to solubility problems shown by HA with a high degree of substitution of tetrazine, this approach was dismissed to accomplish the primary aim of this project. Nevertheless, HA with a low degree of substitution with tetrazines proved useful for attachment of proteins for the construction of superselective probes.

Chapter 3 is focused on the enzymatic synthesis of the Le^x trisaccharide and Gb_3 oligosaccharide that contained an azide at its anomeric position. The synthesis of some of these oligosaccharides required the expression of the enzymes and evaluation of their activity. In addition, it was important to establish the best reaction conditions for carbohydrate synthesis.

Due to the incorporation of an azide in the anomeric position of the oligosaccharides, the synthesis of a hyaluronic acid containing an alkyne was required. For this reason, the attachment

of propargylamine to HA suitable to perform CuAAC cycloadditions is described in Chapter 4. The incorporation of the different carbohydrates in the alkyne derivatized backbone was performed by CuAAC reaction with the azido-derivatized oligosaccharides. These structures were characterised by NMR spectroscopy and size exclusion column chromatography with multi-angle scattering light detector (SEC-MALS) becoming precursors for the mucin-like structures.

Finally, Chapter 5 includes the incorporation of an anchor (biotin or poly-histidine) at the reducing end of the derivatized HA to achieve derivatized polymers suitable for performing binding studies on a surface. Once these structures were accomplished, a glycocalyx model was built and characterized by quartz crystal microbalance with dissipation monitoring (QCM-D) and spectroscopy ellipsometry (SE). Following successful characterization, binding studies between CTB or STxB and the different glycocalyx models built using hyaluronan, lactose-derivatized hyaluronic acid, Lewis^x-derivatized hyaluronic acid and Gb_3-derivatized hyaluronic were monitored by QCM-D and quantified by SE.

CHAPTER 2: CONSTRUCTION OF TETRAZINE-DERIVATIZED HYALURONIC ACID

2.1 Introduction: coupling to hyaluronic acid

Hyaluronic acid (also known as hyaluronan or HA) is a glycocalyx polysaccharide that is part of the glycosaminoglycan family. It performs several functions in the cell membrane, like maintaining its hydration or protect the cell from external agents.[39] Because of its physical and chemical proprieties, hyaluronic acid is also an interesting material to derivatize for production of hydrogels or conjugates with multiple functions including drug-delivery, tissue engineering and making artificial tissues.[131–137]

As shown in figure 2.1, various reactive groups are available that could be used to perform chemical reactions on HA, but the most reactive ones are the carboxylic acid groups on GlcA, existing in their ionized form in solution, and the primary hydroxyl group on GlcNAc. Deacetylation of the *N*-Acetyl group could also be used to provide a reactive amino group. Among these groups, the one which allows more selective reactivity is the carboxylic acid, which is suitable for making amides or esters. Furthermore, derivatization of this group has little impact on the mechanical properties of the polymer.[138,139]

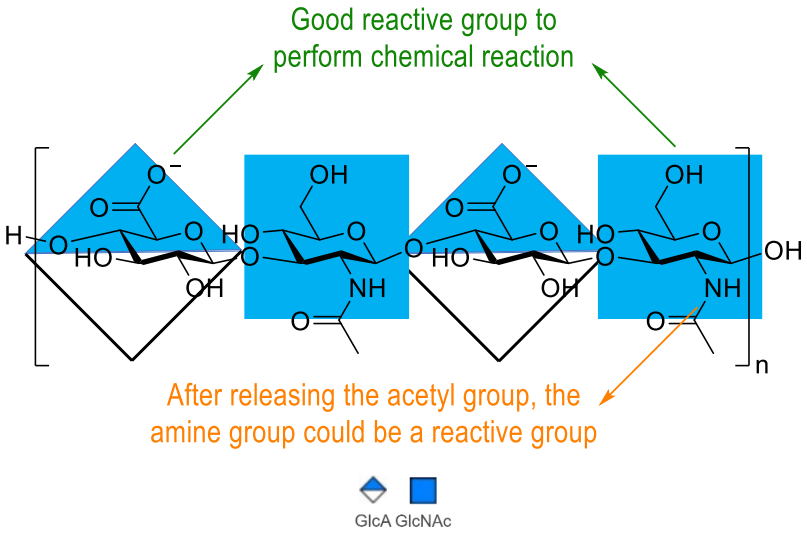

Figure 2.1: Hyaluronic structure and its possible reactive groups suitable to perform chemical reactions.

Several methods have been described to form an amide bond from the carboxylic acid in the HA chain, like using NHS and EDC as activators.[140,141] This well-known reaction has several advantages including the possibility to use both aqueous solution or organic solvents; potential high degree of substitution of the polymer; and the HA sodium salt can be used directly as purchased without any need for other chemical modifications such as deacetylation that would be required for derivatisation of amino groups. However, there are also disadvantages: It has been reported that the pH for amide coupling needs to be acidic (between 3.5 and 4.5 for highest efficiency of

activation which mean that the presence of protons and dissociated carboxyl groups are necessary for the reaction of carbodiimide), however under such conditions the amine is protonated and thus a less reactive; and large amounts of EDC are required because of its hydrolysis (or the active ester intermediate) in water.[139,142,143]

There are other methods for amidations using activators such as 2-chloro-1-methylpyridinium iodide (CMPI),[144] 1,1'-carbonyl-diimidazole (CDI)[145] or triazines, like 2-chloro-4,6-dimethoxy-1,3,5 triazine (CDMT). These last two presented mild reaction conditions and high degree of derivatization on HA.[146] Finally, the formation of the tetrabutylammonium (TBA) hyaluronan salt improves the reactivity of the carboxylic acid, making the amide or ester bond formation easier.[139] However, this methodology requires extra steps increasing the chances for degradation of the backbone, the use of resins for ion exchange and organic solvents such as DMSO giving as a result difficulties during the purification steps.[139,147]

2.2 Synthesis of a tetrazine-derivatized hyaluronic acid

Due to the advantages presented by IEEDA reactivity including the high selectivity; fast rates at low concentration; no requirement for metal catalysis; and compatibility with physiological conditions to perform the cycloaddition, this reaction was a good choice to attach carbohydrates or proteins to HA.[148–150]

Among all the options available, a tetrazine-derivatized hyaluronic acid presents many advantages: the first one is easier calculation of the degree of substitution. Because the molar extinction coefficient (ε) is known, the degree of substitution could be calculated by the UV-visible spectroscopy absorbance as well as by ^{1}H NMR peak integration.[151,152] Moreover, because the tetrazine-derivatized HA would be pink, it would be simple to check the success of the IEDDA reaction, because the polymer would become colourless following the cycloaddition. The reaction could also be performed in the presence of proteins without side reactions. The most suitable functional group in the hyaluronic acid structure for attaching a tetrazine was the carboxylic group, therefore the tetrazine had to contain a free amine to allow an amide bond to be formed as reported by Famili *et al*.[152] (Scheme 2.1).

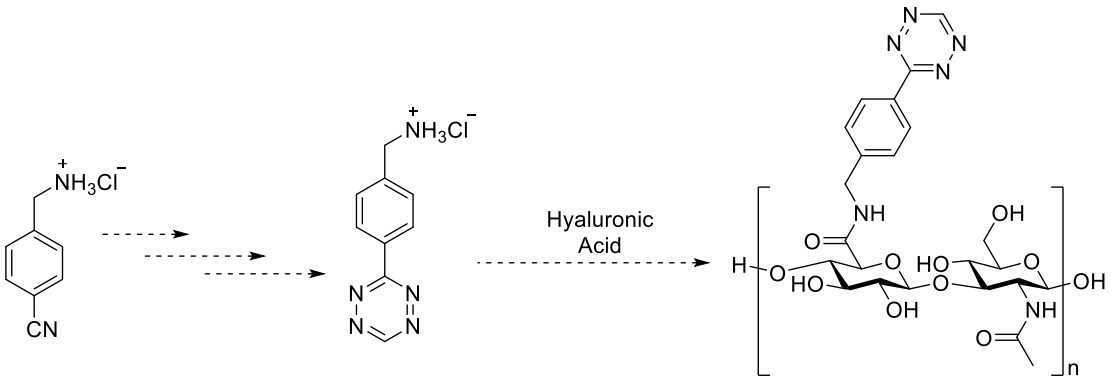

Scheme 2.1: Synthetic plan for a tetrazine-derivatized hyaluronic acid0.

2.2.1 Synthesis of a tetrazine

The synthesis of tetrazine-derivatized hyaluronic acid started by protecting the free amine of 4-(aminomethyl)benzonitrile hydrochloride (**2.0**) with Boc-anhydride (Boc_2O) in basic conditions (TEA) to achieve **2.1**. Then, the synthesis of protected tetrazine **2.2** was performed by reacting **2.1** with formamidine acetate and hydrazine hydrate ($NH_2NH_2{\cdot}H_2O$) in presence of zinc trifluoromethanesulfonate in DMF for 36 h at 30 °C in a sealed flask.[153,154] Finally, the Boc group was removed with HCl in dioxane overnight to finish with (4-(1,2,4,5-tetrazin-3-yl)phenyl) methanamine hydrochloride (**2.3**) (Scheme 2.2).

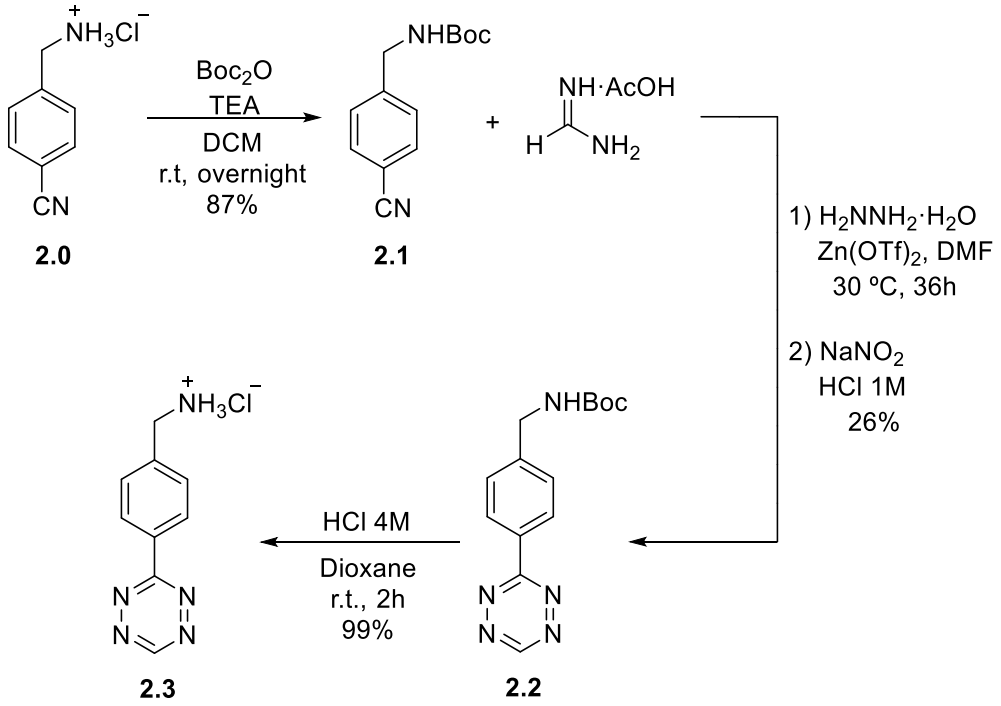

Scheme 2.2: Synthesis of the tetrazine **2.3** available to attach to hyaluronic acid.

Before performing the coupling reaction between **2.3** and hyaluronic acid, a study of reactivity was done with the polysaccharide to optimize the reaction conditions. The procedure followed was

described by Famili *et al*. but the ratios of reagents and activators were changed according the project's needs, use as less as possible of tetrazine as it was hard to synthesize, by reducing the equivalents of **2.3** and increasing the ratios for the activators.[152] Due to the complexity of the tetrazine synthesis, **2.0** was used as a model reagent to couple to the HA instead of tetrazine **2.3** and save this valuable molecule once the conditions of the coupling were established.

2.2.2 Studying the reactivity of the carboxylic acid in hyaluronic acid using 4-(aminomethyl)benzonitrile (2.0)

In this model study, a solution of hyaluronic acid in MES buffer (2-(*N*-morpholino)ethanesulfonic acid) at pH 6 was reacted with 4-(aminomethyl)benzonitrile hydrochloride in presence of 1-ethyl-3-(3-dimethylaminopropyl)carbodiimide (EDC) and *N*-hydroxysuccinimide (NHS) to achieve HA derivatized as the 4-cyanobenzylamide (**2.4**) (Scheme 2.3). The percentage of derivatization of the polymer was calculated by comparing the integrations of the aromatic protons in the ^{1}H NMR spectra with the 3 protons in the acetamide group (Figure 2.2).

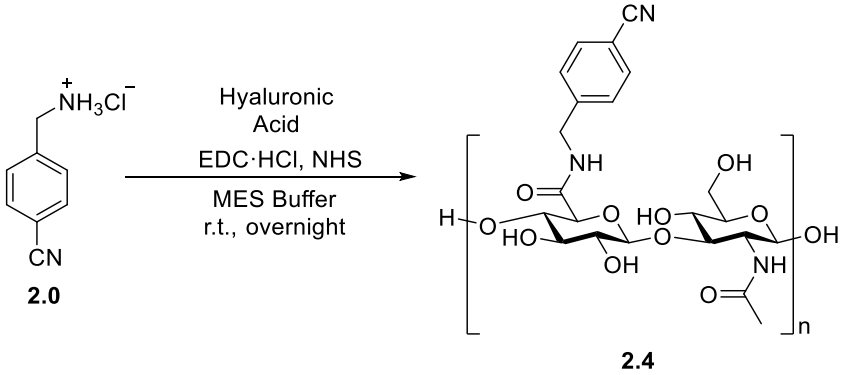

Scheme 2.3: Reaction used in the model study.

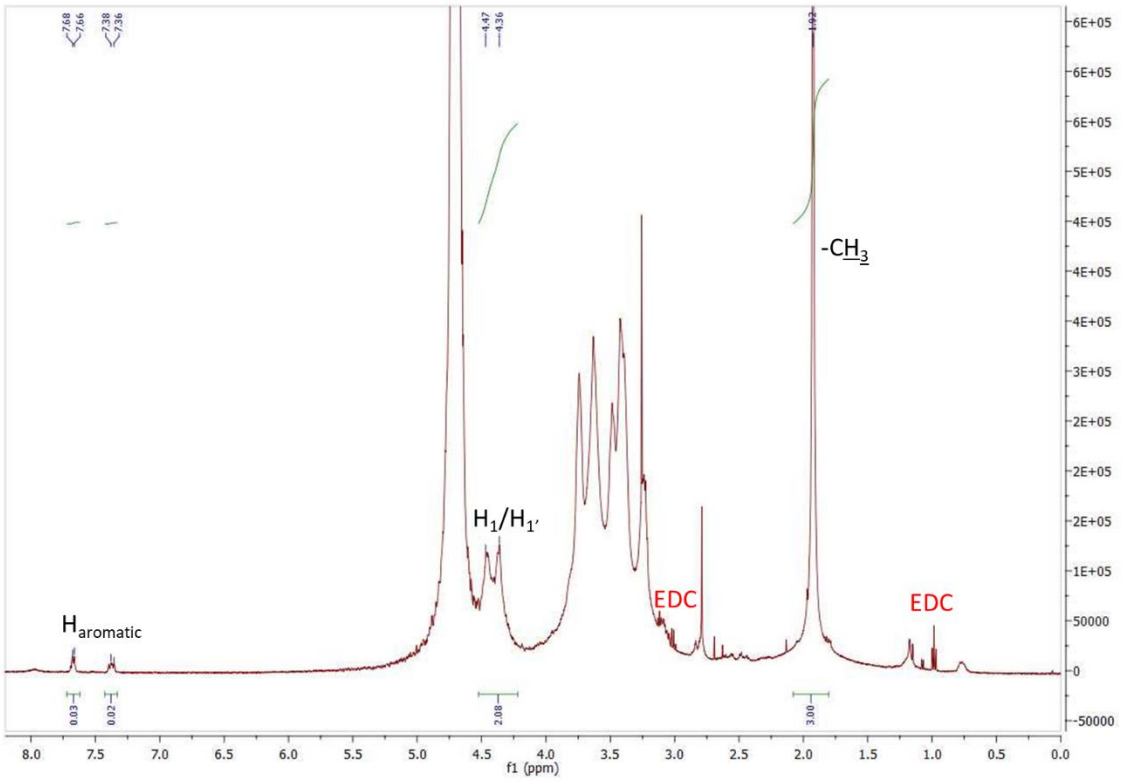

Figure 2.2: ^{1}H NMR spectra of **2.4** to calculate the percantge of derivatization on hyaluronic acid.

To determine the effect of EDC and NHS concentrations on the coupling reaction during the coupling reaction, a set of experiments was performed where the equivalents of EDC was changed while NHS was in a large excess. Also, the ratio of the HA (200 to 500 kDa, 927 carboxylic groups per mol of HA) to amine was kept constant 2 eq. amine per HA carboxylic acid group in all the experiments. The equivalents of EDC were varied while NHS was present in a large excess. The data obtained are presented in Graph 2.1.

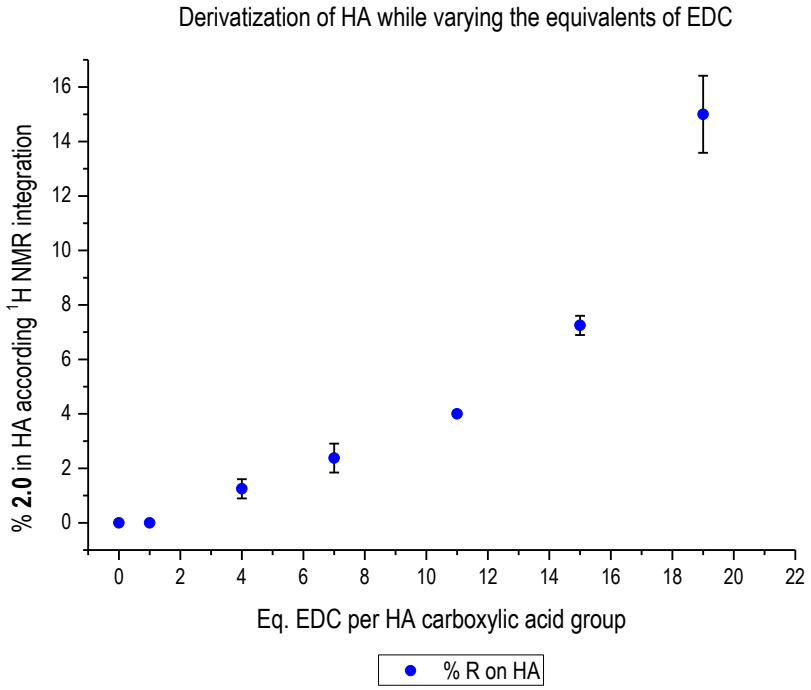

Graph 2.1: Percentage derivatization of HA with 4-(aminomethyl)benzonitrile hydrochloride (**2.0**) vs the ratio of EDC to HA carboxyl. Mean values were average between the two results obtained and the error bars corresponds to the standard deviation.

As seen in Graph 2.1, the relationship between EDC concentration and the derivatization of the HA was not directly proportional, probably because the hydrolysis of the activated carboxylic acid before reacting with the tetrazine. It provided reliable information to guide the design of experiments to achieve low levels of HA derivatization that would be needed for attaching proteins to this polymer. However, it is important to mention that once the ratio of EDC to carboxyl groups was higher than 7:1, extra peaks started to appear in the ^{1}H NMR spectra due to an unknown side reaction. This aspect is discussed in depth in Chapter 4.

According to the data obtained, it can be concluded that the degree of derivatization of the HA depends on the amount of EDC added in the mixture. This hypothesis is also supported by the mechanism of the coupling reaction (Scheme 2.4). Once the carboxylic acid is activated with EDC, then NHS is able to form an active ester which reacts with the free amine of **2.0**. A urea is formed as a side product, and so the EDC is unable to activate another carboxylic acid. However, the NHS structure in unchanged by the reaction, so it is able to react again.[143,155]

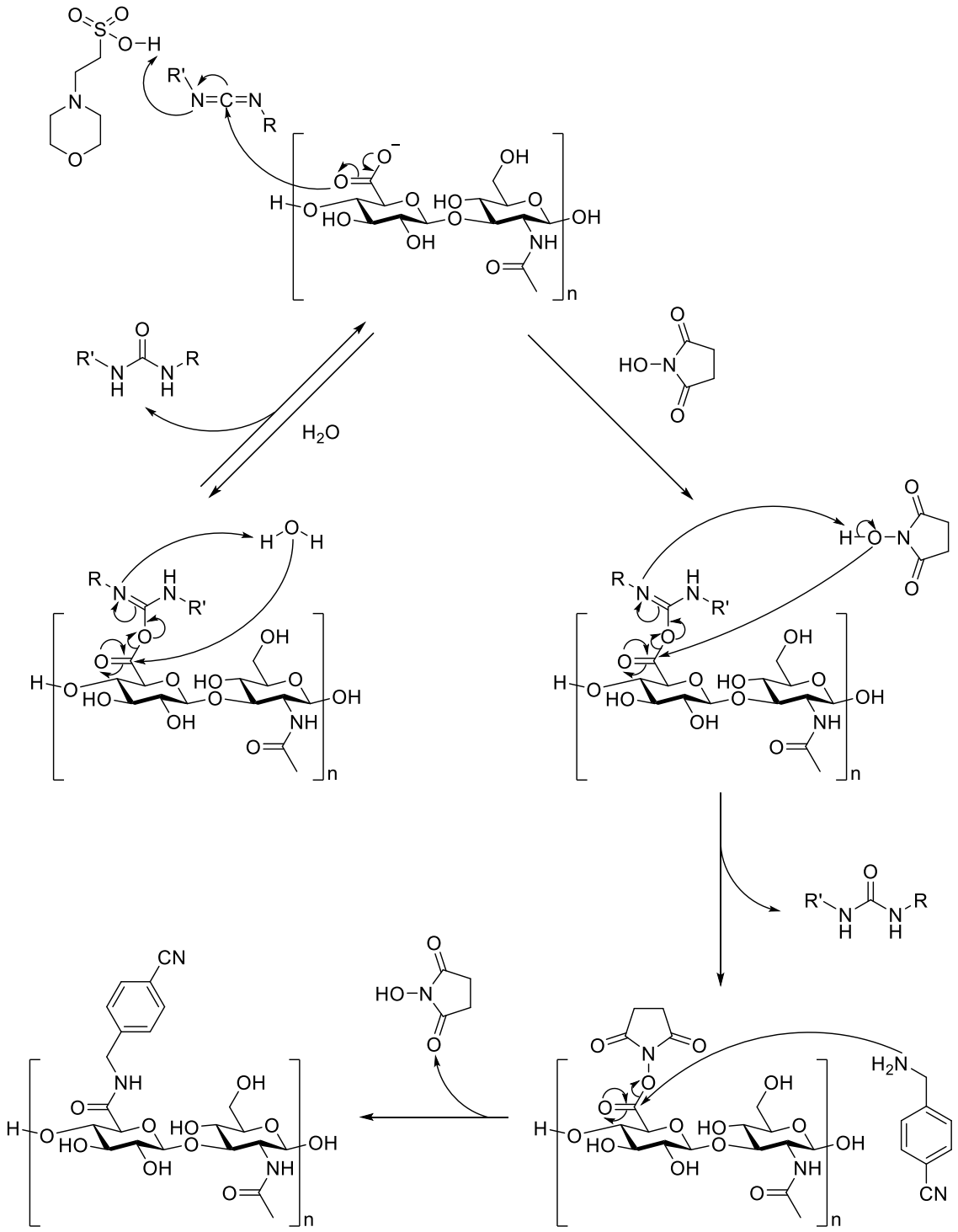

Scheme 2.4: Mechanism of coupling of the HA.

2.2.3 Attaching tetrazine to hyaluronic acid

Once this study of reactivity was done, the same conditions were applied to make a hyaluronic acid derivatized with tetrazine **2.3**. A solution of HA in MES buffer at pH 6 reacted with tetrazine **2.3** in presence of EDC and NHS in the same ratios used in this set of experiments (represented on graph 2.1) to achieve a HA-*g*-Tz (**2.5**) (Scheme 2.5). The degree of derivatization was calculated

by comparing the integrations of the aromatic protons in the ^{1}H NMR spectra with the 3 protons in the acetamide group.

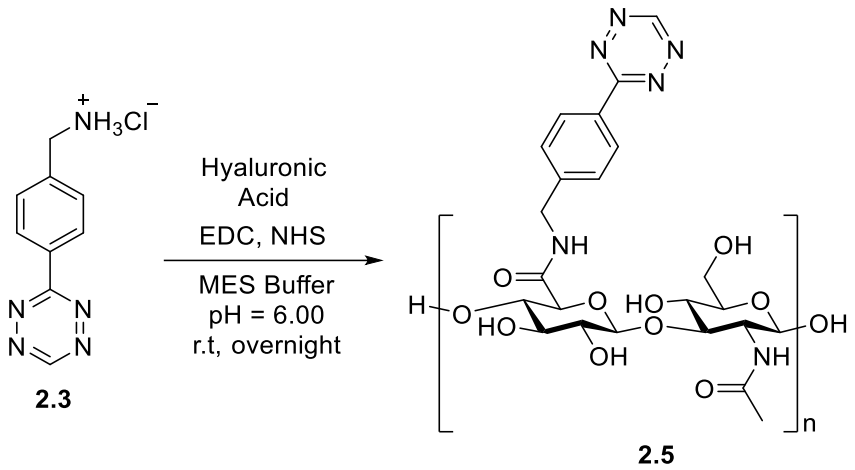

Scheme 2.5: Strategy to couple **2.3** to the hyaluronic acid.

The reaction was repeated four times: two of them following the model according the eq. of EDC and two of them following the ratios described Famili *et al.*[152] Different percentages of derivatization in the polymer were achieved, but the results did not follow the pattern expected from the model studies (Table 2.1).

Table 2.1: Derivatization of HA with Tz **2.3** using different ratios of EDC and NHS.

Test	Eq. HA -COOH	Eq. 2.3	Eq. EDC	Eq. NHS	Percentage derivatization of HA expected	Percentage derivatization of HA found
1*	1	2	9	20	3%	2.5-3%
2*	1	2	13	20	5%	3%
3**	1	1.6	1.5	1	5%	5%
4**	1	2	2	3	10%	6%

* Tests 1 and 2 were performed using the ratios of EDC:HA carboxylic acids established with the model system. The percentages of derivatization expected was calculated by the results obtained in Graph 2. ** Tests 3 and 4 were performed using the ratios of EDC and NHS suggested by Famili *et al.*[152] The percentages of derivatization expected was calculated by the results described following Famili *et al.* protocol.

As can be observed in Table 2.1, the degree of derivatization achieved for entry 1 is similar to the value predicted by the model, but it is lower than the expected value for entry 2 even though the experiments followed the EDC:HA ratios established in the model. This discrepancy may be

due to the behaviour of the final product **2.5**. For the model system, all the reagents and the final product **2.4** were soluble in buffer solution (HEPES 25 mM, NaCl 150 mM) and water. However, once tetrazine **2.3** reacted with HA, the resulting product **2.5** was poorly soluble in buffer, water and several organic solvents (including DMSO, DMF, pyridine or MeOH) and this change may have affected the reactivity of the remaining carboxylic acids present in the polysaccharide. As a result, the conditions used for the model were not applicable for the tetrazine coupling.

Due to the results obtained following the model's conditions, two different experiments were tried using the procedure described by Famili *et al.*[152] As seen in Table 2.1, entries 3 and 4, the degree of derivatization was higher when using fewer equivalents of NHS and EDC. These results indicated that large amounts of either of the activators did not help achieve a higher degree of derivatization of HA.

Even though it was possible to achieve **2.5** with low degree of derivatization following the published protocol once attempts were made to increase the degree of derivatization, the resulting product showed solubility issues due to the mixture of hydrophobic and hydrophilic groups of this polymer: very hydrophilic hyaluronan and very hydrophobic tetrazine groups. Therefore, the construction of mucin-like structures using the tetrazine-derivatized hyaluronic acid was dismissed. For this reason, the incorporation of electron-rich dienophile into carbohydrates (H-Le^y, Le^x or Gb_3) or their attachment to **2.5**, is not described in this chapter. An alternative approach to the synthesis of the mucin-like structures is described in Chapter 3, 4 and 5. Nevertheless, **2.5** was useful for the synthesis of lectin-on-HA using this polymer as a backbone for attaching norbornene-derivatized proteins. This project was performed with PhD student Chunyue Wang in the Faculty of Biological Sciences in the University of Leeds.

2.3 Application example of HA-*g*-Tz: multivalent lectin-on-HA probe for superselective targeting

HA-*g*-Tz **2.5** containing low degree of substitution, between 2 to 6% of tetrazine was the polymer scaffold chosen to synthesize lectin-on HA probes. The lectin chosen for the construction of this structures was CBM40 because it is a monovalent lectin with affinity to G_{M3}, 12 μM, which is overexpressed on melanoma cells. The resulting HA-*g*-CBM40 was designed to show superselectivity for cell surfaces containing G_{M3} meaning that below the threshold density of this oligosaccharide, the probe would not bind to the surface. On the contrary, for densities above the threshold of G_{M3} on the surface, the HA-*g*-CMB40 would bind being possible to discriminate between different surfaces.[156,157] The aim of Chuyue Wang's project was to synthesize these

superselective probes, HA-*g*-CBM40, for the recognition of cancer cells by its affinity to G_{M3} overexpressed on the cell membrane.

2.3.1 Synthesis of a norbornene derivative for protein coupling to HA

As described already, tetrazine-derivatized hyaluronic acid was also useful for the synthesis of superselective probes for cell surface carbohydrates. The synthesis of these structures required the conjugation of multi copies of a monovalent lectin, CBM40, to the **2.5** HA polymer by IEDDA cycloaddition, and therefore the attachment of an electron-rich dienophile to the protein. The molecule chosen to modify the lectin was 5-norbornene-2-carboxylic acid because it was commercially available, it is stable in physiological conditions and reacts fast with tetrazines. Because there was a terminal cysteine on C terminus in CBM40, a maleimide with a linker, four PEGs, was attached to 5-norbornene-2-carboxylic acid to make a bifunctional linker to allow the protein to react with the tetrazine-derivatized hyaluronic acid (Scheme 2.6).

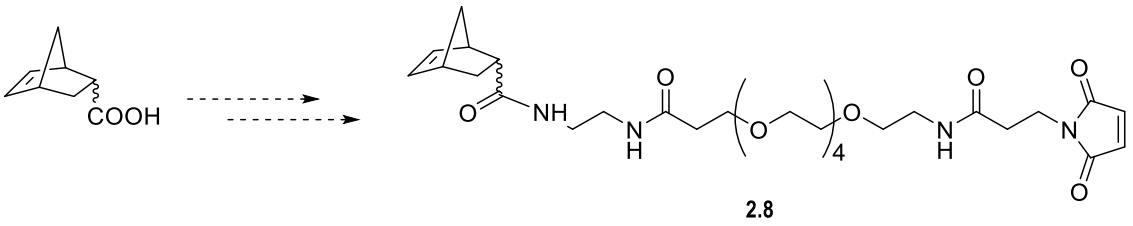

2.8

Scheme 2.6: Synthetic plan for the maleimide-norbornene linker

The synthesis of the norbornene derivative started by forming an amide bond between *N*-Boc-ethylenediamine and norbornene acid in presence of 2-(6-chloro-1H-benzotriazole-1-yl)-1,1,3,3-tetramethylaminium hexafluorophosphate (HCTU) and TEA (Scheme 2.7). Then, the Boc group was removed with TFA to achieve amine **2.7**.

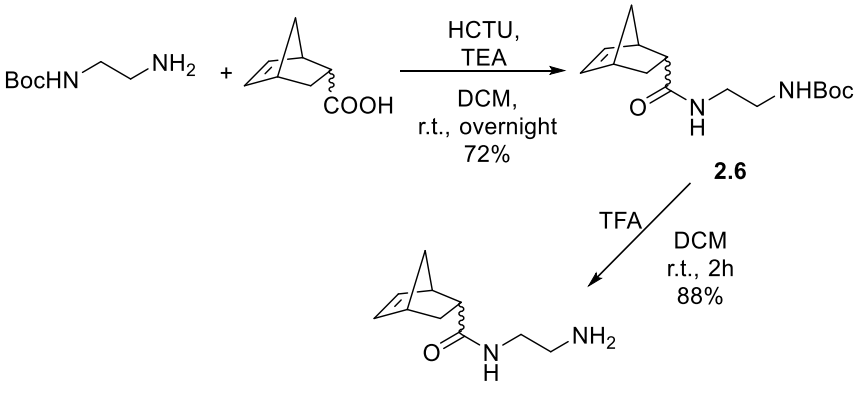

2.7

Scheme 2.7: Synthesis of **2.7**.

Once the amine analogue of the norbornene **2.7** was made, a last coupling was performed with a commercial linker comprising a maleimide with a four repeat units of polyethylene glycol (PEG) linker and a carboxylic acid activated by an NHS from ThermoFisher. For this amide formation, both reagents were reacted in DMF in the presence of TEA to produce **2.8** (Scheme 2.8), ready for coupling to the protein.

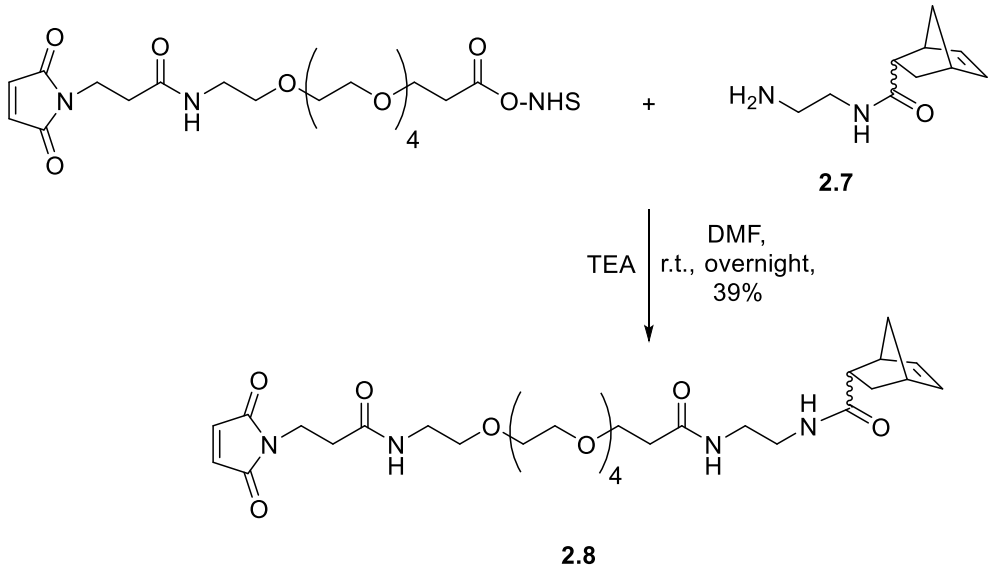

Scheme 2.8: Amide bond formation between **2.7** and Succinimidyl-([*N*-maleimidopropionamido]-tetraethylenglycol) ester ($SM(PEG)_4$).

The addition of **2.8** to the cysteine-modified CBM40 (CBM40-Cys) was performed by Chunyue Wang (University of Leeds). High-resolution electrospray mass spectra showed evidence that the addition of the norbornene analogue via thio-Michael reaction was successful as the mass of the protein increased by 666.35 Da, i.e. the mass of the **2.8** molecule (Figure 2.3).

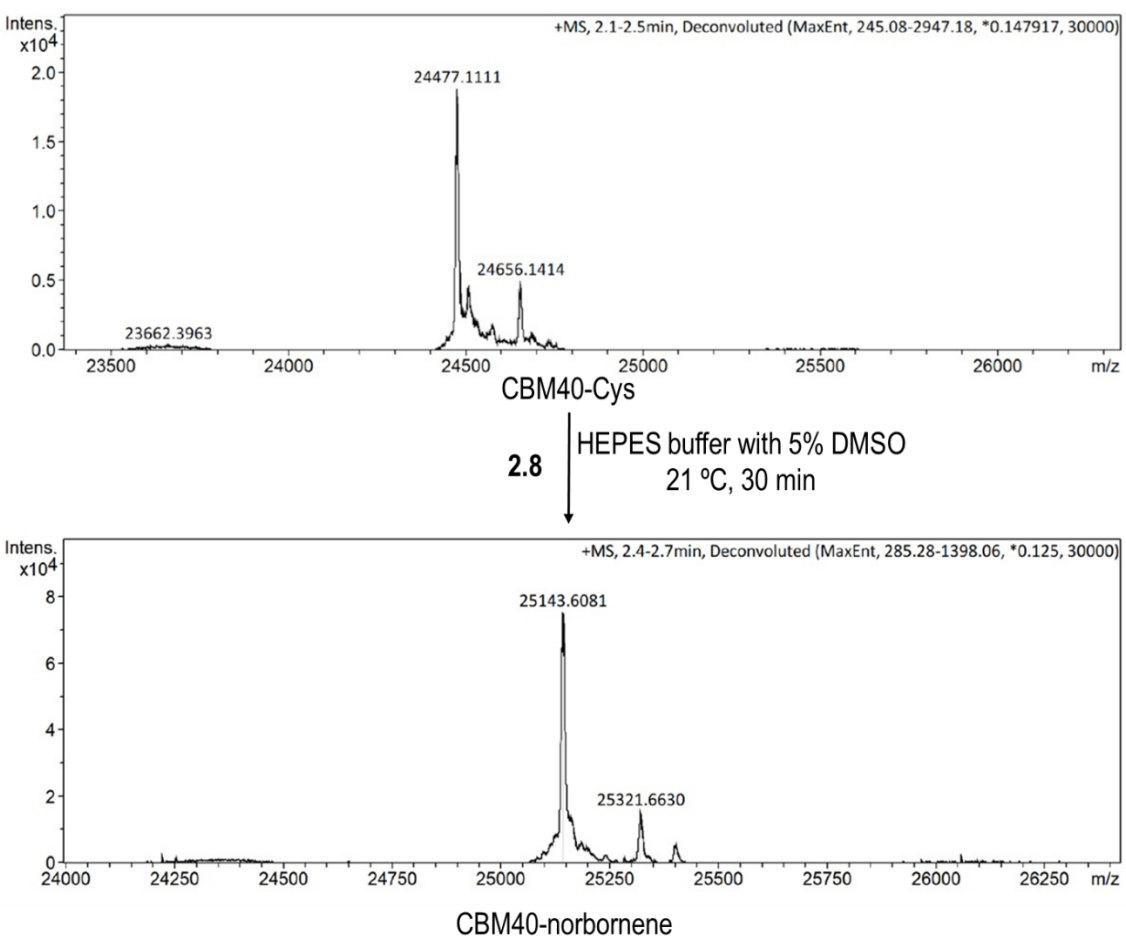

Figure 2.3: High resolution electrospray mass spectra for the addition of **2.8** to CBM40-Cys. The mass of the protein corresponds to 24477 Da while the CBM40-norbornene corresponded to 25143 Da, that is an addition of 666.50 Da.

2.3.2 Construction of a multivalent lectin-on-HA probe: HA-*g*-CBM40

Finally, to ensure if both IEDDA reagents worked as expected and create the desired lectin-on-HA probe, Chunyue Wang performed the corresponding cycloaddition by reacting **2.5** and CBM40-norbornene at near-physiological ionic strength and pH.

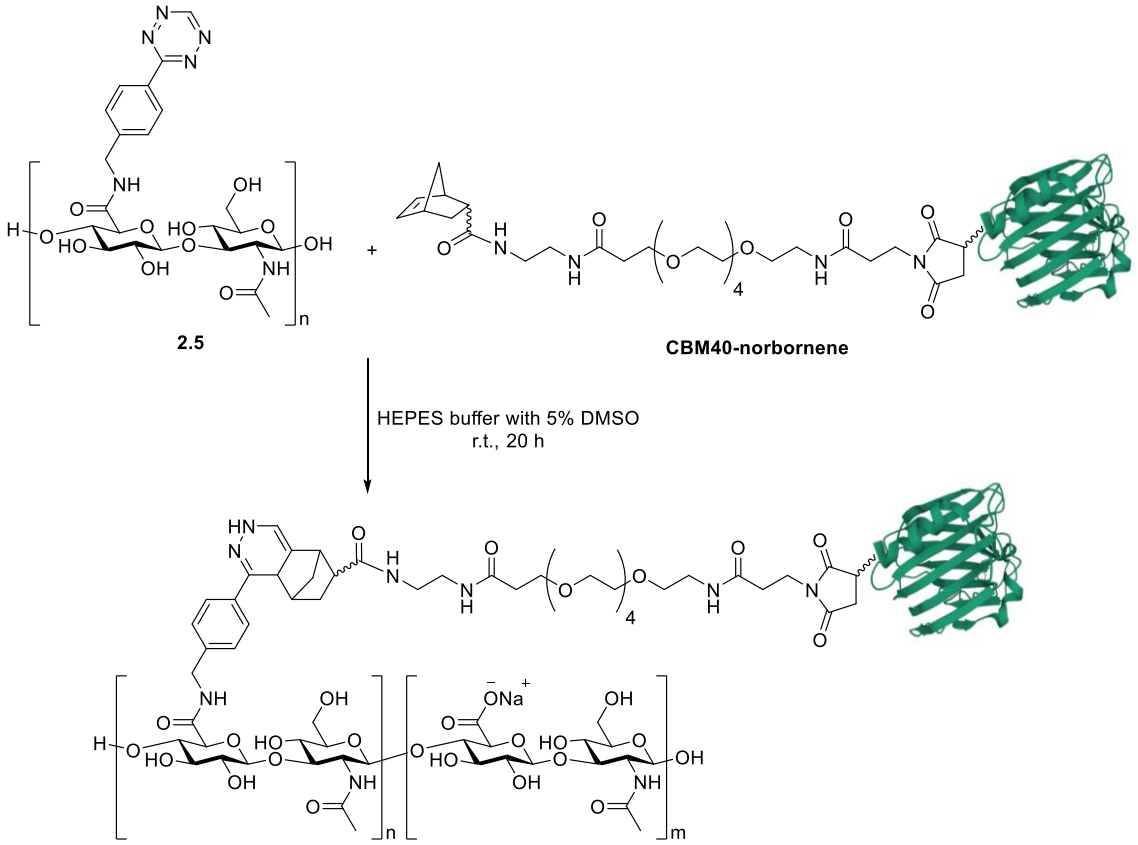

Scheme 2.9: Synthesis of the multivalent probe using **2.5** and CBM40-norbornene as reagents.

Due to the nature of the reagents used, a large (derivatized) polymer with high size dispersity and a derivatized protein with complex amino acid composition, the reaction could not be followed by conventional analysis techniques such as mass spectroscopy, TLC or NMR. Instead, we used UV-visible spectroscopy exploiting that fact that tetrazine **2.5** absorbs light (with an absorption peak at 515 nm) when unreacted but not once reacted. The disappearance or reduction of intensity of this peak provided strong evidences for loss of the tetrazine in the polymer and the IEDDA reaction had worked successfully.

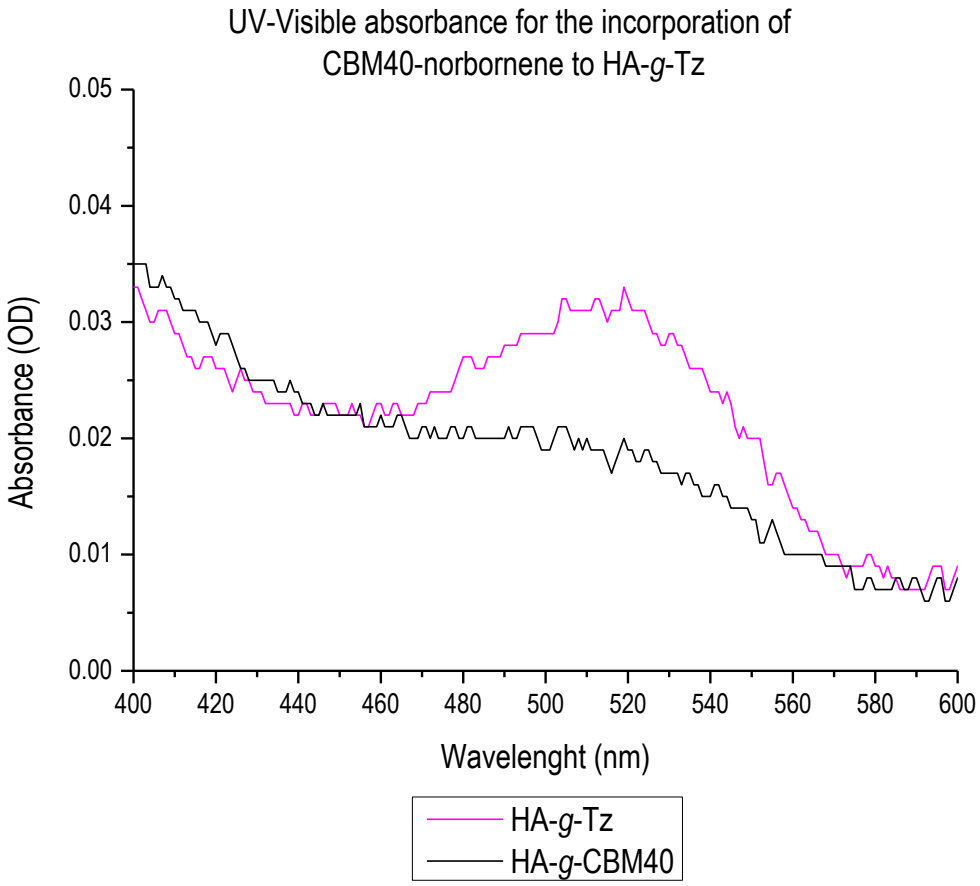

Figure 2.4: UV-Visible spectrum for the IEDDA reaction between **2.5** and CBM40-norbornene.

The resulting multivalent-on-polymer was characterised further by SEC-MALS showing the proteins had been attached giving as a result a mass average molar mass of 564 kDa. This structure was used successfully in binding studies performed by Chunyue Wang, PhD thesis, University of Leeds, 2023. Together, this data showed that the reagents synthesized in this chapter can be used successfully to perform a IEDDA cycloaddition and to form these complex structures. HA-*g*-CBM40 was tested successfully as demonstrated by Chunyue to bind their target glycan G_{M3} supserselectively providing the opportunity to use these types of probes for cancer cell recognition.

2.4 Conclusions

Different aspects were concluded in this first chapter: Tetrazine **2.3** which contained a free amine was synthesised and coupled to the carboxylic acid groups of HA. Model studies for the amide forming reaction were performed using 4-(aminomethyl)benzonitrile hydrochloride and indicated that changing the equivalents of EDC would allow a low degree of substitution on the polymer to be achieved. Unfortunately, the model could not be applied using tetrazine **2.3** as a reagent due to solubility issues in the resulting product **2.5**.

Even though it was not possible to use the model to guide the synthesis of tetrazine-derivatized hyaluronic acid, **2.5** was achieved in low degree of derivatization (between 2.5 and 6% of tetrazines attached on the polymer). As it was impossible to increase the degree of derivatization, the use of tetrazine derivatized polymer **2.5** was discarded to fulfil the aim of this project to make mucin-like glycopolymers. Another approach to synthesize these strcutures is described in Chapter 3, 4 and 5 in this thesis. Luckily, these structures with low degree of substitution were useful for Chunuye Wang to build a superselective probe for detecting cell surface glycans.

The synthesis of the norbornene derivative **2.8** was successful as well as its incorporation onto the protein CBM40-Cys, providing a suitable reagent for the IEDDA cycloaddition with the **2.5** polymer. This reaction between the tetrazine-derivatized hyaluronic acid and the CBM40-norbornene was performed by Chunyue Wang and it gave good results and clear evidence that the polymer and the norbornene analogue reacted successfully with the protein under physiological conditions. Finally, these structures showed a superselective binding to surfaces containing G_{M3} providing the possibility to use them for cancer cells recognition.

CHAPTER 3: ENZYMATIC SYNTHESIS OF AZIDE DERIVATIZED OLIGOSACCHARIDES

3.1 Enzymatic synthesis of oligosaccharides

Oligosaccharides are structures that play an important roles once attached to proteins or lipids in the glycocalyx including signalling, like the blood-group antigens, or adhesion to the cell.[1,158] Biological oligosaccharides have complex structures due to all the possible combinations of monosaccharides, linkage sites in their building blocks and type of bonds (α- or β-glycosidic linkages). For these reasons, the synthesis of oligosaccharides still represents a challenge nowadays.

Different approaches were taken to synthesise oligosaccharides: their chemical synthesis and their enzymatic synthesis.[159] Both of them presented advantages and disadvantages but it has been proved that the synthesis by enzymes is easier than the chemical approach. Even though the chemical synthesis of carbohydrates is well established, it requires several steps of regioselectivity protection and deprotection and complex purifications. Also, its complexity increases as the size of the oligosaccharide becoming synthetic routes with lots of steps and low yields.[159–161]

On the other hand, the enzymatic approach offers a wide range of regiospecificity, stereospecificity and regioselectivity. Moreover, protecting groups and hazardous chemicals are not required and the reaction takes places in mild conditions.[159,162] There are two main enzymes responsible to build these complex structures: the glycotransferases (Scheme 3.1, a) and the glycosidases (Scheme 3.1, b). Both types of enzymes need an acceptor and a donor substrate but it is important to highlight that the normal function needs to be reversed for glycosidases to perform glycosidic bonds between oligosaccharides.[53,161,162]

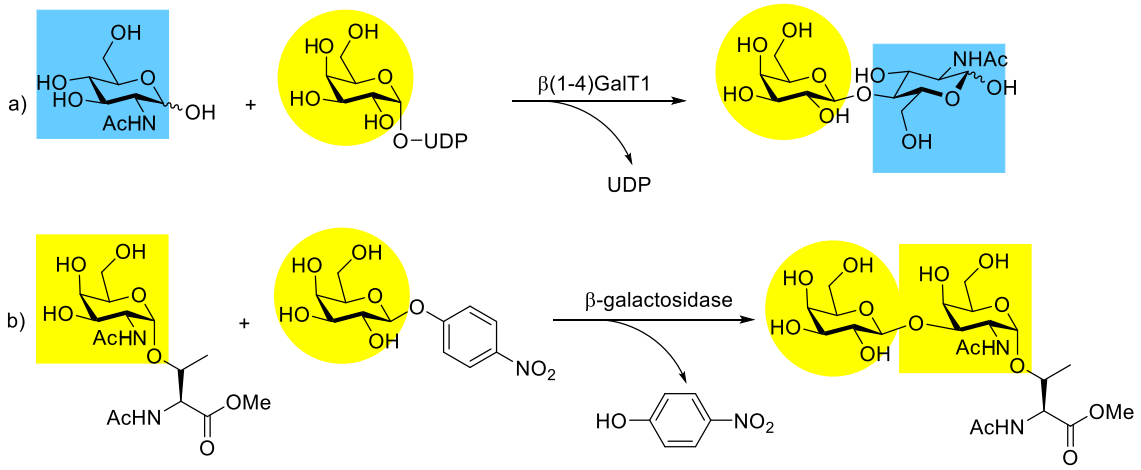

Scheme 3.1: a) Example of glycosidic bond performed by glycotransferase b) Example of glycosidic bond performed by glycosidase.[161]

One other advantage for the enzymatic synthesis of oligosaccharides is the flexibility of the enzymes to use other substrates. Different modifications in the acceptors or donors can provide a

large library of oligosaccharides with different reactive groups in their structures.[163–166] However, to achieve this aim, the tolerance for these modified substrates by the enzymes needs to be studied because the substitution of some positions may make the molecule unrecognisable for the enzyme or inhibit the protein.[167–169]

H-Lewis^y is an oligosaccharide belonging to the Lewis antigens family which can bind to the secondary binding site in Cholera Toxin (Figure 3.1, a).[53,74] Because of its biological importance, several syntheses have been described including the chemical and enzymatic approach. Different chemical approaches to achieves this tetrasaccharide were described but all required several steps, around ten, and overall the yield was not higher than 60%.[170–172] On the other hand, recent approaches using enzymes from *Helicobacter pylori* have also been described.[173–176] These syntheses were less time consuming and they had less steps, just three, than the chemical approaches. Moreover, their substrate did not need any treatment and the yields were much higher (around 60-70%).

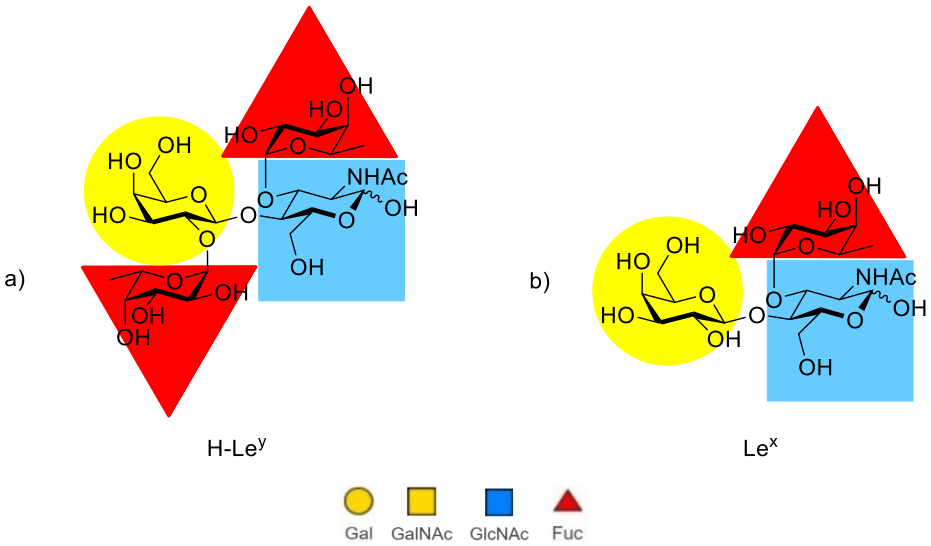

Figure 3.1: a) Structure H-Le^y tetrasaccharide b) Structure Le^x trisaccharide.

The trisaccharide Le^x is also an oligosaccharide from the Lewis antigen family and it can also bind to the secondary bind to CT (Figure 3.1, b).[53,73] Again, both chemical and enzymatic synthesis has been described. However, the chemical synthesis for Le^x was easier than the H-Le^y because it has one monosaccharide less.[177–179] The enzymatic approach is also well-known and again, several of the approaches described for the tetrasaccharide could be used for this trisaccharide too.[174,176,180] To conclude, because the structure of H-Le^y covers the structure of Le^x, its synthesis is well established.

Finally, Gb_3 oligosaccharide is a trisaccharide with high biological importance because several lectins interact with Shiga Toxin and Pertussis Toxin.[62,63,95] The Gb_3 oligosaccharide structure is

Gal-α(1-4)-Gal-β(1-3)-Glc (Figure 3.2). Chemical approaches with multiple steps were described to synthesise this trisaccharide and, even though they were successful, the α(1-4) glycosidic bond between galactose was difficult to achieve.[181–184] However, as it was described for H-Le^y and Le^x, the enzymatic syntheses were the easiest path to achieve this oligosaccharide: LgtC enzyme can perform easily the addition of the terminal Galactose by α(1-4) glycosidic bond.[185–187]

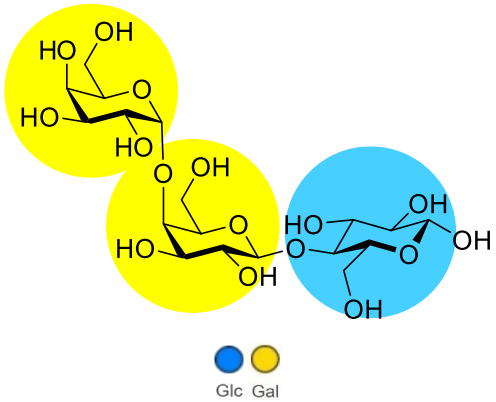

Figure 3.2: Gb_3 oligosaccharide structure.

3.2 New strategy to synthesize mucin-like structures

The synthesis of mucin-like structures could not be achieved by using HA-*g*-tetrazine (**2.5**) due to the solubility issues caused while the degree of substitution was high, more than 6% of tetrazine on HA showed problems of precipitation of the resulting derivatized polymer in aqueous solution. Therefore, there was a need to change the synthetic plan for a pair of bioorthogonal groups that could derivatize HA to high degree of substitution and incorporate to monosaccharides without influence in the enzymatic activity for the synthesis of oligosaccharides.

Aiming for the synthesis of these complex structures and accomplishing the requirements mentioned above, a new strategy was designed using copper(I)-catalysed azide-alkyne cycloaddition. The new synthetic plan included the incorporation of the different pair of reactive groups according Scheme 3.2: an alkyne on HA and an azide on the anomeric position of oligosaccharides.

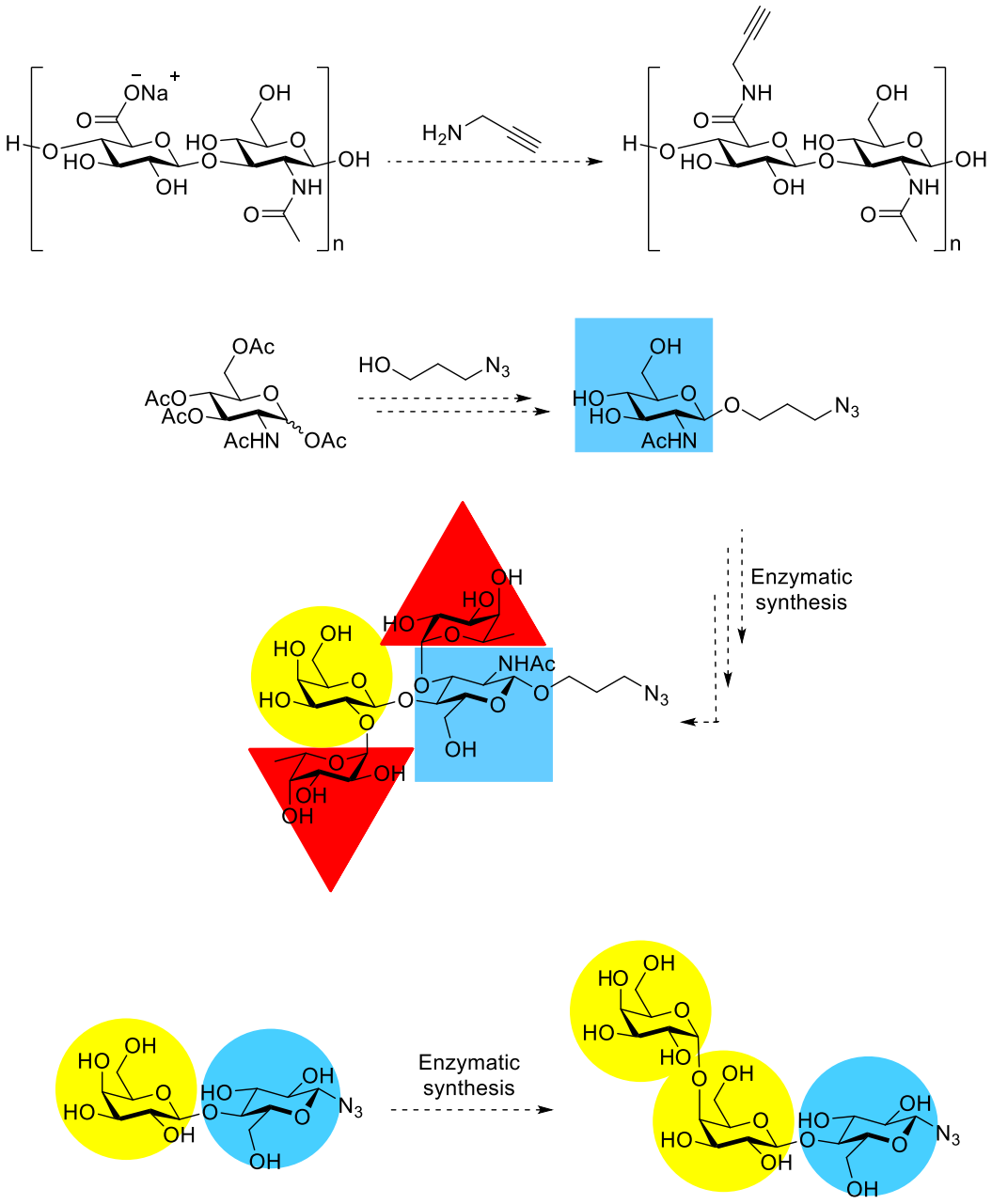

Scheme 3.2: New strategy suggested to build mucin-like structures using CuAAC reactivity.

The incorporation of propargylamine to hyaluronan through an amide bond is widely described in Chapter 4 while the addition of an azide on the anomeric position of GlcNAc and the resulting enzymatic reactions to synthesize H-Le^y and Gb_3 is extensively explained in this chapter.

The advantages for the new synthetic plan included the use of commercially available reagents for the synthesis of propargyl-derivatized HA and several protocols described in the literature to achieve this polymer in high degree of substitution.[140,141,188,189] However, all the attempts and procedures followed to synthesize it are described in Chapter 4.

In terms of the oligosaccharides moiety, this new strategy showed several advantages including the use of reagents already prepared in the laboratory such as lactosyl azide provided by Dr.

Vajinder Kumar (University of Leeds), almost all the enzymes required for the synthesis were provided by Prozomix and the certainty that azidopropyl GlcNAc could perform enzymatic reaction without side reactions degradation of both reagents and the resulting product.[190] In addition, the CuAAC reaction using these oligosaccharides as reagents should react quantitatively with the propargyl-derivatized HA giving as a result the desired mucin-like structures.

3.3 Synthesis of azidopropyl GlcNAc

Due to the change of the derivatization of the polymer, an alkyne instead of a tetrazine, the reactive group incorporated on the H-Le^y moiety changed as well, an azide in spite of a norbornene. Nevertheless, as it has been shown previously, the synthesis of azidopropyl GlcNAc (**3.3**) seemed easy using well-known reactivity of protected sugars.

The new approach started with the formation of the oxazoline of the para-acetylated GlcNAc following by the glycosylation in the anomeric position using 3-azido-1-propanol.[191,192] Once the glycosidic bond was formed (**3.2**), the hydroxyl groups were deprotected in basic conditions (Scheme 3.3). Finally, the resulting product azidopropyl GlcNAc (**3.3**) was suitable for enzymatic reactions.[186,190]

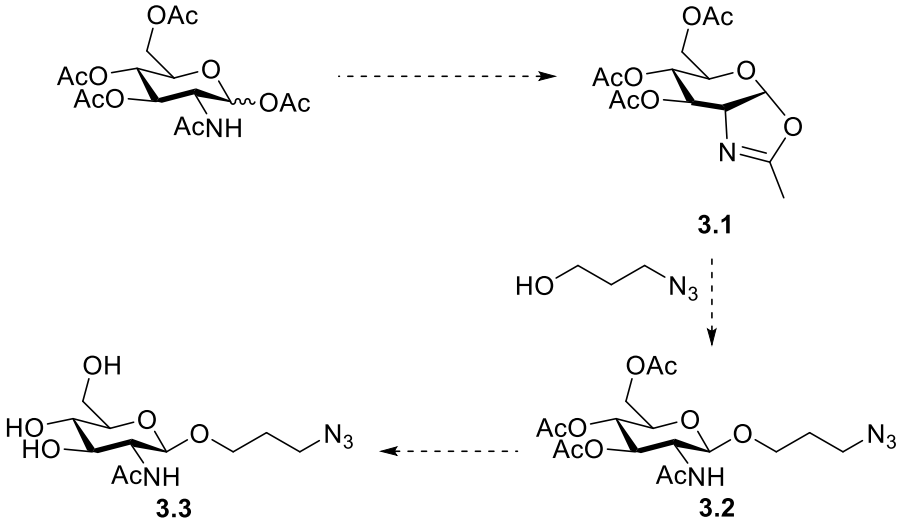

Scheme 3.3: New strategy to attach an azide in para-acetylated GlcNAc.

As it was planned, this synthesis started with the formation of the oxazoline (**3.1**): peracetylated GlcNAc was reacted with trimethylsilyl trifluoromethanesulfonate (TMSOTf) in dichloromethane (DCM) under anhydrous conditions to obtain oxazoline **3.1** (Scheme 3.4).

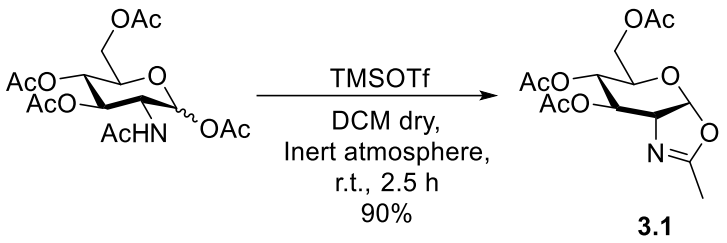

Scheme 3.4: Synthesis of **3.1**.

Once this first step was achieved, the glycosylation reaction was performed between the oxazoline **3.1** and 3-azido-1-propanol in presence of CSA in anhydrous DCE under N_2 to obtain the acetylated 3-azidopropyl glycoside (**3.2**).[191,192] Then, deprotection of the three hydroxyl groups was performed under anhydrous basic conditions to make 3-azidopropyl *N*-acetyl-2-deoxy-β-D-glucopyranoside (**3.3**) (Scheme 3.5).

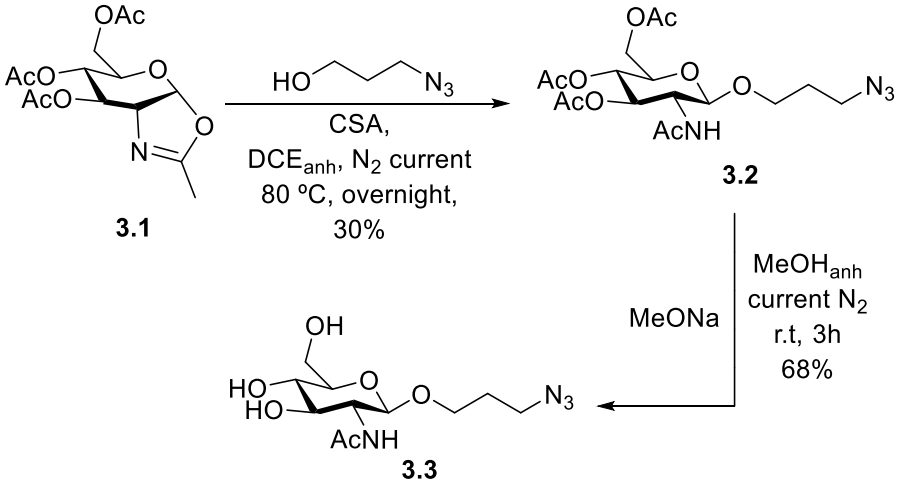

Scheme 3.5: Synthesis of azidopropyl GlcNAc **3.3**.

After this sequence of three straight forwards reactions, deprotected azidopropyl GlcNAc was achieved in a yield high enough, 20%, to perform the enzymatic reactions required for the synthesis of azidopropyl Lewis^x or azidopropyl H-Lewis^y.

3.4 Synthesis of azidopropyl H-Le^y

The synthesis of azidopropyl H-Le^y was performed by enzymatic reactions using azidopropyl GlcNAc (**3.3**) as one of the substrates. Different enzymes are required in order to synthetize azidopropyl H-Le^y: four transferases to construct step by step the tetrasaccharide and the epimerase responsible to change the stereochemistry from UDP-Glc to UDP-Gal. The transferases used during the synthesis were β-1,4-galactosyltransferase 1 (β(1-4)GalT1),[190] GDP-fucose pyrophosphorylase (FKP) from *Bacteroides fragilis*,[190] *Helicobacter pyrol* α-1,3-fucosalytransferase (α(1-3)FucT HP),[190] and *Helicobacter pyrol* α-1,2-fucosalytransferase (α(1-2)FucT HP) while the

epimerase was UDP-Glc-4-epimerase ($Glc(4)_{ep}$). FKP and α(1-2)FucT HP were expressed in the laboratory and β(1-4)GalT1, α(1-3)FucT HP and $Glc(4)_{ep}$ were provided by Prozomix.

As shown in Scheme 3.6, the first step in this synthesis would be the attachment of Gal to GlcNAc derivative **3.3** in its 4 position by a β(1-4) bond. In this first one pot reaction, UDP-Glc was modified to UDP-Gal by $Glc(4)_{ep}$ following by the attachment of UDP-Gal, a donor monosaccharide, to azidopropyl GlcNAc, the acceptor substrate, to synthesise azidopropyl LacNAc (**3.4**).[193] This second step was performed by β(1-4)GalT1.[186]

Once **3.4** was achieved, the next steps were the additions of the fucose (Fuc) to GlcNAc and Gal residues. However, due to the constitution of the enzymes used, these additions needed to be performed in a specific order starting with the attachment of Fuc in the position 4 of GlcNAc residue by an α(1-3) bond and followed by the addition of another Fuc in the position 2 of Gal residue by an α(1-2) bond. According to this premise, the second reaction was performed by reacting Fuc with ATP and GTP using FKP to achieve Fuc-GDP, a donor substrate, which was suitable to react with azidopropyl LacNAc, the acceptor disaccharide, to finish with azidopropyl Le^x (**3.5**). This second step was performed by the transferase α(1-3)FucT HP. Finally, the last fucose was chained to the position 2 of the Gal, repeating the previous modification on Fuc residue to achieve Fuc-GDP using FKP followed by its addition to **3.5** performed by α(1-2)FucT HP. After all these steps, azidopropyl H-Le^y (**3.6**) was accomplished.[173,174]

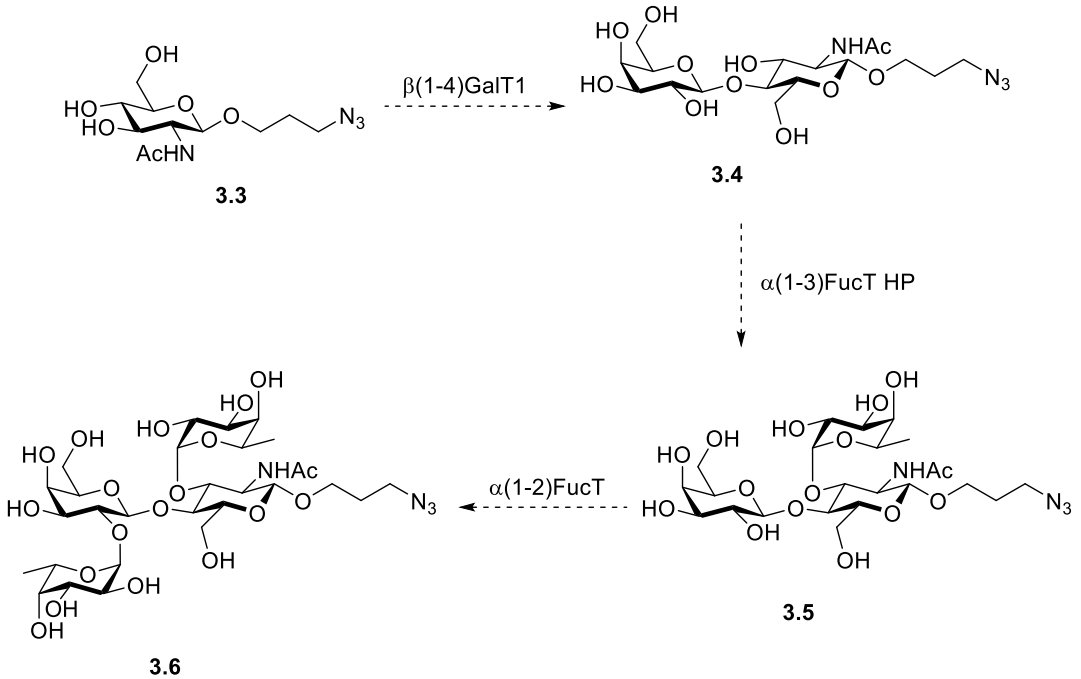

Scheme 3.6: Enzymatic synthesis of azidopropyl H-Le^y (**3.6**).

3.4.1 Expression of enzymes

3.4.1.1 β(1-4)GalT1

As it has been explained in the previous section, β(1-4)GalT1 is a glycotransferase responsible to perform the bond β(1-4) between Gal and **3.3**. This enzyme requires as substrates UDP-Gal as a donor monosaccharide and GlcNAc, wild or derivatives, as an acceptor.[186]

To express this enzyme, a genetic modified *Escherichia coli* (*E. coli* BL21 (DE)) which contain a plasmid with the genetic information of the expression of β(1-4)GalT1 was grown in autoinduction media for 3 h at 37 °C.[194] After this time, the bacteria culture was kept at 18 °C for 48 h to favour the expression of the protein instead of increasing the colony of bacteria. Then, the cells were collected by centrifugation and sonicated to release β(1-4)GalT1 in solution. The protein was isolated by Nickel affinity chromatography and then buffer exchange by diafiltration using a centrifugal ultrafiltration concentrator. Finally, polyacrylamide gel electrophoresis (PAGE) was done to check how pure was the protein (Figure 3.3) and, in addition, was quantified by UV absorption (λ = 280 nm, ε = 108430 cm^{-1}).

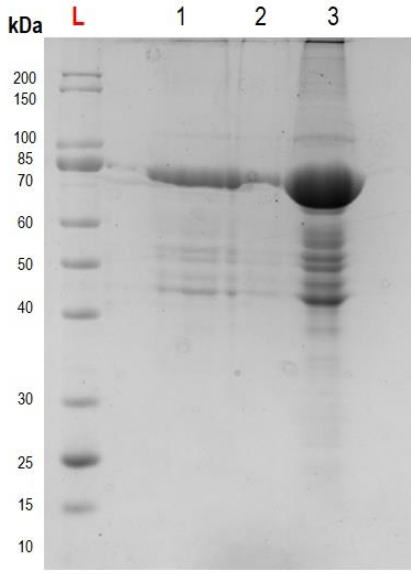

Figure 3.3: SDS-PAGE for β(1-4)GalT1 expression. expression. Lane L referring to the protein mass ladder, lane 1 Flowthrough, lane 2 First washing and lane 3 Elution.

3.3.1.2 FKP

FKP is an enzyme that can phosphorylate the fucose anomeric hydroxy group, and then convert it to GDP-fucose which will be the donor monosaccharide for the fucosyl transferases. *E. coli* BL21 (DE3) cells were freshly transformed with a plasmid for FKP-His tag (*N* terminus) designed and provided by Dr. Kristian Hollingsworth (University of Leeds) to produce a cell stock. Then, the newly transformed bacteria were grown at 37 ºC on 2xYT media for 3.5 h, induced with isopropyl β-D-1-

thiogalactopyranoside (IPTG) and left at 25 ºC overnight. The cells were collected by centrifugation and FKP was released by sonication and purified by a Nickel affinity chromatography followed by two rounds of dialysis in TRIS buffer to remove the imidazole. Finally, an SDS-PAGE gel was run (Figure 3.4) to check the protein purity using an FKP batch provided by Prozomix as reference and the protein concentration was quantified by UV absorption (λ = 280 nm, ε(FKP) = 151315 M^{-1} cm^{-1}).

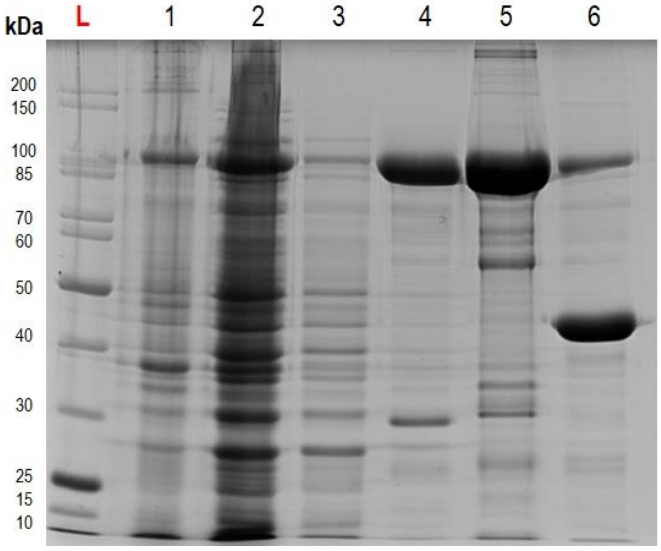

Figure 3.4: SDS-PAGE for FKP expression. expression. Lane L referring to the protein mass ladder, lane 1 Pellet, lane 2 Flowthrough, lane 3 First washing, lane 4 Elution, lane 5 FKP reference and lane 6 old batch of FKP.

3.4.1.3 α(1-2)FucT HP

To attach a Fuc in the 2 position in the Gal and the enzyme chosen to perform this addition is α(1-2)FucT HP using GDP-Fuc as a donor monosaccharide and Le^x or **3.5** as an acceptor oligosaccharide. Expression of the FucT enzyme was studied by preparing minicultures at different temperatures for two types of cells lines (*E. coli* BL21 (DE3) and *E. coli* K12 (SHuffle T7)) harbouring a plasmid encoding His tag-MBP-FucT enzyme designed and provided by Dr. Kristian Hollingsworth. To start this study, three minicultures of each type of cell were shaken at 37 ºC in LB media until their O.D. was up to 0.6, prior to induction by adding IPTG. Once they were induced, one of the falcons was kept at 37 ºC while the other two were transferred to preheated incubators at 18 ºC and 25 ºC, respectively. Then, after 2 hours, 1 mL was taken from each miniculture, centrifuged and frozen at -80 ºC after the media was removed. This process was repeated 4 times (2h, 4h, 6h and overnight). The following day, the cells were resuspended in lysis buffer and sonicated to release the protein. Finally, the samples were centrifuged and the supernatant and pellet were separated to be analysed by SDS-PAGE.

The supernatants for *E. coli* BL21 (DE3) cells were analysed to try to find the protein expressed however, as it can see in Figure 3.5, there is a little protein present in the supernatant. Nevertheless, the SDS-PAGE showed some protein with the expected mass when the cells were grown overnight at 25 ºC after being induced.

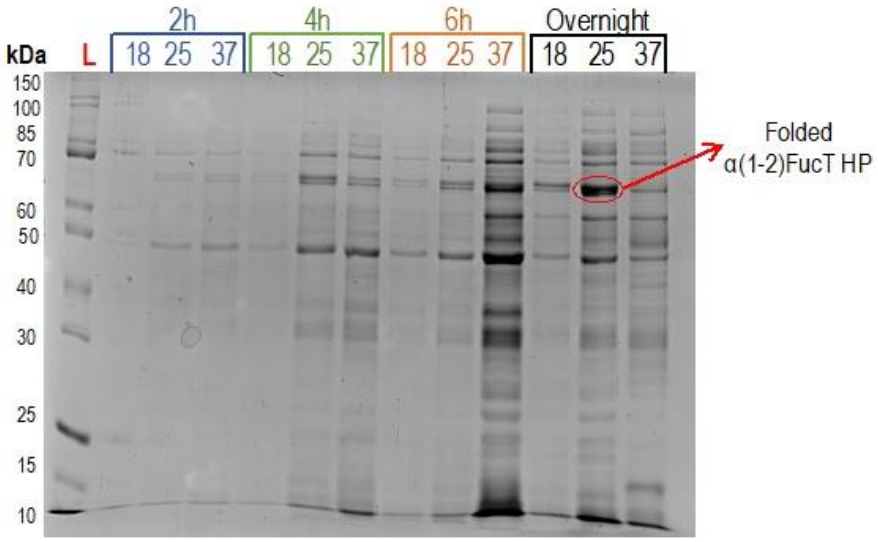

Figure 3.5: SDS-PAGE of the soluble proteins from *E. coli* BL21 (DE3) cells to determine about the best temperature to express α(1-2)FucT HP (from left to right: 18 ºC, 25 ºC and 37 ºC) and expression time (from left to right: 2h, 4h, 6h and overnight). L refers to the protein ladder.

Due to the small amount of α(1-2)FucT HP shown in the SDS-PAGE for the supernatant (soluble proteins), the pellet was also analysed by SDS-PAGE (Figure 3.6). The results shown in the pellet SDS- PAGE revealed, the expression of protein was working well and in large amounts. However, because it was not folded correctly, it was insoluble and appeared in the pellet instead of in the supernatant. Previous attempts in the group to refold the enzyme have thus far been without success so, the unfolded protein could not be recovered. However, this SDS-PAGE gel confirmed the best conditions to express soluble α(1-2)FucT HP is overnight at 25 ºC.

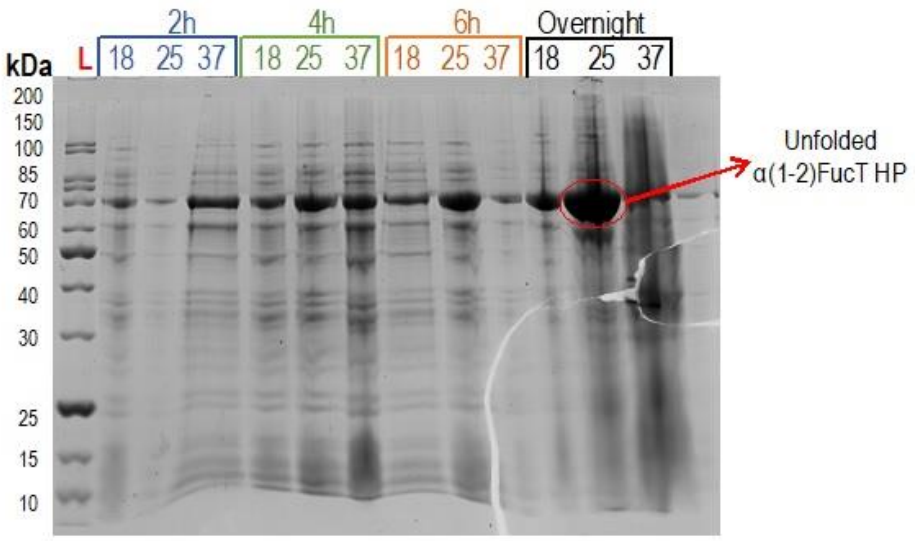

Figure 3.6: SDS-PAGE of the pellet from *E. coli* BL21 (DE3) cells to determine about the best temperature to express α(1-2)FucT HP (from left to right: 18 ºC, 25 ºC and 37 ºC) and expression time (from left to right: 2h, 4h, 6h and overnight). L refers to the protein ladder.

The pellet and supernatant of the *E. coli* K12 (SHuffle T7) were also studied in the hope of achieving better yields for expression of folded α(1-2)FucT HP because this type of cell has a cytosolic difulfide isomerase enzyme used to help the folding of proteins with high number of disulfide bonds, like this enzyme. However, as it can be seen in the SDS-PAGE gel of the soluble protein fraction from *E. coli* K12 (SHuffle T7) (Figure 3.7), there is no substantial improvement in protein expression compared to the supernatant from *E. coli* BL21 (DE3) cells. On the contrary, there is less folded protein in the sample that was incubated overnight at 25ºC.

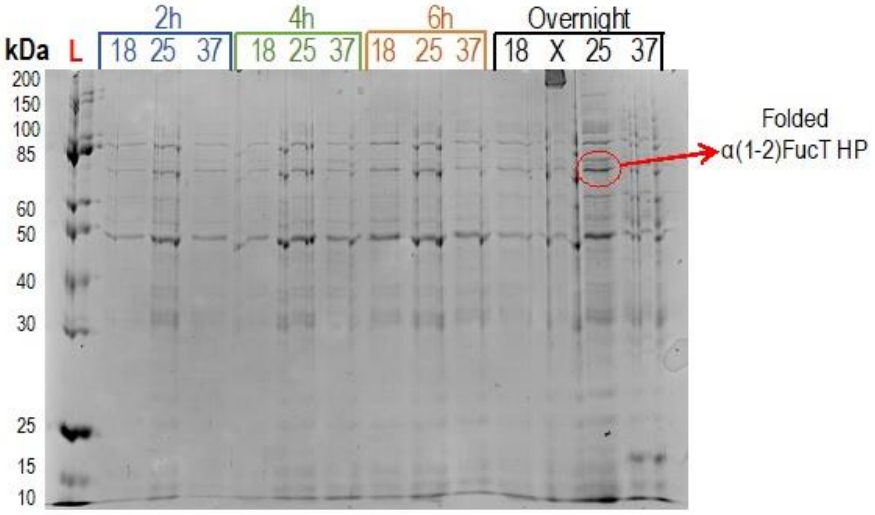

Figure 3.7: SDS-PAGE of the soluble proteins from *E. coli* K12 (SHuffle T7) cells to determine about the best temperature to express α(1-2)FucT HP (from left to right: 18 ºC, 25 ºC and 37 ºC) and expression time (from left to right: 2h, 4h, 6h and overnight). L refers to the protein ladder.

The pellet from this type of cells were also analysed to if there was unfolded protein present. As it can be seen in the SDS-PAGE gel of the pellet (Figure 3.8), there was a large amount of unfolded α(1-2)FucT HP, more than the pellet from the previous type of cells. It can be concluded that *E. coli* K12 (SHuffle T7) offered better expression of the unfolded enzyme and no improvement in the folded protein so it was better to use the *E. coli* BL21 (DE3) cells to express folded α(1-2)FucT HP.

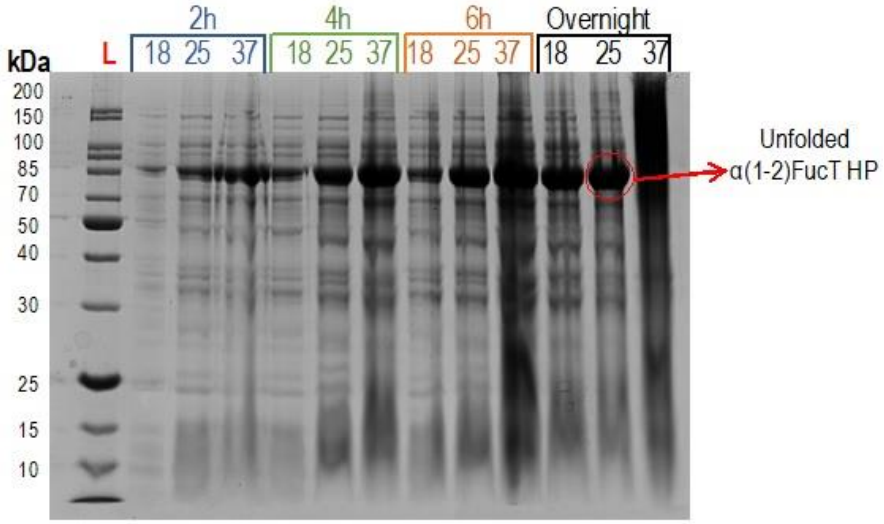

Figure 3.8: SDS-PAGE of the pellet from *E. coli* K12 (SHuffle T7) cells to determine about the best temperature to express α(1-2)FucT HP (from left to right: 18 ºC, 25 ºC and 37 ºC) and expression time (from left to right: 2h, 4h, 6h and overnight). L refers to the protein ladder.

Having concluded the study to determine the best temperature at which to express folded α(1-2)FucT HP, the enzyme was expressed on a big scale. *E. coli* BL21 (DE3) cells were grown in LB media at 37 ºC until the OD was 0.8. Then different amounts of IPTG were added to each culture to check if a lower amount of this inducer component improved the expression of folded enzyme. The final concentration of IPTG was 0.1 mM and 0.01 mM, respectively. Both cultures were left overnight at 25 ºC. The cells were collected by centrifugation and they were resuspended in lysis buffer followed by sonication to release the folded protein. The enzyme was purified by nickel affinity chromatography followed by two rounds of dialysis in TRIS buffer to remove the imidazole. The two different protein expression were analysed by SDS-PAGE (Figure 3.9) and the yield of isolation protein was quantified by UV absorption (λ = 280 nm, ε(α(1-2)FucT HP) = 126545 M^{-1} cm^{-1}).

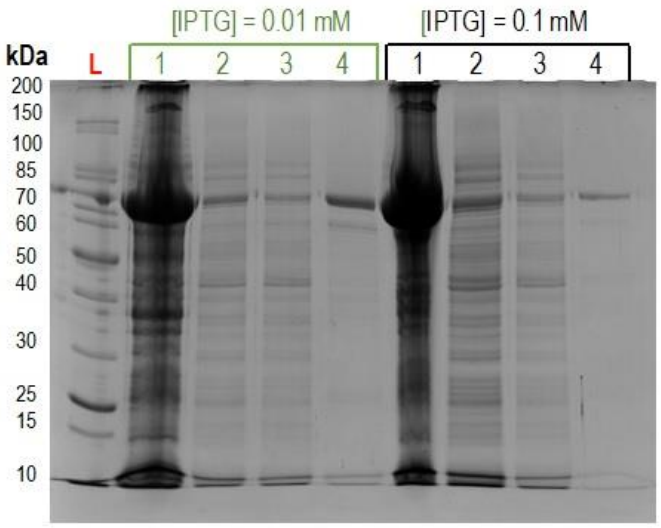

Figure 3.9: SDS-PAGE for α(1-2)FucT HP expression. Lane L referring to the protein mass ladder, lane 1 Pellet, lane 2 Flowthrough, lane 3 First washing and lane 4 Elution.

Even though it can be concluded that the lower amount of IPTG helped to achieve a better yield of folded enzyme, the isolated protein concentrations determined by UV absorption concluded the opposite: the culture that was induced with higher amount of IPTG showed better results. However, as it can be in the SDS-PAGE gel (Figure 3.8), there was a large amount of unfolded protein present in the pellet for both conditions.

3.4.2 Synthesis of azidopropyl Le^x

3.4.2.1 Synthesis of wild Le^x to check the activity of the enzymes

When all the enzymes required were expressed or prepared, the synthesis of H-Le^y started. *N*-Acetyllactosamine (LacNAc) (**3.7**) was synthesised using two enzymes: $Glc(4)_{ep}$ to convert UDP-Glc into UDP-Gal, and β(1-4)GalT1, for the synthesis of LacNAc using UDP-Gal as an donor and GlcNAc as the acceptor substrate (Scheme 3.7). Both reactions took place in the same mixture in presence of Mn^{2+}, which is required for the proper functioning of the β(1-4)GalT1 enzyme, in a TRIS buffer (pH = 8) media.

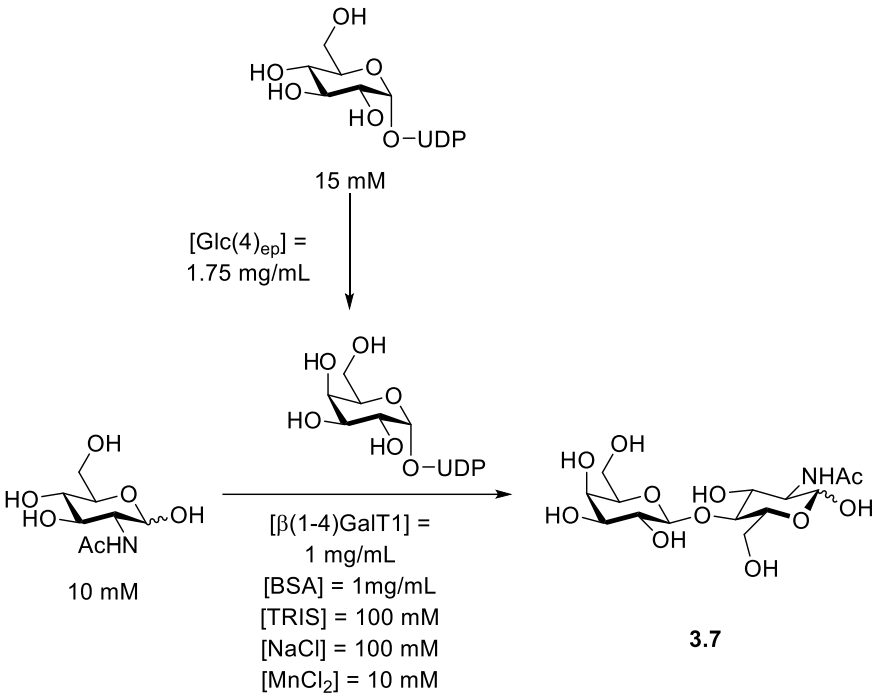

Scheme 3.7: Synthesis of LacNAc using two different enzymes.

Once all GlcNAc had reacted (by its missing evidences in TLC and LC-MS), the next enzymatic reaction to attach a Fuc was performed on the same mixture. In this stage, fucose was added at the position 3 of the GlcNAc to synthesise Lewis^x (Le^x, **3.9**). However, once again, more than one transformation was performed at the same time requiring two different enzymes and several reagents.

The addition of guanosine diphosphate (GDP) to the anomeric position of Fuc was required to transform fucose to a substrate suitable for α(1-2)FucT HP and α(1-3)FucT HP. The enzyme required for this transformation was FKP which is responsible for attaching a phosphate group at the anomeric position of fucose and transfer of guanosine monophosphate (GMP) from guanosine triphosphate (GTP) to the Fuc-1-phosphate to obtain fucosyl guanosine diphosphate (GDP-Fuc) (**3.8**), the donor carbohydrate (Scheme 3.8):

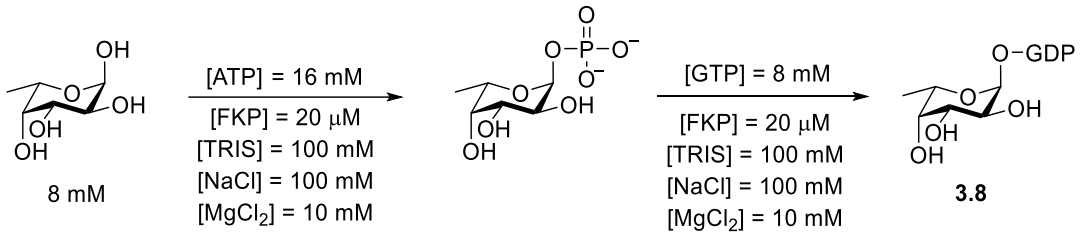

Scheme 3.8: Enzymatic activity of FKP.

Once GDP-Fuc was synthesised, its reaction with LacNAc (acceptor) was catalysed by α(1-3)FucT HP provided by Prozomix to achieve Le^x (Scheme 3.9). To perform the generation of **3.8**

and its addition to **3.7** in one pot reaction a TRIS buffer (pH = 8) was required and the presence of magnesium ion (Mg^{2+}) as the optimized conditions for the enzymes used. These conditions were described to be the best ones for the activity of the enzymes as this protein was stable at pH between 7.4 and 8 and Mg^{2+} was necessary on the binding pocket to complex donor carbohydrates.

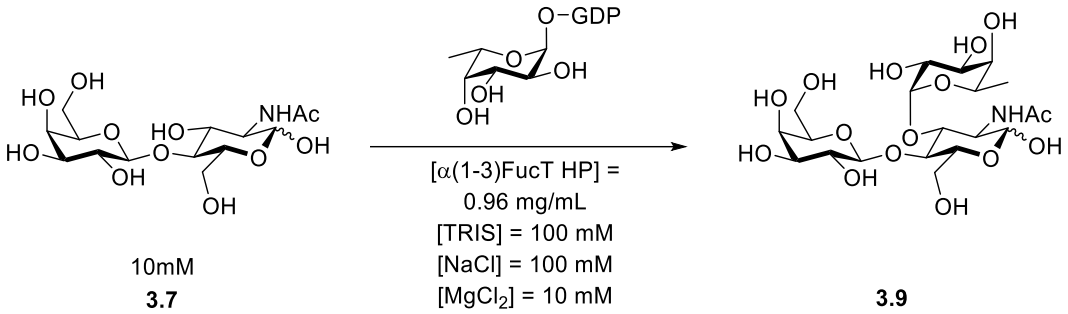

Scheme 3.9: Enzymatic synthesis of Lewis^x.

Once the α(1-2)FucT HP enzyme was expressed, its activity was tested by performing the glycosylation reaction. In the same reaction mixture, GDP-Fuc was synthesised by FKP for transfer by α(1-2)FucT HP to the 2-position of Gal in **3.9** (Scheme 3.10) to achieve H-Le^y. This second step was performed by α(1-2)FucT HP.

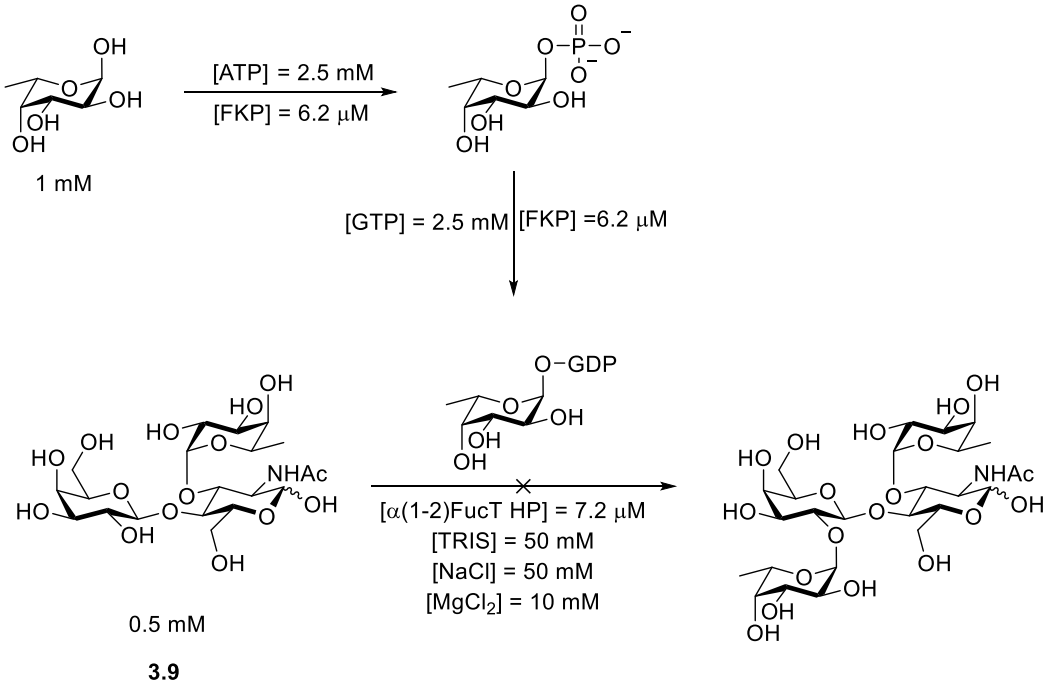

Scheme 3.10: Unsuccessful synthesis of H-Le^y.

The reaction mixture was analysed by TLC and LC-MS and neither test indicated the presence of H-Lewis^y tetrasaccharide. This fact could be due to two different reasons: the inactivity of the enzyme expressed or a mistake in the enzymatic conditions. It would be difficult to identify which of these options could be responsible for the failure of this last step. Although Lewis^y was not made

at this point, all of the enzymatic reactions to make Lewis^x had been found to work and as it is also a ligand for CTB, then our focus switched to optimising this part of the synthesis.

3.4.2.2 Optimisation of the synthesis of azidopropyl Le^x

Once the activity of the enzymes expressed were revise by the formation of wild Le^x, a screening was designed and performed to find the best conditions to synthesise azidopropyl Le^x on a large scale.

Different parameters were reviewed during this screening in each step of this process. For the synthesis of azidopropyl LacNAc, it was monitored the concentration of substrates (UDP-Glc and azidopropyl GlcNAc) while for the formation of azidopropyl Le^x the parameters checked were the concentration of enzymes α(1-3)FucT HP and FKP and the reaction over time. The conditions established by Dr. Kristian Hollingsworth were used as a control experiment in the whole synthesis, because it was well-known its full conversion in all the steps.[190][Work pending of publication]

Due to the presence an azide in the substrate of the enzymes, an imidazolium-based molecule (iTag) derivative with an alkyne (**3.10**, provided by Prof Mª Carmen Galan, University of Bristol) was attached by a CuAAC reaction (Scheme 3.11). The incorporation of this charged moiety to the carbohydrates allowed to quantify the progress of the reaction by ESI-HRMS in each step. Similar methods were described by Prof Mª.Carmen Galan and they were based on the introduction of an iTag to carbohydrates following by their analysis by LC-MS. This method have been used to study different enzymes' activity including several glycotransferase.[195–200] However, the quantitative analysis of the iTag-derivatized oligosaccharide mixtures by ESI-HRMS has been used in the laboratory recently and the corresponding data have not been published yet. [Work pending of publication]

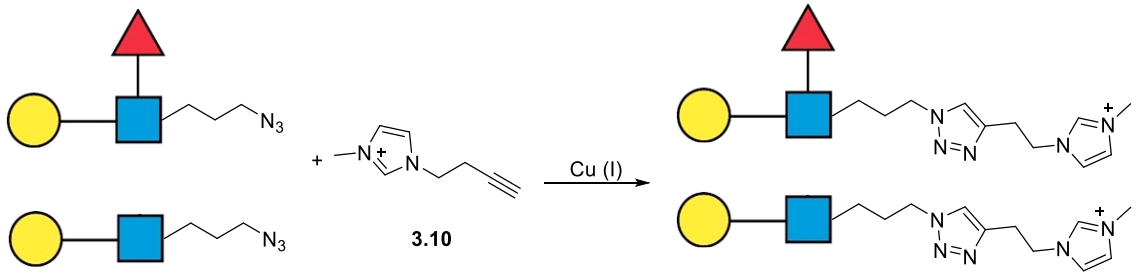

Scheme 3.11: CuAAC reaction between **3.10** and oligosaccharides derivatized with an azide.

The first reaction to check was the synthesis of azidopropyl LacNAc. A big difference was presented between the control conditions and the ones established in this project: the presence of the Glc(4)$_{ep}$ and UDP-Glc (Scheme 3.12). The presence of this enzyme and substrate did not show any inconveniences during the synthesis of wild Le^x however they could have an effect using

azidopropyl GlcNAc as a substrate. Another important fact to highlight was the concentration of substrates in the reaction mixture which could also influence in the progress of the reaction: for the control experiment the concentration of **3.3** was lower than for the conditions established in this project, the new conditions. The concentration of UDP-Gal was also different in both experiments: its concentration was well-known in the beginning of control experiment while the concentration of UDP-Gal was uncertain in the reaction because of the use of $Glc(4)_{ep}$ (Scheme 3.12).

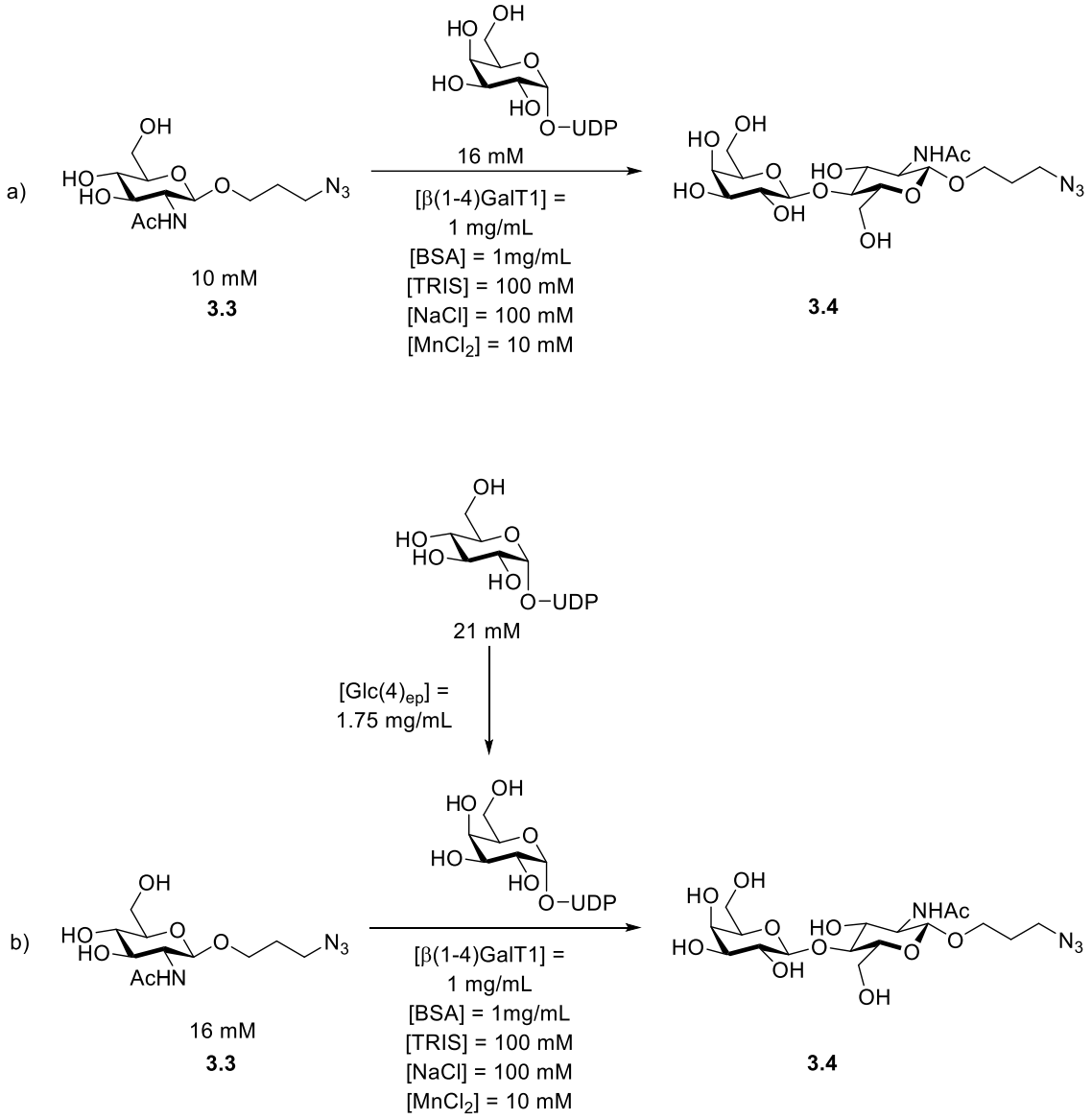

Scheme 3.12: Synthesis of azidopropyl LacNAc a) for the control experiment and b) for the new conditions.

After incubating both reactions at 37 ºC overnight, the CuAAC reaction of **3.4** with **3.10** was performed to analyse both mixtures by ESI-HRMS. As it is shown in the Table 3.1, both enzymatic procedures worked well giving an almost 100% conversion. The conclusion deduced by these

results were that both conditions, the control and the new conditions, worked well for the formation of azidopropyl LacNAc.

Table 3.1: Progress of the enzymatic synthesis of azidopropyl LacNAc overnight at 37 ºC once iTag was attached to the azidopropyl derivatized oligosaccharides and ESI-HRMS was performed three times.

Experiment	% Azidopropyl LacNAc	% Azidopropyl GlcNAc
Control	94.0±0.5	6.0±0.5
New conditions	92.5±0.6	7.5±0.6

After the synthesis of **3.4**, different aspects were tested for the synthesis of azidopropyl Le^x including concentration of FKP, concentration of α(1-3)FucT HP and the time of incubation. All the conditions were tested for both azidopropyl LacNAc mixtures (control and new conditions) to compare results between reactions mixtures. It is important mention that for this step, the FKP used was expressed and provided by Dr. James Ross (University of Leeds).

The procedure followed to perform both studies and comparations was the following one: an aliquot of enzymatic reaction mixture was taken every hour followed by its click reaction with **3.10** in presence of Cu(I) overnight to incorporate the iTag in the mixture of azido-oligosaccharides. The resulting CuAAC mixtures were analysed by ESI-HRMS three times to ensure that the results were reliable.

The first two parameters to check was the effect of α(1-3)FucT HP in the fucosylation and the time required to arrive to full conversion. Four experiments at different concentration of this enzyme (from 1.44 mg/mL to 0.24 mg/mL) were set up while all the others parameters were kept the same to ensure that any change was due to the α(1-3)FucT HP. These four experiments were performed in both azidopropyl LacNAc mixtures, the control one and the new conditions one.

The results obtained for the control mixture of **3.4** were really revealing: first of all, as it is shown in the graph 3.1, all the experiments arrived to full conversion after four hours of incubation. However, as the concentration of α(1-3)FucT HP increased, it seemed that the speed of the reaction decreased. Even though that fact could be surprising, that was due to the probably aggregation of enzyme becoming less effective for the substrate present. Finally, it seemed obvious that the amount of α(1-3)FucT used in the previous experiments was too high for the concentration of substrates and FKP.

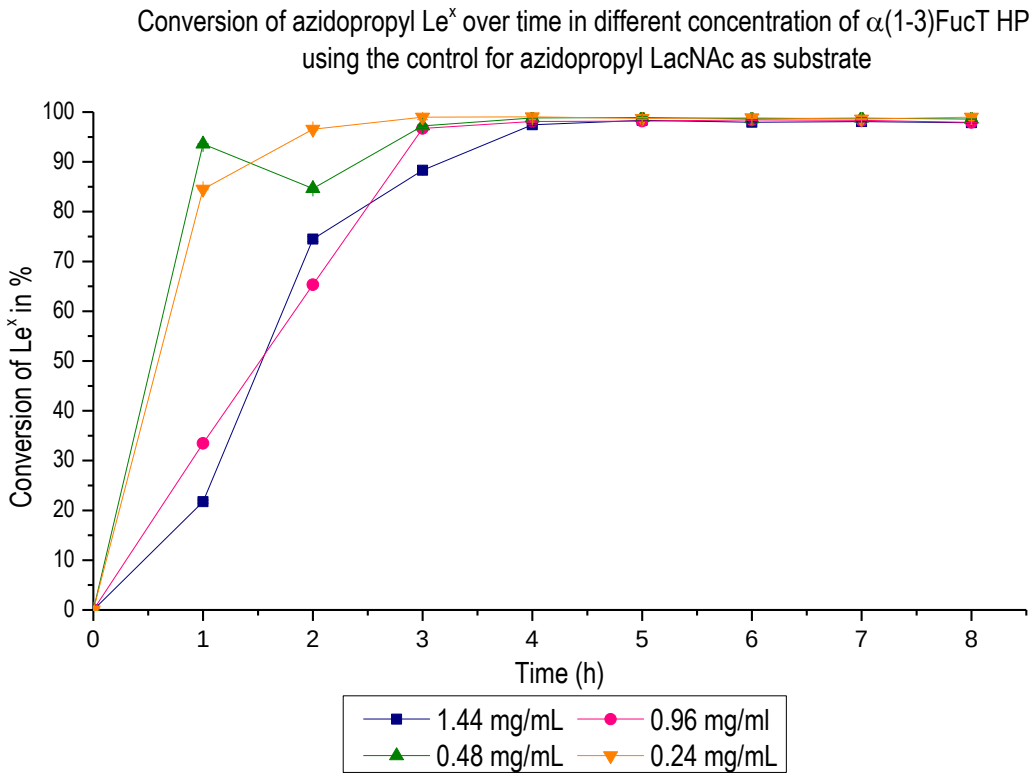

Graph 3.1: Percentage of conversion of azidopropyl Le^x changing the concentration of α(1-3)FucT HP over time using the azidopropyl LacNAc mixture from the control experiment. Mean values were average between the results and the error bars corresponds to the standard deviation.

The results obtained for the new conditions experiment for azidopropyl LacNAc were really revealing as well: first of all, as it is shown in the graph 3.2, all the experiments arrived at full conversion after four hours of incubation too. Again, the highest concentration of α(1-3)FucT HP did show again the slowest speed, even though there was a really big improvement of the speed rate from the third to fourth hour of incubation. On the other hand, the other three concentrations (from 0.96 to 0.24 mg/mL) showed the similar kinetics for this conversion, the 0.96 mg/mL was a little bit slower than the 0.48 and 0.24 mg/mL but at around 2 h all of the experiments were around 90% conversion for **3.5**. Again, it seemed that excessive α(1-3)FucT HP did not help in the rate and extent of the reaction.

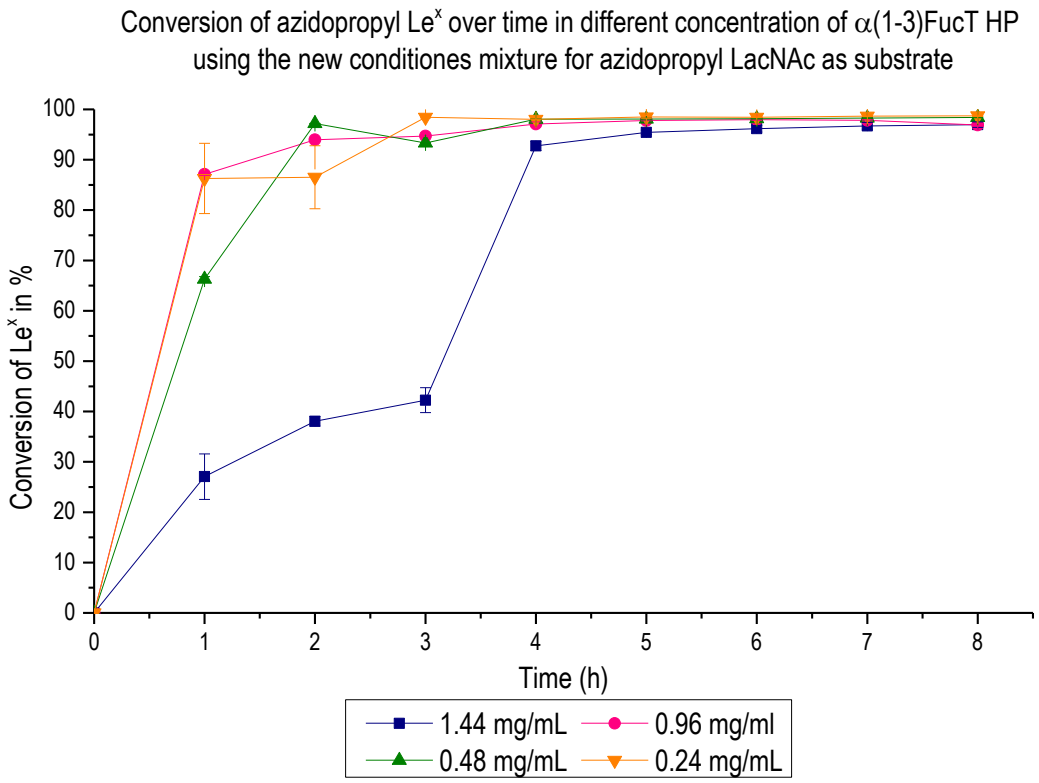

Graph 3.2: Percentage of conversion of azidopropyl Le^x changing the concentration of α(1-3)FucT HP over time using the azidopropyl LacNAc mixture from the new conditions experiment. Mean values were average between the results and the error bars corresponds to the standard deviation.

The others two parameters to revise were the best concentration of FKP and the time to synthesise azidopropyl Le^x. Three different experiments were set up using a range of FKP from 8.8 to 2.2 µM while the others substrates and enzymes were kept constant. These experiments were performed in both **3.4** mixtures, the control one and the new conditions one.

The first experiments to analyse were again the conversion using the control mixture for the azidopropyl LacNAc synthesis. The results obtained were really interesting indeed (graph 3.3): the speed of the reaction decreased as the concentration of FKP was decresed. For the experiment using 8.8 µM of FKP, the speed was fast, at the third hours of incubation there was full conversion, while for the experiment at 2.2 µM of FKP the full conversion was achieved after seven hours of incubation. These results concluded that the speed of the reaction depends on the activity and concentration of FKP, responsible to synthesise GDP-Fuc. At the concentration of substrate established and for a concentration of α(1-3)FucT HP of 0.96 mg/mL, 8.8 µM of FKP showed fastest speed.

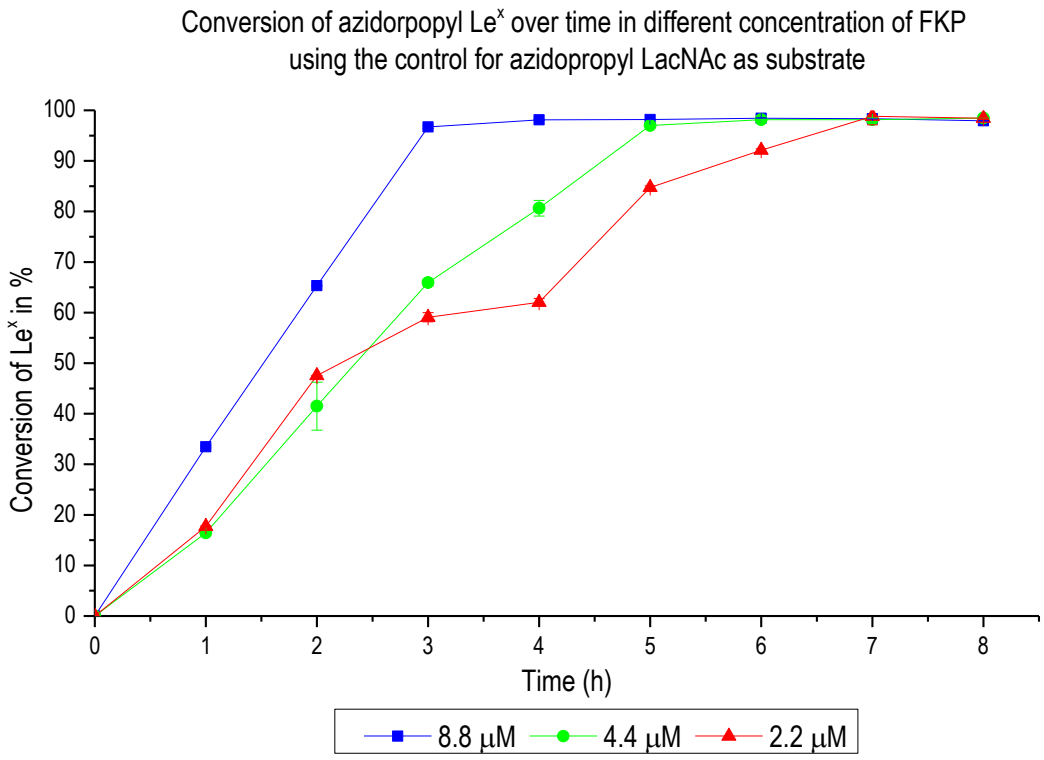

Graph 3.3: Percentage of conversion of azidopropyl Le^x changing the concentration of FKP over time using the azidopropyl LacNAc mixture from the control experiment. Mean values were average between the results and the error bars corresponds to the standard deviation.

For the synthesis of azidopropyl Le^x from the new conditions azidopropyl LacNAc's mixture, the results obtained were really similar to the previous ones (Graph 3.4). Again, all the reactions arrived to full conversion between the fifth and sixth hour of incubation. Furthermore, the synthesis was faster as the concentration of FKP increased becoming the experiment at 8.8 µM of FKP the fastest among the three concentrations tested. In conclusion, the results obtained seemed to agree with the previous experiment: the concentration of FKP controlled the speed of the reaction. Nevertheless, an important fact to highlight is that the speed of this enzymatic reaction seemed faster for the new conditions' mixture for azidopropyl LacNAc than for the control condition ones.

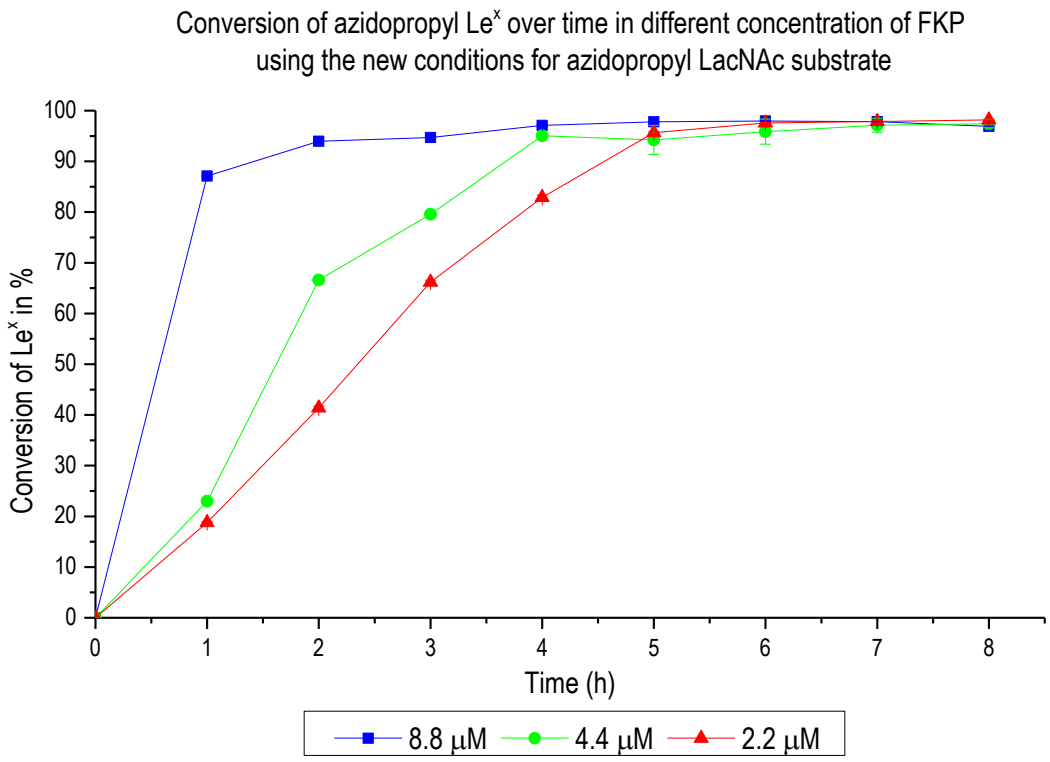

Graph 3.4: Percentage of conversion of azidopropyl Le^x changing the concentration of FKP over time using the azidopropyl LacNAc mixture from the new conditions experiment. Mean values were average between the results and the error bars corresponds to the standard deviation.

After ensuring that the preparation of azidopropyl LacNAc synthesis did not affect the speed of the synthesis of azidopropyl Le^x, it was compared the activity of the FKP expressed in this project and the one provided by Dr. James Ross because previous experiments seemed to indicate that the reaction was not as fast as the screening showed. Then, it was checked the best concentration for α(1-3)FucT HP according to the optimal concentration of FKP (8.8 µM).

Three experiments at different at different concentration of α(1-3)FucT HP (from 1.44 mg/mL to 0.48 mg/mL) were performed keeping the concentration of substrate constant as the previous experiments and 8.8 µM for the FKP expressed in this project previously. These three experiments were performed in **3.4** mixture synthesised using UDP-Glc and Glc(4)$_{ep}$. Because the experiment did not seem to finish after eight hours, like the previous ones, aliquots were taken for 68 hours of incubation.

The results for these experiments presented a different profile that all the data obtained previously (Graph 3.5). First of all, it required around 55 h to achieve more than 90% of conversion from azidopropyl LacNAc to azidopropyl Le^x. Secondly, the reaction was faster as the concentration of α(1-3)FucT HP and, for a concentration of 0.48 mg/mL, the reaction did not go further than

around 70% conversion. Finally, the high concentration of α(1-3)FucT HP did not affect the conversion because the experiments using 1.44 and 0.96 mg/mL were similar, both of them aimed full conversion after 55 hours.

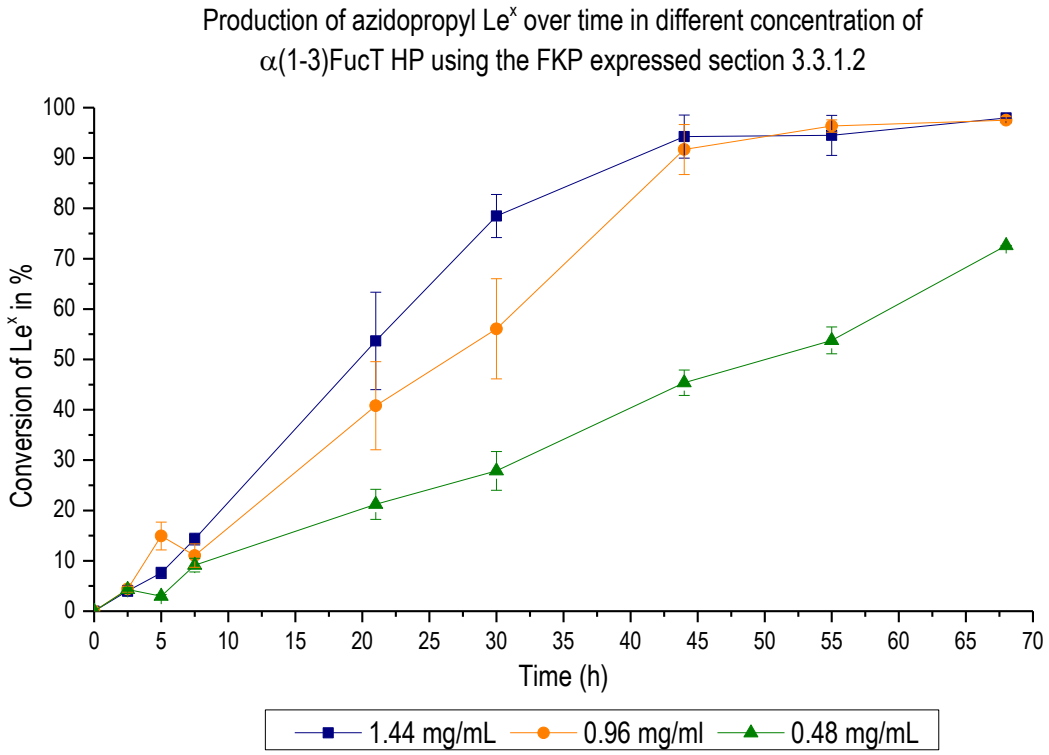

Graph 3.5: Percentage of conversion of azidopropyl Le^x changing the concentration of α(1-3)FucT HP over time using the FKP expressed in this project. Mean values were average between the results and the error bars corresponds to the standard deviation.

As a conclusion, the FKP expressed in this project was not as active as the one provided by Dr. James Ross. Using his enzyme, the reactions were finished by average of five hours while using mine, around 50 hours was required. Moreover, the concentration of α(1-3)FucT could be low because of the high activity of his FKP but using the FKP expressed in this project, the concentration of the fructosyltransferase had to be high. However, these experiments provided an idea about the time of incubation required to achieve full conversion depending of the FKP activity.

All of these experiments were really useful to find the best conditions to synthesise azidopropyl Le^x on a large scale without using a big excess of enzymes or substrates. Also, it provided an idea of the kinetics of the enzymes used in the reaction.

3.4.2.3 Synthesis of azidopropyl Le^x on a large scale

After the screening experiment, the synthesis of azidopropyl Le^x in big scale was performed to synthesize enough oligosaccharide to attach it to alkyne-derivatized hyaluronic acid. Its synthesis

started with the formation of azidopropyl LacNAc by the addition of Gal in the position 4 of azidopropyl GlcNAc following by its fucosylation at the position 3 of the same residue.

3-Azidopropyl *N*-acetyllactosamine (**3.4**) was synthesised in big scale using two enzymes: $Glc(4)_{ep}$ to convert UDP-Glc into UDP-Gal, and β(1-4)GalT1, for the synthesis of **3.4** using UDP-Gal as an donor and azidopropyl GlcNAc as the acceptor substrate (Scheme 3.13). Both reactions took place in the same mixture in the presence of Mn^{2+}, which is required for the proper functioning of the β(1-4)GalT1 enzyme, in a TRIS buffer (pH = 8) media.

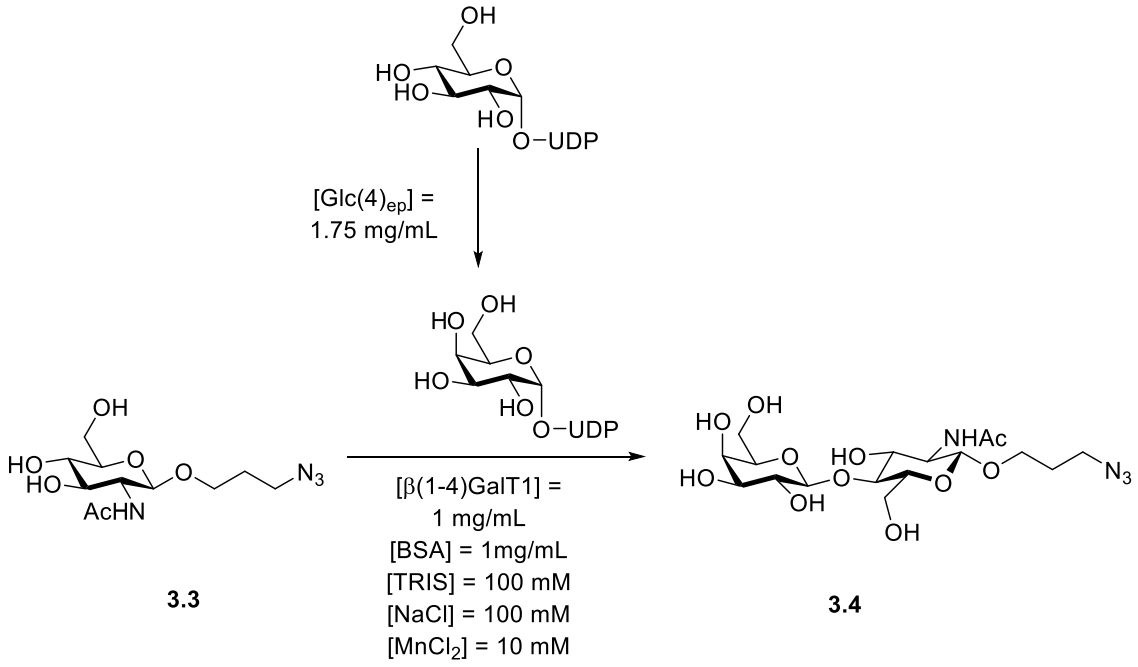

Scheme 3.13: Synthesis of azidopropyl LacNAc using two different enzymes.

Once all **3.3** had reacted (checked by TLC and LC-MS), the next enzymatic reaction was performed on the same mixture. In this stage, fucose was added at the position 3 of the azidopropyl GlcNAc to synthesise azidopropyl Lewis^x. However, once again, more than one transformation was performed at the same time requiring two different enzymes and several reagents: first, Fuc-GDP was synthesised, as it has been explained previously, by FKP using Fuc, ATP and GTP as substrates. Once GDP-Fuc was achieved, its reaction with **3.4** (acceptor) was catalysed by α(1-3)FucT HP to achieve azidopropyl Le^x (Scheme 3.14). To perform the generation of Fuc-GDP and its addition to azidopropyl LacNAc in one pot reaction a TRIS buffer (pH = 8) was required and the presence of magnesium ion (Mg^{2+}) as the optimized conditions for the enzymes used.

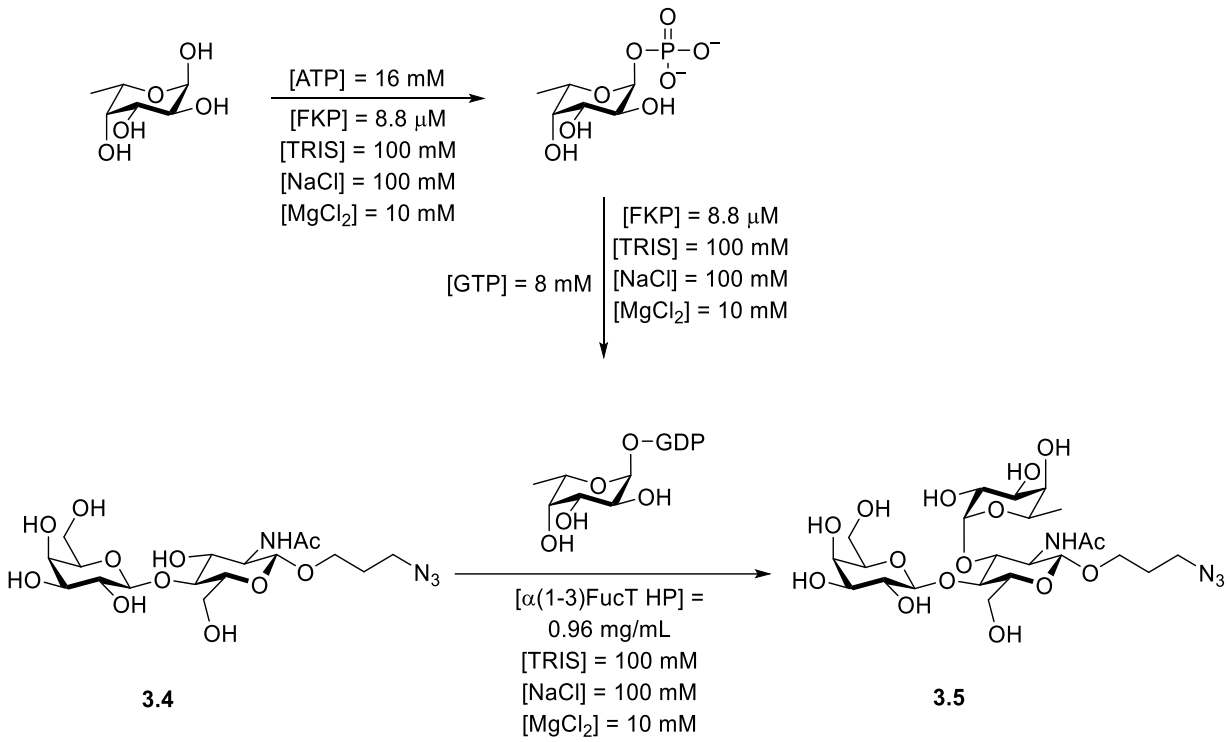

Scheme 3.14: Enzymatic synthesis of azidopropyl Lewis^x.

3.5 Synthesis of Gb_3-N_3

3.5.1 Expression of the enzymes required

As it has been commented previously, the new approach offers flexibility to attach any oligosaccharide-azide to the hyaluronic acid. Because of its importance and utility to perform binding studies with a large number of proteins, Gb_3-N_3 (**3.11**) was synthesised to attach it to HA-*g*-propargyl through CuAAC cycloaddition. Its synthesis can be performed chemically or enzymatically, being this second option easier and faster. The enzymatic synthesis was followed starting with β-D-galactopyranosyl-(1-4)-D-glucopyranosyl azide (Lac-N_3) provided by Dr. Vajinder Kumar (University of Leeds).

The enzymatic synthesis required just one step performed by two different enzymes: $Glc(4)_{ep}$ to convert the cheaper UDP-Glc into UDP-Gal, and α-1,4-galactosyltransferase (LgtC), which transfers a galactosyl residue from UDP-Gal (donor monosaccharide) to Lac-N_3 (acceptor oligosaccharide) forming an α(1-4) bond to the Gal residue. For this reason, the first step to synthesise either Gb_3 oligosaccharide or Gb_3-N_3 was to express LgtC.

E. coli BL21 cells with LgtC-His tag plasmid in provided by Dr. Kristian Hollingsworth were grown for two hours at 37 ºC in auto-induction LB media and it was left overnight at 25 ºC. Then, the cells were recovered by centrifugation and resuspended in lysis buffer. The protein was released by sonicating the suspension and purified by nickel affinity chromatography followed buffer exchange

using a centrifugal ultrafiltration concentrator to remove the imidazole. An SDS-PAGE gel (Figure 3.10) was done to check the degree of purity and the enzyme was quantified by UV absorption (λ = 280 nm, ε(LgtC) = 59735 M^{-1} cm^{-1}).

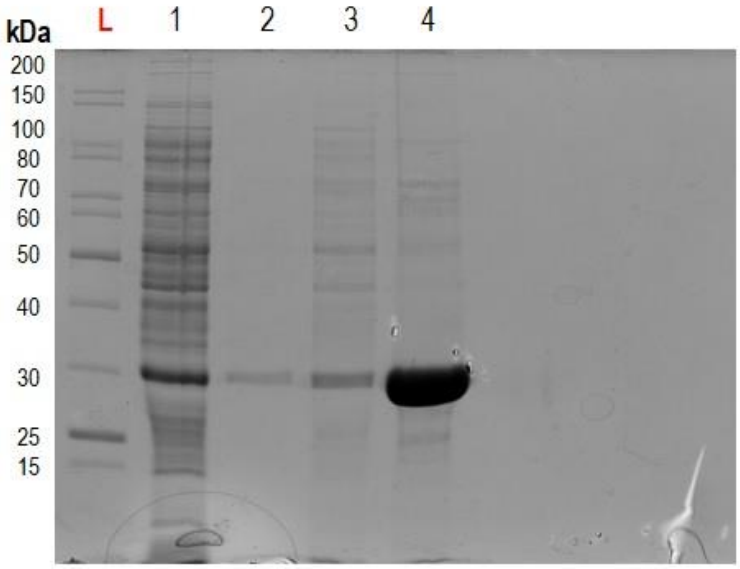

Figure 3.10: PAGE for LgtC expression. Lane L referring to the protein mass ladder, lane 1 Pellet, lane 2 Flowthrough, lane 3 First washing and lane 4 Elution.

Once the enzyme was prepared, the enzymatic reaction to synthesise Gb_3-N_3 was set up: $Glc(4)_{ep}$ and LgtC used UDP-Glc and Lac-N_3 as a substrate respectively in TRIS buffer and in presence of Mn^{2+} to make Gb_3-N_3 (**3.11**) (Scheme 3.15).

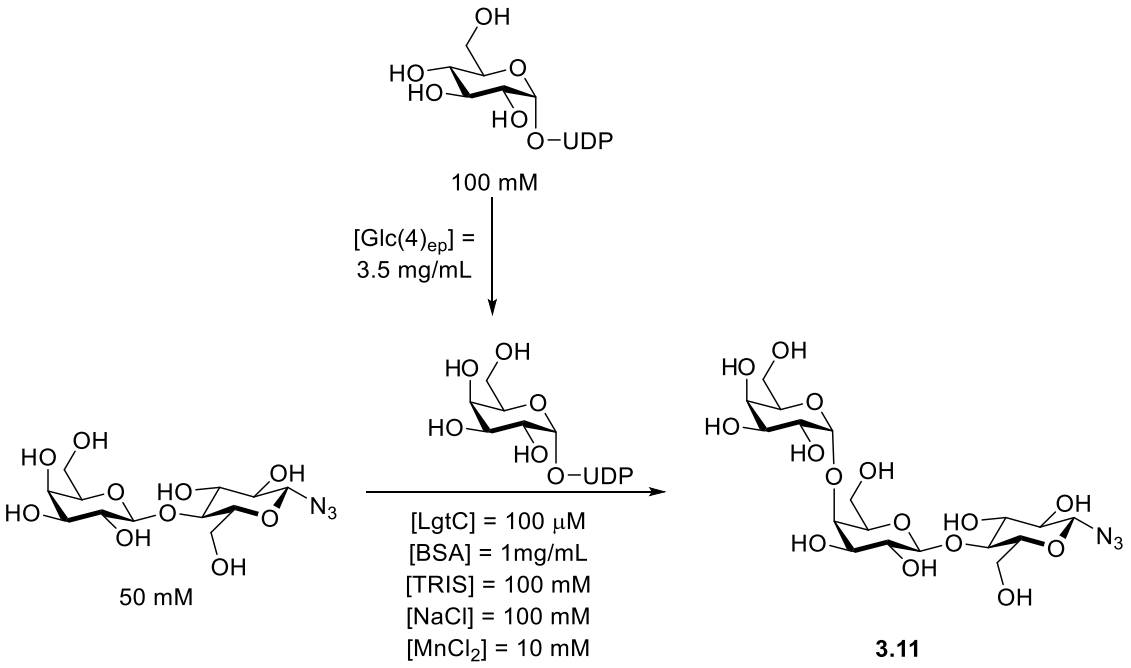

Scheme 3.15: Enzymatic synthesis of Gb_3-N_3 using two enzymes, $Glc(4)_{ep}$ and LgtC in one pot.

3.5.2 Synthesis of Gb_3-N_3 trisaccharide

Even though Gb_3-N_3 was synthesised using the LgtC enzyme, yield of 4%, the reaction did not proceed to completion and the principal product was not Gb_3-N_3 but a side product that has not been identified.

Due to the problems presented in the previous enzymatic synthesis, another enzyme was used to try to improve the yields of Gb_3-N_3 production. The galactosyltransferase enzyme chosen was GalT-Tt 1871 and it was provided by Prozomix.[186] First of all, this enzyme was tested in small scale using Lac-N_3 or Lac and UDP-Gal as substrates (Scheme 3.16):

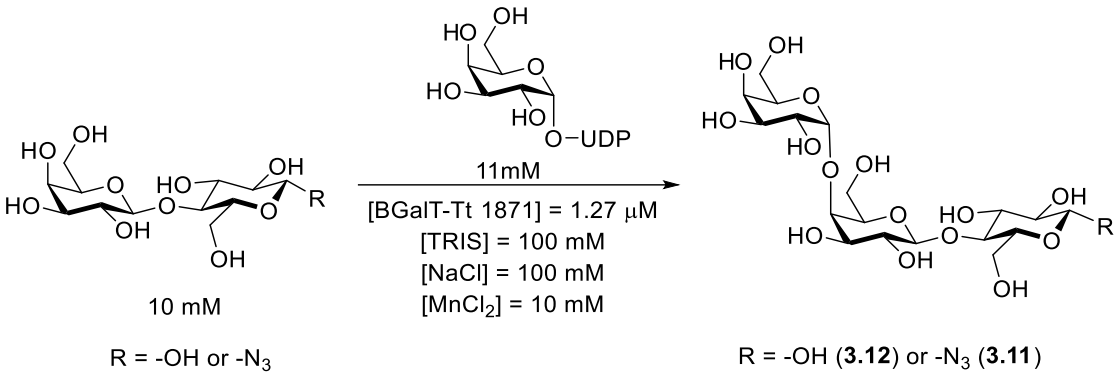

Scheme 3.16: Test reactions to check GalT-Tt 1871 enzyme using Lac-N_3 or Lac as a substrate.

UDP-Gal (donor monosaccharide) was attached to Lac-N_3 or Lac (acceptor oligosaccharide) by GalT-Tt 1871 in TRIS buffer (pH = 8) in presence of Mn^{2+}. This first test worked well and LC-MS and TLC showed evidences for synthesis of Gb_3-N_3 (**3.11**) or Gb_3 oligosaccharide (Gb_3-os, **3.12**). However, there was not full conversion but the crude mixture was cleaner than the one using LgtC as an enzyme. Also, there was not presence of the impurity achieved in the previous enzymatic synthesis.

After this test, the compatibility of GalT-Tt 1871 with $Glc(4)_{ep}$ was studied. Another two test were set up using both enzymes in one pot: $Glc(4)_{ep}$ producing UDP-Gal using UDP-Glc as a substrate and GalT-Tt 1871 attaching this donor monosaccharide to Lac-N_3 or Lac (Scheme 3.17). Both tests were done on a small scale as well and they were followed by LC-MS and TLC.

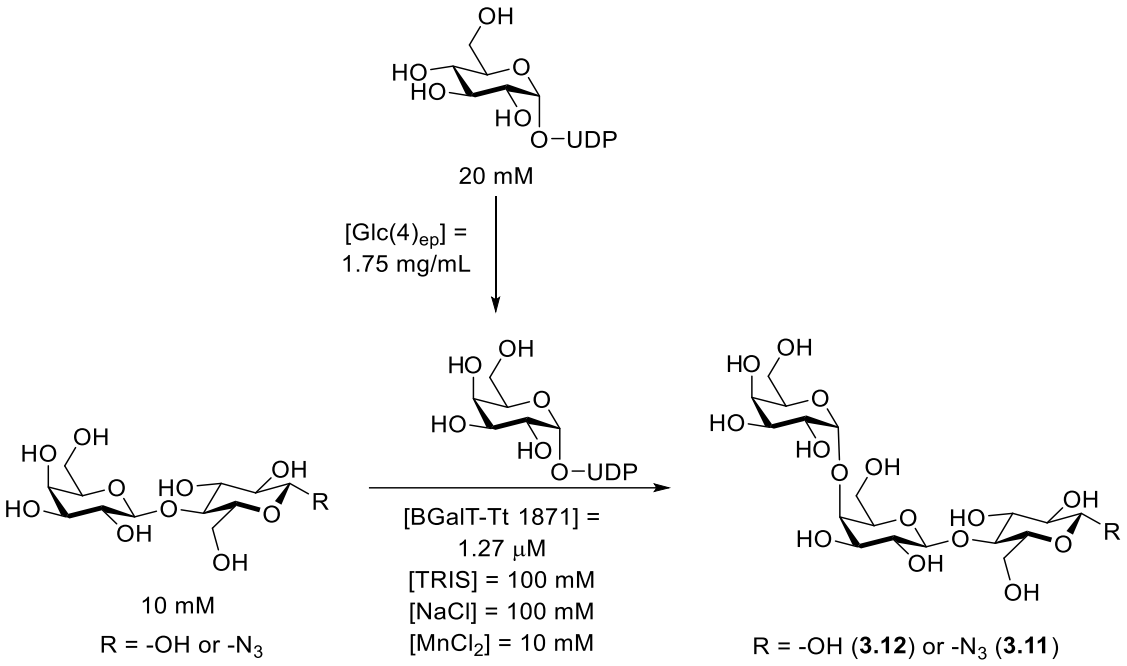

Scheme 3.17: Test reactions to check the compatibility of GalT-Tt 1871 and $Glc(4)_{ep}$ enzymes using $Lac\text{-}N_3$ or Lac as a substrate and UDP-Glc respectively.

In that case, the reaction did not arrive to a full conversion either; there was still presence of Lac or $Lac\text{-}N_3$, but the main product was the trisaccharide and the crude mixture was still cleaner than the one using LgtC as an enzyme. To achieve the full synthesis of Gb_3-os or $Gb_3\text{-}N_3$, the conditions of the reaction needed to be optimised in terms of pH and concentrations of reagents and enzymes.[186]

A set of experiments was set up to try to find the best concentration for the reagents $Lac\text{-}N_3$ and UDP-Glc because, as it has been established by Huang, *et al.*, the best pH was 7.4 even though high activity was found at pH 8.[186] Five experiments were set up following the concentrations presented in Table 3.2 while the concentration of buffer, enzymes, and catalyst were kept the same for all of the reactions as well as the pH. All reactions were left at 37 ºC overnight.

Table 3.2: Concentrations of substrates to try to set up the best conditions for BGalT T1-1871

Test	Concentration $Lac\text{-}N_3$ (mM)	Concentration UDP-Glc (mM)	Full conversion of $Lac\text{-}N_3$ (after overnight)
1	2	4	No
2	4	8	No
3	6	12	No
4	8	16	No
5	10	20	No

The following day all the reaction mixture were analysed by LC-MS and TLC revealing that none of the tests had full conversion of Lac-N_3 to Gb_3-N_3. By TLC and LC-MS was still visible the starting material (**3.11**).

To try to improve the yield and achieve full conversion, more GalT1 Tt-1871 was added to test 1, 2 and 3 leaving another night at 37 ºC while test 4 and 5 were left for two days at 37 ºC. Both attempts to improve yields were not successful after their analysis by TLC and LC-MS. However, it seemed that the conditions for test 4 or 5 provided more product than the conditions for test 1, 2 or 3. For this reason, the conditions set up were the ones in test 5 in future experiments.

Even though the concentrations of reagents were established to achieve the highest yield in the synthesis, there was still an issue during the purification process. Gb_3-N_3 and Lac-N_3 (or Gb_3-os and Lac) had similar size and polarity so it was really hard to obtain the final product pure. As a consequence, Lactase enzyme (BioCare) was introduced in the synthesis to digest Lac-N_3 (or Lac) so the final reaction mixture contained trisaccharides and monosaccharides becoming easier to separate them (Scheme 3.18).

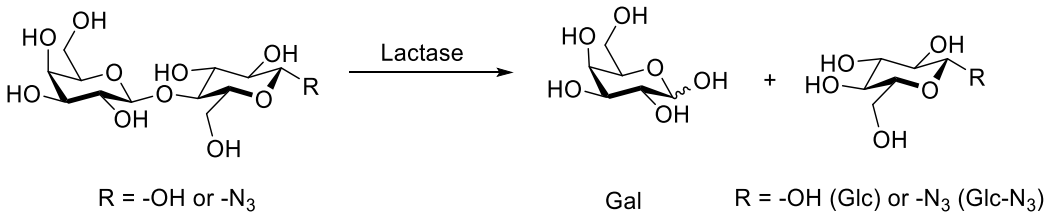

Scheme 3.18: Lactase enzyme reaction.

The incorporation of this new enzyme in the synthesis required to set up the conditions of this last step. Moreover, it was necessary to revise that lactase did not present a side reaction with the modified substrates containing an azide group or did not digest **3.11** or **3.12**. Different test reactions were performed to check these possible side reactions as well as to establish the conditions of the reaction.

The first test started with the synthesis of Gb_3-os using the conditions established on test 5, Table 3.2. The following day, lactase was added to the reaction mixture and left at room temperature. After 2.5 h, the progress of the digestion was analysed by TLC and LC-MS revealing the appearance of a new spot on the TLC as well as the mass of Gal/Glc in the LC-MS spectra. It is also important to highlight that the **3.12** spot did not seem to suffer any change while Lac spot was less intense. Because it seemed that the enzyme was working properly, it was added more lactase and the resulting mixture was left at room temperature for 2 more hours following by its analysis by TLC and LC-MS. Finally, the reaction mixture was left overnight at room temperature

to check if Gb_3-os was digested after long exposition of lactase but it was not according the TLC and LC-MS analysis.

Once the previous test confirmed that, at least Gb_3-os was stable in presence of lactase, the concentration of lactase was set up performing 4 tests described in the Table 3.3:

Table 3.3: Concentration of substates and Lactase to establish the best conditions to use this enzyme.

Test	Concentration of Lac (mM)	Theorical concentration of Gb_3-os (mM)*	Concentration Lactase (units/µL)
1	8.5	-	1
2	8.5	-	0.24
3	-	8.5	1
4	-	9	0.24

*Theorical Concentration of Gb_3-os in the reaction mixture of the previous **3.12** synthesis if there was full conversion, even though it was already known that there was not full conversion because of the presence of Lac by TLC and LC-MS.

All the test reactions were left at room temperature overnight and analysed by TLC and LC-MS. As it was shown by TLC and confirmed by LC-MS, for the Lac tests (entries 1 and 2 in Table 3.3), only test 1 did not contain Lac but Gal and/or Glc. On the other hand, in test 2 there was still large amount of lactose but some was digested as it was also visible Gal and/or Glc. For the test using the reaction mixture of Gb_3-os synthesis (entries 3 and 4 in Table 3.3), the results were similar even though it was harder to analyse due to the presence of several compounds in the mixture. Nevertheless, test 3 did not present lactose by TLC or LC-MS while test 4 contained it was not fully digested. These four reactions provided enough information about the best conditions in terms of concentration to use Lactase in the future.

Finally, it was checked that the conditions set up in the previous test were applicable for Gb_3-N_3 synthesis. For this reason, Gb_3-N_3 was synthetized following by the addition of Lactase respecting the concentrations established on entry 3 in Table 3.3. The reaction mixture was analysed by TLC and LC-MS after 2 hours and 6 hours. After 6 hours, there was not presence of Lac-N_3 and Gb_3-N_3 did not seem to suffer any degradation or side reaction. A last test was done leaving the reaction mixture (Gb_3-N_3 and Lactase) overnight at room temperature but there was not any change respect. In conclusion, Lactase could be used in the synthesis of Gb_3-N_3 without any side reaction or degradation.

After all this test performed, the synthesis of Gb_3-os first and Gb_3-N_3 later was done at big scale using the conditions established in all the test before. The only change done to try to achieve higher

yields was the concentration of epimerase which was increased from 1.75 mg/mL to 3.5 mg/mL This high concentration was the one used to use following LgtC protocol and, by increasing it, the conversion of Glc-UDP to Gal-UDP was faster than the one used in the test and mor useful for big scale reactions.

The synthesis Gb_3-os was performed in one pot using $Glc(4)_{ep}$ to produce UDP-Gal using UDP-Glc as a substrate and GalT-Tt 1871 to attach this donor monosaccharide to Lac (Scheme 3.19). The reaction was left at 37 ºC overnight. In one last attempt to improve the yield of the synthesis, another batch of $Glc(4)_{ep}$ and UDP-Glc were added and the reaction mixture was left another night at 37 ºC. This extra addition seemed to help to synthesise more **3.12** according the TLC spot intensities. Then, Lactase was incorporated to the reaction to digest the remaining Lac overnight at room temperature. The purification was successful and the yield was the highest achieved so far, 70%.

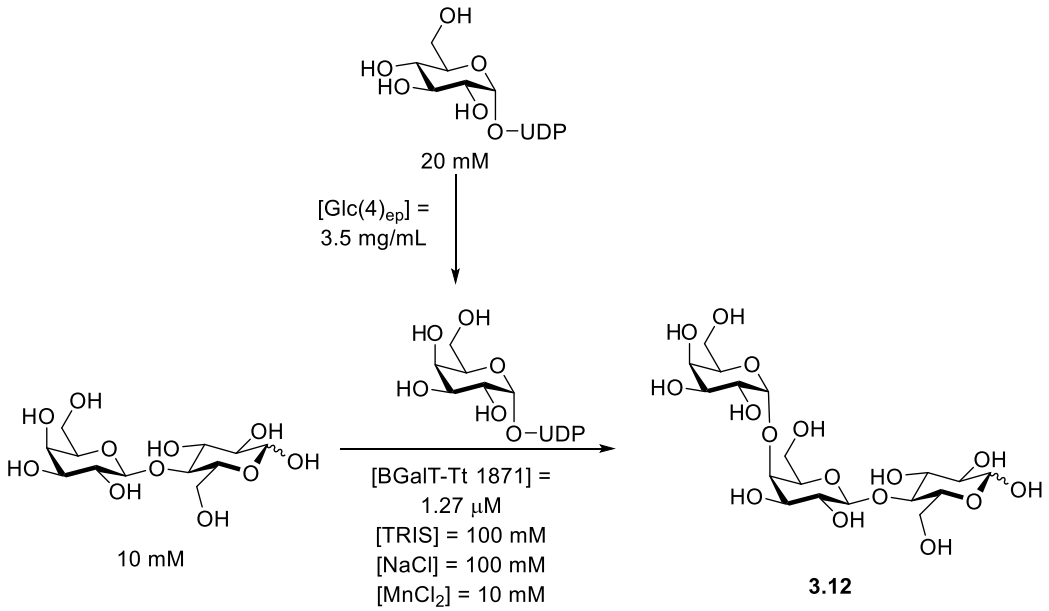

Scheme 3.19: Synthesis of Gb_3-os in big scale.

The synthesis of Gb_3-N_3 at big scale was performed using exactly the same conditions than the ones used for the Gb_3-os synthesis. Nevertheless, the concentration of UDP-Glc was slightly lower (17 mM instead of 20 mM) and the extra addition of $Glc(4)_{ep}$ and UDP-Glc was not possible to perform because there was not enough of this last substrate left. For this reason, in one pot reaction UDP-Glc and Lac-N_3 were the substates for $Glc(4)_{ep}$ and BGalT Tt-1871 respectably to synthetize Gb_3-N_3 in presence of Mn^{2+} (Scheme 3.20). The following day, lactase enzyme was added to digest the remaining Lac-N_3 overnight following by its purification to achieve Gb_3-N_3 in high yield as well, 40%.

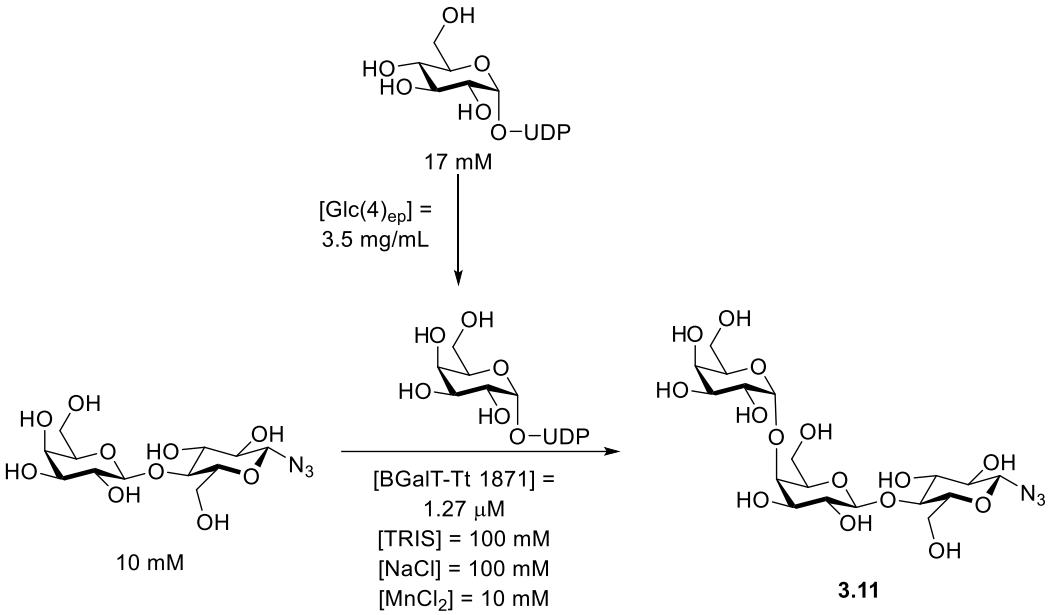

Scheme 3.20: Synthesis of Gb_3-N_3 in big scale.

3.5.3 CuAAC cycloadditions using Gb_3-N_3 as a reagent

All the efforts to synthesise Gb_3-N_3 was invested for its biological significance as well as for the possibility to perform CuAAC cycloadditions with other moieties to achieve different product with several applications, such as binding studies. To accomplish one of the goals of this project as well as to help other researches in the network, the click chemistry was studied to establish the best conditions to perform the CuAAC cycloaddition using Gb_3-N_3 as a reagent.

The reaction performed was the cycloaddition between **3.11** and 5-hexynoic acid in presence of Cu (I) (Scheme 3.21). This metal catalyst was achieved by adding to the reaction mixture $CuSO_4$ and sodium ascorbate because this reagent reduced Cu (II) to the required Cu (I).

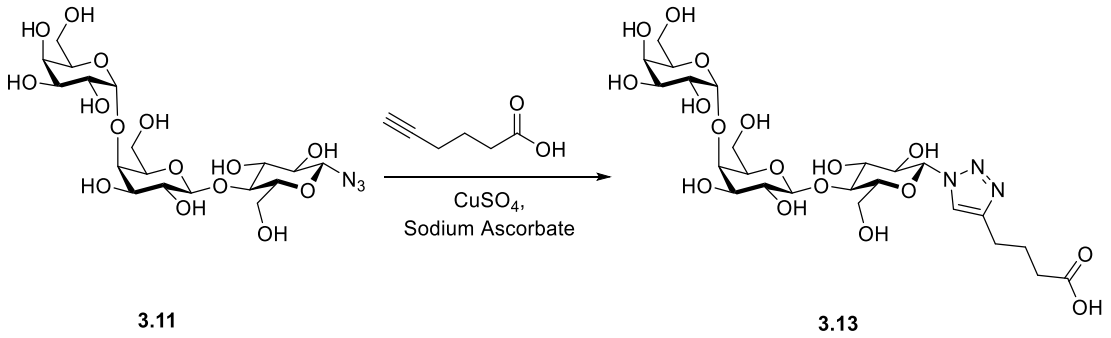

Scheme 3.21: CuAAC cycloaddition between Gb_3-N_3 and 5-hexynoic acid in presence of Cu (I).

Two sets of experiments were performed to set up the best concentration of alkyne, in both sets 5-hexynoic acid, and sodium ascorbate to achieve full conversion of Gb_3-N_3 overnight at room temperature. Consequently, the concentrations of **3.11** and $CuSO_4$ were kept the same in all the experiments so the influence of both substances was constant.

In the first set of experiments, it was studied the role of the alkyne concentration keeping the others three constant being 10 mM for Gb_3-N_3, 15 mM for sodium ascorbate and 5 mM for $CuSO_4$. The concentration of 5-hexynoic acid was tested according Table 3.4. All the reactions were subjected to TLC and LC-MS analysis.

Table 3.4: CuAAC cycloaddition test modifying the concentration of the alkyne (5-hexynoic acid) to try to establish the conditions for full conversion of Gb_3-N_3.

Test	Concentration of 5-hexynoic acid (mM)	Full conversion of Gb_3-N_3
1	10	No
2	15	No
3	20	No
4	25	No

As it was shown by TLC and confirmed by LC-MS, in any of this reaction there was full conversion of Gb_3-N_3 meaning that the concentration of alkyne did not have the key role for this reaction. Nevertheless, by TLC was possible to observe that reactions for entries 1, 2 and 3 had more product than entry 4 meaning that high concentration of alkyne did not help to improve the yield of the reaction.

On the other hand, another set of experiments were performed to check if different concentration of sodium ascorbate made a difference in the cycloaddition. The same reaction was performed as the previous tests. So, the concentrations of Gb_3-N_3, $CuSO_4$ and 5-hexynoic acid were kept constant at 10 mM, 5 mM and 10 mM respectably while the concentration of sodium ascorbate was ranged according Table 3.5. All the reactions were subjected to TLC and LC-MS analysis.

Table 3.5: CuAAC cycloaddition test modifying the concentration of sodium ascorbate to try to establish the conditions for full conversion of Gb_3-N_3.

Test	Concentration of sodium ascorbate (mM)	Full conversion of Gb_3-N_3
1	10	No
2	15	No
3	20	No
4	25	No
5	30	Yes

As it can be observed in the previous Table, at high concentration of sodium ascorbate, there was full conversation of **3.11**. This fact was shown by TLC and confirmed by LC-MS because as

the concentration of sodium ascorbate was increasing, more intense was spot of the product until the experiment for entry 5, where there was only product and no Gb_3-N_3.

To conclude, both set of experiments revealed important information to set up the best conditions to perform CuAAC cycloadditions and achieve full conversion of Gb_3-N_3. It has been demonstrated that the increase of alkyne in the reaction mixture did not help to improve the yield while sodium ascorbate seemed to perform a key role in the reaction ensuring the presence of Cu (I) catalyst.

Due to the CuAAC conditions were set up with the previous test, the incorporation of a biotin to the anomeric position by a CuAAC reaction was performed. For this experiment, alkyne-PEG_4-biotin was reacted with Gb_3-N_3 in same conditions established in entry 5 on the previous Table (Scheme 3.22). However, because the reaction was done in bigger scale, it took 2 days to arrive a full conversion for Gb_3-N_3 and also it was required an extra addition of sodium ascorbate after the first day of reaction to achieve Gb_3-PEG_4-Biotin in 27% yield.

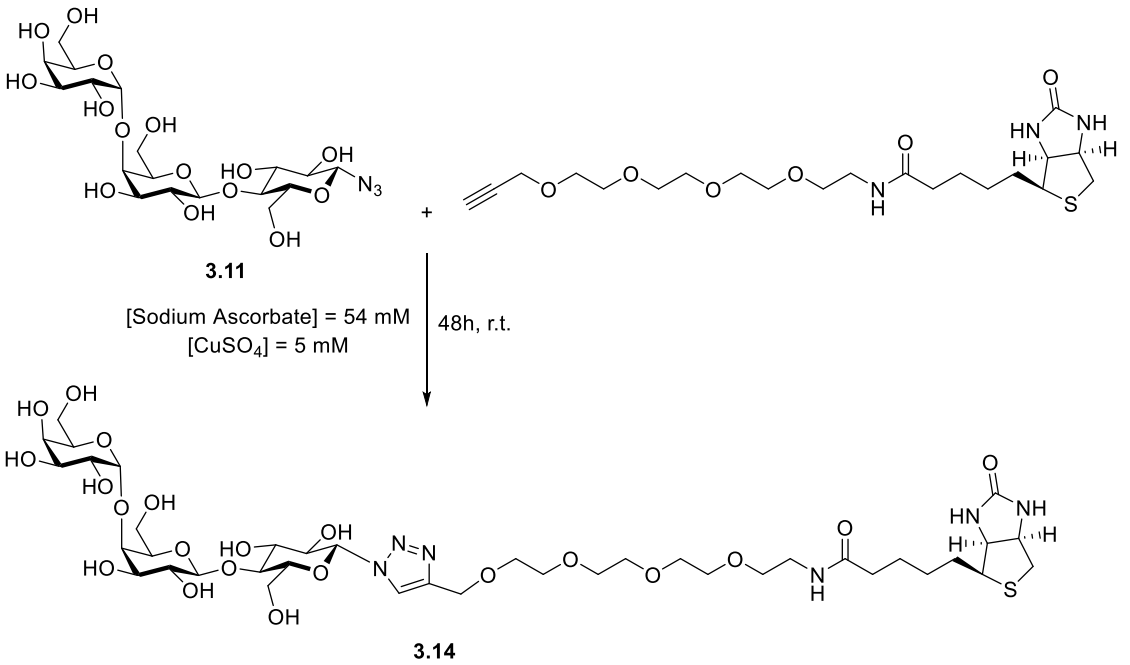

Scheme 3.22: Synthesis of Gb_3-PEG_4-Biotin

This molecule was not used for this project but it was sent to Natalia Denielewicz, who used it for isolate Shiga toxin in a solid support.

3.6 Conclusions

Two different oligosaccharides derivatized with an azide were synthesised successfully: azidopropyl Le^x and Gb_3-N_3. Moreover, as it has been checked for the second oligosaccharide, these molecules could perform CuAAC cycloadditions without side products.

Even though the synthesis of azidopropyl H-Le^y was not successful, the information achieved in terms of the expression of the enzyme was really useful for future approaches. The best conditions to express α(1-2) FucT HP were discovered, however, this enzyme did not show activity in the actual conditions.

On the other hand, revealing information were obtained because of the screening to find the best conditions for the synthesis of azidopropyl Le^x. First of all, the synthesis of the disaccharide **3.4** did not show any improvement or retrogression using $Glc(4)_{ep}$ and UDP-Glc instead of UDP-Gal. The enzymatic mixture for **3.4** did not show any extra issue in the following step neither. Secondly, the kinetics of the addition of Fuc to azidopropyl LacNAc fell on the activity of FKP showing slow reaction's speed as the concentration of FKP decreased for the same batch of enzyme. This conclusion was supporting once different batches of this enzyme were compered, demonstrating that using a less active FKP required longer incubation times (from around five to 50 hours). Finally, high concentration of α(1-3)FucT HP did not help in the reaction speed, on the contrary, low concentration of this enzyme ended with a fast reactions when using the same concentration of FKP, probably because high concentration of fructosyltransferase lead to precipitation of protein giving as a result less active enzyme.

Using all the information achieved on the screening, the best conditions were established using the FKP expressed in this project, even though it was less active than the one used for the screening (provided by Dr. James Ross, University of Leeds). The synthesis of the trisaccharide **3.5** was successful with high yields.

Gb_3-N_3 has also been achieved, an oligosaccharide that will be really useful to incorporate in a polymer to perform binding studies with other lectins like Shiga Toxin. Even though **3.11** has been synthesised, the LgtC galactosyl transferase presented some problems so another enzyme was tested to use instead. BGalT Tt-1871, the new enzyme, was tested by itself and with $Glc(4)_{ep}$ providing a cleaner product mixture than the one achieved by LgtC. Besides, the use of Lactase was studied to achieve an easy purification step. However, the conditions to aim full conversion for this reaction were optimized so the synthesis of **3.11** was successful in high yields. Finally, the conditions to perform CuAAC cycloaddition using Gb_3-N_3 as a reagent were set up allowing to attach successfully a biotin to the trisaccharide for protein (Shiga Toxin) purification purpose.

CHAPTER 4: CONSTRUCTION OF OLIGOSACCHARIDE-DERIVATIZED HYALURONIC ACID USING CuAAC CYCLOADDITION

4.1 Synthetic plan for the construction of oligosaccharide-derivatized hyaluronic acid

For the synthesis of mucin-like structures using hyaluronic acid as a backbone and oligosaccharides derivatized with an azide achieved in Chapter 3, it was required the incorporation of alkyne on the backbone to perform a CuAAC reaction between these two moieties. As it is already described deeply in the previous chapter and studied in Chapter 2, the reactive group on hyaluronan chosen for the incorporation of an alkyne was again the carboxylic acid on the glucuronic acid to avoid side reactions and ensure selectivity on the backbone, aspect difficult to ensure while performing reactions on hydroxyls groups. In addition, this approach offered advantages like the use of a commercially available propargylamine reagent as well as fewer steps for the synthesis of the modified polysaccharides.

Hence, the synthetic plan to aim for the mucin-like structures started by the coupling of propargylamine to hyaluronic acid following by the CuAAC cycloaddition between the resulting HA-*g*-propargyl and the carbohydrates derivatized with an azide as it is shown in Scheme 4.1. The resulting structures were complexes glycopolymers with well-defined structures containing the carbohydrates that could be recognized by some B subunits from the AB_5 toxins: glycopolymer containing Gb_3 for STxB and the structures with Le^x for CTB.

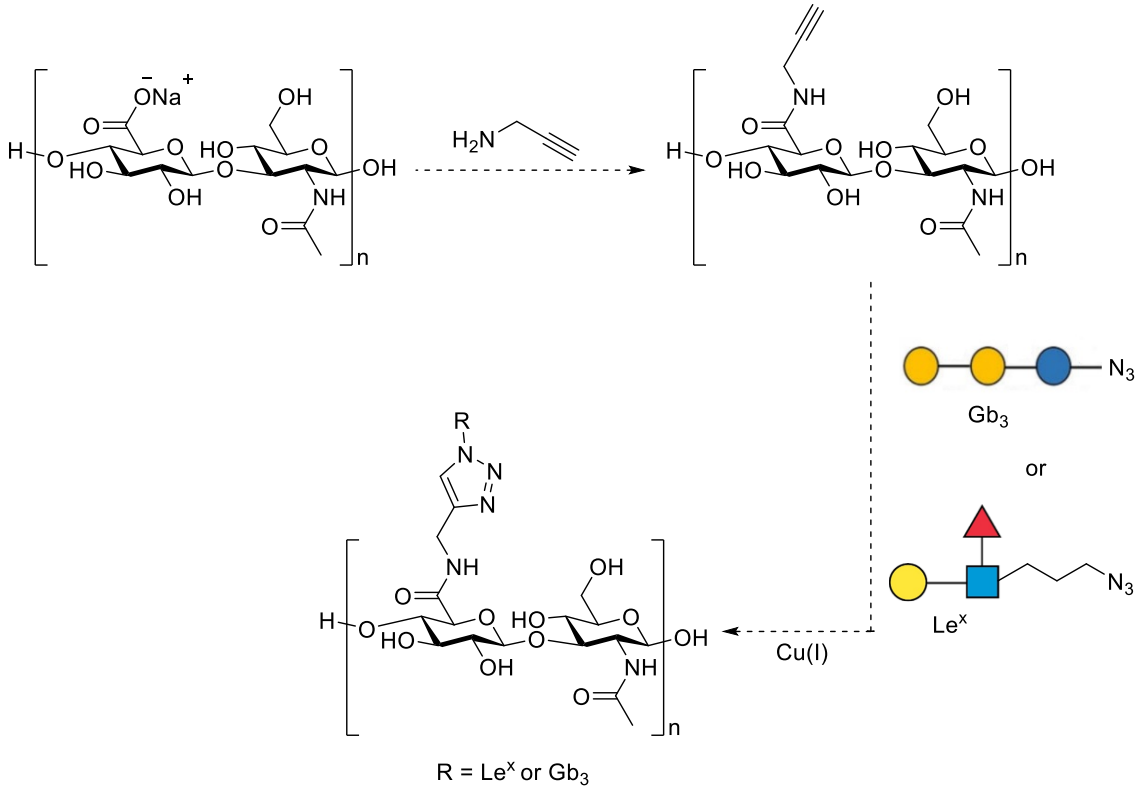

Scheme 4.1: Synthetic plan to derivatize hyaluronan with an alkyne and its following attachment of oligosaccharides to HA.

4.2 Synthesis of alkyne-derivatized hyaluronic acid

The incorporation of alkyne in hyaluronan has been described for formation of hydrogels.[141,188] The incorporation of a propargylamine using EDC and NHS as activators is only one of many procedures that have been described.[140,189] On the other hand, Manzi, G. *et al.* described the synthesis of alkyne-derivatized hyaluronan by forming first the TBA salt of the polymer followed by its reaction with propargyl bromide to form the corresponding propargyl ester.[201] However, the resulting product was not stable showing hydrolysis of the ester bond after two hours in aqueous solution and included an extra step and purification hard to perform for high molecular weight hyaluronan. There are no evidences that degradation could occur for the amide formation in aqueous solution and only one step is required becoming the best choice for the synthesis of alkyne-derivatized hyaluronan. Amide formation between the HA carboxylic acids and propargylamine was chosen because this amine is small, soluble in water or buffer and commercially available.

4.2.1 Coupling using EDC and NHS as activators

As described in Chapter 2, the formation of amide bonds over HA could be performed by using different activators. The model of Chapter 2 established that different proportions of EDC and NHS gave, as a result, different levels of derivatization of HA while maintaining the ratio for the free amine during the coupling. For this reason, and making the assumption that propargylamine presents similar reactivity as 4-(aminomethyl)benzonitrile, coupling conditions established in one of the model reactions was performed. The conditions applied were similar to those which gave highest derivatization in the model (around 15% derivatization). However, in an attempt to increase the degree of derivatization, and because propargylamine was commercially available, the ratio for the amine was increased from two to four equivalents per repeat unit.

Therefore, a solution of HA in MES buffer was reacted with propargylamine (four equivalents per HA carboxylic acid group) in presence of large excess of EDC (20 equivalent per HA carboxylic acid group) and NHS (19 equivalents per HA carboxylic acid group) to achieve HA-*g*-propargyl (**4.1**) (Scheme 4.2; Table 4.1, Column 1) after extensive dialysis of the product. Proportion for activators were established in the model described in Chapter 2. The percentage of derivatization of the polymer was calculated by integration of the ^{1}H NMR spectrum taking the 3 protons in the acetamide group as a reference and comparing to the integration ≡C<u>H</u> from the propargylamide (Figure 4.2).

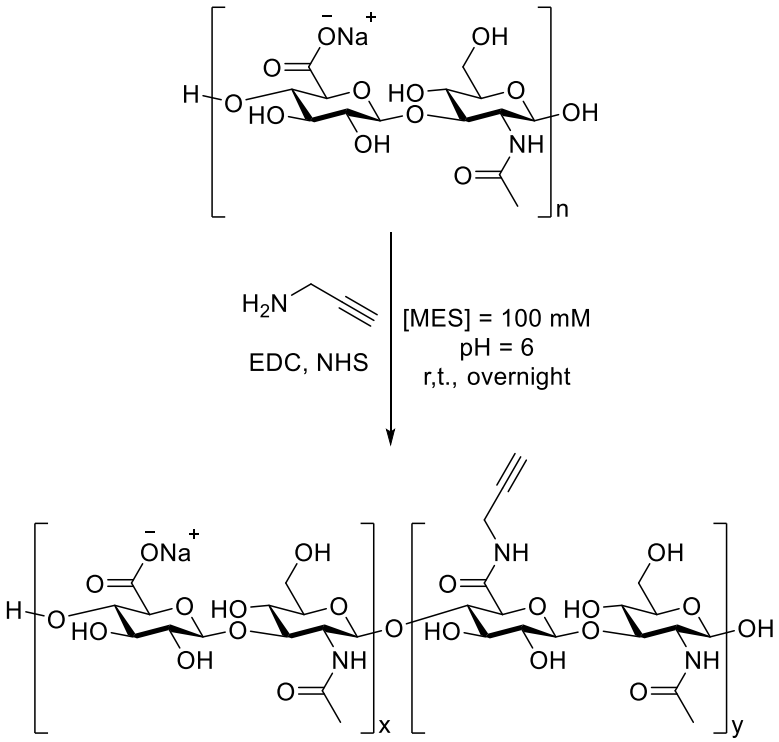

4.1

Scheme 4.2: First attempt to attach propargylamine to hyaluronic acid.

This sample of HA-*g*-propargyl **4.1** showed a profile in the ^{1}H NMR spectrum that seemed to contain some extra peaks than the expected ones. First of all, there were three extra peaks appeared in the spectrum from 3.0 to 2.3 ppm: a multiplet from 2.91 to 2.88 ppm, another multiplet from 2.70 to 2.59 ppm and a last really complex multiplet from 2.47 to 2.39 ppm. These peaks were relatively broad indicating that their presence was not due to impurities in the sample but molecules attached to the polymer. This hypothesis was reinforced by the fact that the sample was dialysed several times and the presence of these peaks did not show any change. For the region of the spectrum, it was expected to find the proton for terminal alkyne from the propargylamide, as it has been previously reported,[140,141,188] however it was impossible to identify which one of these peaks corresponded to ≡C<u>H</u> and, because there was more than one peak together, the degree of derivatization could not be calculated. Moreover, these extra peaks in less intensity were also shown in other published work meaning that side reactions were seen previously but not described.[140,141] Different possibilities for their origin were considered: the coupling between HA and MES buffer; a side reaction from the propargylamine; or attachment of the NHS to the carboxylic acids.

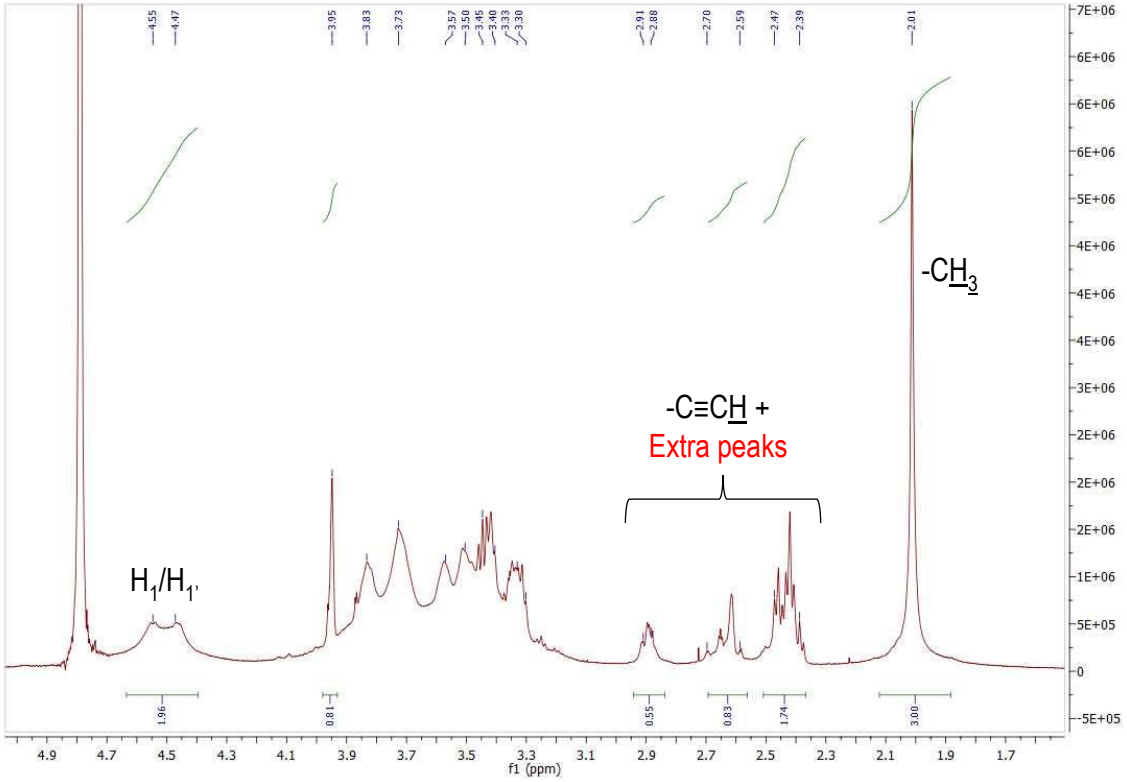

Figure 4.2: ^{1}H NMR of the HA-*g*-propargyl **4.1** and its extra peaks from 3 to 2.3 ppm due to unknown side reactions.

Aiming for HA-*g*-propargyl pure without side products attached on the backbone, a further five different conditions were tested as described in Table 4.1.

Table 4.1: Different conditions tested to achieve a HA-*g*-propargyl pure.

Reagent	Test 1[L]	Test 2[†]	Test 3[‡]	Test 4[‡]	Test 5	Test 6
HA*	1 eq.	1 eq.	1 eq.	1 eq.	1 eq.	1 eq.
Propargylamine*	4 eq.	2 eq.	4 eq.	4 eq.	4 eq.	-
1-Amino-3-butyne*	-	-	-	-	-	4 eq.
EDC*	20 eq.	2 eq.	6 eq.	6 eq.	20 eq.	20 eq.
NHS*	19 eq.	3 eq.	5 eq.	5 eq.	19 eq.	19 eq.
MES buffer pH = 4 (50 mM)**	-		3.3 mL	10 mL	-	-
MES buffer pH = 6 (100 mM)**	7 mL	7 mL	-	-	-	7 mL
H_2O**	-	-	-	-	7 mL	-
Concentration HA	4 mg/mL	4 mg/mL	15 mg/mL	4 mg/mL	4 mg/mL	4 mg/mL
Extra peaks between 2 and 3 ppm in ^{1}H NMR	**YES**	**YES**	**YES + Extra peaks and EDC**	**YES + Extra peaks and EDC**	**YES**	**YES**

*The reagents (HA, propargylamine and 1-amino-3-butyne) and the activators are described in terms of the number of molar equivalents (eq.) relative to -COOH in HA.

** Total reaction volume.

[L] Test based on the model established in Chapter 2 in this thesis.

[†] Test following the same ratios used to synthesize the tetrazine-derivatized hyaluronic acid (**2.5**) following the protocol described by Famili *et al.*[152]

[‡] Tests following the procedure described by Crescenzi *et al.*[140,141]

Test 2 was set up following the protocol used to produce tetrazine-derivatized hyaluronic acid (Table 4.1, Column 2, Test 2),[152] however, this experiment also resulted in the presence of the same side products. These impurities were not as intense as the ones in Test 1, therefore, the synthesis of these molecules was related to the equivalents of activators used. Nevertheless, it is important to highlight that these peaks were not present in tetrazine-derivatized hyaluronic acid product meaning that the change of amine in this coupling influenced to the formation of these side products. As it occurred in Test 1, the spectrum showed three multiplets from 3.0 to 2.3 ppm indicating the overlap of signals from different moieties attached to HA (Figure 4.3, green). For this reason, it was not possible to calculate the percentage of derivatization by ^{1}H NMR spectroscopy because the absence of an isolated peak for ≡C<u>H</u> between 3.0 to 2.3 ppm.

Two further experiments were performed using the protocol described by Crescenzi *et al.*[140,141] In both experiments, the ratios between hyaluronan, propargylamine and activators were the same, but Test 3 (Table 4.1, Column 3) used a higher hyaluronic acid concentration (15 mg/mL) as described in the procedure by Crescenzi *et al.,* while in Test 4 (Table 4.1, Column 4) the hyaluronic acid concentration was 4 mg/mL as used in all my previous experiments. Neither experiment provided clean HA-*g*-propargyl and the proportions of the side products were similar to Test 1 as it was observed on the spectrum (Figure 4.3, blue). Multiplets from 2.70 to 2.59 ppm and from 2.47 to 2.39 ppm were also shown but not explained on the ^{1}H NMR spectra in the work published by Crescenzi *et al.*[140,141] but the integration of these peaks were much lower than the same ones for the samples synthesized in this project. Additional singlet peaks at 3.9 ppm and 2.9 ppm on the spectrum also appeared making the spectrum even more difficult to interpret (Figure 4.3, blue). In addition, even after ten and five dialysis for Test 3 and Test 4 respectively, there was presence of EDC attached to HA due to the presence of broad peaks at 3.2 ppm, 1.9 ppm and 1.2 ppm.

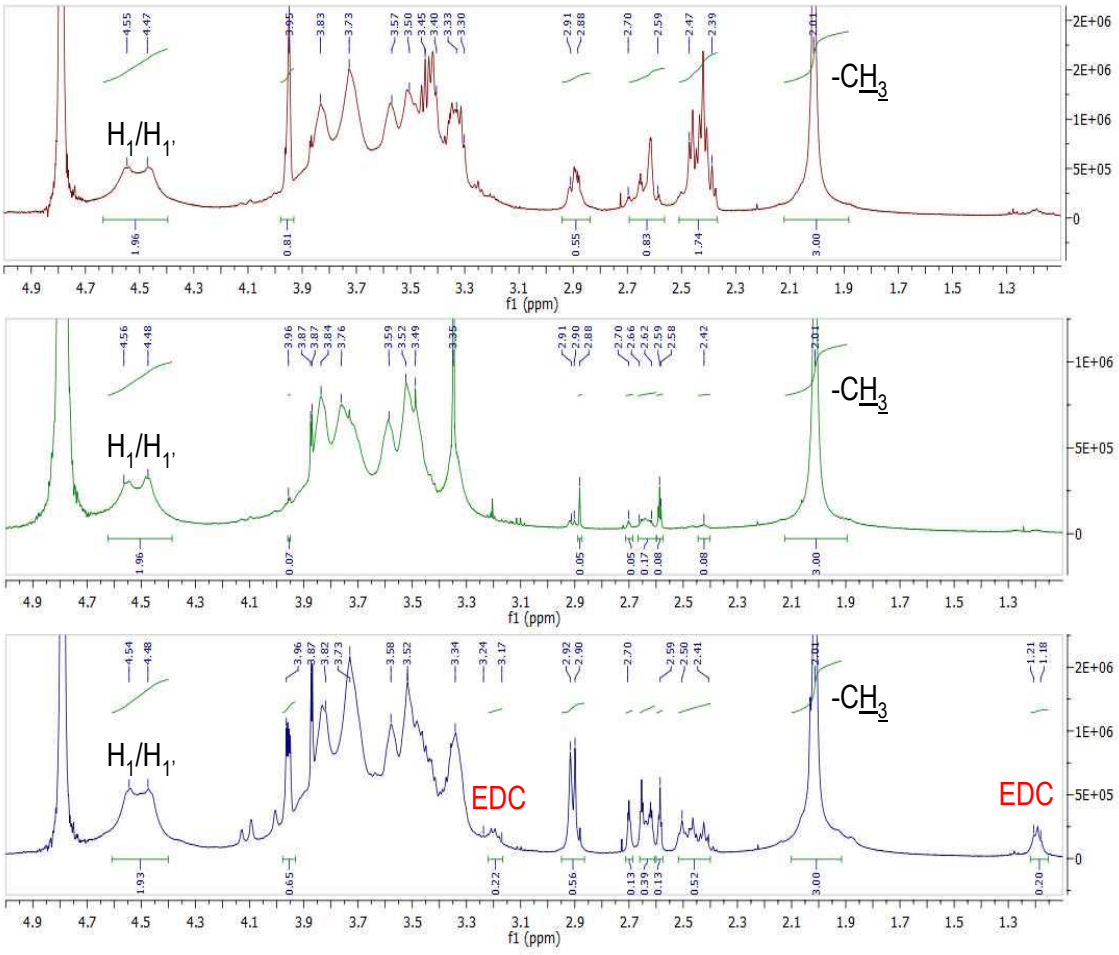

Figure 4.3: ^{1}H NMR spectrum of the HA-*g*-propargyl (**4.1**, Table 4.1, Test 1) in red; ^{1}H NMR spectrum of the HA-*g*-propargyl (**4.1**, Table 4.1, Test 2) in green; and ^{1}H NMR spectrum of the HA-*g*-propargyl (**4.1**, Table 4.1, Test 4) in blue.

After analysing the three ^{1}H NMR spectra for Test 1, 2 and 3 on Table 4.1, it could be concluded that the side reactions were closely related to the amount of activators used for the coupling: less equivalents of EDC and NHS provided less side products attached to the polymer. However, it was not possible to conclude if this fact was due to the presence of others components in the reaction mixture (e.g. the buffer) or the reagent used for the reaction, propargylamine.

As none of the previous procedures provided a clean product, subsequent experiments were designed to test each hypothesis for the origin of the extra peaks. To test if the extra peaks in the ^{1}H NMR were due to covalent addition of the buffer to the hyaluronic acid backbone, an experiment was set up in which the buffer was replaced by water as solvent (Table 4.1, Column 5). The conditions for this experiment were otherwise the same as used in Test 1 because that product contained less impurities compared with the other products made. However, the same extra peaks were observed in the same proportion as for Test 1, demonstrating that they did not originate from reaction of the buffer.

The second hypothesis tested was that these extra peaks were caused by a side reaction of propargylamine. Therefore, in Test 6 (Table 4.1, Column 6), the proportions of reagents were kept the same as Test 1 but propargylamine was changed to 1-amino-3-butyne. The resulting products were not clean either: the extra peaks between 3.0 and 2.3 ppm appeared again in similar proportions as before and, because of the complexity of the spectrum, it was not possible to calculate the degree of derivatization

The third hypothesis considered was that the extra peaks could arise from the presence of NHS ester groups in the product. To check this possibility, the coupling reaction was first repeated as in Test 1 (Table 4.1, Column 1). After three rounds of dialysis to remove extra reagents and side products, the solution of HA-*g*-propargyl was divided into three aliquots to keep one sample as a control and to try two different treatments with hydroxylamine to remove any remaining NHS esters (Scheme 4.3).

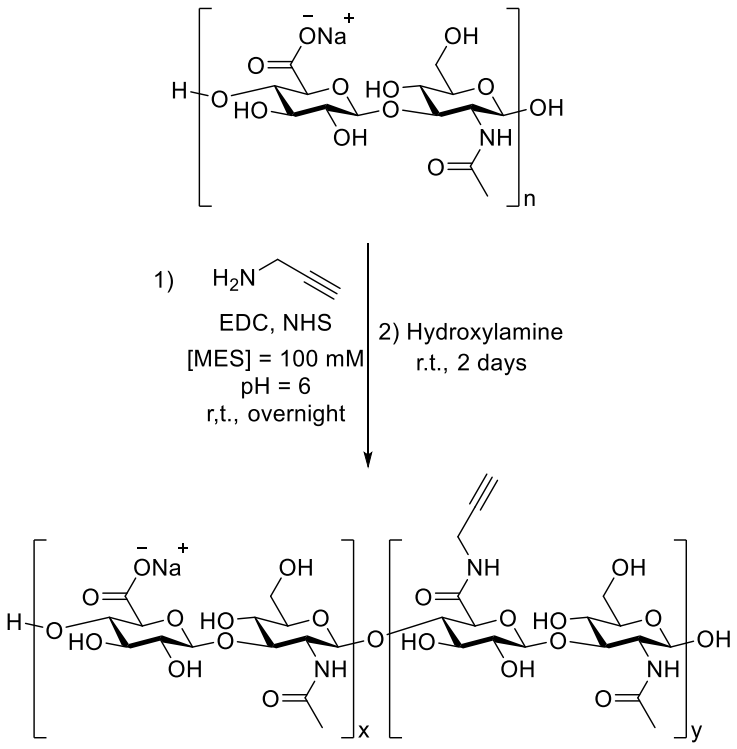

4.1 1a/ 4.1 1b

Scheme 4.3: Test to attach propargylamine to HA followed by its treatment with hydroxylamine.

Hydroxylamine (50% w/v aqueous solution) was added to two of the samples of HA-*g*-propargyl, to achieve the amounts described in Table 4.2 to quench the reaction as it was described by Araújo *et al*.[202] The reactions were left for two days at room temperature followed by purification by dialysis. For Test 1a (Table 4.2, entry 2) it was assumed that all the carboxylic acids in the HA were still activated so the ratio of carboxylic acid/hydroxylamine was kept 1:1. For Test 1b (Table 4.2, entry

3), a large excess of hydroxylamine was added. Finally, there was a control experiment (Table 4.2, entry 1) without hydroxylamine treatment to compare this HA-*g*-propargyl with the ones under hydroxylamine treatments. The percentage of derivatization of the polymer was calculated by integration of the ^{1}H NMR spectrum taking the 3 protons in the acetamide group as a reference and comparing to the integration ≡C<u>H</u> from the propargylamide or the disappearance of some of the extra peaks between 3.0 and 2.3 ppm.

Table 4.2: Treatment of Test 1 reaction mixture with hydroxylamine to remove any remaining NHS esters in the HA.

Test	Equivalents of hydroxylamine according µmols –COOH in HA
Control experiment	-
Test 1a	1 eq.
Test 1b	20 eq.

All three of the resulting HA-*g*-propargyl samples still had the extra peaks from 3.0 to 2.3 ppm, but the integration of these signals differed between experiments as shown in Figure 4.4. As the amount of hydroxylamine increased, the integration of the extra peaks, as well as the signals assumed to be the propargylamine CH_2 at 2.92 ppm, decreased. This observation is clearly seen for the peaks at 2.92 ppm: in the ^{1}H NMR spectrum for the control sample (blue spectrum), its integration relative to the 3 proton acetamide signal was around 0.7 while in the Test 1a spectrum (green) the integration was 0.5 and in the Test 1b spectrum (red) it was 0.3. Moreover, it was not possible to isolate any of the peaks between 3.0 and 2.3 ppm, therefore, it was not possible to assign the ≡C<u>H</u> from the propargylamide either.

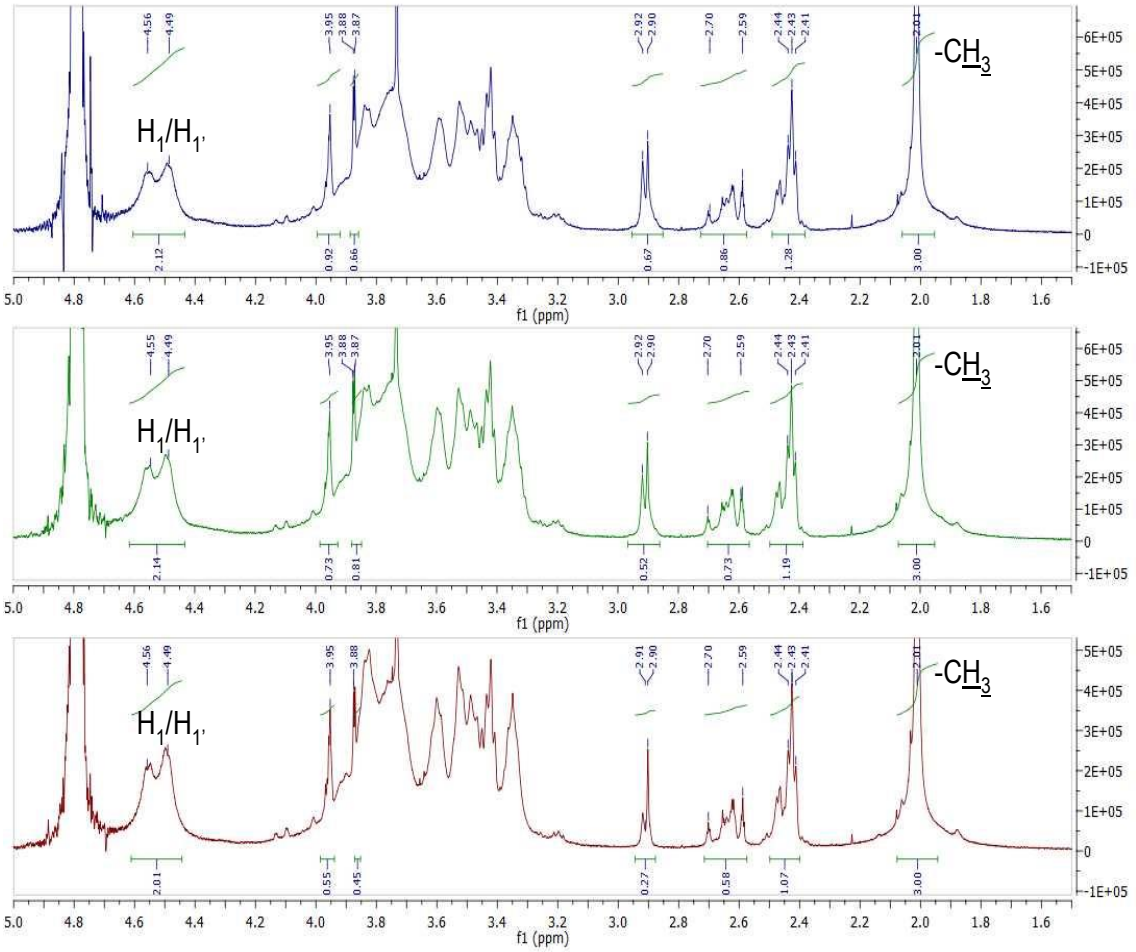

Figure 4.4: ^{1}H NMR spectrum of the HA-*g*-propargyl (**4.1**) without hydroxylamine treatment (Control) in blue; ^{1}H NMR spectrum of the HA-*g*-propargyl (**4.1 1a**) with Treatment 1 of hydroxylamine in green; and ^{1}H NMR spectrum of the HA-*g*-propargyl (**4.1 1b**) with Treatment 2 of hydroxylamine in red.

Even though the hydroxylamine treatment seemed to reduce the amount of side products attached to HA, the final products were still not pure. For this reason, it was concluded that the hypothesis of the origin of these extra peaks was not (entirely) due to the NHS still attached to the polymer.

As these treatments were partially successful, a similar approach was investigated. Assuming that the side products were not attached by amide bonds to HA, because that could only be derived from propargylamine (the only reagent with a free amine), it could be possible to hydrolyse bonds between the HA and these side products or cross-linking of the same or different polymer chains (e.g. any ester bonds) under mild basic conditions without breaking the backbone or the amide bonds.[203–205]

Following this hypothesis, another coupling reaction of HA was performed followed by a purification under basic conditions. This time, the synthesis of HA-*g*-propargyl (**4.1 B**) was performed again as for Test 1 (Table 4.1, Column 1), and a first dialysis was performed to remove

unattached side products. Then dialysis in a solution of sodium hydroxide (NaOH) at pH 10 was performed to hydrolyse any possible ester bonds (Scheme 4.4).

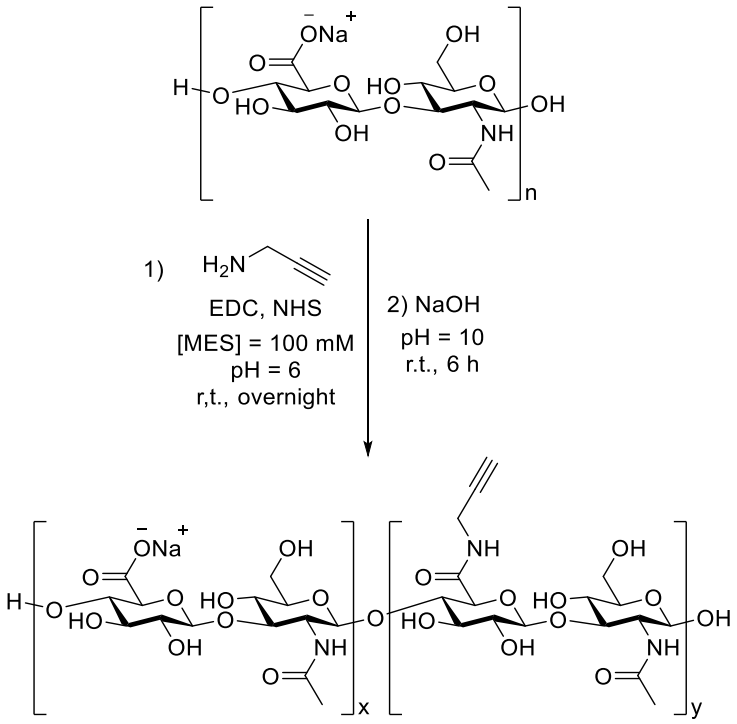

4.1 B

Scheme 4.4: Test to attach propargylamine to HA followed by its treatment in alkaline conditions.

The results of this treatment were not satisfactory either. As shown in the ^{1}H NMR spectra (Figure 4.5), there were still extra peaks from 3.0 to 2.3 ppm due to unknown compounds or molecules attached to HA. However, as for the samples treated with hydroxylamine, the amount of these side products, by ^{1}H NMR integration, was lower after the basic treatment (Figure 4.5, blue spectrum). Moreover, the complexity of these peaks decreased becoming easier to identify the multiplicity of the peaks: as an example, the apparent triplet at 2.91 ppm in the red spectrum (Figure 4.5, sample without basic treatment) became two singlets in the blue spectrum (Figure 4.5, sample with basic treatment). The reason for this phenomenon could be that side products were removed from the polymer backbone, even though it was not enough to achieve pure HA-*g*-propargyl.

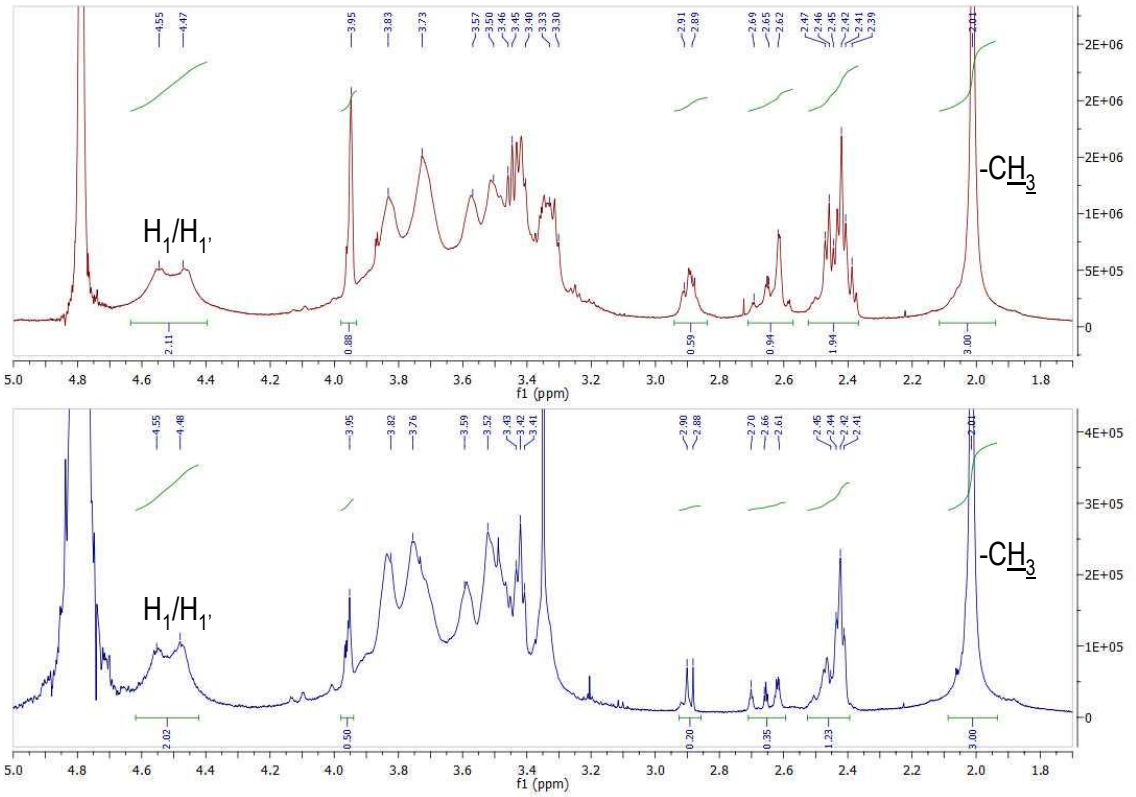

Figure 4.5: ^{1}H NMR spectrum of the HA-*g*-propargyl (**4.1**) without basic treatment (Control) in red. ^{1}H NMR spectrum of the HA-*g*-propargyl (**4.1 B**) after basic treatment in blue.

These combined experiments provided a lot of information that proved difficult to analyse again because the overlap of signals or the number of extra peaks on the ^{1}H NMR spectrum. However, some conclusions were deduced from these tests: the production and attachment to the polymer chain of side products was directly related to the excess of activators and, because of the complexity of the spectra achieved, it was not possible to know the degree of derivatization. The origin of these side products was due to the activators used and they seemed to be covalently attached to HA. On the other hand, all the attempts to remove these side products failed in part, while reducing the amount and even removing some of the extra peaks in the ^{1}H NMR spectra, but never removing all of them to achieve a clean final product of HA-*g*-propargyl.

Other published procedures used a smaller size of hyaluronic acid than the one used in the experiments presented here, from few oligosaccharide to 50 kDa and 200-500 kDa respectively.[206–210] For this reason, one last aspect to consider was the effect of the size of the polymer on the extra peaks appearing in the ^{1}H NMR spectra of the reaction products. For this reason, two different coupling reactions were performed using a small hyaluronic acid (from 40 to 50 kDa (HA_{ss})), which was small enough to see if there would be any improvement in its reactivity, but big enough for the purposes of this project.

In both reactions, HA_{ss} was dissolved in MES buffer followed by the addition of an excess of EDC, NHS and propargylamine according to the table 4.3 to achieve HA_{ss}-*g*-propargyl. One of the coupling reactions performed followed the protocol described by Hartwell *et al.*[206] (Table 4.3, Column 2, HA_{ss}-*g*-propargyl (**4.2 Test 3**)), which was the same proportions described by Crescenzi *et al.*[140,141] but using an HA about 16 kDa instead of the 200 kDa hyaluronan, while the other amide formation was following the conditions from Test 1 in Table 4.1 (Table 4.3, Column 1, HA_{ss}-*g*-propargyl (**4.2 Test 1**)). The percentage of derivatization of the polymer was calculated by integration of the ^{1}H NMR spectrum taking the 3 protons in the acetamide group as a reference and comparing to the integration ≡C<u>H</u> from the propargylamide.

Table 4.3: Derivatization of HA_{ss} following the ratios described by my model (Column 1, HA_{ss}-*g*-propargyl (**4.2 Test 1**)) and following the same ratios described by Crescenzi/Hartwell *et al.*[140,141,206] (column 1, HA_{ss}-*g*-propargyl (**4.2 Test 2**)).

Reagent/buffer	Test 1 from Table 4.1 (4.2 Test 1)	Test 3 from Table 4.1 (4.2 Test 2)
HA_{ss} (-COOH groups)	1 eq.	1 eq.
Propargylamine	4 eq.	4 eq.
EDC	20 eq.	6 eq.
NHS	19 eq.	5 eq.
MES buffer (50 mM) pH 4	-	3.3 mL
MES buffer (100 mM) pH 6	7 mL	-
Concentration HA	4 mg/mL	15 mg/mL
Extra peaks	**Yes + EDC**	**Yes + EDC**

Even though the size of the new hyaluronic acid, 40-50 kDa, was closer to the one used by Hartwell *et al.*, 16 kDa, the results obtained were not satisfactory. The solubility for HA_{ss} was much better than the previous reagent used, 200-500 kDa, but the same side products seemed to be synthesized during the coupling in similar proportions (Figure 4.6) as seen before in Test 1 and Test 3 from Table 4.1. This fact indicated that the change of the size in the polymer did not affect the reactivity for this coupling giving as a result similar impurities. As can be seen in both ^{1}H NMR spectra (Figure 4.6), neither of the products were clean as both showed the presence of extra peaks of from 3.0 to 2.3 ppm. Moreover, there was still some EDC present in the sample after the purification process but for **4.2 Test 1** it was much higher (around 20%) than **4.2 Test 2** (around 5%).

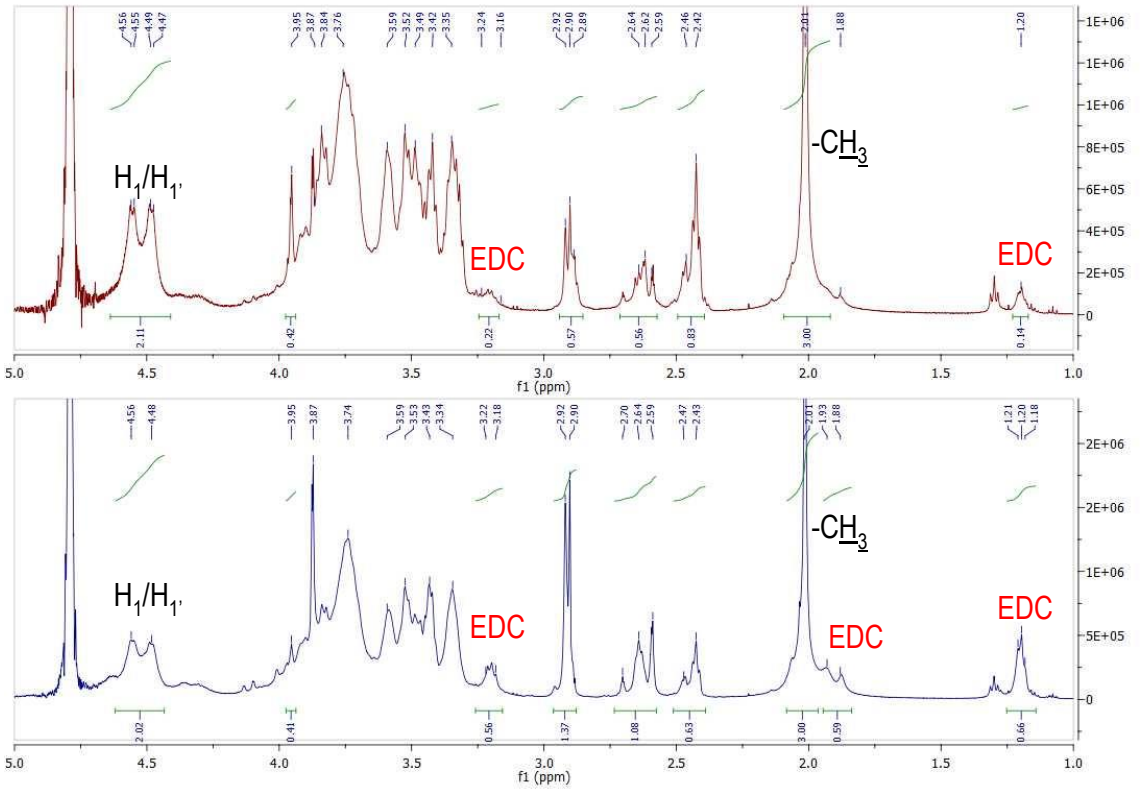

Figure 4.6: ^{1}H NMR spectra for HA_{ss}-*g*-propargyl (**4.2 Test 2**) synthesized as described by Crescenzi/Hartwell *et al.*[140,141,206] in red and HA_{ss}-*g*-propargyl (**4.2 Test 1**) synthesized as described in Test 1 from Table 4.1 in blue.

Although the hyaluronan used in these last experiments was smaller than that used throughout the project, the outcome of the amide coupling reaction was similar to that seen for the larger HA used in the preceding experiments. The side products attached to the polymer chain were still present in the HA_{ss}-*g*-propargyl (**4.2 Test 2** and **4.2 Test 1**) but their amounts, according the ^{1}H NMR integration, were slightly different than the ones for the HA-*g*-propargyl **4.1** (Test 1 and 3 from Table 4.1) in some cases: for Test 1 using 200-500 kDa and 40-50 kDa respectively, the multiplet between 2.7 and 2.6 ppm showed similar integration while for the multiplet 2.5-2.3 ppm and the multiplet 2.9-2.8 ppm, the integration changed significantly. For the samples **4.1** Test 3 from Table 4.1 and **4.2 Test 2** achieved by following the protocol described by Crescenzi/Hartwell *et al.*[140,141,206], the size of hyaluronan did not seem to have any effect as the impurities attached to the polymer showed similar integration for the three extra multiplets (2.9-2.8, 2.7-2.6 and 2.5-2.3 ppm). Another issue to consider was the purity of the HA_{ss}-*g*-propargyl: some activators, like EDC attached to HA, were still present in the final product suggesting that their purification was more complicated than the larger HA as these peaks were not present in Figure 4.3.

For all these reasons, it was finally concluded that coupling using EDC and NHS as activators would not be successful, although such reactions had been described with better results but never

with completely clean products as it was mentioned previously.[141,140] All the hypotheses suggested to solve the problem of the synthesis and attachment of side products to the polymer were never completely successful but factors like side reactions with buffer, propargylamine or the cross-linking of chains through an ester bond were discarded as a origin of these extra peaks between 3.0 and 2.3 ppm. In addition, the only analysis suitable to check the composition of these big structures was ^{1}H NMR spectroscopy making it difficult to identify the structure of these impurities.

4.2.2 Coupling using DMTMM as activator

There are other methods described in the literature to make amide bonds in HA from the carboxylic acid apart from the coupling using carbodiimides: the use of triazines like 2-chloro-4,6,-dimethoxy-1,3,5-triazine (CDMT)[146,211] as activators or 4-(4,6-dimethoxy-1,3,5-triazin-2-yl)-4-methyl-morpholinium chloride (DMTMM).[138,212,213] that presented mild reaction conditions and high degree of derivatization on HA. Several coupling reactions of HA have been described using DMTMM as activator, with products having clean ^{1}H NMR data, however none of them used propargylamine as one of the reagents.[212,214] The activator DMTMM is a triazine compound which reacts with carboxylic acids releasing *N*-methylmorpholine (NMM). The activated ester is a highly reactive intermediate that can form an amide bond with a free amine (Scheme 4.5).[212,213] Moreover, these coupling reactions of hyaluronan presented several positive features like the possibility to perform the reaction in aqueous solvent without needing to monitor the pH, and high efficiency and degree of substitution on the polymer chain.[215]

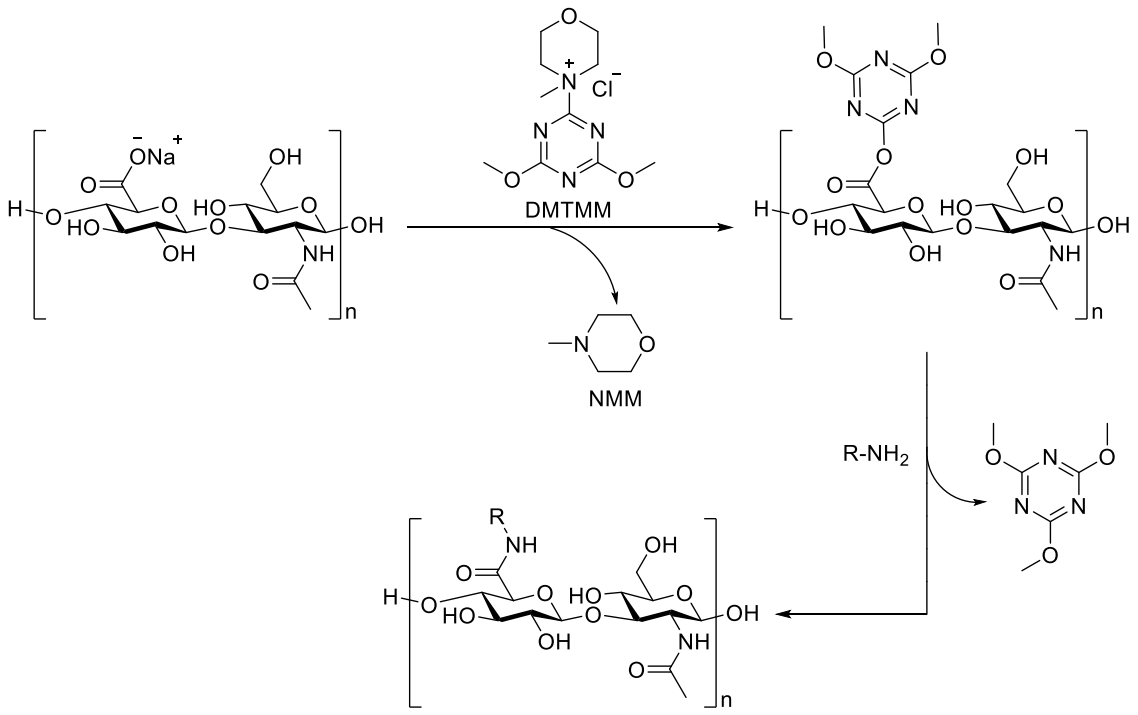

Scheme 4.5: Mechanism of amide coupling of HA using DMTMM as activator.[212]

Following all the promising information found, a new batch of experiments was attempted in which hyaluronan was reacted with DMTMM and propargylamine in MES buffer following the same ratios described by Yu *et al*. for furylamine (one eq. and one eq. respectively per HA carboxylic acid group) (Scheme 4.6).[216] The percentage of derivatization of the polymer was calculated by integration of the ^{1}H NMR spectrum taking the 3 protons in the acetamide group as a reference and comparing to the integration ≡C<u>H</u> from the propargylamide.

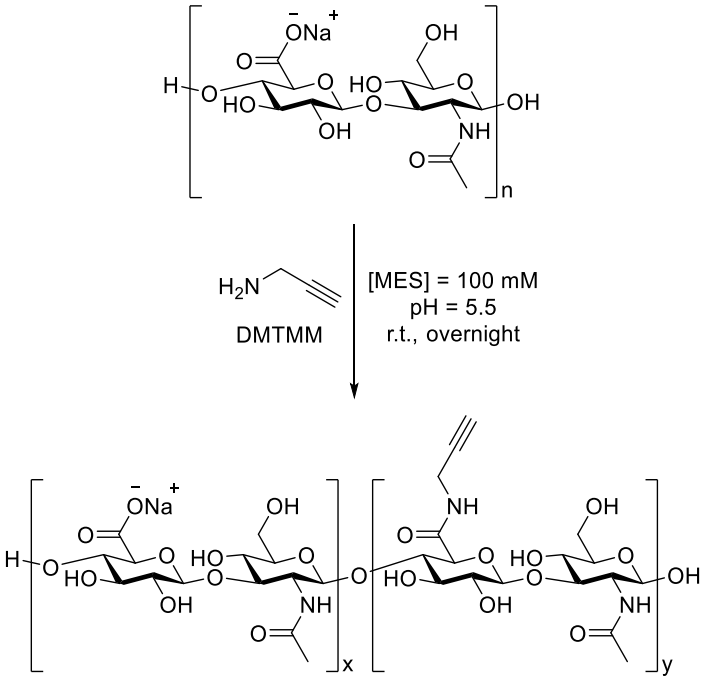

4.3

Scheme 4.6: Coupling between propargylamine and hyaluronan using DMTMM as activators in MES buffer.

The resulting HA-*g*-propargyl (**4.3**) was analysed by ^{1}H NMR spectroscopy (Figure 4.7) as well as ^{1}H-^{1}H COSY and HSQC providing new and clear data about alkyne-derivatized hyaluronan. Several points were concluded after analysing and comparing these data with literature.[217] First of all, the peak corresponding to the alkyne proton appeared at 2.70 ppm, impossible to identify in the previous spectra because it was hidden behind the impurities. Secondly, the assumption that the sharp peak at 3.95 ppm corresponded to the -CH_2- from the propargylamide was wrong, on the contrary, in the correct product these protons were a pair of doublets from 4.13 to 3.97 ppm (Figure 4.7), which, in retrospect, were also visible in some earlier spectra. Although the multiplicity of this peak was surprising at the beginning, it could be explained because the chirality of the polymer, therefore, these protons are diastereotopic. Lastly, this coupling reaction was very clean and did

not present any extra peaks in any part of the ^{1}H NMR spectrum and its degree of derivatization was high enough for the aim of the project at around 20%.

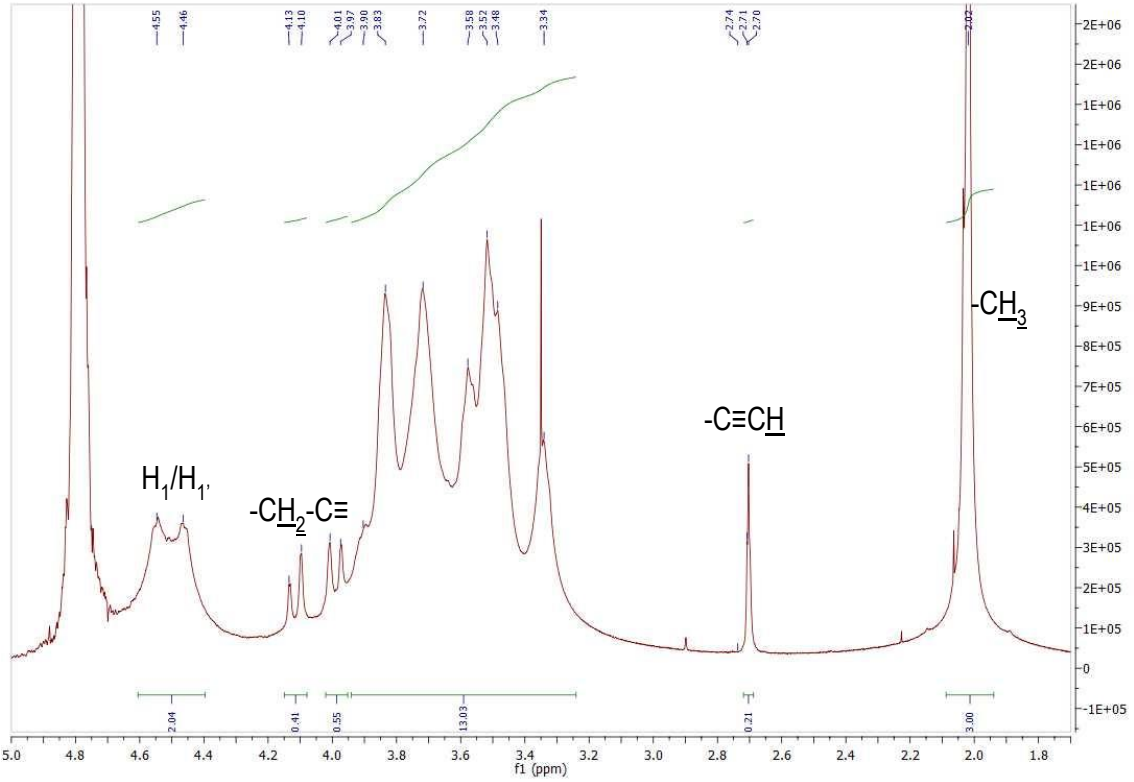

Figure 4.7: ^{1}H NMR for HA-*g*-propargyl (**4.3**) synthesized using DMTMM.

Because of the success of this reaction, other couplings using DMTMM as activator were performed to try to achieve a higher degree of substitution and create a library of HA-*g*-propargyl polymers suitable for click reactions with the azido-derivatized oligosaccharides that had been synthesized. To achieve this aim, three more reactions were set up with increasing eq. of DMTMM and propargylamine following the ratios described at table 4.4.

Table 4.4: Derivatization over HA using different proportions of DMTMM and propargylamine.

Reagents	Amounts for Test 1 (µmol)	Amounts for Test 2 (µmol)	Amounts for Test 3 (µmol)	Amounts for Test 4 (µmol)
HA (-COOH groups)	1 eq.	1 eq.	1 eq.	1 eq.
Propargylamine	1 eq.	3 eq.	6 eq.	10 eq.
DMTMM	1 eq.	3 eq.	6 eq.	10 eq.
Concentration HA	4 mg/mL	4 mg/mL	4 mg/mL	4 mg/mL
% Propargyl in HA	**20±2%***	**38±1%***	**50±1%***	**45%**

* Experiments repeated twice to provide an average and range of the integration achieved.

Changing the concentrations of DMTMM and propargylamine did not seem to affect the purity of the final products, all reactions providing really clean ^{1}H NMR spectra, while the degree of substitution increased significantly as the amount of DMTMM and propargylamine added in the reaction increased. It is important to highlight that other authors have routinely calculated degree of derivatisation after conversion of alkynes to triazoles where the data achieved was more reliable due to the presence of an aromatic proton.[218]

4.3. Incorporation of oligosaccharides on alkyne-derivatized hyaluronic acid

Oligosaccharides were attached to HA-*g*-propargyl by a CuAAC reaction in aqueous solution. However, even though it is a well-known reaction with high yields, the click procedure needed to be tested. In order to set up the conditions for this procedure, a reaction with Lac-N_3 provided Dr. Vajinder Kumar (University of Leeds) was tested first. The resulting structure, HA-*g*-Lac, would be useful as a control glycopolymer for binding studies because lactose binds weakly to CTB and does not bind to VTB (also known as Shiga Toxin, STx).[219,220] Once the reaction conditions were established, the incorporation of Le^x and Gb_3 to HA-*g*-propargyl could be done to make more complex structures that would be expected to bind with higher affinity to CTB and Shiga Toxin B subunit (STxB), respectively.

4.3.1 Establishing the CuAAC conditions: Incorporation of Lactose on the polymer

The first conditions tested for making HA-*g*-Lac were those described by Charlot *et al*.: the ratio of alkyne to azide was 1:1; no additives like TBTA to complex Cu(I) were added to avoid difficulties in purification.[218] Assuming that the degree of propargyl substitution for **4.3** was around 20%, a CuAAC reaction was performed with Lac-N_3 in presence of $CuSO_4$ and sodium ascorbate to achieve HA-*g*-Lac (**4.4**) (Scheme 4.7).

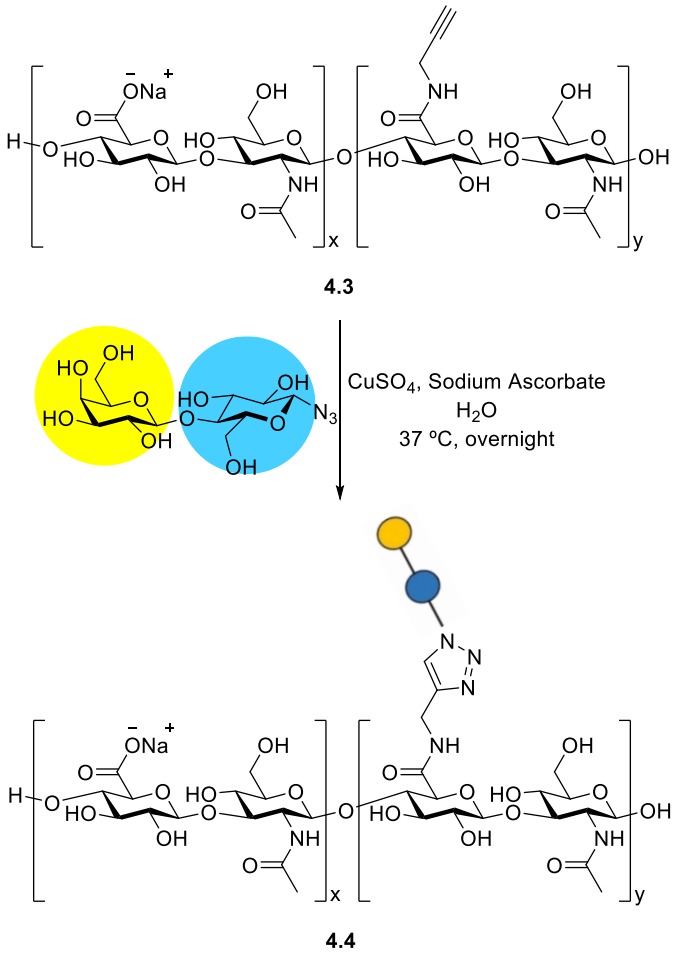

Scheme 4.7: Click reaction between **4.3** and Lac-N_3 to achieve HA-*g*-Lac (**4.4**).

The results of this test were satisfactory because, as can be seen in the red spectrum of **4.4** (Figure 4.8), there was no peak at 2.7 ppm corresponding to the alkyne proton from **4.3**, and the peaks from 4.1 to 3.9 ppm for the propargyl methylene group moved from their positions from the blue spectrum (**4.3**, starting material) to the red spectrum (**4.4**, product) due to formation of the triazole ring. Moreover, there was no presence of unexpected side reactions giving a really clean final product. The only aspect to take into consideration was the apparent degree of substitution because it decreased from around 20% for alkyne groups in **4.3** to around 13% for lactosyl groups in **4.4**. The reason for this decrease was probably due to the manual integration accuracy for the measurement on the ^{1}H NMR spectrum for **4.3** rather the loss of propargyl groups during the CuAAC reaction. Despite this change, the degree of derivatization was still around the same order so it was concluded that this methodology would work really well for future attachment of other oligosaccharides to HA-*g*-propargyl.

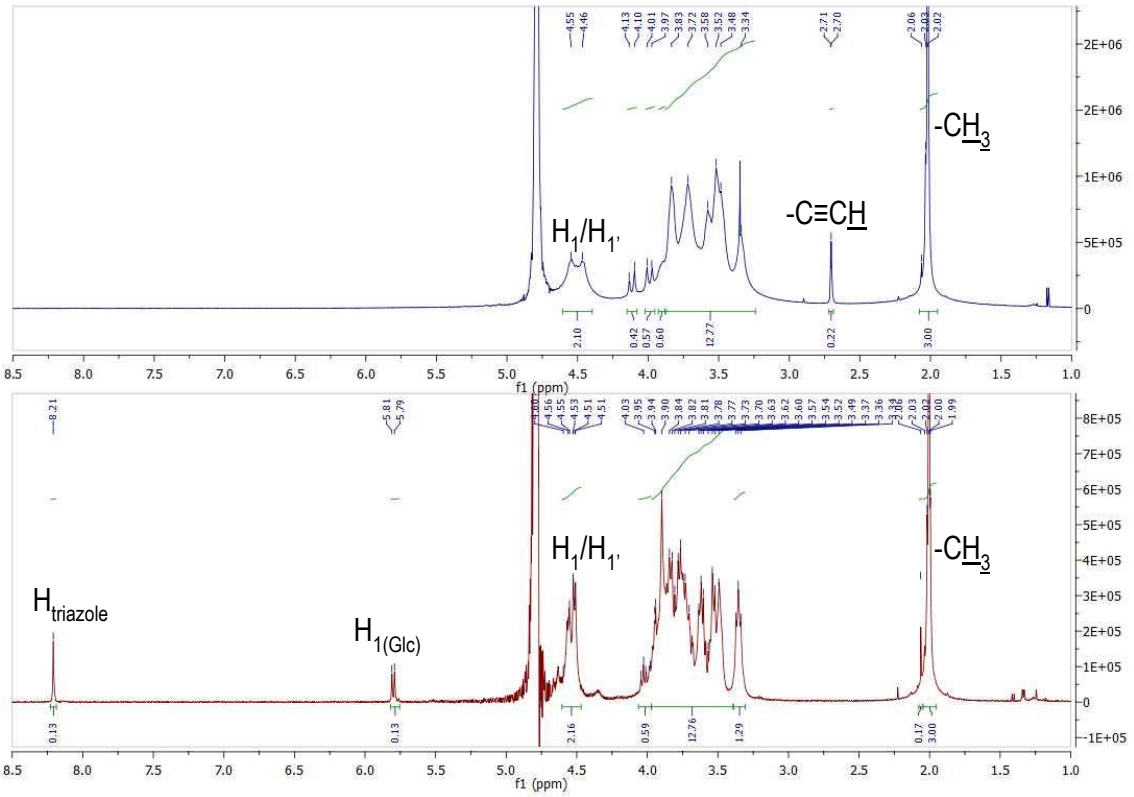

Figure 4.8: ^{1}H NMR for HA-*g*-propargyl (**4.3**) as starting material in blue and ^{1}H NMR for HA-*g*-Lac (**4.4**) as product in red.

Having obtained good results for the HA-*g*-propargyl reaction with lactosyl azide, other aspects of the reaction were taken into consideration to provide best yields and products. The first aspect to revise was for possible degradation of the glycopolymer during the CuAAC reaction. The hyaluronan chain could show some degradation in the presence of free copper(II) ions, giving smaller sizes of products. To check this hypothesis, two experiments were set up to produce HA-*g*-Lac **4.4** in the presence or absence of the chelation agent tris(3-hydroxypropyltriazolylmethyl)amine (THPTA).[124,206,221] The resulting products were analysed by ^{1}H NMR, which provided the degree of derivatization, and size exclusion chromatography with multi-angle light scattering (SEC-MALS) detector, which provided the average molecular weight (M_w) and dispersity (Đ) for the polymers.[210,222] This type of characterization was not described before for polymers like **4.3** or the subsequent triazole products.

Both HA-*g*-Lac polymers contained around 12% lactosyl groups according the integrations of ^{1}H NMR spectra (Table 4.5, entry 1). On the other hand, the SEC-MALS analysis showed that the reaction in presence of THPTA produced a glycopolymer twice the molecular weight of the reaction that did not contain the chelation agent (Table 4.5, entry 2). Moreover, the dispersity (Đ) for the

reaction without THPTA was also higher than the one using this chemical meaning that there was more degradation of the backbone during this step of the synthesis (Table 4.5, entry 3).

Table 4.5: Differences between the resulting **4.4** achieved in the presence or absence of THPTA during an overnight CuAAC cycloaddition.

	CuAAC without THPTA	**CuAAC with THPTA**
% of Lac in HA	12%	11%
M_w	35 kDa	72 kDa
Đ	1.67	1.41

The results obtained in these tests concluded that the presence of THPTA during the CuAAC reaction provided bigger products of higher molecular mass than in the absence of this chelation agent. Moreover, the degree of derivatization was not affected by the presence of THPTA so the other glycopolymers synthesized followed this methodology.

Another aspect investigated in the synthesis of glycan-derivatized HA was the reactivity of the alkyne groups. Although the CuAAC cycloaddition is described as fast and quantitative, even for polymers,[189,206,223,224] this project required full conversion from alkyne to triazole to achieve the highest degree of derivatization on hyaluronan. On the other hand, as described in Chapter 3, the synthesis of the different oligosaccharide could not be done on gram scale because of the amount of the enzyme required, so it was not possible to employ a large excess of Gb_3 or Le^x. For this reason, experiments were performed using different concentrations of lactosyl azide to optimise the conversion of alkyne to triazole. In this case, a CuAAC reaction was performed using HA-*g*-propargyl with a degree of derivatization around 37% and Lac-N_3 in presence of $CuSO_4$, THPTA and sodium ascorbate to achieve HA-*g*-Lac (**4.4**) (Scheme 4.8).

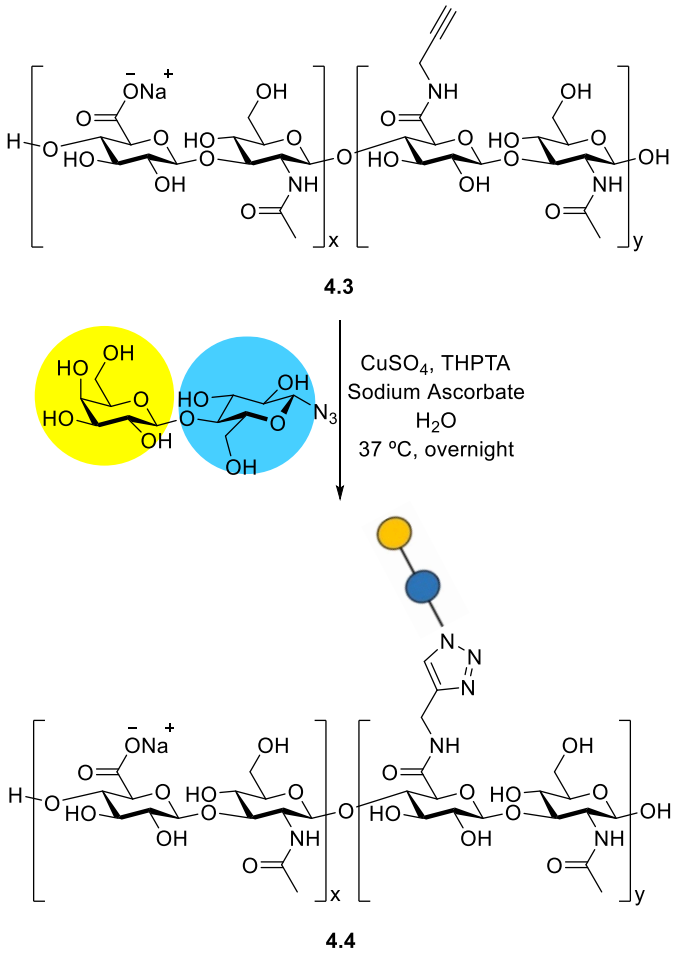

Scheme 4.8: CuAAC reaction between **4.3** (37% propargyl groups) and Lac-N_3 to achieve HA-*g*-Lac (**4.4**).

Two different concentrations of Lac-N_3 (one eq. or two eq. per HA alkyne group) were tested and the resulting products were analysed by ^{1}H NMR spectroscopy calculating the percentage of derivatization of the polymer by comparing the triazole proton at 8.21 ppm and the lactosyl anomeric proton at 5.80 ppm, which had similar integrations, to the 3 protons in the acetamide group as a reference. In both cases the results were the same meaning that an equimolar ratio between alkyne and azide was enough for the alkynes to fully react.

Even though the presence of THPTA seemed to reduce the disintegration of the backbone, this issue was particularly pronounced using other azido-derivatized carbohydrates, especially azydopropyl Lewis^x as explained further in this chapter. For this reason, a final experiment was performed to evaluate the effect of the reaction time. In this case, a reaction was set up using the 50% alkyne **4.3** and the same conditions as the previous experiment using THPTA. Aliquots were taken at 2 hours, 5 hours and overnight (12 h) for analysis by ^{1}H NMR spectroscopy (Figure 4.9) and SEC-MALS (Table 4.6).

Table 4.6: SEC-MALS analysis for the **4.3**, **4.4 (5h)** and **4.4 (overnight (12h))** providing the average molecular weight (Mw) and the dispersity (Đ).

Sample	Mw	Đ
4.3	140.0 kDa	1.03
4.4 (5h)	114.2 kDa	1.18
4.4 (overnight (12h))	59.7 kDa	1.60

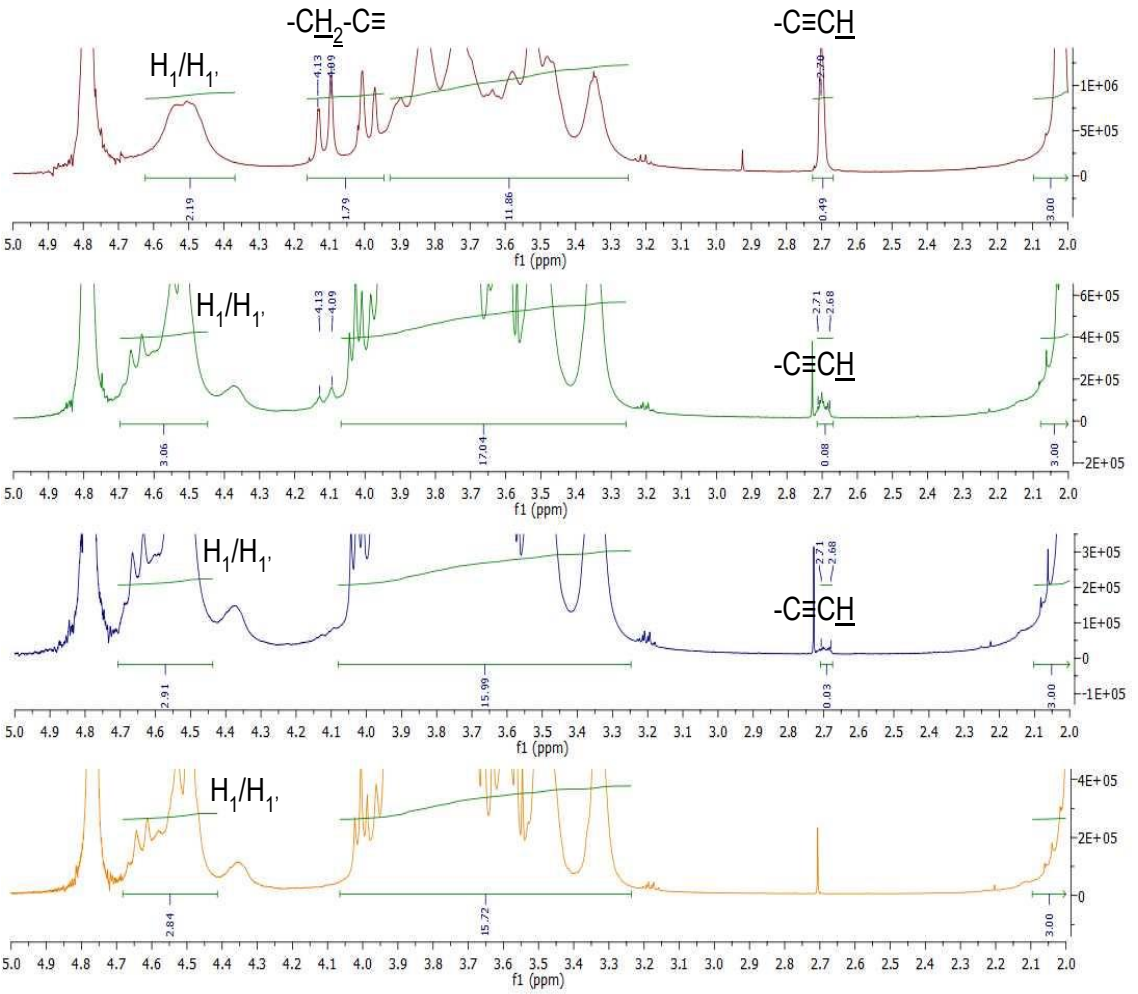

Figure 4.9: ^{1}H NMR for HA-*g*-propargyl (**4.3**) as starting material in red, ^{1}H NMR for HA-*g*-Lac (**4.4**) for 2 hours reaction in green, ^{1}H NMR for HA-*g*-Lac (**4.4**) for 5 hours reaction in blue and ^{1}H NMR for HA-*g*-Lac (**4.4**) for overnight (12 h) reaction in orange.

The results of the ^{1}H NMR analysis were clear, the full conversion of the polymer was after long periods of time, at least more than 5 hours, because before this time there was still presence of free alkyne in the polymer. However, it seemed likely that the reaction could be stop before 12 hours. However, it seemed likely that the reaction could be stop before 12 hours, which could be beneficial as SEC-MALS revealed that the longer the hyaluronic acid was in presence of Cu^{2+}, the greater the disintegration of the backbone resulting in smaller glycopolymers. There is literature

precedent for degradation of HA in the presence of Cu^{2+} or Fe^{2+} ions, although most studies also include hydrogen peroxide which facilitates the production of hydroxyl radicals.[222,225–227]

It was concluded after this experiment that to achieve a balance between disintegration and full conversion, the time reaction optimum was around 7 hours. Unfortunately, this data was achieved after the synthesis of the library glycopolymers due to the limited access to the SEC-MALS equipment established in the University of Manchester. However, the following synthesis of glycopolymers were synthetized having "short" overnight reactions, between 8 and 10 hours.

4.3.2 Synthesis of Lewis^x-derivatized hyaluronic acid

Conjugation of azidopropyl Le^x to HA-*g*-propargyl by a copper-catalyzed cycloaddition was required to make a polymer suitable to bind to the secondary binding site of CTB. Therefore, once the reaction conditions had been optimised using lactosyl azide, the same conditions were applied to synthesize HA-*g*-Le^x (**4.5**): azidopropyl Le^x and HA-*g*-propargyl **4.3** were mixed in the presence of $CuSO_4$, THPTA and sodium ascorbate to obtain **4.5** (Scheme 4.9).

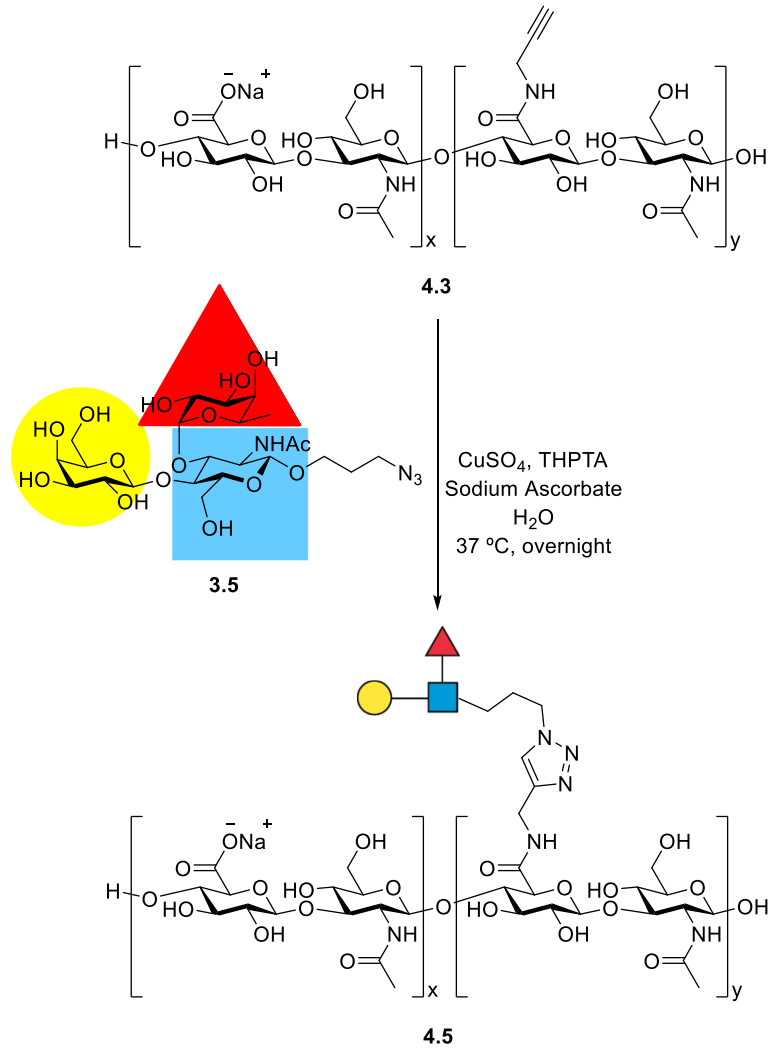

Scheme 4.9: Click reaction between **4.3** and azidopropyl Le^x to achieve HA-*g*-Le^x (**4.5**).

This overnight reaction was performed twice with different HA-*g*-propargyl with different percentage of alkyne, 39% and 50%, to synthesize two glycopolymers containing different degree of substitution of Le^x (20% and 33%). For **4.5** with a 20% derivatization, there was no free alkyne in the resulting product but the degradation of the backbone was higher than expected providing a small polymer (10 kDa). For HA-*g*-Le^x containing 33% Le^x, there was still 4% of free alkyne but the resulting structure was 3 times bigger than the previous synthesized with a M_w equal to 30 kDa (Figure 4.10). The reason of this fact was unknown but it was concluded that azidopropyl Le^x showed different reactivity than the Lac-N_3, probably due to the propyl moiety. Despite the small sizes of both polymers, the one with highest degree of derivatization (33%) was suitable to perform binding studies described in Chapter 5.

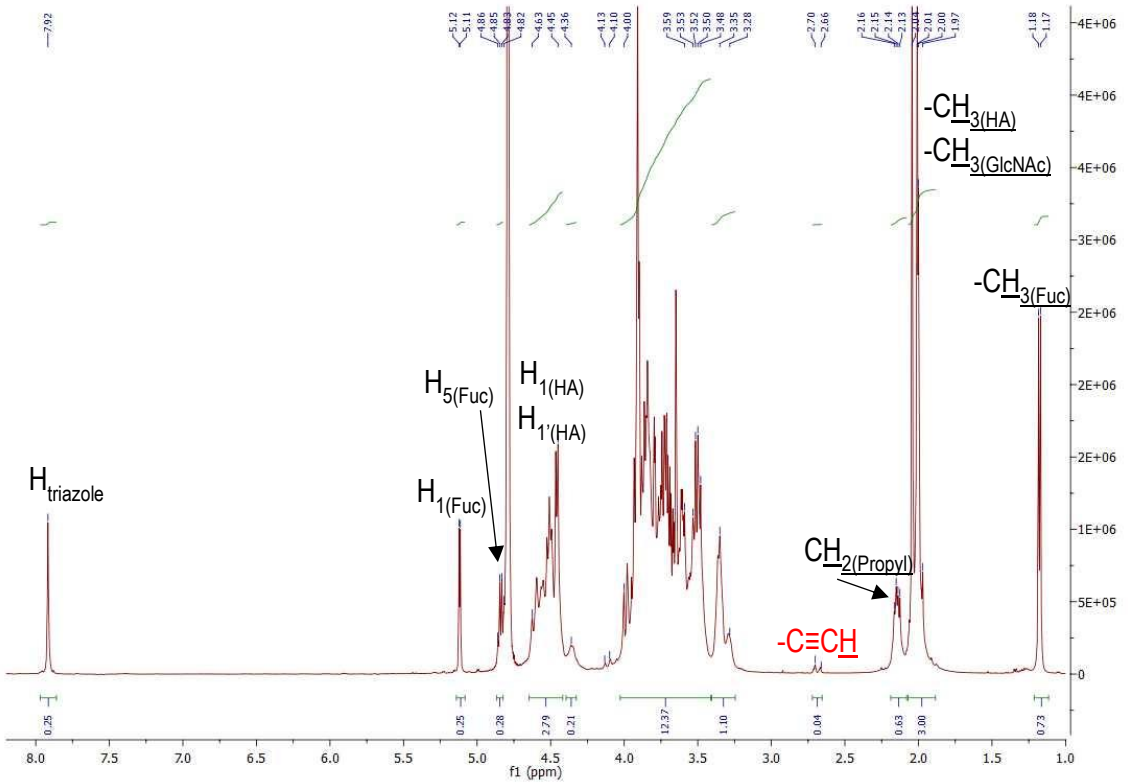

Figure 4.10: ^{1}H NMR spectrum for **4.5** containing 33% Le^x.

4.3.3 Synthesis of Gb_3-derivatized hyaluronic acid

Finally, to perform binding studies with Shiga Toxin B-subunit, a polymer containing Gb_3 oligosaccharide was required. In this case, and because the trisaccharide contained the azide in the same position than the lactosyl azide used during the tests described in the previous section, the reactivity expected in terms of degradation and full conversion of alkyne was the same. Applying the same conditions set up for the synthesis for **4.4**, Gb_3-N_3 and **4.3** (50% of alkyne) were reacted in presence of $CuSO_4$, THPTA and sodium ascorbate to achieve HA-*g*-Gb_3 (**4.6**) (Scheme 4.10).

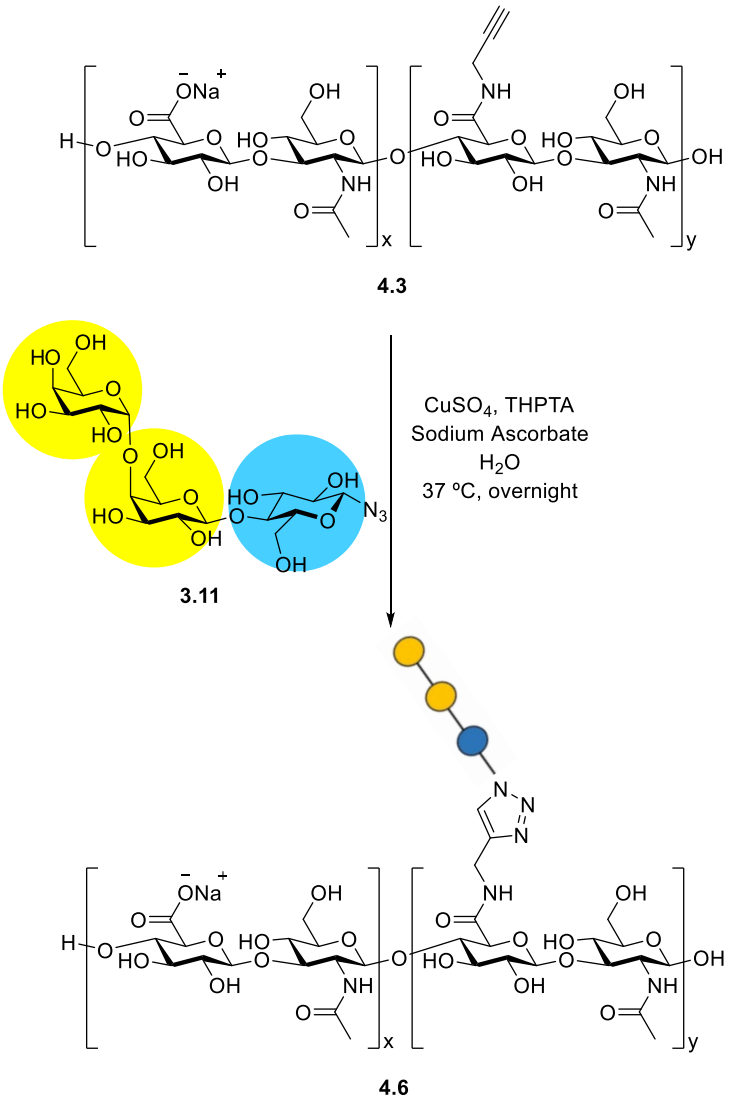

Scheme 4.10: Click reaction between **4.3** and Gb_3-N_3 to achieve HA-*g*-Gb_3 (**4.6**).

This reaction was performed only once giving as a result a product with high degree of derivatization (35%) (Figure 4.11) according the integration of ^{1}H NMR spectrum and large enough (89 kDa) to form a good brush layer for the binding studies described as well in Chapter 5. However, once again the alkyne did not show full conversion to triazole as it can be observed in Figure 4.11 that there was still 6% of the peak corresponding to -C≡C<u>H</u> from **4.3**.

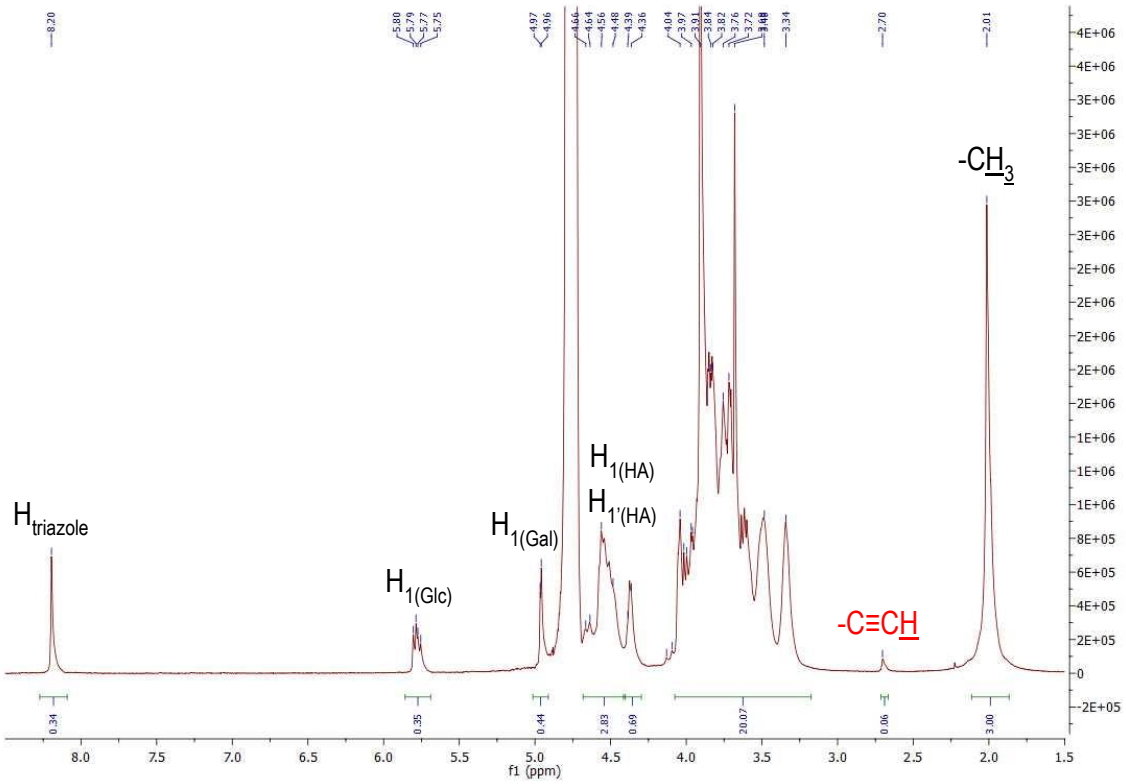

Figure 4.11: ^{1}H NMR spectrum for **4.6** containing 35% Gb_3.

4.4 Conclusions

The synthesis of pure HA-*g*-propargyl was achieved despite issues described using NHS and EDC as activators. It was concluded that these chemicals attached side products to the backbone of HA giving extra peaks that proved difficult to analyse by ^{1}H NMR. Although all the components of this coupling reaction were changed, added or removed to attempt to achieve pure HA-*g*-propargyl **4.3**, it became obvious that the extra peaks in the proton NMR spectra were due to both activators: NHS and EDC. Despite the use of these activators in Chapter 2, the high concentration of NHS and EDC required to achieve high degree of derivatization lead to attachment of side products to the backbone while using propargylamine as amine for the coupling. In addition, the methodologies described by Crescenzi e*t al.*[140,141] for larger HA, 200 kDa, or by Hartwell et al.[206] for small hyaluronan chains, 16 kDa, also showed these side products in less intensity than the samples achieved in this project applying the same protocol without explaining their origin. These protocols showed purification problems as well making difficult to remove remaining activators as EDC.

In contrast, a high degree of derivatization was achieved when the activator was changed to DMTMM, a methodology well established to perform amide bonds using other amines as reagents (e. g. furylamine) but not using propargylamine.[212,215,216] It provided good results in terms of degree

of derivatization and purity of the resulting HA-*g*-propargyl. Four conditions were investigated to achieve a small library of pure HA-*g*-propargyl **4.3** with different degrees of derivatization from 20 to 50% substitution with alkyne groups according to ^{1}H NMR integrations comparing the alkyne signal at 2.7 ppm with the three protons in the acetamide group at 2.0 ppm. For all the products, there were no extra peaks in the proton NMR spectra and the resulting polymers contained high degree of substitution.

Once the HA-*g*-propargyl was prepared in pure form, and with a high degree of derivatization, the CuAAC cycloaddition was tested using Lac-N_3. Different parameters were investigated to establish the optimal reaction conditions for maximising the size of the resulting glycopolymer and the full conversion from alkyne to triazole.

To check if there was degradation of the hyaluronan chain during the CuAAC reaction, two reactions were set up in the presence or absence of a chelation agent, THPTA. After analysing the products **4.4** of different CuAAC reactions by SEC-MALS, it was concluded that the presence of free Cu (II) favoured the degradation of the polymer backbone. After this test, all the CuAAC reaction were performed with THPTA present to maximise the size of the resulting glycopolymers.

Another aspect investigated was the reactivity of the alkyne. To ensure full conversion from alkyne to triazole, different concentrations of Lac-N_3 were tested. It was found that a ratio 1:1 between alkyne groups and azide-derivatized oligosaccharides was sufficient to allow high conversion to the triazole products, and higher concentrations of lactosyl azide did not provide any advantage.

A last experiment was performed to check the degradation of the backbone taking aliquots of the click reaction at different time points. The data revealed more degradation of the glycopolymer when the reaction time was longer, however, for short reaction times there was still alkyne present by ^{1}H NMR analysis. It was concluded that the optimal time reaction was between 8 and 10 hours to provide a compromise between full conversion and maintaining integrity of the backbone.

After all the information compiled from the preliminary experiments, the best conditions for the CuAAC reaction were applied to achieve successfully HA-*g*-Le^x and HA-*g*-Gb_3 with a degree of derivatization, in both cases of around 34%. The main difference between the resulting glycopolymers was their size: probably due to the propyl moiety in **4.5**, this glycopolymer was smaller (30 kDa) than the **4.6** (89 kDa). Despite this difference between materials, both were suitable for binding studies as described in Chapter 5.

.

CHAPTER 5: SELF-ASSEMBLY OF GLYCOCALYX MODELS FROM MUCIN ANALOGOUES TO PROBE TOXIN-GLYCOCALYX INTERACTIONS

5.1 Introduction: Creating a glycocalyx model and interacting with AB_5 toxins

Cholera Toxin and Shiga Toxin, as explained in the introduction, are lectins with affinity for different oligosaccharides on the cell surface and, because of this recognition, these toxins can infect cells.[34,67,73,99] However, due to the complexity and the large number of different oligosaccharides present in the glycocalyx, it is hard to establish a mechanism for the first recognitions and binding of these toxins by cells. Attempts to have a better understanding for the interactions between toxins and glycocalyx were tried in cells by suppressing the expression of enzymes responsible to synthesize oligosaccharides but these experiments did not lead to a clear conclusion about which carbohydrates CT or STx could recognize in the extracellular matrix.[34,67] In addition, the current models to mimic the glycocalyx are simple and, even though they provide good overview about how these lectins infect the host cell, it still lacks from the first binding between the glycans on the cell membrane and the toxins.[100]

Due to the lack of realistic models to study the binding between carbohydrates present on the cell membrane and AB_5 toxins, it seems a good approach to design a more complex glycocalyx model than the ones previously described with a defined organisation and known glycan density, mucin-like structures, to observe the interaction between AB_5 toxins and this model alike to the cell membrane, therefore, it would be possible to have an idea about the first recognition and interaction from these proteins on the cell membrane. This model would be presented as a film, similar to the one created by mucins on the glycocalyx on cells, capable to form brushes where proteins could be trapped inside if there is binding between the glycans and the lectins from AB_5 toxins. This chapter covers the synthesis of mucin-like structures as building blocks for glycocalyx models, the construction of glycocalyx models, and their applications for the analysis of toxin binding. Specifically, the interaction with STxB was analysed with mucin-like structures containing Gb_3, and the interaction with CTB was analysed with mucin-like structures derivatized with Le^x.

To build these glycocalyx models, it was required a technique that could perform the monitoring binding processes including the assembly of the glycocalyx models on a surface and their interaction with the proteins. Quartz crystal microbalance with dissipation (QCM-D) and spectroscopic ellipsometry (SE) were the techniques chosen because they accomplish the requirement previously mentioned by different parameters. QCM-D could follow the binding process by monitoring the mechanical properties of the film through changes in frequency and dissipation of a quartz crystal, deeply explained in section 5.1.1, providing data regarding the effective size of the mucin-like structures, which provides an idea about the length of the glycopolymer once packed in these films, and softness of the film created.[228,229] SE monitors

binding processes by calculating the areal mass density of glycopolymer and/or mucin-like structure with lectin through changes of the polarisation of light, described deeply in section 5.5.2.[228]

Firstly, the incorporation of an anchorage to the glycopolymers was required to graft these structures to a surface. The resulting structures with anchor tag were used as building blocks for glycocalyx models to achieve a film. The surface to build these models were silica-coated QCM-D sensors for QCM-D analyses, and silicon wafer with a native oxide coating for SE analysis. Both these surfaces similarly facilitate the formation of supported lipid bilayers (SLBs), the platform of choice for the glycocalyx models. SLBs reproduce salient properties of the cell membrane, notably the organisation as a lipid bilayer and the fluidity of lipids in the membrane plane. The lipid composition of the SLB was tuned to afford incorporation of glycopolymers according to their anchor tag: biotinylated lipids, along with a streptavidin (SAv) monolayer attach the mucin-like structures with a biotin on the reducing end (Scheme 5.1a); lipids with Ni^{2+}-NTA attach the glycopolymer derivatized with a poly-histidine via Ni (II) (Scheme 5.1b).

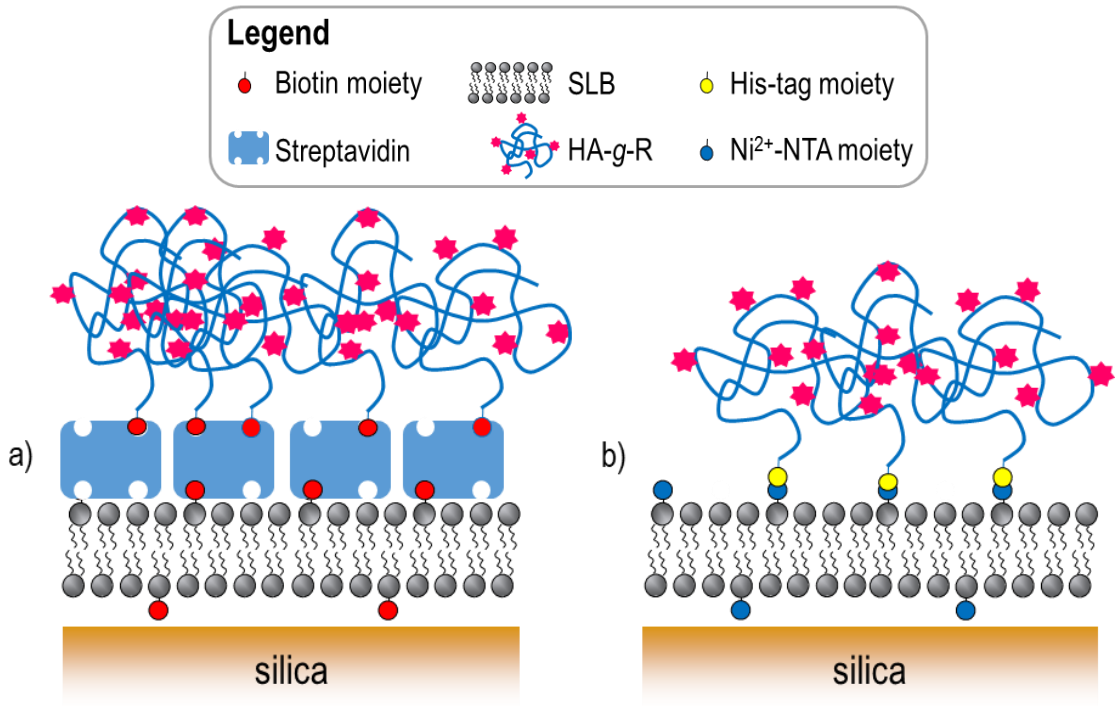

Scheme 5.1: Schemes of the different assemblies to build the glycocalyx model, however, the elements on the sketches are not drawn in scale a) Glycopolymer assembly on an SLB containing a fraction of biotinylated lipids coated with a SAv monolayer to create glycocalyx models. b) Glycocalyx model on SLBs containing a fraction of Ni^{2+}-NTA labelled lipids.

5.1.1 Quartz crystal microbalance with dissipation monitoring (QCM-D)

A technique was required to analyse the formation of glycocalyx models and toxin binding. Quartz crystal microbalance with dissipation monitoring (QCM-D) is a method to monitor

biomolecular binding processes, and to analyse the mechanical properties of thin films, at surfaces in a liquid environment. This technique can be used in a wide range of substrates and it can perform the measurement of thickness, absorbed material and viscoelasticity of films analysed.[228] The changes on the surface are recorded (with a time resolution in the range of a second and better) in situ without labels.[230]

5.1.1.1 QCM-D working principle

QCM-D measures changes in the frequency (Δf) and dissipation (ΔD) of a quartz crystal resonator. Variations in Δf and ΔD are the consequence of the changes on the surface of quartz crystal surface. To a first approximation, Δf relates to the mass adsorbed per unit area, and ΔD relates to the softness of the interfacial film. In QCM-D, changes in frequency and dissipation are recorded as a function of time by using a 'ring-down' method, summarized by the following steps:[228,230–232]

1. The active component to make the measurement is a quartz crystal disk sandwiched between two gold electrodes. Application of an alternating current (AC) near a resonance frequency of the disk causes the shear oscillation of the disk. The fundamental resonance frequency is on the order of 5 MHz (Figure 5.1).

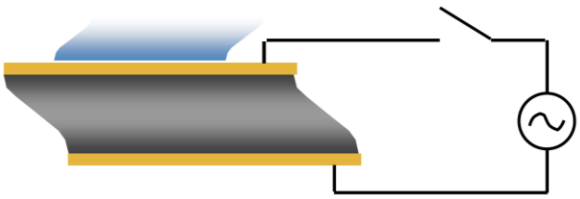

Figure 5.1: Scheme of the setup of the quartz crystal disk (grey crystal) with the two gold electrodes (in yellow) sheared by the AC applied owing to the piezoelectric properties of quartz.[228]

2. Then the external AC field is turned off giving as a result the free oscillation of the sensor with exponentially decaying amplitude. This decaying oscillation is recorded and from a fitting of the curve, the resonance frequency f and the energy dissipation D are extracted. This recording is made at the fundamental resonance (i = 1) and at six overtones (i = 3, 5, 7, 9, 11 and 13), corresponding to standing shear waves in the disk with i the number of nodes.[231]
3. Steps 1 and 2 are repeated with a time resolution of less than 1 s, and changes in f_i and D_i are monitored. Relevant for further analysis are the normalised frequency shifts $\Delta F_i = \Delta f_i / i$ and the dissipation shifts ΔD_i.

5.1.1.2 Models to fit QCM-D data

Different models are described in the literature to fit the data achieved according the nature of the film: homogenous or monolayers of discrete nanoscale objects.[230,232] Laterally homogenous films are films in which the length scale of the sample's internal structure is smaller than the film thickness.[228] Films of end-grafted polymers, such as mucin analogues, are typically homogeneous as per the above definition. For homogenous films, well established models to describe the QCM-D data are: the Sauerbrey model[229,233,234] and the viscoelastic model[234–238]

For films that are sufficiently rigid, the Sauerbrey model can be applied meaning that the mass of the material absorbed is proportional to the change in frequency:[229,233,239]

$$\Delta m = -C \times \Delta F \tag{5.1}$$

where Δm is the adhered mass per unit surface area (also called areal mass density), C is the sensor's mass sensitivity constant and it is specific to the sensor, and ΔF is the normalised frequency shift.

This model can only be applied for films with $\Delta D \approx 0$, more specifically, $|\Delta D/\Delta F| \ll 4 \times 10^{-7}$ Hz^{-1} (for a sensor crystal with $F_1 \approx 5$ MHz).[230] In this case, the areal mass density can be extracted keeping in mind that this measurement would contain the mass of the adsorbate and the solvent in the film. The benefit of the Sauerbrey model is its simplicity. It provides the areal mass density and the thickness of the film once the previous parameter was divided by the effective density of the film. This density takes into consideration the solvent and the macromolecules constituting the film.[240]

The viscoelastic model can be applied when the film is thick and soft enough for the QCM-D to be sensitive to the mechanical properties of the surface-bound film. This is the case when the film exhibits a non-zero dissipation ($\Delta D > 0$).[230] In the viscoelastic model, dissipation and frequency depend on the thickness, density, shear viscous modulus (related to the viscosity) and shear elastic modulus of the film as well as the density and viscosity of the bulk solution.[229,235,241] The dependencies are quite complex, and numerical fitting of the data is required to extract the film properties from the QCM-D responses (ΔD and ΔF at several overtones). In many instances of practical relevance, the density and viscosity of the bulk solution can be kept constant to a good approximation, and the density of the film can be approximated reasonably well. In this case, the thickness, the viscosity and the elastic modulus of the film can be obtained with the viscoelastic model.

Contrary to the previous models described, films formed by monolayers of discrete nanoscale objects need another mathematical treatment for the data interpretation.[232] These types of films are not appropriately described by the viscoelastic model. Additional hydrodynamic effects and energy

dissipation phenomena can become relevant in monolayers of discrete objects that are not taken into account in the viscoelastic model. The quantitative analysis of films of discrete nanoscale objects is generally more complex and will not be covered in detail here. Of note, however, the Sauerbrey equation can be applied for dense monolayers of nanoscale objects to estimate the areal mass density of the monolayer (included coupled solvent) and, more importantly, the height of the objects above the surface.[229,230]

5.1.1.3 QCM-D application for the present project

Due to the capability to monitor binding processes at surfaces in real time, QCM-D is a useful (and well-established) tool to probe the formation of biomolecular films at surfaces.[142,229,242,243] It was here used to analyse the formation, the quality and some physical properties (thickness and softness) of model glycocalyces, and to initially study the binding of toxins to model glycocalyces.

5.1.2 Spectroscopic ellipsometry (SE)

Spectroscopic ellipsometry (SE) is an optical technique that measures the change of the polarisation of light upon reflection at an interface.[244,245] This technique is non-destructive, non-contact and non-invasive and it can be used to characterize, among other things, the composition, roughness and thickness of materials or films.[246–248] Similar to QCM-D, SE can be deployed for the time-resolved characterisation of organic thin films at the solid-liquid interface.[228] However, SE and QCM-D assess different information about the film, making the two techniques complementary. SE is able to quantify the thickness, refractive index and areal mass density (excluding any trapped solvent) of organic thin films, whereas QCM-D measured the thickness, mechanical properties and the areal mass density (including trapped solvent).

5.1.2.1 SE working principle

Light is an electromagnetic wave described by the oscillation of two fields that propagate in the same direction yet are perpendicular to each other: the magnetic field and the electric field. The orientation of the electromagnetic field defines the polarisation of light. In conventional light sources, the emitted light rays have varying polarisations and the light is called non-polarised. Polarising filters let one specific angle of polarisation pass, and block all other angles, thus creating linearly polarised light. Upon reflection at an interface, the polarisation of light changes. The polarisation of light is very sensitive to changes in the optical properties of the interface, and therefore measuring the change of polarisation upon reflection can provide valuable information about the interface itself.

In a general case, linearly polarised light, upon reflection, becomes elliptically polarised, meaning that the electric and magnetic field vectors change their spatial direction and amplitude with time, describing an ellipse in the plane perpendicular to the direction of light propagation (Figure 5.2).[245,247,249] This ellipse gives ellipsometry its name.

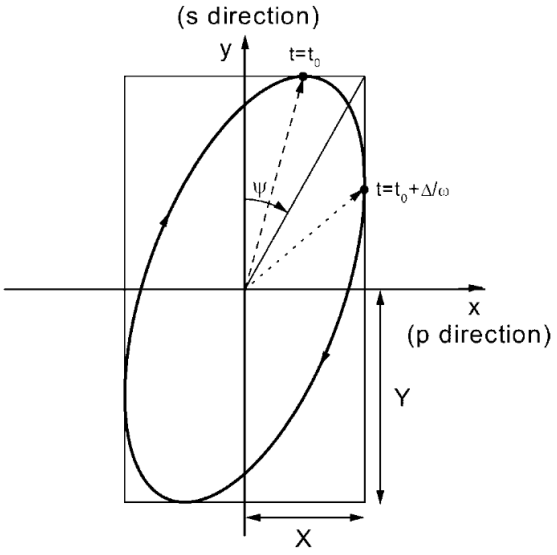

Figure 5.2: Elliptically polarised light. Directions *p* and *s* are defined with respect to the plane of incidence of light being *p* the direction parallel to the plane of incidence, and *s* is the direction perpendicular to the plane of incidence. The ellipsometric angle Ψ describes the orientation of the ellipse, which is defined by the relative amplitudes of *s* and *p* components of the polarised light. The ellipsometric angle Δ (not shown here) is the phase difference between the *s* and *p* components of the polarised light. The positive values for the *z* axis are pointing towards the reader, and define the direction of light propagation.

SE determines the dielectric functions of the light once it has been reflected at the sample interface, relying on changes in the two ellipsometric angles ψ and Δ (Figure 5.2).[244,247,249] For *in-situ* spectroscopic ellipsometry, the changes in these parameters are recorded as a function of the wavelength (λ) (ranging from 400 to 1000 nm in the setup used in this work) and the angle of incidence (θ).[228,248] To monitor these changes, the ellipsometer requires the following fundamental parts in two optical arms (Figure 5.3): light source and polarizer, and analyser and detector. Optionally, compensators before and after reflecting the light at the sample are added to be able to sample the full range of ellipsometric angles. The orientation of the two optical arms, with the reflecting sample in the middle, defines the angle of incidence (θ) (Figure 5.3).[247,249]

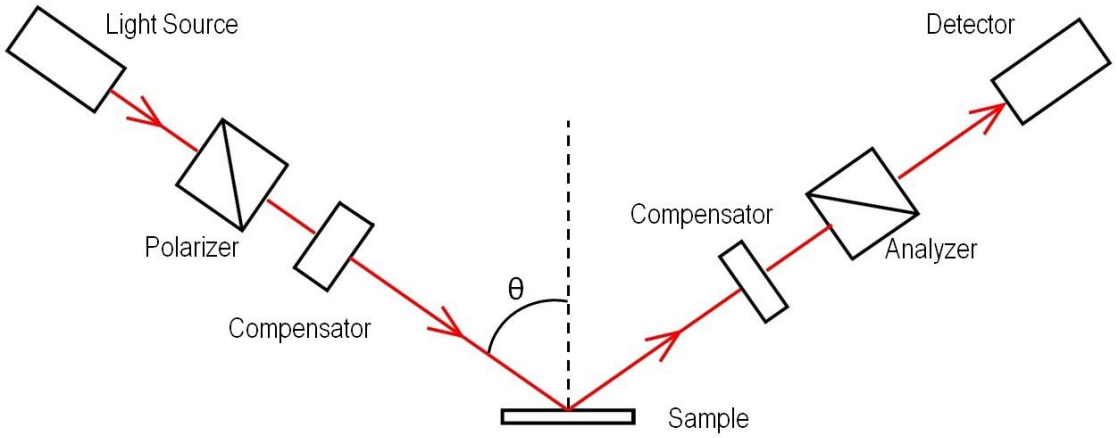

Figure 5.3: Schematic of the light path and principal optical components in an ellipsometer.

5.1.2.2 SE data analysis

The polarised light beam can be decomposed into two parts, one parallel to the plane of incidence (*p*) and the other perpendicular to the plane of incidence (*s*). The changes in the ellipse can be described as modifications in the amplitude ratio and the phase difference between these two parts (Figure 5.4). Changes in ψ(λ) and Δ(λ) are described using the ratio between the changes in the coefficients of each plane, reflection in the plane (R_p) and reflection out of the plane (R_s), according to:[250–252]

$$\rho = \frac{R_p}{R_s} = \tan\Psi e^{i\Delta} \tag{5.2}$$

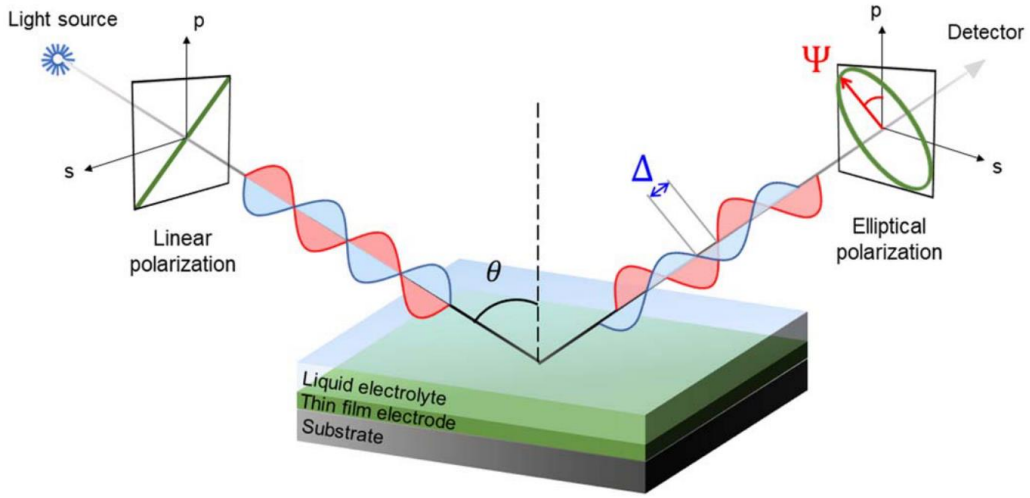

Figure 5.4: SE set up where *p* (in blue) and *s* (in red) polarised parts are described before and after reflection at an angle of incidence θ. Shown are the changes caused by the sample giving as a result the ellipsometric angles ψ and Δ.[253]

An appropriate optical model is required to extract the interface optical properties from the SE data. Because ψ(λ) and Δ(λ) depend non-linearly on the optical properties, numerical fitting is

required.[248] The optical model must duly consider the different interfacial layers and the medium that the polarized light traverses, to achieve an accurate interpretation of the data.[251,254] For each of the layers, there would be its dielectric function relying on the complex (in the mathematical definition, with the imaginary unit i) refractive index (N) which is defined by the refractive index (n) and the extinction coefficient (k):

$$\varepsilon = (N)^2 = (n + ik)^2 \tag{5.3}$$

Assuming each layer to be homogeneous, the optical properties of the layers, both non-absorbing ($k = 0$) or with a complex index of refraction ($k \neq 0$), are fully described by the thickness and the wavelength-dependent refractive index of the sample.[228]

Most organic thin films and solutions, including those relevant here, are non-absorbing ($k = 0$). The optical properties of such media are appropriately described by dispersion models.[247] The Cauchy equation describes the wavelength dispersion of the refractive index well: [251,252,254–256]

$$n(\lambda) = A + \frac{B}{\lambda^2} + \frac{C}{\lambda^4} \tag{5.4}$$

Here *A*, *B* and *C* are the so-called Cauchy parameters. In practice, C is often close to zero and can be neglected, leaving two parameters (*A* and *B*) to describe the wavelength dependence of the refractive index.

For the purposes of this thesis, the most interesting parameter that can be derived from SE is the surface density of surface bound molecules. Different approaches can be applied to extract the molecular surface density (Γ) from the SE data, depending on the type of the layers considered. This parameter can be extracted by areal mass density (m, ng×cm^{-2}), which is measured by SE, if known the M_w of the sample analysed. For thicker films, from a few nm to a few 10 nm, two models are described, De Feijter[247,255] and Lorentz-Lorenz approach[228,248,257], while for thinner or ultra-thin films, there are the Stenberg approach[246,258] and Linear averaging approach.[228,259] Nevertheless, these will not be explained because this project does not involve them.

The De Feijter approach considers transparent solvated layers immersed in a transparent ambient solution with refractive index n_{amb}. In this case:

$$\Gamma = \frac{d(n - n_{\mathrm{amb}})}{\mathrm{d}n/\mathrm{d}c} \tag{5.5}$$

where d is the layer thickness, n is the layer refractive index, and $\mathrm{d}n/\mathrm{d}c$ is the refractive index increment for the molecules in the layer (e.g., proteins, lipids or glycans).[228,247,251,254,255,260]

In summary, the most relevant parameters accessible by SE are the thickness and refractive index, and ultimately the areal mass density and molecular surface density, of biomolecular films. These aspects are relevant when analysing a film because they provide quantitative data in terms

of concentration of ligand on the surface relevant while studying the interaction of these films with biomolecules such as proteins.

5.1.2.2 SE application for the present project

SE is a precise tool to obtain information about the thickness and areal mass density of biomolecular films, as well as dynamic changes in films for *in situ* experiments.[247,248,256] In the context of this thesis, SE was used to quantify the surface density of glycopolymers in the model glycoalyces, and the binding of toxins to the model glycocalyces.

5.2 Incorporation of anchor to oligosaccharide-derivatized hyaluronic acid.

The incorporation of an anchor to the structures whose synthesis was described in Chapter 4 was crucial to perform binding studies such as QCM-D or SE, and the nature of this anchor needed to be compatible with the lipid bilayers used in this type of experiments. Among all the possibilities, one of the most used is biotinylated lipids, followed by the addition of streptavidin and, finally, a biotinylated sample.[261–263] Another system commonly used involves lipids with Ni^{2+}-NTA headgroups, in which a nickel (II) ion that has been complexed to nitrilotriacetic acid (NTA).

Applying these two possibilities to perform the binding studies with the proteins from the AB_5 family, needed a biotin or a poly-histidine peptide to be attached to the hyaluronic acid. Moreover, the addition of these anchors had to be at a single position in the hyaluronic acid to avoid having more than one anchor group for streptavidin or Ni^{2+}-NTA lipids. The best position for chemical attachment of the anchor was at the reducing end of the hyaluronic acid because it presents a unique chemical reactivity and there is only one reducing end per hyaluronic acid (Scheme 5.2).[264–266]

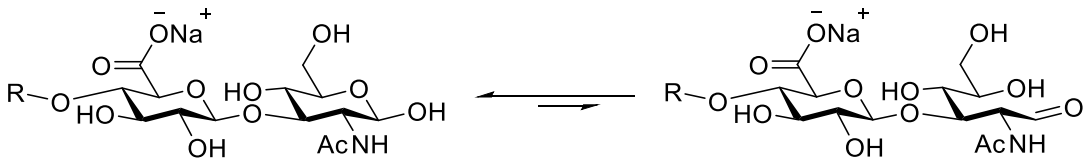

Scheme 5.2: Chemical structure of the reducing end of hyaluronic acid.

5.2.1 Incorporation of biotin at the reducing end of oligosaccharide-derivatized hyaluronic acid.

Hydrazone ligation was the common approach for the functionalization of GAGs,[266,267] but a methodology to attach a biotin in the reducing end on these polysaccharides has been well established by Thakar *et al*.[264] using oxime ligation. In this case, a biotin derivatized with

hydroxylamine reacted with the reducing end of HA or Heparan Sulfate (HS) using aniline as a catalyst, as it is shown in Scheme 5.3.[264,268]

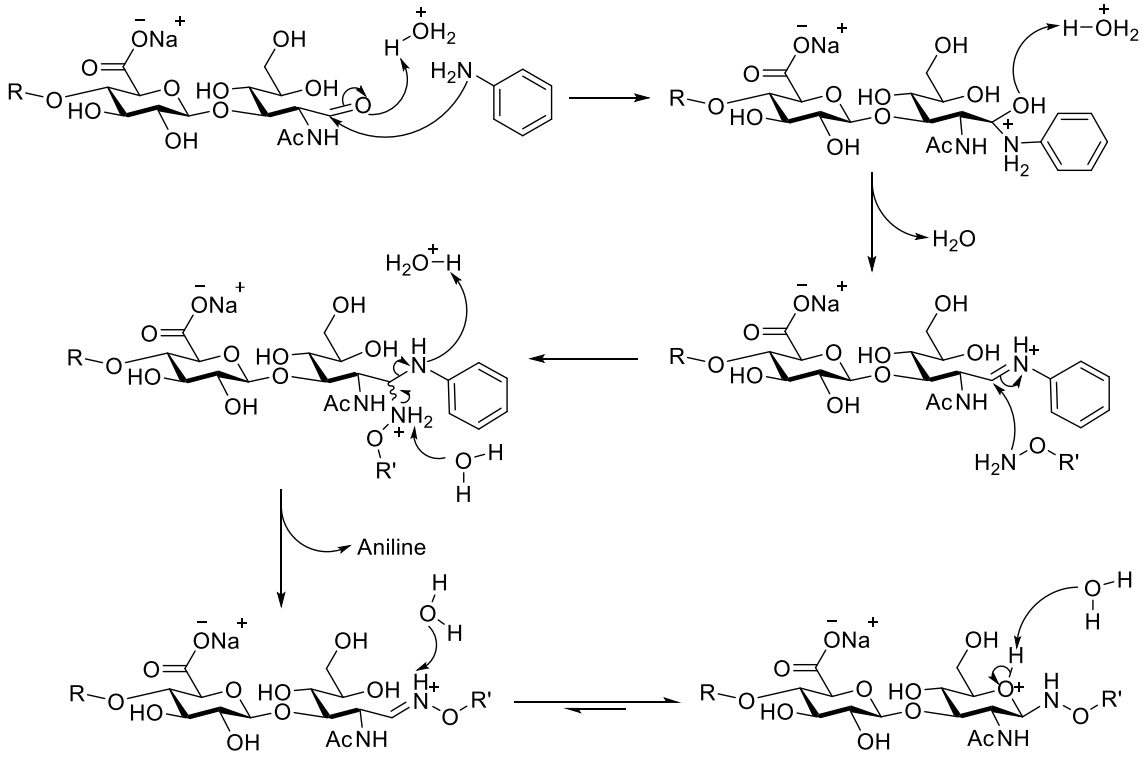

Scheme 5.3: Oxime ligation mechanism using aniline as a catalyst.

First of all, it was checked that the procedure described was reproducible using pure hyaluronic acid. Two reactions were set up using HA with different sizes (200-500 kDa and 40-50 kDa) and alkoxyamine PEG_4-biotin (Sigma-Aldrich) and aniline as a catalyst in presence of sodium acetate to perform the reaction at pH around 7 and achieve HA-Biotin (**5.1**) (Scheme 5.4). These polymers were useful for the QCM-D studies as building blocks to construct the different glycocalyx models as it is described in section 5.3 in this chapter.

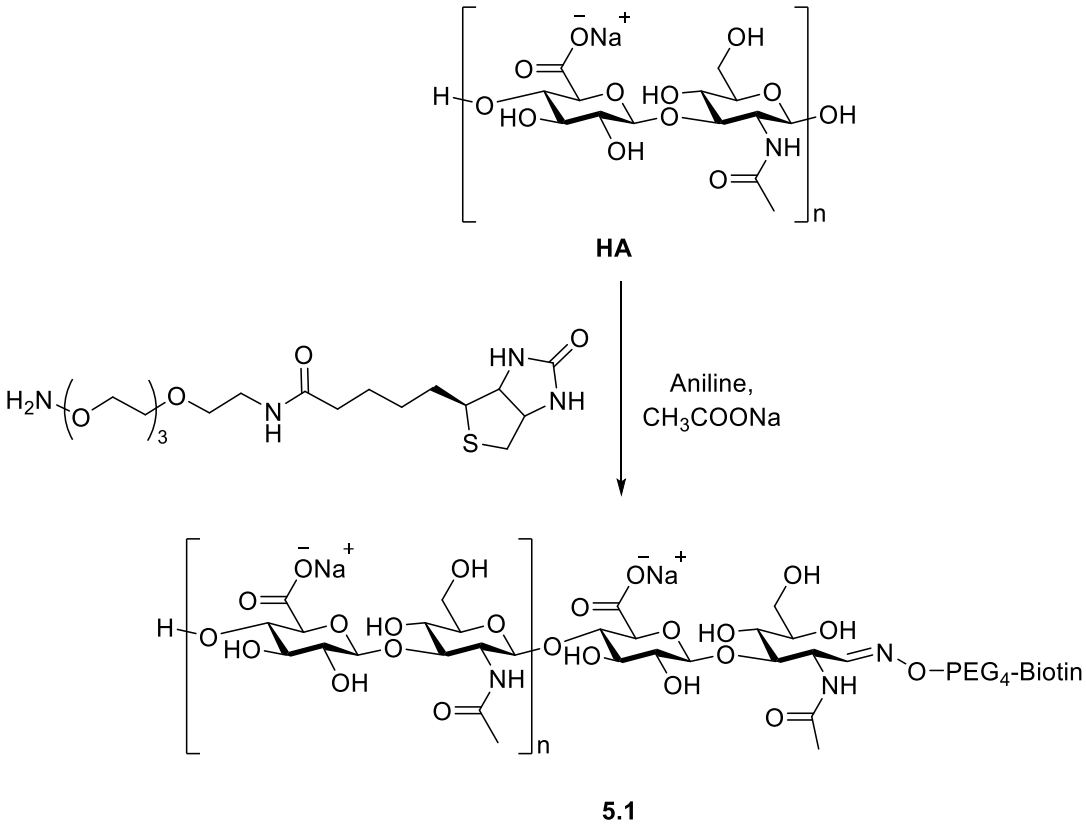

Scheme 5.4: Attachment of biotin to the reducing end to produce **5.1**.

Because the reaction worked as expected showing clear response as it is described in section 5.3 (Figure 5.6), the same conditions were applied for HA-*g*-Lac (**4.4**), HA-*g*-Le^x (**4.5**) and HA-*g*-Gb_3 (**4.6**). Both glycopolymers were reacted with alkoxyamine PEG_4-biotin using aniline as a catalyst in presence of sodium ascorbate to aim (HA-*g*-Lac)-Biotin (**5.2**), (HA-*g*-Le^x)-Biotin (**5.3**) and (HA-*g*-Gb_3)-Biotin (**5.4**) respectively (Scheme 5.5)

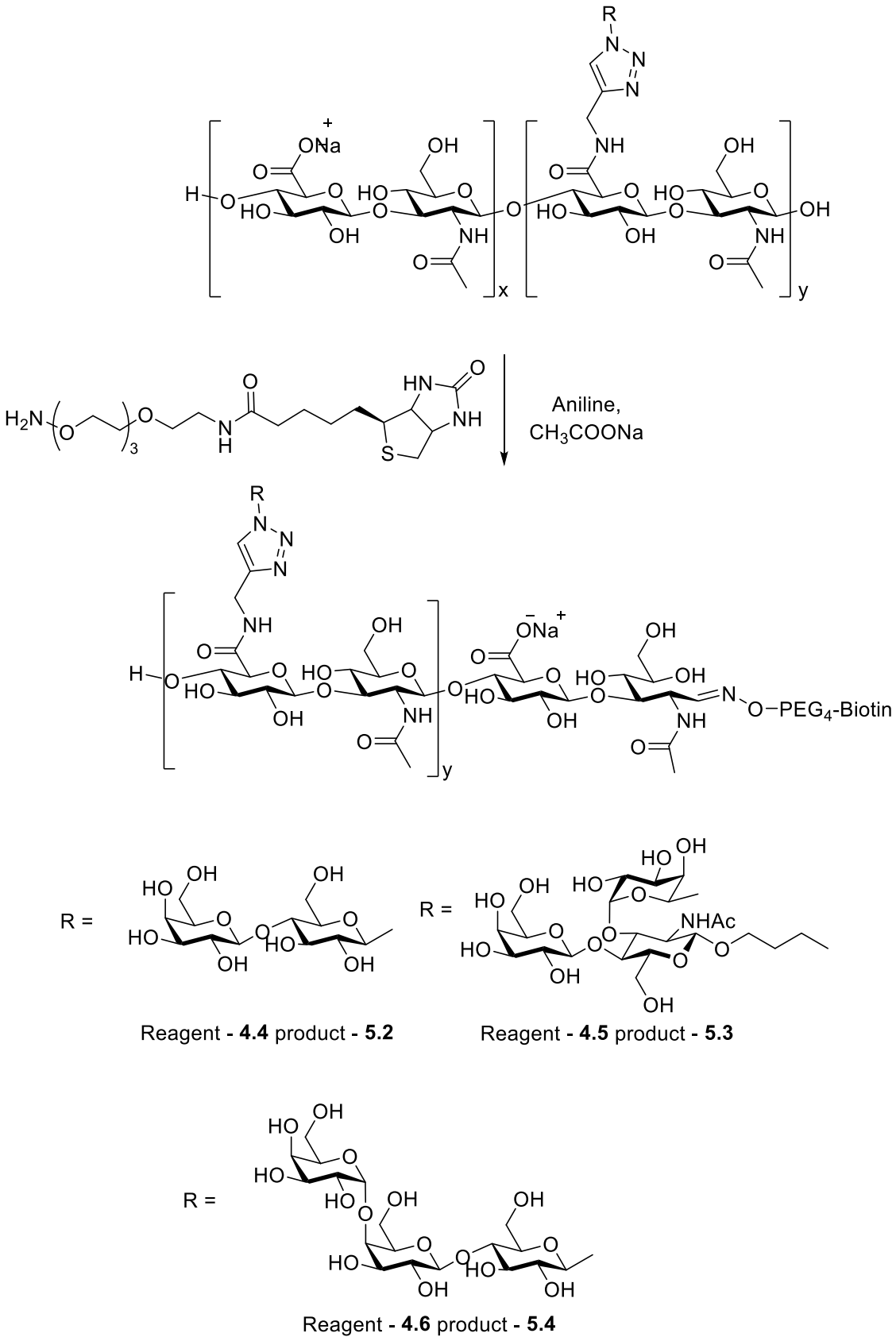

Scheme 5.5: Synthesis of biotinylated glycopolymers **5.2**, **5.3** and **5.4** from HA-*g*-Lac **4.4**, HA-*g*-Le^x **4.5** and HA-*g*-Gb$_3$ **4.6**, respectively.

Glycopolymers **5.2**, **5.3** and **5.4** were used as building blocks for the glycocalyx models on the QCM-D or SE sensors which were coated with biotinylated lipids and streptavidin, as described in the subsequent sections in this chapter.

5.2.2 Incorporation of a His-tag at the reducing end of oligosaccharide-derivatized hyaluronic acid.

Another system discussed above involved the use of Ni^{2+}-NTA lipids because it offers different advantages like avoiding the stiffness provided by the streptavidin or the possibility to add glycolipids to the surface to have a more realistic glycocalyx model having different types of glycoconjugate. An alternative way to anchor the glycopolymers is to use a combination of Ni^{2+}-NTA lipids and a poly-histidine (His-tag) on the polysaccharide

Although the nature of the anchor was changed, the chemical reaction to incorporate the anchor into the glycopolymer was not modified. Consequently, the poly-histidine synthesized required the incorporation of an alkoxyamine group (Scheme 5.6) to be able to perform oxime ligation with the reducing end of the derivatized hyaluronic acid.

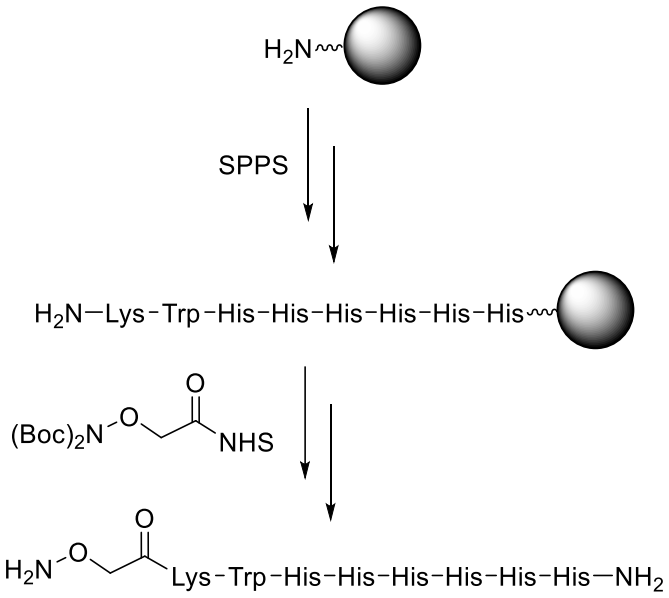

5.5

Scheme 5.6: Plan to synthesize an aminooxy-poly-histidine tag for attachment to the glycopolymers.

5.2.2.1 Synthesis of the His-tag

Solid Phase Peptide Synthesis (SPPS) was used to synthesize the required poly-histidine tag. The target peptide (Scheme 5.5) was designed to have six histidine residues, a tryptophan (Trp) to provide a UV-visible amino acid to simplify HPLC purification and for quantification purposes, and a lysine (Lys) to incorporate a free amine to attach interesting moieties like a fluorescent tag. Finally,

2-[(bis-Boc)amino]oxyacetic acid would be attached at the N-terminus of the peptide to provide the alkoxyamine group that was crucial for the goal of this peptide.

Following this plan, six protected histidine (His) were coupled manually to a Fmoc-rink amide methylbenzhydryl amine (MBHA) resin. Each coupling was checked by heating some resin in a saturated solution of ninhydrin in MeOH: if some of the beats were blue, meaning there was free amine groups, the coupling was not successful. After the addition of these six His, a mini cleavage was performed to ensure the purity of the resulting peptide because the coupling of His could trigger side reaction. Even though the purity of the resulting peptide at this stage was not really high, less than 40%, more than one peak was shown in the analytical HPLC as well as LC-MS, a boc protected tryptophan (Trp), followed by a boc protected lysine (Lys) and 2-[(bis-Boc)amino]oxyacetic acid were added to the peptide sequence. Finally, deprotection using TFA and triisopropylsilane (TIS) gave H_2N-O-Lys-Trp-His_6-NH_2 (**5.5**) (Scheme 5.7).

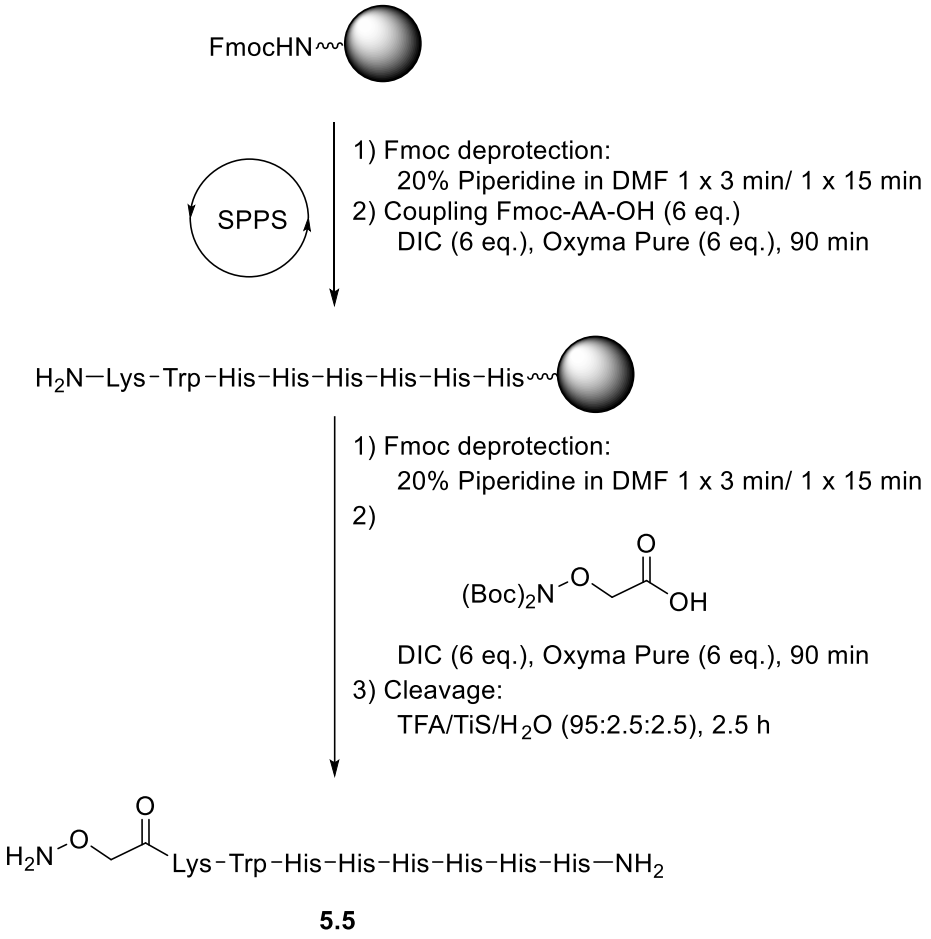

5.5

Scheme 5.7: Manual SPPS for the peptide H_2N-O-Lys-Trp-His_6-NH_2.

The purification of this peptide became challenging as well, even though the couplings were checked in each step, more than one peak with similar intensities were shown in the HPLC making difficult to identify the product. In addition, once different peaks seemed isolated and analysed by

LC-MS, more than one peak was revealed with different masses forcing an extra purification. Moreover, the yield of this synthesis was not high either, instead of achieving 246 mg only 1.3 mg was isolated and clean by HPLC, but, luckily, the material required for the incorporation of this His-tag into the glycopolymer was not large.

5.2.2.2 Incorporation of His-tag to the reducing end of the polymer

The incorporation of a poly-histidine at the reducing end of GAGs has not been described before. For this reason, although the oxime ligation should work as for the alkoxyamine PEG_4-biotin used in the previous section, it was not known if that would be the result of this reaction.

To check the oxime ligation, HA-*g*-Gb_3 was reacted with peptide **5.5** using aniline as a catalyst in presence of sodium acetate to achieve (HA-*g*-Gb_3)-Lys-Trp-His_6-NH_2 glycopolymer (**5.6**) suitable to bind to Ni^{2+}-NTA lipids bilayers in QCM-D or SE (Scheme 5.8), described in sections 5.3 and 5.4 in this chapter.

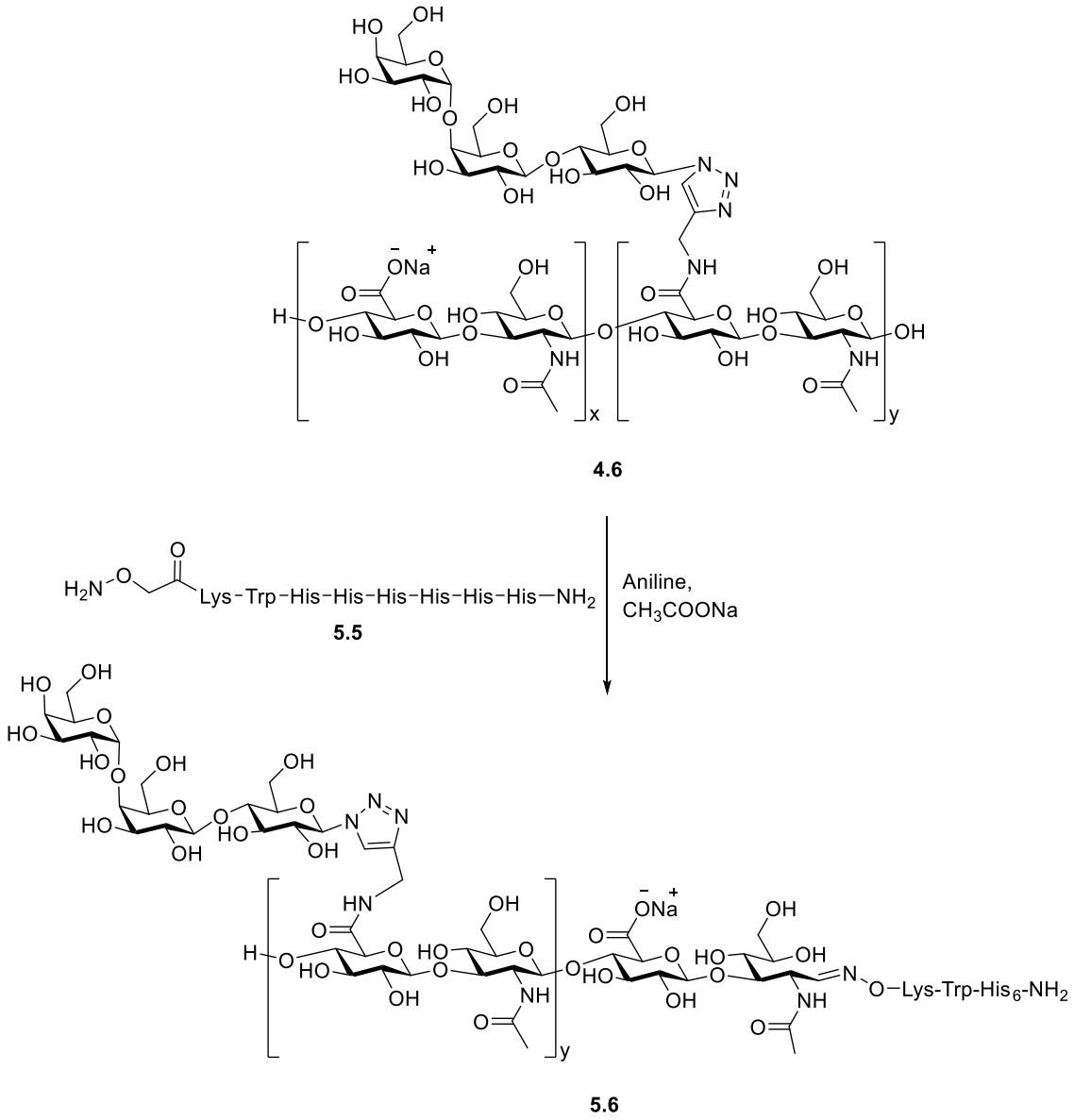

Scheme 5.8: Attachment by oxime ligation of **5.5** and **4.6**.

Although the synthesis of peptide **5.5** was more difficult than expected due to the number of histidine residues in the sequence, the incorporation of the poly-histidine tag to derivatize glycopolymer **4.6** was successful. The resulting glycopolymer with a His-tag at its reducing end (**5.6**) was also used as a building block to construct glycocalyx models that did not require streptavidin monolayer systems, as described in the following section in this chapter.

5.3 Construction of glycocalyx models

5.3.1 Constructing glycocalyx models using biotinylated glycopolymers

QCM-D was used to check for the correct formation of the SLB and the SAv monolayer, and for successful attachment of the glycopolymers *via* their biotin. A representative experiment is shown in Figure 5.5.

Small unilamellar vesicles (SUVs) containing 5 mol-% of biotinylated phospholipids (DOPE-CAP-B) along with inert DOPC lipids for SLB formation were provided by Dr. Xiaoli Zhang (University of Leeds). The 5 mol-% of biotinylated lipids here are expected to be sufficient for the formation of a dense monolayer of SAv.[269] (4-(2-hydroxyethyl)-1-piperazineethanesulfonic acid) (HEPES) buffered saline (150 mM NaCl) solution (HBS, pH 7.4) was used as running buffer, to maintain the pH and ionic strength at close-to-physiological conditions.

The QCM-D frequency shifts (ΔF, blue lines) and dissipation shifts (ΔD, red lines) were recorded over time. Two experiments were performed in parallel: both used the same SAv-on-SLB platform with one using the biotinylated (HA-*g*-Lac)-B (**5.2**) glycopolymer (Figure 5.5b, lines with square symbols) and the other the non-biotinylated HA-*g*-Lac **4.4** (Figure 5.5b, lines with triangle symbols) as a control to test for non-specific binding.

The experiment started with the addition of the biotinylated SUVs (Figure 5.5b, from 11 to 32 min) which produced a final decrease in ΔF about -27 Hz, and a slight increase in ΔD about 0.1×10^{-6}, as expected for the formation of a good-quality supported lipid bilayer without patches. The QCM-D response also shows the classical feature of vesicle adhesion and spreading.[270,271] Up to around 15 min, there is a decrease in ΔF and a concomitant increase in ΔD reflecting the adhesion of SUVs on the surface. After reaching extrema, there is an increase of ΔF and a decrease of ΔD which reflect the rupture and spreading of SUVs to form a planar SLB. Subsequently, SAv was incubated (Figure 5.5b, from 42 to 57 min). The responses of ΔF, a decrease by -25 Hz, and ΔD, an increase by 0.5×10^{-6}, are consistent with the formation of a streptavidin monolayer that is suitable to anchor biotinylated structures. In addition, as can be seen in the rinse step (Figure 5.5b, from 57 to 68 min), there was no change of dissipation or frequency meaning that the surface coating was fully stable under flow in HBS.

Finally, incubations for non-biotinylated and biotinylated HA-*g*-Lac were performed (Figure 5.5b, 68-114 min). The non-biotinylated control (line with triangle symbols) did not show any detectable response in ΔF or ΔD, while for the biotinylated glycopolymer there was a clear response in ΔF (a decrease of around 45 Hz) and ΔD (an increase of around 12×10^{-6}), which was stable upon subsequent rinsing in working buffer. These two experiments demonstrate successful and specific anchorage of the glycopolymer *via* the strong biotin-streptavidin bond. In addition, the change in dissipation is rather large (e.g., compared to the SAv monolayer) and indicates the formation of a soft film.

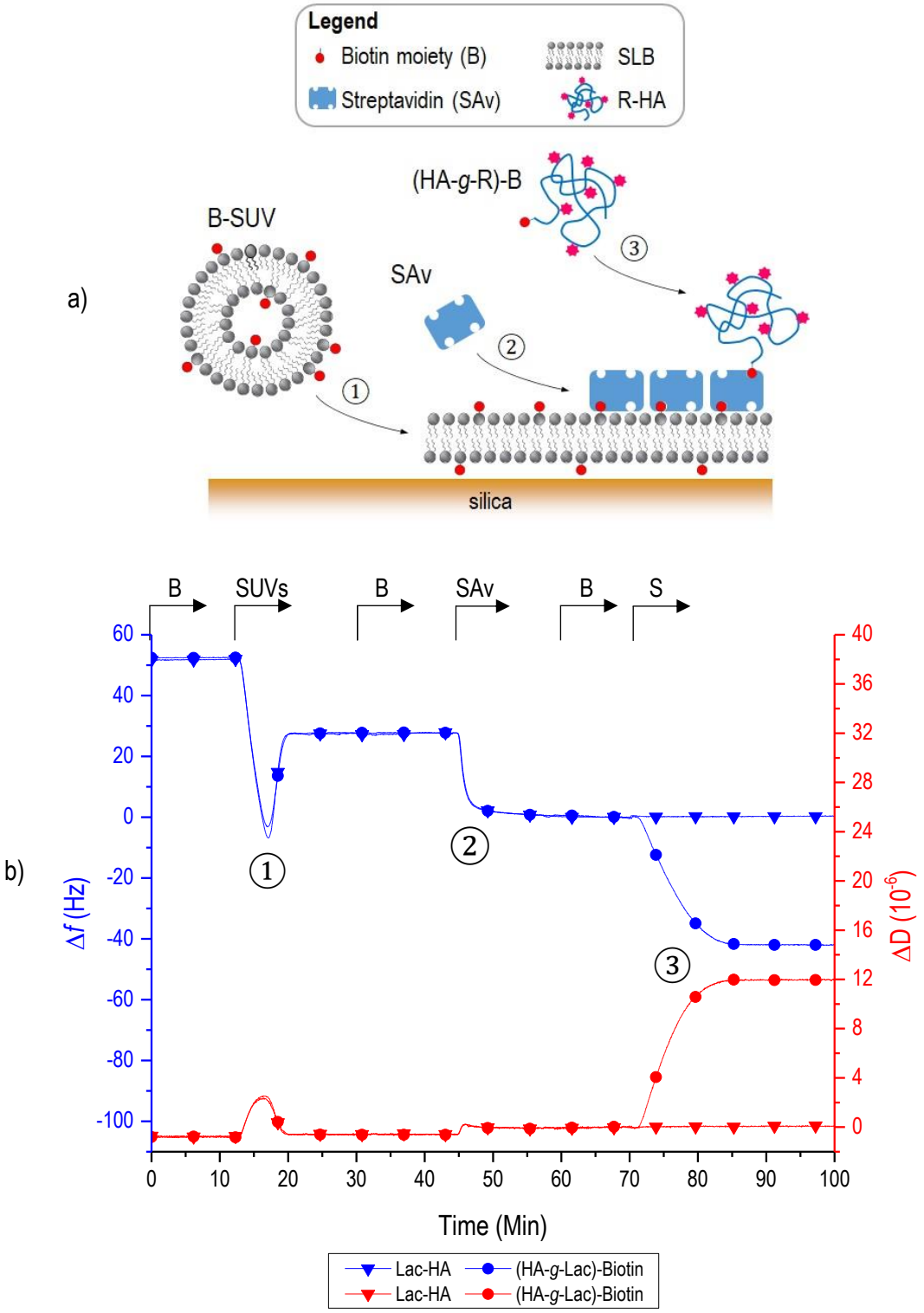

Figure 5.5. (a) Scheme for the supramolecular self-organisation process to form glycocalyx models: (1) adsorption of SUVs with biotinylated lipids on the silica surface, and their subsequent rupture to form an SLB, (2) Binding of SAv by at least two biotins from the biotinylated SLB to form a monolayer,[263] (3) anchorage of the biotinylated glycopolymer. (b) Quartz crystal microbalance with dissipation monitoring (QCM-D) data demonstrating successful anchorage of (HA-*g*-Lac)-Biotin on a SAv-on-SLB surface. Shown are data for the formation of a supported lipid bilayer (from SUVS containing 5 mol-% biotinylated lipids),

subsequent binding of streptavidin to monolayer coverage, and ultimately the addition of HA-*g*-Lac (as a control) or (HA-*g*-Lac)-biotin. Abbreviations: B - working buffer (HBS; HEPES 10 mM, NaCl 150 mM, pH 7.4), SUVs – small unilamellar vesicles (DOPC:DOPE-CAP-B 95:5 (mol:mol)) , SAv – Streptavidin, S – sample: HA-*g*-Lac or (HA-*g*-Lac)-biotin. Arrows atop the graph indicate the start of incubation with each – samples as indicated. Incubation conditions: B-SUVs – 50 µg/mL, SAv – 20 µg/mL, S – 20 µg/mL. All solutions were prepared in working buffer ((HBS; HEPES 10 mM, NaCl 150 mM, pH 7.4)

Taken together, these results were really promising because they confirmed successful anchorage of the newly synthesised glycopolymers, and successful formation of SLB-anchored glycopolymer brushes as model glycocalyces.

Once (HA-*g*-Lac)-Biotin **5.2** (Figure 5.6, line with circle symbols) was tested, the remaining glycopolymers with a biotin at the reducing end, including HA-Biotin **5.1** (200-500 kDa) (Figure 5.6, lines with triangle symbols), (HA-*g*-Le^x)-Biotin **5.3** (Figure 5.6, lines with diamond symbols) and (HA-*g*-Gb_3)-Biotin **5.4** (Figure 5.6, lines with square symbols) were also checked for their binding on a SAv-on-SLB anchor surface by QCM-D. While there was no binding for the unbiotinylated glycopolymers (Data showed in Chapter 9, Section 9.2), all the mucin-like structures containing the biotin at the reducing end were successfully and stably attached to the SAv monolayer surface, evidencing the strong and specific binding *via* SAv/biotin bonds.

For the glycopolymers **5.2**, **5.3** and **5.4**, a dense brush similar to the glycocalyx was achieved while **5.1** (200-500 kDa) did not form a dense film due to contamination of the sample with free biotin. As it can be observed in Figure 5.6, lines with triangle symbols, there was binding between SAv and **5.1** (200-500 kDa) until 87 min. However, once it was performed the step of rinsing with working buffer, there was not any change on the surface neither in ΔF or ΔD. If there was steric hindrance between chains in this film, once the rinsing step was being performed, **5.1** chains would have rearranged realising extra material from the surface and these changes would have been recorded by ΔF or ΔD, a slight increase for frequency shift and minor increase for dissipation shift. A more in-depth characterization of these films will be undertaken in section 5.4 in this chapter. However, as it can be observed by the increase in the dissipation shift (from around 7 to 12 $\times$ 10^{-6} depending on the sample), the derivatized hyaluronic acid with oligosaccharides generally created a soft and dense film similar to the glycocalyx but with well-defined structures.

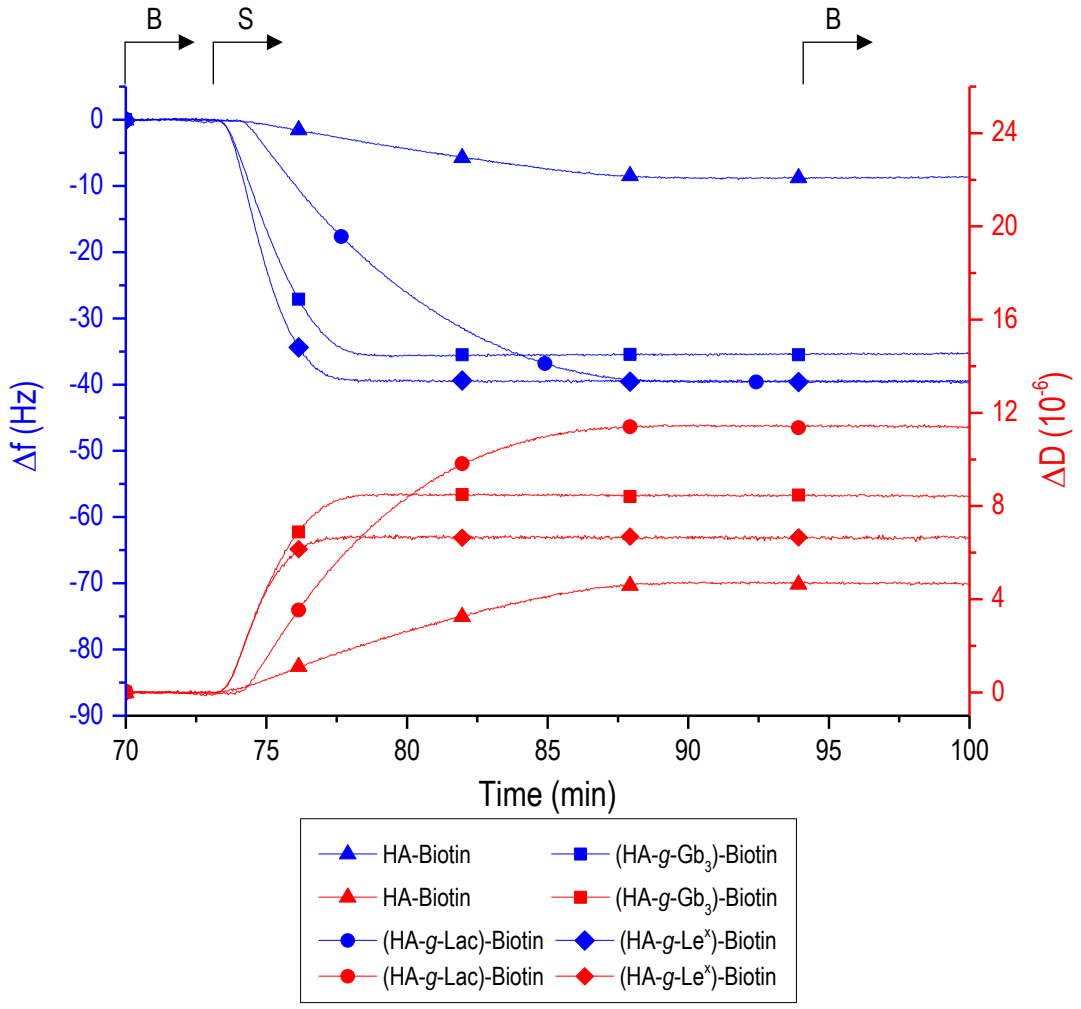

Figure 5.6: QCM-D data demonstrating successful incorporation of the biotinylated glycopolymers on a SAv-on-SLB surface. This surface was built as the one described in Figure 5.1 but it is not shown. Shown (as lines with symbols) are data for the addition of HA-Biotin (**5.1**, 200-500 kDa) (line with triangle symbols), (HA-*g*-Lac)-Biotin (**5.2**) (line with circle symbols), (HA-*g*-Le^x)-Biotin (**5.3**) (line with diamond symbols) and (HA-*g*-Gb_3)-Biotin (**5.4**) (line with square symbols). Abbreviations: B - working buffer (HEPES 10 mM, NaCl 150 mM, pH 7.4), S – samples: **5.1** (200-500 kDa), **5.2**, **5.3** and **5.4**. Arrows atop the graph indicate the start of incubation with each –samples as indicated. Incubation conditions: S – 20 µg/mL. All solutions were prepared in working buffer ((HBS; HEPES 10 mM, NaCl 150 mM, pH 7.4)

In summary, it was concluded that polymers **5.1**, **5.2**, **5.3** and **5.4** were building blocks suitable to construct a glycocalyx model as they accomplish the following requirements: they could be anchored *via* the stable binding between SAv and the biotin on the glycopolymers.

5.3.2 Constructing glycocalyx models using glycopolymers derivatized with a His-tag

Even though the biotinylated glycopolymers were good building blocks for a glycocalyx model, the constitution of the SAv monolayer was not alike the endothelial cell membrane, formed by lipids

(including glycolipids and phospholipids) and some proteins and glycoproteins as well).[271] Moreover, to create a dense film it is required a saturated surface of streptavidin not allowing to add glycolipids accessible for the lectins because these would be blocked by the SAv monolayer. On the other hand, the use of Ni^{2+}-NTA glycolipids gives the chance to achieve a model similar to the cell glycocalyx, in terms of components, but using well-defined structures: glycolipids in the surface and a dense brush of mucin-like structures.

Aiming for models that combine two types of glycan structures, glycolipids and glycopolymers, it was checked by QCM-D if the mucin-like structures with a poly-histidine tag at the reducing end were suitable for anchorage to SLBs. SUVs for SLB formation contained 5 mol-% of chelator lipids (monitor) along with inert DOPC lipids. HBS was again used as working buffer to but supplemented with 2 mM $NiCl_2$ during the SLB formation process to load the NTA with nickel ions and facilitate the SUV binding and rupture.[259]

The SLB formation process as monitored by QCM-D is shown in Figure 5.7. As for the biotinylated SUVs, the NTA-presenting SUVs showed the two-phase response in ΔF and ΔD characteristic for adhesion and subsequent rupture and spreading of SUVs. Final responses were ΔF = -28 Hz and ΔD = 0.1 $\times$ 10^{-6}, consistent with an SLB of high quality (i.e., with few residual intact SUVs remaining). Moreover, there was no change of ΔF or ΔD upon rinsing in buffer, demonstrating the SLB was stable under flow, as desired.

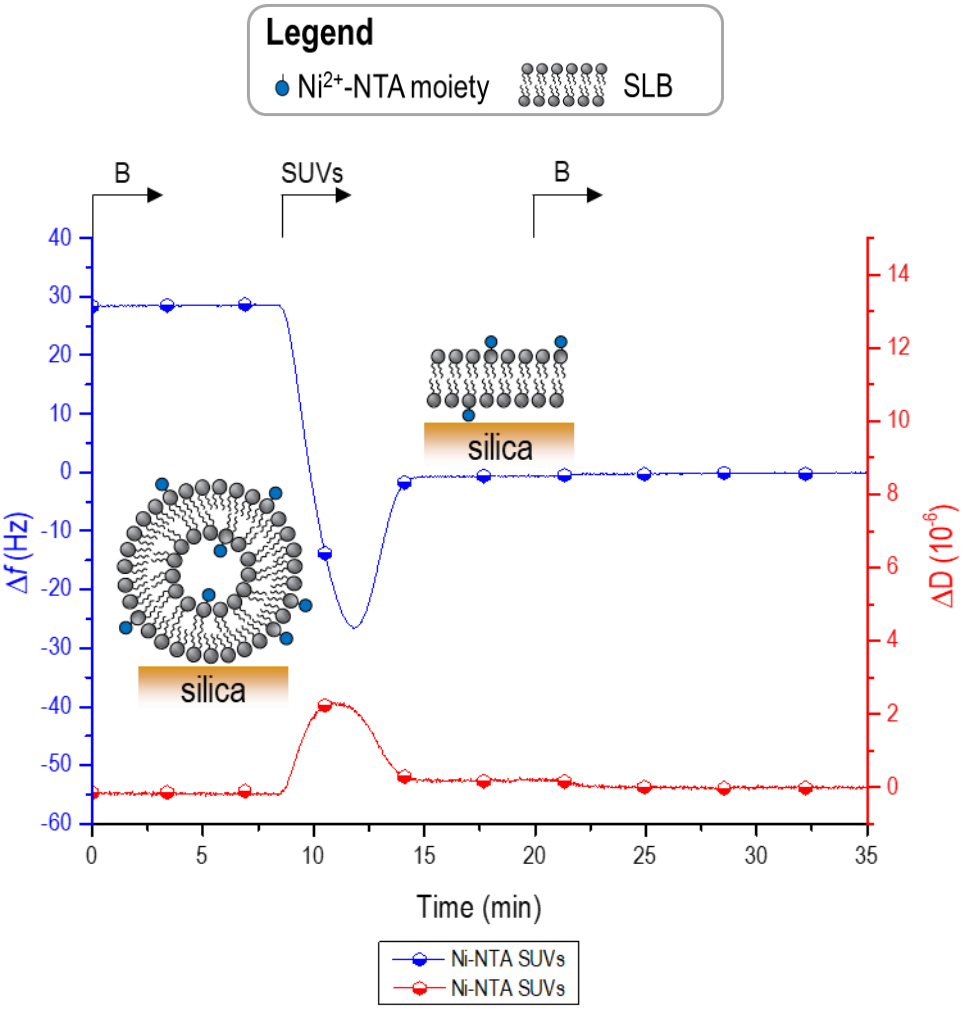

Figure 5.7: Formation of Ni^{2+}-NTA presenting SLB recorded by QCM-D. Abbreviations: B - working buffer (HEPES 10 mM, NaCl 150 mM, pH 7.4), SUVs – small unilamellar vesicles (Ni^{2+}-NTA DODA: DOPC lipids 95:5 (mol:mol). Arrows atop the graph indicate the start of incubation with each –samples as indicated. Incubation conditions: SUVs – 50 µg/mL. The solution was prepared in working buffer (HBS; HEPES 10 mM, NaCl 150 mM, pH 7.4)

The Ni^{2+}-NTA presenting SLBs were used to test for anchorage of: the glycopolymer control **4.6** (Figure 5.8a, lines with triangle symbols) without poly-histidine tag, the poly-histidine peptide **5.5** (Figure 5.8b, lines with hexagon symbols), and the poly-histidine tagged glycopolymer **5.6** (Figure 5.8b, lines with star symbols). The control glycopolymer without tag did not show any response in ΔF or ΔD (Figure 5.8a, from 43 to 90 min), while for the tagged glycopolymer (Figure 5.8b, lines with star symbols; from 44 to 102 min) there was a strong response in ΔF (a decrease of around 50 Hz) and ΔD (an increase of around 9×10^{-6}), which was stable upon HBS rinsing. These data evidence a stable and specific anchorage via the poly-histidine tag and the Ni^{2+} presented by the NTA-displaying surface. These evidences lead to the conclusion that a film built using (HA-*g*-Gb_3)-

K-W-H_6-NH_2 was soft and dense, as it was indicated by the values in frequency and dissipation shifts, giving as a result a suitable glycocalyx model. The peptide tag itself also gave a clear response in ΔF, although this was much smaller than for the glycopolymer with peptide anchor (Figure 5.8b, lines with hexagon symbols; from 44 to 102 min). From the frequency shift, $\Delta F = -$ 5 Hz, a film thickness of 1 nm can be estimated, which is consistent with the peptides forming a very thin film. The dissipation shift for the peptide film also remained relatively small, $\Delta D \approx 0.5 \times 10^{-6}$, consistent with a more rigid film being formed. These results also provided good conclusions: only structures containing the poly-histidine could bind to the Ni^{2+}-NTA supported lipid bilayer and they were stable over time meaning that, even though the flexibility of the SLB, once the structures were anchored, they were not removed.

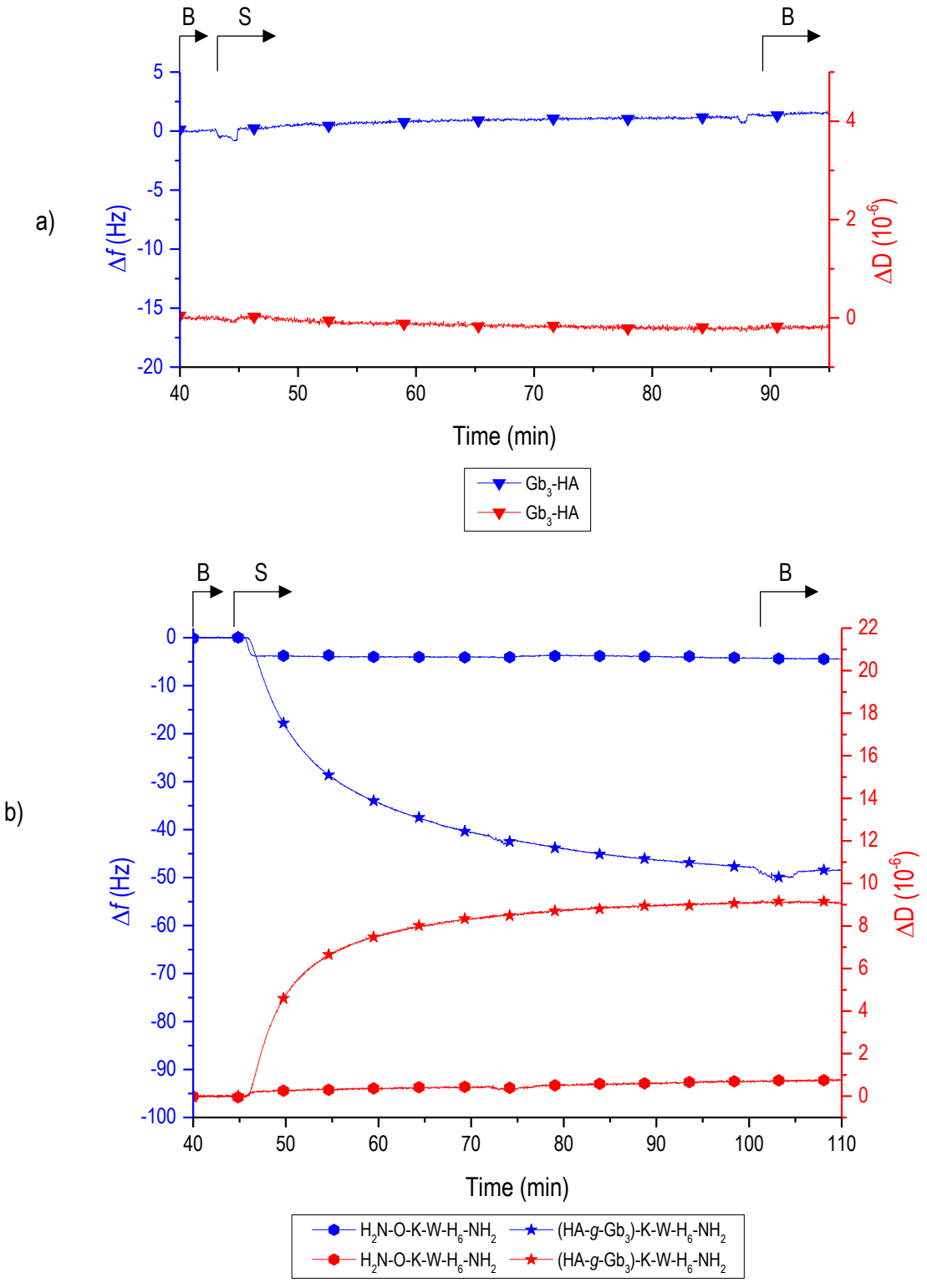

Figure 5.8. (a) QCM-D measurements demonstrating the absence of non-specific interactions between HA-*g*-Gb_3 and a Ni^{2+}-NTA -presenting SLB. Shown are data for the addition of HA-*g*-Gb_3 **4.6** (line with down triangle symbols). (b) QCM-D measurements demonstrating successful incorporation of the poly-histidine derivatized polymers in a biosensor surface. Shown are data for the addition of H_2N-O-K-W-H_6-NH_2 **5.5** (line with hexagon symbols) and (HA-*g*-Gb_3)-K-W-H_6-NH_2 **5.6** (line with star symbols). Abbreviations: B -working

buffer (HEPES 10 mM, NaCl 150 mM, pH 7.4), S - **4.6**, **5.5** and **5.6**. Arrows atop the graph indicate the start of incubation with each –samples as indicated. Incubation conditions: S – 20 μg/mL. All solutions were prepared in working buffer (HBS; HEPES 10 mM, NaCl 150 mM, pH 7.4).

These promising data indicate that structures like (HA-*g*-Gb_3)-Lys-Trp-His_6-NH_2, glycopolymers derivatized with a poly-histidine, are suitable to build a glycocalyx models.

5.4 Characterization of the size of glycopolymers in glycocalyx models

Having established successful anchorage of the mucin-like structures to different surfaces, the next goal was to characterise the average size of the glycopolymers, and the grafting density of glycopolymers. QCM-D and SEC-MALS were used to analyse the glycopolymer size on the surface and in solution, respectively, and SE was used to quantify the glycopolymer surface density.

5.4.1 Glycopolymer size characterization by QCM-D and SEC-MALS

The dissipation and frequency responses, as measured by QCM-D, provide information about the size of the polymer attached to the surface, as first described for DNA by Tsortos *et al.*[272] and later for HA (and other glycosaminoglycans) by Srimasorn *et al.*[273] Srimasorn *et al.* demonstrated that the $\Delta D/-\Delta f$ ratio increases monotonically yet non-linearly with HA size. Three different non-linear functions were established to serve as calibration curves for three overtones (i = 3, 5 and 7), which can be used to estimate the effective mean size of HA (and other glycosaminoglycans) that are end-grafted to a surface. The calibration curves provide the number of disaccharides in the linear hyaluronan chains, from which the molecular mass of the HA sample can be computed (1 HA disaccharide has a molecular mass of 400 Da).

Assuming that mucin-like structures behave as plain HA chains, the contour length of the glycopolymers could be estimated using the QCM-D based method (including the non-linear standard curves) established by Srimasorn *et al*. This assumption is based on the idea that the backbone of the glycopolymer is hyaluronan and that the molecules attached on HA were also carbohydrates, which had similar in hydrophilicity than the disaccharide of the polymer, and their volume were small.

The size obtained by this QCM-D based is a measure of the mean glycopolymer size when attached on the surface, and can be compared with the size determined by SEC-MALS analysis for the glycopolymer in solution. Ideally, the sizes measured by QCM-D and SEC-MALS should be equal. Previous work by Srimasorn *et al* demonstrated, however, that for GAGs with a high degree of dispersity, the mean chain length on the surface tends to be inferior to the mean chain length in solution, owing to preferential binding of shorter chains. Aiming to have a better understanding of

the size of the mucin-like structures in the glycocalyx model, the QCM-D and SEC-MALS analyses were applied to the newly synthesised glycopolymers.

The first step towards applying the method by Srimasorn *et al.* was to establish parametric plots of $\Delta D/-\Delta F$, a measure of the film softness, against -ΔF, a measure of the glycopolymer coverage on the surface, from the QCM-D data for glycopolymer binding. These data are shown in Figure 5.5 for biotinylated HA (HA-Biotin **5.1** (both 200-500 kDa and 40-50 kDa) and HA derivatives (HA-*g*-Lac)-Biotin **5.2**, (HA-*g*-Le^x)-Biotin **5.3** and (HA-*g*-Gb$_3$)-Biotin **5.4**).

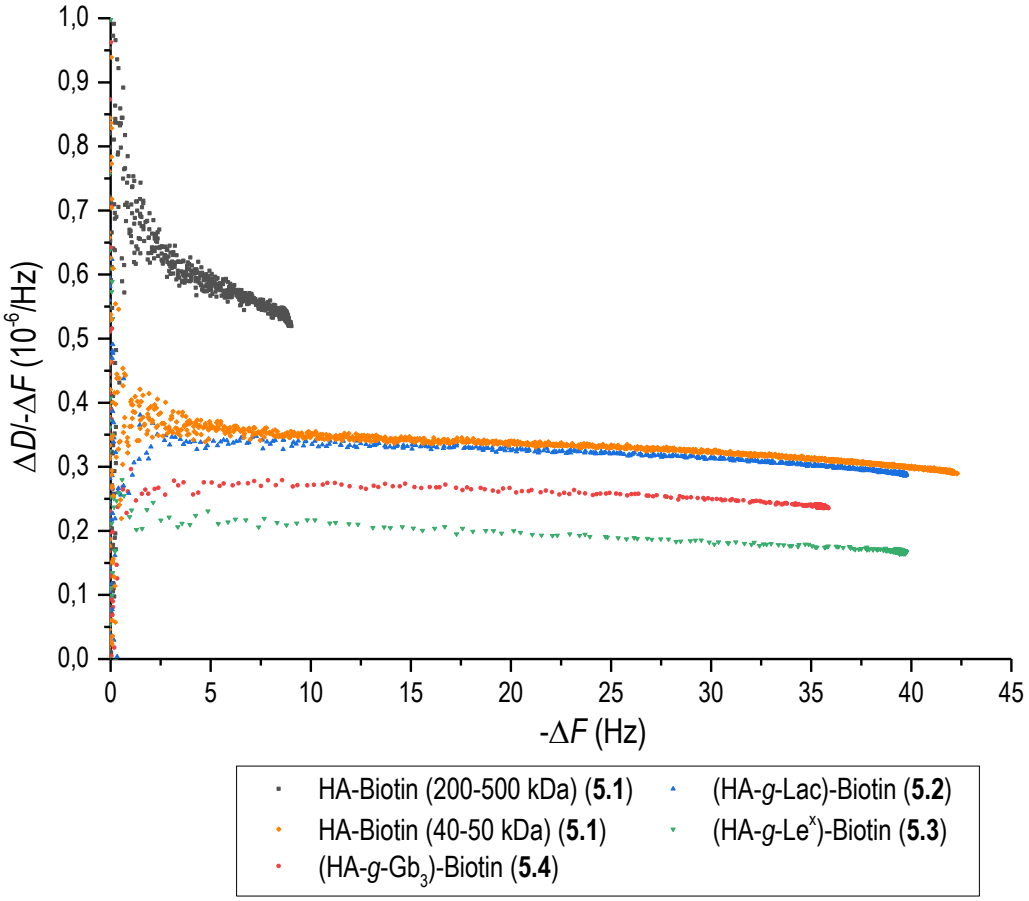

Graph 5.1: Parametric plot of $\Delta D/-\Delta F$ against -ΔF for the formation of films of **5.1** (both 200-500 kDa (Figure 5.2) and 40-50 kDa (Graph 9.3, Chapter 9), **5.2** (Figure 5.2), **5.3** (Figure 5.2) and **5.4** (Figure 5.2).

The parametric plot discriminates quite well by their size the different glycopolymers. At a given $-\Delta F$ value, a larger polymers is expected to have larger $\Delta D/-\Delta F$ values, and a smaller polymers a comparatively smaller $\Delta D/-\Delta F$ value. This first qualitative analysis identifies the plain HA-biotin (200-500 kDa) as being the largest, and the (HA-*g*-Lac)-biotin as having a size comparable to HA-biotin (40-50 kDa), with (HA-*g*-Gb$_3$)-biotin being smaller and (HA-*g*-Le^x)-biotin smaller still. As a first conclusion, all the carbohydrate-derivatised HA were quite small compared to the starting HA material used to make them (200-500 kDa).

Srimasorn *et al.* considered the $\Delta D/-\Delta F$ ratio at $-\Delta F$ = 2.5 Hz for further quantitative analysis of polymer length. It is important to mention that this approach was established for glycosaminoglycans, including pure HA, but it was unknown if HA-based mucin-like structures (i.e., with side chains) could also be analysed with this method.[273] The relationship between the $\Delta D/-\Delta F$ ratio and the polymer length (expressed in number of disaccharides n_{ds}) for the fifth overtone is:[273]

$$n_{\mathrm{ds}} = \frac{\Delta D}{-\Delta f} \Big/ \frac{10^{-6}}{\mathrm{Hz}} \times \left(37.15 \frac{\mathrm{Hz}}{10^{-6}} \cdot \frac{\Delta D}{-\Delta f} + 23.83\right) \times \left(\frac{12.53 + \left(3.259 \frac{\mathrm{Hz}}{10^{-6}} \cdot \frac{\Delta D}{-\Delta f}\right)^{-6.775}}{1 + \left(3.259 \frac{\mathrm{Hz}}{10^{-6}} \cdot \frac{\Delta D}{-\Delta f}\right)^{-6.775}}\right) \quad (5.8)$$

The results of this analysis are reported in Graph 5.2, and confirm the deduced size trend. It is notable that the spread in apparent glycopolymer length is quite large, with the values for (HA-*g*-Le^x)-Biotin and (HA-*g*-Gb$_3$)-Biotin being, respectively, 22 and 10 times smaller than the HA (200-500 kDa) starting material, consistent with a high degree of degradation as already discussed in Chapter 4.

To confirm the robustness of the glycopolymer size estimation, the QCM-D analysis was performed not only for the 5th overtone, but also for overtones 3 and 7. Details are presented in Chapter 7, Section 7.9.2, and only the final results are reported in Graph 7.1 and Graph 7.2. The three overtones generally produced consistent results (within the experimental error). One exception is the HA (200-500 kDa) polymer where the 3rd overtone generated a marginally large glycopolymer length. Overall, these data confirm robust length estimation.

The calculation of n_{ds} by SEC-MALS data (Chapter 9, Section 9.1) followed the formula:

$$n_{ds} = \frac{M_{w(\mathrm{glycopolymer})}}{(1 - \%\ \mathrm{carbohydrate}) \times M_{w(\mathrm{HA\ disaccharide})} + \%\ \mathrm{carbohydrate} \times M_{w(\mathrm{HA-carbohydrate})}} \quad (5.9)$$

with $M_{w(\mathrm{glycopolymer})}$ being the mass of the glycopolymer measured by SEC-MALS, % carbohydrate the degree of substitution calculated by ^{1}H NMR, $M_{w(\mathrm{HA\ disaccharide})}$ = 0.378 kDa the mass of a hyaluronan disaccharide and $M_{w(\mathrm{HA\text{-}carbohydrate})}$ the mass of a HA disaccharide unit with the carbohydrate side chain attached. SEC-MALS also provided the Đ, which provided an idea of the size dispersion in each sample. It is important to highlight that glycopolymers without biotin or poly-histidine were analysed by SEC-MALS after checking that the addition of these tags did not change the length of the chains.

Having analysed the effective mean length of the surface-anchored glycopolymer chains (by QCM-D), it was interesting to see how these results compare with the mean length of the free

glycopolymer chains in the solutions that were used for surface anchorage, as determined by SEC-MALS. These data are also reported in Graph 5.2.

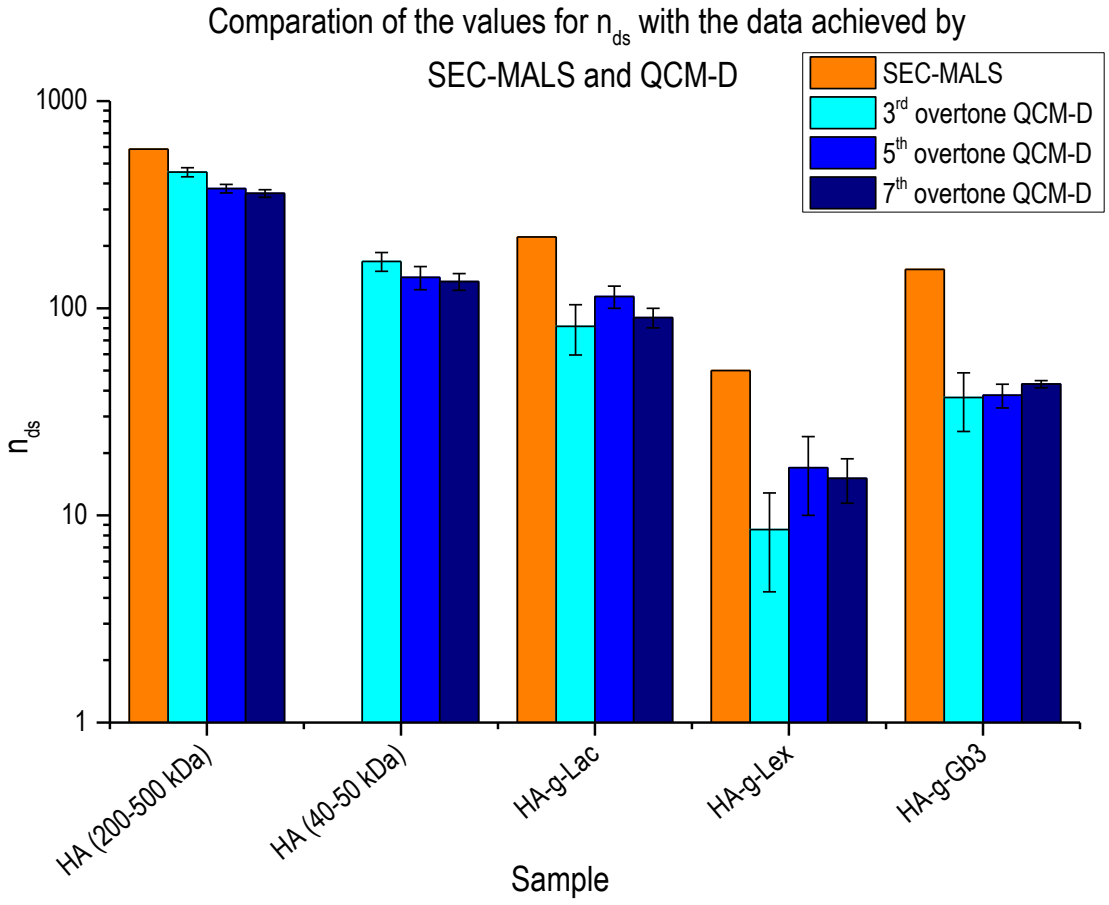

Graph 5.2: Bar plot for the mean number of disaccharides n_{ds}, represented in logarithmic scale, in the HA backbone according SEC-MALS analysis (orange) and QCM-D analysis (for overtones 3, light blue, 5, blue, and 7, dark blue). For plain HA, a size range of 200–500 kDa would correspond to n_{ds}= 300-1250, and a size range of 40-50 kDa to n_{ds} = 100-120. The SEC-MALS data for plain HA (40-50 kDa) was not available. Mean values were calculated as the average and error bars as the standard deviation of values for QCMD.

The glycopolymer lengths reported by QCM-D vs. SEC-MALS differed quite substantially: values obtained by QCM-D tended to be smaller than those obtained by SEC-MALS. The difference was particularly large for (HA-*g*-Le^x)-Biotin and (HA-*g*-Gb$_3$)-Biotin. On the other hand, (HA-*g*-Lac)-Biotin and HA-Biotin showed results in the similar range, not the same numbers but without relatively big changes.[270]

The differences in the results shown in Graph 5.2 could be due to several reasons: the first to take into consideration were the analytical properties of both techniques. While the M_w achieved by SEC-MALS, the samples were in solution forming random coils, for the QCM-D the samples were attach to a surface and factors such as steric hindrance or the selectivity for small polymer

from the surface could easily divert the final results to low values. Another aspect to highlight was the nature of the samples here analysed. Even though these glycopolymers had a hyaluronan backbone, they had been modified with carbohydrates attached through a triazole, and these modifications might change the behaviour of the polymer as well as the conformation that they formed once attached to the surface. Nevertheless, using both techniques the glycopolymers could be analysed properly either in solution or in a surface. The results using both techniques were in similar range but different in absolute value for each sample and provided an average for the contour length of the mucin-like structures in the models created.

5.4.2 Calculation of areal mass density and thickness of the film by SE

SE was used to characterise the glycopolymer surface density and the thickness of the model glycocalyx films. Figure 5.9a provides a representative dataset, obtained for glycopolymer (HA-*g*-Le^x)-Biotin, as an example, while Figure 5.5b showed the dataset for **5.6**. The sample incubation steps were the same as for the QCM-D assay for both types of assemblies tested: SAv-on-SLB or Ni^{2+}-NTA SLB. For the biotinylated structures (Figure 5.9a), SE experiments started by the addition of biotinylated SUVs for supported lipid bilayer formation (Figure 5.9a, ①), followed by streptavidin to form a SAv monolayer (Figure 5.9a, ②), and the biotinylated glycopolymer of choice to form a model glycocalyx (Figure 5.9a, ③). On the other hand, SE experiment for (HA-*g*-Gb_3)-K-W-H_6-NH_2 began with the incubation of Ni^{2+}-NTA SUVs (Figure 5.9b, ①) followed by the addition of the glycopolymer derivatized with a His-tag (Figure 5.9b, ③). Incubation conditions were essentially as established by QCM-D, though the times of sample incubation were longer to ensure full saturation/equilibration of the binding steps.

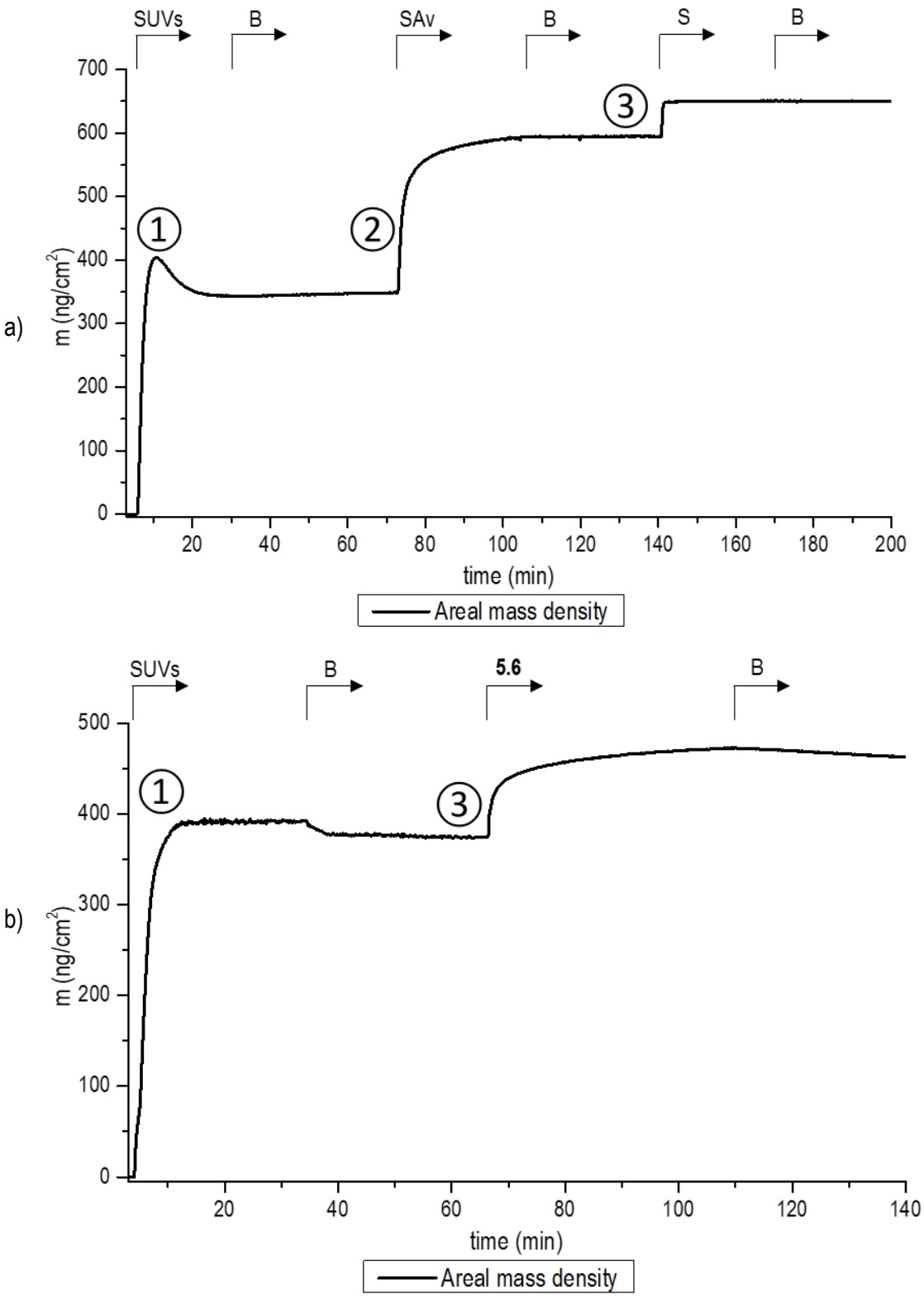

Figure 5.9. Graph of areal mass density against time (a) for the formation of a biotinylated SLB, and the following incubation of SAv to form a monolayer and the addition of the glycopolymer (b) for the formation of Ni^{2+}-NTA SLB following by the incubation of (HA-*g*-Gb_3)-K-W-H_6-NH_2. Abbreviations: B - working buffer (HBS; HEPES 10 mM, NaCl 150 mM, pH 7.4), SUVs – small unilamellar vesicles (DOPC:DOPE-CAP-B 95:5 (mol:mol)) or (Ni^{2+}-NTA DODA: DOPC lipids 95:5 (mol:mol)), SAv – Streptavidin, S – sample: (HA-*g*-Le^x)-

Biotin, **5.6** – (HA-*g*-Gb_3)-K-W-H_6-NH_2. Arrows atop the graph indicate the start of incubation with each – samples as indicated. All solutions were prepared in working buffer (HBS; HEPES 10 mM, NaCl 150 mM, pH 7.4).

Different parameters including the thickness d, areal mass density m and the molar surface density (just for SAv (Γ_{SAv})) were analysed for the formation of the SLBs, both biotinylated or Ni^{2+}-NTA, and the subsequent SAv monolayer in SE experiments. The results of these analyses are reported in Table 5.1

Table 5.1: SE results for the glycopolymers for the formation of biotynilated SLB (B-SLB, entry one), SAv monolayer (entry 2) and Ni^{2+}-NTA SLB (entry three).

Sample	m (ng·cm^{-2})	*d* (nm)	M_w (kDa)	Γ_{SAv} (pmol·cm^{-2})
B-SLB	359.7 ± 0.8	7.9 ± 0.2	-	-
SAv	213.3 ± 1.1	4.4 ± 0.1	60	3.5 ± 0.0
Ni^{2+}-NTA SLB	374.0 ± 0.4	9.1 ± 0.1	-	-

The data achieved for the analysis of the SLB-on-SAv surfaces revealed lower Γ_{SAv} than the one reported by Dubacheva *et al.*,[263] being more precise, 1 pmol/cm^2 less than the values provided by Richter and co-workers.[263] The differences between the values achieved in this project and the ones described in the literature could be due to different reasons including short time of incubation of SAv or the quality of the biotinylated SUVs used, in terms of percentage of biotin. The values for both SLB were similar providing reliable data about the good formation of this layer.

Three glycopolymers were analysed for their thickness d and areal mass density m by SE: the biotinylated **5.3** and **5.4** on a SAv monolayer, and the polyhistidine-tagged **5.6** on a Ni^{2+}-NTA SLB. Table 5.2 reports the properties of the fully formed glycopolymer films.

Table 5.2: SE results for the glycopolymers (HA-*g*-Le^x)-Biotin **5.3** and (HA-*g*-Gb_3)-Biotin **5.4** on a SAv-on-SLB surface, and for (HA-*g*-Gb_3)-K-W-H_6-NH_2 **5.6** on a Ni^{2+}-NTA SLB. DS (column 2) corresponds to the degree of substitution calculated by ^{1}H NMR

Sample	DS	m (ng·cm^{-2})	*d* (nm)	$M_{w,\ gpip}$ (kDa)	Γ_{glycan} (pmol·cm^{-2})	c_{glycan} (mM)
5.3*	32%	66.1 ± 0.4	-	1.831	36.1 ± 0.1	-
5.4	35%	65.5 ± 0.2	10.4 ± 0.7	1.717	38.2 ± 0.1	7 ± 1
5.6	35%	87.6 ± 0.3	8.4 ± 0.4	1.717	51.0 ± 0.2	14 ± 5

5.3*: The values for *d* after the fitting the results to the model were not reliable, therefore, the results could not be used for further experiments.

The values for the third column, $M_{w,\mathrm{pgip}}$, refers to the molecular mass per target glycan (Le^x or Gb_3) moiety in the polymer. It is equivalent to the total mass of the glycopolymer divided by the number of target glycans (Le^x or Gb_3) in the polymer, yet can be obtained more straightforwardly from the degree of substitution, DS, as $M_{w,\mathrm{pgip}} = (1/DS - 1)M_{w,\mathrm{HA2}} + M_{w,\mathrm{HA2-der}}$, where $M_{w,\mathrm{HA2}}$ = 378 Da is the molecular mass of a plain HA disaccharide, and $M_{w,\mathrm{HA2-der}}$ is the mass of an HA disaccharide derivatised with the target glycan. The glycan surface density was calculated as $\Gamma_{\mathrm{glycan}} = m/M_{w,\mathrm{pgip}}$, and the glycan concentration in the film as $c_{\mathrm{glycan}} = \Gamma_{\mathrm{glycan}}/d$.

As shown in Table 5.2, similar results for the areal mass density (first column) were achieved for the two biotinylated glycopolymers, (HA-*g*-Le^x)-Biotin and (HA-*g*-Gb_3)-Biotin, while the areal density was approximately 50% higher for the glycopolymer derivatized with the poly-histidine, (HA-*g*-Gb_3)-K-W-H_6-NH_2. These results seemed sensible according the nature of the surface used to attach the mucin-like structures. Because the number of binding sites in SAv, no more than two glycopolymers per protein could be attached providing similar areal density, however, Ni^{2+}-NTA SLB provided a full surface where **5.6** could be anchored with the only impediment of steric hindrance and electrostatic charge between polymers. For this reason, the areal density for the **5.6** was higher than **5.3** or **5.4**.

As a conclusion, SE experiments provided information about the glycan density of the glycopolymer films created with the different anchorage systems (SAv monolayer or Ni^{2+}-NTA SLB) giving similar results for biotinylated glycopolymers and a denser film for the poly-histidine derivatized polymer. Finally, it was also possible to estimate the concentration of glycan epitopes in the film containing Gb_3, useful for the binding studies with lectins.

5.5 Toxin interaction with the glycocalyx models

Having established the preparation glycocalyx models, and characterised their thickness and target glycan density, the next step was to validate that these structures interact with the target toxins, CTB and STxB.

Shiga Toxin is known to contain 15 binding sites in its B subunit that recognize Gb_3 ceramide. The K_d for the monovalent interaction of an individual Gb_3 moiety with STxB is about 1 mM. The study of STxB in an environment alike glycocalyx has not been done yet. However, due to the multivalency of this protein, it is expected to show higher affinity for multivalent structures.[67,99] With the here established glycocalyx models, the glycans are presented in a defined organisation and

with controlled density. This now enables quantitative analysis of the effect of such presentation on the avidity and specificity of toxin binding. As illustrated before, QCM-D offers a really good set up to monitor the formation of a glycocalyx model forming a dense brush of glycopolymers attached in a surface as well as to record any binding with proteins to the film created. The incubation of the lectin of interest, in this case the STxB, in these films could provide key information about how this toxin interact with the glycocalyx including the minimum density of glycan required for binding with the protein on the film.

On the other hand, B subunit of Cholera Toxin contains two different binding sites, the primary binding site which binds strongly to GM_1 ganglioside, and the secondary binding site which can bind H-Le^y or Le^x.[34,73] However, it is unknown how CTB interacts with the glycocalyx of the endothelial cells. Aiming to achieve better and more information about the approach of CTB when there is the first interaction with the glycocalyx, QCM-D experiments were performed. The goal was to create a model similar to the glycocalyx, a dense film of glycopolymers big enough to make a brush where proteins could get trapped inside.

5.5.1 STxB binding to glycocalyx models presenting Gb_3

Initial experiments aimed to establish the specific binding of STxB in glycocalyx models presenting Gb_3. Two different aspects were the first to check: the non-specific binding of STxB (either a SAv monolayer, or a Ni^{2+}-NTA presenting SLB) and the recognition of this protein for at least one mucin-like structure with Gb_3.

Tests started with the SAv monolayer based platform, by QCM-D. In a set of two parallel experiments, STxB binding to a (HA-*g*-Gb_3)-Biotin film (Figure 5.10, lines with square symbols) was compared with STxB binding to a bare SAv monolayer (Figure 5.10, lines with triangle symbols). The QCM-D frequency and dissipation shifts confirmed that glycopolymer **5.6** was successfully anchored to the SAv monolayer. The responses at saturation (ΔF = -35 Hz and ΔD = 8 $\times 10^{-6}$) were not quite as high as reported in Figure 5.6, suggesting that there was some biotin contamination in this batch of biotinylated glycopolymer that limited the surface density; however, this was not a concern for the present assay. After rinsing the reminding (HA-*g*-Gb_3)-Biotin, a first incubation of STxB (0.4 μM) was performed in both experiments (Figure 5.10, 110-130 min). Whilst there was no measurable response for the plain SAv monolayer experiment (lines with triangle symbols), there was a clear decrease in ΔF, around -7 Hz, as well as an increase in ΔD, by 1×10^{-6}, for the Gb_3 containing model glycocalyx (lines with quare symbols), confirming specific recognition of the glycocalyx. After rinsing the protein from both systems, a second incubation of STxB (2 μM) was performed (Figure 5.10, 150-170 min). The results were the same than the

previous protein incubation but different in magnitude: the experiment containing (HA-*g*-Gb_3)-Biotin showed a steep decrease in in ΔF (-17 Hz), lower than the previous protein incubation (-7 Hz, Figure 5.10), and a similar increase in ΔD as the previous incubation (1 $\times 10^{-6}$). In addition, the binding between mucin-like analogue and protein was reversible as the protein was rinsed without issues while buffer was passing through the film. For the experiment without glycopolymer, again there was not response neither in ΔF and ΔD showing more and better evidences that STxB and the SAv monolayer did not bind non-specifically.

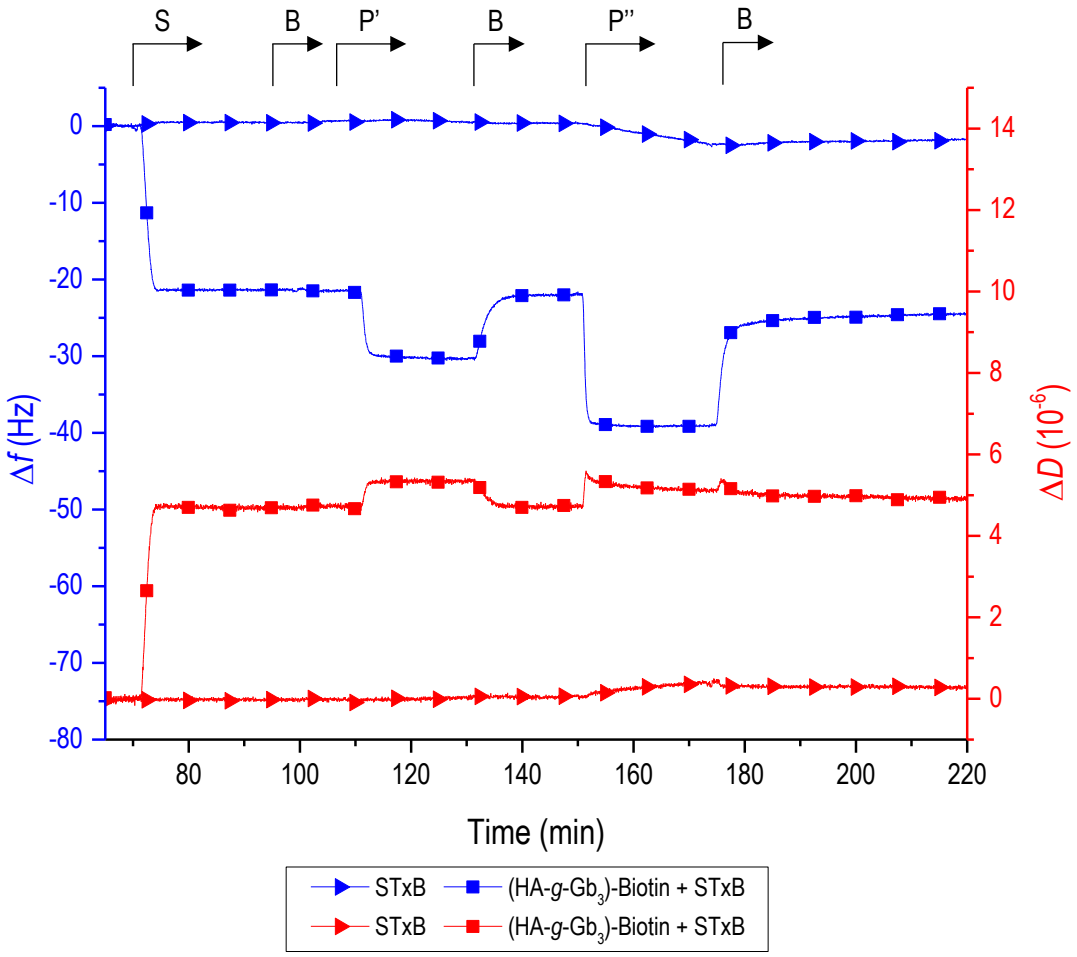

Figure 5.10: QCM-D measurements demonstrating specific binding of STxB in a Gb_3 presenting model glycocalyx. Shown are data for the addition **5.4** (lines with square symbols) + STxB and just the protein by itself (right triangle). Abbreviations: B -working buffer (HBS 10 mM, NaCl 150 mM, pH 7.4), S -**5.4**, P'- STxB, P'' – STxB. Arrows atop the graph indicate the start of incubation with each –samples as indicated. Incubation conditions: S – 20 µg/mL, P' – 0.4 µM and P'' – 2 µM. All solutions were prepared in working buffer (HBS; HEPES 10 mM, NaCl 150 mM, pH 7.4).

The results for this preliminary experiment were really promising: first of all, STxB did not show binding with the SAv monolayer meaning that any decrease in frequency shift or increase in

dissipation shift recorded on QCM-D experiment was due to the binding between this lectin and the glycopolymers. Moreover, even though the K_d for one binding site of STxB and Gb_3 oligosaccharide is high (2 mM), there was clear binding between **5.4** and STxB at a much low concentration of the lectin presumably because the multibinding interaction.

In order to verify that the binding shown in the previous experiment was because of the recognition of Gb_3 oligosaccharide by STxB and not because of non-specific binding between any glycopolymer and the lectin, another experiment was performed. In this case, all the biotinylated glycopolymers were incubated in different chambers followed by the incubation of STxB (Figure 5.11).

In four experiments where biotinylated SLB and SAv monolayer were already set up successfully, HA-Biotin **5.1** (40-50 kDa, Figure 5.11, lines with triangle symbol), (HA-*g*-Lac)-Biotin **5.2** (Figure 5.11, lines with circle symbol), (HA-*g*-Le^x)-Biotin **5.3** (Figure 5.11, lines with diamond symbol) and (HA-*g*-Gb_3)-Biotin **5.4** (Figure 5.11, lines with square symbol) were incubated. The decrease in ΔF as well as the increase in ΔD had the values expected as Figure 5.6 providing convincing data about the full saturation of the surfaces with these structures. After rinsing any possible glycopolymer left in the solution, incubations with STxB (0.4 μM and 2 μM) were performed. As it is shown in Figure 5.11, from 135 to 150 min and from 160 to 176 min respectively, only (HA-*g*-Gb_3)-Biotin (Figure 5.11, lines with square symbol) showed some reversible binding with the lectin because there were steep decreases in ΔF and a slight increase in ΔD for the second lectin incubation. These results seemed to indicate for the differences in the frequency shift. Higher as the concentration of the protein increased, that there was a dependent relationship between STxB concentration and the binding in the film. The other three glycopolymers did not show any response.

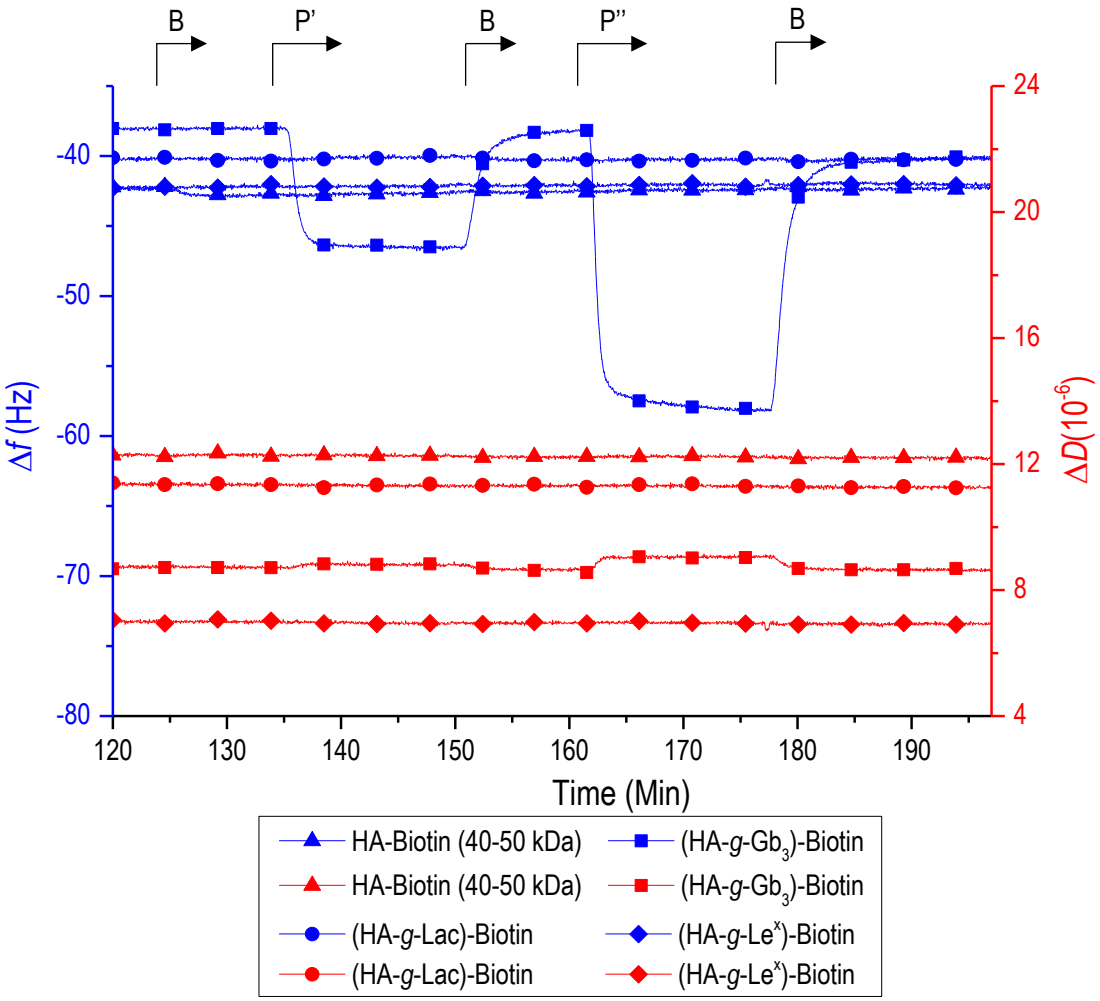

Figure 5.11: QCM-D measurements demonstrating successful interaction between a glycopolymer containing Gb_3 oligosaccharide and STxB no interaction between glycopolymers without Gb_3 oligosaccharide and STxB once all the films were built. Shown are data for the productive interaction between (HA-*g*-Gb_3)-Biotin **5.4** (line with square symbol) and STxB and the lack of interaction of STxB with HA-Biotin **5.1** (line with triangle symbol), (HA-*g*-Lac)-Biotin **5.2** (line with circle symbol) and (HA-*g*-Le^x)-Biotin **5.3** (line with diamond symbol). Abbreviations: B -working buffer (HBS 10 mM, NaCl 150 mM, P'- STxB, P'' – STxB. Arrows atop the graph indicate the start of incubation with each sample as indicated. Incubation conditions: P' – 0.4 μM and P'' – 2 μM. All solutions were prepared in working buffer (HBS; HEPES 10 mM, NaCl 150 mM, pH 7.4).

For the last preliminary experiment, the SLB was changed: instead of using the biotinylated SUVs and SAv monolayer approach, it was used just the SUVs containing 5 mol-% Ni^{2+}-NTA. However, due to the change of the nature of the surface, it was required to check that STxB did not show any non-specific binding with the Ni^{2+}-NTA SLB.

In order to check this aspect, two QCM-D experiments were performed once the Ni^{2+}-NTA SLB was set up successfully as the frequency and dissipation shift were similar, -28 Hz and 0.1 $\times 10^{-6}$

to the previous experiment in Figure 5.7. As it can be shown in the control experiment in Figure 5.12 (line with right triangle symbols, 90-110 min and 120-140 min), STxB did not interact with the chelator surface meaning that there was not any non-specific binding between Ni^{2+}-NTA lipids and the lectin. On the second experiment, after successfully created the Ni^{2+}-NTA SLB surface, (HA-*g*-Gb_3)-Lys-Trp-His_6-NH_2 was incubated (Figure 5.12, line with start symbols, 35-77 min) creating a dense glycopolymer brush containing Gb_3 oligosaccharide. Then, incubations with STxB (0.4 μM and 2 μM) were performed (Figure 5.12, line with star symbols, 90-110 min and 120-140 min respectively) showing an immediate response in ΔF (around – 10 Hz and -25 Hz) but none in ΔD.

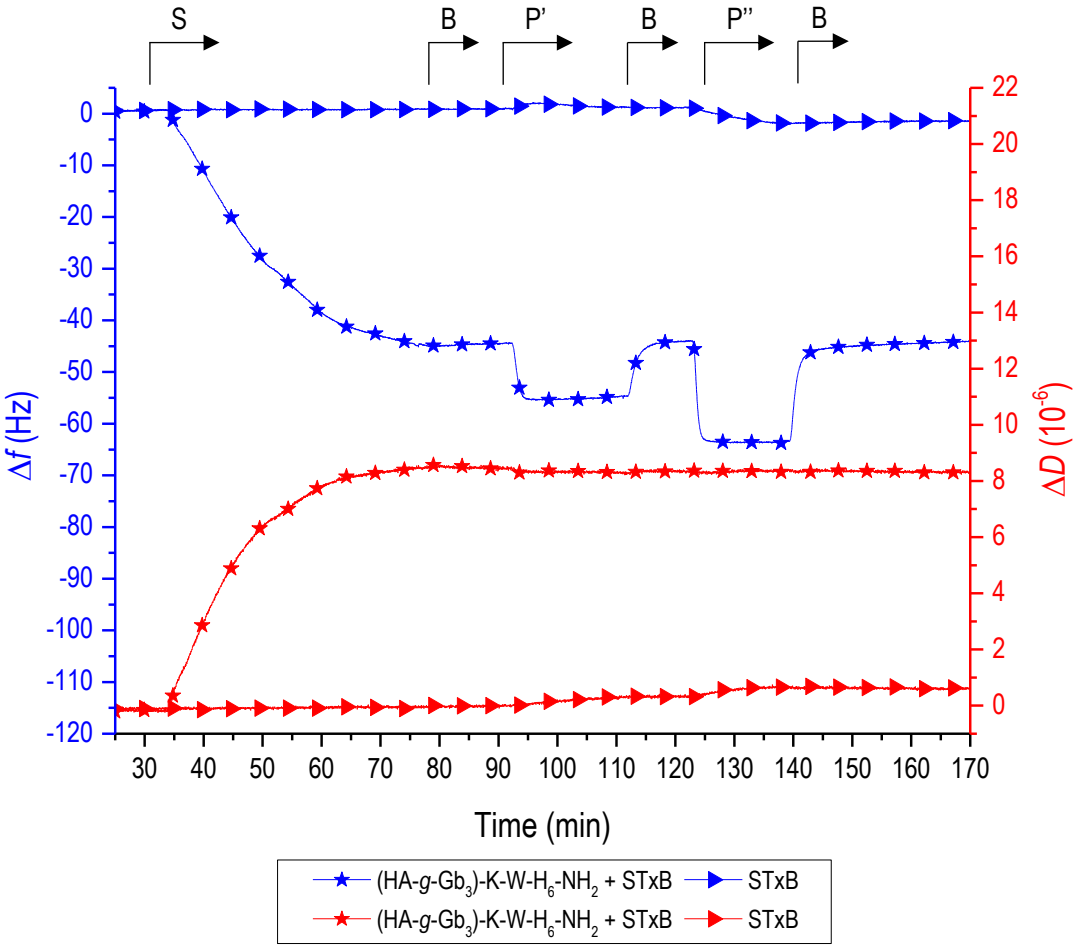

Figure 5.12: QCM-D measurements demonstrating successful interaction between a glycopolymer and STxB and the control for non-specific interaction between Ni^{2+}-NTA SLB and STxB. Shown are data for the addition **5.6** (line with stars symbols) + STxB and just the protein by itself (line with right triangle symbols). Abbreviations: B -working buffer (HEPES 10 mM, NaCl 150 mM, pH 7.4), S - **5.6**, P'- STxB, P'' – STxB. Arrows atop the graph indicate the start of incubation with each sample as indicated. Incubation conditions: **5.6** – 40 μg/mL, P' – 0.4 μM and P'' – 2 μM. All solutions were prepared in working buffer (HBS; HEPES 10 mM, NaCl 150 mM, pH 7.4).

As a conclusion, STxB bound specifically to model glycocalyces presenting Gb_3 oligosaccharides (**5.4** and **5.6**). Binding was reversible and in a lectin concentration dependent manner. Finally, the type of glycopolymer anchorage did not significantly affect STxB binding, except perhaps for subtle impact on film rigidity depending on surface type and glycopolymer surface coverage.

5.5.2 CTB binding to glycocalyx models presenting Le^x

As it was done for STxB, once the synthesis of biotinylated glycopolymers was successful and non-specific binding occurred between derivatized HA and SAv monolayer, it was necessary to ensure that CTB would not show interaction with the SAv-on-SLB or Ni^{2+}-NTA SLB. Moreover, it was also necessary to check that this lectin could just recognize polymers containing Le^x and not any glycopolymer.

Aiming to verify these aspects of CTB, different QCM-D control experiments were performed including the incubation of the lectin with just SAv monolayer or Ni^{2+}-NTA SLB and the exposure of this protein with different glycopolymers.

The first verification was the presence or absence of non-specific binding between CTB and SAv monolaryer. For this reason, in two chambers containing SAv-on-SLB, one film using (HA-*g*-Le^x)-Biotin was built successfully (Figure 5.13, line with diamond symbols, 70-105 min). Then, incubations of CTB were performed from 129 to 156 min at concentration 0.34 μM and from 179 to 228 min at concentration 1.75 μM in both systems. While there was no response neither in ΔF and ΔD for the SAv monolayer system (Figure 5.13, line with left triangle symbols), there was a slight decrease in ΔF, around -2 Hz or -10 Hz respectively, for the surface that contained the Lewis^x derivatized structures meaning that there was a possible and weak binding between CTB and the glycopolymer (Figure 5.13, line with diamond symbols).

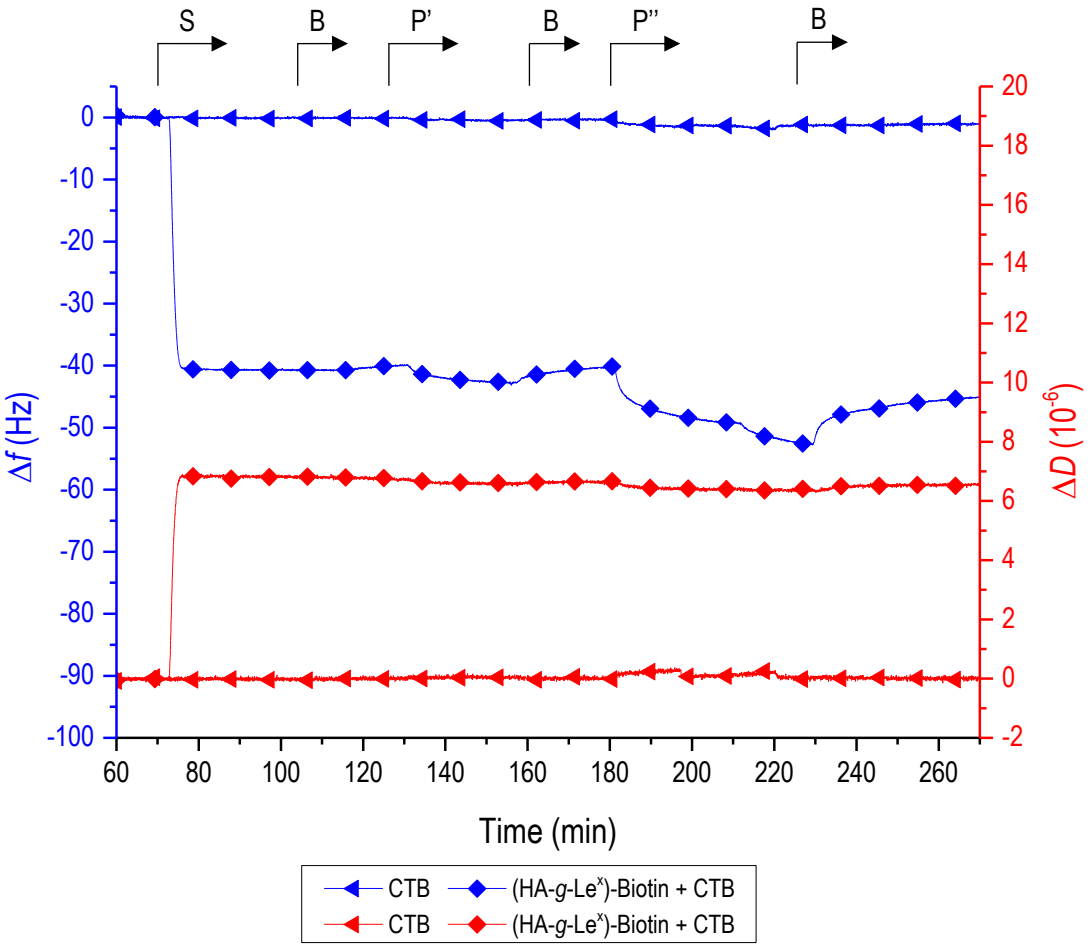

Figure 5.13: QCM-D measurements demonstrating successful interaction between a glycopolymer and CTB and the control for non-specific interaction between SAv monolayer and CTB. Shown are data for the addition **5.3** (line with diamond symbols) + CTB and just the protein by itself (line with left triangle symbols). Abbreviations: B -working buffer (HEPES 10 mM, NaCl 150 mM, pH 7.4), S -**5.3**, P'- CTB, P''– CTB. Arrows atop the graph indicate the start of incubation with each sample as indicated. Incubation conditions: **5.3** – 20 µg/mL, P' – 0.34 µM and P'' – 1.75 µM. All solutions were prepared in working buffer (HBS; HEPES 10 mM, NaCl 150 mM, pH 7.4).

As the protein did not show non-specific binding for SAv monolayer and aiming to ensure that CTB could only recognize the Lewis^x structures, another sparingly QCM-D experiment was performed using all the library of biotinylated glycopolymers achieved: HA-biotin (Figure 5.14, line with triangle symbols), (HA-*g*-Gb$_3$)-Biotin (Figure 5.14, line with square symbols), (HA-*g*-Lac)-Biotin (Figure 5.14, line with circle symbols) and (HA-*g*-Le^x)-Biotin (Figure 5.14, line with diamond symbols). Different concentrations of the CTB (0.7 and 3.5 µM) were tested to have better understanding of the system and ensure good resolution of the signal. In this first case, none of the glycopolymers showed any response except **5.3**, which showed a small decrease in ΔF, around -

2 Hz. For the second incubation, the results were the same than the previous one but, as the concentration of the protein increased, the response was clearer: decrease in ΔF, around -8 Hz, and a slightly increase in ΔD, around 0.1×10^{-6} for the film containing **5.3**. However, once CTB was rinse to the chamber, it did not seem that all was removed from the biotinylated Lewis^x polymer brush because the frequency shift did not achieve the same value than before adding the protein.

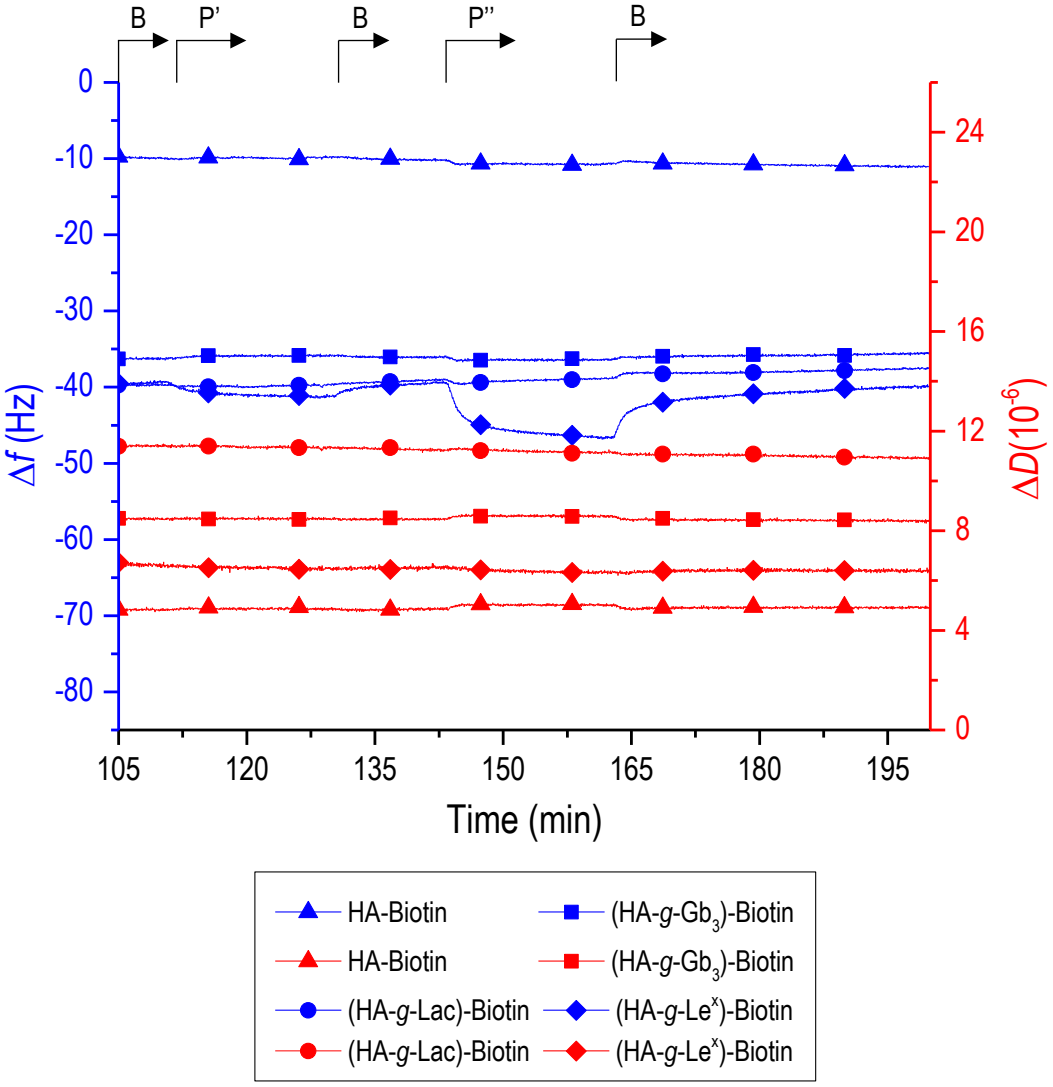

Figure 5.14: QCM-D measurements demonstrating successful interaction between a glycopolymer containing Le^x oligosaccharide and CTB no interaction between glycopolymers without Le^x oligosaccharide and CTB. Shown are data for the interaction between **5.3** (line with diamond symbols) and CTB and the non-interaction between **5.1** (line with triangle symbols), **5.2** (line with circle symbols) and **5.4** (line with square symbols) with CTB. Abbreviations: B -working buffer (HEPES 10 mM, NaCl 150 mM, pH 7.4), P'-CTB, P''– CTB. Arrows atop the graph indicate the start of incubation with each sample as indicated. Incubation conditions: P' – 0.7 μM and P'' – 3.5 μM. All solutions were prepared in working buffer (HBS; HEPES 10 mM, NaCl 150 mM, pH 7.4).

These results were also really interesting and helpful to have better understanding how this protein interacts with these glycopolymers. To begin with, only (HA-*g*-Le^x)-Biotin bind to CTB in the two concentrations of CTB tested while the other glycopolymer did not show any response. Moreover, different information about this binding was also achieved for the Lewis^x derivatized system: because frequency did not seem to arrive to equilibrium, it could suggest that most of the protein binds to the Lewis^x derivatized film but not at once, so slowly the film was enriched with CTB. The same happened while rinsing the protein from the system, most of the CTB was removed but some was still bound to the film and it was almost impossible to remove all. This profile seemed to indicate that it is difficult to the protein to bind to the film but once it was in a ligand multivalent environment, the affinity increased dramatically.

The conclusions from these studies were the following ones: first of all, CTB did not show non-specific binding to the SAv monolayer meaning that all the responses recorded in the QCM-D were due to oligosaccharide-CTB bonds. The responses were due to the only recognition of Lewis^x derivatized structure from CTB but the binding and unbinding process seemed slow and suggested that some of the protein was "trapped" in the brush once had bind to the film.

Finally, as it was done for STxB, a last preliminary experiment was performed which, the SLBs was changed: instead of using a NTA containing 5 mol-% of biotinylated phospholipids, it was used SUVs containing 5 mol-% of Ni^{2+}-NTA to attach structures with a His-tag.

The first control was to check if CTB showed any non-specific binding with this chelate surface. For this reason, in a chamber where Ni^{2+}-NTA SLB surface was successfully achieved, CTB at 0.34 μM was incubated (Figure 5.15, line with left triangle symbols) from 120 to 150 min. As it can be seen in Figure 5.15, a steep decrease in ΔF (around -25 Hz) and a relevant increase in ΔD (around 3 x 10^{-6}) was recorded once the lectin was present in the system. Moreover, after 30 min of CTB incubation, there was an attempt to remove the lectin from the Ni^{2+}-NTA SLB but after 15 min (Figure 5.15, line with left triangle symbols, 150-168 min), there was not much change in frequency shift (it was kept around -25 Hz) while the dissipation shift decreased a little bit (around 1 x 10^{-6}). These results indicated that the binding between the Ni^{2+} and CTB was too strong for the lectin to be removed from the surface once bound. Finally, a rinse with a solution of 500 mM imidazole (Figure 5.15, line with left triangle symbols, 168-194 min) following by the incubation of buffer was able to remove all the protein from the surface to end up in the initial conditions of the experiment: Ni^{2+}-NTA SLB.

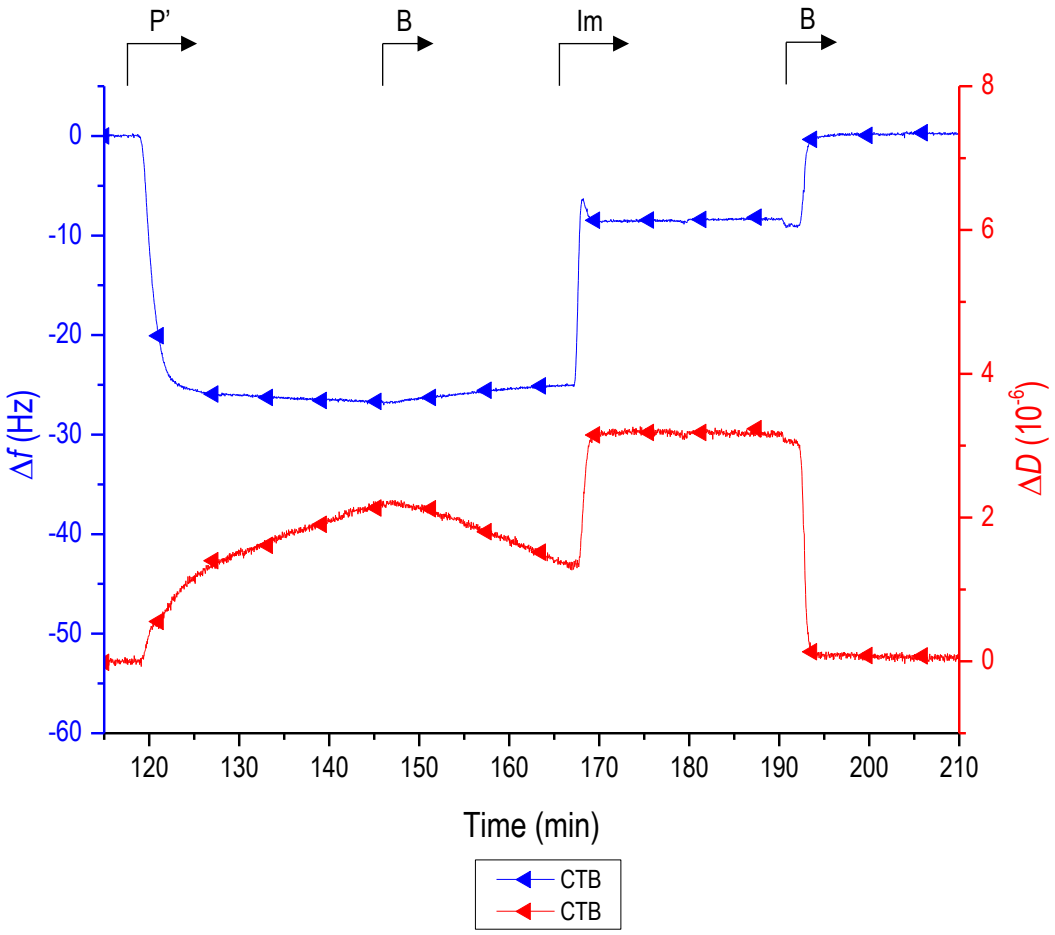

Figure 5.15: QCM-D measurements demonstrating interaction between Ni^{2+}-NTA SLB and CTB. Shown are data for the addition just the protein by itself (left triangle) following by the rinsing of CTB with imidazole. Abbreviations: B -working buffer (HEPES 10 mM, NaCl 150 mM, pH 7.4), P'- CTB, Im- Imidazole. Arrows atop the graph indicate the start of incubation with each sample as indicated. Incubation conditions: P' – 0.34 µM and Im – 500 µM. All solutions were prepared in working buffer (HBS; HEPES 10 mM, NaCl 150 mM, pH 7.4).

After achieving these results, it was clear that this Ni^{2+}-NTA SLB surface could not be used when CTB was involved due to its strong interaction. After studying the structure of this lectin, it was concluded that the binding with Nickel surface was due to free five histidines present on the bottom of the protein. Actually, these histidines are used to purify the protein by Nickel affinity column, so it was not surprising the results achieved because both surfaces are similar. This binding only could be broken by the presence of imidazole, which could replace the CTB as this molecule was smaller and their affinity for Nickel higher than the protein.

5.6 Glycan density dependent binding of multivalent toxins

Once it was checked that the glycocalyx model was suitable to study STxB and CTB binding with the different mucin-like structures and that these lectins only showed binding with their corresponding oligosaccharides (STxB-Gb_3 and CTB-Le^x), more complex systems were designed to aim for better understanding of these proteins. As it has been recorded in the previous QCM-D experiments, the frequency shift for both proteins had bigger responses while the lectin concentration was higher. This effect seemed to indicate that there was a relationship between the concentration of STxB or CTB and the concentration of their corresponding oligosaccharide on the surface. To prove this hypothesis, complex glycocalyx models, which involved more than one glycopolymer, were designed to modify the glycan density in the surface and check how the protein interacted with them.

5.6.1 Gb_3 density dependent binding of STxB

Aiming to check if the binding of STxB was related of the concentration of Gb_3 oligosaccharide on the surface, a mixture of (HA-*g*-Gb_3)-Biotin, used as a target polymer, and (HA-*g*-Lac)-Biotin, used as the inert glycopolymer to achieve a dense film, with similar sizes (89 kDa and 114 kDa respectively) was used to create different films over the SAv-on-SLB surface.

To control the percentage of Gb_3 on the surface, subsequent additions of polymers were performed: four experiments with 5 mol% biotinylated SLB following by the addition of streptavidin were established successfully. Then, (HA-*g*-Gb_3)-Biotin **5.4** was incubated different times as it is shown in Figure 5.16: from 74 to 79 (Figure 5.16, line with half triangle symbols), 82 (Figure 5.16, line with half diamond symbols), 87 (Figure 5.16, line with half circle symbols) and to 107 (Figure 5.16, line with full square symbols) min, which correspond to full saturation of Gb_3 derivatized structures. For the first three experiment, aiming for full saturation in the surface as well, (HA-*g*-Lac)-Biotin **5.2** was incubated from 117 to 135 min until the both ΔF and ΔD arrive to equilibrium. The percentage of the Gb_3 on the surface was calculated following the relation $\Delta F/\Delta F_{max}$ being ΔF the value achieved on the equilibrium once rinsing and ΔF_{max} the value for the saturation using **5.4**. Four densities of Gb_3 oligosaccharide were achieved: 37% Gb_3 in Lac (lines with half triangle symbols), 61% Gb_3 in Lac (lines with half diamond symbols), 85% Gb_3 in Lac (lines with half circle symbols) and 100% Gb_3 (lines with full square symbols).

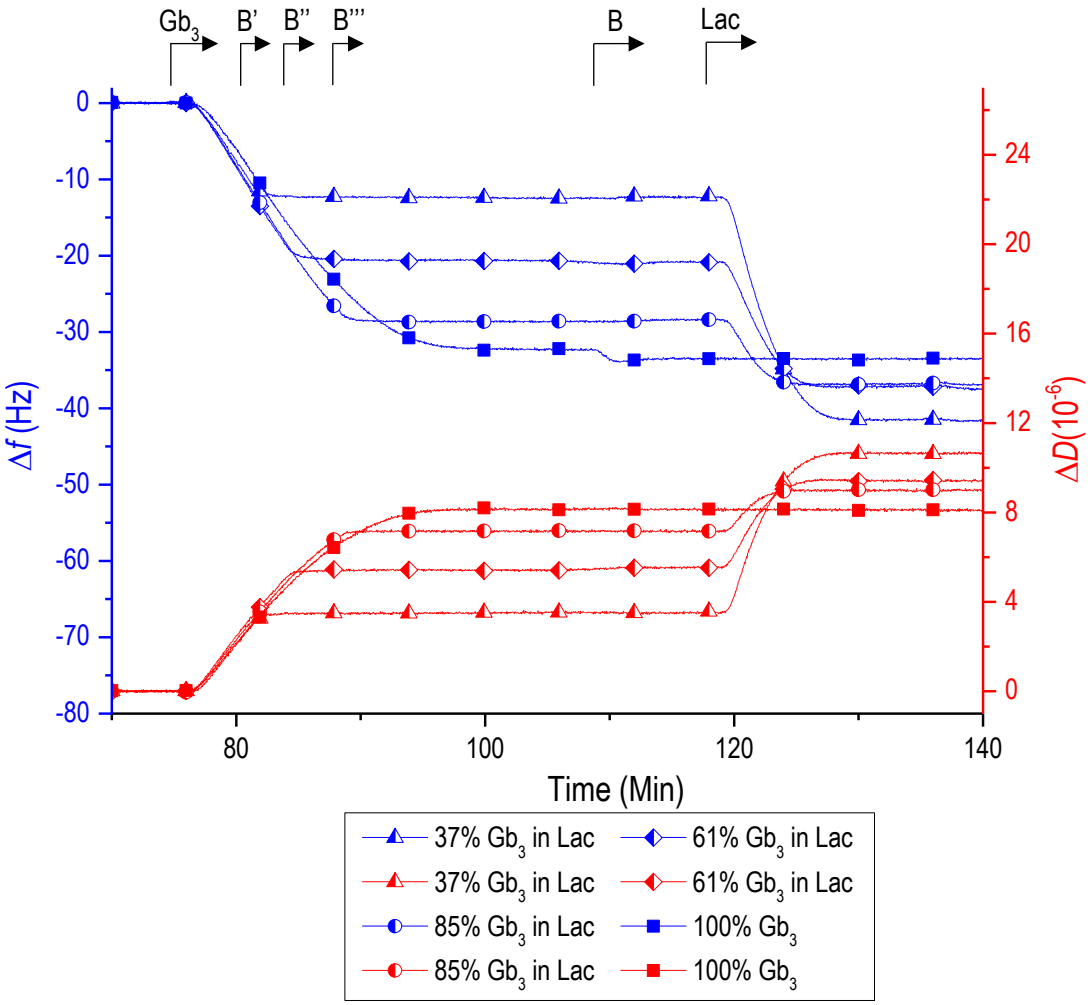

Figure 5.16: QCM-D measurements demonstrating the formation of complexes glycocalyx models using different glycopolymers. Shown are data for the formation of a surface containing 37% (line with half triangle symbols), 61% (line with half diamond symbols) and 85% (line with half circle symbols) Gb_3 oligosaccharide in Lac and full saturation Gb_3 surface (line with square symbols). Abbreviations: B -working buffer (HEPES 10 mM, NaCl 150 mM, pH 7.4) in all experiments, B' -working buffer (HEPES 10 mM, NaCl 150 mM, pH 7.4) in the 37% Gb_3 experiment, B'' -working buffer (HEPES 10 mM, NaCl 150 mM, pH 7.4) in the 61% Gb_3 experiment, B''' -working buffer (HEPES 10 mM, NaCl 150 mM, pH 7.4) in the 85% Gb_3 experiment, Gb3 – (HA-*g*-Gb_3)-Biotin, Lac – (HA-*g*-Lac)-Biotin. Arrows atop the graph indicate the start of incubation with each sample as indicated. Incubation conditions: Gb3 – 20 µg/mL and Lac – 20 µg/mL. All solutions were prepared in working buffer (HBS; HEPES 10 mM, NaCl 150 mM, pH 7.4).

Once these four glycocalyx models were achieved, the STxB incubation took place (Figure 5.17). The first one was from 145 to 166 min, at a concentration of 0.4 µM. For the lowest density of Gb_3 (line with half triangle symbols) the changes in frequency and dissipation shifts were barely significant while, as the concentration of Gb_3 increased, the responses in ΔF increased in magnitude to -2 Hz, -5 Hz and -7 Hz for 61% Gb_3, 85% Gb_3 and 100% Gb_3, respectively. As

expected, binding was fully reversible upon rinsing in HBS. A second incubation of STxB was performed at 2 μM from 183 to 200 min for the 37% Gb_3 in Lac system (line with half triangle symbols), and from 183 to 204 min for the remaining 3 surfaces (61% Gb_3 in Lac (line with half diamond symbols), 85% Gb_3 in Lac (line with half circle symbols) and 100% Gb_3 (line with full square symbols)). The results were overall comparable, although with equilibrium responses of higher magnitude consistent with the expected dose-dependent binding of STxB: -16 Hz, -14 Hz, -10 Hz and -3 Hz for 100%, 85%, 61% and 37% Gb_3, respectively. However, all the systems kept similar values for the increase of ΔD, around 0.5 $\times$ 10^{-6}, so it did not seem that the changes in dissipation shift were directly related to the concentration of Gb_3 in the film. Finally, the lectin was rinsed from the chambers proving different results: the total avidity of the STxB was shown for the film containing less Gb_3 (37%) while for the surfaces with high density of Gb_3 (61%, 85% and 100%) some lectin was still present. This effect was not shown in dissipation shift, while for all the systems their value decrease as none protein was incubated.

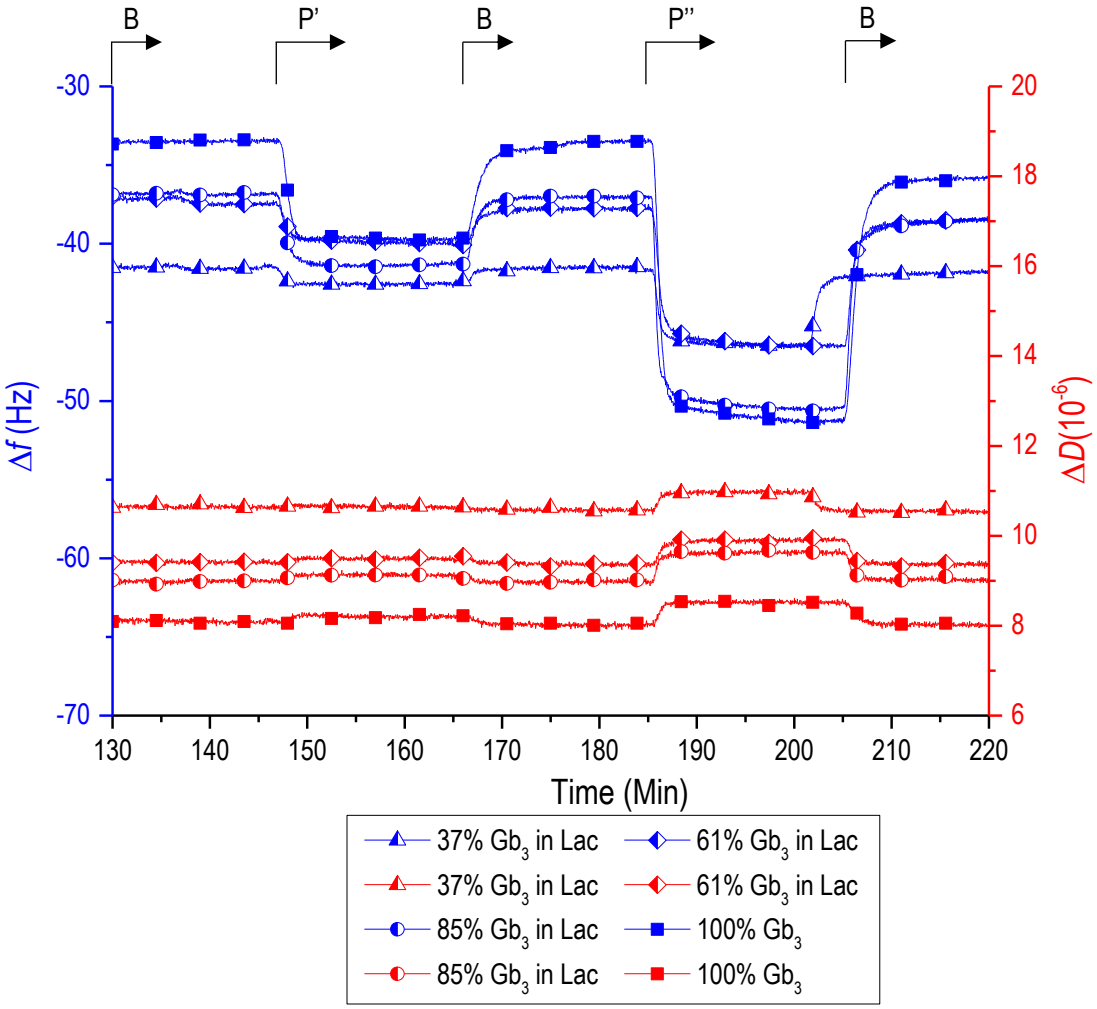

Figure 5.17: QCM-D measurements demonstrating successful interaction between a glycopolymer containing different percentages of Gb_3 oligosaccharide and STxB. Shown are data for the interaction

between surfaces containing 37% (line with half triangle symbols), 61% (like with half diamond symbols) and 85% (line with half circle symbols) Gb_3 oligosaccharide in Lac and full saturation Gb_3 surface (line with square symbols) and STxB. Abbreviations: B -working buffer (HEPES 10 mM, NaCl 150 mM, pH 7.4), P'-STxB, P'' – STxB. Arrows atop the graph indicate the start of incubation with each sample as indicated. Incubation conditions: P'– 0.4 µM and P'' – 2 µM All solutions were prepared in working buffer (HBS; HEPES 10 mM, NaCl 150 mM, pH 7.4).

To analyse quantitatively the dependence of STxB binding on the concentration of Gb_3 oligosaccharide on the surface, the negative equilibrium frequency shifts, $-\Delta F_{\mathrm{eq,STxB}}$, at a given STxB concentration were used as a measure of STxB binding and compared across the four Gb_3 surface densities. The results are shown in Graph 5.3 as a double-logarithmic plot.

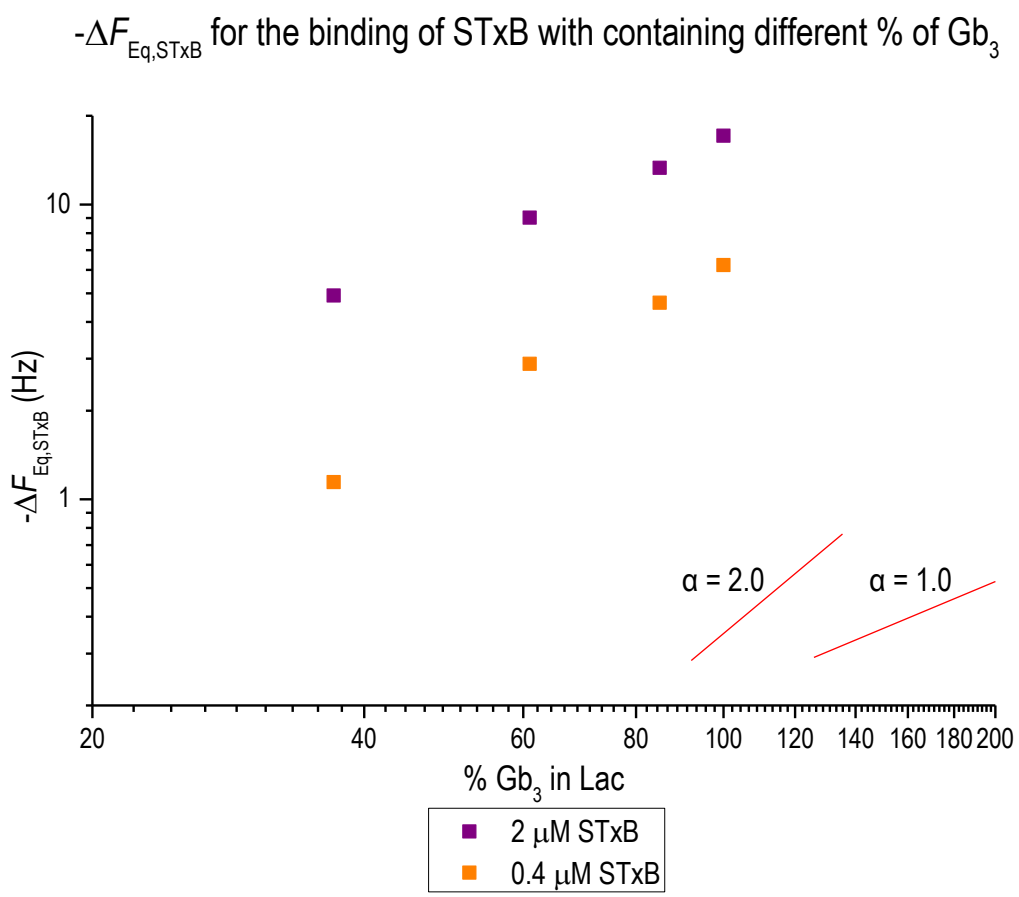

Graph 5.3: Plot in logarithmic scale of $-\Delta F_{\mathrm{eq,STxB}}$, a measure of STxB binding, against the percentage of Gb_3 glycopolymers on the surface, as a measure of Gb_3 oligosaccharide concentration. Data were extracted from Figure 5.13, with data for 0.4 µM and 2 µM STxB colour coded as indicated. The red lines with slope α = 1 and 2 are indicated for reference.

The results of this graph were really revealing. The data points for each of the two tested STxB concentrations fell onto a single line. The slope is close to 1 for 2 µM STxB implies that the protein

binding increased proportionally to the concentration of Gb_3 oligosaccharides on the surface. That the slope for 0.4 μM is larger than one is an important finding, because it suggests a strong (superlinear) dependence of STxB binding on the Gb_3 concentration. The superlinear dependence implicates that STxB is able to sharply discriminate glycocalyces by their comparative Gb_3 concentration. Such an effect, which is now commonly termed 'superselective' recognition, is a sign of multivalent interaction of STxB with the Gb_3-rich model glycocalyx. This effect has previously been shown for other multivalent binding processes.[274,275] For 0.4 μM STxB, a slope close to two implies that an increase in Gb_3 concentration by a factor of 2 leads to a $2^2 = 4$ fold increase in STxB binding. These results were really promising but QCM-D was not sensitive enough to confirm these conclusions, therefore, a more sensitive technique, like SE, was required to achieve further information.

5.6.2 Le^x density dependent binding of CTB

Once the preliminary data was recoded, complexes systems could be designed to achieve more information about how CTB's affinity was related to the concentration of Lewis^x in the surface. For this reason, a mixture of HA-Biotin and (HA-*g*-Le^x)-Biotin in similar size (40-50 kDa and 30 kDa respectively) was used in different ration of Lewis^x over the same SAv-on-SLB.

Four experiments again were set up at the same time again but all started incubating biotinylated SUVs and the SAv to form a dense monolayer. Then, (HA-*g*-Le^x)-Biotin **5.3** was incubated for different times (from 66 to 69, 71, 73 and 86 min) to achieve a range of Lewis^x concentration on the surface (Figure 5.18) according the ΔF values. To aim for saturation in the surface, the first three chambers were also incubated with HA-Biotin (40-50 kDa) (Figure 5.18). The percentage of the Le^x on the surface was calculated following the relation $\Delta F/\Delta F_{max}$ being ΔF the value achieved on the equilibrium once rinsing and ΔF_{max} the value for the saturation using **5.3**. As a result, four different systems were built: 40% Le^x in HA (line with half triangle symbols, Figure 5.18), 62.5% Le^x in HA (line with half square symbols, Figure 5.18), 82.5% Le^x in HA (line with half circle symbols, Figure 5.18) and 100% Le^x (line with full diamond symbols, Figure 5.18).

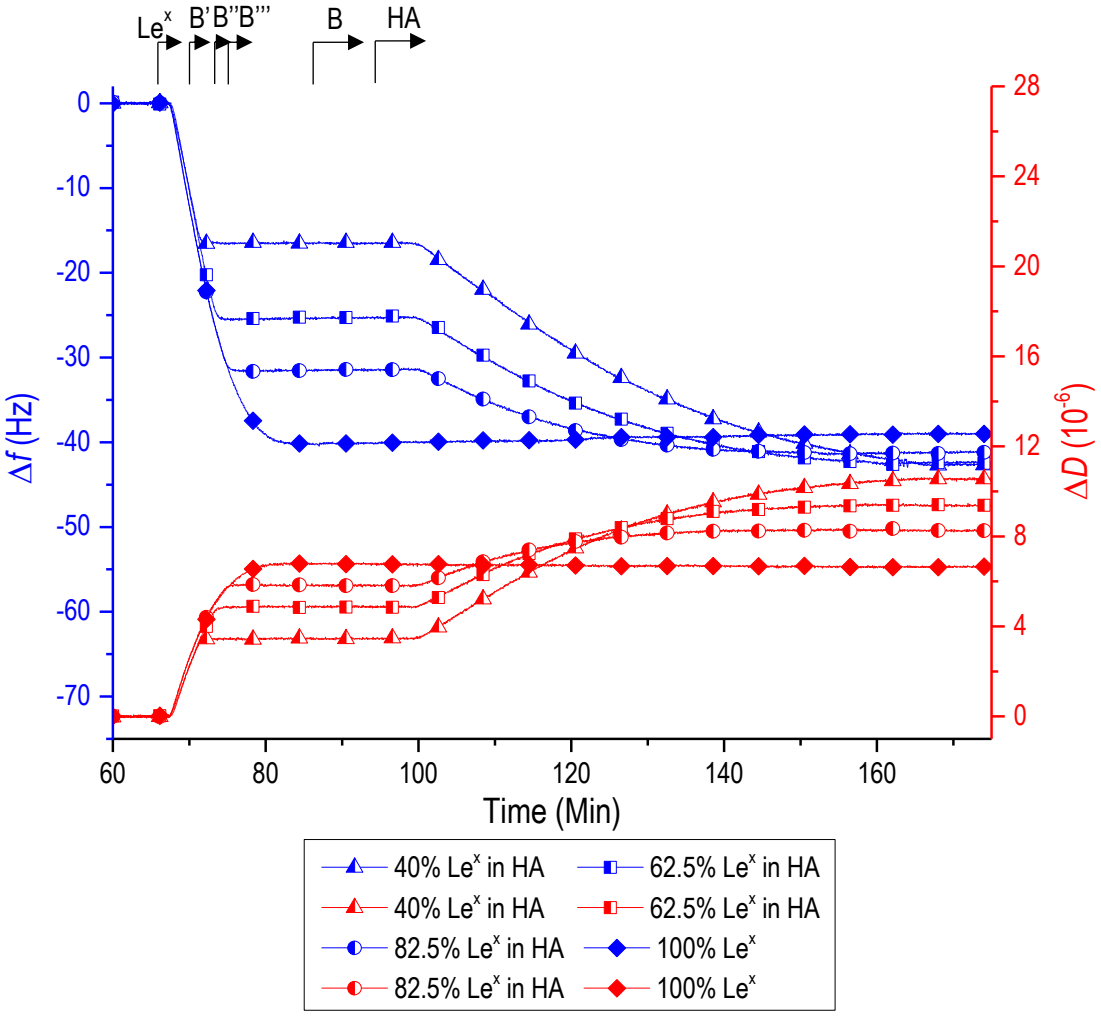

Figure 5.18: QCM-D measurements demonstrating the formation of complexes glycocalyx models using different glycopolymers. Shown are data for the formation of a surface containing 40% (line with half triangle symbols), 62.5% (line with half square symbols) and 82.5% (line with half circle symbols) Le^x oligosaccharide in HA and full saturation Le^x surface (line with diamond symbols). Abbreviations: B -working buffer (HEPES 10 mM, NaCl 150 mM, pH 7.4) in all experiments, B' -working buffer (HEPES 10 mM, NaCl 150 mM, pH 7.4) in the 40% Le^x experiment, B" -working buffer (HEPES 10 mM, NaCl 150 mM, pH 7.4) in the 62.5% Le^x experiment, B"' -working buffer (HEPES 10 mM, NaCl 150 mM, pH 7.4) in the 82.5% Le^x experiment, Le^x – (HA-*g*- Le^x)-Biotin, HA – HA-Biotin. Arrows atop the graph indicate the start of incubation with each sample as indicated. Incubation conditions: Le^x– 20 µg/mL and HA – 20 µg/mL All solutions were prepared in working buffer (HBS; HEPES 10 mM, NaCl 150 mM, pH 7.4).

After the construction of these systems, two different concentrations of CTB were incubated to monitor the responses for ΔF and ΔD. Firstly, CTB at 0.7 µM was incubated in all the chambers from 175 to 200 min showing interesting results: first of all, all systems showed decrease in the ΔF while there was no change in ΔD (Figure 5.19). As it was expected, higher concentration of Lewis^x in the brush provided higher response in the frequency shift showing a change about -3.5 Hz, -1.5

Hz and -0.5 Hz for the surfaces contain 100%, 82.5% and 62.5% Le^x respectively. Another interesting aspect to take into consideration is the unbinded CTB while rinsing: all the protein could only be removed for the systems with 40% and 62.5% Le^x in the film (half triangle and half square respectively, Figure 5.15) while some CTB was kept in the film after this step for the systems containing 82.5% and 100% Le^x in HA (line with half circle symbols and full diamond symbols respectively, Figure 5.19). At this point, CTB was incubated at higher concentration (3.5 μM) in all the chambers (222-229 min). Again, there was not any change in the dissipation shift for any of the systems while the frequency shift revealed a lot of information. As it happened in the previous CTB incubation, the decrease in ΔF was bigger as the concentration of Le^x in the film increased for all the systems being -9 Hz, -5 Hz, -2 Hz and 0.5 Hz for the surfaces contain 100%, 82.5%, 62.5% and 40% Le^x respectively. Moreover, only the experiment with 40% of Le^x in the brush (line with half triangle symbols, Figure 5.19) was capable to recover the same frequency shift before protein incubation. For the rest of experiments, not all the CTB could be rinsed from their systems as it is shown in Figure 5.19 (line with half square symbols, half circle symbols and full diamond symbols).

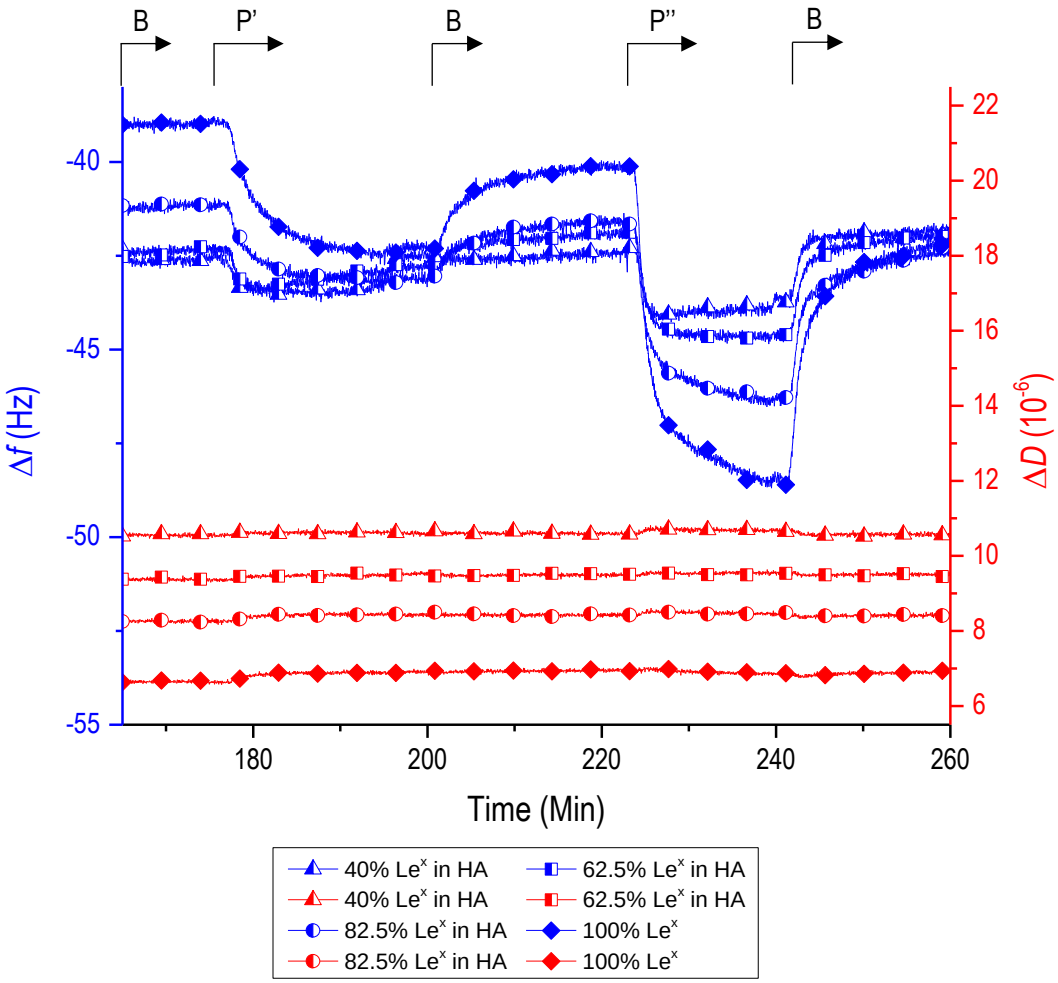

Figure 5.19: QCM-D measurements demonstrating successful interaction between a glycopolymer containing different percentages of Le^x oligosaccharide and CTB. Shown are data for the interaction between surfaces containing 40% (line with half triangle symbols), 62.5% (line with half square symbols) and 82.5% (line with half circle symbols) Le^x in HA and full saturation Le^x surface (line with full diamond symbols) and CTB. Abbreviations: B -working buffer (HEPES 10 mM, NaCl 150 mM, pH 7.4), P'- CTB, P'' – CTB. Arrows atop the graph indicate the start of incubation with each sample as indicated. Incubation conditions: P'– 0.7 µM and P'' – 3.5 µM All solutions were prepared in working buffer (HBS; HEPES 10 mM, NaCl 150 mM, pH 7.4).

The dependence of CTB binding on Le^x concentration was analysed analogous to the case of STxB and Gb_3. Two of the 8 CTB incubations did not arrive to equilibrium, and the frequency shift at the end of the incubation process was used in these cases instead as a lower limit of the binding response. The results are shown in graph 5.4:

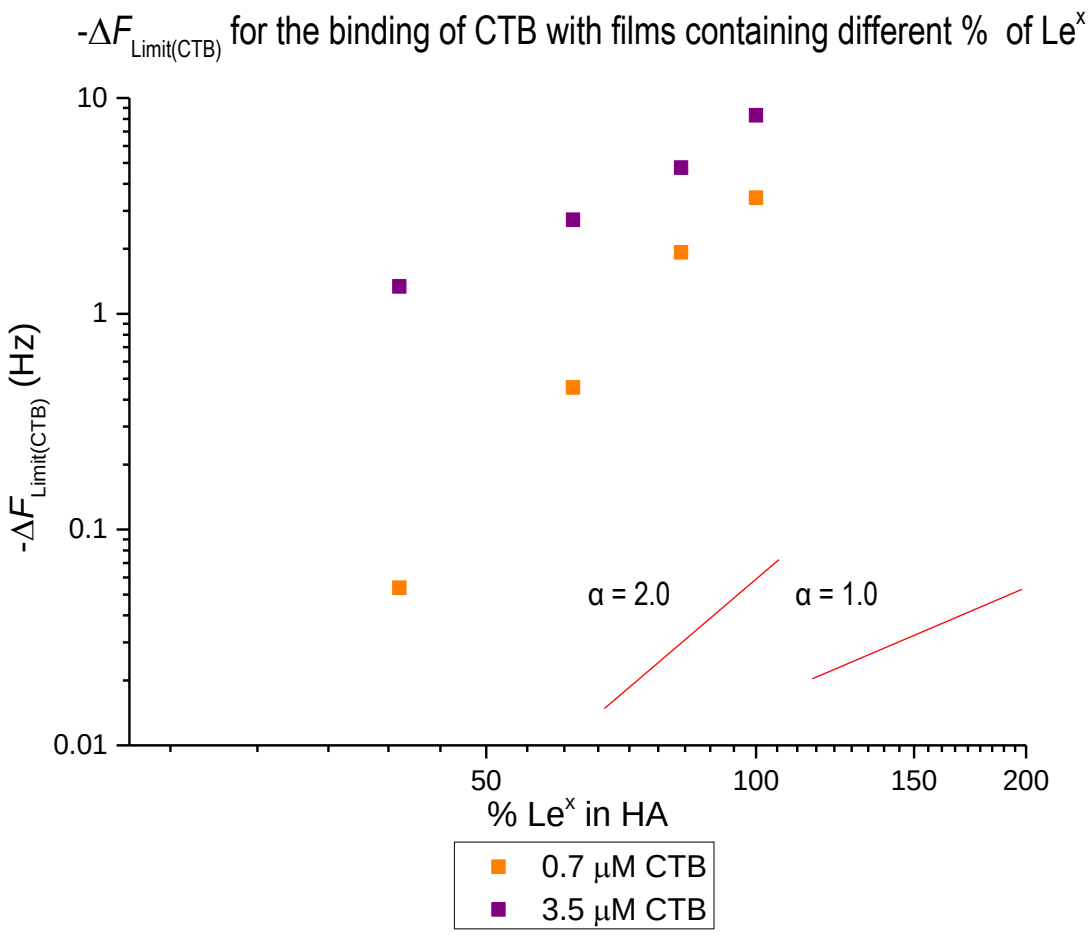

Graph 5.4: Plot in logarithmic scale of $-\Delta F_{Limit(CTB)}$ against the concentration of Le^x in HA in percentage. It is important that for this experiment the values for frequency shift on the y axis corresponds to the lower limit on the binding response.

The results of this graph were appealing. Whilst the data for each of the two CTB concentrations did not fall on a line in the logarithmic plot, the local slopes where generally higher than one meaning that CTB, as STxB, recognises its glycan ligand in the glycocalyx model superselectively. The maximal slopes on the lines were α_{max} = 2 for 3.5 μM CTB, and even larger than 2 for 0.7 μM CTB, indicating that the quality of superselectivity is enhanced for CTB compared to STxB. Nevertheless, it is important to highlight that this data needed more accuracy because, as it is shown in Figure 5.19, the technique was not sensitive enough for the small changes on the surface. As STxB, to confirm these conclusions a more sensitive technique, like SE, was required to achieve further information.

5.7 Quantifying the avidity of toxin binding to the model glycocalyces

To achieve quantitative data regarding the glycocalyx models previously described, SE technique was chosen to calculate the number of proteins per surface attached to the glypolymers as well as a K_d for the lectins with this surface.

Once the experiment was done successfully, the data required a mathematical treatment to check if it could be fitted to the Langmuir isotherm. If that was the case, information regarding the protein analysed could be deduced from it like the K_d or the partition coefficient (*PC*), the equilibrium constant obtained dividing the concertation of the protein in the film by the concentration of protein in the bulk solution.[259,276–278] The data's analysis is described in the following sections for each system in a SAv monolayer: (HA-*g*-Gb_3)-Biotin with STxB and (HA-*g*-Le^x)-Biotin with CTB.

5.7.1 Strength of STxB binding to a Gb_3-rich glycocalyx model

The titration experiment started by the successful achievement of a SAv-on-SLB layer. Then, **5.4** was incubated giving as a result a film with an areal mass density and thickness (65.5 ± 0.1 ng·cm^{-2} and 10.4 ± 1.2 nm) described in section 5.4.2 in this chapter for the same sample. The similarity of the values achieved provided reliable data about the quality if the film. Then, seven additions of STxB from 0.04 to 4 μM were performed for the titration experiments successfully followed by the rinse of all the protein in one step as it is shown in Figure 5.20.

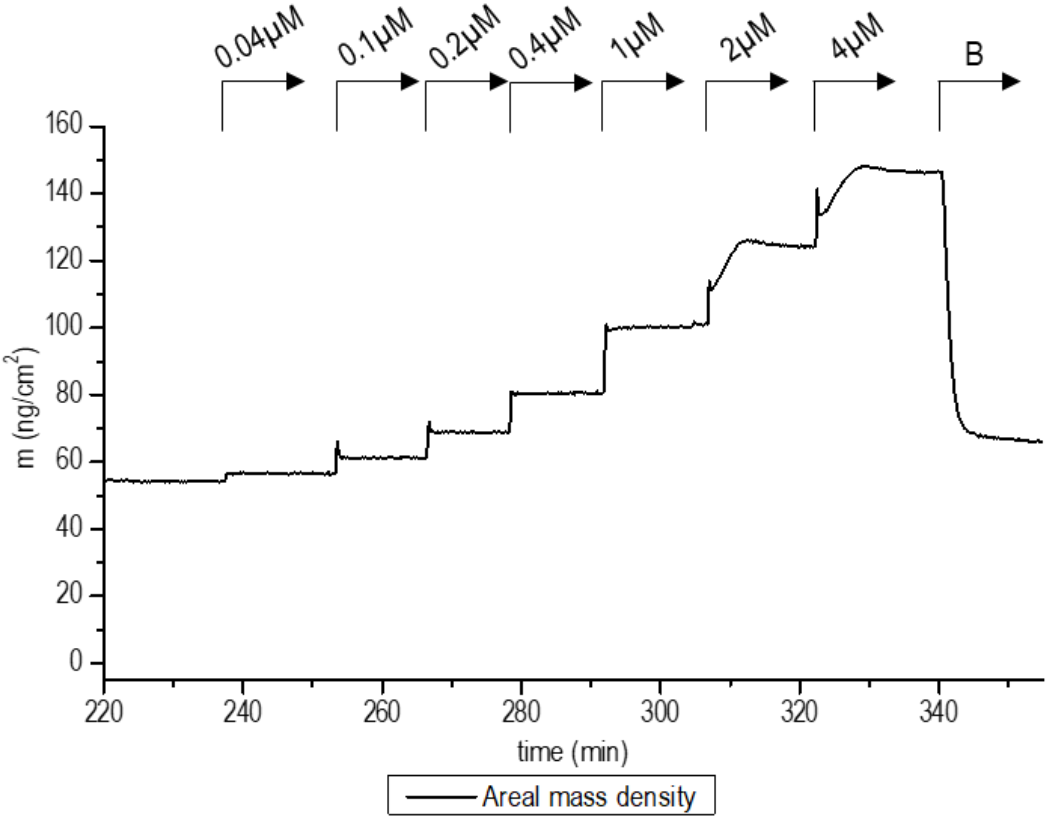

Figure 5.20: Graph of areal mass density against time for the construction of a film using (HA-*g*-Gb_3)-Biotin followed by the multiple steps of STxB additions at increasing concentration. Abbreviations: B -working buffer (HBS 10 mM, NaCl 150 mM, pH 7.4). Numbers atop the arrows indicate the concentration of STxB in the measurement chamber.

The areal mass densities at equilibrium, m_{eq}, were extracted from the time-resolved data, converted to molecular surface densities ($\Gamma_{\mathrm{eq}} = m_{\mathrm{eq}}/M_W$ being $M_w = 40$ kDa for the STxB) and plotted as a function of the STxB concentration. (Graph 5.5, blue circle). Then, the Langmuir isotherm was fitted (Graph 5.5, red line) according to Formula 5.6.

$$\Gamma = \Gamma_{max} \frac{[STxB]^n}{K_d^n + [STxB]^n} \tag{5.6}$$

where it was established $n = 1$.

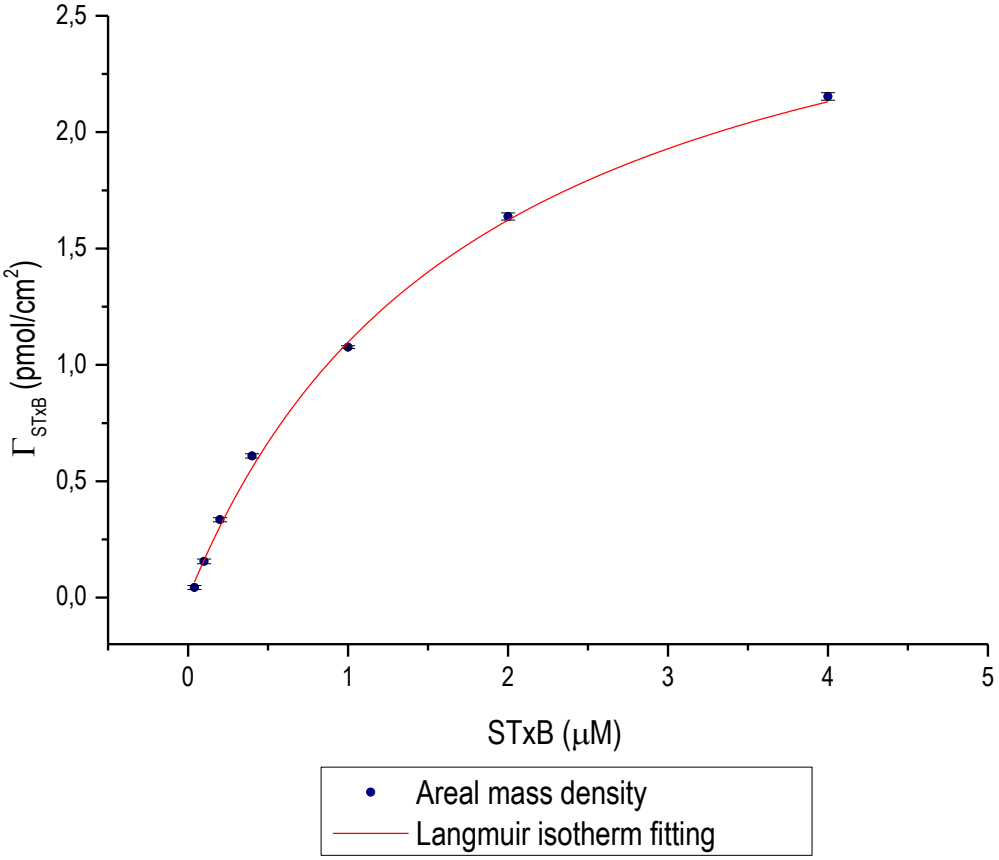

Graph 5.5: Graph representing Γ_{STxB} against STxB concentration (blue circle) and Langmuir Isotherm fitting (red line).

The data was reproduced very well with the best-fit Langmuir isotherm, providing an avidity of K_d = 1.8 ± 0.2 μM and a maximum STxB surface density Γ_{max} = 3.1 ± 0.2 pmol/cm^2. For comparison, total surface density of Gb_3 oligosaccharides was 31.2 ± 0.2 pmol/cm^2. The proportion between sugar and protein thus was 10 Gb_3 or more per 1 STxB pentamer.

Finally, it was also possible to calculate the partition coefficient, $PC = \Gamma_{max}/K_d d$, which describes the ratio of STxB in the film versus in the bulk solution. Here, d is the thickness of the model glycocalyx. With the established input values, *PC* = 137 ± 80 for STxB in a film built with (HA-*g*-Gb_3)-Biotin. This value represents an enrichment of lectin on the film of about two orders of magnitude meaning a that there was a substantial amount of protein absorbed on the film.

Several preliminary data was achieved from this titration experiment and its mathematical analysis including a K_d for the binding site in a dense Gb_3 oligosaccharide surface and the maximum areal mass density for STxB in this type of films, being quite high (3.1 ± 0.2 pmol/cm^2) if compared with the glycan one (31.2 ± 0.2 pmol/cm^2). Interestingly, the K_d for STxB in this film decreased by a factor of 1100 indicating that in an environment enrich with Gb_3, the multivalency

of the protein could decrease the K_d and have better affinity for the glycocalyx model from 2 mM for a single binding site of STxB to a 1.8 μM for the whole protein in this film.

5.7.2 Strength of CTB binding to a Le^x-rich model glycocalyx

Similar information as the one obtained for STxB could be extracted as well for the secondary binding site of CTB. Again, after achieving a successful SAv monolayer once a biotinylated supported lipid bilayer was formed, (HA-*g*-Le^x)-Biotin was incubated to fulfil a film rich in Le^x described in section 5.4.2 in this chapter (66.1 ± 0.2 ng·cm^{-2}). Finally, nine additions of CTB from 0.2 to 20 μM were added to perform successfully the titration experiment for this system as it is shown in Figure 5.21.

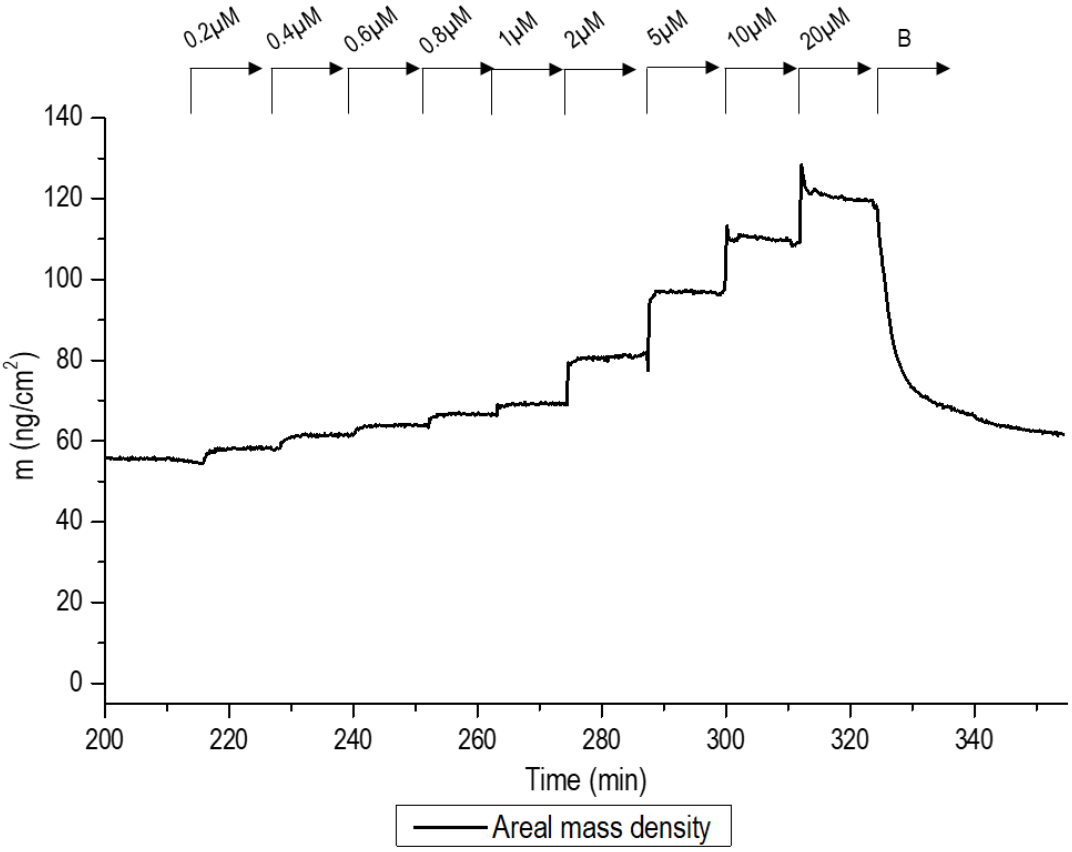

Figure 5.21 Graph of areal mass density against time for the construction of a film using (HA-*g*-Le^x)-Biotin, shown already in Figure 5.5a, followed by the multiple steps of CTB additions at increasing concentration. Abbreviations: B -working buffer (HBS 10 mM, NaCl 150 mM, pH 7.4). Numbers atop the arrows indicate the concentration of CTB in the measurement chamber.

Then, as it was done for the STxB too, the areal mass density for CTB (Γ_{CTB}) was plotted against the concentration of CTB (Graph 5.6, purple circle) following by the fitting the data in the Langmuir

isotherm (Graph 5.6, red line) following formula 5.6 in the previous section and establishing $n = 1$.

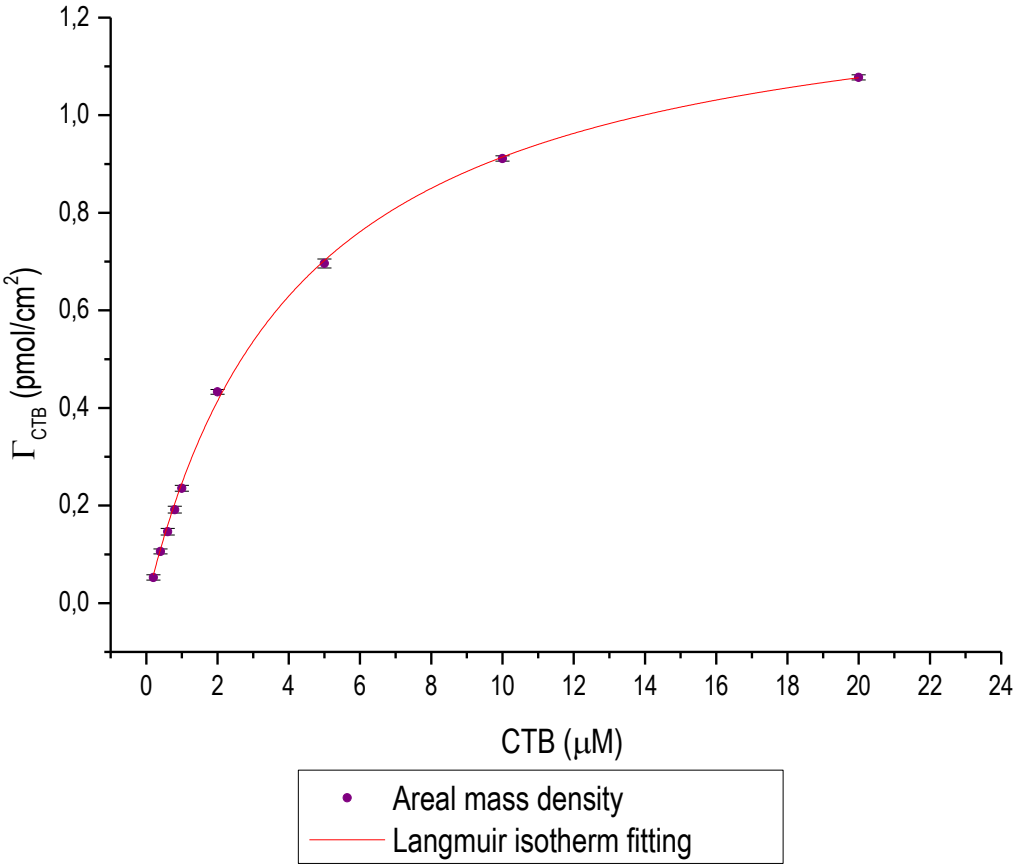

Graph 5.6: Graph representing Γ_{CTB} against CTB concentration (purple circle) and Langmuir Isotherm fitting (red line).

As it can be seen in the Graph 5.16, the fitting provided interesting information about the secondary binding site of CTB. The first parameter achieved for the Langmuir fitting was the K_d for this lectin in a film enrich with Le^x, 4.33 ± 0.16 μM. Furthermore, the maximum Γ_{CTB} was also calculated giving as a result 1.3 ± 0.02 pmol/cm^2. Once this value was compared with the total concentration of glycan on the surface (36.1 ± 0.1 pmol/cm^2), the relationship between glycan was lectin was 27.6 Le^x: 1 CTB, much higher than the previous system.

This preliminary experiment provided good information to have a better understand how CTB interact with the glycocalyx, being more specific, this model enriched with Le^x. First of all, a K_d for the secondary binding site again decreased by the order of 2000 because of the multivalency offered by the protein in a highly dense glycan surface: from 10 ± 3 mM for a single binding site to 4.33 ± 0.16 μM in this films for the whole lectin.[73] Nevertheless, not much protein could be bound to the film as it indicated $\Gamma_{CTB(max)}$, which is quite low (1.3 ± 0.02 pmol/cm^2) once compared by the

areal density of the carbohydrate (36.1 ± 0.1 pmol/cm^2). One hypothesis to explain why this effect occurred could be due to the size of the glycopolymer: because it was not really big, only 30 kDa, it might be that the film was not big enough to contain more proteins on it making $\Gamma_{CTB(max)}$ low.

5.8 Conclusions

Several aspects regarding the structures of mucin-like structures, their use to construct of glycocalyx models and their interaction with AB_5 toxins were concluded in this chapter.

First, the reducing end of glycopolymers synthesized in Chapter 4 was able to react with derivatized hydroxylamines and, it was thus possible to attach either biotin or poly-histidine at the reducing end of plain HA, HA-*g*-Lac, HA-*g*-Le^x and HA-*g*-Gb_3. The resulting mucin-like structures were suitable as building blocks for the design and construction of glycocalyx models on supported lipid bilayers. The manual synthesis of the poly-histidine with a terminal hydroxylamine, even though it presented some challenges, was finally successful including extra amino acids for its characterization (tryptophan for absorbance quantification) and ligation of other moieties (the lysine with a free amine for addition of a fluorophore).

Second, the resulting mucin-like structures (**5.1, 5.2**, **5.3**, **5.4** and **5.6**) were suitable to build a glycocalyx model, as characterized by QCM-D and SE. Glycopolymers were stably anchored to a SAv-on-SLB via biotin tags, and to Ni^{2+}-NTA presenting SLBs via poly-histidine tags. QCM-D analysis facilitated analysis of the mean length of the backbone of surface-anchored glycopolymers, and compare with the glycopolymer size in solution as determined by SEC-MALS. As a rule, the mean size of surface-grafted glycopolymers appeared smaller than in solution. Reasons of the discrepancy could be differences on the analysis, random coils in solution in SEC-MALS *versus* attached samples on a surface in QCM-D, and the assumption (important for QCM-D) that these glycopolymers would behave as pure hyaluronan in their chain mechanics. In addition, QCM-D analysis was influenced by the preference of the attachment of smaller chains on the surface and, hence, the results could be diverted to smaller sizes than the actual sample. In terms of SE characterization, (HA-*g*-Le^x)-Biotin and (HA-*g*-Gb_3)-Biotin showed similar areal mass density, around 35 pmol·cm^{-2}, while (HA-*g*-Gb_3)-K-W-H_6-NH_2 had higher areal mass density, 51 pmol·cm^{-2} suggesting that the absence of SAv monolayer provided the possibility to build denser films using the same glycopolymer.

Third, one of the most revealing conclusions was the interactions between the glycocalyx models and two lectins from AB_5 toxins, CTB and STxB. STxB showed reversible binding to Gb_3 derivatised glycopolymers and did not show any binding with the other glycopolymers (HA-Biotin, (HA-*g*-Le^x)-Biotin and (HA-*g*-Lac)-Biotin) or the surfaces (neither SAv monolayers or Ni^{2+}-NTA SLB)

tested. On the other hand, CTB also revealed binding with (HA-*g*-Le^x)-Biotin while there was no recognition for HA-Biotin **5.1**, (HA-*g*-Lac)-Biotin **5.2** and (HA-*g*-Gb_3)-Biotin **5.4** or SAv monolayers. Although QCM-D recorded binding between **5.3** and CTB, the reversibility of the process was not as fast as STxB showing long time to remove the protein from the film. Finally, this protein could not be used in Ni^{2+}-NTA SLB because it bound to the surface using histidines present on the bottom of its structure.

Fourth, salient properties of the binding on the selected lectins and glycan ligands (STxB-Gb_3 and CTB-Le^x) could be quantified in the model glycocalyx context. Model glycocalyces with tunable glycan ligand content were accomplished by building films of mixed glycopolymer content resulting in different percentages of ligand (Gb_3 or Le^x) in an inert background (HA or HA-*g*-Lac). Binding studies indicated superselective recognition of the target glycans by both lectins, with CTB showing an enhanced quality of superselective (glycan density dependent) binding.

Finally, information regarding the K_d and how STxB interacts with a multivalent polymer (**5.4**) could be extracted by the titration experiment performed using SE. It was possible to calculate the K_d of the binding sites in STxB, 1.8 ± 0.2 μM, showing evidences that in a film enrich with Gb_3 this lectin increased dramatically its affinity with this oligosaccharide. Moreover, the value *PC* confirmed the enrichment of two order of magnitude of lectin in the film. On the other hand, similar data could be extracted for CTB in a film containing 100% Le^x (**5.3**): again, the K_d for the secondary binding site decreased for a factor of 2000 because of the use of a multivalent polymer, from 2 mM to 4.33 ± 0.16 μM.

CHAPTER 6: CONCLUSIONS AND FUTURE WORK

6.1 Conclusions

6.1.1 Synthesis of mucin-like structures to create building blocks for a glycocalyx model

The principal aim of this project, the synthesis of mucin-like structures to perform binding studies, was achieved successfully. For the accomplishment of these structures, the CuAAC reaction was performed between propargyl-hyaluronic acid and oligosaccharides derivatized with an azide, azidopropyl Le^x and Gb_3-N_3, giving as a result a library of glycopolymers with well-defined structures. An anchor was successfully attached on one end of each glycopolymer, making the resulting mucin-like structures suitable to be grafted on a surface and perform binding studies with CTB and STxB. Nevertheless, different aspects were concluded during this process releated to both the synthesis of the glycopolymers and their subsequent application in glycocalyx models outlined in the next sections.

6.1.1.1 Synthesis of propargyl hyaluronic acid

For the accomplishment of mucin-like structures using CuAAC reactivity, incorporation of an alkyne onto the selected hyaluronic acid backbone was required with a high degree of substitution. As this polymer contains a carboxylic acid in its repeating unit, amide bond formation with propargylamine was selected to make an alkyne-derivatized HA. However, the synthesis of propargyl hyaluronic acid was more difficult than expected because of side reactions presented by some of the coupling conditions.

Using EDC and NHS as activators in large excess (20 and 19 molar equivalents, respectively, relative to carboxylic acid), gave as a result the presence of extra peaks in the proton NMR spectrum making impossible to conclude the degree of derivatization of alkyne in the polymer. These extra peaks were also shown in previous work published without explanation.[140,141] Different hypotheses were considered for the origin of these extra peaks including side reactions with the buffer or the amine reagent, the cross-linking of polymer chains or the presence of unreacted activated esters. However, after testing each of these hypotheses by performing different coupling conditions, or post-reaction treatments such as the addition of hydroxylamine or alkaline solution at pH = 10, the results were the same. The concentration of activators and HA were also changed aiming for an improvement of the final product purity, but without success. After all these failed experiments, it was that the extra peaks caused by EDC and NHS could not be completely excluded from the products, and the best approach to achieve propargyl hyaluronic acid was by changing the activators.

The second method investigated for making a clean propargyl hyaluronic acid with high degree of derivatization was a coupling using DMTMM as an activator described by Yu *et al*. for a coupling

between HA and furylamine with excellent results.[215,216] Nevertheless, this methodology was not tested before using HA and propargylamine. The reaction using equimolar ratio of DMTMM, propargylamine and carboxylic acid in HA resulted in a clean propargyl hyaluronic acid with 20% of backbone carboxylic acid groups substituted with alkynes according to its ^{1}H NMR spectrum. This reaction was performed using four different conditions providing pure products with a range from 20 to 50% of alkyne substitution in HA.

6.1.1.2 Enzymatic synthesis of oligosaccharides derivatized with an azide at the anomeric position

For the construction of mucin-like structures, two different oligosaccharides derivatized with an azide were synthesised successfully: azidopropyl Le^x, as it can be recognized by CTB, and Gb_3-N_3, because it binds to STxB. Moreover, the synthesis of these two oligosaccharides provided revealing information regarding the enzymes used.

The screening experiments performed to set up the best conditions to make azidopropyl Le^x led to two different conclusions: firstly, the use of $Glc(4)_{ep}$ to epimerise UDP-Glc in situ instead of using UDP-Gal directly did not have a negative effect on the synthesis of azidopropyl LacNAc or the following fucosylation to achieve azidopropil Le^x. Secondly, it was concluded that generation of GDP-Fuc was the rate-limiting step under the conditions you investigated for the synthesis of the trisaccharide: decreasing the concentration of FKP resulted in slower rates for the same amount α(1-3)FucT HP, while decreasing the concentration of α(1-3)FucT HP, while keeping the same concentration of FKP, did not show any changes on reaction rate. Using an FKP preparation provided by Dr. James Ross (University of Leeds), the synthesis of Le^x-propan-N_3 was performed successfully on a large scale by applying the best conditions found in the screening experiments.

For the synthesis of Gb_3-N_3, the use of BGalT Tt-1871, the new enzyme,[186] with $Glc(4)_{ep}$ did show good activity and provided the opportunity to synthesize this trisaccharide on a big scale, 150 mg, with good yields, 57%.

6.1.1.3 Construction of mucin-like structures suitable to perform binding studies on surfaces

The construction of the mucin-like structure was successfully achieved by performing a CuAAC cycloaddition between the pure propargyl hyaluronic acid (50% alkyne) and the azide-derivatized oligosaccharides including Lac-N_3, provided by Dr. Vajinder Kumar (University of Leeds), azidopropyl Le^x and Gb_3-N_3. Although these reactions resulted in full conversion of alkyne to triazole, some degradation of the backbone was observed by SEC-MALS analysis providing smaller glycopolymers: 136 kDa propargyl hyaluronic acid was converted to 35 kDa for HA-*g*-Lac. THPTA was added to the click reaction, significantly reducing the degradation as Cu(I) was

chelated,[279] e.g., CuAAC reaction using the same 136 kDa propargyl hyaluronic acid, the resulting HA-*g*-Lac had a size of 72 kDa when there was chelating agent in the reaction mixture.

A library of glycopolymers was achieved successfully following the protocol using THPTA with no, or barely any, free alkyne in the resulting products: HA-*g*-Lac (11%), HA-*g*-Le^x (30%) and HA-*g*-Gb_3 (35%). A biotin or poly-histidine was attached to the reducing end anomeric position through oxime ligation to provide an anchor for attaching the glycopolymers to a surface. The success of these reaction was analysed by QCM-D, where using different surfaces including SAv-on-SLB for biotinylated glycopolymers including HA-Biotin (200-500 kDa and 40-50 kDa), (HA-*g*-Lac)-Biotin, (HA-*g*-Le^x)-Biotin and (HA-*g*-Gb_3)-Biotin. To check the success of the incorporation of poly-hisitidine to derivatized hyaluronan, (HA-*g*-Gb_3)-K-W-H_6-NH_2, a QCM-D experiment was performed assembling the glycopolymers on Ni^{2+}-NTA SLB surface. All of these structures accomplished the requirements to build a glycocalyx model: long chains of polymer (HA), containing high percentage of oligosaccharide (from 11% to 35%) and with a single biotin or poly-histidine anchor.

6.1.2 Construction of glycocalyx models and their characterization by QCM-D and SE

Five biotinylated glycopolymers were attached successfully on a SAv-on-SLB surface, with QCM-D providing strong evidence for the stability of the resulting film. The mean length of the derivatized hyaluronan structures grafted on the surface was also characterized by QCM-D while assuming that their mechanical properties were similar to pure HA. Nevertheless, the values achieved by this type of analysis were smaller than the ones provided by SEC-MALS, around 25% smaller for (HA-*g*-Le^x)-Biotin and HA-*g*-Gb_3)-Biotin, indicating that other aspects had to be taken into consideration to compare both analyses like the preference by QCM-D for smaller chains or the differences of disposition of the chain while attached on a surface or dissolved in buffer. (HA-*g*-Gb_3)-K-W-H_6-NH_2 was also successfully attached to Ni^{2+}-NTA SLB and the resulting film was also stable becoming a good glycocalyx model.

The quantitative analysis of these films was performed by SE offering a deeper understanding of the composition of these films. Only three glycopolymers were analysed on their respective surfaces: (HA-*g*-Le^x)-Biotin and (HA-*g*-Gb_3)-Biotin on a SAv monolayer and (HA-*g*-Gb_3)-K-W-H_6-NH_2 on a Ni^{2+}-NTA SLB. The mucin analogue areal mass densities for carbohydrates (Le^x or Gb_3) were determined to be around 35 pmol·cm^{-2} for biotinylated glycopolymers and 51 pmol·cm^{-2} for poly-histidine tag structures suggesting that Ni^{2+}-NTA SLBs can afford denser films than the SAv monolayers.

6.1.3 Toxin interactions with the glycocalyx model and quantification of the avidity of these proteins with the model surfaces.

Another aim of this project was the use of these glycocalyx models to achieve better understanding regarding the recognition of STxB or CTB by multivalent glycans such as the mucin-like structures. The glycocalyx models provided a good scenario to check if these lectins could bind to these films to evaluate how strong or weak binding would be to provide an idea about how these proteins interact with the glycocalyx on the cell membrane. Preliminary QCM-D and SE binding experiments between STxB and Gb_3 derivatized structure, or CTB and Le^x glycopolymers reinforced the conclusion that these glycocalyx models were suitable to study these lectins in a way that was not possible before.

6.1.3.1 Interaction between Shiga Toxin B subunit and films containing Gb_3 trisaccharide and its quantification

SE experiments also revealed quantitative information regarding the binding between STxB and Gb_3. Titration experiments were performed in a film built with (HA-*g*-Gb_3)-Biotin at a selected glycan surface density, and fitting of the resulting data to the Langmuir isotherm provided a K_d = 1.8 ± 0.2 μM for the pentamer, much lower than the individuals K_d for each binding site (between 2 to 6 mM depending on the binding site 1, 2 or 3).[67,99] In addition, the maximum STxB surface density was Γ_{max} = 3.1 ± 0.2 pmol/cm^2 giving a ratio between sugar and protein of 10 Gb_3 or more per 1 StxB pentamer.

After exposing STxB to different films containing plain HA or glycopolymers derivatized with Lac, Le^x and Gb_3, the only clear (and reversible) binding recorded by QCM-D was between this lectin and films made of (HA-*g*-Gb_3)-Biotin or (HA-*g*-Gb_3)-K-W-H_6-NH_2. Changing the density of this glycan on the surface by mixing different proportions (HA-*g*-Gb_3)-Biotin and (HA-*g*-Lac)-Biotin also provided interesting information regarding the protein. This experiment suggested a superselective recognition of Gb_3 in the glycocalyx models by STxB meaning that the lectin is able to sharply discriminate glycocalyces by their comparative Gb_3 concentration

SE results combined with the QCM-D experiments suggested that in a multivalent environment such as the glycocalyx model created in this project gave accurate information regarding how the pentamer interacts with the glycocalyx model which includes a lower K_d than the previously described for monovalent binding reported in the literature and a superselective approach regarding the recognition of the ligand by this lectin.[67,99]

6.1.3.2 Interaction between the secondary binding site of Cholera Toxin B subunit and films containing Le^x trisaccharide and its quantification

SE titration experiments between a film made by (HA-*g*-Le^x)-Biotin and CTB provided unknown information about the secondary binding site of this lectin. Langmuir isotherm was fitted to the data achieved in this experiment giving as a result a K_d of 4.33 ± 0.16 μM for the pentamer, much lower than 10 mM reported in the literature for the monovalent interaction.[83] Moreover, the maximum CTB surface density was Γ_{max} = 1.3 ± 0.02 pmol/cm^2, not a high value probably due to the small size (30 kDa by SEC-MALS analysis) of the glycopolymer used to build the film. However, once this value was compared with the total concentration of glycan on the surface (36.1 ± 0.1 pmol/cm^2), the relationship between glycan and lectin was 27.6 Le^x : 1 CTB pentamer, much higher than STxB-Gb_3.

CTB was exposed to the different glycocalyx models built using plain HA or glycopolymers including (HA-*g*-Lac)-Biotin, (HA-*g*-Le^x)-Biotin and (HA-*g*-Gb_3)-Biotin. QCM-D was used to monitor any binding between CTB and the films, which revealed that only structures containing Le^x trisaccharide were recognized by CTB. The density of this glycan on the surface was changed by mixing plain HA with (HA-*g*-Le^x)-Biotin and, as for STxB, CTB showed superselective recognition relying on the glycan density on the surface.

The combination between results obtained by QCM-D and SE revealed that CTB showed superselective recognition for Le^x on the surface, which was not known previously because of the lack of appropriate models, and there was a considerable decrease of the K_d of the secondary binding site in a multivalency environment, from 10 mM described for a single pocket to 4.33 ± 0.16 μM for the pentamer.

6.2 Future work

The use of these models to discover new aspects of the recognition of these lectins have been demonstrated using QCM-D and SE. However, the resulting models built with mucin-like structures grafted on surfaces like SAv-on-SLB or Ni^{2+}-NTA lack complexity once compared to the cell glycocalyx. For this reason, different aspects could be improved to achieve models more similar to the glycocalyx on the cell membrane as described in the following sections.

6.2.1 Ensuring representative size of mucin-like structures and homogeneity of different glycans in the glycocalyx model

Degradation of the backbone during reactions performed on the polymer has been observed by SEC-MALS analyses, resulting in smaller products than the reactants. In addition, to create a good

glycocalyx model, these structures need to be long enough that the proteins are able to penetrate the film created by the mucin-like structures. For these reasons, improved synthetic methodology that ensures long chains with low dispersity in size would be needed to achieve consistency in the resulting products.

This issue could be solved by following different strategies including changing the polymer backbone or shortening the CuAAC reaction time to avoid HA chain cleavage and studying the reactivity of the different oligosaccharides because the data seemed to indicate that azidopropyl Le^x had different reactivity to Gb_3-N_3 or Lac-N_3: the polymers containing the first trisaccharide with the propyl tale were three times shorter than the oligosaccharides with the azide attached directly to the anomeric position.

It was possible to achieve different glycan densities on the film, as described in section 5.6.1 and 5.6.2, by using mixtures of different biotinylated glycopolymers. However, the homogeneity of these films was not alike to those found in cell membranes because individual chains contained exclusively one of the binding ligands (Gb_3 for STxB and Le^x for CTB) increasing the local density of that glycan dramatically. Aiming to reduce this effect and ensure the homogeneity on the film created in terms of an even distribution of glycans across the surface, it would be interesting for the complexity of the structure to attach more than one oligosaccharide to the same chain by reacting propargyl hyaluronic acid with different ratios of oligosaccharides derivatized with an azide resulting structures similar as the one shown in Figure 6.1.

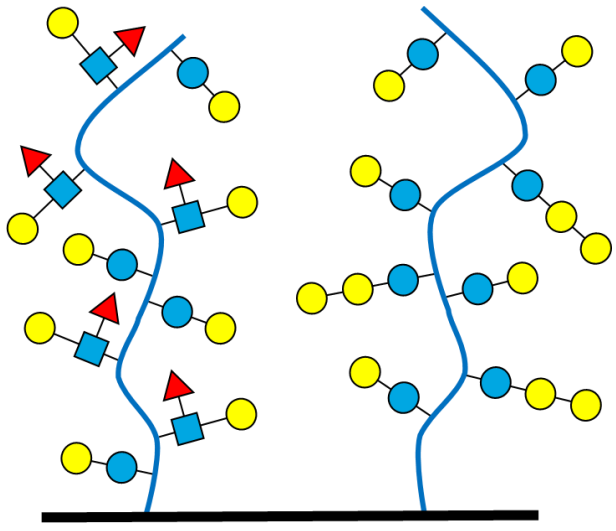

Figure 6.1: Scheme of the glycopolymers containing more than one type of oligosaccharide on the chain.

Once these mucin-like structures were synthesized, films could be built using them as building blocks giving as a result glycocalyx models with homogenous ligand density across the surface but microheterogeneity of glycan types present. CTB and STxB could be incubated in these films to

check if the affinity for these new films, similar to the actual cell glycocalyx, was similar, higher or lower than the binding shown in the films created in this project. These experiments would provide a better idea about how these lectins interact with the cell glycocalyx and which surface density of ligands is required for these proteins to show binding.

6.2.2 Construction of complex glycocalyx models with more than one building block

Another field that seems promising to study more deeply is the use of Ni^{2+}-NTA SLB and His-tag glycopolymers to create complex glycocalyx models. These mucin-like structures can potentially be combined with glycolipids resulting in a dense film created by these two different building blocks as shown in Figure 6.2. Results achieved using such glycocalyx models could be more reliable to extrapolate the first recognition of these proteins on the cell membrane and how their diffusion across the glycocalyx is regulated.

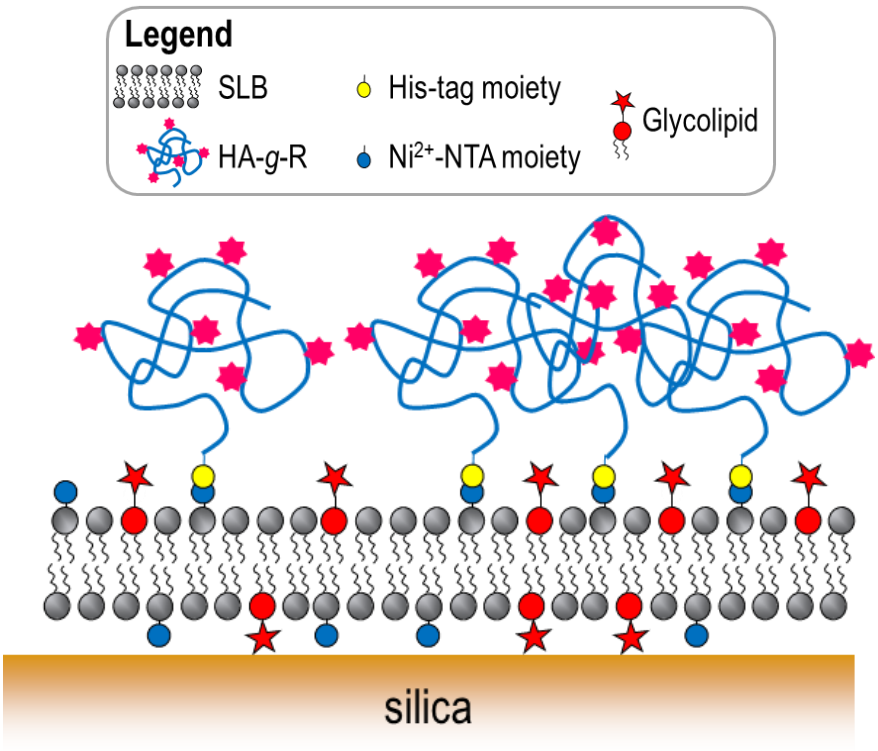

Figure 6.2: Complex glycocalyx model using poly-histidine tagged glycopolymers attached to a Ni^{2+}-NTA SLB containing glycolipids.

These systems would provide a new wide range of possibilities including the combination of different glycans and their location in the model providing the opportunity to design models more alike to the cell glycocalyx for the lectin studies. As an example, for STxB a good glycocalyx model would be the incorporation of Gb_3 glycolipid and Lac or Le^x glycopolymers attached to the combined

Gb_3/Ni^{2+}-NTA SLB. This model would contain the same disposition of glycans that STxB would find on the native glycocalyx.

These models also offer the possibility to study other aspects of the lectins including the steric hindrance that the protein could face from the glycopolymers to recognize the glycolipid target or if the presence of the ligand (Gb_3 for STxB and Le^x for CTB) is required on the mucin-like structure for the initial binding of these proteins to the glycocalyx model.

6.2.3 Incorporation of mucin-like structures into giant unilamellar vesicles (GUVs) to observe internalization of proteins

The use of giant unilamellar vesicles (GUVs) as artificial cell membrane models has been described as good glycocalyx model where glycolipids,[100,102] glycopeptides or glyoconjugates are incorporated.[3] Among the work already described, the use of GUVs containing Gb_3 ceramide provided a better understanding about the recognition by STx for this trisaccharide and the following internalization on these vesicles.[100,102] However, the main problem of this model is the lack of native glycocalyx features like steric constraints in membrane interactions, an aspect that the mucin-like structures could provide. For this reason and aiming to achieve better understanding of how STx or CT bind firstly to the glycocalyx followed by their internalization, the incorporation of the glycopolymers in GUVs seems a good strategy to achieve this goal.

The typical composition of GUVs is DOPC and cholesterol but Ni^{2+}-NTA or biotinylated lipids could also be incorporated into the vesicle structures providing anchorage for the grafting of streptavidin and biotinylated mucin-like structures, or molecules containing a poly-histidine tag such as (HA-*g*-Gb_3)-K-W-H_6-NH_2. As in the previous section, a mixture of glycolipids of interest and mucin-like structures with different glycans could be attached to these GUVs. In addition, fluorophores could be attached to the proteins to be studied, the GUVs and the mucin-like structures to allow visualization by confocal microscope, as in the work described by Römer *et al.*[100]

As an example of this idea, and taking again STx as the subject to study, fluorescently-labelled GUVs containing Gb_3 ceramide and Ni^{2+}-NTA lipids could be built, followed by the incorporation of a fluorescently-labelled mucin-like structure tagged with a poly-histidine like (HA-*g*-Lac)-K(fluorophore)-W-H_6-NH_2 resulting in a fluorescent glycocalyx model built with two different components. Finally, fluorescent STx could be incubated with these structures and monitored by confocal microscopy to observe how the lectin interacts with this glycocalyx model and if STx was internalized in the GUVs or not.

The mucin-like structures offer a wide range of possibilities: the glycopolymers could be compatible with glycolipids to assembly models more similar to native glycocalyx and monitor the

binding of proteins using techniques such as QCM-D or SE. Moreover, they could be introduced in GUVs to improve the current models of glycocalyx described in this field. These complex structures are good tools which could be used to have better understanding about the binding process of lectins that remain unknown nowadays.

CHAPTER 7: EXPERIMENTAL SECTION

7.1 Materials and methods

All dried solvents used were obtained from the School of Chemistry dry solvent system or otherwise dried according to standard methods. All solvents used for flash chromatography were HPLC grade except acetone which was GPR grade. The glassware for reactions performed under dry conditions were kept in the oven overnight and under N_2 atmosphere during the reaction. Materials and reagents used came from Sigma-Aldrich/Merk, Fisher Scientifics, Alfa Aeaser, Fisher, Fluorochem or Carbosynth.

^{1}H NMR, ^{13}C NMR, ^{1}H-^{1}H COSY and ^{1}H-^{13}C HSQC spectra were recorded on Bruker AV-NEO 500-CP or Bruker AV3HD-400 spectrometers. Chemical shifts are given in parts per million (ppm) referenced either to an internal standard (TMS) or to the residual solvent signal.[280] The following abbreviations are used to describe ^{1}H NMR signals: s = singlet, d = doublet, t = triplet, q = quartet, quint = quintet, sx =sextuplet, sp = septuplet, dd= double doblet, dt = double triplet and ddd = double double doublet.

Electrospray (ES+) ionisation mass spectra were obtained on a Bruker HCT-Ultra mass spectrometer and high-resolution ES+ were performed on a Bruker Daltonics MicroTOF mass spectrometer and LC-MS analysis performed on Brucker AmaZon X series LC-MS spectrometer Lyophilisation carried out using Virtis Benchtop K freeze dryer. Centrifugation was performed using an Eppendorf Centrifuge 5810.

Aluminium foil coated with silica gel (60 F, 1.2 mm) for thin layer chromatography was from Merck. To visualize the spots several methods and reagents were used depending on the nature of the analytes: UV light (254 nm), 1% solution of potassium permanganate in water, 5% solution of sulfuric acid in methanol, 5% H_2SO_4/methanol solution or orcinol solution (20.2 mM)/ H_2SO_4 (0.9 M) in water.

Flash chromatography was used to purify products. Chromatogel silica gel (35-70 μm) was used as stationary phase. Mixtures of organic solvents used as eluents are listed in each experimental method. Alternatively, a Biotage flash purification system was used to purify products using 10 g or 100 g SNAP stationary phase cartridges and a mixture of organic solvents as eluents described in each experimental method. Size exclusion chromatography was performed using a Biogel P2 column attached to a GE Pharmacia ÄKTA Prime FPLC system.

Polymers were loaded onto a Superdex-75 10/300 (GE) column running at a flow rate of 0.75 ml/min in PBS (pH 7.4). Samples eluting from the column passed through a Wyatt Helios 18-angle laser photometer with the 13th detector replaced with a Wyatt QELS detector for the simultaneous measurement of hydrodynamic radius. This was coupled to a Wyatt Optilab TrEX refractive index

detector and the hydrodynamic radius, molecular mass moments and concentrations of the resulting peaks were analysed using Astra V6.

7.2 Synthesis of small molecules

7.2.1 tert-Butyl (4-cyanobenzyl)carbamate (2.1)

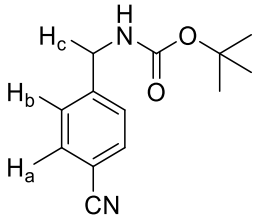

4-(Aminoethyl) benzonitrile hydrochloride (1 g, 5.9 mmol, 1 eq.) and di-*tert*-butyl dicarbonate (Boc_2O) (1.44 g, 6.5 mmol, 1.01 eq.) were dissolved in 25 mL of DCM followed by the addition of TEA (2 mL, 15 mmol, 2.5 eq.). The mixture was stirred overnight at room temperature. Then, 20 mL of DCM was added and the resulting solution was cleaned with 100 mL of 10% (v/v) HCl solution in water. The aqueous layer was extracted with DCM (2 × 20 mL). The combined organic layer was dried over $MgSO_4$ and concentrated under vacuum to achieve 1.3 g of **2.1** as a white solid in 87% yield.

TLC (Hexane/EtOAc 80:20): R_f = 0.25

^{1}H NMR (500 MHz, $CDCl_3$): δ 7.62 (d, *J* = 8.3 Hz, 2H, H_a); 7.39 (d, *J* = 8.3 Hz, 2H, H_b); 4.97 (br. s, 1H, -NH-); 4.37 (d, *J* = 5.5 Hz, 2H, H_c); 1.46 (s, 9H, -C-($C\underline{H}_3$)$_3$).

^{13}C NMR (100 MHz, $CDCl_3$): δ 156.0 (O-(<u>C</u>=O)-NH-), 144.8 (-<u>C</u>$_q$-CH_c-NH), 132.6 (-<u>C</u>H_a-), 127.9 (-<u>C</u>H_d-), 118.9 (-<u>C</u>≡N), 111.3 (-<u>C</u>$_q$-C≡N), 80.2 (-<u>C</u>-(CH_3)$_3$), 44.3 (-<u>C</u>H_c-), 28.5 (-C-(<u>C</u>H_3)$_3$).

ESI HRMS (positive mode): *m/z*: Found 255.1101 $[M+Na]^+$ calc for $C_{13}H_{16}N_2O_2Na$ 255.1109.

7.2.2 *tert*-Butyl (4-(1,2,4,5-tetrazin-3-yl)benzyl)carbamate (2.2)[153]

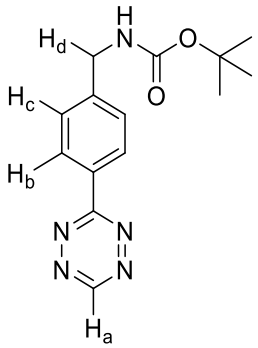

tert-Butyl (4-cyanobenzyl)carbamate **2.1** (224 mg, 1 mmol, 1 eq.), $Zn(OTf)_2$ (180 mg, 0.5 mmol, 0.5 eq.) and formamidine acetate (1.54 g, 15 mmol, 15 eq.) were weighed in a 100 mL round bottomed flask (RBF), and sealed with a septum and parafilm. Then, using a syringe, $NH_2NH_2 \cdot H_2O$ (2.4 mL, 50 mmol, 50 eq.) in DMF (0.7 mL) were added to the mixture. The reaction was stirred for 36 h at 30 °C (oil bath) as a sealed system. Then, the sealed RBF was removed from the heating and opened. The initial product was oxidised by addition of a solution of $NaNO_2$ (1.70 g, 20 mmol, 20 eq.) in 15 mL of water followed by the dropwise addition of a solution 1M HCl in water until the pH was 2. The resulting mixture was diluted in 80 mL of water and extracted repeatedly with DCM (40 mL) until the organic extracts were not red. The combined organic extracts were dried over $MgSO_4$ and concentrated under vacuum. The resulting red solid was purified using a SNAP 100 g biotage column (elution with hexane/EtOAc from 90:10 to 50:50). A red-pink solid was achieved, which was further purified by silica gel column chromatography (elution 100% DCM) to achieve a pure pink solid **2.2** (61 mg, 26%).

TLC (Hexane/EtOAc 75:25): R_f = 0.32

^{1}H NMR (500 MHz, $CDCl_3$): δ 10.20 (s, 1H, H_a); 8.55 (d, *J* = 8.4 Hz, 2H, H_b); 7.50 (d, *J* = 8.4 Hz, 2H, H_c); 5.11 (br. s, 1H, -NH-); 4.43 (d, *J* = 6.1 Hz, 2H, H_d); 1.46 (s, 9H, -C-(C$\underline{H}_3$)$_3$).

^{13}C NMR (100 MHz, $CDCl_3$): δ 166.2 (-$\underline{C}_q$-Ph), 157.7 (-$\underline{C}H_a$-), 155.9 (O-($\underline{C}$=O)-NH-), 144.6 (-$\underline{C}_q$-CH_d-NH-), 130.4 (-$\underline{C}_q$-Tz), 128.5 (-$\underline{C}H_b$-), 128.0 (-$\underline{C}H_c$-), 79.8 (-$\underline{C}$-$(CH_3)_3$), 44.2 (-$\underline{C}H_d$-), 28.3 (-C-($\underline{C}H_3$)$_3$).

ESI HRMS (positive mode): *m/z*: Found 310.1277 $[M+Na]^+$ calc for $C_{14}H_{17}N_5O_2Na$ 310.1279.

7.2.3 (4-(1,2,4,5-Tetrazin-3-yl)phenyl)methanamine hydrochloride (2.3)

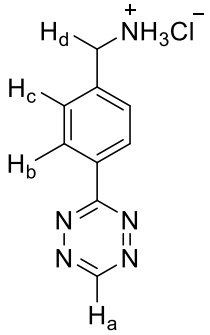

tert-Butyl (4-(1,2,4,5-tetrazin-3-yl)benzyl)carbamate **2.2** (55 mg, 0.19 mmol, 1 eq.) was dissolved in 2 mL of a solution 4M HCl in dioxane for 2 h. The resulting mixture was dried under vacuum to achieve a red/pink solid **2.3** (40 mg, 99%).

TLC (EtOAc 100 %): R_f = 0.21

^{1}H NMR (500 MHz, CD_3OD): δ 10.30 (s, 1H, H_a); 8.60 (d, *J* = 8.3 Hz, 2H, H_b); 7.67 (d, *J* = 8.3 Hz, 2H, H_c); 4.20 (s, 2H, H_d).

^{13}C NMR (100 MHz, CD_3OD): δ 167.3 (-$\underline{C}_q$-Ph), 159.5 (-CH_a-), 139.4 (-$\underline{C}_q$-CH_d-NH_3), 134.3 (-$\underline{C}_q$-Tz), 130.9 (-CH_b-), 129.8 (-CH_c-), 43.9 (-CH_d-).

ESI HRMS (positive mode): *m/z*: Found 188.0925 $[M+H]^+$ calc for $C_9H_{10}N_5$ 188.0936.

7.2.4 Mixture *endo*- and *exo*-2-(2'-*tert*-butoxycarbamatoethyl)-carboxamidonorborn-5-ene (2.6)

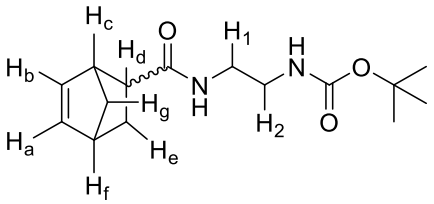

HCTU (707 mg, 1.7 mmol, 1.2 eq.) and a mixture *endo*- and *exo*-5-norbornene-2-carboxylic acid (175 µL, 1.2 mmol, 1 eq.) were dissolved in 5 mL of pyridine. The reaction was stirred for 15 min to activate the carboxylic acid followed by dropwise addition of a solution of *N*-Boc-ethylenediamine (274 mg, 1.7 mmol, 1.2 eq.) in 2 mL of pyridine. The resulting mixture was stirred for 2 h at room temperature. Then, the solvent was removed under vacuum and the resulting oil was dissolved in 50 mL of DCM. The organic solution was washed twice with 10% (v/v) HCl solution in water (2 × 50 mL) and the aqueous layer was back-extracted with DCM (2 × 20 mL). The combined organic layer was dried over $MgSO_4$ and concentrated under vacuum. The resulting yellow oil was purified by silica gel column (elution DCM/MeOH mixture from 100:0 to 92:8) to afford the title product **2.6** as a white solid (*endo*:*exo* 1:0.3, 263 mg, 66%).

TLC (DCM/MeOH 95:5): Rf = 0.51

^{1}H NMR (400 MHz, $CDCl_3$)

Endo isomer: δ 6.20 (dd, *J* = 3.1 Hz, *J* = 5.7 Hz, 1H, H_a); 5.95 (dd, *J* = 2.9 Hz, *J* = 5.7 Hz, 1H, H_b); 5.00 (s, 1.21H, -NH-); 3.31-3.18 (m, 4H, H_1 and H_2); 3.12 (s, 1H, H_c); 2.89 (s, 1H, H_f); 2.85 (dt, *J* = 4.1 Hz, *J* = 9.3 Hz, 1H, H_d); 1.90 (ddd, *J* = 3.6 Hz, *J* = 9.2 Hz, *J* = 12.0 Hz, 1H, H_e); 1.43-1.42 (m, 10H, H_g and *tert*-butyl group); 1.32 (ddd *J* = 2.7 Hz, *J* = 4.5 Hz, *J* = 12.0 Hz, 1H, $H_{e'}$); 1.27 (d, *J* = 8.2 Hz, 1H, $H_{g'}$).

Exo isomer: δ 6.12 (dd, *J* = 2.9 Hz, *J* = 5.5 Hz, 1H, H_a); 5.95 (dd, *J* = 3.0 Hz, *J* = 5.5 Hz, 1H, H_b); 5.00 (s, 2H, -NH-); 3.31-3.18 (m, 2H, H_1 and H_2); 2.91 (s, 2H, H_c and H_f); 2.00 (dd, *J* = 3.2 Hz, *J* = 7.7 Hz, 1H, H_d); 1.90 (m, 1H, H_e); 1.66 (d, *J* = 8.3 Hz, 1H, H_g); 1.43-1.42 (m, 4H, $H_{g'}$ and *tert*-butyl group); 1.32 (m, 1H, H_e).

^{13}C NMR (100 MHz, $CDCl_3$)

Endo isomer: δ 175.2 (-(C=O)-NH-), 157.3 (O-(C=O)-NH-), 137.8 (-CH_a-), 132.4 (-CH_b-), 79.8 (C-$(CH_3)_3$), 50.1 (-CH_g-), 46.2 (-CH_c-), 44.9 (-CH_d-), 42.8 (-CH_f-), 40.8 (-CH_1- or -CH_2-), 40.4 (-CH_1- or -CH_2-), 29.8 (-CH_e-), 28.5 (C-$(CH_3)_3$).

Exo isomer: δ 175.2 (-(C=O)-NH-), 157.3 (O-(C=O)-NH-), 138.3 (-CH_a-), 136.1 (-CH_b-), 79.8 (C-$(CH_3)_3$), 47.2 (-CH_g-), 46.5 (-CH_c-), 44.7 (-CH_d-), 41.7 (-CH_f-), 40.8 (-CH_1- or -CH_2-), 40.4 (-CH_1- or -CH_2-), 30.6 (-CH_e-), 28.5 (C-$(CH_3)_3$).

ESI HRMS (positive mode): *m/z*: Found 303.1687 $[M+Na]^+$ calc for $C_{15}H_{24}N_2O_3Na$ 303.1679.

7.2.5 Mixture *endo* and *exo* of 2-(2'-*tert*-butoxycarbamatoethyl)-carboxamidonorborn-5-ene (2.7)

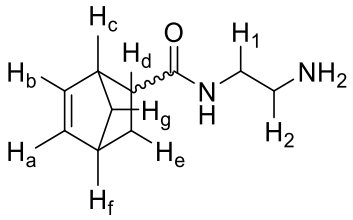

endo/exo-2-(2'-*tert*-Butoxycarbamatoethyl)-carboxamidonorborn-5-ene **2.6** (201 mg, 0.7 mmol, 1 eq.) was dissolved in 5 mL of DCM and cooled to 0ºC in an ice-bath. Then, 2 mL of TFA were added carefully to the solution. After 2 h, the TFA and the solvent was removed under a N_2 stream and it was dried under vacuum. The resulting oil was purified by silica gel column (elution with DCM/MeOH/TEA, 95:5:2) to achieve **2.7** as a yellow-brown oil (*endo*:*exo* 1:1, 186 mg, 88%).

TLC (DCM/MeOH/TEA 80:20:10): Rf = 0.21

^{1}H NMR (400 MHz, CD_3OD)

Endo isomer: δ 6.18 (dd, *J* = 3.1 Hz, *J* = 5.3 Hz, 1H, H_a); 5.99 (dd, *J* = 2.5 Hz, *J* = 5.4 Hz, 1H, H_b); 3.20 (t, *J* = 6.3 Hz, 2H, H_1); 3.16-3.13 (m, 1H, H_f/H_c) 2.92 (dt, *J* = 9.6 Hz, *J* = 3.8 Hz, 1H, H_d); 2.86-2.82 (m, 1H, H_f/H_c); 2.68 (t, *J* = 6.3 Hz, 2H, H_2); 1.91-1.83 (m, 1H, H_e); 1.43-1.38 (m, 2H, $H_{e'}$ and H_g); 1.37-1.30 (m, 1H, $H_{g'}$).

Exo isomer: δ 6.15-6.14 (m, 2H, H_a and H_b); 3.25 (t, *J* = 6.3 Hz, 2H, H_1); 2.86-2.82 (m, 2H, H_f and H_c); 2.72 (t, *J* = 6.3 Hz, 2H, H_2); 2.14-2.11 (m, 1H, H_d); 1.91-1.83 (m, 1H, H_e); 1.70-1.68 (m, 1H, H_g); 1.43-1.38 (m, 1H, $H_{e'}$); 1.37-1.30 (m, 2H, $H_{g'}$).

^{13}C NMR (100 MHz, CD_3OD)

Endo isomer: δ 178.42 (-(C=O)-NH-), 138.72 (-CH_a-), 132.89 (-CH_b-), 50.80 (-CH_g-), 47.47 (-CH_f-/-CH_c-), 45.35 (-CH_d-), 43.95 (-CH_f-/-CH_c-), 40.82 (-CH_2-), 38.27 (-CH_1-), 30.01 (-CH_e-).

Exo isomer: δ 179.82 (-(C=O)-NH-), 139.06 (-CH_a-), 137.18 (-CH_b-), 48.41 (-CH_f-/-CH_c-), 47.07 (-CH_g-), 45.19 (-CH_d-), 42.75 (-CH_f-/-CH_c-), 40.90 (-CH_2-), 38.39 (-CH_1-), 31.11 (-CH_e-).

ESI HRMS (positive mode): *m/z*: Found 181.1340 $[M+H]^+$ calc for $C_{10}H_{17}N_2O$ 181.1335.

7.2.6 Mixture *endo* and *exo* maleimide-PEG$_6$-norbornene (2.8)

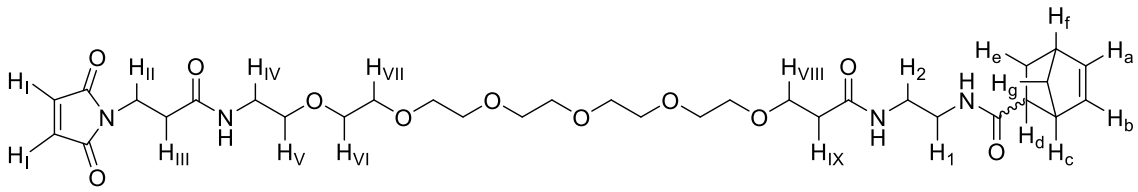

Maleimide-PEG$_6$-CO-NHS from TermoFisher (19.98 mg, 33.2 µmol, 1 eq.) and a mixture *endo*- and *exo*-2-(2'-tert-butoxycarbamatoethyl)-carboxamidonorborn-5-ene **2.7** (6.84 mg, 36.4 µmol, 1.1 eq.) were dissolved in 1 mL of DMF. Then, TEA (5 µL, 36.4 µmol, 1.1 eq.) was added to the mixture and the resulting reaction was stirred overnight at room temperature. The crude mixture was dried under vacuum and the resulting oil was purified by silica gel column (elution with DCM/MeOH from 96:4 to 90:10) to achieve **2.8** as a colorless oil (*endo*:*exo* 1:0.6, 8.56 mg, 39%).

TLC (DCM/MeOH 90:10): Rf = 0.69

^{1}H NMR (500 MHz, CD_3OD)

Endo isomer: δ 7.86 (s, 1H, -NH-); 7.62 (s, 1H, -NH-); 6.82 (s, 2H, H_I); 6.16 (dd, *J* = 3.0 Hz, *J* = 5.7 Hz, 1H, H_a); 5.90 (dd, *J* = 3.0 Hz, *J* = 5.7 Hz, 1H, H_b); 3.77 (t, *J* = 6.8 Hz, 2H, H_{II}); 3.73 (t, *J* = 6.1 Hz, 2H, H_{VII}); 3.64-3.61 (m, 16H, O-CH_2-CH_2-O); 3.50 (t, *J* = 6.1 Hz, 2H, H_2); 3.30-3.28 (m, 2H, H_1); 3.27-3.24 (m, 2H, H_{IV}); 3.14 (s, 1H, H_c/H_f); 2.92-2.88 (m, 2H, H_d and H_c/H_f); 2.48-2.43 (m, 4H, H_{III} and H_{IX}); 1.89-1.84 (m, 1H, H_e); 1.42-1.38 (m, 3H, H_g, $H_{g'}$ and $H_{e'}$).

Exo isomer: δ 7.86 (s, 0.62H, -NH-); 7.62 (s, 1H, -NH-); 6.82 (s, 2H, H_I); 6.15-6.13 (m, 2H, H_a and H_b); 3.77 (t, *J* = 6.8 Hz, 2H, H_{II}); 3.72 (t, *J* = 6.1 Hz, 2H, H_{VII}); 3.64-3.61 (m, 16H, O-CH_2-CH_2-O); 3.50 ((t, *J* = 6.1 Hz, 2H, H_2); 3.30-3.28 (m, 2H, H_1); 2.92-2.88 (m, 2H, H_c and H_f); 2.48-2.43 (m, 4H,

H_{III} and H_{IX}); 2.12-2.09 (m, 1H, H_d); 1.89-1.84 (m, 1H, H_e); 1.68 (d, *J* = 8.2 Hz, 1H, H_g); 1.42-1.38 (m, 2H, $H_{g'}$ and $H_{e'}$) pm.

^{13}C NMR (100 MHz, CD_3OD)

Endo isomer: δ 177.3 (-(C=O)-NH-CH_1-), 174.4 (-(C=O)-NH-CH_2-), 173.1 (-(C=O)-NH-), 172.2 ((C=O)-N-), 138.6 (-CH_a-), 135.5 (CH_I=) 133.1 (-CH_b-), 71.6 (O-CH_2-), 71.5 (O-CH_2-), 71.4 (O-CH_2-), 71.3 (O-CH_2-), 71.2 (O-CH_2-), 70.4 (-CH_2-), 68.2 (-CH_{VIII}-), 50.8 (-CH_g-), 47.5 (-$CH_{c/f}$-), 45.4 (-CH_d-), 44.0 (-CH_f-), 40.4 (-CH_{IV}-), 40.2 (-CH_1- or -CH_2-), 40.1 (-CH_1- or -CH_2-), 37.7 (-$CH_{III/IX}$-), 35.7 (-$CH_{III/IX}$-), 35.5 (-CH_V-), 30.0 (-CH_e-).

Exo isomer: δ 178.7 (-(C=O)-NH-CH_1-), 174.4 (-(C=O)-NH-CH_2-), 173.1 (-(C=O)-NH-), 172.2 ((C=O)-N-), 139.1 (-$CH_{a/b}$-), 137.3 (-CH_b-), 135.5 (CH_I=), 71.6 (O-CH_2-), 71.5 (O-CH_2-), 71.4 (O-CH_2-), 71.3 (O-CH_2-), 71.2 (O-CH_2-), 70.4 (-CH_2-), 68.2 (-CH_{VIII}-), 59.3 (-$CH_{f/c}$-), 47.1 (-CH_g-), 45.3 (-CH_d-), 42.8 (-CH_f-), 40.4 (-CH_{IV}-), 40.2 (-CH_1- or -CH_2-), 40.1 (-CH_1- or -CH_2-), 37.7 (-$CH_{III/IX}$-), 35.7 (-$CH_{III/IX}$-), 35.5 (-CH_V-), 31.2 (-CH_e-)..

ESI HRMS (positive mode): *m/z*: Found 667.3554 $[M+H]^+$ calc for $C_{32}H_{51}N_4O_{11}$ 667.3549.

7.2.7 2-methyl-(3,4,6-tri-*O*-acetyl-1,2-dideoxy-α-D-glucopyranoso)[1,2-d]-2-oxazoline (3.1)

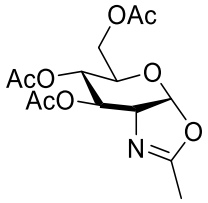

TMSOTf (0.6 mL, 2.8 mmol, 1.1 eq.) was added to a solution of 1,3,4,6-tetra-O-acetyl-*N*-acetylglucosamine (1 g, 2.57 mmol, 1 eq.) dry DCM (25 mL) under N_2. The reaction was stirred for 1.5 h at room temperature. Then, TEA (1.5 mL) was added to the mixture and the solvents were removed under vacuum to obtain a yellow-brown oil. The resulting product was purified by silica gel column chromatography (elution with hexane/ethyl acetate (EtOAc) from 50:50 to 10:90). Finally, **3.1** was obtained as a colourless oil (760 mg, 90%).

TLC (Hexane/ EtOAc 3:1): R_f = 0.22

^{1}H NMR (400 MHz, $CDCl_3$): δ 5.95 (d, *J* = 7.6 Hz, 1H, H_1); 5.26 (t, *J* = 2.4 Hz, 1H, H_3); 4.93 (ddd, *J* = 1.3 Hz, *J* = 2.0 Hz, *J* = 9.3 Hz, 1H, H_4); 4.17-4.10 (m, 3H, H_2, H_6, H_6'); 3.61 (dt, *J* = 4.3 Hz, *J* = 8.9 Hz, 1H, H_5); 2.12 (s, 3H, Me); 2.10 (s, 3H, Me); 2.9 (d, *J* = 1.8 Hz, 3H, Me); 2.08 (s, 3H, Me).

^{13}C NMR (100 MHz, $CDCl_3$): δ 170.6 (Me-(C=N)-O-), 169.6 (-(C=O)-Me), 169.2 (-(C=O)-Me), 166.7 (-(C=O)-Me), 99.4 (C_1), 70.4 (C_3), 68.4 (C_4), 67.6 (C_5), 65.0 (C_2), 63.4 (C_6), 21.0 (-CH_3), 20.9 (-CH_3), 20.8 (-CH_3), 14.2 (-CH_3).

ESI MS (positive mode): *m/z*: Found 352.1021 $[M+Na]^+$ calc for $C_{14}H_{19}NO_8Na$ 352.1008.

7.2.8 3-Azidopropyl 2-acetamido-3,4,6-tri-*O*-acetyl-β-D-glucopyranoside (3.2)[191,192]

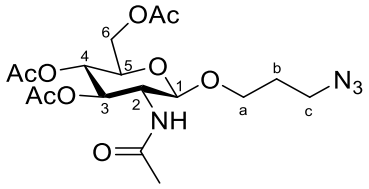

A solution of oxazoline **3.1** (954 mg, 2.9 mmol, 1 eq.) in dry DCE (40 mL) under N_2 was heated for 30 min to ensure that the solution was at 80 ºC. Then, CSA (336 mg, 1.45 mmol, 0.5 eq.) and 3-azido-1-propanol (0.4 mL, 4.3 mmol, 1.5 eq.) were added to the **3.1** solution and the reaction mixture was left stirring overnight at 80 ºC. The following day, the mixture was colled to room temperature and 20 mL of DCM was added. The solution was washed three times with 60 mL of a saturated solution of sodium bicarbonate ($NaHCO_3$). The organic layer was dried over $MgSO_4$ and dried under vacuum. The brown oil obtained was purified using a SNAP 25 g biotage column (elution with Hexane/EtOAc from 50:50 to 100% EtOAc) to achieve **3.2** as a white solid (370 mg, 30%).

TLC (EtOAc 100%): R_f = 0.38

^{1}H NMR (500 MHz, $CDCl_3$): δ 5.61 (d, *J* = 8.9 Hz, 1H, -NH-); 5.22 (dd, *J* = 10.6 Hz, *J* = 9.3 Hz, 1H, H_3); 4.93 (t, *J* = 9.6 Hz, 1H, H_4); 4.61 (d, *J* = 8.3 Hz, 1H, H_1); 4.24 (dd, *J* = 12.3 Hz, *J* = 4.8 Hz, 1H, H_6); 4.13 (dd, *J* = 12.3 Hz, *J* = 2.5 Hz, 1H, $H_{6'}$); 3.97-3.89 (m, 2H, H_2, H_a); 3.69 (ddd, *J* = 10.0 Hz, *J* = 4.8 Hz, *J* = 2.5 Hz, 1H, H_5); 3.58 (ddd, *J* = 9.7 Hz, *J* = 8.3 Hz, *J* = 4.7 Hz, 1H, $H_{a'}$); 3.40-3.32 (m, 2H, H_c); 2.08 (s, 3H, CH_3); 2.02 (s, 3H, CH_3); 2.01 (s, 3 H, CH_3); 1.95 (s, 3H, CH_3); 1.77-1.74 (m, 2H, H_b).

^{13}C NMR (125 MHz, $CDCl_3$): 171.1 (-(C=O)-OCH_3), 170.8 (-(C=O)-OCH_3), 170.3 (-(C=O)-$NHCH_3$), 169.5 (-(C=O)-OCH_3), 101.2 (C_1), 72.5 (C_3), 72.0 (C_5), 68.6 (C_4), 66.2 (CH_a), 62.0 (C_6), 54.5 (C_2), 48.0 (CH_c), 28.9 (CH_b), 23.3 (-NH-CH_3), 20.8 (-CH_3), 20.7 (-CH_3) and 20.6 (-CH_3).

ESI MS (positive mode): *m/z* Found 431.08 $[M+H]^+$ calc for $C_{19}H_{26}N_4O_9$ 431.35.

7.2.9 3-azidopropyl *N*-acetamido -β-D-glucopyranoside (3.3)[191,192]

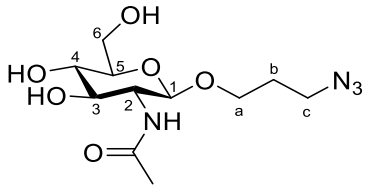

To solution of **3.2** (370 mg, 0.86 mmol, 1 eq.) in dry MeOH (5 mL) under N_2 was added 1.5 mL of 0.5 M sodium methoxide (MeONa) solution in $CHCl_3$. The mixture was stirred at room temperature for 3 hours. Then, it was neutralized with DOWEX-50 H^+ resin and the suspension as filtered. The resulting solution was dried under vacuum to achieve **3.3** as a white solid (177 mg, 68%)

TLC (DCE/MeOH/AcOH/H_2O 50:30:25:10): R_f = 0.59

^{1}H NMR (500 MHz, CD_3OD): δ 4.38 (d, *J* = 8.4 Hz, 1H, H_1); 3.95 (dt, *J* = 10.0 Hz, *J* = 5.6 Hz, 1H, H_a); 3.88 (dd, *J* = 11.9 Hz, *J* = 2.2 Hz, 1H, H_6); 3.70-3.62 (m, 2H, H_2, H_6'); 3.56 (ddd, *J* =10.0 Hz, *J* = 7.3 Hz, *J* = 5.2 Hz, 1H, $H_{a'}$); 3.44 (dd, *J* = 10.4 Hz, *J* = 8.4 Hz, 1H, H_4); 3.38 (t, *J* = 6.7 Hz, 2H, H_c); 3.33-3.29 (under CD_2HOD peak, H_3); 3.26 (ddd, *J* = 9.7 Hz, *J* = 5.7, *J* = 2.2 Hz, 1H, H_5); 1.84-1.78 (m. 2H, H_b).

^{13}C NMR (125 MHz, CD_3OD): δ 173.7 (-(C=O)-$NHCH_3$), 102.8 (C_1), 78.0 (C_5), 75.6 (C_4), 72.1 (C_3), 67.1 (CH_a), 62.8 (C_6), 57.4 (C_2), 48.9 (CH_c), 30.1 (CH_b) and 23.0 (-$NHCH_3$).

ESI MS (positive mode): *m/z* Found 305.14518 $[M+H]^+$ calc for $C_{11}H_{21}N_4O_6$ and found 327.1275 $[M+Na]^+$ calc for $C_{11}H_{20}N_4O_6Na$.

7.2.10 (*N*-[1-(1-{α-D-galactopyranosyl-1,4-β-D-galactopyranosyl-1,4-β-D-glucopyranosyl}-1H-1,2,3-triazol-4-yl)-2,5,8,11-tetraoxatridecan-13-yl]-5-[(3aS,4S,6aR)-2-oxohexahydro-1H-thieno[3,4-d]imidazol-4-yl]pentanamide (3.14)

Gb_3-PEG_4-biotin was synthesised by adding the following components (Table 7.1) to a 50 mL falcon tube. The alkyne-PEG4-biotin reagent was purchased from Sigma-Aldrich 764213.

Table 7.1: Reagents used to make compound **3.14**

Reagent	stock solution concentration	Final concentration	volume/mass added
Gb_3-N_3 (3.11)	-	5 mM	15 mg
Sodium ascorbate	500 mM	30 mM	132 µL
Alkyne-PEG_4-biotin	250 mM	10 mM	88 µL
$CuSO_4$	500 mM	5 mM	22 µL
H_2O	-	-	1958 µL

The reaction was left overnight (first night) at room temperature. The following day it was checked by TLC and mass spectrometry and, because there was no Gb_3-N_3 remaining, 22 µL of a Gb_3-N_3 stock solution (500 mM) in mQ water and 132 µL of sodium ascorbate stock solution (500 mM) were added to the mixture. The reaction was left overnight (second night) at room temperature following by TLC and mass spectrometry analysis the following day. As the alkyne-PEG_4-biotin had not fully reacted and there was no Gb_3-N_3 remaining, another 30 µL of a Gb_3-N_3 stock solution (500 mM) in mQ water and 132 µL of sodium ascorbate stock solution (500 mM) were added to the falcon tube. The reaction mixture was left overnight (third night) at room temperature. The following day, the reaction mixture was subjected to mass spectrometry and TLC analysis to check the absence of Alkyne-PEG_4-Biotin.

The reaction mixture was freeze dried to remove the solvent. The resulting brown solid was dissolved in 250 µL of water and purified by size exclusion chromatography (Biogel P2 resin) using aqueous ammonium formate (20 mM) as eluent to obtain Gb_3-PEG_4-Biotin **3.14** (5.7 mg, 27%).

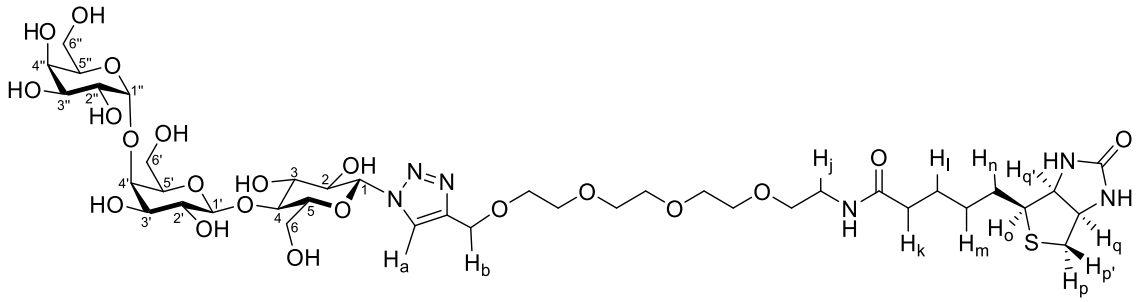

TLC (DCE/MeOH/AcOH/H_2O 50:30:25:10): R_f = 0.33

^{1}H NMR (500 MHz, D_2O): δ 8.29 (s, 1H, H_a); 5.81 (d, *J* = 9.3 Hz, 1H, H_1); 4.96 (d, *J* = 3.9 Hz, 1H, $H_{1''}$); 4.74 (s, 2H, H_b); 4.61-4.58 (m, 1H, $H_{q'}$); 4.57 (d, *J* = 7.8 Hz, 1H, $H_{1'}$); 4.41 (dd, *J* = 8.1 Hz, *J* = 4.6 Hz, 1H, H_q); 4.38 (t, *J* = 6.4 Hz, 1H, $H_{5''}$); 4.07-4.06 (m, 1H, H_2) 4.05 (dd, *J* = 3.3 Hz, *J* = 0.9 Hz, 1H, $H_{4'}$); 4.00-3.96 (m, 2H, H_6, $H_{6'}$); 3.94-3.93 (m, 1H, $H_{4''}$); 3.91-3.89 (m, 3H, -CH_2-, $H_{5'}$); 3.89-8.87

(m, 1H, H_6); 3.86-3.85 (m, 1H, H_4); 3.84-3.81 (m, 1H, $H_{2''}$); 3.78-3.77(m, 1H, $H_{3''}$); 3.77-3.75 (m, 3H, -CH_2-, $H_{3'}$); 3.71 (dd, *J* = 6.8 Hz, *J* = 2.3 Hz, 4H, -CH_2-, $H_{6''}$); 3.69-3.68 (m, 8H, -CH_2-, H_3, H_5); 3.64-3.60 (m, 3H, -CH_2-, $H_{2'}$); 3.38 (t, *J* = 5.4 Hz, 2H, H_j); 3.32 (qt, *J* = 4.3 Hz, 1H, H_o); 2.98 (dd, *J* = 13.0 Hz, *J* = 5.1 Hz, 1H, H_p); 2.77 (d, *J* = 13.0 Hz, 1H, $H_{p'}$); 2.25 (t, *J* = 7.3 Hz, 2H, H_k); 1.75-1-54 (m, 4H, H_l, H_m or H_n); 1.44-1.35 (m, 2H, H_l, H_m or H_n).

^{13}C NMR (125 MHz, D_2O): δ 176.9 (-CO-NH-), 165.3 (-NH-CO-NH-), 144.2 (-HC=C-), 124.3 (CH_a), 103.2 ($C_{1'}$), 100.2 ($C_{1''}$), 87.2 (C_1), 77.7 (C_3/C_5), 77.5 ($C_{4'}$), 77.3 (C_4), 75.4 ($C_{3''}$), 74.5 (C_3/C_5), 72.1 (C_2), 72.0 ($C_{3'}$), 70.8 ($C_{5''}$/$C_{2'}$) 70.7 ($C_{5''}$/$C_{2'}$), 69.6 (CH_2), 69.5 (CH_2), 69.5 (CH_2), 69.5 (CH_2), 69.3 (CH_2), 69.1 (CH_2), 69.0 (CH_2/$C_{2''}$/$C_{5'}$/$C_{4''}$), 68.9 (CH_2/$C_{2''}$/$C_{5'}$/$C_{4''}$), 68.5 (CH_2/$C_{2''}$/$C_{5'}$/$C_{4''}$), 63.0 (CH_2), 63.0 (CH_b), 62.0 ($CH_{q'}$), 60.4 ($C_{6''}$), 60.3 ($C_{6'}$), 60.2 (CH_q), 59.6 (C_6), 55.3 (CH_o), 39.6 (CH_p), 38.8 (CH_j), 35.4 (CH_k), 27.8 (CH_l/CH_m/CH_n), 27.6 (CH_l/CH_m/CH_n) and 25.0 (CH_l/CH_m/CH_n).

ESI HRMS (positive mode): m/z: Found 987.4080 $[M+H]^+$ calc for $C_{39}H_{67}N_6O_{21}S$ 987.4002.

7.3 Solid Phase Peptide Synthesis

7.3.1 General reagents and procedures

All amino acids, resins and coupling reagents were purchased from Novabiochem and used without further purification. Fritted polypropylene tubes (10 mL) were purchased from Supelco (Merek) and were used for all solid phase reactions. Agitation of solid phase reaction mixtures was achieved by rotation on a Stuart blood rotator at room temperature. Peptides were synthesised using Rink Amide MBHA resin (loading 0.5 mmol/g).

Peptides were analysed by HPLC using an Agilent 1290 affinity LC system equipped with an Ascentis Express 10 cm × 2.1 mm, 2.7 µm ES-C_{18} peptide column (0.5 ml min^{-1}) and ultraviolet (UV) detection at 220-280 nm. The peptide column was run with a gradient from 0.1% TFA/5% MeCN (*v/v*) in H_2O to 0.1% TFA/95% MeCN (*v/v*) in H_2O over 10 minutes.

7.3.2 Standard procedure for manual solid phase peptide synthesis

7.3.2.1 Preparation of the resin

Fmoc-protected Rink amide resin methylbenzhydryl amine (MHBA) was weighed in a polypropylene syringe fitted with a polyethylene filter disc. It was first washed with DCM (3 × syringe volume); DMF (3 × syringe volume), MeOH (3 × syringe volume) and DCM (3 × syringe volume). Fmoc removal was achieved by reaction with 20% piperidine in DMF (1 syringe volume × 3 min + 1 syringe volume × 15 min); followed by washing with DMF (2 × syringe volume) and DCM (3 × syringe volume).

7.3.2.2 Peptide coupling

Incorporation of protected amino acids was accomplished by using 6 eq. of both Fmoc-amino acid, Oxyma Pure and DIC dissolved in the minimum amount of DMF. Coupling reactions were rotated for 90 min at room temperature. Afterwards, the resin was washed with DCM (3 × syringe volume), DMF (3 × syringe volume) and MeOH (3 × syringe volume). If the coupling was not complete, as assessed by heating some resin beads in a saturated solution of ninhydrin in MeOH, it was repeated using another 3 eq. of the reagents.

After the coupling of the first 6 amino acids, a mini cleavage was performed to check the purity of the peptide.

Incorporation of 2-[(Bis-Boc)amino]oxyacetic acid on the peptide (*N*-terminal position) was accomplished by using 6 eq. each of this molecule, Oxyma Pure and DIC. Coupling reaction was left for 90 min at room temperature. The coupling was checked by heating some resin beads in a saturated solution of ninhydrin in MeOH.

7.3.2.3 Mini cleavage

A small sample of beads from the isolated deprotected amino acid-resin were exposed to 1 mL of the cleavage cocktail (95:2.5:2.5 (v/v/v) TFA/H_2O/TIS) for 45 minutes. The filtrate was collected and the mixture was evaporated under a N_2 stream. The remaining solid was dissolved in MeOH, filtered and analysed by LCMS.

7.3.3 Cleavage and isolation

Deprotection and cleavage was carried out by reaction with a 95:2.5:2.5 (v/v/v) TFA/H_2O/TIS mixture (1 mL for 100 mg of resin) for 2.5 h at room temperature. The filtrate was then collected and resin was washed with TFA (5 mL or until the filtrate was not orange) which was added to the filtrate; then TFA was evaporated under a N_2 stream. The crude product was precipitated with diethyl ether. The peptide dissolved in water was lyophilized, purified by HPLC, quantified by UV-Visible spectroscopy and characterized by mass spectroscopy.

7.3.4 Synthesis of peptide H_2N-O-K-W-H_6-NH_2 5.5

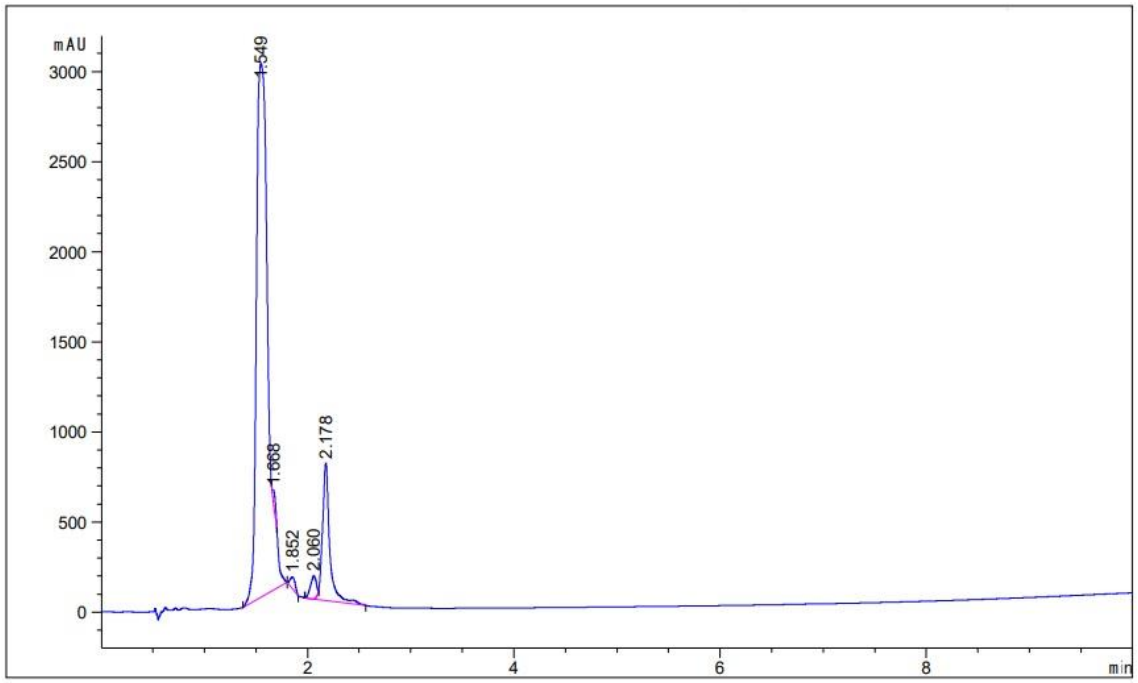

Peptide was synthesised using methodology described in section 7.3.2 and 7.3.3.

Yield: 4.86 mg, 3%

ESI HRMS (positive mode): m/z: Found 1227.5819$[M+H]^+$ calc for $C_{55}H_{71}N_{24}O_{10}$ 1227.5712.

LCMS (positive mode): m/z: Found 410.53 $[M+3H]^{3+}/3$ calc for $[C_{55}H_{70}N_{24}O_{10} + 3H]^{3+}/3$ 410.11.

7.4 Synthesis of Hyaluronic Acid Derivatives

7.4.1 4-(Aminomethyl)benzonitrile-derivatized Hyaluronic Acid (2.4)

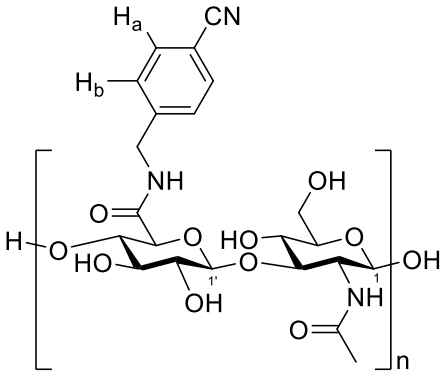

Hyaluronic acid (15 mg, 39.4 µmol -COOH, 1 eq.) was dissolved in MES buffer (3.75 mL, 100 mM, pH = 6.0). 4-Aminobenzyl cyanide (13.3 mg, 79 µmol, 2 eq.), EDC (151.1 mg, 788 µmol, 20 eq.) and the corresponding amount of NHS (Table 7.2) were weighed in a glass vial. Then, the hyaluronic acid solution was transferred to the glass vial containing all the other reagents, and it was vortexed until all the solid reagents were dissolved. The mixture was placed on a rocker overnight at room temperature. The crude product was transferred to a dialysis bag (SnakeSkin

dialysis tubing: 7000 MWCO) and it was purified by dialysis at room temperature, first against NaCl solution (3.5 g/L) for 24 h and then water for 24 h. The resulting solution was freeze-dried and analysed by ^{1}H NMR.

* The amount of NHS was changed depending of each experiment on the set of experiments (see table 7.2).

Table 7.2: Amounts used for NHS

Experiment	NHS		
Test	mg	µmol	eq.
0	0	0	0
1	4.5	39.4	1
2	18.3	157.6	4
3	31.8	275.8	7
4	49.9	433.4	11
5	68.1	591.0	15
6	86.2	748.6	19

^{1}H NMR (500 MHz, D_2O): δ 7.78-7.73 (m, H_a); 7.48-7.43(m, H_b); 4.55-4.46 (m, 2H, H_1 and $H_{1'}$); 2.02 (s, 3H, CH_3-CO-NH-).

7.4.2 (4-(1,2,4,5-Tetrazin-3-yl)phenyl)methanamine-derivatized Hyaluronic Acid (2.5)

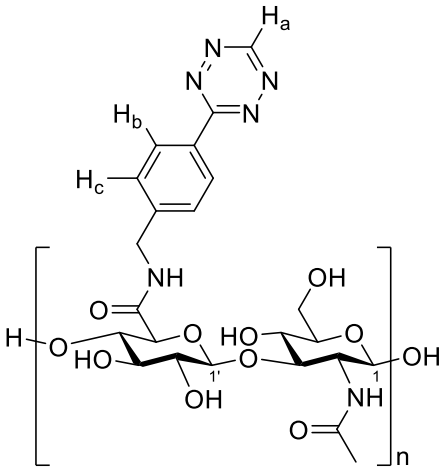

Method 1 based on the 4-(aminomethyl)benzonitrile model:

- 2.5% HA-*g*-Tz

Hyaluronic acid (28 mg, 73.8 µmol -COOH, 1 eq.) was dissolved in MES buffer (7 mL, 100 mM, pH = 6.0). Tetrazine **2.3** (30 mg, 146.4 µmol, 2 eq.), NHS (169 mg, 1472 µmol, 20 eq.) and EDC (127 mg, 662.4 µmol, 9 eq.) were weighed in a glass vial. Then, the hyaluronic acid solution was

transferred to the glass vial containing all the other reagents, and it was vortexed until all the solid reagents were dissolved. The mixture was placed on a rocker overnight at room temperature. The crude product was transferred to a dialysis bag (SnakeSkin dialysis tubing: 7000 MWCO) and it was purified by dialysis at room temperature, successively against NaCl solution (2.5 g/L) for 24 h; water for 24 h; NaCl solution (9 g/L) for 24 h; and water for 6 h. The resulting solution was freeze-dried and analysed by ^{1}H NMR.

^{1}H NMR (500 MHz, D_2O): δ 10.38-10.36 (m, 0.02H, H_a); 8.50-8.45 (m, 0.05H, H_b); 7.66-7.57 (m, 0.04, H_c); 4.54-4.46 (m, 2H, H_1 and $H_{1'}$); 2.01 (s, 3H, C<u>H$_3$</u>-CO-NH-).

- 3% HA-*g*-Tz

Hyaluronic acid (28 mg, 73.8 µmol -COOH, 1 eq.) was dissolved in MES buffer (7 mL, 100 mM, pH = 6.0). Tetrazine **2.3** (30 mg, 146.4 µmol, 2 eq.), NHS (169 mg, 1472 µmol, 20 eq.) and EDC (183.5 mg, 957 µmol, 13 eq.) were weighed in a glass vial. Then, the hyaluronic acid solution was transferred to the glass vial containing all the other reagents, and it was shaken until all the solid reagents were dissolved. The mixture was shaken gently overnight at room temperature. The crude product was transferred to a dialysis bag (SnakeSkin dialysis tubing: 7000 MWCO) and it was purified by dialysis at room temperature, successively against NaCl solution (5.5 g/L) for 24 h; water for 24 h; water for 24 h; NaCl solution (7 g/L) for 24 h; and water for 24 h. The resulting solution was freeze-dried and analysed by ^{1}H NMR.

^{1}H NMR (500 MHz, D_2O): δ 10.38-10.36 (m, 0.02H, H_a); 8.50-8.45 (m, 0.06H, H_b); 7.66-7.57 (m, 0.06H, H_c); 4.54-4.46 (m, 2H, H_1 and $H_{1'}$); 2.01 (s, 3H, C<u>H$_3$</u>-CO-NH-).

<u>Method 2 using ratios of reagents employed by Famili *et al.*:</u>[152]

- 4% HA-*g*-Tz

Hyaluronic acid (28.5 mg, 39.4 µmol -COOH, 1 eq.), **2.3** (28 mg, 125.5 µmol, 1.6 eq.), NHS (8 mg, 75 µmol, 1 eq.) and EDC (22 mg, 112.5 µmol, 1.5 eq.) were weighed in a 10 mL round bottom flask. Then, MES buffer (7.12 mL, 100 mM, pH = 6.0) and a drop of pyridine were added to the solid reagents. The mixture was stirred overnight at room temperature. An attempt to purify the product by size exclusion chromatography was not successful, and crude product was transferred to a dialysis bag (SnakeSkin dialysis tubing: 7000 MWCO) and it was purified by dialysis at room temperature, successively against NaCl solution (2.5 g/L) for 24 h and water for 24 h. The solution was freeze-dried and analysed by ^{1}H NMR.

^{1}H NMR (500 MHz, D_2O): δ 10.38-10.36 (m, 0.02H H_a); 8.50-8.45 (m, 0.04H, H_b); 7.66-7.57 (m,0.04H, H_c); 4.54-4.46 (m, 2H, H_1 and $H_{1'}$); 2.01 (s, 3H, $C\underline{H_3}$-CO-NH-).

- 5% HA-*g*-Tz

Hyaluronic acid (15 mg, 39.4 µmol -COOH, 1 eq) was weighed in a 15 mL falcon tube and it was dissolved in MES buffer (3.75 mL, 100 mM, pH = 6.0). NHS (13 mg, 113.4 µmol, 3 eq.) and EDC (14 mg, 75.6 µmol, 2 eq.) were added to the HA solution and which was left for 30 min. Then, **2.3** (16 mg, 75.6 µmol, 2 eq.) was added and the mixture was vortexed to achieve a red cloudy solution. The mixture was placed on a rocker overnight at room temperature. The crude product was transferred to a dialysis bag (SnakeSkin dialysis tubing: 7000 MWCO) and it was purified by dialysis at room temperature, successively against NaCl solution (7.5 g/L) for 24 h and water for 24 h. The resulting suspension was freeze-dried and analysed by ^{1}H NMR.

^{1}H NMR (500 MHz, D_2O): δ 10.38-10.36 (m, 0.5H, H_a); 8.50-8.45 (m, 0.10H, H_b); 7.66-7.57 (m, 0.11H, H_c); 4.54-4.46 (m, 2H, H_1 and $H_{1'}$); 2.01 (s, 3H, $C\underline{H_3}$-CO-NH-).

SEC-MALS (HEPES buffer 10 mM, NaCl 150 mM. pH 7.4): M_n 115 kDa, M_w 204 kDa, Đ 1.77, R_h 46.6 nm.

7.4.3 HA-*g*-Propargyl(4.1)[140,141,152]

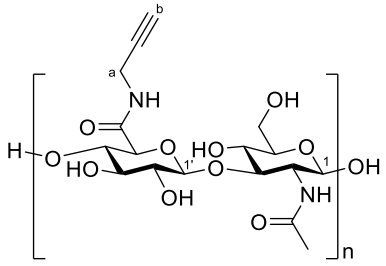

Hyaluronic acid (28 mg, 84 µmol -COOH, 1 eq.) was weighed in a 10 mL glass vial and dissolved in MES buffer (7 mL, 100 mM, pH = 6.0) by shaking gently overnight at room temperature. EDC* and NHS** (Table 7.3) were added in this order to the HA solution and the carboxylic acid were activated for 20 min. This step released gas bubbles. Then, the amine molecule*** (Table 7.3) was added to the solution. The mixture was placed on a rocker overnight at room temperature. The crude product was transferred to a dialysis bag (SnakeSkin dialysis tubing: 7000 MWCO) and it was purified by dialysis at room temperature, successively against NaCl solution (1 M) for 24 h followed by four dialysis against water, each for 24 h. The resulting suspension was freeze-dried and analysed by ^{1}H NMR.

Table 7.3: Amounts of EDC, NHS and propargylamine/1-amino-3-butyne used in coupling reactions

Exp	EDC*			NHS**			Amine molecule***		
	mg	µmol	eq.	mg	µmol	eq.	µL	µmol	eq.
4.1 Test 1	352	1680	20	172	1596	19	21	336	4
4.1 Test 5†	352	1680	20	172	1596	19	21	336	4
4.1 Test 6‡	352	1680	20	172	1596	19	27.8	336	4
4.1 Test 1a/1b┼	352	1680	20	172	1596	19	21	336	4
4.1 Test 1 B⊤	352	1680	20	172	1596	19	21	336	4
4.1 Test 2	35.2	168	2	28.5	251	3	10.5	168	2
4.2 Test 1ᴸ	279	1460	20	160	1387	19	18.7	292	4

4.1 Test 5†: This experiment was performed in water, not in MES buffer

4.1 Test 6‡: This experiment was performed using 1-amino-3-butyne as amine instead of propargylamine.

4.2 Test1ᴸ : For this experiment, the HA used was 40-50 kDa.

4.1 Test 1a/1b┼: The crude product mixture was divided between 3 falcon tubes, two of which were treated with hydroxylamine (1680 µmol and 84 µmol respectively) for 2 days before purification by dialysis as described in the method above.

4.1 Test 1B⊤: The crude product mixture was purified by dialysis at room temperature, successively against NaCl solution (1 M) for 24h; NaOH solution (pH = 10); and four dialysis against water, each for 24h.

7.4.4 HA-*g*-Propargyl(4.2)[206]

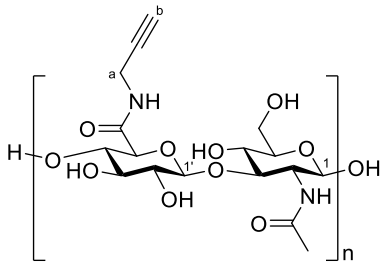

Hyaluronic acid (50 mg, 126 µmol, -COOH, 1 eq.) was weighed in a 15 mL falcon tube, dissolved in MES buffer (50 mM, pH = 4.0) according Table 7.4, last column, and placed on a rocker overnight at room temperature. EDC* and NHS** (Table 7.4) were added in this order to the HA solution and the carboxylic acid groups were activated for 20 min. This step released gas bubbles. Then, propargylamine*** (Table 7.4) was added to the solution. The mixture was placed on a rocker overnight at room temperature. The crude product was transferred to a dialysis bag (SnakeSkin dialysis tubing: 7000 MWCO) and it was purified by dialysis at room temperature,

successively against NaCl solution (1 M) for 24 h followed by four dialysis against water, each for 24 h. The resulting suspension was freeze-dried and analysed by ^{1}H NMR.

Table 7.4: Amounts used for EDC, NHS and Propargylamine.

Exp	EDC*			NHS**			Propargylamine***			MES
	mg	µmol	eq.	mg	µmol	eq.	µL	µmol	eq.	mL
4.1 Test 3	144	755	6	73	629	5	32	504	4	3.3
4.1 Test 4	144	755	6	73	629	5	32	504	4	10
4.2 Test 2‡	151	786	6	75	655	5	33.6	534	4	3.3

4.12‡: For this experiment, the HA used was 40-50 kDa.

7.4.5 HA-*g*-Propargyl(4.3)[216]

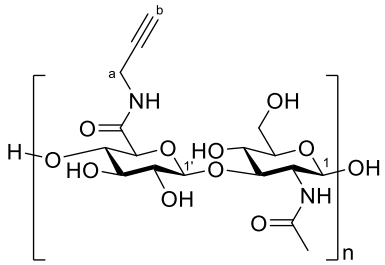

Hyaluronic acid (50 mg, 125.5 µmol -COOH, 1 eq.) was dissolved in MES buffer (15 mL, 100 mM, pH = 5.5) overnight at room temperature while placed on a rocker. The following day DMTMM* (Table 7.5) was added to HA solution and the carboxylic acid groups were activated for 10 min followed by the addition of propargylamine** (Table 7.5). The mixture was placed on a rocker overnight at room temperature. The crude product was transferred to a dialysis bag (SnakeSkin dialysis tubing: 7000 MWCO) and it was purified by dialysis at room temperature, successively against NaCl solution (1 M) for 24 h followed by four dialysis against water, each for 24 h. The resulting solution was freeze-dried and analysed by ^{1}H NMR and multi-angle light scattering (MALS).

Table 7.5: Amounts used for DMTMM and Propargylamine.

Experiment	DMTMM*			Propargylamine**		
4.3	mg	µmol	eq.	µL	µmol	eq.
Test 1	35	125.5	1	8	125.5	1
Test 2	105	376.5	3	24	376.5	3
Test 3	210	753	6	48	753	6
Test 4	350	1255	10	80	1255	10

For Test **1**:

^{1}H NMR (500 MHz, D_2O): 4.51 (d, 2H, H_1 and $H_{1'}$); 4.05 (dd, *J* = 62.4 Hz, *J* = 18.0 Hz, H_a); 3.91-3.30 (m), 2.71 (s, 0.21H, H_b); 2.02 (s, 3H, CO-C$\underline{H_3}$).

SEC-MALS (HEPES buffer 10 mM, NaCl 150 mM. pH 7.4): M_n 115 kDa, M_w 139 kDa, Đ 1.20, R_h 37.7 nm.

For Test **2**:

^{1}H NMR (500 MHz, D_2O): 4.51 (d, 2H, H_1 and $H_{1'}$); 4.05 (dd, *J* = 62.4 Hz, *J* = 18.0 Hz, H_a); 3.91-3.30 (m), 2.71 (s, 0.19H, H_b); 2.02 (s, 3H, CO-C$\underline{H_3}$).

SEC-MALS (HEPES buffer 10 mM, NaCl 150 mM. pH 7.4): M_n 97 kDa, M_w 112 kDa, Đ 1.43, R_h 37.0 nm.

For Test **3**:

^{1}H NMR (500 MHz, D_2O): 4.5 (s, 2H, H_1 and $H_{1'}$); 4.05 (dd, *J* = 61.7 Hz, *J* = 17.7 Hz, H_a); 3.94-3.27 (m), 2.70 (s, 0.57H, H_b); 2.02 (s, 3H, CO-C$\underline{H_3}$).

SEC-MALS (HEPES buffer 10 mM, NaCl 150 mM. pH 7.4): M_n 137 kDa, M_w 140 kDa, Đ 1.03, R_h 43.4 nm.

For Test **4**:

^{1}H NMR (500 MHz, D_2O): 4.53 (d, 2H, H_1 and $H_{1'}$); 4.05 (dd, *J* = 60.9 Hz, *J* = 17.6 Hz, H_a); 3.94-3.25 (m), 2.70 (s, 0.45H, H_b); 2.02 (s, 3H, CO-C$\underline{H_3}$).

SEC-MALS (HEPES buffer 10 mM, NaCl 150 mM. pH 7.4): M_n 136 kDa, M_w 176 kDa, Đ 1.29, R_h 39.8 nm.

7.4.6 HA-*g*-Lac (4.4)

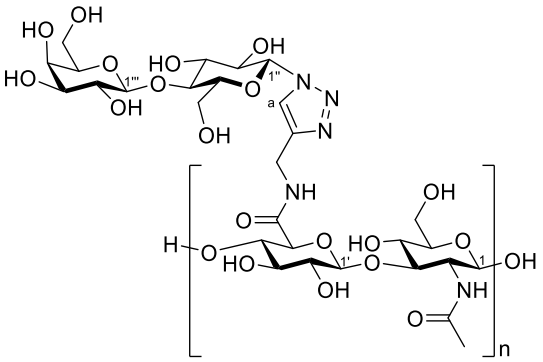

Method 1: Synthesis without THPTA:[218]

The following components (Table 7.6) were added to a two mL Eppendorf tube. All the stocks were in water.

Table 7.6: Summary of stock solutions and final concentrations in the CuAAC reaction using **4.3**.

Reagent	Stock	Final concentration	V (µL)
HA-*g*-Propargyl 4.3	5 mM*	4 mM	1500
Lac-N_3	400 M	4 mM	18.75
$CuSO_4$	500 mM	0.2 mM	0.75
Sodium ascorbate	500 mM	4 mM	15
H_2O	-	-	340.5

* Concentration of alkyne groups

The reaction mixture was incubated at 37 ºC overnight. Then, the crude product was transferred to a dialysis bag (SnakeSkin dialysis tubing: 7000 MWCO) and it was purified by dialysis at room temperature, successively against ethylenediaminetetraacetic acid solution (10 mM EDTA) for 24 h and two dialysis against water, each for 24 h. The resulting solution was freeze-dried and analysed by ^{1}H NMR spectroscopy and SEC-MALS.

^{1}H NMR (500 MHz, D_2O): δ 8.21 (s, 0.12H, H_a); 5.80 (d, *J* = 9.2 Hz, 0.13H, H_1''); 4.54-4.49 (m, 2.14H H_1 and $H_{1'}$); 4.08-3.44 (m); 3.42-3.27 (m), 2.02 (s, 3H, CO-CH_3).

SEC-MALS (HEPES buffer 10 mM, NaCl 150 mM, pH 7.4): M_n 22 kDa, M_w 35 kDa, Đ 1.67, R_h 17.1 nm.

Method 2: Synthesis with THPTA:[206]

The following components (Table 7.7) were added to a two mL Eppendorf tube. All the stocks were in water.

Table 7.7: Summary of stock solutions and final concentrations in the CuAAC reaction using **4.3**.

Reagent	Order of addition	Stock	Final concentration	V (µL)
HA-*g*-Propargyl 4.3	6	5 mM *	4 mM	1500
Lac-N_3	2	400 M	4 mM	18.4
$CuSO_4$	3	500 mM	1.2 mM	4.42
Sodium ascorbate	4	500 mM	30 mM	110.4
THPTA	5	500 mM	8 mM	29.44
H_2O	1	-	-	207.34

* Concentration of alkyne groups

The reaction mixture was incubated at 37 ºC overnight. Then, the crude product was transferred to a dialysis bag (SnakeSkin dialysis tubing: 7000 MWCO) and it was purified by dialysis at room temperature, successively against ethylenediaminetetraacetic acid solution (10 mM EDTA) for 24 h and two dialysis against water, each for 24 h. The resulting solution was freeze-dried and analysed by ^{1}H NMR spectroscopy and SEC-MALS.

^{1}H NMR (500 MHz, D_2O): δ 8.21 (s, 0.11H, H_a); 5.80 (d, *J* = 9.2 Hz, 0.13H, H_1''); 4.54 (m, 2H H_1 and $H_{1'}$); 4.08-3.44 (m); 3.42-3.27 (m), 2.02 (s, 3H, CO-C$\underline{H_3}$).

SEC-MALS (HEPES buffer 10 mM, NaCl 150 mM, pH 7.4): M_n 51 kDa, M_w 72 kDa, Đ 1.41, R_h 22.3 nm.

7.4.7 HA-*g*-Lewis^x (4.5)

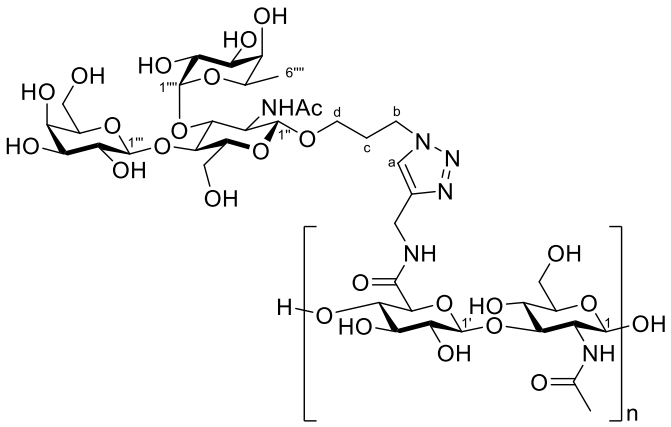

HA-*g*-Propargyl **4.3** (Test 3, 50% derivatization alkyne, 22.2 mg, 0.029 mmol alkyne) was dissolved overnight in 5.8 mL of water in a 15 mL Falcon tube. The following day, the stock solutions listed in Table 7.8 were added. All the stocks were in water.

Table 7.8: Summary of stock solutions and final concentrations in the CuAAC reaction to synthesize **4.5**.

Reagent	Order of addition	Stock	Final concentration	V
HA-*g*-Propargyl 4.3	6	5 mM*	4 mM	5.8 mL
Azidopropyl Le^x (3.5)	2	400 M	4 mM	72.5 µL
$CuSO_4$	3	500 mM	1.2 mM	17.4 µL
Sodium ascorbate	4	500 mM	30 mM	434 µL
THPTA	5	500 mM	8 mM	116 µL
H_2O	1	-	-	790.1 µL

* Concentration of alkyne groups

The reaction mixture was incubated at 37 ºC overnight. Then, the crude product was transferred to a dialysis bag (SnakeSkin dialysis tubing: 7000 MWCO) and it was purified by dialysis at room temperature, successively against ethylenediaminetetraacetic acid solution (10 mM EDTA) for 24 h and two dialysis against water, each for 24 h. The resulting solution was freeze-dried and analysed by ^{1}H NMR spectroscopy and SEC-MALS.

^{1}H NMR (500 MHz, D_2O): δ 7.92 (s, 0.3H, H_a); 5.12 (d, J = 3.9 Hz, 0.3H, $H_{1''''}$); 4.85 (q, J = 6.5 Hz, 0.3H, $H_{5''''}$); 4.63 – 4.45 (m, 2.6H, H1, $H_{1'}$, $H_{1''}$ and $H_{1'''}$); 4.00 – 3.28 (m, 13H); 2.16 – 2.13 (m, 0.6H, H_c); 2.04 – 1.97 (m, 3.9H, CO-CH_3 and CO-$CH_{3''}$); 1.17 (d, J = 6.6Hz, 0.9H, $H_{6''''}$).

SEC-MALS (HEPES buffer 10 mM, NaCl 150 mM, pH 7.4): M_n 27.4 kDa, M_w 29.8 kDa, Đ 1.23, R_h 15.9 nm.

7.4.8 HA-*g*-Gb_3 (4.6)

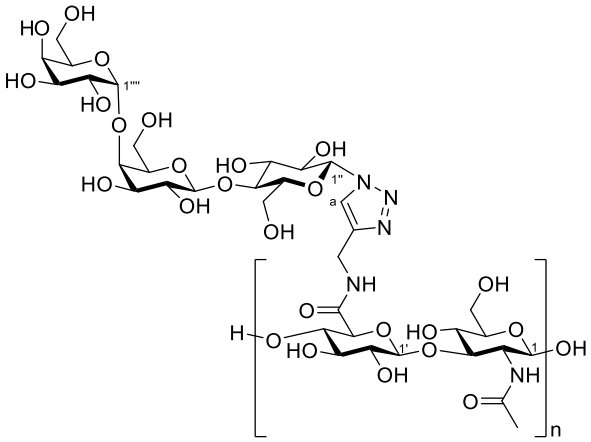

HA-*g*-Propargyl **4.3** (Test 3, 50% derivatization alkyne, 22.7 mg, 0.029 mmol alkyne) was dissolved overnight in 5.8 mL of water in a 15 mL Falcon tube. The following day, the stock solutions listed in Table 7.9 were added. All the stocks were in water.

Table 7.9: Summary of stock solutions and final concentrations in the CuAAC reaction to synthesize **4.6**.

Reagent	Order of addition	Stock	Final concentration	V
HA-*g*-Propargyl 4.3	6	5 mM*	4 mM	5.8 mL
Gb_3-N_3 (3.11)	2	400 M	4 mM	72.5 µL
$CuSO_4$	3	500 mM	1.2 mM	17.4 µL
Sodium Ascorbate	4	500 mM	30 mM	434 µL
THPTA	5	500 mM	8 mM	116 µL
H_2O	1	-	-	790.1 µL

* Concentration of alkyne groups

The reaction mixture was incubated at 37 ºC overnight. Then, the crude product was transferred to a dialysis bag (SnakeSkin dialysis tubing: 7000 MWCO) and it was purified by dialysis at room temperature, successively against ethylenediaminetetraacetic acid solution (10 mM EDTA) for 24 h and two dialysis against water, each for 24 h. The resulting solution was freeze-dried and analysed by ^{1}H NMR spectroscopy and SEC-MALS.

^{1}H NMR (500 MHz, D_2O): δ 8.21 (s, 0.35H, H_a); 5.82-5.76 (m, 0.35H, H_1''); 4.97 (d, *J* = 3.9 Hz, 0.37H, H_1''''); 4.57-4.49 (m, 2H H_1 and $H_{1'}$); 4.08-3.44 (m); 3.42-3.27 (m), 2.02 (s, 3H, CO-C$\underline{H_3}$).

SEC-MALS (HEPES buffer 10 mM, NaCl 150 mM, pH 7.4): M_n 64.7 kDa, M_w 89.2 kDa, Đ 1.38, R_h 26.9 nm.

7.4.9 Biotinylation of hyaluronic acid (5.1)[264]

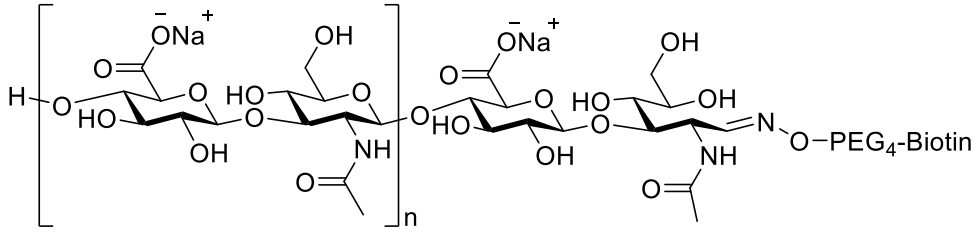

A solution of hyaluronic acid (final concentration 25 µM, 5 mg/mL) was transferred to a 200 µL Eppendorf tube. Then, sodium acetate (final concentration 50 mM), aniline (final concentration 20 mM) and EZ-link Alkoxyamine PEG_4-Biotin (ThermoFisher; final concertation 75 µM) were added following the order described. The reaction mixture was incubated overnight at 37 ºC in a thermocycler at 300 rpm. The following day, the product was purified using a desalting column (Pd-10 G-25M with MWCO = 5000 Da; GE Healthcare) taking elution aliquots of 250 µL. The resulting fractions were analysed to check for the presence of the polysaccharide by spotting 3 µL onto a

TLC plate, which was dried and dipped in a solution of orcinol (20.2 mM) and sulfuric acid (0.9 M) in water, and heating with a heat gun. Fractions containing HA were then analysed by QCM-D using a streptavidin monolayer as described in Section 7.8.2, to determine which fractions contained 5.1.

7.4.10 Biotinylation of glycopolymers 5.2, 5.3 and 5.4

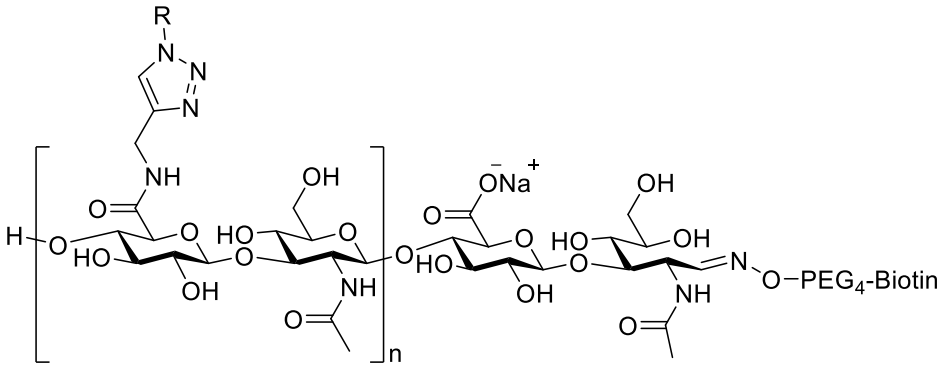

R= Lac **5.2** R= Propyl Le^x **- 5.3** R= Gb_3 - **5.4**

A solution of glycopolymer (**4.4**, **4.5** or **4.6**; final concentration 25 µM, 5 mg/mL) was transferred to a 200 µL Eppendorf. Then, sodium acetate (final concentration 50 mM), aniline (final concentration 20 mM) and EZ-link Alkoxyamine PEG_4-Biotin (ThermoFisher; final concertation 75 µM) were added following the order described. The reaction mixture was incubated overnight at 37 ºC at 300 rpm in a thermocycler. The following day, the product was purified using a desalting column (Pd-10 G-25M with MWCO = 5000 Da; GE Healthcare) taking aliquots of 250 µL. The resulting fractions were analysed to check for the presence of the polysaccharide by spotting 3 µL onto a TLC plate, which was dried and dipped in a solution of orcinol (20.2 mM) and sulfuric acid (0.9 M) in water, and heating with a heat gun. Fractions containing HA were then analysed by QCM-D using a streptavidin monolayer as described in Section 7.8.2, to determine which fractions contained **5.2**, **5.3** or **5.4** respectively.

7.4.11 Addition of polyhistidine to HA-*g*-Gb_3 4.6

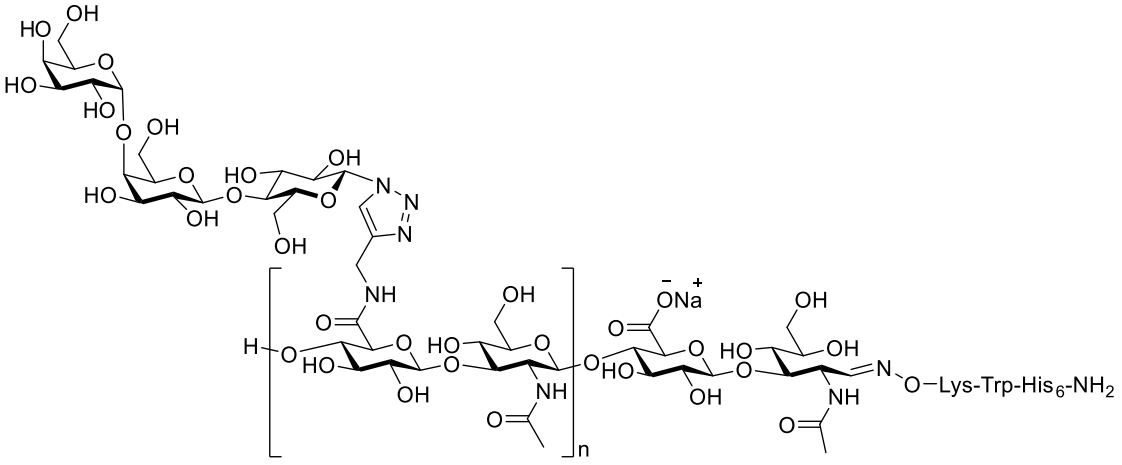

5.6

A solution of HA-*g*-Gb_3 **4.6** (final concentration 25 µM (or 5 mg/mL)) was transferred to a 200 µL Eppendorf. Then, sodium acetate (final concentration 50 mM), aniline (final concentration 20 mM) and peptide **5.5** (final concertation 75 µM) were added following the order described. The reaction mixture was incubated overnight at 37 ºC at 300 rpm in a thermocycler. The following day, the product was purified using a desalting column (Pd-10 G-25M with MWCO = 5000 Da; GE Healthcare) taking elution aliquots of 250 µL. The resulting fractions were analysed to check for the presence of the polysaccharide by spotting 3 µL onto a TLC plate, which was dried and dipped in a solution of orcinol (20.2 mM) and sulfuric acid (0.9 M) in water, and heating with a heat gun. Fractions containing HA were then analysed by QCM-D using a streptavidin monolayer as described in Section 7.8.2, to determine which fractions contained **5.6**.

7.5 Expression of proteins

7.5.1 Common buffers, solutions and media

7.5.1.1 Buffer and solutions

All solutions were made 15 mΩ water (ELGA PURLAB classic), adjusting pH with 5 M NaOH and/or 5 M HCl.

TRIS stock Buffer: NaCl 1 M, TRIS 1 M, 5 mg of DNAse and 1 tablet of protease inhibitor adjusted to pH 8.

Imidazole stock buffer: 200 mM TRIS (pH 8.0), 200 mM NaCl, 2 M Imidazole.

Bradford test: 2 mL of Protein Assay Dye Reagent Concentrate from Bio-Rad diluted in 10 mL of mQ water.

Kanamycin stock solution: 50 mg/mL

Ampicillin stock solution: 100 mg/mL

IPTG solution: 500 mM IPTG

Glycerol solution: 80% (*v/v*) glycerol in water.

7.5.1.2 Bacterial growth media

Quantities for 1 L of media:

LB autoinduction (Formamedium) – 34.85 g

LB growth media (LB): 25 g (10 g Tryptone, 5 g Yeast extract, 10 g NaCl)

2xYT growth media: 16 g Tryptone, 10 g Yeast extract, 5 g NaCl

LB agar media (LB-Agar): 25 g LB media, 15 g Agar

7.5.1.3 SDS PAGE buffers

5× SDS-PAGE loading buffer: 250 mM Tris, 10% (w/v) SDS, 1.0 M DTT, 50% (v/v) glycerol, 0.01% (w/v) bromophenol blue.

SDS-PAGE running buffer: 25 mM Tris-base, 192 mM Glycine, 0.1% (w/v) SDS.

Coomassie stain: Coomassie G250 (0.625% (w/v), 40% (v/v) methanol, 10% (v/v) acetic acid.

Coomassie destain: 40% (v/v) methanol, 10% (v/v) acetic acid.

SDS-PAGE loading buffer: 50 mM TRIS-HCl (pH 6.8), 2% (*w/v*) SDS, 10% (*v/v*) glycerol, 100 mM DTT, 12.5 mM EDTA, 0.02% (*w/v*) bromophenol blue.

7.5.2 Standard protocols for protein expression

7.5.2.1 Expression of protein β(1-4)GalT1

A stab was taken from a stock of *E.coli* BL21(DE3)omp8 cells containing the plasmid encoding the protein to be expressed and it was used to inoculate 5 mL of LB growth medium containing Kanamycin (50 µg/mL) in a 50 mL falcon tube. The starter culture was incubated overnight at 37°C, and then used to inoculate 1 L LB autoinduction media containing Kanamycin (50 mg/L). This culture was incubated at 37 °C for 3 h and, then at 18 °C for 48 h. The bacterial cells were isolated by centrifugation at 10,000 x *g* for 15 min. The supernatant was discarded and the bacterial pellet was suspended in 50 mL of TRIS lysate buffer (200 mM TRIS, 200 mM NaCl, pH 8.0, DNAase I and a tablet of Protease Inhibitor).

The bacterial suspension was sonicated for 2 min and allowed to rest for 1 min in an ice-bath and the process was repeated 3 times. The resulting lysate was cleared by centrifugation at 48,000 x *g* for 30 min and the pellet was discarded. The brown solution was purified using a Nickel-NTA affinity column and washing with TRIS buffer (200 mM TRIS, 200 mM NaCl, pH 8.0, 40 mL) for the flowthrough, TRIS buffer (200 mM TRIS, 200 mM NaCl, pH 8.0, 20 mM Imidazole, 60 mL) for the

first wash and eluted with elution buffer (200 mM TRIS, 200 mM NaCl, pH 8.0, 200 mM Imidazole, 40 mL) until Bradford test was negative. All the aliquots which contained protein were combined together and concentrated using a 10 kDa MWCO ultrafiltration concentrator. The sample was diluted and concentrated three times with the storage buffer (100 mM TRIS, 100 mM NaCl, pH 8.0) using the 10 kDa MWCO ultrafiltration concentrator to remove the imidazole.

The resulting solution of β(1-4)GalT1 was quantified by UV absorption (λ = 280 nm, ε = 108430 cm^{-1}) giving a final concentration of 44.6 μM. Finally, sodium dodecylsulfate polyacrylamide gel electrophoresis (SDS-PAGE) was performed to check the purity of the protein solution (Figure 7.1).

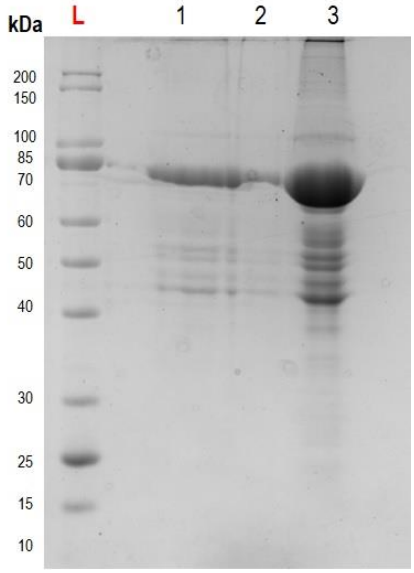

Figure 7.1: SDS-PAGE for β(1-4)GalT1 purification on Ni-NTA resin. Lane L is the protein mass ladder, lane 1 is the flowthrough, lane 2 is the first wash and lane 3 is the elution with imidazole.

7.5.2.2 Expression of FKP

A stab was taken from a stock of *E.coli* BL21(DE3)omp8 cells containing the plasmid encoding the protein to be expressed and it was used to inoculate 5 mL of 2xYT growth medium containing ampicillin (100 μg/mL) in a 50 mL falcon tube. The starter culture was incubated overnight at 37 °C, and then used to inoculate 400 mL 2xYT growth media containing ampicillin (100 mg/L). This culture was incubated at 37 °C for 3.5 h (until OD_{600} = 0.668) and induced by adding IPTG stock solution (400 μL) and leaving at 25 °C overnight. The bacterial cells were isolated by centrifugation at 10,000 x *g* for 15 min. The supernatant was discarded and the bacterial pellet was suspended in 10 mL of TRIS buffer (200 mM TRIS, 200 mM NaCl, pH 8.0, DNAase I and a tablet of Protease Inhibitor).

The bacterial suspension was sonicated for 2 min and allowed to rest for 1 min and the process was repeated twice. The resulting lysate was cleared by centrifugation at 30,000 x *g* for 40 min and

the pellet was discarded. The brown solution was loaded onto a Nickel-NTA affinity column and washed with washing buffer (200 mM TRIS, 200 mM NaCl, pH 8.0, 40 mL or until the Bradford test was negative) and eluted with elution buffer 6 (200 mM TRIS, 200 mM NaCl, pH 8.0, 300 mM Imidazole, 30 mL or until Bradford test was negative). The resulting protein was dialysed twice against TRIS buffer (100 mM TRIS, 100 mM NaCl, pH 8.0) at 4 ºC to remove the remaining imidazole.

The resulting FKP solution was concentrated using a 10 kDa MWCO ultrafiltration concentrator and quantified by UV absorption (λ = 280 nm, ε = 151315 cm^{-1}) giving a final concentration of 39.0 µM. The enzyme was stored in 10% glycerol solution in TRIS buffer (100 mM TRIS, 100 mM NaCl, pH 8.0) at 4 ºC. Finally, SDS-PAGE was performed to check the purity of the protein solution (Figure 7.2).

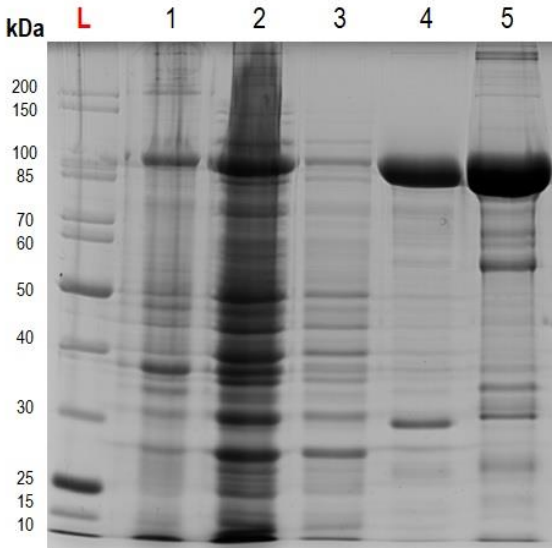

Figure 7.2: SDS-PAGE for FKP expression and purification. Lane L is the protein mass ladder, lane 1 is the cell lysate pellet, lane 2 is the flowthrough from the Ni-NTA column, lane 3 is the first wash, lane 4 is the elution step, lane 5 is an FKP reference sample expressed and purified by Dr. Kristian Hollingsworth.

7.5.2.3 Expression of protein α(1-2)FucT HP

A stab was taken from a stock of *E.coli* BL21(DE3)omp8 cells containing the plasmid encoding the protein to be expressed and it was used to inoculate 5 mL of LB growth medium containing kanamycin (50 µg/mL) in a 50 mL falcon tube. The starter culture was incubated overnight at 37 °C, and then used to inoculate 400 mL LB growth media containing kanamycin (50 mg/L). This culture was incubated at 37 °C for 3.5 h (until OD_{600} = 0.883) and induced by adding IPTG stock solution (80 µL or 8 µL, to give final IPTG concentrations of either 0.1 mM or 0.01 mM) and the culture was incubated at 25 °C overnight. The bacterial cells were isolated by centrifugation at 10,000 x *g* for 15 min. The supernatant was discarded and the bacterial pellet was suspended in

10 mL of TRIS buffer (200 mM TRIS, 200 mM NaCl, pH 8.0, DNAase I and a tablet of Protease Inhibitor).

The bacterial suspension was sonicated for 2 min and allowed to rest for 1 min and the process was repeated twice. The resulting lysate was cleared by centrifugation at 30,000 x *g* for 40 min and the pellet was discarded. The brown solution was loaded onto a Nickel-NTA affinity column and washed washing buffer (200 mM TRIS, 200 mM NaCl, pH 8.0, 40 mL or until the Bradford test was negative) and eluted with elution buffer 6 (200 mM TRIS, 200 mM NaCl, pH 8.0, 300 mM Imidazole, 30 mL or until Bradford test was negative). The resulting protein was dialysed twice against TRIS buffer (100 mM TRIS, 100 mM NaCl, pH 8.0) at 4 ºC to remove the remaining imidazole.

The resulting solution of α(1-2)FucT HP solution was concentrated using a 10 kDa MWCO ultrafiltration concentrator and quantified by UV absorption (λ = 280 nm, ε = 126545 cm^{-1}) giving the following results:

- For the culture induced using 0.1 mM IPTG, the final concentration of α(1-2)FucT HP was 31.5 µM, final volume 300 µL.
- For the culture induced using 0.01 mM IPTG, the final concentration of α(1-2)FucT HP was 22.4 µM, final volume 500 µL.

The enzyme was stored in 50% glycerol solution in TRIS buffer (100 mM TRIS, 100 mM NaCl, pH 8.0) at -20 ºC. Finally, SDS-PAGE was performed to check the purity of the protein solution (Figure 7.3).

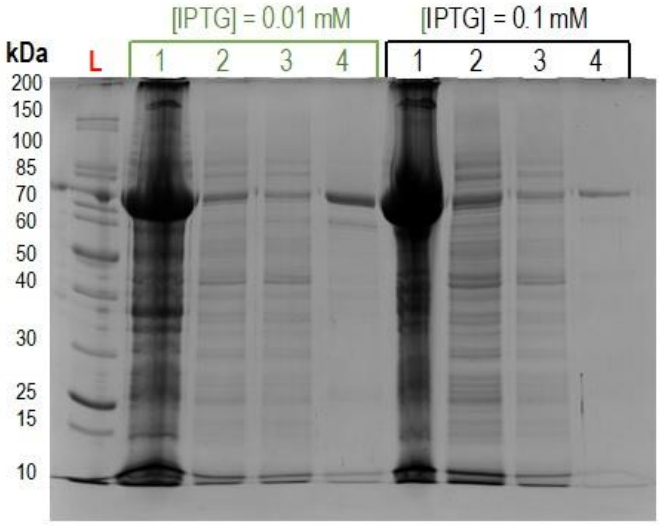

Figure 7.3: SDS-PAGE for α(1-2)FucT HP purification. Lane L is the protein mass ladder, lane 1 is the cell lysate pellet, lane 2 is the flowthrough from the Ni-NTA column, lane 3 is the first wash and lane 4 is the elution.

7.5.2.4 Expression of protein LgtC

A stab was taken from a stock of *E.coli* BL21(DE3) cells containing the plasmid encoding the protein to be expressed and it was used to inoculate 5 mL of LB growth medium containing kanamycin (50 µg/mL) in a 50 mL falcon tube. The starter culture was incubated overnight at 37 °C, and then used to inoculate 500 mL LB autoinduction growth media containing kanamycin (50 mg/L). This culture was incubated at 37 °C for 2 h and, then at 25 °C overnight. The bacterial cells were isolated by centrifugation at 10,000 x *g* for 15 min. The supernatant was discarded and the bacterial pellet was suspended in 10 mL of TRIS buffer (200 mM TRIS, 200 mM NaCl, pH 8.0, DNAase I and a tablet of Protease Inhibitor).

The bacterial suspension was sonicated for 2 min and allowed to rest for 1 min and the process was repeated twice. The resulting lysate was cleared by centrifugation at 30,000 x *g* for 40 min and the pellet was discarded. The brown solution was loaded onto a Nickel-NTA affinity column and washing buffer (200 mM TRIS, 200 mM NaCl, pH 8.0, 70 mL or until the Bradford test was negative) and eluted with elution buffer 6 (200 mM TRIS, 200 mM NaCl, pH 8.0, 300 mM Imidazole, 60 mL or until Bradford test was negative). The sample was diluted and concentrated three times with TRIS buffer (100 mM TRIS, 100 mM NaCl, pH 8.0) using a 10 kDa MWCO ultrafiltration concentrator to remove the imidazole.

The resulting solution of LgtC solution was quantified by UV absorption (λ = 280 nm, ε = 59735 cm^{-1}) giving a final concentration was 119.7 µM (final volume 1500 µL). The enzyme was stored in 40% glycerol solution in TRIS buffer (100 mM TRIS, 100 mM NaCl, pH 8.0) at -20 ºC. Finally, SDS-PAGE was performed to check the purity of the protein solution (Figure 7.4).

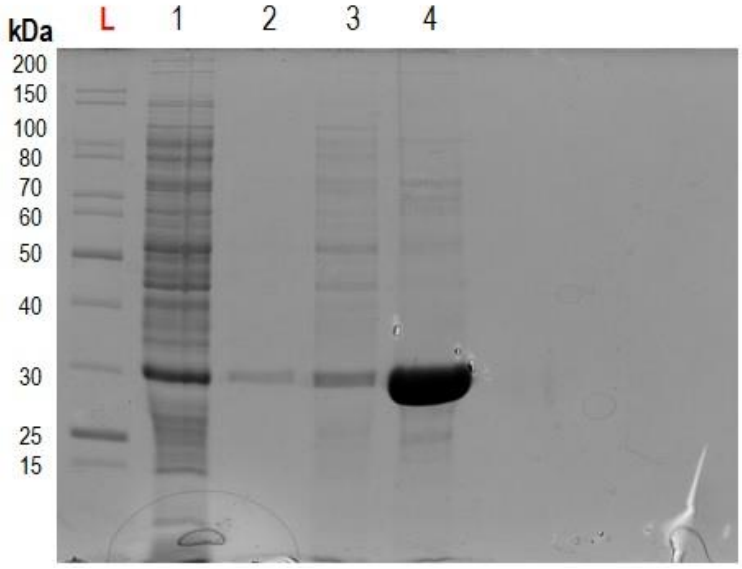

Figure 7.4: PAGE for LgtC purification. Lane L is the protein mass ladder, lane 1 is the cell lysate pellet, lane 2 is the flowthrough from the Ni-NTA column, lane 3 is the first wash and lane 4 is the elution step

7.5.3 Standard protocol for protein analysis

7.5.3.1 SDS-PAGE

Finally, a polyacrylamide gel electrophoresis (PAGE) was done to check the purification grade of the protein solution using BioRad tetragel apparatus The resolving gel was prepared using the recipe in Table 7.10 (column 2) adding TEMED last, the solution was poured immediately into a fixed Bio-Rad 1.50 mm gel cast, and left to set with a layer isopropanol was added to the surface of resolving gel to produce a flat surface. *tert*-Butanol was poured on top of the resolving gel to produce a flat surface and the gel was left to set. The isopropanol was decanted off of the set resolving gel, the stacking gel, prepared according Table 7.10 (column 3) adding TEMED last, was poured on top and the plastic comb inserted to create sample wells. The gel was again left to set at room temperature. Samples for analysis were prepared by mixing 10 µL of protein sample with 10 µL SDS loading buffer and 10 µL aliquots were loaded into the sample wells. Electrophoresis was performed at 180 V in SDS running buffer. After 45 minutes the gels were removed and stained with instant blue for at least 1 h before being stored in water until the gel was imaged.

Table 7.10: Materials for preparing SDS-PAGEs.

Reagents	12% Resolving Gel	Stacking Gel
H_2O	4.25 mL	3.32 mL
1.5 M Tris pH 8.8	2.53 mL	-
0.5 M Tris pH 6.8	-	94.5 µL
40% (*w/v*) Acrylamide	3.00 mL	625 µL
10% (*w/v*) SDS	100 µL	50 µL
10% (w/v) APS	150 µL	50 µL
TEMES	10 µL	5 µL

7.6 Protocol for enzymatic reactions

7.6.1 Synthesis of azidopropyl Le^x (3.5).

7.6.1.1 Reagents and stock solutions:

All solutions were prepared using purified water with a resistivity of at least 15 MΩ

- UDP-Glc (500 mM) in water
- Azidopropyl GlcNAc (**3.3**)
- L-Fucose
- Solution of ATP (400 mM) and GTP (200 mM) in 100 mM TRIS buffer at pH = 8
- β(1-4)GalT1 (2.7 mg/mL) suspension in ammonium sulfate solution

- $Glc(1\text{-}4)_{ep}$ (11.9 mg/mL) suspension in ammonium sulfate solution
- FKP (90 µM) in 100 mM TRIS buffer at pH = 8.0 containing 10% glycerol (*v/v*)
- α(1-3)FucT HP (4.8 mg/mL) suspension in ammonium sulfate solution
- Bovine serum albumin (BSA; 100 mg/mL) in water
- TRIS buffer: 1 M TRIS, 1 M NaCl at pH = 8
- $MnCl_2$ (1 M) in water
- $MgCl_2$ (500 mM) in water

7.6.1.2 Procedure:

The following components (Table 7.11) were added to a 15 mL Falcon tube to synthesize azidopropyl LacNAc **3.4**.

Table 7.11: Reagents used to make azidopropyl LacNAc **3.4**.

Reagent	Stock solution	Final concentration	Quantity
Azidopropyl GlcNAc 3.3 *	-	16 mM	12.5 mg
UDP-Glc	500 mM	21 mM	153.2 µL
β(1-4)GalT1**	2.6 mg/mL	1 mg/mL	383 µL
$Glc(1\text{-}4)_{ep}$**	17.5 mg/mL	1.75 mg/mL	38.3 µL
BSA	100 mg/ mL	1 mg/ mL	1417.1 µL
TRIS	1 M	100 mM	383 µL
$MnCl_2$***	1 M	10 mM	38.3 µL
H_2O	-	-	1417.1 µL

Azidopropyl GlcNAc * was added as a solid.

For β(1-4)GalT1** and $Glc(1\text{-}4)_{ep}$**, the volumes indicated were taken from a stock ammonium sulfate suspension and centrifuged to discard the supernatant. The solid protein was resuspended in equal volume to the original sulfate suspension in water and added to the mixture.

$MnCl_2$*** was added as the last reagent because it can be oxidized.

The resulting mixture was incubated for two nights at 37 °C. The reaction mixture was subjected to mass spectrometry and TLC analysis to check if the reaction was successful. The starting material was not present in either test, therefore, it was transferred to a 50 mL Falcon tube and the following components (Table 7.12) were added to the same tube to perform the fucosylation reaction:

Table 7.12: Reagents used to convert azidopropyl LacNAc to axidopropyl Le^x (**3.5**).

Reagent	Stock solution	Final concentration	Quantity
Crude LacNAc	16 mM	4 mM	3830 µL
Fucose	500 mM	8 mM	245 µL
ATP	400 mM	16 mM	613 µL
GTP	200 mM	8 mM	
α(1-3)FucT HP**	4.8 mg/mL	0.96 mg/mL	3064 µL
FKP	90 µM	8.8 µM	1480 µL
TRIS	1 M	100 mM	1532 µL
$MgCl_2$	500 mM	10 mM	306.4 µL
H_2O	-	-	4.25 mL

α(1-3)FucT HP**, the volume indicated was taken from a stock ammonium sulfate suspension and centrifuged to discard the supernatant. The solid protein was resuspended in equal volume to the original sulfate suspension in water and added to the mixture.

The resulting mixture was incubated for two days at 37 °C. The reaction mixture was subjected to mass spectrometry and TLC analysis to check if the reaction was finished. There was no azidopropyl LacNAc **3.4**, starting material.

7.6.1.3 Purification:

The proteins in the product mixture were removed using a 10 kDa MWCO ultrafiltration concentrator. The resulting aqueous solution was mixed with silica and dried under vacuum to achieve a white powder, which was loaded onto a SNAP 10 g Biotage column to perform silica gel chromatography (elution EtOAc/MeOH from 95:5 to 100% MeOH). The fractions which contained oligosaccharide (visualised on a TLC plate by dipping in a solution of 10% (*v/v*) sulphuric acid in MeOH and heating) were combined together and the solvent was removed under vacuum. The remaining syrup was dissolved in 2 mL of water and purified by size exclusion chromatography (Biogel P2 resin) using ammonium formate (20 mM) as eluent to obtain **3.5** (9.23 mg, 37%).

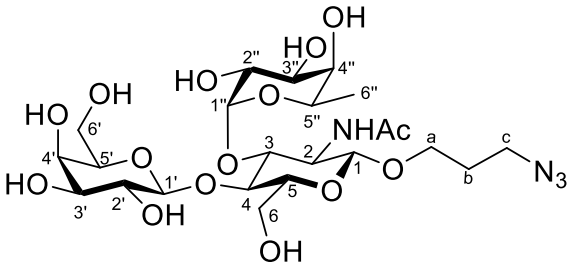

TLC (DCE/MeOH/AcOH/H_2O 50:30:25:10): R_f = 0.30

^{1}H NMR (500 MHz, D_2O): δ 5.11 (d, *J* = 4.0 Hz, 1H, $H_{1''}$); 4.84 (q, *J* = 6.5 Hz, 1H, $H_{5''}$); 4.54 (d, *J* = 8.1 Hz, 1H, H_1); 4.45 (d, *J* = 7.8 Hz, 1H, $H_{1'}$); 4.00 (dd, *J* = 12.4, *J* = 2.3 Hz, 1H, H_6); 3.98-3.92 (m, 1H, H_a); 3.92-3.83 (m, 6H, H_2, H_3, $H_{3'}$, H_4, $H_{4'}$, H_{6a}); 3.79 (d, *J* = 2.7 Hz. 1H, $H_{4''}$); 3.76-3.64 (m, 5H, $H_{2''}$, $H_{3'}$, $H_{6'}$, $H_{a'}$); 3.61-3.57 (m, 2H, H_5, $H_{5'}$); 3.49 (dd, *J* = 9.9, *J* = 7.8 Hz, 1H, $H_{2'}$); 3.42-3.32 (m, 2H, H_c); 2.04 (s, 3H, CH_3-CO-NH-); 1.84 (p, *J* = 6.5 Hz, 2H, H_b); 1.17 (d, *J* = 6.6 Hz, 3H, $H_{6''}$).

^{13}C NMR (126 MHz, D_2O): δ 174.2 (-CO-), 101.8 ($C_{1'}$), 100.9 (C_1), 98.6 ($C_{1''}$), 75.3 (C_5/$C_{5'}$), 74.9 (C_3/C_4/C_5/$C_{5'}$), 73.3 (C_3/C_4), 72.4 ($C_{3'}$), 71.9 ($C_{4''}$), 71.0 ($C_{2'}$), 69.2 ($C_{3''}$), 68.3 ($C_{4'}$), 67.7 ($C_{2''}$), 67.2 (CH_a), 66.7 ($C_{5''}$), 61.5 ($C_{6'}$), 59.7 (C_6), 55.8 (C_2), 47.7 (CH_c), 28.1 (CH_b), 22.2 (CO-CH_3) and 15.3($C_{6''}$).

m/z Found 613.2568 $[M+H]^+$ calc for $C_{23}H_{41}N_4O_{15}$ and found 635.2574 $[M+Na]^+$ calc for $C_{23}H_{40}N_4O_{15}Na$.

7.6.2 Synthesis of Le^x (3.9).

7.6.2.1 Reagents and stock solution:

- UDP-Glc
- L-Fucose
- Solution of ATP (400 mM) and GTP (200 mM) in 100 mM TRIS buffer at pH = 8
- β(1-4)GalT1 (2.7 mg/mL) suspension in ammonium sulfate solution
- $Glc(1\text{-}4)_{ep}$ (11.9 mg/mL) suspension in ammonium sulfate solution
- FKP (90 µM) in 100 mM TRIS buffer at pH = 8.0 containing 10% glycerol (*v/v*)
- α(1-3)FucT HP (4.8 mg/mL) suspension in ammonium sulfate solution
- Bovine serum albumin (BSA; 100 mg/mL) in water
- TRIS buffer: 1 M TRIS, 1 M NaCl at pH = 8
- $MnCl_2$ (1 M) in water
- $MgCl_2$ (500 mM) in water

7.6.2.2 Procedure:

The following components (Table 7.13) were added to a 50 mL Falcon tube to synthesize LacNAc.

Table 7.13: Reagents used to make LacNAc.

Reagent	Stock solution	Final concentration	Quantity
GlcNAc*	-	10 mM	46.5 mg
UDP-Glc*	-	15 mM	181.4 mg
β(1-4)GalT1**	2.6 mg/mL	1 mg/mL	7.9 mL
Glc(1-4)$_{ep}$**	17.5 mg/mL	1.75 mg/mL	2.1 mL
BSA	20 mg/ mL	1 mg/ mL	525 µL
TRIS	1 M	100 mM	2.1 mL
$MnCl_2$***	1 M	10 mM	210 µL
H_2O	-	-	8.22 mL

GlcNAc* and UDP-Glc* were added as a solid in the mixture.

For β(1-4)GalT1** and Glc(1-4)$_{ep}$**, the volumes indicated were taken from a stock ammonium sulfate suspension and centrifuged to discard the supernatant. The solid protein was resuspended in equal volume to the original sulfate suspension in water and added to the mixture.

$MnCl_2$*** was added as the last reagent because it can be oxidized.

The resulting mixture was incubated overnight at 37 °C. The reaction mixture was subjected to mass spectrometry and TLC analysis to check if the reaction was successful. The starting material was not present in either test, therefore, the following components and solutions were added (Table 7.14) to perform the next enzymatic synthesis: the addition the Fuc on the position 3 of the GlcNAc by a linkage α(1-3).

Table 7.14: Reagents used to make Le^x **3.9**.

Reagent	Stock solution	Final concentration	Quantity
LacNAc in the Crude	10 mM	4 mM	21 mL
Fuc*	-	8 mM	68.9 mg
ATP	150 mM	16 mM	5.6 mL
GTP	150 mM	8 mM	2.8 mL
α(1-3)FucT HP**	4.8 mg/mL	0.96 mg/mL	10.5 mL
FKP	200 µM	20 µM	5.25 mL
TRIS	1 M	100 mM	2.1 mL
$MgCl_2$	500 mM	10 mM	5.25 mL
H_2O	-	-	1.05 mL

Fuc* was added as a solid in the mixture.

α(1-3)FucT HP**, the volume indicated were taken form a precipitated protein stock in ammonium sulfate and spined down to discard the supernatant.. The solid protein was resuspended in equal volume to the original sulfate suspension in water and added to the mixture.

The resulting mixture was incubated overnight at 37 °C. The reaction mixture was subjected to mass spectrometry and TLC analysis to check if the reaction was finished. There was no LacNAc, starting material.

7.6.2.3 Purification:

First, the mixture was spined down using a spinner concentrator to remove all the proteins. The resulting water solution was mixed with silica and dried under vacuum to achieve a white powder completely dry. This dry loading was purified using a SNAP 10 g biotage column (elution EtOAc/MeOH from 90:10 to 100% MeOH). The fraction which contained oligosaccharide (observed by TLC using a solution of sulphuric acid (H_2SO_4) 10% (*v/v*) in MeOH) were joined together and the solvent was removed under vacuum. The remaining syrup was dissolved in 2 mL of water and purified by size exclusion column (Biogel P2 resin) using water as eluent to obtain Le^x. (14 mg, 13%)

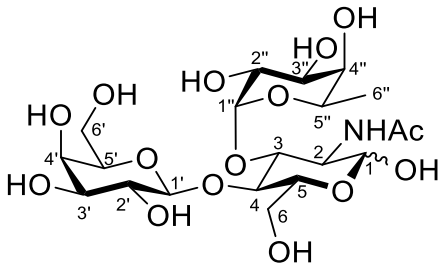

TLC (MeOH/EtOAc 60:40): R_f = 0.17

^{1}H NMR (500 MHz, D_2O): (Proportion Le^x(β)/Le^x(α) 0.6:1) δ 5.10 (t, *J* = 4.0 Hz, 2H, $H_{1''}$ and $H_{1(\alpha)}$); 4.84 (q, *J* = 6.7 Hz, 1.6H, $H_{5''}$); 4.72 (d, J = 8.0 Hz, 0.6 H, $H_{1(\beta)}$); 4.46 (d and d, *J* = 7.8 Hz, *J* = 7.7 Hz, 1.6H, $H_{1'}$); 4.15 (dd, *J* = 10.3 Hz, *J* = 3.5 Hz, 1H, $H_{2(\alpha)}$); 4.02-3.93 (m, 4H, $H_{3(\alpha)}$, $H_{6(\beta)}$, $H_{4(\alpha)}$, $H_{6(\alpha)}$); 3.91-3.88 (m, 4H, $H_{2(\beta)}$, $H_{3''}$, $H_{4'}$); 3.87-3.83 (m, 1.6H, $H_{6(\beta)}$); 3.79 (d, *J* = 2.9 Hz, 1.6H, $H_{4''}$); 3.76-3.60 (m, 5.6H, $H_{6'}$, $H_{6'}$, $H_{2''}$); 3.64-3.63 (m, 1.6H, $H_{3'}$); 3.61-3.58 (m, 2.1H, $H_{5'}$, $H_{5(\alpha)}$); 3.52-3.47 (m, 1.6H, $H_{2'}$); 2.03 (s, 3.4H, C<u>H</u>$_3$-CO-NH-); 1.23 (d, *J* = 6.6 Hz, 0.6H, $H_{6''}$); 1.17 (d and d, *J* = 6.6 Hz, *J* = 6.6 Hz, 3.6H, $H_{6''}$) .

^{13}C NMR (126 MHz, D_2O): δ 174.40 (-<u>C</u>O-), 174.18 (-<u>C</u>O-), 101.77 ($C_{1'}$), 98.58 ($C_{1''}$), 94.69 ($C_{1(\beta)}$), 91.05 ($C_{1(\alpha)}$), 75.41 ($C_{5'}$/$C_{5(\alpha)}$), 73.25 (C_3/C_4/C_5), 72.79 (C_3/C_4/C_5), 72.41 ($C_{3'}$), 71.88 ($C_{4''}$), 71.29

($C_{2'}$), 71.01 (C_3/C_4/C_5), 69.23 ($C_{3''}$/$C_{4'}$), 68.32 ($C_{3''}$/$C_{4'}$), 67.67 ($C_{2''}$), 66.64 ($C_{5''}$), 61.15 ($C_{6'}$), 59.65 (C_6), 56.90 ($C_{2(\beta)}$), 54.06 ($C_{2(\alpha)}$), 22.20 (CO-$\underline{C}H_{3(\alpha/\beta)}$), 21.94 (CO-$\underline{C}H_{3(\alpha/\beta)}$), 15.25 ($C_{6''}$).

ESI HRMS (positive mode): *m/z*: Found $[M+Na]^+$ 552.1898 calc for $C_{20}H_{35}NNaO_{15}$ 552.1904.

7.6.3 Synthesis of Gb_3-N_3 (3.11) using LgtC as the glycosyltransferase.

7.6.3.1 Reagents and stock solution:

- UDP-Glc
- Lac-N_3 provided by Vajinder Kumar (University of Leeds)
- LgtC (399 µM) in a solution of 40% glycerol (*v/v*) in mQ water.
- Glc(1-4)$_{ep}$ (11.9 mg/mL) suspension in ammonium sulfate solution
- Bovine serum albumin (BSA; 100 mg/mL) in water
- TRIS buffer: 1 M TRIS, 1 M NaCl at pH = 8
- $MnCl_2$ (1 M) in water

7.6.3.2 Procedure:

The following components (Table 7.15) were added to a 15 mL Falcon tube to synthesize Gb_3-N_3.

Table 7.15: Reagents used to make Gb_3-N_3, **3.11**

Reagent	Stock solution	Final concentration	Quantity
Lac-N_3*	-	50 mM	138 mg
UDP-Glc*	-	100 mM	428 mg
LgtC	399 µM	100 µM	1.85 mL
Glc(1-4)$_{ep}$**	17.5 mg/mL	3.5 mg/mL	1.48 mL
BSA	20 mg/ mL	1 mg/ mL	74 µL
TRIS	1 M	100 mM	740 µL
$MnCl_2$***	1 M	10 mM	74 µL
H_2O	-	-	3.182 mL

Lac-N_3* and UDP-Glc* were added as a solid in the mixture.

For Glc(1-4)$_{ep}$**, the volume indicated were taken form a precipitated protein stock in ammonium sulfate and spined down to discard the supernatant. The solid protein was resuspended in equal volume to the original sulfate suspension in water and added to the mixture

$MnCl_2$*** was added as the last reagent because it can be oxidized.

The resulting mixture was incubated overnight at 37 °C. The reaction mixture was subjected to mass spectrometry and TLC analysis to check if the reaction was. There was not starting material Lac-N_3.

7.6.3.3 Purification:

First, the mixture was spined down using a spinner concentrator to remove all the proteins. The resulting water solution was mixed with silica and dried under vacuum to achieve a white powder completely dry. This dry loading was purified using a SNAP 10 g biotage column (elution EtOAc/MeOH from 90:10 to 100% MeOH). The fraction which contained oligosaccharide (observed by TLC using a solution of orcinol in 95:5 mQ water/H_2SO_4) were joined together and the solvent was removed under vacuum. The remaining syrup was dissolved in 2.5 mL of water and purified by size exclusion column (Biogel P2 resin) using an ammonium formate (NH_4HCOO) solution (40 mM) in mQ water as eluent to obtain Gb_3-N_3 (7.2 mg, 4%).

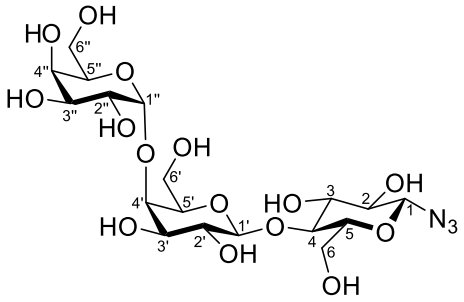

TLC (MeOH/EtOAc 60:40): R_f = 0.10

^{1}H NMR (500 MHz, D_2O): δ 4.95 (d, *J* = 3.9 Hz, 1H, $H_{1''}$); 4.79-4.76 (d, lies under D_2O peak, 1H, H_1); 4.51 (d, *J* = 7.7 Hz, 1H, $H_{1'}$); 4.35 (t, *J* = 6.6 Hz, 1H, $H_{5''}$); 4.03 (t, J = 3.73 Hz, 1H, $H_{4'}$); 3.99 (dd, *J* = 12.3 Hz, *J* = 1.2 Hz, 1H, H_6); 3.95-3.91 (m, 2H, $H_{6'}$, $H_{4''}$); 3.89 (d, *J* = 3.2 Hz, $H_{5'}$); 3.87-8.86 (m, 1H, H_6); 3.84 (m, 1H, H_4); 3.83-3.82 (m, 1H, $H_{2''}$); 3.79-3.77(m, 2H, $H_{3''}$); 3.74 (dd, *J* = 10.3 Hz, *J* = 3.2 Hz, 1H, $H_{3'}$); 3.71 (dd, *J* = 2.5 Hz, *J* = 7.0 Hz, 2H, $H_{6''}$); 3.68-3.66 (m, 2H, H_3, H_5); 3.59-3.55 (m, 1H, $H_{2'}$); 3.30 (t, *J* = 8.6 Hz, 1H, H_2).

^{13}C NMR (126 MHz, D_2O): δ 103.2 ($C_{1'}$), 100.3 ($C_{1''}$), 89.9 (C_1), 77.9 (C_3/C_5), 77.3 ($C_{4'}$) 77.1 ($C_{4'}$), 75.4 ($C_{3''}$), 74.3 (C_3/C_5), 72.6 (C_2), 72.1 ($C_{3'}$), 70.8 ($C_{5''}$/$C_{2'}$) 70.8 ($C_{5''}$/$C_{2'}$), 69.1 ($C_{2''}$/$C_{5'}$/$C_{4''}$), 69.0 ($C_{2''}$/$C_{5'}$/$C_{4''}$), 68.5 ($C_{2''}$/$C_{5'}$/$C_{4''}$), 60.4 ($C_{6''}$), 60.3 ($C_{6'}$) and 59.7 (C_6).

ESI HRMS (positive mode): *m/z*: Found $[M+H]^+$ 530.9173 calc for $C_{18}H_{31}N_3O_{15}$ 530.1825.

7.6.4 Synthesis of Gb_3-N_3 (3.11) using BGalT T1-1871 as the glycosyltransferase and lactase to degrade unreacted lactosyl azide.

7.6.4.1 Reagents and stock solution:

- UDP-Glc
- Lac-N_3 provided by Vajinder Kumar (University of Leeds)
- BGalT Tt-1871 (6.33 µM) suspension in ammonium sulfate solution
- $Glc(1\text{-}4)_{ep}$ (11.9 mg/mL) suspension in ammonium sulfate solution
- TRIS buffer: 1 M TRIS, 1 M NaCl at pH = 8.0
- $MnCl_2$ (1 M) in water
- Lactase enzyme (5 units/µL) in water and glycerol.

7.6.4.2 Procedure:

The following components (Table 7.16) were added to a 50 mL Falcon tube to synthesize Gb_3-N_3.

Table 7.16: Reagents used to make Gb_3-N_3, **3.11**

Reagent	Stock solution	Final concentration	Quantity
Lac-N_3*	-	10 mM	104 mg
UDP-Glc*	-	17 mM	285 mg
BGalT Tt-1871**	6.33 µM	3 µM	12.6 mL
$Glc(1\text{-}4)_{ep}$**	17.5 mg/mL	3.5 mg/mL	5.6 mL
TRIS	1 M	100 mM	2.8 mL
$MnCl_2$***	1 M	10 mM	280 µL
H_2O	-	-	6.72 mL

Lac-N_3* and UDP-Glc* were added as a solid in the mixture.

For BGalT Tt-1871** and $Glc(1\text{-}4)_{ep}$**, the volume indicated were taken form a precipitated protein stock in ammonium sulfate and spined down to discard the supernatant. The solid protein was resuspended in equal volume to the original sulfate suspension in water and added to the mixture.

$MnCl_2$*** was added as the last reagent because it can be oxidized.

The resulting mixture was incubated overnight at 37 °C. The reaction mixture was subjected to mass spectrometry and TLC analysis to check if UDP-Glc was present on the mixture. Because of its absence, Lactase enzyme was added to the mixture (5 mL) and left at room temperature overnight.

7.6.4.3 Purification:

First, the mixture was spined down using a spinner concentrator to remove all the proteins. The resulting water solution was mixed with silica and dried under vacuum to achieve a white powder completely dry. This dry loading was purified using a SNAP 100 g biotage column (elution EtOAc/MeOH from 95:5 to 100% MeOH). The fraction which contained oligosaccharide (observed by TLC using a solution of orcinol in 95:5 mQ water/H_2SO_4) were joined together and the solvent was removed under vacuum. The remaining syrup was dissolved in 1 mL of water and purified by size exclusion column (Biogel P2 resin) using an ammonium formate (NH_4HCOO) solution (20 mM) in mQ water as eluent to obtain Gb_3-N_3 (116.7 mg, 39%). Analytical data was the same as listed in section 7.6.3.3.

7.6.5 Synthesis of Gb_3-N_3 (3.11) using BGalT T1-1871 as the glycosyltransferase.

7.6.5.1 Reagents and stock solution:

- UDP-Glc
- Lac-N_3 provided by Vajinder Kumar (University of Leeds)
- BGalT Tt-1871 (6.33 µM) suspension in ammonium sulfate solution
- $Glc(1\text{-}4)_{ep}$ (11.9 mg/mL) suspension in ammonium sulfate solution
- TRIS buffer: 1 M TRIS, 1 M NaCl at pH = 8.0
- $MnCl_2$ (1 M) in water

7.6.5.2 Procedure:

The following components (Table 7.17) were added to a 50 mL Falcon tube to synthesize Gb_3-N_3.

Table 7.17: Reagents used to make Gb_3-N_3, **3.11**

Reagent	Stock solution	Final concentration	Quantity
Lac-N_3*	-	10 mM	165 mg
UDP-Glc*	-	20 mM	509 mg
BGalT Tt-1871**	6.33 µM	3 µM	20 mL
$Glc(1\text{-}4)_{ep}$**	17.5 mg/mL	3.5 mg/mL	9 mL
TRIS	1 M	100 mM	4.5 mL
$MnCl_2$***	1 M	10 mM	450 µL
H_2O	-	-	11 mL

Lac-N_3* and UDP-Glc* were added as a solid in the mixture.

For BGalT Tt-1871** and $Glc(1\text{-}4)_{ep}$**, the volume indicated were taken form a precipitated protein stock in ammonium sulfate and spined down to discard the supernatant. The solid protein was resuspended in equal volume to the original sulfate suspension in water and added to the mixture. $MnCl_2$*** was added as the last reagent because it can be oxidized.

The resulting mixture was incubated overnight at 37 °C. The reaction mixture was subjected to mass spectrometry and TLC analysis. There was not presence of UDP-Glc and Lac-N_3.

7.6.5.3 Purification:

First, the mixture was spined down using a spinner concentrator to remove all the proteins. The resulting water solution was mixed with silica and dried under vacuum to achieve a white powder completely dry. This dry loading was purified using a SNAP 10 g biotage column (elution EtOAc/MeOH from 60:40 to 100% MeOH). The fraction which contained oligosaccharide (observed by TLC using a solution of orcinol in 95:5 mQ water/H_2SO_4) were joined together and the solvent was removed under vacuum. The remaining syrup was dissolved in 1 mL of water and purified by size exclusion column (Biogel P2 resin) using an ammonium formate (NH_4HCOO) solution (20 mM) in mQ water as eluent to obtain Gb_3-N_3 (139.2 mg, 57%). Analytical data was the same as listed in section 7.6.3.3.

7.6.6 Synthesis of Gb_3-os (oligosaccharide) (3.12) using BGalT T1-1871 as the glycosyltransferase and lactase to degrade unreacted lactosyl azide.

7.6.6.1 Reagents and stock solution:

- UDP-Glc
- Lactose
- BGalT Tt-1871 (6.33 µM) suspension in ammonium sulfate solution
- $Glc(1\text{-}4)_{ep}$ (11.9 mg/mL) suspension in ammonium sulfate solution
- TRIS buffer: 1 M TRIS, 1 M NaCl at pH = 8.0
- $MnCl_2$ (1 M) in water
- Lactase enzyme (5 units/µL) in water and glycerol.

7.6.6.2 Procedure:

The following components (Table 7.18) were added to a 15 mL Falcon tube to synthesize Gb_3-os.

Table 7.18: Reagents used to make Gb_3-N_3, **3.12**

Reagent	Stock solution	Final concentration	Quantity
Lac*	-	10 mM	56 mg
UDP-Glc*	-	20 mM	185 mg
BGalT Tt-1871**	6.33 µM	3 µM	6.8 mL
Glc(1-4)$_{ep}$**	17.5 mg/mL	3.5 mg/mL	3.28 mL
TRIS	1 M	100 mM	1.64 µL
$MnCl_2$***	1 M	10 mM	164 µL
H_2O	-	-	4.51 mL

Lac* and UDP-Glc* were added as a solid in the mixture.

For BGalT Tt-1871** and Glc(1-4)$_{ep}$**, the volume indicated were taken form a precipitated protein stock in ammonium sulfate and spined down to discard the supernatant. The solid protein was resuspended in equal volume to the original sulfate suspension in water and added to the mixture.

$MnCl_2$*** was added as the last reagent because it can be oxidized.

The resulting mixture was incubated two nights at 37 °C. The reaction mixture was subjected to mass spectrometry and TLC analysis. Because there was still Lac, 100 mg of Glc-UDP and 3.3 mL of stock of Glc(1-4)$_{ep}$ was added to the mixture and it was incubated overnight at 37 ºC. Then, the crude was analysed by mass spectrometry and TLC showing Lac. For this reason, 3 mL of Lactase was added and left at room temperature overnight. The resulting mixture was purified.

7.6.6.3 Purification:

First, the mixture was spined down using a spinner concentrator to remove all the proteins. The resulting water solution was mixed with silica and dried under vacuum to achieve a white powder completely dry. This dry loading was purified using a SNAP 10 g biotage column (elution EtOAc/MeOH from 95:5 to 100% MeOH). The fraction which contained oligosaccharide (observed by TLC using a solution of orcinol in 95:5 mQ water/H_2SO_4) were joined together and the solvent was removed under vacuum. The remaining syrup was dissolved in 1 mL of water and purified by size exclusion column (Biogel P2 resin) using an ammonium formate (NH_4HCOO) solution (20 mM) in mQ water as eluent to obtain Gb_3-olgs (62.4 mg, 66%).

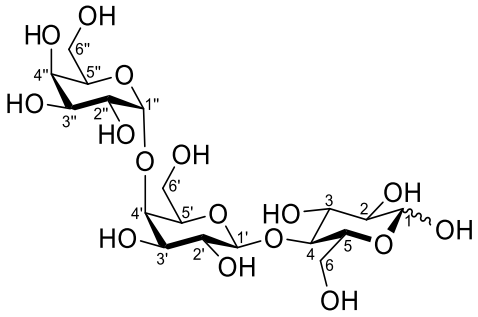

TLC (DCE/MeOH/AcOH/H_2O 50:30:25:10): R_f = 0.14

^{1}H NMR (400 MHz, D_2O): (Proportion $Gb_3(\beta)/Gb_3(\alpha)$ 1:1) δ 5.23 (d, *J* = 3.8 Hz, 1H, $H_{1(\alpha)}$); 4.95 (d, *J* = 3.9 Hz, 2H, $H_{1''}$); 4.67 (d, *J* = 8.0 Hz, 1H, $H_{1(\beta)}$); 4.52 (d, *J* = 7.8 Hz, 2H, $H_{1'}$); 4.36 (t, *J* = 6.3 Hz, 2H, $H_{5''}$); 4.04 (t, *J* = 3.1 Hz, 2H, $H_{4'}$); 3.99-3.88 (m, 7H, $H_{4''}$, $H_{5'}$, $H_{6(\beta)}$, $H_{6'}$); 3.87-3.74 (m, 10H, $H_{2'}$, $H_{2''}$, $H_{3(\alpha)}$, $H_{3'}$, $H_{3''}$, $H_{4(\beta)}$, $H_{6''}$); 3.71 (dd, , *J* = 5.7 Hz, *J* = 1.9 Hz, 4H, $H_{6''}$); 3.69-3.56 (m, 8H, $H_{2(\alpha)}$, $H_{2'}$, $H_{3(\beta)}$, $H_{4(\alpha)}$, $H_{5(\beta)}$, $H_{5(\alpha)}$, $H_{6(\alpha)}$); 3.28 (t, *J* = 8.5 Hz, 1H, $H_{2(\beta)}$).

^{13}C NMR (126 MHz, D_2O): δ 103.2 ($C_{1'}$), 100.4 ($C_{1''}$), 95.7 ($C_{1\beta}$), 91.8 ($C_{1\alpha}$), 78.6 ($C_{5\alpha}/C_{1\beta}/C_{3\alpha}/C_{3\beta}/C_{4\alpha}/C_{4\beta}$), 78.5 ($C_{5\alpha}/C_{1\beta}/C_{3\alpha}/C_{3\beta}/C_{4\alpha}/C_{4\beta}$), 77.3 ($C_{4'}$), 75.4 ($C_{3''}$), 74.8 ($C_{5\alpha}/C_{1\beta}/C_{3\alpha}/C_{3\beta}/C_{4\alpha}/C_{4\beta}$), 74.4 ($C_{5\alpha}/C_{1\beta}/C_{3\alpha}/C_{3\beta}/C_{4\alpha}/C_{4\beta}$), 73.9 ($C_{2\beta}$), 72.1 ($C_{3'}$), 71.4 ($C_{5\alpha}/C_{1\beta}/C_{3\alpha}/C_{3\beta}/C_{4\alpha}/C_{4\beta}$), 71.2 ($C_{2\alpha}/C_{2'}/C_{5''}$), 70.8 ($C_{2\alpha}/C_{2'}/C_{5''}$), 70.8 ($C_{2\alpha}/C_{2'}/C_{5''}$), 70.1 ($C_{5\alpha}/C_{1\beta}/C_{3\alpha}/C_{3\beta}/C_{4\alpha}/C_{4\beta}$), 69.1 ($C_{2''}/C_{5'}/C_{4''}$), 68.9 ($C_{2''}/C_{5'}/C_{4''}$), 68.5 ($C_{2''}/C_{5'}/C_{4''}$), 60.4 ($C_{6''}$), 60.3 ($C_{6'}$), 60.0 ($C_{6\alpha}$), 59.84 ($C_{6\beta}$).

ESI LRMS (positive mode): *m/z*: Found $[M+Na]^+$ 527.16 calc for $C_{18}H_{30}O_{16}Na$ 527.25.

7.7 Protocol for enzymatic screening reactions

7.7.1 Synthesis of azidopropyl LacNAc and its quantification by mass spectrometry using an iTag.

This section describes the protocol for the experiments described in section 3.4.2.2. Different methodologies were tested to check if the incorporation of UDP-Glc-4-epimerase ($Glc(1\text{-}4)_{ep}$) and UDP-Glc instead of UDP-Gal had any negative effect for the synthesis of azidopropyl LacNAc (**3.4**). Control conditions were established by Dr. Kristian Hollingsworth[work pending to publish] while New conditions were suggested in this project.

7.7.1.1 Reagents and stock solution:

- Solution of UDP-Glc (500 mM) in mQ water
- Solution of UDP-Gal (100 mM) in mQ water.

- Solution of azidopropyl GlcNAc (**3.3**) (500 mM) in mQ water.
- β(1-4)GalT1 (2.7 mg/mL) suspension in ammonium sulfate solution
- $Glc(1\text{-}4)_{ep}$ (17. mg/mL) suspension in ammonium sulfate solution
- Bovine serum albumin (BSA; 100 mg/mL) in water
- TRIS buffer: 1 M TRIS, 1 M NaCl at pH = 8
- $MnCl_2$ (1 M) in water
- $MgCl_2$ (500 mM) in water
- Solution of THTPA (50 mM) in mQ water.
- Solution of $CuSO_4$ (50 mM) in mQ water.
- Solution of clickable iTag **3.10** (10 mM) in mQ water provided by Prof. M ª Carmen Galan (University of Bristol).
- Solution of Sodium Ascorbate (NaAsc) (50 mM) in mQ water.

7.7.1.2 Procedure:

The corresponding amounts from the stock were transferred according Table 7.19 to synthesize azidopropyl LacNAc (**3.4**) in two 1.5 mL Eppendorf.

Table 7.19: Reagents used to make azidopropyl LacNAc (**3.4**) by different methodologies

		Control conditions	New conditions
Reagent	**Stock solution**	**Final concentration**	**Quantity**
3.3	500 mM	10 mM	16 mM
UDP-Gal	100 mM	16 mM	-
UDP-Glc	500 mM	-	21 mM
β(1-4)GalT1**	2.6 mg/mL	1 mg/mL	1 mg/mL
$Glc(1\text{-}4)_{ep}$**	17.5 mg/mL	-	1.75 mg/mL
BSA	20 mg/ mL	1 mg/ mL	1 mg/ mL
TRIS	1 M	100 mM	100 mM
$MnCl_2$***	1 M	10 mM	10 mM

For β(1-4)GalT1** and $Glc(1\text{-}4)_{ep}$**, the volume indicated were taken form a precipitated protein stock in ammonium sulfate and spined down to discard the supernatant. The solid protein was resuspended in equal volume to the original sulfate suspension in water and added to the mixture.

$MnCl_2$*** was added as the last reagent because it can be oxidized.

The reaction mixtures were incubated overnight at 37 ºC.

7.7.1.3 Click reaction and quantification:

The following day, an aliquot of each Eppendorf was taken and the protein was precipitated by the addition of MeOH (table 7.20, entry 8) to quench the enzymatic reaction. Then, a CuAAC reaction was performed with the clickable iTag **3.10** following the conditions listed in Table 7.20.

Table 7.20: Reagents used add iTag **3.10** to a mixture of azido-derivatized oligosaccharides.

		Control CuAAC reaction		New cond. CuAAC reaction	
Reagent	Stock	Final Conc.	Quantity	Final Conc.	Quantity
3.4 ContM*	10 mM	0.5 mM	2.5 µL	-	-
3.4 NewC**	16 mM	-	-	0.5 mM	1.5 µL
3.10	10 mM	0.5 mM	2.5 µL	0.5 mM	2.5 µL
THPTA	50 mM	5 mM	5 µL	5 mM	5 µL
$CuSO_4$	50 mM	5 mM	5 µL	5 mM	5 µL
NaAsc	50 mM	10 mM	10 µL	10 mM	10 µL
MeOH	-	-	25 µL	-	26 µL

3.4 ContM* refers to the azidopropyl LacNAc enzymatic mixture using the Control conditions

3.4 NewC** refers to the azidopropyl LacNAc enzymatic mixture using the New conditions

Both reactions were left overnight at room temperature. The following day, both Eppendorfs of the click reaction mixture were spined down at 13.000 x *g* for 2 min. Then, 2 µL of the supernatant was diluted in 198 µL mQ water in a mass-spectrometry vial to analyse by ESI-HRMS.

7.7.2 Synthesis of azidopropyl Le^x and its quantification.

7.7.2.1 Reagents and stock solution:

- LacNAc enzymatic mixture for the control experiment (**3.4** Control M)
- LacNAc enzymatic mixture for the control experiment (**3.4** New Cond)
- Solution of L-Fucose (500 mM) in mQ water
- Solution of ATP (400 mM) and GTP (200 mM) in 100 mM TRIS buffer at pH = 8
- α(1-3)FucT HP (4.8 mg/mL) suspension in ammonium sulfate solution
- FKP (223 µM) in a solution of 10% glycerol (*v/v*) in 100 mM TRIS buffer at pH = 8.0 provided by Dr. James Ross (University of Leeds)
- FKP (123 µM) in a solution of 10% glycerol (*v/v*) in 100 mM TRIS buffer at pH = 8.0
- Solution of $MgCl_2$ (1M) in mQ water
- TRIS buffer: 1 M TRIS, 1 M NaCl at pH = 8
- Solution of THTPA (50 mM) in mQ water.

- Solution of $CuSO_4$ (50 mM) in mQ water.
- Solution of clickable iTag **3.10** (10 mM) in mQ water provided by Prof. M ª Carmen Galan (University of Bristol).
- Solution of Sodium Ascorbate (NaAsc) (50 mM) in mQ water.

7.7.2.2 Procedure:

In six 500 µL Eppendorfs, the corresponding amounts from the stock were transferred for the following table 7.21 to synthesize azidopropyl Le^x (**3.5**) using **3.4** Control Mixture (**3.4** Control M).

Table 7.21: Reagents used in Lewis^x test reactions 1-6.

		Test 1	Test 2	Test 3	Test 4	Test 5	Test 6
Reagent	**Stock**	**Final Conc.**	**Final Conc.**	**Final Conc.**	**Final Conc.**	**Final Conc.**	**Final Conc.**
3.4 Control M.	10 mM	4 mM	4 mM	4 mM	4 mM	4 mM	4 mM
Fuc	500 mM	8 mM	8 mM	8 mM	8 mM	8 mM	8 mM
ATP	400 mM	16 mM	16 mM	16 mM	16 mM	16 mM	16 mM
GTP	200 mM	8.8 mM	8.8 mM	8.8 mM	8.8 mM	4.4 mM	2.2 mM
α(1-3)FucT HP*	4.8 mg/mL	1.44 mg/mL	0.96 mg/mL	0.48 mg/mL	0.24 mg/mL	0.96 mg/mL	0.96 mg/mL
FKP**	223 µM	8.8 µM	8.8 µM	8.8 µM	8.8 µM	8.8 µM	8.8 µM
TRIS	1 M	100 mM	100 mM	100 mM	100 mM	100 mM	100 mM
$MgCl_2$	1 M	10 mM	10 mM	10 mM	10 mM	10 mM	10 mM

α(1-3)FucT HP*, the volume indicated were taken form a precipitated protein stock in ammonium sulfate and spined down to discard the supernatant. The solid protein was resuspended in water and added to the mixture.

FKP** it was provided by Dr. James Ross

The six experiments were incubated at 37 ºC. Every hour, 2.5 µL of enzymatic mixture was taken from each Eppendorf and quenched by the addition of 8.5 µL of MeOH. This procedure was repeated for eight hours.

On the other hand, in six 500 µL Eppendorfs, the corresponding amounts from the stock were transferred for the following table 7.22 to synthesize azidopropyl Le^x (**3.5**) using **3.4** New conditions (**3.4** New Cond.).

Table 7.22: Summary of the reagents and their concentrations initials and final to perform the enzymatic reaction for each experiment.

		Test 1	Test 2	Test 3	Test 4	Test 5	Test 6
Reagent	**Stock**	**Final Conc.**	**Final Conc.**	**Final Conc.**	**Final Conc.**	**Final Conc.**	**Final Conc.**
3.4 New Cond.	16 mM	4 mM	4 mM	4 mM	4 mM	4 mM	4 mM
Fuc	500 mM	8 mM	8 mM	8 mM	8 mM	8 mM	8 mM
ATP	400 mM	16 mM	16 mM	16 mM	16 mM	16 mM	16 mM
GTP	200 mM	8.8 mM	8.8 mM	8.8 mM	8.8 mM	4.4 mM	2.2 mM
α(1-3)FucT HP*	4.8 mg/mL	1.44 mg/mL	0.96 mg/mL	0.48 mg/mL	0.24 mg/mL	0.96 mg/mL	0.96 mg/mL
FKP**	223 µM	8.8 µM	8.8 µM	8.8 µM	8.8 µM	8.8 µM	8.8 µM
TRIS	1 M	100 mM	100 mM	100 mM	100 mM	100 mM	100 mM
$MgCl_2$	1 M	10 mM	10 mM	10 mM	10 mM	10 mM	10 mM

α(1-3)FucT HP*, the volume indicated were taken form a precipitated protein stock in ammonium sulfate and spined down to discard the supernatant. The solid protein was resuspended in water and added to the mixture.

FKP** for this experiment was provided by Dr. James Ross.

The six experiments were incubated at 37 ºC. Every hour, 2.5 µL of enzymatic mixture was taken from each Eppendorf and quenched by the addition of 8.5 µL of MeOH. This procedure was repeated for eight hours.

Finally, in three 500 µL Eppendorfs, the corresponding amounts from the stock were transferred for the following table 7.23 to synthesize azidopropyl Le^x (**3.5**) using **3.4** New conditions (**3.4** New Cond.) using FKP expressed in this project.

Table 7.23: Summary of the reagents and their concentrations initials and final to perform the enzymatic reaction for each experiment.

		Test 1	Test 2	Test 3
Reagent	**Stock**	**Final Conc.**	**Final Conc.**	**Final Conc.**
3.4 New Cond.	16 mM	4 mM	4 mM	4 mM
Fuc	500 mM	8 mM	8 mM	8 mM
ATP	400 mM	16 mM	16 mM	16 mM
GTP	200 mM	8.8 mM	8.8 mM	8.8 mM
α(1-3)FucT HP*	4.8 mg/mL	1.44 mg/mL	0.96 mg/mL	0.48 mg/mL
FKP**	123 µM	8.8 µM	8.8 µM	8.8 µM
TRIS	1 M	100 mM	100 mM	100 mM
$MgCl_2$	1 M	10 mM	10 mM	10 mM

α(1-3)FucT HP*, the volume indicated were taken form a precipitated protein stock in ammonium sulfate and spined down to discard the supernatant. The solid protein was resuspended in water and added to the mixture.

FKP** was expressed in this project.

The three experiments were incubated at 37 ºC. In different times (2.5 h, 5 h, 7.5 h, 21 h, 30 h, 44 h, 55 h, 68 h), 2.5 µL of enzymatic mixture was taken from each Eppendorf and quenched by the addition of 8.5 µL of MeOH.

7.7.2.3 Click reaction and quantification:

For all the enzymatic mixtures quenched (2.5 µL enzymatic mixture and 8.5 MeOH µL), the CuAAC reaction was performed according table 7.24.

Table 7.24: Summary of the reagents and their concentrations initials and final to perform the addition of iTag **3.10** in mixture of azido-derivatized oligosaccharides for each experiment.

		CuAAC reaction	
Reagent	Stock	Final Conc.	Quantity
Enzymatic reaction in MeOH	0.9 mM	0.5 mM	11 µL
3.10	10 mM	0.5 mM	1 µL
THPTA	50 mM	5 mM	2 µL
$CuSO_4$	50 mM	5 mM	2 µL
NaAsc	50 mM	10 mM	4 µL

The reaction was left overnight at room temperature. The following day, the Eppendorfs of the click reaction mixture were spined down at 13.000 x *g* for 2 min. Then, 2 µL of the supernatant was diluted in 198 µL mQ water in a mass-spectrometry vial to analyse by ESI-HRMS.

7.8 Preparation of small unilamellar lipid vesicles (SUVs)

1,2-Dioleoyl-sn-glycero-3-phosphocholine (DOPC) (3.361 mg, 4.27 µmol, 127.9 µL from stock 26.27 g/L in chloroform) and nitrilotriacetic acid (tris-NTA) dioctadecylamine (0.347 mg, 0.22 µmol, 438.6 µL from stock 0.79 g/L in chloroform) were transferred to a glass vial to achieve a mixture 95:5 molar ratio DOPC/tris-NTA. The resulting mixture of lipids was dried under N_2 stream and, once a thin film was achieved, it was left in a desiccator for 2 hours under vacuum. Then, 1854 µL of HEPES buffer (HEPES 10 mM, NaCl 150 mM at pH 7.4) was added to the vial and five freeze/thaw cycles were performed by immersing the vials in dry ice followed by submerging in hot water. The vial was also vortexed between immersions, giving a homogeneous, milky solution. Finally, the suspension was sonicated for 15 min in an ice-water bath using a tip sonication (Fisher Scientific) in pulse mode (1 s on/1 s off) at 30% duty cycle to achieve a transparent colourless solution and centrifuged (12.100 x *g*) for 10 min to remove any insoluble impurity. The SUVs were stored in an inert atmosphere (N_2) in the fridge until used.

7.9 Protocol for experiments in QCM-D and sizing mucin-like structures in overtones 3 and 7

7.9.1 QCM-D experiment protocol

7.9.1.1 Preparation of sensors and working buffer

Silica coated sensors (QSX303, Biolin Scientific, Västra Frölunda, Sweden) were cleaned for 30 min in 2% SDS solution in water and, after blow-drying in N_2 gas, exposed to UV/ozone chamber (ProCleaner™ plus Bioforce nanoscience) treatment for 30 min.

QCM-D experiment were run with 4 independent flow modules using the Q-Sense E4 system (Biolin Scientific). Flow modules were connected to a syringe pump (Legato, World Precision Instruments) to operate in withdraw mode at 20 µL/min. For all the experiments, the working temperature was set to 23 ºC and the working buffer (HEPES 10 mM, NaCl 150 mM at pH = 7.4) was degassed (using a bath sonicator in pulsed 'degas' mode) for 25 min.

Changes in the sensors' resonance frequency (Δf_i) and dissipation (ΔD_i) were continuously recorded for six overtones (i = 3, 5, 7, 9, 11 and 13) with sub-second time resolution. Whilst data for one or a few selected overtones are typically presented, all other overtones gave qualitatively similar information. Normalised frequency shifts, $\Delta F_i = \Delta f_i / i$, are presented throughout.

7.9.1.2 QCM-D signal calibration

The change in ΔD_3 upon filling the fluidic system of each module with buffer was used to confirm the fluid volume above the sensor was well filled and free from air bubbles ($\Delta D_3 > 159 \times 10^{-6}$ was considered appropriate). Next, buffer was left to flow over the sensors for at least 30 min to let the QCM-D signals equilibrate. Changes in $|\Delta f| < 2$ Hz / hour were considered sufficiently small as baseline drifts.

7.9.1.3 QCM-D experiment protocol[281]

All QCM-D experiments were performed with supported lipid bilayers (SLBs) as model membranes on which model glycocalyces were subsequently built and interactions with lectins analysed.

Experiments started by flowing buffer for 10 min to establish a baseline, followed by SLB formation through incubation of SUVs (50 µg/mL) for 20 min, or until the responses in ΔF and ΔD were in equilibrium. Any material left was rinsed with working buffer (HEPES 10 mM, NaCl 150 mM at pH = 7.4) for 10 min. For experiments using biotinylated glycopolymers, streptavidin (SAv; 20 µg/mL) from Sigma-Aldrich was incubated on biotin-presenting SLBs for 15 min, or until ΔF was between -25 and -26 Hz representing a close-to-complete SAv monolayer following by the rinsing step for 10 min with working buffer (HEPES 10 mM, NaCl 150 mM at pH = 7.4). Next, the samples were incubated according Table 7.25 in different experiments:

Table 7.25: Concentration of the different samples and its time of incubation for QCM-D experiments. Samples **4.4**, **4.5**, **4.6**, STxB and CTB (Table 7.24, entry 1, 5 and 6) were incubated by themselves to check their (non)binding with the surface tested including SAv monolayer or tris-NTA SLB in presence of 5mM $NiCl_2$ (Ni^{2+}-NTA) as control experiments. To remove any structure attached to the Ni^{2+}-NTA SLB, imidazole was incubated as final step. Samples from **5.1** to **5.4** (Table 7.24, entry 2) were incubated in SAv monolayer following by the incubation of STxB or CTB (Table 7.24, entry 5 and 6) to check binding between the mucin-like structures and lectins. Samples **5.5** and **5.6** (Table 7.24, entry 3 and 4) were incubated in tris-NTA in presence of 5 mM $NiCl_2$ following by the incubation of STxB (Table 7.24, entry 5) to check binding between these structures and the lectin. To remove any structure attached to the Ni^{2+}-NTA SLB, imidazole was incubated as final step.

Sample	Concentration	Incubation time
4.4, **4.5** or **4.6**	20 µg/mL	1 hour*
5.1, **5.2**, **5.3** or **5.4**	20 µg/mL	1 hour*
5.5	20 µg/mL	30 min
5.6	20 µg/mL or 40 µg/mL	30 min
STxB	0.4 µM or 2 µM	20-30 min
CTB	0.34 µM, 0.7 µM or 3.5 µM	20-30 min
Imidazole	500 mM	30 min

*The time established was 1 hour but, if the system reached equilibrium before that time, the rinsing step was performed in advance.

After each sample incubation, working buffer (HEPES 10 mM, NaCl 150 mM at pH = 7.4) was flown for 10 min to rinse away any sample remaining in the solution phase, before incubating the next sample.

7.9.2 Estimating the contour length of the HA backbone by QCM-D (overtones *i* = 3 and 7)

Chapter 5, section 5.4.1, focused on *i* = 5 for the estimation of the number of disaccharides n_{ds} in the backbone of the synthesised glycopolymers, using the method by Srimasorn *et al.*[281]. Here, complementary data is provided for *i* = 3 and 7.

7.9.2.1 Overtone 3rd

Time-resolved QCM-D responses, $\Delta F_3(t)$ and $\Delta D_3(t)$, for the binding of the biotinylated derivatized hyaluronan samples (**5.1** - both 200-500 kDa and 40-50 kDa, **5.2**, **5.3** and **5.4**) were graphed as parametric plots of $\Delta D/-\Delta F$ against $-\Delta F$.

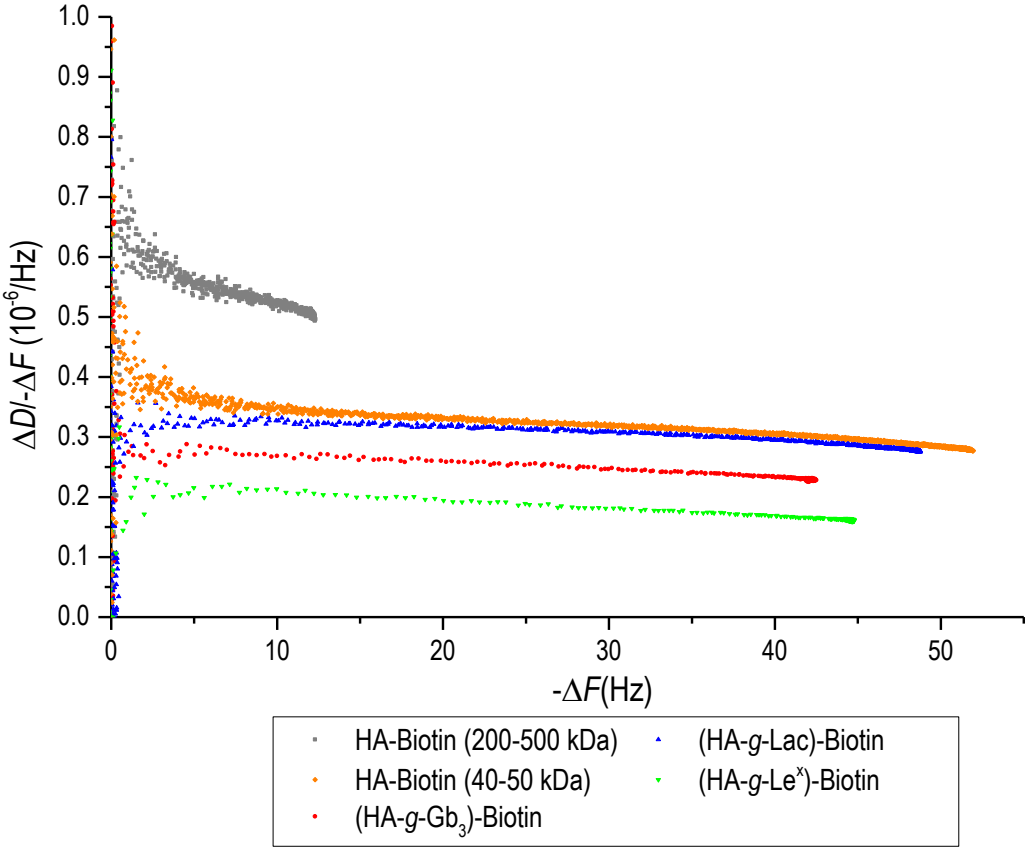

Graph 7.1: Parametric plots (*i* = 3) for **5.1** (both 200-500 kDa and 40-50 kDa), **5.2**, **5.3** and **5.4** (colour coded as indicated in the caption).

$\Delta D/-\Delta F$ at -ΔF = 2.5 Hz was extracted from the parametric plots by applying the average and standard deviation function on Excel, and inserted in Equation 7.1, to calculate the number of disaccharides in the HA backbone of the glycopolymer, as established by Srimasorn *et al.*[281]

$$n_{\mathrm{ds}} = 32.66 \times \left(\frac{\Delta D}{-\Delta f} \Big/ \frac{10^{-6}}{Hz}\right)^{0.9907} \times \left(1 + \frac{58.78}{1+e^{\left(2.291\frac{Hz}{10^{-6}}\cdot\frac{\Delta D}{-\Delta f}\right)^{-2.277}}}\right) \qquad (7.1)$$

The results of this analysis are listed in Table 7.26.

Table 7.26: n_{ds} estimated from *i* = 3. The mean value and the standard deviation were calculated applying the average function and the standard deviation function on Excel.

Sample	QCM-D	
	$\Delta D/-\Delta F$	n_{ds}
5.1 (200-500 kDa)	0.59 ± 0.02	454 ± 23
5.1 (40-50 kDa)	0.38 ± 0.01	168 ± 18
5.2	0.32 ± 0.02	82 ± 23
5.3	0.21 ± 0.03	9 ± 4
5.4	0.27 ± 0.02	37 ± 11

7.9.2.2 Overtone 7th

Finally, the data was plotted for the binding of the biotinylated derivatized hyaluronan (**5.1** (both 200-500 kDa and 40-50 kDa), **5.2**, **5.3** and **5.4**) $\Delta D/-\Delta f$ against -Δf for 7th overtone.

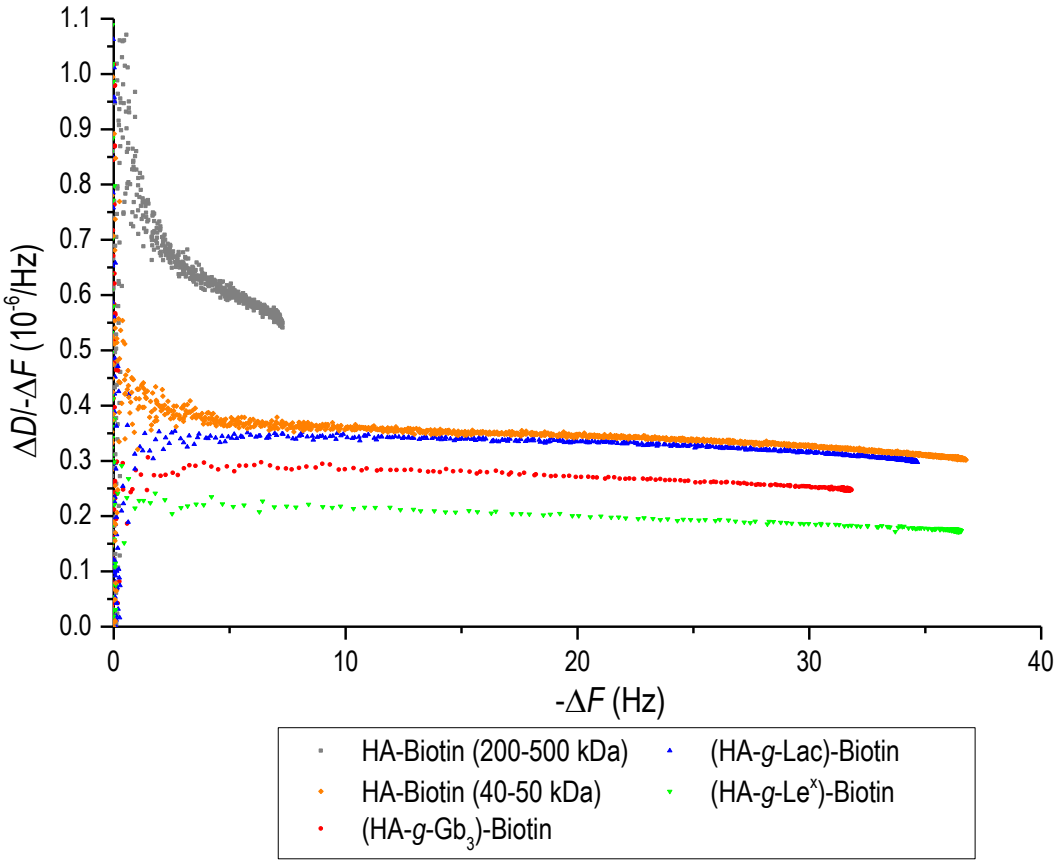

Graph 7.2: Parametric plots (*i* = 7) for **5.1** (both 200-500 kDa and 40-50 kDa), **5.2**, **5.3** and **5.4** (colour coded as indicated in the caption).

$\Delta D/-\Delta F$ at -ΔF = 2.5 Hz was extracted from the parametric plots by applying the average and standard deviation function on Excel, and inserted in Equation 7.2, to calculate the number of disaccharides in the HA backbone of the glycopolymer, as established by Srimasorn *et al.*[281]

$$n_{ds} = \frac{\Delta D}{-\Delta f} / \frac{10^{-6}}{Hz} \times (17.5 \frac{Hz}{10^{-6}} \cdot \frac{\Delta D}{-\Delta f} + 20.2) \times (\frac{16.99+\left(3.125\frac{Hz}{10^{-6}}\cdot\frac{\Delta D}{-\Delta f}\right)^{-5.128}}{1+\left(3.125\frac{Hz}{10^{-6}}\cdot\frac{\Delta D}{-\Delta f}\right)^{-5.128}} \quad (7.2)$$

The results obtained once applied the formula are described at Table 7.27.

Table 7.27: n_{ds} estimated from *i* = 7. The mean value and the standard deviation were calculated applying the average function and the standard deviation function on Excel.

Sample	QCM-D	
	$\Delta D/-\Delta f$	n_{ds}
5.1 (200-500 kDa)	0.67 ± 0.02	358 ± 15
5.1 (40-50 kDa)	0.39 ± 0.01	135 ± 12
5.2	0.34 ± 0.01	90 ± 10
5.3	0.22 ± 0.01	15 ± 4
5.4	0.28 ± 0.01	43 ± 3

7.10 SE experiment protocol

Ellipsometry measures changes in the polarisation of light, specifically, the ellipsometric angles Δ and ψ, upon reflection at the surface of interest. As the polarisation of light is very sensitive to changes in the optical properties of the surface, it can be used to characterize the thickness and refractive index of thin organic surface coatings. From these parameters, the surface density of molecules can be quantified. This surface was installed in an open cuvette with intermittent stirring according the needs of the experiment.

7.10.1 SE protocol for experiments

7.10.1.1 Preparation of the sensing surface and working buffer

Silicon wafer pieces with a thin oxide coating (BT Electronics (Les Ulis, France)) were used as sensing surfaces. They were cleaned for 30 min in 2% SDS solution in water, then blow-dried in a N_2 stream, and exposed to UV/ozone for at least 30 min just before use. The working buffer (HEPES 10 mM, NaCl 150 mM, pH = 7.4) was degassed for 25 min.

7.10.1.2 Experimental setup

The main SE device was a spectroscopic rotating compensator ellipsometer (M2000V; J.A. Woollam; NE, USA) with a horizontal plane of light incidence. Ellipsometric data were acquired over

a range of wavelengths λ, from 380 to 1000 nm, at 70° angle of incidence and a time resolution of ~ 5s. A custom-built cuvette (108 µL) was used for the real time *in situ* analysis of binding processes.[259] CompleteEASE software (J. A. Woollam) was used for data acquisition and analysis.

7.10.1.3 Surface calibration

A characterisation of the optical properties of the bare surface was required prior to the use foro binding studies, to determine the optical properties of the native oxide coating and to verify proper alignment of the cuvette windows and surface. A freshly cleaned wafer piece, immersed in working buffer was used for this step.

A three-layer model (sol - ambient buffer solution, SiO2 - native silicon oxide, silicon) was applied to fit the ellipsometric data, Δ and ψ as a function of the wavelength λ, and to extract the refractive index $n(\lambda)$ and the thickness d of the oxide layer. The ambient solution and the oxide film were treated as transparent Cauchy media, described by a wavelength dependence $n(\lambda) = A + B/\lambda^2$. The optical properties of the working buffer were set to $A_{\mathrm{sol}} = 1.325$ and $B_{\mathrm{sol}} = 0.00322$.[263,282] The optical properties of the silicon were set to tabulated values (provided by J. A. Woollam). The optical parameter B of the silicon oxide coating was set to B_{SiO2} = 0.0159 (consistent with previous work). The thickness d_{SiO2} and the optical parameter A_{SiO2} of the silicon oxide coating, and the angle of incidence, where adjustable parameters in the fit.

Values obtained in a typical experiment were A_{SiO2} = 2.411 ± 0.062 and d_{SiO2} = 1.01 ± 0.17 nm, with an error in the angle of incidence below 0.1 degrees. The normalised χ^2 value was lower than 1.6, that is close to 1, indicated a fit of good quality. These three adjustable parameters were fixed going forward when analysing biomolecular binding to the surface.

7.10.1.4 Protocol for SE titration experiment

Then, different materials and samples were injected directly into the open cuvette, which was filled with buffer. The samples were incubated according Table 7.28 and Table 7.29:

Table 7.29: Concentration of the different samples and its time of incubation for SE experiments for experiments on biotinylated SLB and SAv monolayer. Sample **5.3** (Table 7.28, entry 3) was incubated in SAv monolayer following by the incubation of CTB (Table 7.28, entry 5) to perform the titration experiment.

Sample **5.4** (Table 7.28, entry 3) was incubated in SAv monolayer following by the incubation of STxB (Table 7.28, entry 4) to perform the titration experiment.

Sample	Concentration	Time incubation
SUVs (95:5 molar ratio DOPC/DOPE-cap-B)	50 µg/mL	30 min
SAv	20 µg/mL	30 min
5.3 or **5.4**	20 µg/mL	30 min
STxB	From 0.2 to 100 µM	10-15 min*
CTB	From 0.2 to 10 µM	10-15 min*

*The time established was at least 10 min, or until the system was in equilibrium, before the following addition or the rinse step.

Table 7.29: Concentration of the different samples and its time of incubation for SE experiments for experiments on Ni^{2+}-NTA SLB. Sample **5.6** (Table 7.29, entry 2) was incubated after the formation of the Ni^{2+}-NTA SLB and following by the incubation of STxB (Table 7.29, entry 3) to perform a binding experiment between the film and the lectin.

Sample	Concentration	Time incubation
SUVs (95:5 DOPC/tris-NTA-DODA)	50 µg/mL	30 min
5.6	40 µg/mL	30 min
STxB	2 µM	30 min

For all the experiment, to remove the material or samples from the cuvette, buffer was flown for 30 min, always stirring to ensure homogeneity in solution.

7.10.1.5 Quantification of material adsorbed on the surface

A five-layer model (sol - ambient buffer solution, bml2 - mucin like layer (with bound lectins), bml1 - SLB with SAv layer, SiO2 - native silicon oxide, silicon) was used. The two biomolecular layers were treated as transparent Cauchy media (see above) with $B_{\mathrm{sol}} = B_{\mathrm{bml2}} = B_{\mathrm{bml1}} = 0.00322$, reflecting that the wavelength dispersion of the solvated layers is not sensitively affected by the biomolecules. During the processes of SLB and SAv monolayer formation, the thickness d_{bml2} was set to zero, and A_{bml1} and d_{bml1} were the adjustable fit parameters. Once the SLB and SAv layers had formed, A_{bml1} and d_{bml1} was fixed, and A_{bml2} and d_{bml2} were the adjustable fit parameters during the processes of mucin-like layer formation and lectin binding/unbinding. The χ^2 values for the fits were typically below 2.0, indicating a fit of high quality, although occasionally (for some sample injections) a moderately higher value was obtained due to light scattering caused by big particles before dissolving them.

The De Feijter equation was used to extract the areal mass density of biomolecules from the thickness and optical properties of the biomolecular layers

$$m = \frac{d_{\mathrm{bml}} \times (n_{\mathrm{bml}} - n_{\mathrm{solvent}})}{\mathrm{d}n/\mathrm{d}c} = \frac{d_{\mathrm{bml}} \times (A_{\mathrm{bml}} - 1.325)}{\mathrm{d}n/\mathrm{d}c}. \quad (7.3)$$

The refractive index increments $\mathrm{d}n/\mathrm{d}c$ depend on the type of biomolecule, and the used values were 0.18 cm^3/g for proteins, 0.169 cm^3/g for lipids and 0.15 cm^3/g for HA and glycopolymers under the assumption that the derivatized hyaluronan behaved as pure HA for the calculations. For molecules with a defined molecular mass M_w, the molar surface density can be derived as

$$\Gamma = \frac{m}{M_w} \quad (7.4)$$

CHAPTER 8: Bibliography

1. Reitsma S, Slaaf DW, Vink H, Van Zandvoort MAMJ, Oude Egbrink MGA. The endothelial glycocalyx: Composition, functions, and visualization. *Pflugers Arch Eur J Physiol*. 2007;454(3):345-359. doi:10.1007/s00424-007-0212-8
2. Tarbell JM, Pahakis MY. Mechanotransduction and the glycocalyx. *J Intern Med*. 2006;259(4):339-350. doi:10.1111/j.1365-2796.2006.01620.x
3. Purcell SC, Godula K. Synthetic glycoscapes: Addressing the structural and functional complexity of the glycocalyx. *Interface Focus*. 2019;9(2). doi:10.1098/rsfs.2018.0080
4. Varki A. Biological roles of oligosaccharides : all of the theories are correct. *Glycobiology*. 1993;3(2):97-130.
5. Varki A. Biological roles of glycans. *Glycobiology*. 2017;27(1):3-49. doi:10.1093/glycob/cww086
6. Shurer CR, Kuo JCH, Roberts LDM, et al. Physical Principles of Membrane Shape Regulation by the Glycocalyx. *Cell*. 2019;177(7):1757-1770.e21. doi:10.1016/j.cell.2019.04.017
7. Pries AR, Secomb TW, Gaehtgens P. The endothelial surface layer. *Pflugers Arch Eur J Physiol*. 2000;440(5):653-666. doi:10.1007/s004240000307
8. Honigfort D, Zhang M, Verespy S, Godula K. Engineering of spectator glycocalyx structures to evaluate molecular interactions at crowded cellular boundaries. *Faraday Discuss*. 2019;219:138-153. doi:10.1039/c9fd00024k
9. Varki A, Cummings RD, Aebi M, et al. Symbol Nomenclature for Graphical Representations of Glycans. *Glycobiology*. 2015;25(12):1323-1324. doi:10.1093/glycob/cwv091
10. Van Den Steen P, Rudd PM, Dwek RA, Opdenakker G. Concepts and principles of O-linked glycosylation. *Crit Rev Biochem Mol Biol*. 1998;33(3):151-208. doi:10.1080/10409239891204198
11. Hounsell EF, Davies MJ, Renouf D V. O-linked protein glycosylation structure and function. *Glycoconj J*. 1996;13(1):19-26. doi:10.1007/BF01049675
12. Stanley P, Moremen KW, Lewis NE, Taniguchi N, Aebi M. Chapter 9 N-Glycans. In: *Essentials of Glycobiology*. 4th Editio. Cold Spring Harbor Laboratoy Press; 2022:[internet]. doi:10.1101/glycobiology.4e.9
13. Aebi M. N-linked protein glycosylation in the ER. *Biochim Biophys Acta - Mol Cell Res*. 2013;1833(11):2430-2437. doi:10.1016/j.bbamcr.2013.04.001
14. Schwarz F, Aebi M. Mechanisms and principles of N-linked protein glycosylation. *Curr Opin*

Struct Biol. 2011;21(5):576-582. doi:10.1016/j.sbi.2011.08.005

15. Mellquist JL, Kasturi L, Spitalnik SL, Shakin-Eshleman SH. The amino acid following an Asn-X-Ser/Thr sequon is an important determinant of N-linked core glycosylation efficiency. *Biochemistry*. 1998;37(19):6833-6837. doi:10.1021/bi972217k
16. Elbein AD. The role of N-linked oligosaccharides in glycoprotein function. *Trends Biotechnol*. 1991;9(1):346-352. doi:10.1016/0167-7799(91)90117-Z
17. Stepper J, Shastri S, Loo TS, et al. Cysteine S-glycosylation, a new post-translational modification found in glycopeptide bacteriocins. *FEBS Lett*. 2011;585(4):645-650. doi:10.1016/j.febslet.2011.01.023
18. Lote CJ, Weiss JB. Identification in urine of a low-molecular-weight highly polar glycopeptide containing cysteinyl-galactose. *Biochem J*. 1967;105(3):37P-54P. doi:10.1042/bj1050037p
19. Hofsteenge J, Müller DR, de Beer T, Löffler A, Richter WJ, Vliegenthart JFG. New Type of Linkage between a Carbohydrate and a Protein: C-Glycosylation of a Specific Tryptophan Residue in Human RNase Us. *Biochemistry*. 1994;33(46):13524-13530. doi:10.1021/bi00250a003
20. Sandhof K. Sphingolipidoses. *J Clin Phatologies*. 1973;27(8):94-105.
21. Hakomori S. Organization and function of glycosphingolipids in membrane. *Proc Japan Acad Ser B Phys Biol Sci*. 2005;81(6):189-203. doi:10.2183/pjab.81.189
22. Merrill AH. Sphingolipid and Glycosphingolipid Metabolic Pathways in the Era of Sphingolipidomics. *Chem Rev*. 2011;111:6387-6422.
23. Fahy E, Subramaniam S, Murphy RC, et al. Update of the LIPID MAPS comprehensive classification system for lipids. *J Lipid Res*. 2009;50:S9-S14. doi:10.1194/jlr.R800095-JLR200
24. Keusch JJ, Manzella SM, Nyame KA, Cummings RD, Baenziger JU. Cloning of GB3 synthase, the key enzyme in globo-series glycosphingolipid synthesis, predicts a family of α1,4-glycosyltransferases conserved in plants, insects, and mammals. *J Biol Chem*. 2000;275(33):25315-25321. doi:10.1074/jbc.M002630200
25. Tarabuso AL. Fabry disease. *Skinmed*. 2011;9(3):173-177.
26. Nudelman A, Kannagi R, Parsons M, et al. A Glycolipid Antigen Associated with Burkitt Lymphoma Defined by a Monoclonal Antibody. *Science (80-)*. 1983;220(4596):509-511.
27. Distler U, Souady J, Hülsewig M, et al. Shiga toxin receptor Gb3Cer/CD77: Tumor-association and promising therapeutic target in pancreas and colon cancer. *PLoS One*. 2009;4(8). doi:10.1371/journal.pone.0006813

28. Melton-Celsa AR. Shiga Toxin (Stx) Classi fi cation , Structure , and Function. *Microbiol Spectr*. 2014;2(4):EHEC-0024-2013. doi:10.1128/microbiolspec.EHEC-0024-2013.Correspondence
29. Schnaar RL. Glycolipid-mediated cell-cell recognition in inflammation and nerve regeneration. *Arch Biochem Biophys*. 2004;426(2):163-172. doi:10.1016/j.abb.2004.02.019
30. Aureli M, Grassi S, Prioni S, Sonnino S, Prinetti A. Lipid membrane domains in the brain. *Biochim Biophys Acta - Mol Cell Biol Lipids*. 2015;1851(8):1006-1016. doi:10.1016/j.bbalip.2015.02.001
31. Todeschini AR, Hakomori S. Functional role of glycosphingolipids and gangliosides in control of cell adhesion, motility, and growth, through glycosynaptic microdomains. *Biochim Biophys Acta - Gen Subj*. 2008;1780(3):421-433. doi:10.1016/j.bbagen.2007.10.008
32. Yu RK, Tsai Y, Ariga T, Yanagisawa M. Structures , Biosynthesis , and Functions of Gangliosides-an Overview. *J Oleo Sci*. 2011;60(10):537-544.
33. Ledeen RW, Wu G, Lu Z-H, Kozireski-Chuback D, Fang Y. The role of GM1 and other gangliosides in neuronal differentiation. Overview and new finding. *Ann N Y Acad Sci*. 1998;845:161-175.
34. Cervin J, Wands AM, Casselbrant A, et al. GM1 ganglioside-independent intoxication by Cholera toxin. *PLoS Pathog*. 2018;14(2):e1006862. doi:10.1371/journal.ppat.1006862
35. Sasisekharan R, Raman R, Prabhakar V. Glycomics Approach To Structure-Function Relationships of Glycosaminoglycans. *Annu Rev Biomed Eng*. 2006;8(1):181-231. doi:10.1146/annurev.bioeng.8.061505.095745
36. Gandhi NS, Mancera RL. The structure of glycosaminoglycans and their interactions with proteins. *Chem Biol Drug Des*. 2008;72(6):455-482. doi:10.1111/j.1747-0285.2008.00741.x
37. Shimida K, Kobayashi M, Kimura S, Nishinaga M, Tekeuchi K, Ozawa T. Anticoagulant heparin-like glycosaminoglycans on endothelial cell surface. *Jpn Circ J*. 1991;55:1016-1021.
38. Bernfield M, Götte M, Park PW, Reizes O, Fitzgerald ML, Lincecum J. Functions of Cell Surface Heparan Sulfate Proteoglycans. *Annu Rev Biomed Eng*. 1999;68:729-777.
39. Dicker KT, Gurski LA, Pradhan-Bhatt S, Witt RL, Farach-Carson MC, Jia X. Hyaluronan: A simple polysaccharide with diverse biological functions. *Acta Biomater*. 2014;10(4):1558-1570. doi:10.1016/j.actbio.2013.12.019
40. Laurent TC, Laurent UB, Fraser JRE. The structure and function of hyaluronan: An overview. *Immunol Cell Biol*. 1996;74:A1-A7. doi:10.1055/s-2006-939550
41. Bansil R, Turner BS. Mucin structure, aggregation, physiological functions and biomedical

applications. *Curr Opin Colloid Interface Sci*. 2006;11(2-3):164-170. doi:10.1016/j.cocis.2005.11.001

42. Dekker J, Rossen JWA, Büller HA, Einerhand AWC. The MUC family: An obituary. *Trends Biochem Sci*. 2002;27(3):126-131. doi:10.1016/S0968-0004(01)02052-7
43. Martínez-Sáez N, Peregrina JM, Corzana F. Principles of mucin structure: Implications for the rational design of cancer vaccines derived from MUC1-glycopeptides. *Chem Soc Rev*. 2017;46(23):7154-7175. doi:10.1039/c6cs00858e
44. Pinzón Martín S, Seeberger PH, Varón Silva D. Mucins and Pathogenic Mucin-Like Molecules Are Immunomodulators During Infection and Targets for Diagnostics and Vaccines. *Front Chem*. 2019;7:710. doi:10.3389/fchem.2019.00710
45. Hattrup CL, Gendler SJ. Structure and Function of the Cell Surface (Tethered) Mucins. *Annu Rev Physiol*. 2008;70(1):431-457. doi:10.1146/annurev.physiol.70.113006.100659
46. Carson DD. The Cytoplasmic Tail of MUC1 : A Very Busy Place. *Sci Signal*. 2008;1(27):pe35.
47. Senapati S, Das S, Batra SK. Mucin-interacting proteins : from function to therapeutics. *Trends Biochem Sci*. 2009;35(4):236-245. doi:10.1016/j.tibs.2009.10.003
48. Bhaskar KR, Turner BS, Lamont JT, et al. Viscous fingering of HCl through gastric mucin. *Nature*. 1992;360(6403):458-461. doi:10.1038/360458a0
49. Hollingsworth MA, Swanson BJ. Mucins in cancer: protection and control of the cell surface. *Nat Rev Cancer*. 2004;4:45-60. doi:10.1038/nrc1251
50. McDermott KM, Crocker PR, Harris A, et al. Overexpression of Muc1 reconfigures the binding properties of tumor cells. *Int J Cancer*. 2001;94:783-791.
51. Xu LL, Townsend SD. Synthesis as an Expanding Resource in Human Milk Science. *J Am Chem Soc*. 2021;143:11277-11290. doi:10.1021/jacs.1c05599
52. Blanas A, Sahasrabudhe NM, Rodríguez E, van Kooyk Y, van Vliet SJ. Fucosylated antigens in cancer: An alliance toward tumor progression, metastasis, and resistance to chemotherapy. *Front Oncol*. 2018;8:1-14. doi:10.3389/fonc.2018.00039
53. Stanley P, Cummings RD. *Essentials of Glycobiology 3rd Edition, Chapter 14: Structures Common to Different Glycans*. 3rd ed. (Varki A, ed.).; 2017.
54. Hellstrom I, Garrigues J, Garrigues U, Hellstrom KE. Highly Tumor-reactive , Internalizing , Mouse Monoclonal Antibodies to Ley-related Cell Surface Antigens. *Cancer Res*. 1990;50:2183-2190.
55. Hou R, Jiang L, Liu D, et al. Lewis(y) antigen promotes the progression of epithelial ovarian cancer by stimulating MUC1 expression. *Int J Mol Med*. 2017;40(2):293-302.

doi:10.3892/ijmm.2017.3009

56. Baldus SE, Zirbes TK, Thakran J, Thiele J, Schneider PM, Dienes HP. Lewis y antigen (CD174) and apoptosis in gastric and colorectal carcinomas : *Histol Histopathol*. 2006;21:503-510. doi:10.14670/HH-21.503
57. Madjd Z, Parsons T, Watson NFS, Spendlove I, Ellis I, Durrant LG. Research article High expression of Lewis y / b antigens is associated with decreased survival in lymph node negative breast carcinomas. *Breast Cancer Res*. 2005;7(5):780-787. doi:10.1186/bcr1305
58. Ma Z, Yang H, Peng L, et al. Expression of the Carbohydrate Lewis Antigen, Sialyl Lewis A, Sialyl Lewis X, Lewis X, and Lewis Y in the Placental Villi of Patients With Unexplained Miscarriages. *Front Immunol*. 2021;12(May):1-12. doi:10.3389/fimmu.2021.679424
59. Pendu JLE, Marionneau S, Cailleau-thomas A, Rocher J, Le B, Clement M. ABH and Lewis histo-blood group antigens in cancer. *AMPIS*. 2001;109(1):9-31.
60. Nakagoe T, Fukushima K, Nanashima A, et al. Expression of Lewisa, sialyl Lewisa, Lewis(x) and sialyl Lewis(x) antigens as prognostic factors in patients with colorectal cancer. *Can J Gastroenterol*. 2000;14(9):753-760. doi:10.1155/2000/149851
61. Merritt EA, Hol WG. AB5 toxins. *Curr Opin Struct Biol*. 1995;5(2):165-171. doi:10.1016/0959-440X(95)80071-9
62. Beddoe T, Paton AW, Le Nours J, Rossjohn J, Paton JC. Structure, biological functions and applications of the AB5 toxins. *Trends Biochem Sci*. 2010;35(7):411-418. doi:10.1016/j.tibs.2010.02.003
63. Fan E, Merritt EA, Verlinde CLMJ, Hol WGJ. AB5 toxins: Structures and inhibitor design. *Curr Opin Struct Biol*. 2000;10(6):680-686. doi:10.1016/S0959-440X(00)00152-4
64. Sixma TK, Kalk KH, van Zanten BAM, et al. Refined structure of escherichia coli heat-Labile enterotoxin, a close relative of cholera toxin. *J Mol Biol*. 1993;230(3):890-918. doi:10.1006/jmbi.1993.1209
65. den Akker F van, Sarfaty S, Twiddy EM, Connell TD, Holmes RK, Hol WG. Crystal structure of a new heat-labile enterotoxin, LT-IIb. *Structure*. 2004;4(6):665-678. doi:10.1016/s0969-2126(96)00073-1
66. Stein PE, Boodhoo A, Armstrong GD, Cockle SA, Klein MH, Read RJ. The crystal structure of pertussis toxin. *Structure*. 1994;2(1):45-57. doi:10.1016/S0969-2126(00)00007-1
67. St Hilaire PM, Boyd MK, Toone EJ. Interaction of the Shiga-like Toxin Type B-Subunit with Its Carbohydrate Receptor. *Biochemistry*. 1994;33(48):14452-14463.
68. Ling H, Boodhoo A, Hazes B, et al. Structure of the Shiga-like Toxin I B-Pentamer Complexed with an Analogue of Its Receptor Gb3. *Biochemistry*. 1998;37(7):1777-1788.

69. Shimizu H, Field RA, Homans SW. Solution Structure of the Complex between the B-Subunit Homopentamer of Verotoxin VT-1 from Escherichia coli and the Trisaccharide Moiety of Globotriaosylceramide. *Biochemistry*. 1998;37(31):11078-11082.
70. Witvliet MH, Burns DL, Brennan MJ, Poolman JT, Manclark CR. Binding of pertussis toxin to eucaryotic cells and glycoproteins. *Infect Immun*. 1989;57(11):3324-3330.
71. Cholera, 2016. *Wkly Epidemiol Rec*. 2017;92(36):521-536. http://www.who.int/wer
72. European Centre for Disease Prevention and Control. Communicable Disease Threats Report, Week 48. *Commun Dis Threat Rep*. Published online 2022:1-21.
73. Heim JB, Hodnik V, Heggelund JE, Anderluh G, Krengel U. Crystal structures of cholera toxin in complex with fucosylated receptors point to importance of secondary binding site. *Sci Rep*. 2019;9(1):1-14. doi:10.1038/s41598-019-48579-2
74. Holmner Å, Mackenzie A, Krengel U. Molecular basis of cholera blood-group dependence and implications for a world characterized by climate change. *FEBS Lett*. 2010;584(12):2548-2555. doi:10.1016/j.febslet.2010.03.050
75. Heggelund JE, Burschowsky D, Bjørnestad VA, Hodnik V, Anderluh G, Krengel U. High-Resolution Crystal Structures Elucidate the Molecular Basis of Cholera Blood Group Dependence. *PLoS Pathog*. 2016;12(4):1-19. doi:10.1371/journal.ppat.1005567
76. Stoll BJ, Hossain KMB. Predisposition for cholera of individuals with o blood. *Am J Epidemiol*. 1985;121(6):791-796.
77. Zhang RG, Westbrook ML, Nance S, et al. The three-dimensional crystal structure of cholera toxin. *J Mol Biol*. 1995;251(4):563-573. doi:10.1006/jmbi.1995.0456
78. Merritt EA, Sarfaty S, Akker FVD, Hoir CL, Martial JA, Hol WGJ. Crystal structure of cholera toxin B-pentamer bound to receptor. *Protein Sci*. Published online 1994:166-175.
79. Kuziemko GM, Stroh M, Stevens RC. Cholera toxin binding affinity and specificity for gangliosides determined by surface plasmon resonance. *Biochemistry*. 1996;35(20):6375-6384. doi:10.1021/bi952314i
80. Turnbull WB, Precious BL, Homans SW. Dissecting the Cholera Toxin-Ganglioside GM1 Interaction by Isothermal Titration Calorimetry. *J Am Chem Soc*. 2004;126(4):1047-1054. doi:10.1021/ja0378207
81. Holmner Å, Lebens M, Teneberg S, Ångström J, Ökvist M, Krengel U. Novel binding site identified in a hybrid between cholera toxin and heat-labile enterotoxin: 1.9 Å crystal structure reveals the details. *Structure*. 2004;12(9):1655-1667. doi:10.1016/j.str.2004.06.022
82. Mandal PK, Branson TR, Hayes ED, et al. Towards a structural basis for the relationship

between blood group and the severity of El Tor cholera. *Angew Chemie - Int Ed*. 2012;51(21):5143-5146. doi:10.1002/anie.201109068

83. Cervin J, Boucher A, Youn G, et al. Fucose-Galactose Polymers Inhibit Cholera Toxin Binding to Fucosylated Structures and Galactose-Dependent Intoxication of Human Enteroids. *ACS Infect Dis*. 2020;6:1192-1203. doi:10.1021/acsinfecdis.0c00009
84. De Haan L, Hirst TR. Cholera toxin: A paradigm for multi-functional engagement of cellular mechanisms (Review). *Mol Membr Biol*. 2004;21(2):77-92. doi:10.1080/09687680410001663267
85. Machin DC, Williamson DJ, Fisher P, et al. Sortase-modified cholera toxoids show specific Golgi localization. *ChemRXiv*.:10.26434/chemrxiv.9125201.v1. doi:10.26434/chemrxiv.9125201.v1
86. Scheutz F, Teel LD, Beutin L, et al. Multicenter Evaluation of a Sequence-Based Protocol for Subtyping Shiga Toxins and Standardizing Stx Nomenclature. *J Clin Microbiol*. 2012;50(9):2951-2963. doi:10.1128/JCM.00860-12
87. Lingwood CA, Law H, Richardson S, et al. Glycolipid binding of purified and recombinant Escherichia coli produced verotoxin in vitro. *J Biol Chem*. 1987;262(18):8834-8839. doi:10.1016/s0021-9258(18)47490-x
88. Karmali MA, Petrie M, Lim C, Fleming PC, Arbus GS, Lior H. The Association Between Idiopathic Hemolytic Uremic Syndrome and Infection by Verotoxin-Producing Escherichia coli. *J Infect Dis*. 1985;151(5):775-782.
89. Karmali MA. Infection by Shiga Toxin-Producing Escherichia coli. *Mol Biotechnol*. 2004;26:117-122.
90. Beutin L, Miko A, Krause G, et al. Identification of Human-Pathogenic Strains of Shiga Toxin-Producing Escherichia coli from Food by a Combination of Serotyping and Molecular Typing of Shiga Toxin Genes . *Appl Environ Microbiol*. 2007;73(15):4769-4775. doi:10.1128/AEM.00873-07
91. Fraser ME, Fujinaga M, Cherney MM, et al. Structure of Shiga toxin type 2 (Stx2) from Escherichia coli O157:H7. *J Biol Chem*. 2004;279(26):27511-27517. doi:10.1074/jbc.M401939200
92. Miller DJ, Ravikumar K, Shen H, Suh J, Kerwin SM, Robertus JD. Structure-Based Design and Characterization of Novel Platforms for Ricin and Shiga Toxin Inhibition. *J Med Chem*. 2002;45(1):90-98.
93. Endo Y, Tsurugi K, Yutsudo T, Takeda Y, Ogasawara T, Igarashi Z. Site of action of a Vero toxin (VT2) from Escherichia coli 0157 : H7 and of Shiga toxin on eukaryotic ribosomes

RNA N-glycosidase activity of the toxins. *Eur J Biochem*. 1988;50:45-50.

94. Hovde CJ, Calderwood SB, Mekalanos JJ, Collier RJ. Evidence that glutamic acid 167 is an active-site residue of Shiga-like toxin I. *PNAS*. 1988;85:2568-2572. doi:10.1073/pnas.85.8.2568
95. Fraser ME, Chernaia MM, Kozlov Y V, James MNG. Crystal structure of the holotoxin from Shigella dysenteriae at 2.5 A resolution. *Nat Struct Biol*. 1994;1:59-64.
96. Menge C. Molecular Biology of Escherichia coli Shiga Toxins ' Effects on Mammalian Cells. *Toxins (Basel)*. 2020;12(5):345.
97. Nyholm P, Zheng Z, Nore R, Binnington-boyd B, Lingwood CA. Two distinct binding sites for globotriaosyl ceram ide on verotoxins : identification by molecular modelling and confirmation using deoxy analogues and a new glycolipid receptor for all verotoxins. *Chem Biol*. 1996;3(4):263-275.
98. Kitova EN, Kitov PI, Paszkiewicz E, et al. Affinities of Shiga toxins 1 and 2 for univalent and oligovalent Pk-trisaccharide analogs measured by electrospray ionization mass spectrometry. *Glycobiology*. 2007;17(10):1127-1137. doi:10.1093/glycob/cwm081
99. Shimizu H, Field RA, Homans SW, Donohue-Rolfe A. Solution Structure of the Complex between the B-Subunit Homopentamer of Verotoxin VT-1 from Escherichia coli and the Trisaccharide Moiety of Globotriasylceramide. *Biochemistry*. 1998;37(31):11078-11082.
100. Windschiegl B, Orth A, Romer W, et al. Lipid Reorganization Induced by Shiga Toxin Clustering on Planar Membranes. *PLoS One*. 2009;4(7):e6238. doi:10.1371/journal.pone.0006238
101. Sandvig K, Bergan J, Dyve A, Skotland T, Torgersen ML. Toxicon Endocytosis and retrograde transport of Shiga toxin. *Toxicon*. 2010;56(7):1181-1185. doi:10.1016/j.toxicon.2009.11.021
102. Romer W, Berland L, Gaus K, et al. Shiga toxin induces tubular membrane invaginations for its uptake into cells. *Nature*. 2007;450(29):670–675. doi:10.1038/nature05996
103. Sandvig K, Lyngaas M, Andersen H, Bo R. Clathrin-independent endocytosis : from nonexisting to an extreme degree of complexity. *Histochem Cell Biol*. 2008;129:267-276. doi:10.1007/s00418-007-0376-5
104. Garred O, Van Duers B, Sandvig K. Furin-induced Cleavage and Activation of Shiga Toxin. *J Biol Chem*. 1995;270(18):10817-10821. doi:10.1074/jbc.270.18.10817
105. Gaynor EC, Emr SD. COPI-independent anterograde transport: Cargo-selective ER to Golgi protein transport in yeast COPI mutants. *J Cell Biol*. 1997;136(4):789-802. doi:10.1083/jcb.136.4.789

106. Lang K, Chin JW. Cellular Incorporation of Unnatural Amino Acids and Bioorthogonal Labeling of Proteins. *Chem Rev*. 2014;114(9):4764-4806. doi:10.1021/cr400355w
107. Ramström O. Scientific Background on the Nobel Prize in Chemistry 2022 Click Chemistry and Bioorthogonal Chemistry The Nobel Committee for Chemistry. *R Swedish Acad Sci*. 2022;50005.
108. Meldal M, Diness F. Recent Fascinating Aspects of the CuAAC Click Reaction. *Trends Chem*. 2020;2(6):569-584. doi:10.1016/j.trechm.2020.03.007
109. Dieterich DC, Lee JJ, Link AJ, Graumann J, Tirrell DA, Schuman EM. Labeling, detection and identification of newly synthesized proteomes with bioorthogonal non-canonical amino-acid tagging. *Nat Protoc*. 2007;2(3):532-540. doi:10.1038/nprot.2007.52
110. Ngo JT, Champion JA, Mahdavi A, et al. Cell-selective metabolic labeling of proteins. *Nat Chem Biol*. 2009;5(10):715-717. doi:10.1038/nchembio.200
111. Dommerholt J, Rutjes FPJT, van Delft FL. Strain-Promoted 1,3-Dipolar Cycloaddition of Cycloalkynes and Organic Azides. *Top Curr Chem*. 2016;374(2):1-20. doi:10.1007/s41061-016-0016-4
112. Saxon E, Bertozzi CR. Cell Surface Engineering by a Modified Staudinger Reaction. *Science (80-)*. 2000;287:2007-2011.
113. Paris C, Brun O, Pedroso E, Grandas A. Exploiting protected maleimides to modify oligonucleotides, peptides and peptide nucleic acids. *Molecules*. 2015;20(4):6389-6408. doi:10.3390/molecules20046389
114. Sánchez A, Pedroso E, Grandas A. Easy introduction of maleimides at different positions of oligonucleotide chains for conjugation purposes. *Org Biomol Chem*. 2012;10(42):8478-8483. doi:10.1039/c2ob26514a
115. Baldwin AD, Kiick KL. Tunable degradation of maleimide-Thiol adducts in reducing environments. *Bioconjug Chem*. 2011;22(10):1946-1953. doi:10.1021/bc200148v
116. Oliveira BL, Guo Z, Bernardes GJL. Inverse electron demand Diels-Alder reactions in chemical biology. *Chem Soc Rev*. 2017;46(16):4895-4950. doi:10.1039/c7cs00184c
117. Huisgen R. Kinetics and reaction mechanisms: Selected examples from the experience of forty years. *Pure Appl Chem*. 1989;61(4):613-628. doi:10.1351/pac198961040613
118. Tornøe CW, Christensen C, Meldal M. Peptidotriazoles on solid phase: [1,2,3]-Triazoles by regiospecific copper(I)-catalyzed 1,3-dipolar cycloadditions of terminal alkynes to azides. *J Org Chem*. 2002;67(9):3057-3064. doi:10.1021/jo011148j
119. Meldal M, Tomøe CW. Cu-catalyzed azide - Alkyne cycloaddition. *Chem Rev*. 2008;108(8):2952-3015. doi:10.1021/cr0783479

120. Kolb HC, Finn MG, Sharpless KB. Click Chemistry: Diverse Chemical Function from a Few Good Reactions. *Angew Chemie - Int Ed*. 2001;40(11):2004-2021. doi:10.1002/1521-3773(20010601)40:11<2004::AID-ANIE2004>3.0.CO;2-5

121. Tang W, Becker ML. "Click" reactions: A versatile toolbox for the synthesis of peptide-conjugates. *Chem Soc Rev*. 2014;43(20):7013-7039. doi:10.1039/c4cs00139g

122. Kennedy DC, McKay CS, Legault MCB, et al. Cellular consequences of copper complexes used to catalyze bioorthogonal click reactions. *J Am Chem Soc*. 2011;133(44):17993-18001. doi:10.1021/ja2083027

123. Nairn NW, Bariola PA, Graddis TJ, et al. Cysteine as a Monothiol Reducing Agent to Prevent Copper-Mediated Oxidation of Interferon Beta during PEGylation by CuAAC. *Bioconjug Chem*. 2015;26(10):2070-2075. doi:10.1021/acs.bioconjchem.5b00320

124. Hong V, Presolski SI, Ma C, Finn MG. Analysis and optimization of copper-catalyzed azide-alkyne cycloaddition for bioconjugation. *Angew Chemie - Int Ed*. 2009;48(52):9879-9883. doi:10.1002/anie.200905087

125. Venkateswara Rao B, Dhokale S, Rajamohanan PR, Hotha S. A tetrazine templated method for the synthesis of ternary conjugates. *Chem Commun*. 2013;49(92):10808-10810. doi:10.1039/c3cc46634e

126. Willems LI, Li N, Florea BI, Ruben M, Van Der Marel GA, Overkleeft HS. Triple bioorthogonal ligation strategy for simultaneous labeling of multiple enzymatic activities. *Angew Chemie - Int Ed*. 2012;51(18):4431-4434. doi:10.1002/anie.201200923

127. Yang J, Šečkute J, Cole CM, Devaraj NK. Live-cell imaging of cyclopropene tags with fluorogenic tetrazine cycloadditions. *Angew Chemie - Int Ed*. 2012;51(30):7476-7479. doi:10.1002/anie.201202122

128. Beckmann HSG, Niederwieser A, Wiessler M, Wittmann V. Preparation of carbohydrate arrays by using Diels-Alder reactions with inverse electron demand. *Chem - A Eur J*. 2012;18(21):6548-6554. doi:10.1002/chem.201200382

129. Karver MR, Weissleder R, Hilderbrand SA. Synthesis and evaluation of a series of 1,2,4,5-tetrazines for bioorthogonal conjugation. *Bioconjug Chem*. 2011;22(11):2263-2270. doi:10.1021/bc200295y

130. Wagner JA, Mercadante D, Nikic I, Lemke EA, Gräter F. Origin of Orthogonality of Strain-Promoted Click Reactions. *Chem - A Eur J*. 2015;21(35):12431-12435. doi:10.1002/chem.201501727

131. Saravanakumar G, Deepagan VG, Jayakumar R, Park JH. Hyaluronic acid-based conjugates for tumor-targeted drug delivery and imaging. *J Biomed Nanotechnol*.

2014;10(1):17-31. doi:10.1166/jbn.2014.1761

132. Collins MN, Birkinshaw C. Hyaluronic acid based scaffolds for tissue engineering - A review. *Carbohydr Polym*. 2013;92(2):1262-1279. doi:10.1016/j.carbpol.2012.10.028
133. Tiwari S, Bahadur P. Modified hyaluronic acid based materials for biomedical applications. *Int J Biol Macromol*. 2019;121:556-571. doi:10.1016/j.ijbiomac.2018.10.049
134. Trombino S, Servidio C, Curcio F, Cassano R. Strategies for hyaluronic acid-based hydrogel design in drug delivery. *Pharmaceutics*. 2019;11(8):1-17. doi:10.3390/pharmaceutics11080407
135. Chen B, Miller RJ, Dhal PK. Hyaluronic acid-based drug conjugates: State-of-the-art and perspectives. *J Biomed Nanotechnol*. 2014;10(1):4-16. doi:10.1166/jbn.2014.1781
136. Platt VM, Szoka FC. reviews Anticancer Therapeutics : Targeting Macromolecules and Nanocarriers to Hyaluronan or CD44 , a Hyaluronan Receptor. 2008;(1):36777-36781.
137. Csapó E, Szokolai H, Juhász Á, Varga N, Janovák L, Dékány I. Cross-linked and hydrophobized hyaluronic acid-based controlled drug release systems. *Carbohydr Polym*. 2018;195(February):99-106. doi:10.1016/j.carbpol.2018.04.073
138. Bulpitt P, Aeschlimann D. New strategy for chemical modification of hyaluronic acid: Preparation of functionalized derivatives and their use in the formation of novel biocompatible hydrogels. *J Biomed Mater Res*. 1999;47(2):152-169. doi:10.1002/(SICI)1097-4636(199911)47:2<152::AID-JBM5>3.0.CO;2-I
139. Schanté CE, Zuber G, Herlin C, Vandamme TF. Chemical modifications of hyaluronic acid for the synthesis of derivatives for a broad range of biomedical applications. *Carbohydr Polym*. 2011;85(3):469-489. doi:10.1016/j.carbpol.2011.03.019
140. di Meo C, Panza L, Campo F, et al. Novel types of carborane-carrier hyaluronan derivatives via “click chemistry.” *Macromol Biosci*. 2008;8(7):670-681. doi:10.1002/mabi.200700304
141. Crescenzi V, Cornelio L, Di Meo C, Nardecchia S, Lamanna R. Novel hydrogels via click chemistry: Synthesis and potential biomedical applications. *Biomacromolecules*. 2007;8(6):1844-1850. doi:10.1021/bm0700800
142. Schneider A, Picart C, Senger B, Schaaf P, Voegel JC, Frisch B. Layer-by-layer films from hyaluronan and amine-modified hyaluronan. *Langmuir*. 2007;23(5):2655-2662. doi:10.1021/la062163s
143. Nakajima N, Ikada Y. Mechanism of Amide Formation by Carbodiimide for Bioconjugation in Aqueous Media. *Bioconjug Chem*. 1995;6(1):123-130. doi:10.1021/bc00031a015
144. Magnani A, Rappuoli R, Lamponi S, Barbucci R, Ettore V. Novel Polysaccharide Hydrogels : Characterization and Properties. *Polym Adv Technol*. 2000;11:488-495.

145. Maroda M, Bodnár M, Berkó S, et al. Preparation and investigation of a cross-linked hyaluronan nanoparticles system. *Carbohydr Polym*. 2011;83(3):1322-1329. doi:10.1016/j.carbpol.2010.09.039

146. Bergman K, Elvingson C, Hilborn J, Svensk G, Bowden T. Hyaluronic acid derivatives prepared in aqueous media by triazine-activated amidation. *Biomacromolecules*. 2007;8(7):2190-2195. doi:10.1021/bm0701604

147. Gramlich WM, Kim IL, Burdick JA. Synthesis and orthogonal photopatterning of hyaluronic acid hydrogels with thiol-norbornene chemistry. *Biomaterials*. 2013;34(38):9803-9811. doi:10.1016/j.biomaterials.2013.08.089

148. Blackman ML, Royzen M, Fox JM. Tetrazine ligation: Fast bioconjugation based on inverse-electron-demand Diels-Alder reactivity. *J Am Chem Soc*. 2008;130(41):13518-13519. doi:10.1021/ja8053805

149. Devaraj NK, Weissleder R, Hilderbrand SA. Tetrazine-based cycloadditions: Application to pretargeted live cell imaging. *Bioconjug Chem*. 2008;19(12):2297-2299. doi:10.1021/bc8004446

150. Devaraj NK, Weissleder R. Biomedical Applications of Tetrazine Cycloadditions. *Acc Chem Res*. 2011;44(9):816-827.

151. Zhang H, Dicker KT, Xu X, Jia X, Fox JM. Interfacial bioorthogonal cross-linking. *ACS Macro Lett*. 2014;3(8):727-731. doi:10.1021/mz5002993

152. Famili A, Rajagopal K. Bio-Orthogonal Cross-Linking Chemistry Enables in Situ Protein Encapsulation and Provides Sustained Release from Hyaluronic Acid Based Hydrogels. *Mol Pharm*. 2017;14(6):1961-1968. doi:10.1021/acs.molpharmaceut.7b00067

153. Yang J, Karver MR, Li W, Sahu S, Devaraj NK. Metal-catalyzed one-pot synthesis of tetrazines directly from aliphatic nitriles and hydrazine. *Angew Chemie - Int Ed*. 2012;51(21):5222-5225. doi:10.1002/anie.201201117

154. Luo Z, Rosenberg AJ, Liu H, Han J, Tu Z. Syntheses and in vitro evaluation of new S1PR1 compounds and initial evaluation of a lead F-18 radiotracer in rodents. *Eur J Med Chem*. 2018;150:796-808. doi:10.1016/j.ejmech.2018.03.035

155. Sheehan JC, Cruickshank PA, Boshart GL. A Convenient Synthesis of Water- Sol uble Carbodiimides. *J Org Chem*. 1960;26:2525.

156. Dubacheva G V., Curk T, Auzély-Velty R, Frenkel D, Richter RP. Designing multivalent probes for tunable superselective targeting. *Proc Natl Acad Sci U S A*. 2015;112(18):5579-5584. doi:10.1073/pnas.1500622112

157. Carlson CB, Mowery P, Owen RM, Dykhuizen EC, Kiessling LL. Selective Tumor Cell

Targeting Using Low-Affinity, Multivalent Interactions. *ACS Chem Biol*. 2007;2(2):119-127.

158. Feizi T. Oligosaccharides that mediate mammalian cell-cell adhesion. *Curr Opin Struct Biol*. 1993;3(5):701-710. doi:10.1016/0959-440X(93)90053-N

159. Nilsson KGI. Enzymatic synthesis of oligosaccharides. *Trends Biotechnol*. 1988;6(10):256-264. doi:doi.org/10.1016/0167-7799(88)90058-3.

160. Paulsen H. Haworth Memorial Lecture. Synthesis of complex oligosaccharide chains of glycoproteins. *Chem Soc Rev*. 1984;13(1):15-45. doi:10.1039/CS9841300015

161. Seeberger PH, Finney N, Rabuka D, Bertozzi CR. Chapter 49 - Chemical and Enzymatic Synthesis of Glycans and Glycoconjugates. In: *Essentials of Glycobiology*. 2nd Editio. Cold Spring Harbor Laboratoy Press; 2009. http://www.ncbi.nlm.nih.gov/books/NBK1956/

162. Monsan P, Paul F. Enzymatic synthesis of oligosaccharides. *FEMS Microbiol Rev*. 1995;16(2-3):187-192. doi:10.1111/j.1574-6976.1995.tb00165.x

163. Soriano del Amo D, Wang W, Besanceney C, et al. Chemoenzymatic synthesis of the sialyl Lewis X glycan and its derivatives. *Carbohydr Res*. 2010;345(9):1107-1113. doi:10.1016/j.carres.2010.03.032

164. Agard NJ, Bertozzi CR. Chemical Approaches To Perturb, Profile, and Perceive Glycans. *Acc Chem Res*. 2009;42(6):788-797.

165. Brown CD, Rusek MS, Kiessling LL. Fluorosugar chain termination agents as probes of the sequence specificity of a carbohydrate polymerase. *J Am Chem Soc*. 2012;134(15):6552-6555. doi:10.1021/ja301723p

166. Hsu TL, Hanson SR, Kishikawa K, Wang SK, Sawa M, Wong CH. Alkynyl sugar analogs for the labeling and visualization of glycoconjugates in cells. *Proc Natl Acad Sci U S A*. 2007;104(8):2614-2619. doi:10.1073/pnas.0611307104

167. Okeley NM, Alley SC, Anderson ME, et al. Development of orally active inhibitors of protein and cellular fucosylation. *Proc Natl Acad Sci U S A*. 2013;110(14):5404-5409. doi:10.1073/pnas.1222263110

168. Gloster TM, Zandberg WF, Heinonen JE, Shen DL, Deng L, Vocadlo DJ. Hijacking a biosynthetic pathway yields a glycosyltransferase inhibitor within cells. *Nat Chem Biol*. 2011;7(3):174-181. doi:10.1038/nchembio.520

169. Rillahan CD, Antonopoulos A, Lefort CT, et al. Global metabolic inhibitors of sialyl- and fucosyltransferases remodel the glycome. *Nat Chem Biol*. 2012;8(7):661-668. doi:10.1038/nchembio.999

170. Hindsgaul O, Norberg T, Le Pendu J, Lemieux RU. Synthesis of type 2 human blood-group antigen determinants. *Carbohydr Res*. 1982;109:109-142. http://dx.doi.org/10.1016/0008-

6215(82)84034-2

171. Mandal PK, Turnbull WB. Studies on the synthesis of Lewis-y oligosaccharides. 2011;346:2113-2120. doi:10.1016/j.carres.2011.07.002

172. Yamazaki Y, Sezukuri K, Takada J, Obata H, Kimura S, Ohmae M. Synthesis of type 2 Lewis antigens via novel regioselective glycosylation of an orthogonally protected lactosamine diol derivative. *Carbohydr Res*. 2016;422:34-44. doi:10.1016/j.carres.2016.01.003

173. Wang G, Boulton PG, Chan NWC, Palcic MM, Taylor DE. Novel Helicobacter pylori α1,2-fucosyltransferase, a key enzyme in the synthesis of Lewis antigens. *Microbiology*. 1999;145(11):3245-3253. doi:10.1099/00221287-145-11-3245

174. Rasko DA, Wang G, Monteiro MA, Palcic MM, Taylor DE. Synthesis of mono- and di-fucosylated type I Lewis blood group antigens by Helicobacter pylori. *Eur J Biochem*. 2000;267(19):6059-6066. doi:10.1046/j.1432-1327.2000.01683.x

175. Stein DB, Lin YN, Lina CH. Characterization of Helicobacter pylori α1,2-fucosyltransferase for enzymatic synthesis of tumor-associated antigens. *Adv Synth Catal*. 2008;350(14-15):2313-2321. doi:10.1002/adsc.200800435

176. Tsai TW, Fang JL, Liang CY, et al. Exploring the Synthetic Application of Helicobacter pylori α1,3/4-Fucosyltransferase FucTIII toward the Syntheses of Fucosylated Human Milk Glycans and Lewis Antigens. *ACS Catal*. Published online 2019:10712-10720. doi:10.1021/acscatal.9b03752

177. Ellervik U, Magnusson G. A high yielding chemical synthesis of sialyl Lewis x tetrasaccharide and Lewis x trisaccharide; examples of regio- and stereodifferentiated glycosylations. *J Org Chem*. 1998;63(25):9314-9322. doi:10.1021/jo981203x

178. Nicolaou KC, Hummel CW, Bockovich N., Wong CH. Stereocontrolled Synthesis of Sialyl Lex, the Oligosaccharide Binding Ligand to ELAM-I (Sialyl = A/-acetylneuramin). *J Chem Soc*. 1995;(870):3810-3815.

179. Nicolaou KC, Bockovich N., Carcanague DR. Total Synthesis of Sulfated Lex and Lea-Type Oligosaccharide Selectin Ligands. *J Am Chem Soc*. 1993;(10):8843-8844.

180. Pudelko M, Bull J, Kunz H. Chemical and chemoenzymatic synthesis of glycopeptide selectin ligands containing sialyl lewis X structures. *ChemBioChem*. 2010;11(7):904-930. doi:10.1002/cbic.201000029

181. Nicolaou KC, Caulfield T, Kataoka H, T K. A Practical and Enantioselective Synthesis of Glycosphingolipids and Related Compounds. Total Synthesis of Globotriaosylceramide (Gb3). *J Am Chem Soc*. 1988;110:7910-7912.

182. Hansen HC, Magnusson G. Synthesis of some amino and carboxy analogs of galabiose ; evaluation as inhibitors of the pilus protein PapG J96 from Escherichia coli. 1998;307:233-242.

183. Miura T, Tsujino S, Satoh A, Goto K, Mizuno M. Fluorescence modification of Gb3 oligosaccharide and rapid synthesis of oligosaccharide moieties using fluorous protective group. *Tetrahedron*. 2005;61:6518-6526. doi:10.1016/j.tet.2005.05.001

184. Hashimoto S, Sakamoto H, Honda T, Abe H, Nakamura S, Ikegami S. " Armed-Disarmed " Glycosidation Strategy Based on Glycosyl Donors and Acceptors Carrying Phosphoroamidate as a Leaving Group : A Convergent Synthesis of Giobotriaosylceramide Shun-iehi Hashimoto ,* t Hiroki Sakamoto , t Takeshi Honda , t 1 Hiroshi Abe ,. *Tetrahedron Lett*. 1997;38(52):8969-8972.

185. Zhang J, Kowal P, Fang J, Andreana P, Wang PG. Efficient chemoenzymatic synthesis of globotriose and its derivatives with a recombinant a - (1 " 4) -galactosyltransferase. *Carbohydr Res*. 2002;337:969-976.

186. Huang K, Marchesi A, Hollingsworth K, et al. Biochemical characterisation of an α1,4 galactosyltransferase from Neisseria weaveri for the synthesis of α1,4-linked galactosides. *Org Biomol Chem*. 2020;18:3142-3148. doi:10.1039/d0ob00407c

187. Yan F, Gilbert M, Wakarchuk WW, Brisson J, Whitfield DM. Chemoenzymatic Iterative Synthesis of Difficult Linkages of Oligosaccharides on Soluble Polymeric Supports. *Org Lett*. 2001;3(21):3265-3268.

188. Mortisen D, Peroglio M, Alini M, Eglin D. Tailoring thermoreversible hyaluronan hydrogels by "click" chemistry and RAFT polymerization for cell and drug therapy. *Biomacromolecules*. 2010;11(5):1261-1272. doi:10.1021/bm100046n

189. Piluso S, Hiebl B, Gorb SN, Kovalev A, Lendlein A, Axel T. Hyaluronic acid-based hydrogels crosslinked by copper-catalyzed azide-alkyne cycloaddition with tailorable mechanical properties. *Int J Artif Organs*. 2011;34(2):192-197. doi:10.5301/IJAO.2011.6394

190. Valverde P, Vendeville JB, Hollingsworth K, et al. Chemoenzymatic synthesis of 3-deoxy-3-fluoro-l-fucose and its enzymatic incorporation into glycoconjugates. *Chem Commun*. 2020;56(47):6408-6411. doi:10.1039/d0cc02209h

191. Nuti E, Cuffaro D, Andrea FD, et al. Sugar-Based Arylsulfonamide Carboxylates as Selective and Water-Soluble Matrix Metalloproteinase-12 Inhibitors. *ChemMedChem*. 2016;11:1626-1637. doi:10.1002/cmdc.201600235

192. Willems MMJHP, Zom GG, Meeuwenoord N, et al. Design , automated synthesis and immunological evaluation of NOD2-ligand – antigen conjugates. *Beilstein J Org Chem*.

2014;10:1445-1453. doi:10.3762/bjoc.10.148

193. Koizumi S, Endo T, Tabata K, Ozaki A. Large-scale production ofUDP-galactose and globotriose by coupling metabolically engineered bacteria. *Nat Biotechnol*. 1998;16:847-850.

194. Rosano GL, Ceccarelli EA. Recombinant protein expression in Escherichia coli: Advances and challenges. *Front Microbiol*. 2014;5(APR):1-17. doi:10.3389/fmicb.2014.00172

195. Naven TJP, Harvey DJ. Cationic Derivatization of Oligosaccharides with Girard ' s T Reagent for Improved Performance in Matrix-assisted Laser DesorptiodIonization and Electrospray Mass Spectrometry. *Rapid Commun Mass Spectrom*. 1996;10(April):829-834.

196. Galan MC, Tran AT, Bernard C. Ionic-liquid-based catch and release mass spectroscopy tags for enzyme monitoring. *Chem Commun*. 2010;46:8968-8970. doi:10.1039/c0cc04224b

197. Tran A, Burden R, Racys DT, Galan MC. Ionic catch and release oligosaccharide synthesis (ICROS). *Chem Commun*. 2011;44(0):4526-4528. doi:10.1039/c0cc05580h

198. Galan MC, Tran AT, Bromfield K, Ernst B. Ionic-liquid-based MS probes for the chemo-enzymatic synthesis of oligosaccharides†. *Org Biomol Chem*. 2012;10:7091-7097. doi:10.1039/c2ob25855b

199. Sittel I, Galan MC. Chemo-enzymatic synthesis of imidazolium-tagged sialyllactosamine probes. *Bioorg Med Chem Lett*. 2015;25(19):4329-4332. doi:10.1016/j.bmcl.2015.07.049

200. Galan MC, Jones RA, Tran AT. Recent developments of ionic liquids in oligosaccharide synthesis : the sweet side of ionic liquids. *Carbohydr Res*. 2013;375:35-46. doi:10.1016/j.carres.2013.04.011

201. Manzi G, Zoratto N, Matano S, et al. "Click" hyaluronan based nanohydrogels as multifunctionalizable carriers for hydrophobic drugs. *Carbohydr Polym*. 2017;174:706-715. doi:10.1016/j.carbpol.2017.07.003

202. Araújo M, Bidarra SJ, Alves PM, Valcarcel J, Vázquez JA, Barrias CC. Coumarin-grafted blue-emitting fluorescent alginate as a potentially valuable tool for biomedical applications. *J Mater Chem B*. 2020;8(4):813-825. doi:10.1039/c9tb01402k

203. Tokita Y, Okamoto A. Hydrolytic degradation of hyaluronic. *Polym Degrad Stab*. 1995;48:269-273.

204. Gatej I, Popa M, Rinaudo M. Role of the pH on Hyaluronan Behavior in Aqueous Solution. *Biomacromolecules*. 2005;6:61-67.

205. Maleki A, Kjøniksen A-L, Nystro B. Effect of pH on the Behavior of Hyaluronic Acid in Dilute and Semidilute Aqueous Solutions. *Macromol Symp*. 2008;274:131-140. doi:10.1002/masy.200851418

206. Hartwell BL, Pickens CJ, Leon M, Berkland C. Multivalent Soluble Antigen Arrays Exhibit High Avidity Binding and Modulation of B Cell Receptor-Mediated Signaling to Drive E ffi cacy against Experimental Autoimmune Encephalomyelitis. *Biomacromolecules*. 2017;18:1893-1907. doi:10.1021/acs.biomac.7b00335

207. Snetkov P, Zakharova K, Morozkina S, Olekhnovich R, Uspenskaya M. Hyaluronic acid: The influence of molecular weight on structural, physical, physico-chemical, and degradable properties of biopolymer. *Polymers (Basel)*. 2020;12(8). doi:10.3390/polym12081800

208. Pouyani T, Prestwich GD. Functionalized Derivatives of Hyaluronic Acid Oligosaccharides: Drug Carriers and Novel Biomaterials. *Bioconjug Chem*. 1994;5(4):339-347. doi:10.1021/bc00028a010

209. Coradini D, Pellizzaro C, Miglierini G, Daidone MG, Perbellini A. Hyaluronic acid as drug delivery for sodium butyrate: Improvement of the anti-proliferative activity on a breast-cancer cell line. *Int J Cancer*. 1999;81(3):411-416. doi:10.1002/(sici)1097-0215(19990505)81:3<411::aid-ijc15>3.0.co;2-f

210. Pravata L, Braud C, Boustta M, et al. New amphiphilic lactic acid oligomer - Hyaluronan conjugates: Synthesis and physicochemical characterization. *Biomacromolecules*. 2008;9(1):340-348. doi:10.1021/bm700843m

211. Kunishima M, Kawachi C, Morita J, Terao K, Iwasaki F, Tani S. 4-(4,6-Dimethoxy-1,3,5-triazin-2-yl)-4-methylmorpholinium chloride: An efficient condensing agent leading to the formation of amides and esters. *Tetrahedron*. 1999;55(46):13159-13170. doi:10.1016/S0040-4020(99)00809-1

212. Farkaš P, Bystrický S. Efficient activation of carboxyl polysaccharides for the preparation of conjugates. *Carbohydr Polym*. 2007;68(1):187-190. doi:10.1016/j.carbpol.2006.07.013

213. Zhou Y, Petrova SP, Edgar KJ. Chemical synthesis of polysaccharide – protein and polysaccharide – peptide conjugates : A review. *Carbohydr Polym*. 2021;274:118662.

214. Nimmo CM, Owen SC, Shoichet MS. Diels-alder click cross-linked hyaluronic acid hydrogels for tissue engineering. *Biomacromolecules*. 2011;12(3):824-830. doi:10.1021/bm101446k

215. D'Este M, Eglin D, Alini M. A systematic analysis of DMTMM vs EDC/NHS for ligation of amines to Hyaluronan in water. *Carbohydr Polym*. 2014;108(1):239-246. doi:10.1016/j.carbpol.2014.02.070

216. Yu F, Cao X, Li Y, Zeng L, Yuan B, Chen X. An injectable hyaluronic acid/PEG hydrogel for cartilage tissue engineering formed by integrating enzymatic crosslinking and Diels-Alder "click chemistry." *Polym Chem*. 2014;5(3):1082-1090. doi:10.1039/c3py00869j

217. Gemma E, Hulme AN, Jahnke A, Jin L, Lyon M, Mu RM. DMT-MM mediated functionalisation of the non-reducing end of glycosaminoglycans. *Chem Commun*. 2007;(26):2686-2688. doi:10.1039/b617038b

218. Charlot LIA, Tizzotti M, Labeau M, Hamaide T, Drockenmuller E, Fleury E. Synthesis of Thermosensitive Guar-Based Hydrogels with Tunable Physico-Chemical Properties by Click Chemistry. 2010;48:2733-2742. doi:10.1002/POLA

219. Kumar V, Turnbull WB. Carbohydrate inhibitors of cholera toxin. *Beilstein J Org Chem*. 2018;14:484-498. doi:10.3762/bjoc.14.34

220. Branson TR, Turnbull WB. Bacterial toxin inhibitors based on multivalent scaffolds. *Chem Soc Rev*. 2013;42(11):4613-4622. doi:10.1039/c2cs35430f

221. Hong V, Steinmetz NF, Manchester M, Finn MG. Labeling live cells by copper-catalyzed alkyne-azide click chemistry. *Bioconjug Chem*. 2010;21(10):1912-1916. doi:10.1021/bc100272z

222. Praest BM, Greiling H, Kock R. Effects of oxygen-derived free radicals on the molecular weight and the polydispersity of hyaluronan solutions. *Carbohydr Res*. 1997;303(2):153-157.

223. Seelbach RJ, Fransen P, Peroglio M, et al. Multivalent dendrimers presenting spatially controlled clusters of binding epitopes in thermoresponsive hyaluronan hydrogels. *Acta Biomater*. 2014;10(10):4340-4350. doi:10.1016/j.actbio.2014.06.028

224. Borke T, V MBB, Najberg M, Ilina P, Bhattacharya M. Hyaluronic Acid Graft Copolymers with Cleavable Arms as Potential Hyaluronic Acid Graft Copolymers with Cleavable Arms as Potential Intravitreal Drug Delivery Vehicles. *Macromol Biosci*. 2018;18(1). doi:10.1002/mabi.201700200

225. Soltes L, Stankovska M, Brezova V, et al. Hyaluronan degradation by copper (II) chloride and ascorbate : rotational viscometric , EPR spin-trapping, and MALDI – TOF mass spectrometric investigations. *Carbohydr Res*. 2006;341(17):2826-2834. doi:10.1016/j.carres.2006.09.019

226. Soltes L, Brezova V, Stankovska M, Kogan G, Gemeiner P. Degradation of high-molecular-weight hyaluronan by hydrogen peroxide in the presence of cupric ions. *Carbohydr Res*. 2006;341(5):639-644. doi:10.1016/j.carres.2006.01.014

227. Jahn M, Baynes JW, Spiteller G. The reaction of hyaluronic acid and its monomers , glucuronic acid and N -acetylglucosamine , with reactive oxygen species. *Carbohydr Res*. 1999;321:228-234.

228. Richter RP, Rodenhousen KB, Eisele NB, Schubert M. Chapter 11 Coupling Spectroscopic

Ellipsometry and Quartz Crystal Microbalance to Study Organic Films at the Solid-Liquid Interface. In: Hinrichs K, Eichhorn K, eds. *Ellipsometry of Functional Organic Surfaces and Films*. Vol 52. Springer, Cham; 2018:391-417. doi:10.1007/978-3-642-40128-2

229. Easley AD, Ma T, Eneh CI, Yun J, Thakur RM, Lutkenhaus JL. A practical guide to quartz crystal microbalance with dissipation monitoring of thin polymer films. *J Polym Sci*. 2022;60(7):1090-1107. doi:10.1002/pol.20210324
230. Reviakine I, Johannsmann D, Richter RP. Hearing what you cannot see and visualizing what you hear: Interpreting quartz crystal microbalance data from solvated interfaces. *Anal Chem*. 2011;83(23):8838-8848. doi:10.1021/ac201778h
231. Rodahl M, Hook F, Krozer A, Brzezinski P, Kasemo B. Quartz crystal microbalance setup for frequency and Q -factor measurements in gaseous and liquid environments rneasurements in gaseous and liquid environments. *Rev Sci Instrum*. 1995;66(7):3924-3930. doi:10.1063/1.1145396
232. Chen Q, Xu S, Liu Q, Masliyah J, Xu Z. QCM-D study of nanoparticle interactions. *Adv Colloid Interface Sci*. 2016;233:94-114. doi:10.1016/j.cis.2015.10.004
233. Shpigel N, Levi MD, Aurbach D. EQCM-D technique for complex mechanical characterization of energy storage electrodes : Background and practical guide. *Energy Storage Mater*. 2019;21:399-413. doi:10.1016/j.ensm.2019.05.026
234. Alexander TE, Lozeau LD, Camesano TA. QCM-D characterization of time-dependence of bacterial adhesion. *Cell Surf*. 2019;5:100024. doi:10.1016/j.tcsw.2019.100024
235. Wang S, Li F, Easley AD, Lutkenhaus JL. Real-time insight into the doping mechanism of redox-active organic radical polymers. *Nat Mater*. 2019;18:69-76. doi:10.1038/s41563-018-0215-1
236. Johannsmann D. Viscoelastic , mechanical , and dielectric measurements on complex samples with the quartz crystal microbalance. *Phys Chem Chem Phys*. 2008;10:4516-4534. doi:10.1039/b803960g
237. Cho N, Frank CW, Kasemo B, Höök F. Quartz crystal microbalance with dissipation monitoring of supported lipid bilayers on various substrates. *Nat Protoc*. 2010;5(6):1096-1106. doi:10.1038/nprot.2010.65
238. Van Der Westen R, Sharma PK, De Raedt H, Vermue I, Van der Mei HC, Busscher HJ. Elastic and viscous bond components in the adhesion of colloidal particles and fibrillated streptococci to QCM-D crystal surfaces with different hydrophobicities using Kelvin – Voigt and Maxwell models. *Phys Chem Chem Phys*. 2017;19:25391-25400. doi:10.1039/c7cp04676f

239. Shpigel N, Levi MD, Sigalov S, Daikhin L, Aurbach D. In Situ Real-Time Mechanical and Morphological Characterization of Electrodes for Electrochemical Energy Storage and Conversion by Electrochemical Quartz Crystal Microbalance with Dissipation Monitoring. *Acc Chem Res*. 2018;51:69-79. doi:10.1021/acs.accounts.7b00477

240. Hook F, Kasemo B. Variations in Coupled Water , Viscoelastic Properties , and Film Thickness of a Mefp-1 Protein Film during Adsorption and Cross-Linking : A Quartz Crystal Microbalance with Dissipation Monitoring , Ellipsometry , and Surface Plasmon. *Anal Chem*. 2001;73(24):5796-5804.

241. Voinova M V, Rodahl M, Jonson M, Kasemo B. Viscoelastic Acoustic Response of Layered Polymer Films at Fluid-Solid Interfaces : Continuum Mechanics Approach Viscoelastic Acoustic Response of Layered Polymer Films at Fluid-Solid Interfaces : Continuum Mechanics Approach. *Phys Scr*. 1999;59:391-396.

242. Bütergerds D, Cramer C, Schönhoff M. pH-Dependent Growth Laws and Viscoelastic Parameters of Poly-l-Lysine/Hyaluronic Acid Multilayers. *Adv Mater Interfaces*. 2017;4(1). doi:10.1002/admi.201600592

243. Eisele NB, Andersson FI, Frey S, Richter RP. Viscoelasticity of thin biomolecular films: A case study on nucleoporin phenylalanine-glycine repeats grafted to a histidine-tag capturing QCM-D sensor. *Biomacromolecules*. 2012;13(8):2322-2332. doi:10.1021/bm300577s

244. Aspnes DE. Spectroscopic ellipsometry — A perspective. *J Vac Sci Technol A*. 2013;31(5):058502. doi:10.1116/1.4809747

245. Schubert M. Another century of ellipsometry. *Ann Phys*. 2006;15(7-8):480-497. doi:10.1002/andp.200510204

246. Rothen A. The Ellipsometer , an Apparatus to Measure Thicknesses of Thin Surface Films. *Rev Sci Instrum*. 1945;12(2):26-30.

247. Tompkins HG, Irene EA, eds. *Polarized Light and Ellipsometry*. William Andrew; 2005.

248. Arwin H. Adsorption of Proteins at Solid Surfaces. In: Hinrich K, Eichhorn K-J, eds. *Ellipsometry of Functional Organic Surfaces and Films*. Springer, Cham; 2014:29-46. doi:10.1007/978-3-642-40128-2

249. Garcia-Caurel E, De Martino A, Gaston J-P, Yan L. Application of Spectroscopic Ellipsometry and Mueller Ellipsometry to Optical. *Appl Spectrosc*. 2013;67(1):1-21. doi:10.1366/12-06883

250. Postava K, Maziewski A, Yamaguchi T, Ossikovski R. Null ellipsometer with phase modulation. *Opt Express*. 2004;12(24):4536-4540.

251. Luciani L, Denoyel R. Adsorption of polydisperse surfactants on solid surfaces: An

ellipsometric study. *J Colloid Interface Sci*. 1997;188(1):75-80. doi:10.1006/jcis.1996.4724

252. Arwin H, Welin-Klintstrom S, Jansson R. Off-Null Ellipsometry Revisited: Basic Considerations for Measuring Surface Concentrations at Solid/Liquid Interface. *J Colloid Interface Sci*. 1993;156:377-382.

253. Cazorla Soult M, Siller V, Zhu X, et al. Spectroscopic Ellipsometry for Operando Monitoring of (De)Lithiation-Induced Phenomena on LiMn 2 O 4 and LiNi 0.5 Mn 1.5 O 4 Electrodes . *J Electrochem Soc*. 2022;169(4):040501. doi:10.1149/1945-7111/ac5ceb

254. Werner C, Eichhorn KJ, Grundke K, Simon F, Grählert W, Jacobasch HJ. Insights on structural variations of protein adsorption layers on hydrophobic fluorohydrocarbon polymers gained by spectroscopic ellipsometry (part I). *Colloids Surfaces A Physicochem Eng Asp*. 1999;156(1-3):3-17. doi:10.1016/S0927-7757(99)00007-2

255. Berlind T, Poksinski M, Tengvall P, Arwin H. Formation and cross-linking of fibrinogen layers monitored with in situ spectroscopic ellipsometry. *Colloids Surfaces B Biointerfaces*. 2010;75(2):410-417. doi:10.1016/j.colsurfb.2009.09.013

256. Arwin H. Application of ellipsometry techniques to biological materials. *Thin Solid Films*. 2011;519(9):2589-2592. doi:10.1016/j.tsf.2010.11.082

257. Cuypers PA, Corsel JW, Janssen MP, Kop JM, Hermens WT, Hemker HC. The adsorption of prothrombin to phosphatidylserine multilayers quantitated by ellipsometry. *J Biol Chem*. 1983;258(4):2426-2431. doi:10.1016/s0021-9258(18)32943-0

258. Stenberg M, Nygren H. Use of the Isoscope Ellipsometer in the Study of Adsorbed Proteins and Biospecific Binding Reactions. *J Phys (Paris), Colloq*. 1983;44(12):83-86. doi:10.1051/jphyscol:19831017

259. Eisele NB, Frey S, Piehler J, Görlich D, Richter RP. Ultrathin nucleoporin phenylalanine-glycine repeat films and their interaction with nuclear transport receptors. *EMBO Rep*. 2010;11(5):366-372. doi:10.1038/embor.2010.34

260. Berlind T, Pribil GK, Thompson D, Woollam JA, Arwin H. Effects of ion concentration on refractive indices of fluids measured by the minimum deviation technique. *Phys Status Solidi Curr Top Solid State Phys*. 2008;5(5):1249-1252. doi:10.1002/pssc.200777897

261. Richter RP, Hock KK, Burkhartsmeyer J, et al. Membrane-grafted hyaluronan films: A well-defined model system of glycoconjugate cell coats. *J Am Chem Soc*. 2007;129(17):5306-5307. doi:10.1021/ja068768s

262. Baranova NS, Nilebäck E, Haller FM, et al. The inflammation-associated protein TSG-6 cross-links hyaluronan via hyaluronan-induced TSG-6 oligomers. *J Biol Chem*. 2011;286(29):25675-25686. doi:10.1074/jbc.M111.247395

263. Dubacheva G V., Araya-Callis C, Geert Volbeda A, et al. Controlling Multivalent Binding through Surface Chemistry: Model Study on Streptavidin. *J Am Chem Soc*. 2017;139(11):4157-4167. doi:10.1021/jacs.7b00540

264. Thakar D, Migliorini E, Coche-guerente L, et al. A quartz crystal microbalance method to study the terminal functionalization of glycosaminoglycans †. *Chem Commun*. 2014;50:15148-15151. doi:10.1039/C4CC06905F

265. Goff RD, Thorson JS. Neoglycosylation and neoglycorandomization: Enabling tools for the discovery of novel glycosylated bioactive probes and early stage leads. *Medchemcomm*. 2014;5(8):1036-1047. doi:10.1039/c4md00117f

266. Godula K, Bertozzi CR. Synthesis of glycopolymers for microarray applications via ligation of reducing sugars to a poly(acryloyl hydrazide) scaffold. *J Am Chem Soc*. 2010;132(29):9963-9965. doi:10.1021/ja103009d

267. Saesen E, Sarrazin S, Laguri C, et al. Insights into the mechanism by which interferon-γ basic amino acid clusters mediate protein binding to heparan sulfate. *J Am Chem Soc*. 2013;135(25):9384-9390. doi:10.1021/ja4000867

268. Thygesen MB, Munch H, Sauer J, et al. Nucleophilic catalysis of carbohydrate oxime formation by anilines. *J Org Chem*. 2010;75(5):1752-1755. doi:10.1021/jo902425v

269. Migliorini E, Thakar D, Sadir R, et al. Biomaterials Well-de fi ned biomimetic surfaces to characterize glycosaminoglycan- mediated interactions on the molecular , supramolecular and cellular levels. *Biomaterials*. 2014;35(32):8903-8915. doi:10.1016/j.biomaterials.2014.07.017

270. Srimasorn S, Souter L, Green DE, et al. A quartz crystal microbalance method to quantify the size of hyaluronan and other glycosaminoglycans on surfaces. *Sci Rep*. 2022;12(1). doi:10.1038/s41598-022-14948-7

271. Richter RP, Bérat R, Brisson AR. Formation of solid-supported lipid bilayers: An integrated view. *Langmuir*. 2006;22(8):3497-3505. doi:10.1021/la052687c

272. Tsortos A, Papadakis G, Gizeli E. Shear acoustic wave biosensor for detecting DNA intrinsic viscosity and conformation: A study with QCM-D. *Biosens Bioelectron*. 2008;24(4):836-841. doi:10.1016/j.bios.2008.07.006

273. Srimasorn S, Souter L, Green DE, et al. A quartz crystal microbalance method to quantify the size of hyaluronan and other glycosaminoglycans on surfaces. *Sci Rep*. 2022;12(1):1-19. doi:10.1038/s41598-022-14948-7

274. Martinez-Veracoechea FJ, Frenkel D. Designing super selectivity in multivalent nano-particle binding. *PNAS*. 2011;108(27):10963-10968. doi:10.1073/pnas.1105351108

275. Curk T, Dubacheva G V, Brisson AR, Richter RP. Controlling Superselectivity of Multivalent Interactions with Cofactors and Competitors. *J Am Chem Soc*. 2022;144(38):17346-17350.
276. Su EJ, Jeeawoody S, Herr AE. Protein diffusion from microwells with contrasting hydrogel domains. *APL Bioeng*. 2020;3(2). doi:10.1063/1.5078650
277. Zahn R, Osmanović D, Ehret S, et al. A physical model describing the interaction of nuclear transport receptors with FG nucleoporin domain assemblies. *Elife*. 2016;5:1-21. doi:10.7554/eLife.14119
278. Wagner RS, Kapinos LE, Marshall NJ, Stewart M, Lim RYH. Promiscuous binding of karyopherinβ1 modulates FG nucleoporin barrier function and expedites NTF2 transport kinetics. *Biophys J*. 2015;108(4):918-927. doi:10.1016/j.bpj.2014.12.041
279. Chen H, Qin J, Hu Y. Efficient degradation of high-molecular-weight hyaluronic acid by a combination of ultrasound, hydrogen peroxide, and copper ion. *Molecules*. 2019;24(3). doi:10.3390/molecules24030617
280. Gottlieb HE, Kotlyar V, Nudelman A. NMR Chemical Shifts of Common Laboratory Solvents as Trace Impurities. *J Org Chem*. 1997;62:7512-7515. doi:10.1109/TPS.2011.2168830
281. Srimasorn S, Souter L, Green DE, et al. A quartz crystal microbalance method to quantify the size of hyaluronan and other glycosaminoglycans on surfaces. *Sci Rep*. 2022;12(1). doi:10.1038/s41598-022-14948-7
282. Carton I, Brisson AR, Richter RP. Label-Free Detection of Clustering of Membrane-Bound Proteins. *Anal Chem*. 2010;82(22):9275-9281.

CHAPTER 9: APENDIX

9.1 SEC-MALS results

9.1.1 HA-*g*-Tz 5% (2.5)

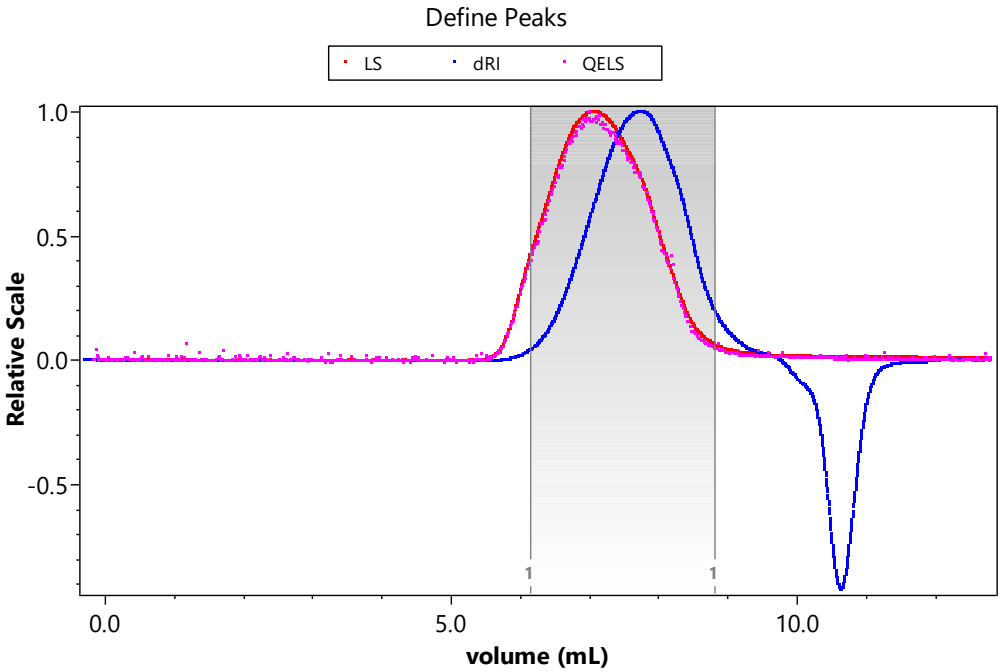

Figure 9.1: Chromatogram of the Size Exclusion Column following by the Multi-Angle Light Scattering detector data. Red and pink dots represent the data regarding the light scattering measurement and the quasi-elastic light scattering respectively while blue dots represent the refractive index of the sample. The blue region represents the surface of the peak.

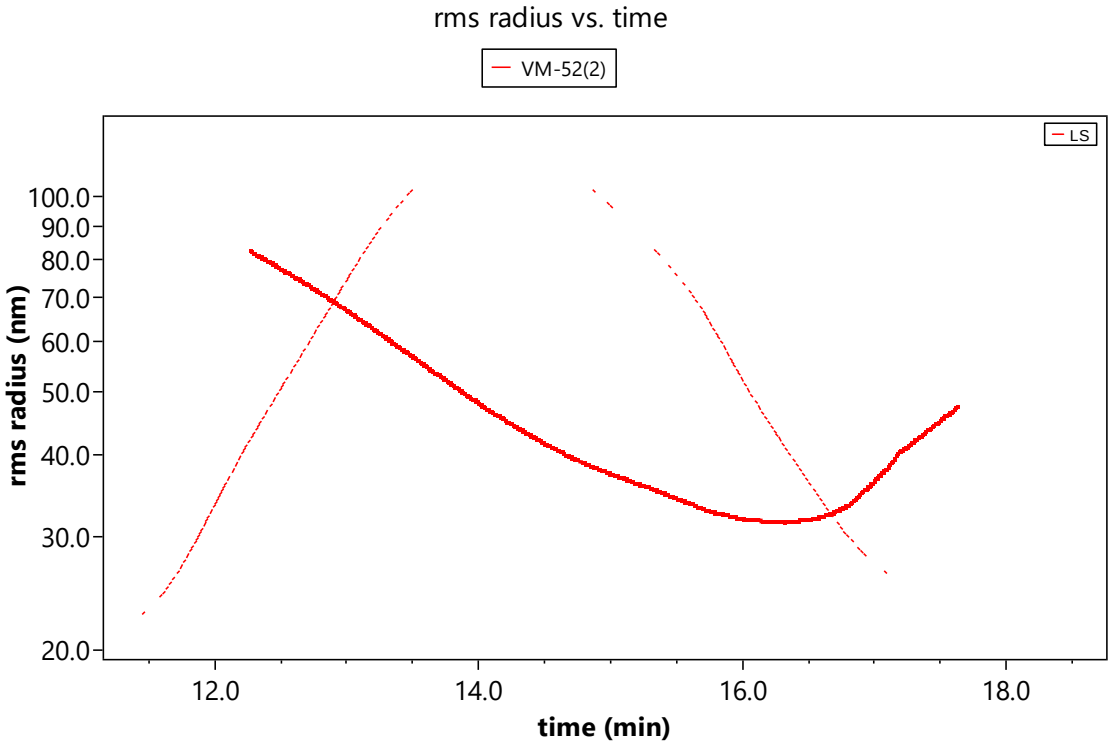

Figure 9.2: Representation of the radius of gyration (rms radius in nm) versus the time according the peak selected in the SEC chromatogram.

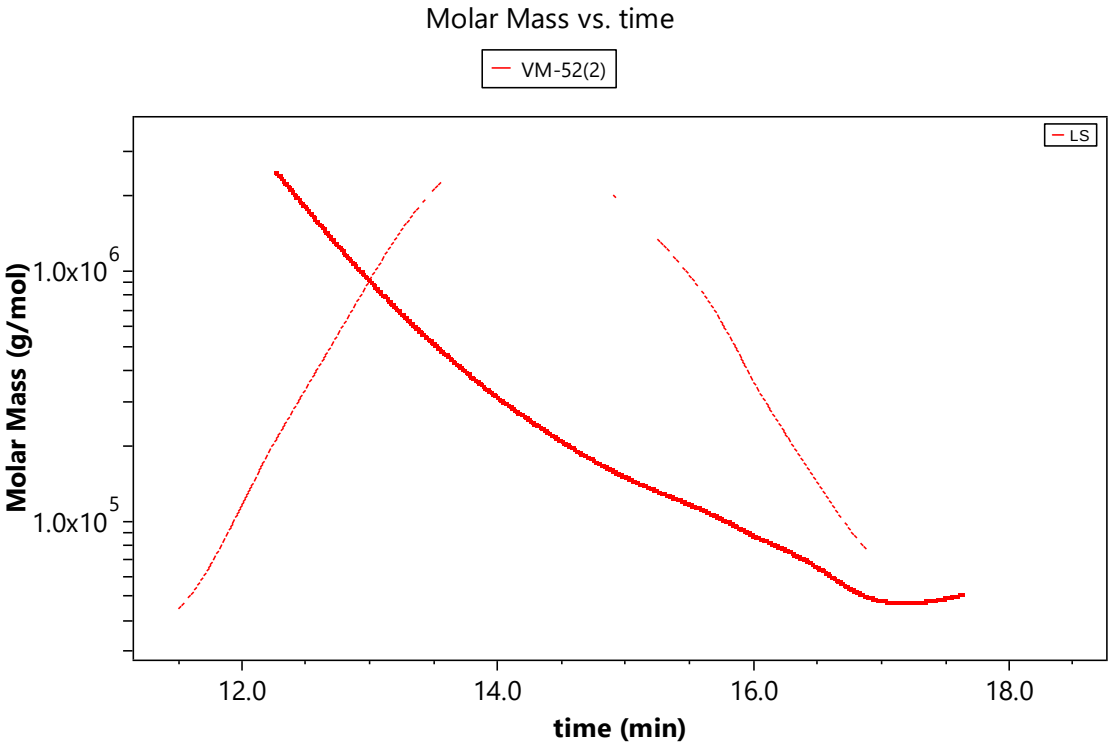

Figure 9.3: Representation of the molar mass (in g/mol) versus the time according the peak selected in the SEC chromatogram.

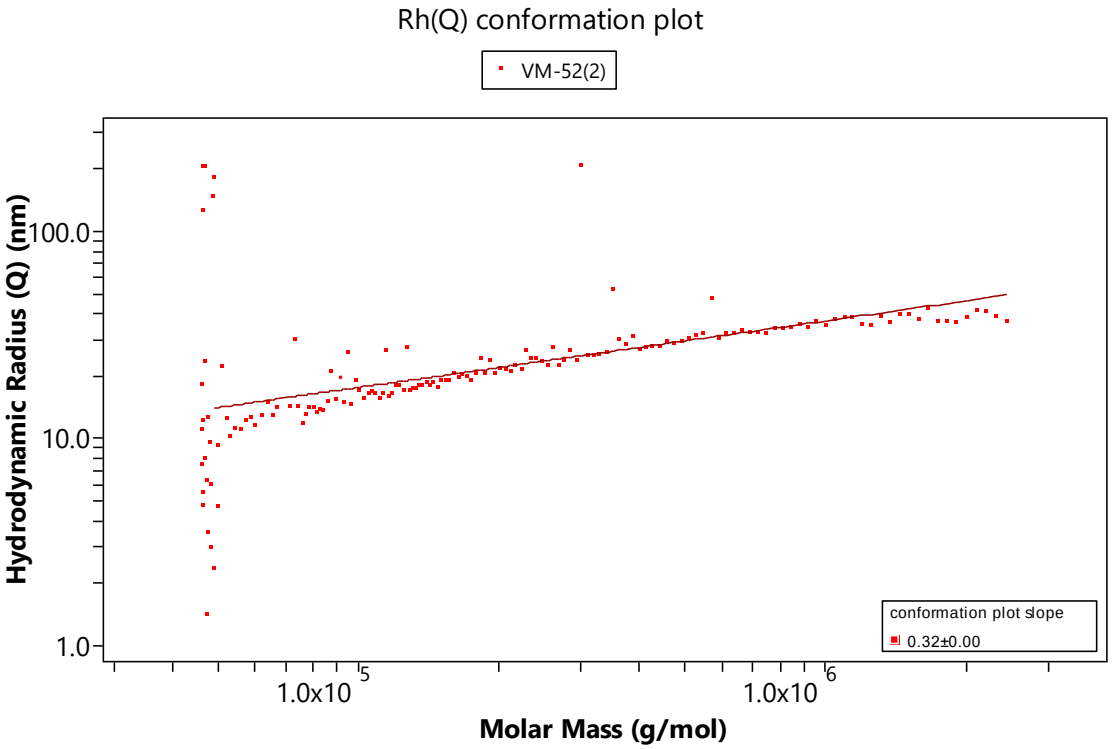

Figure 9.4: Plot of the hydrodynamic radius (Q in nm) versus the molar mass (in g/mol) of the peak selected in the SEC chromatogram.

9.1.2 HA-*g*-Propargyl(4.3)

9.1.2.1 Test 1 (20%)

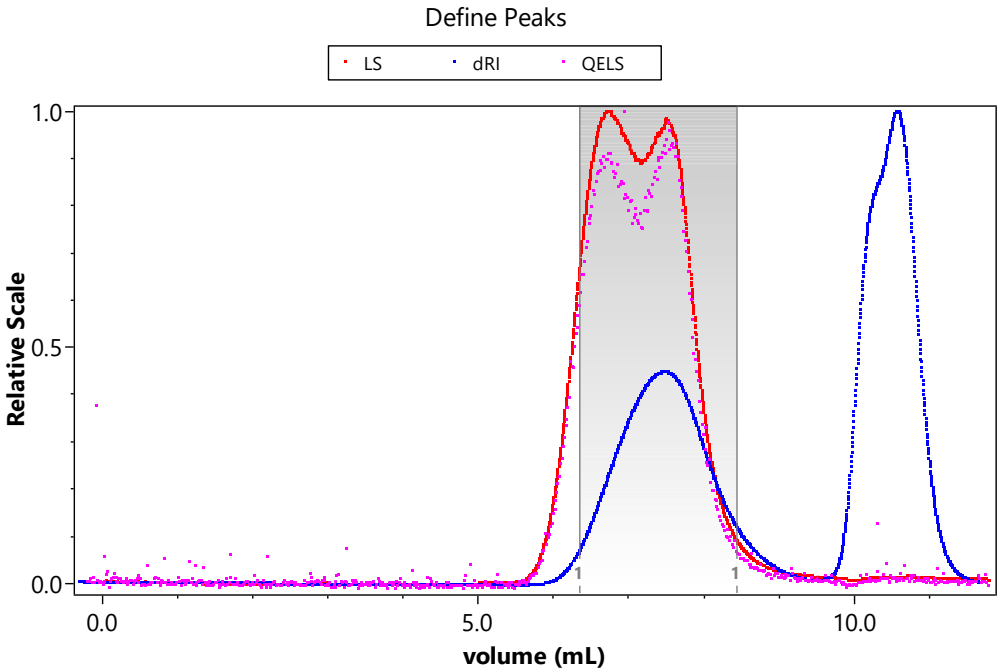

Figure 9.5: Chromatogram of the Size Exclusion Column following by the Multi-Angle Light Scattering detector data. Red and pink dots represent the data regarding the light scattering measurement and the quasi-elastic light scattering respectively while blue dots represent the refractive index of the sample. The blue region represents the surface of the peak.

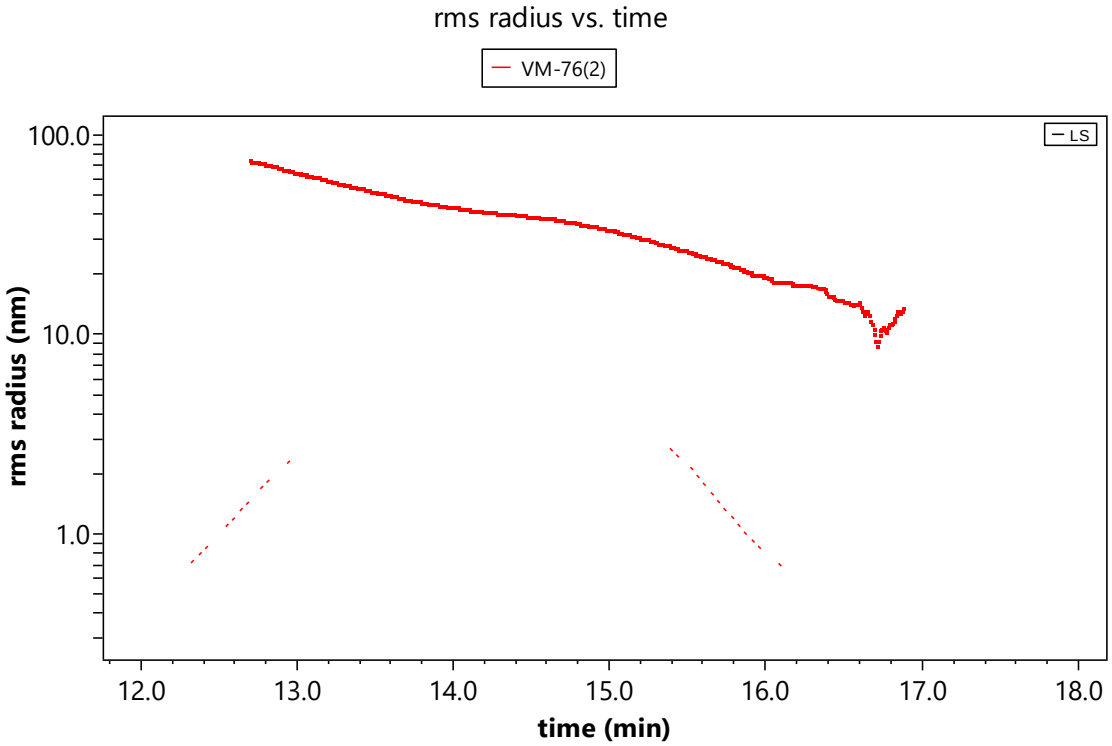

Figure 9.6: Representation of the radius of gyration (rms radius in nm) versus the time according the peak selected in the SEC chromatogram.

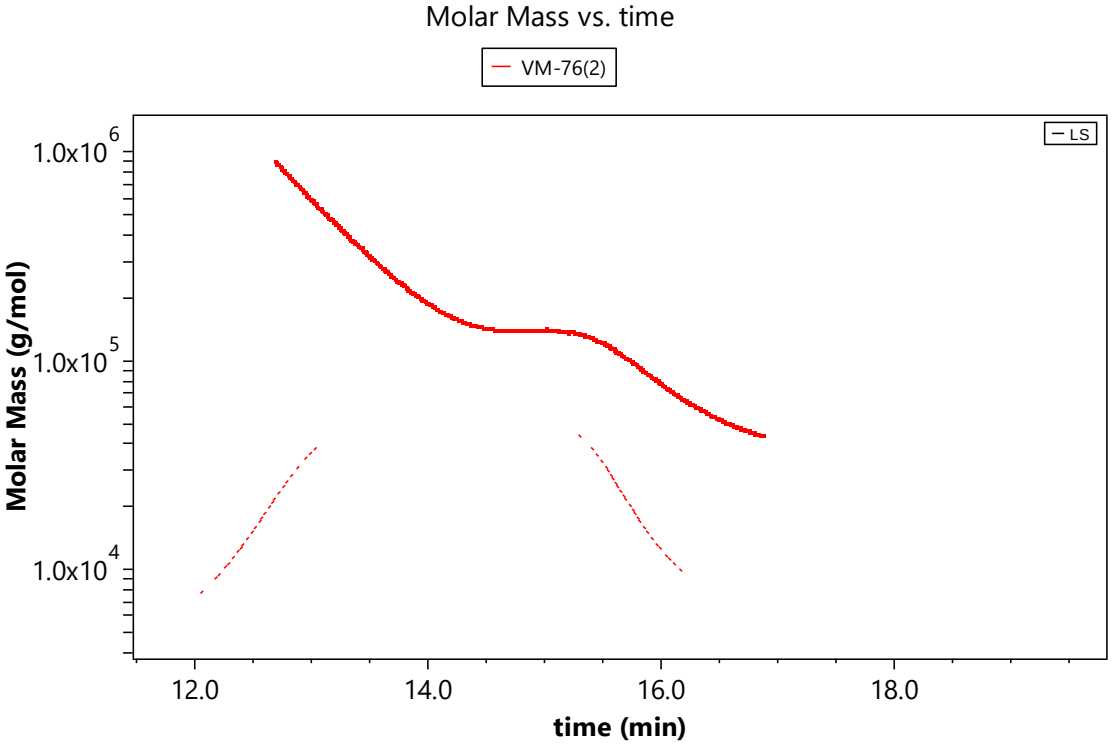

Figure 9.7: Representation of the molar mass (in g/mol) versus the time according the peak selected in the SEC chromatogram.

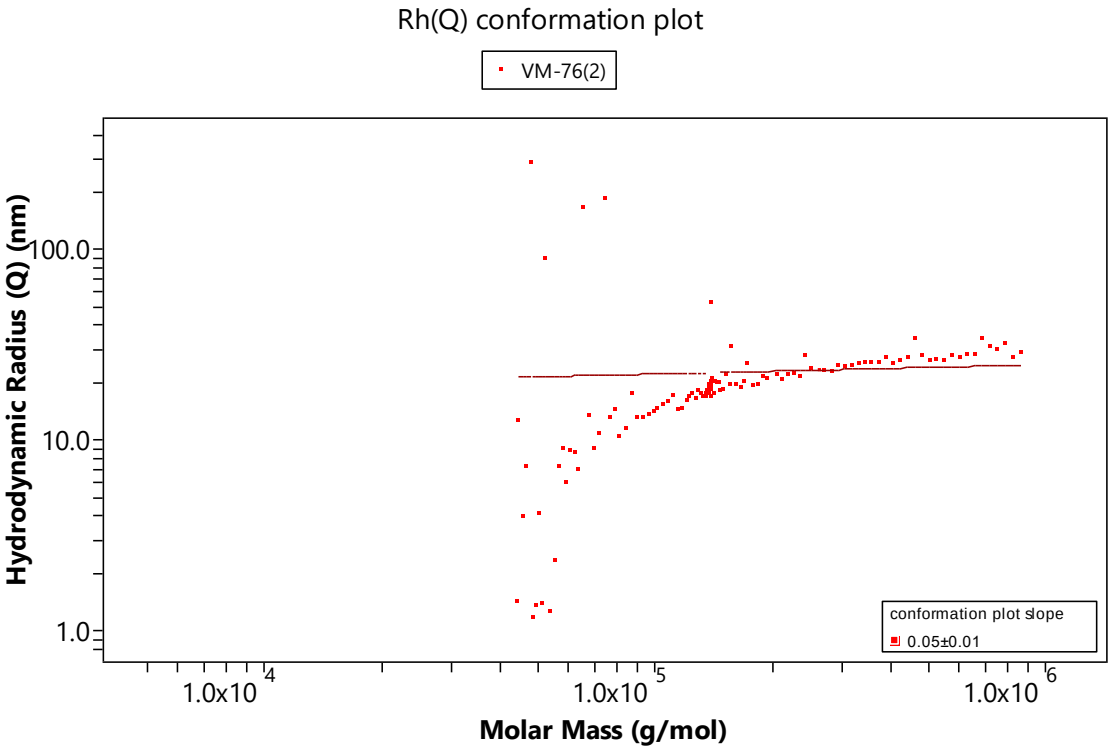

Figure 9.8: Plot of the hydrodynamic radius (Q in nm) versus the molar mass (in g/mol) of the peak selected in the SEC chromatogram.

9.2.1.2 Test 2 (20%)

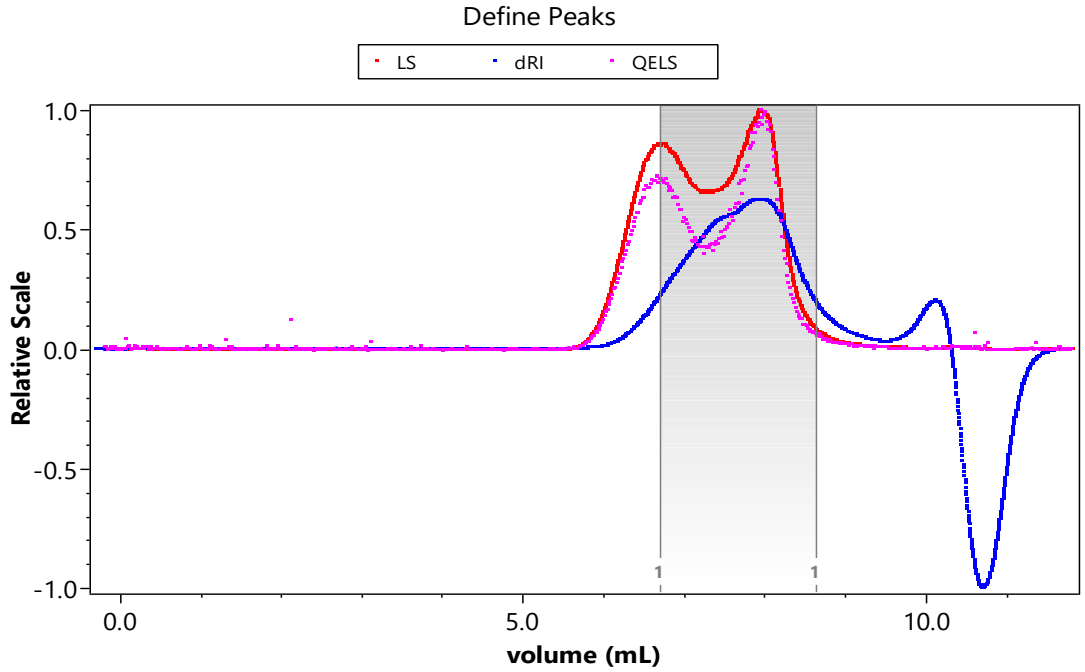

Figure 9.9: Chromatogram of the Size Exclusion Column following by the Multi-Angle Light Scattering detector data. Red and pink dots represent the data regarding the light scattering measurement and the quasi-elastic light scattering respectively while blue dots represent the refractive index of the sample. The blue region represents the surface of the peak.

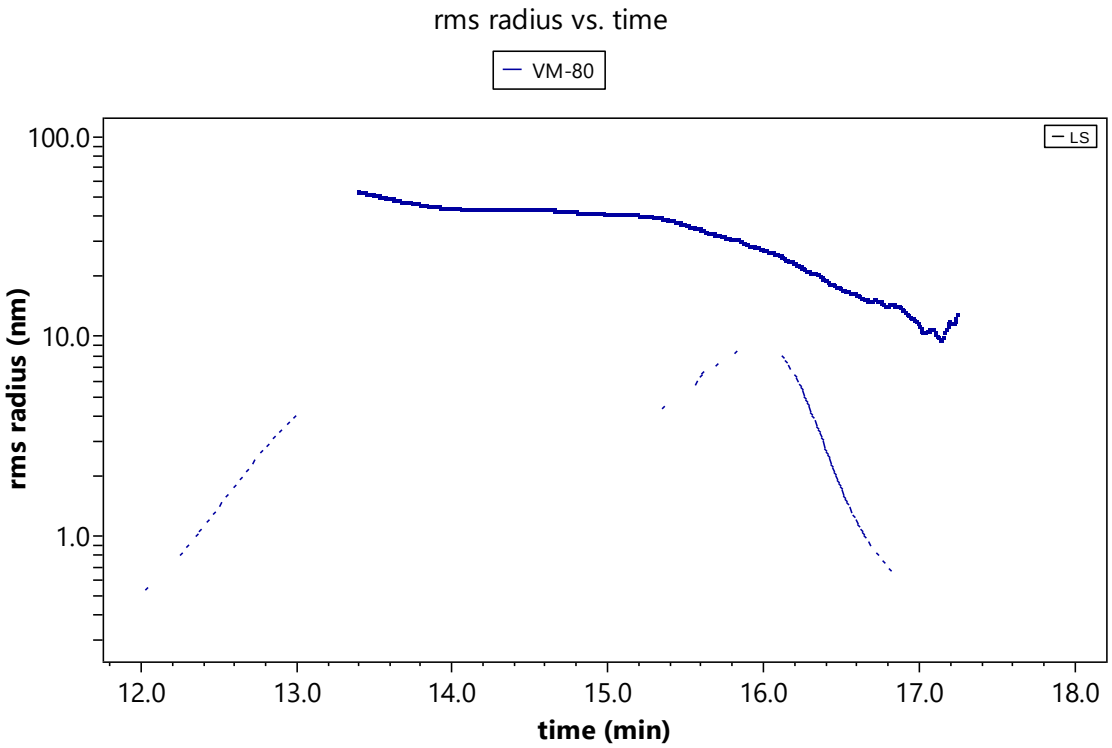

Figure 9.10: Representation of the radius of gyration (rms radius in nm) versus the time according the peak selected in the SEC chromatogram.

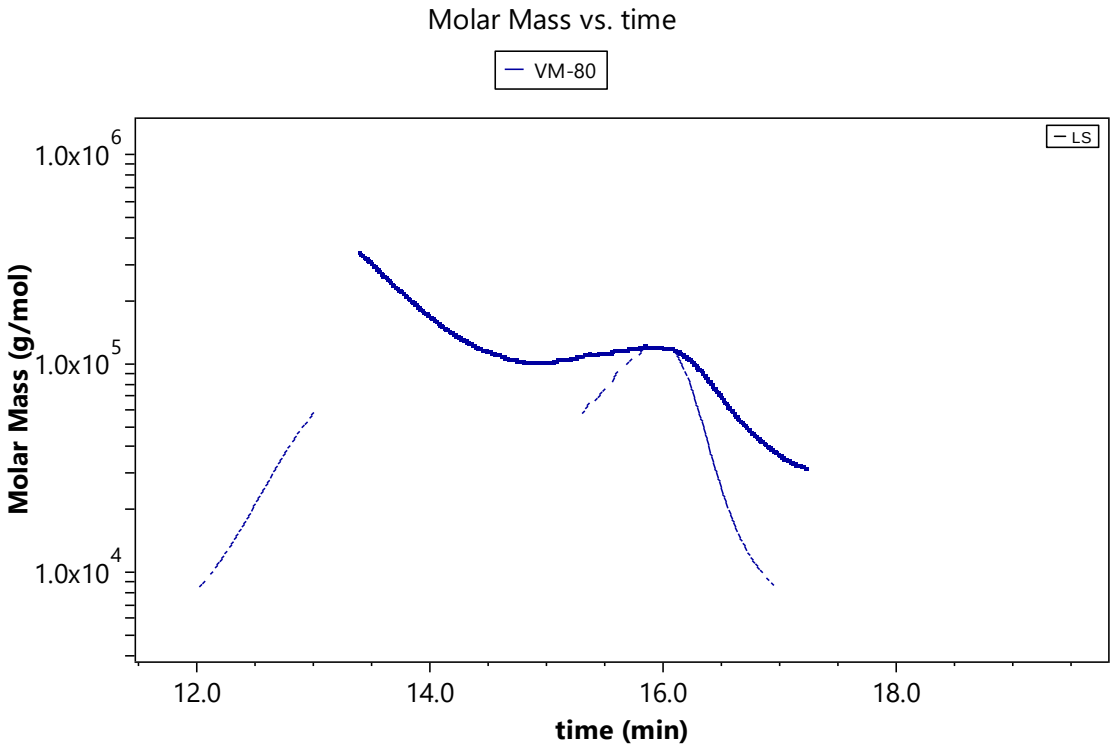

Figure 9.11: Representation of the molar mass (in g/mol) versus the time according the peak selected in the SEC chromatogram.

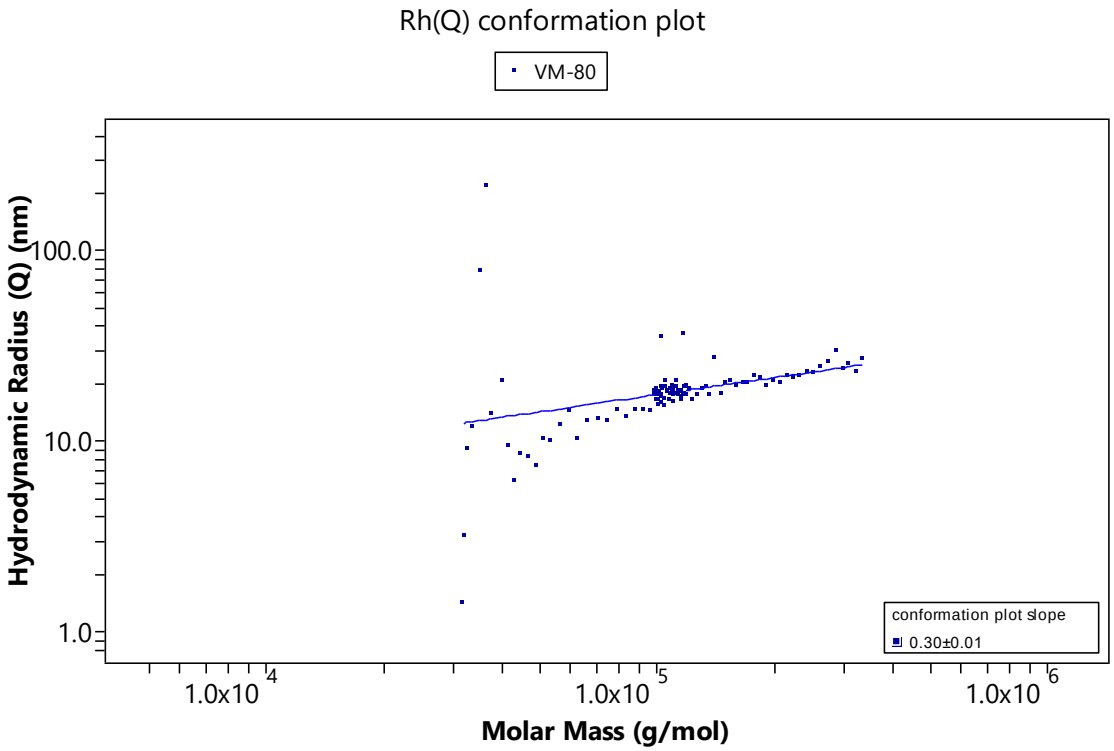

Figure 9.12: Plot of the hydrodynamic radius (Q in nm) versus the molar mass (in g/mol) of the peak selected in the SEC chromatogram.

9.1.2.3 Test 3 (50%)

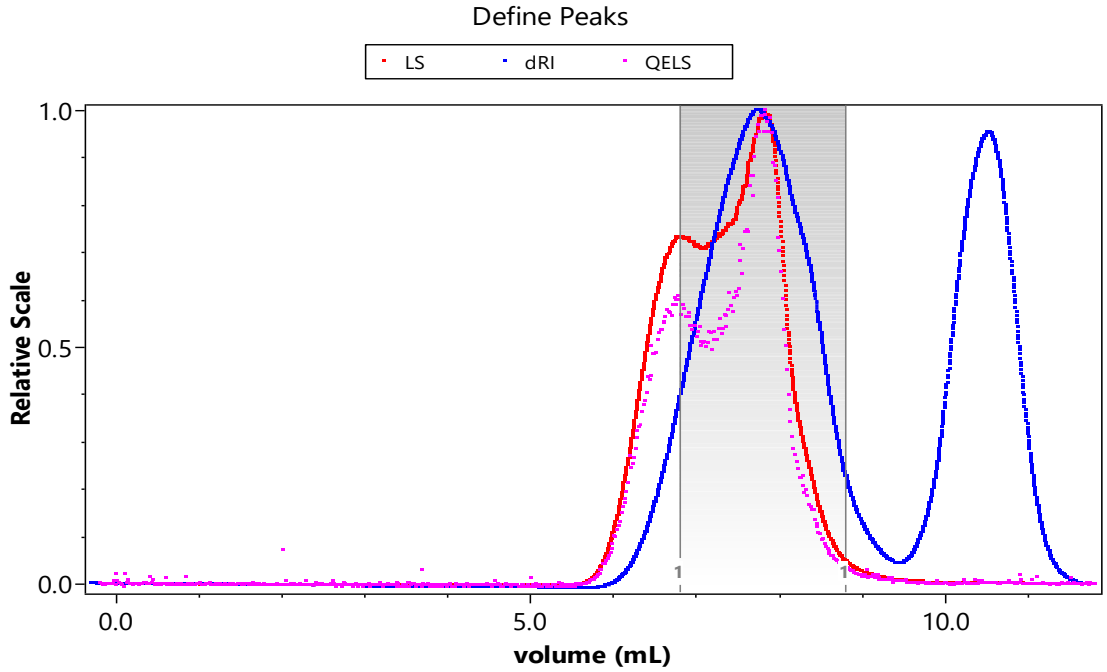

Figure 9.13: Chromatogram of the Size Exclusion Column following by the Multi-Angle Light Scattering detector data. Red and pink dots represent the data regarding the light scattering measurement and the quasi-elastic light scattering respectively while blue dots represent the refractive index of the sample. The blue region represents the surface of the peak.

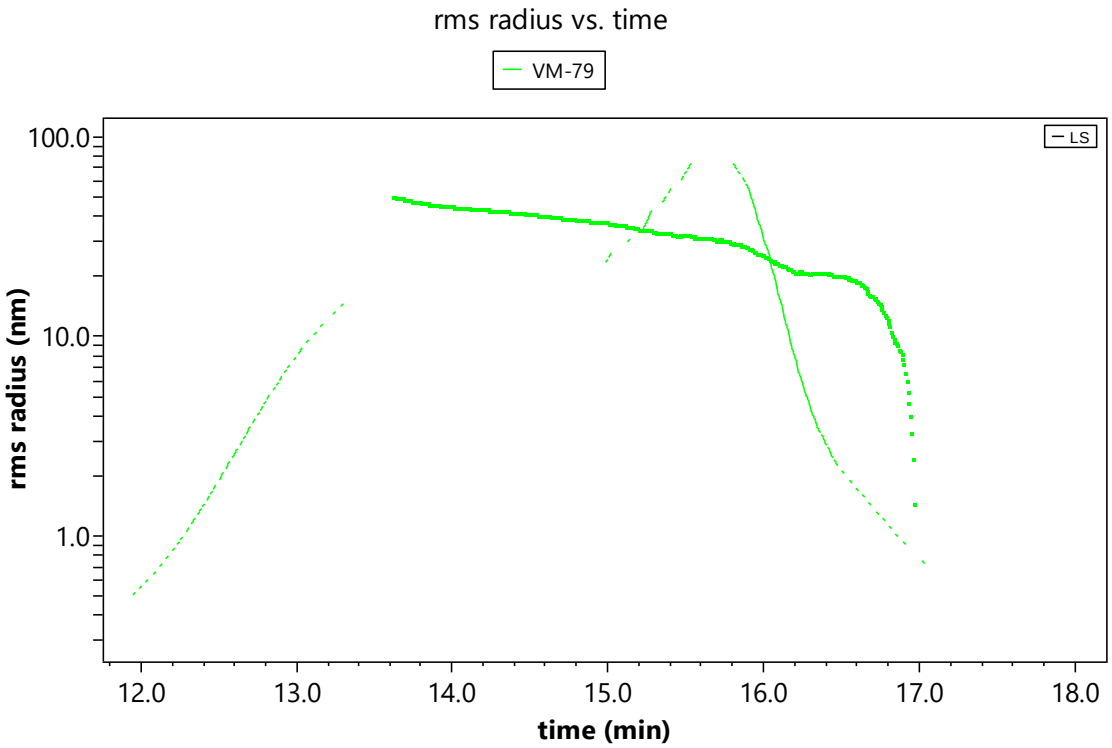

Figure 9.14: Representation of the radius of gyration (rms radius in nm) versus the time according the peak selected in the SEC chromatogram.

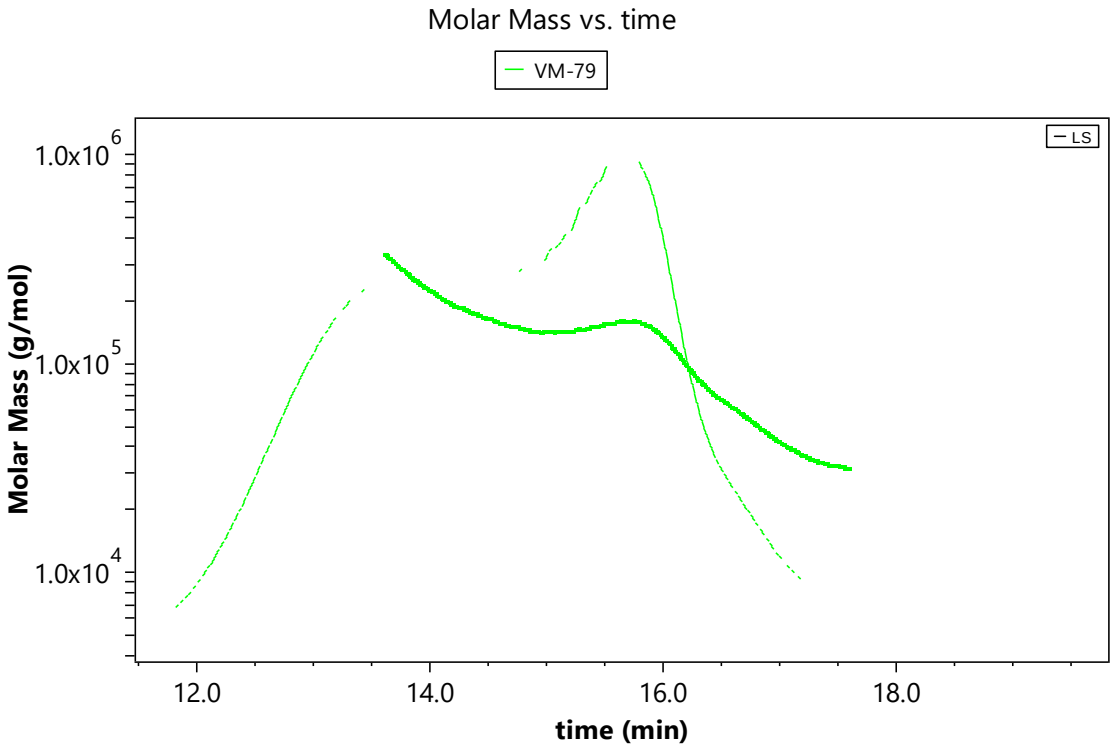

Figure 9.15: Representation of the molar mass (in g/mol) versus the time according the peak selected in the SEC chromatogram.

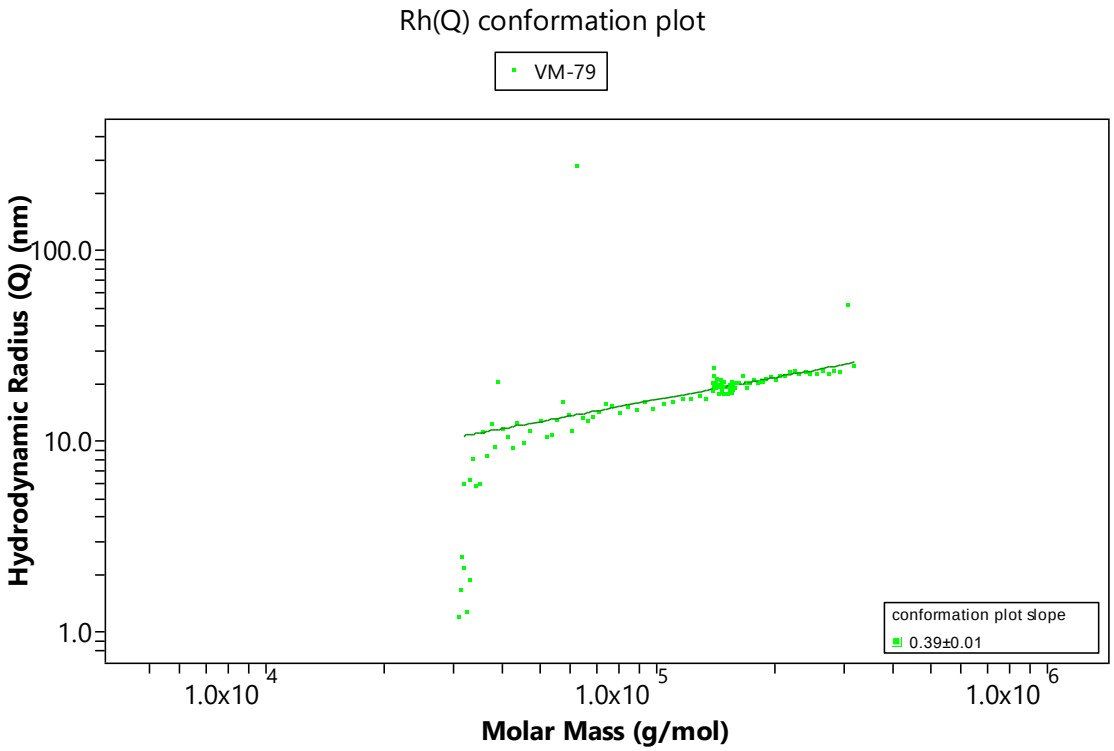

Figure 9.16: Plot of the hydrodynamic radius (Q in nm) versus the molar mass (in g/mol) of the peak selected in the SEC chromatogram.

9.1.2.4 Test 4 (45%)

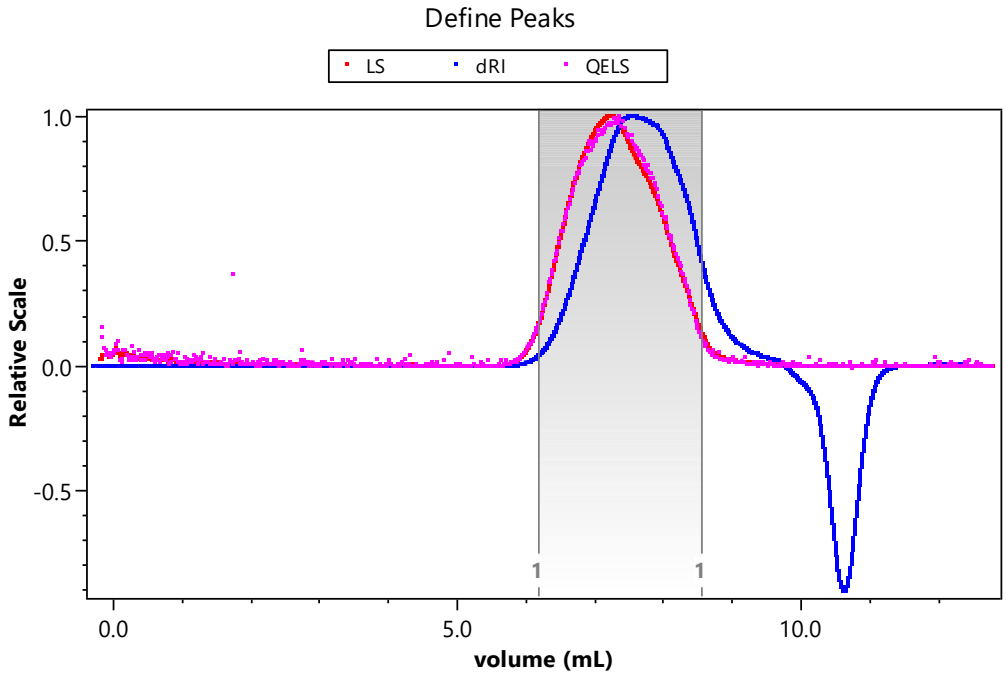

Figure 9.17: Chromatogram of the Size Exclusion Column following by the Multi-Angle Light Scattering detector data. Red and pink dots represent the data regarding the light scattering measurement and the quasi-elastic light scattering respectively while blue dots represent the refractive index of the sample. The blue region represents the surface of the peak.

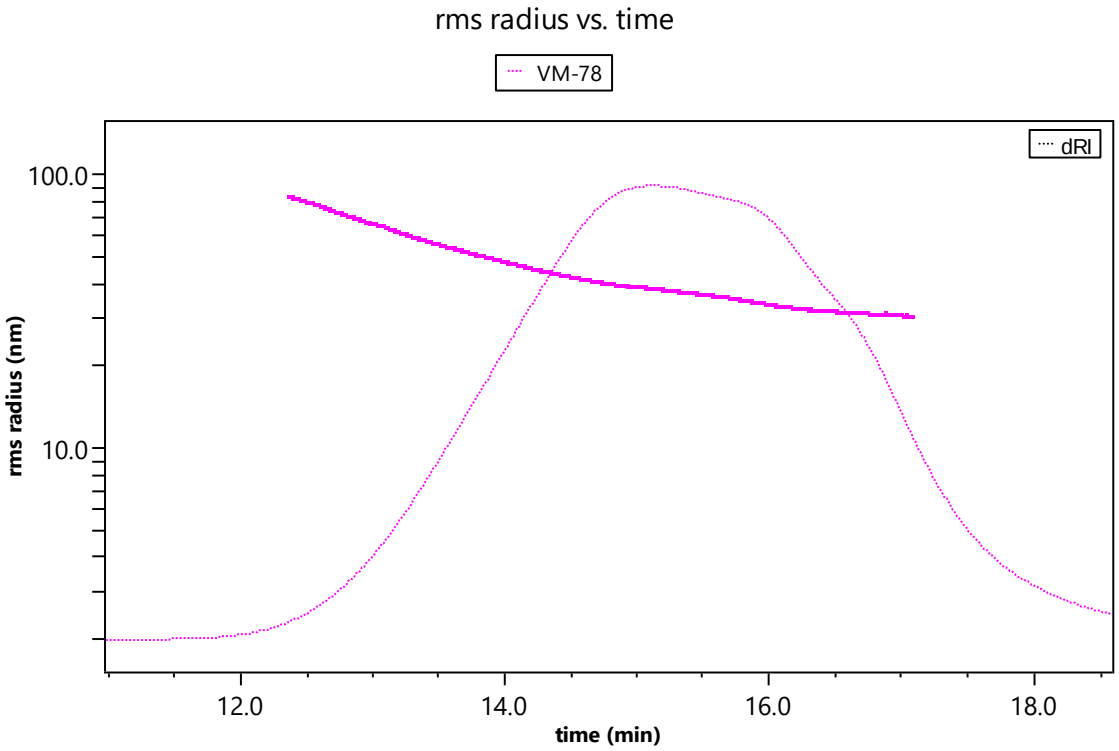

Figure 9.18: Representation of the radius of gyration (rms radius in nm) versus the time according the peak selected in the SEC chromatogram.

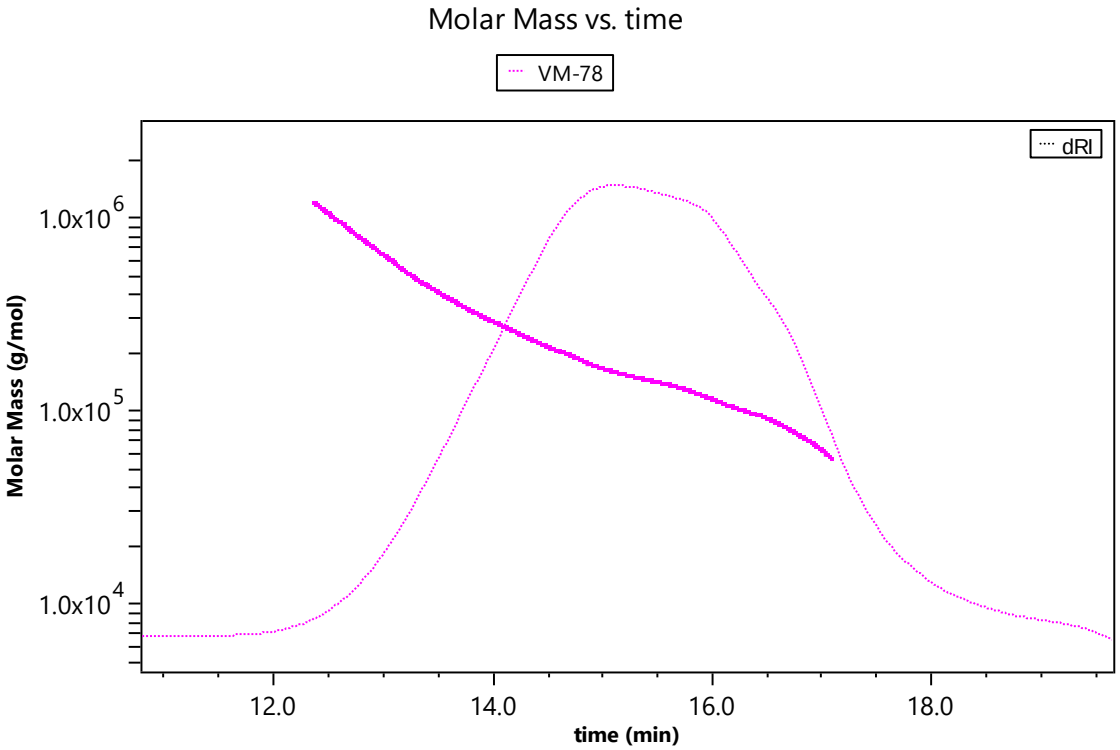

Figure 9.19: Representation of the molar mass (in g/mol) versus the time according the peak selected in the SEC chromatogram.

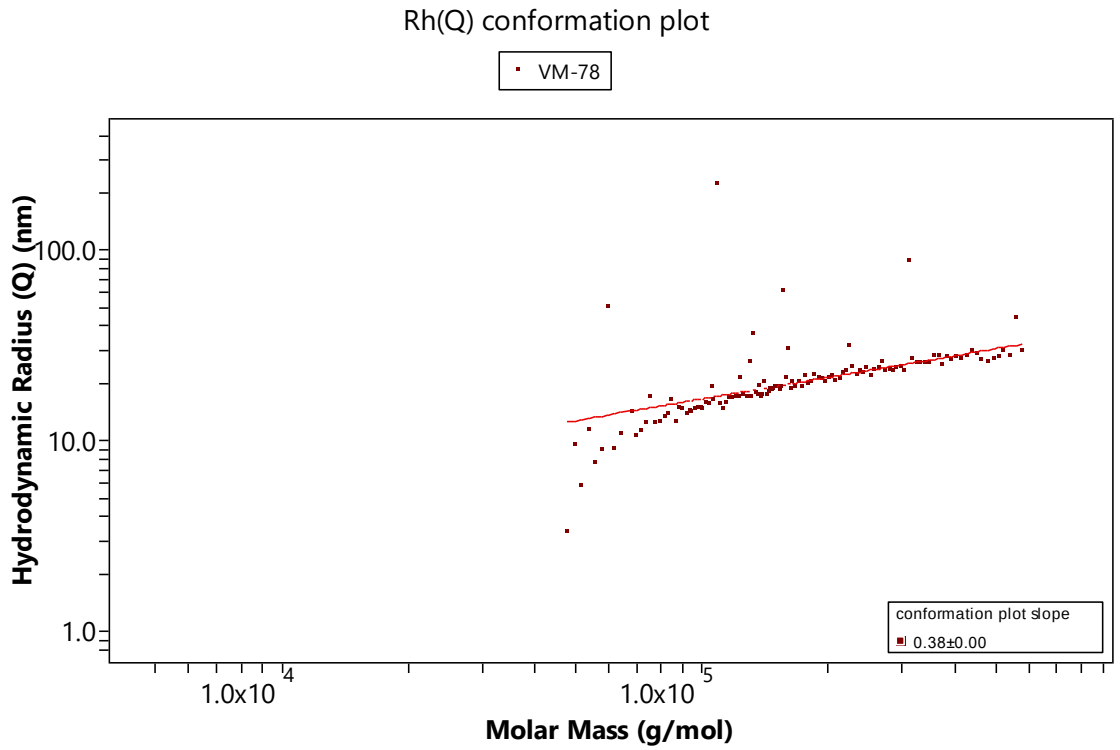

Figure 9.20: Plot of the hydrodynamic radius (Q in nm) versus the molar mass (in g/mol) of the peak selected in the SEC chromatogram.

9.1.3 HA-*g*-Lac (4.4)

9.1.3.1 Without THPTA

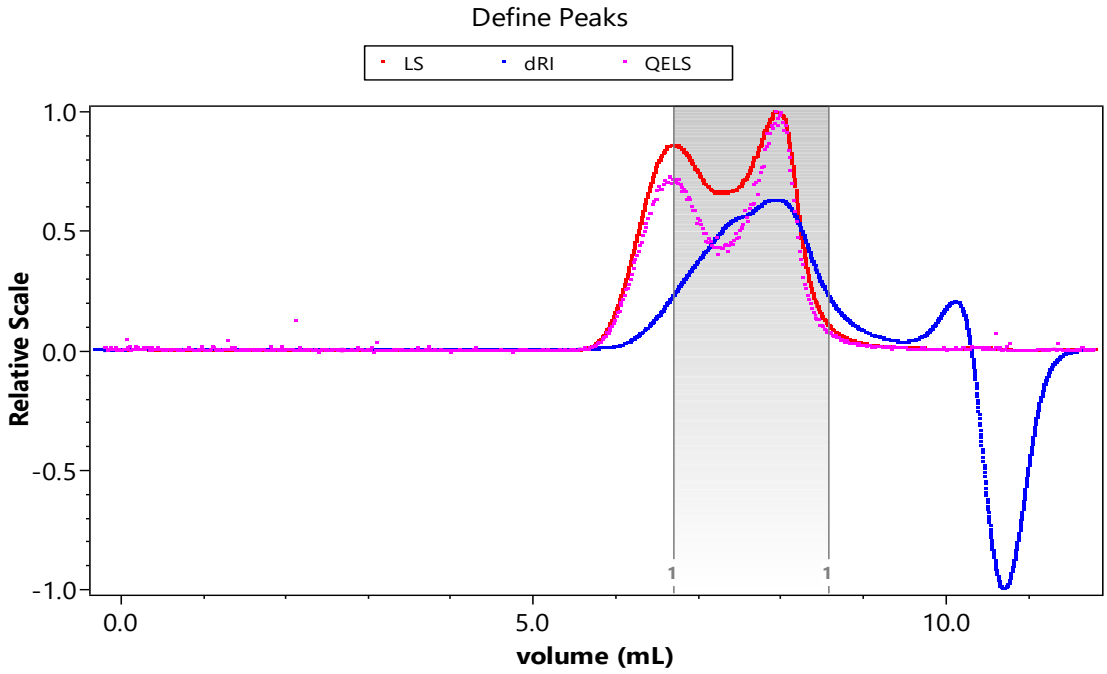

Figure 9.21: Chromatogram of the Size Exclusion Column following by the Multi-Angle Light Scattering detector data. Red and pink dots represent the data regarding the light scattering measurement and the quasi-elastic light scattering respectively while blue dots represent the refractive index of the sample. The blue region represents the surface of the peak.

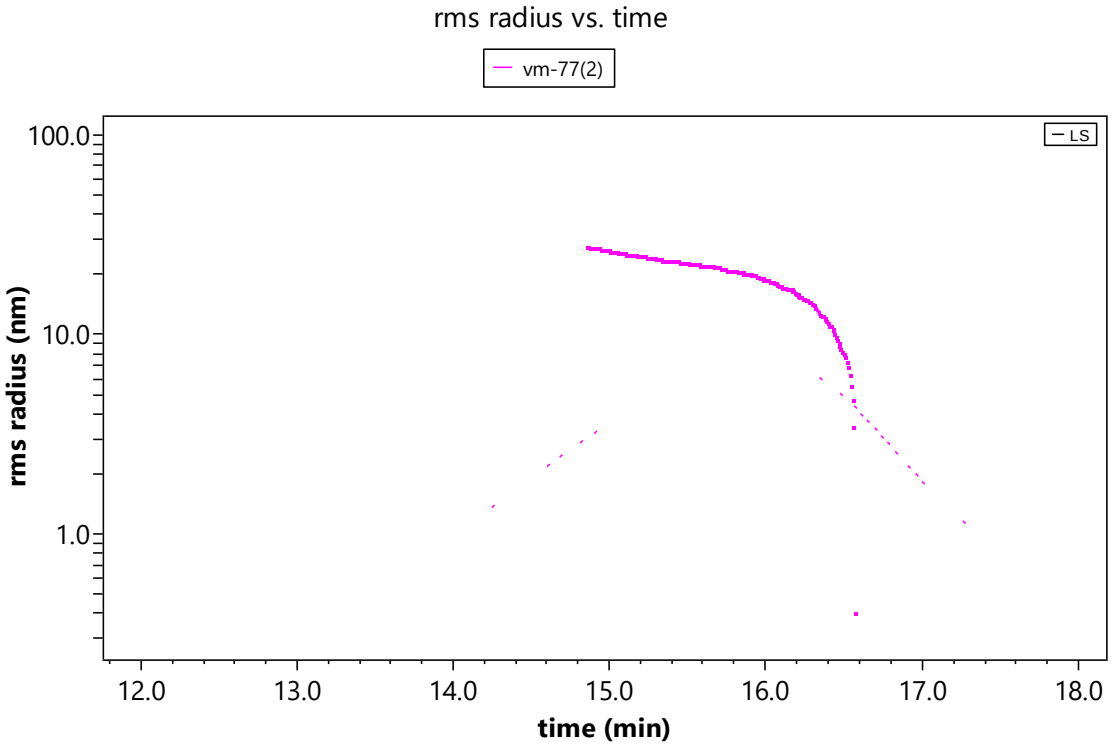

Figure 9.22: Representation of the radius of gyration (rms radius in nm) versus the time according the peak selected in the SEC chromatogram.

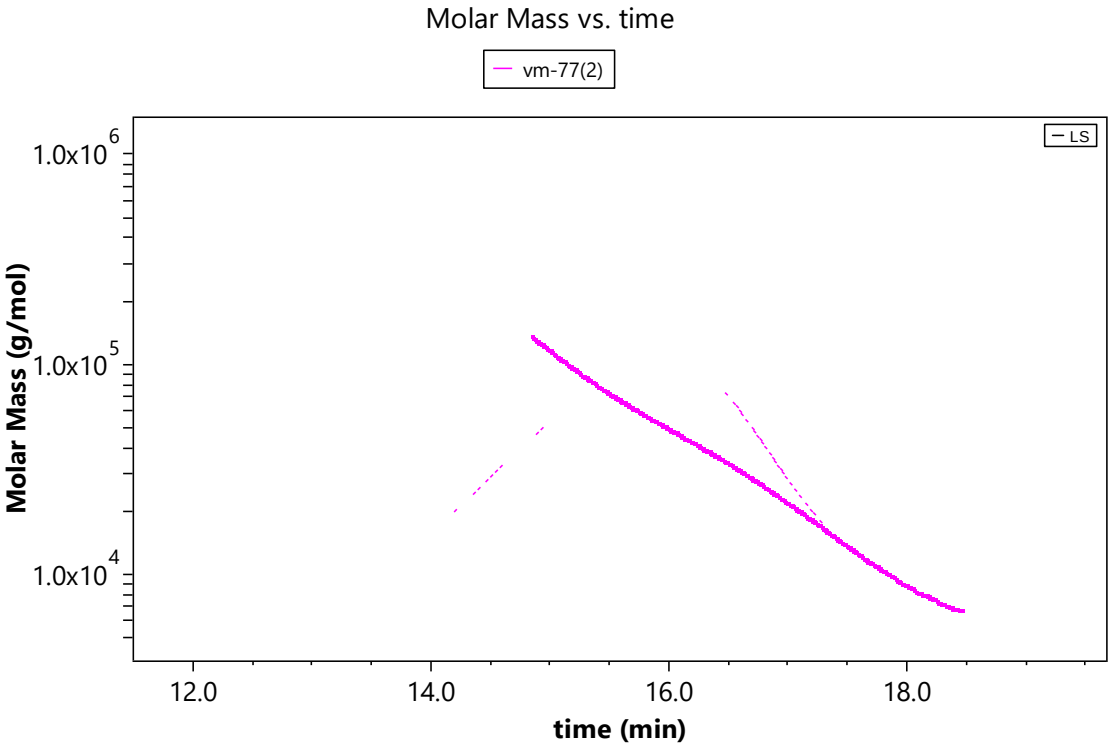

Figure 9.23: Representation of the molar mass (in g/mol) versus the time according the peak selected in the SEC chromatogram.

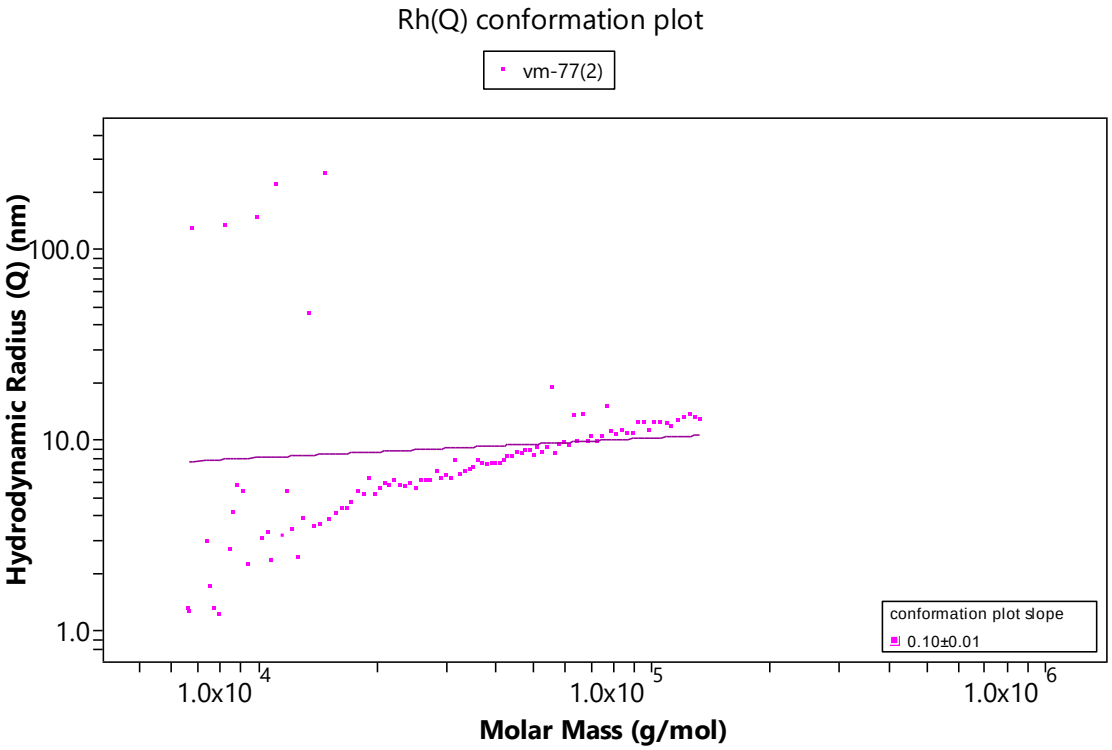

Figure 9.24: Plot of the hydrodynamic radius (Q in nm) versus the molar mass (in g/mol) of the peak selected in the SEC chromatogram.

9.1.3.2 With THPTA

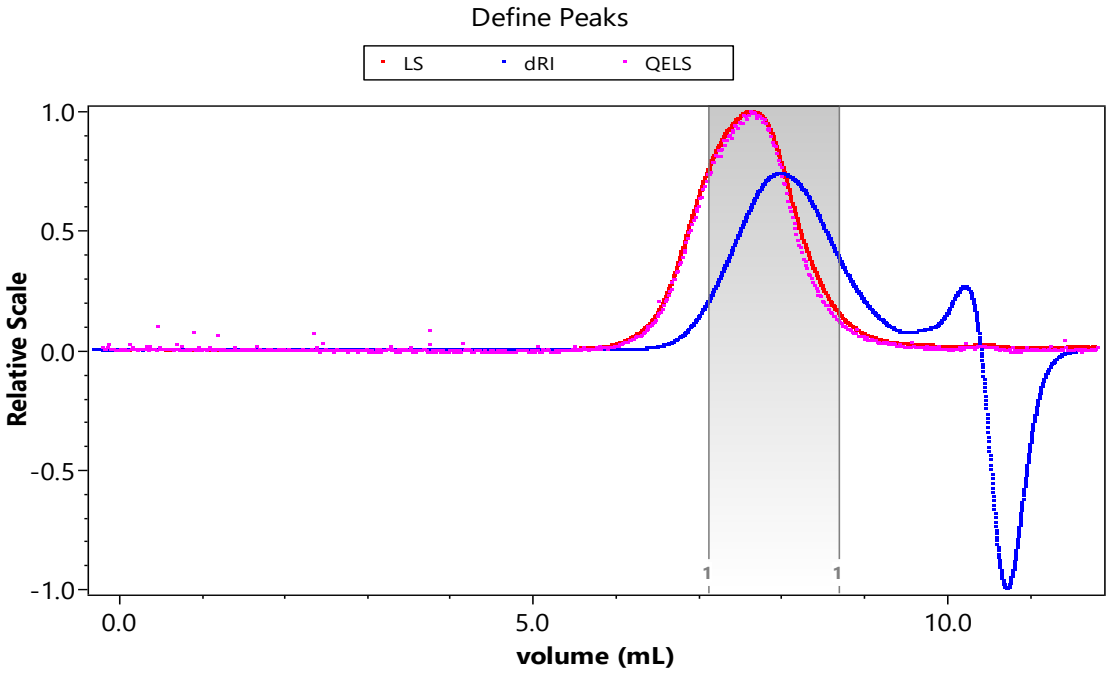

Figure 9.25: Chromatogram of the Size Exclusion Column following by the Multi-Angle Light Scattering detector data. Red and pink dots represent the data regarding the light scattering measurement and the quasi-elastic light scattering respectively while blue dots represent the refractive index of the sample. The blue region represents the surface of the peak.

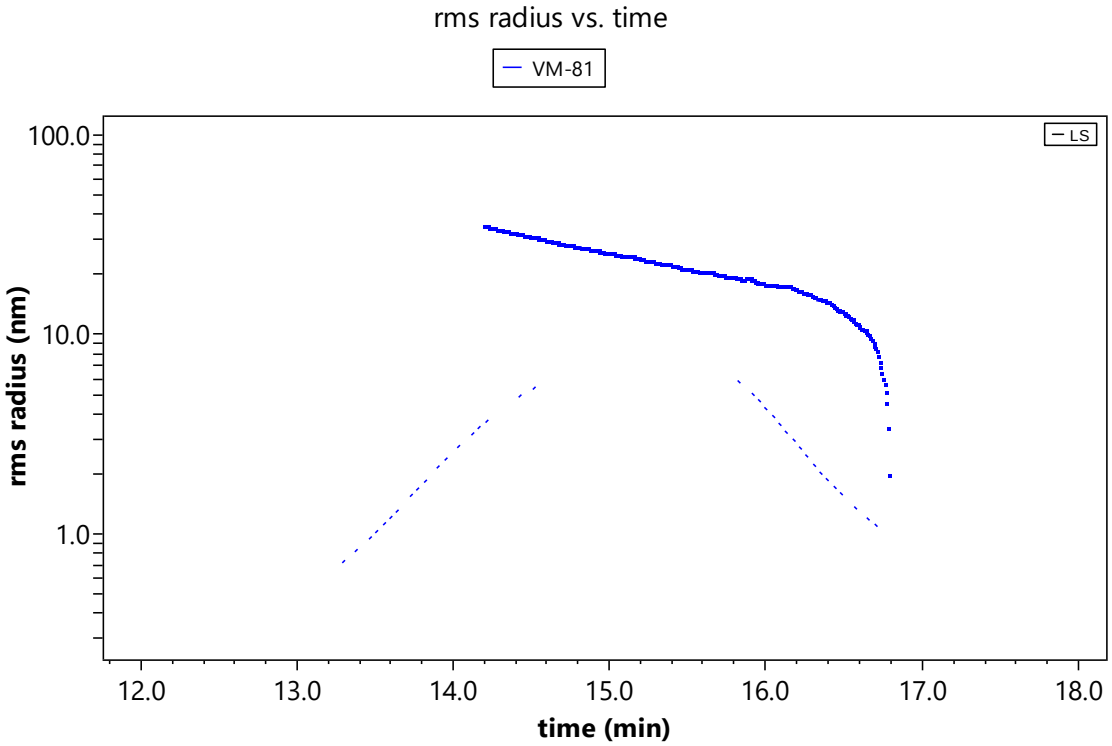

Figure 9.26: Representation of the radius of gyration (rms radius in nm) versus the time according the peak selected in the SEC chromatogram.

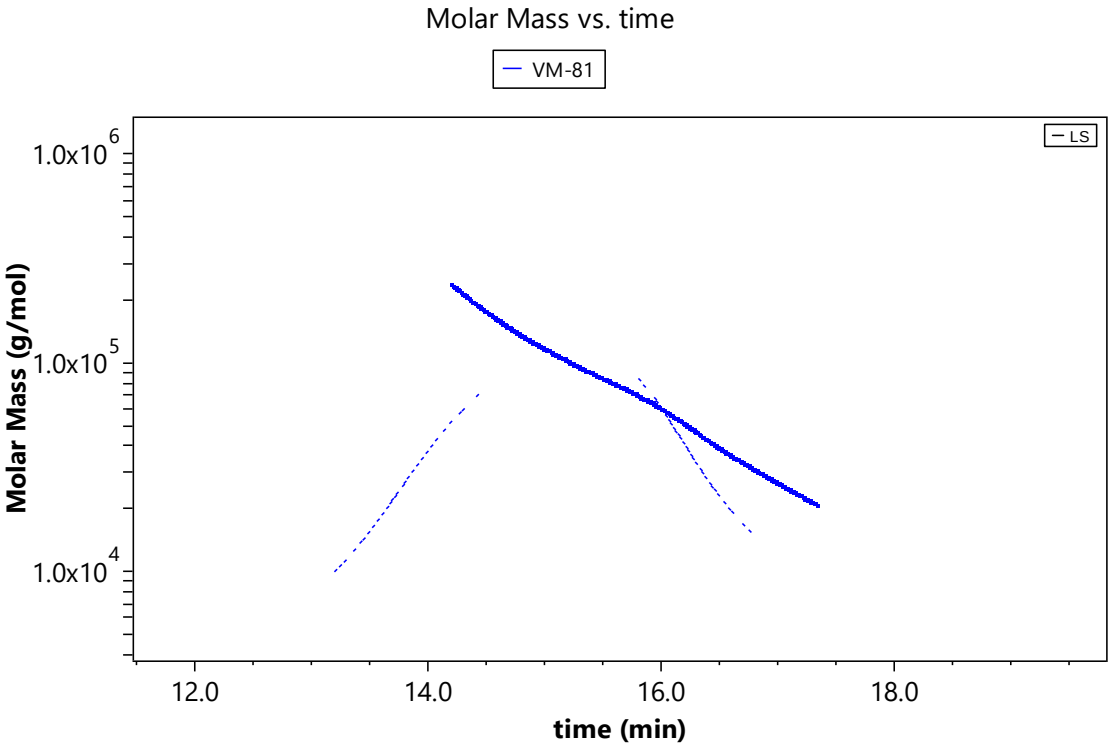

Figure 9.27: Representation of the molar mass (in g/mol) versus the time according the peak selected in the SEC chromatogram.

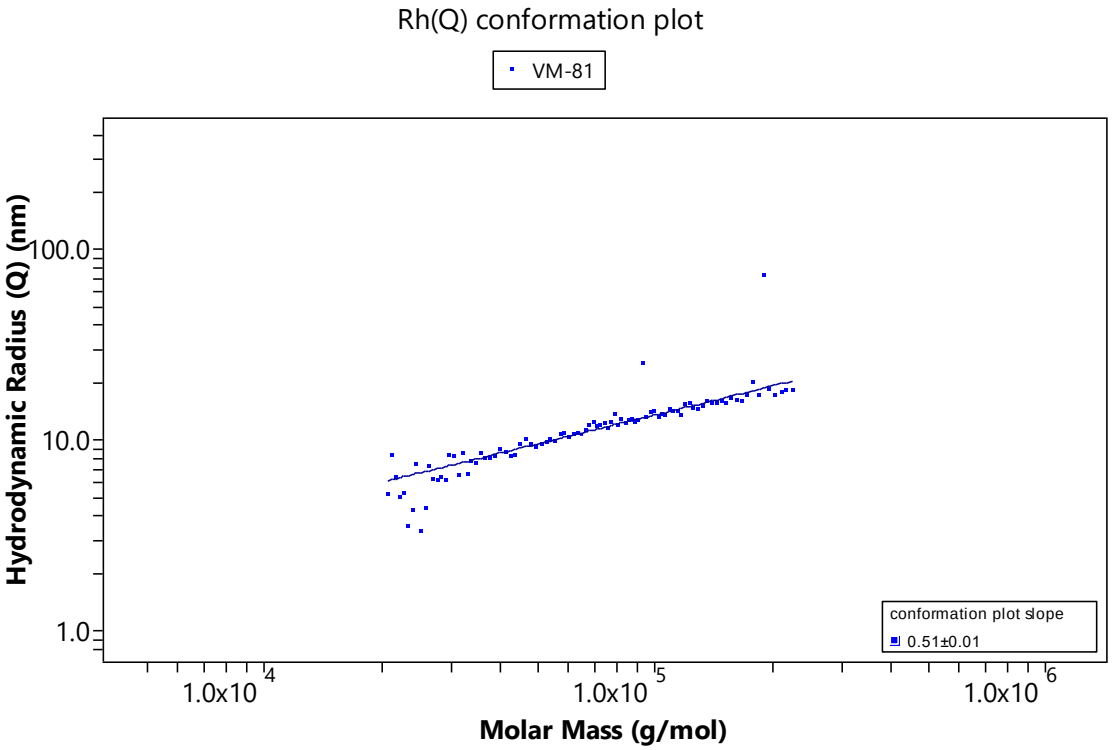

Figure 9.28: Plot of the hydrodynamic radius (Q in nm) versus the molar mass (in g/mol) of the peak selected in the SEC chromatogram.

9.1.4 HA-*g*-Lewis^{x} (4.5)

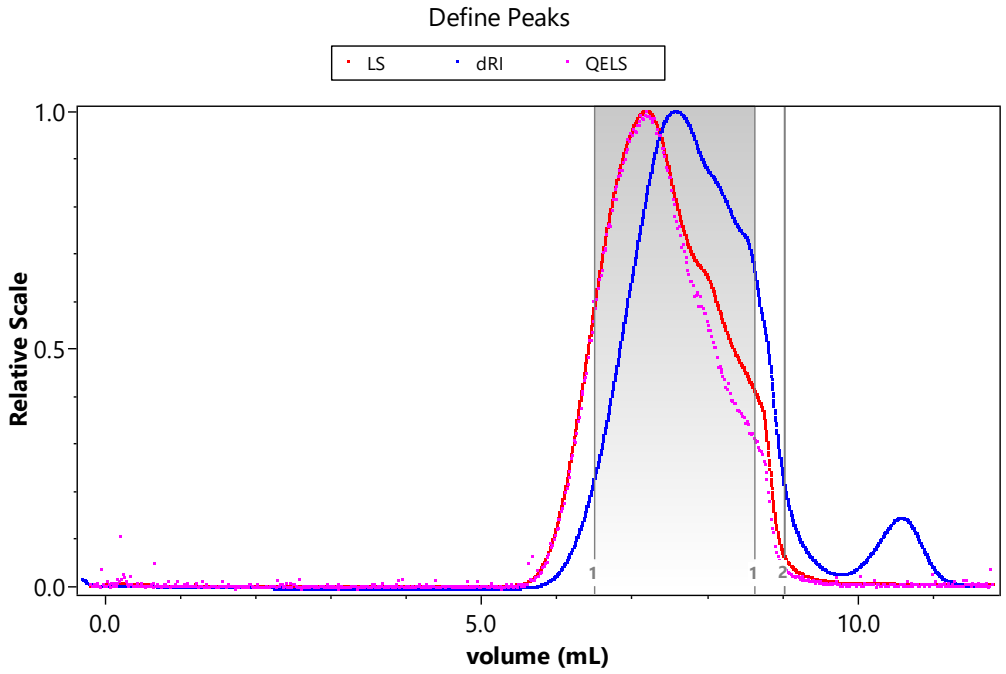

Figure 9.29: Chromatogram of the Size Exclusion Column following by the Multi-Angle Light Scattering detector data. Red and pink dots represent the data regarding the light scattering measurement and the quasi-elastic light scattering respectively while blue dots represent the refractive index of the sample. The blue region represents the surface of the peak.

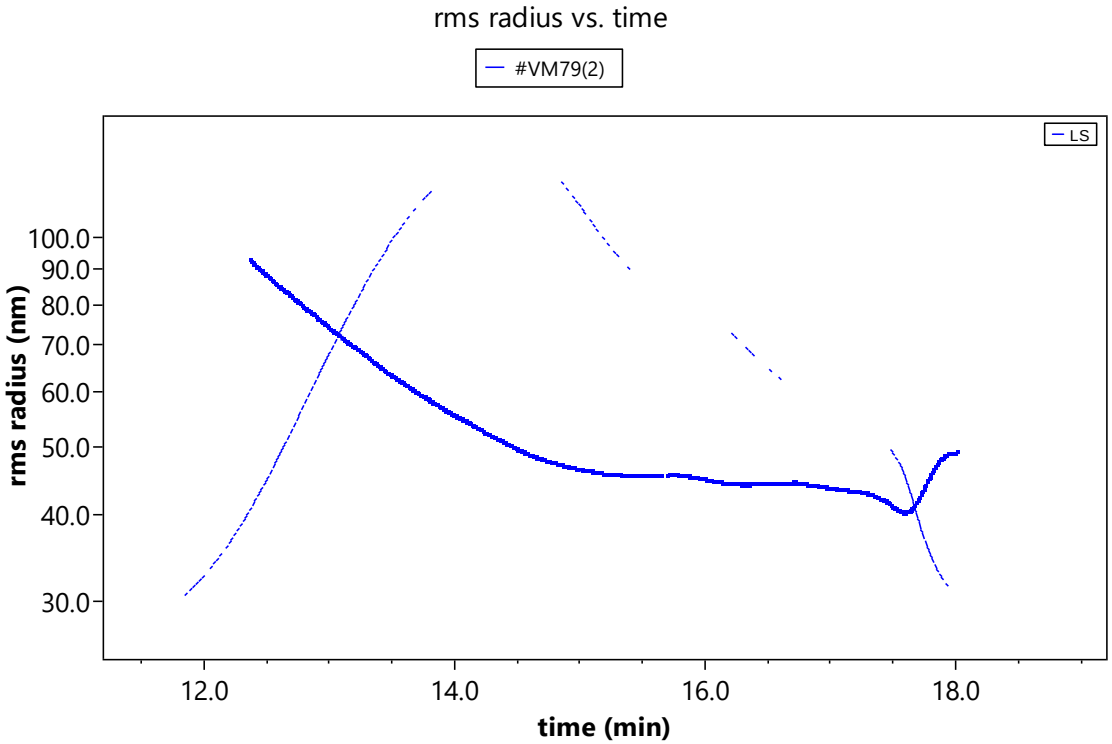

Figure 9.30: Representation of the radius of gyration (rms radius in nm) versus the time according the peak selected in the SEC chromatogram.

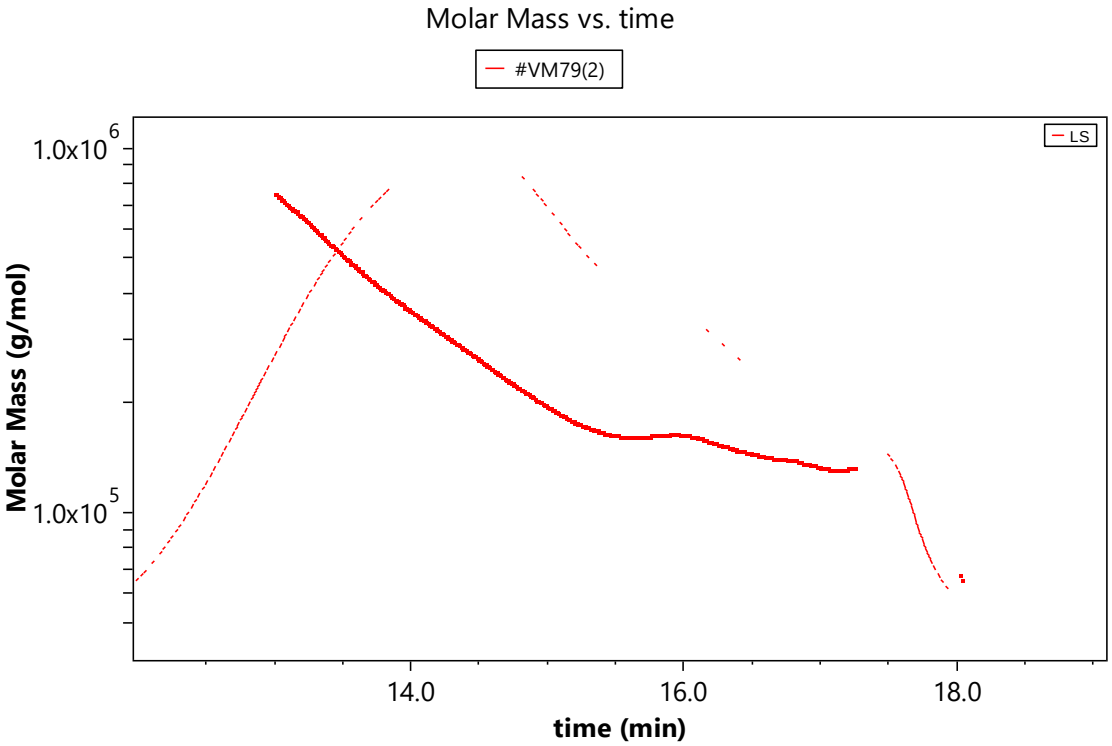

Figure 9.30: Representation of the molar mass (in g/mol) versus the time according the peak selected in the SEC chromatogram.

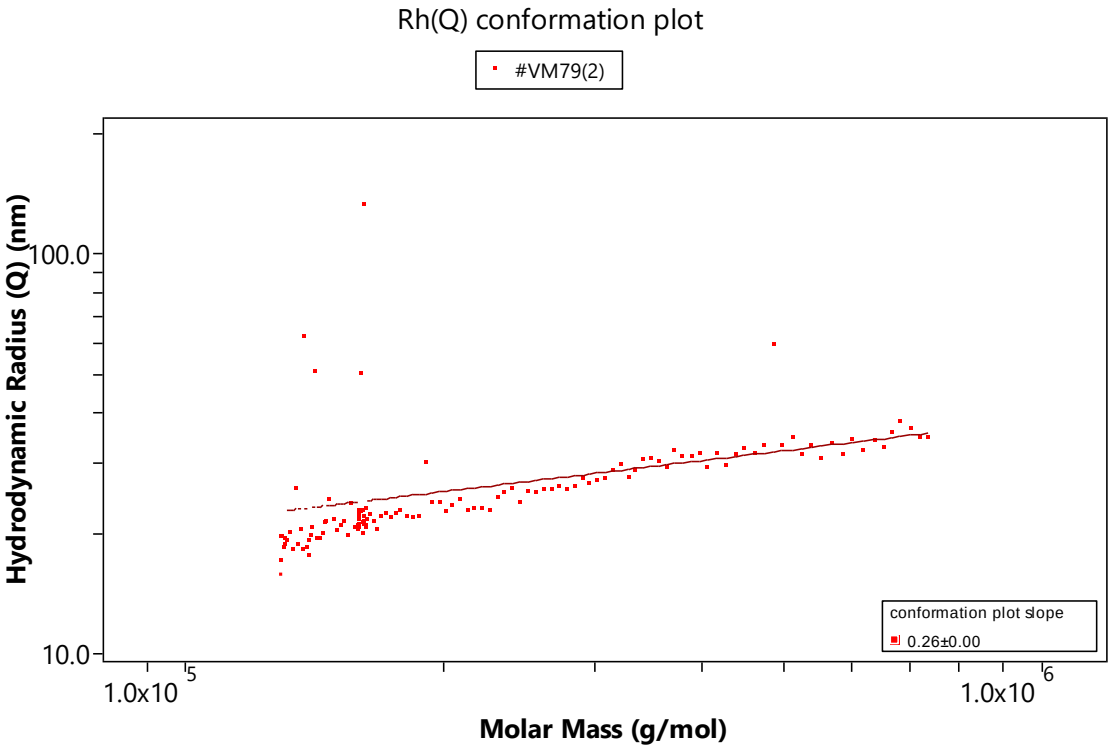

Figure 9.32: Plot of the hydrodynamic radius (Q in nm) versus the molar mass (in g/mol) of the peak selected in the SEC chromatogram.

9.1.5 HA-*g*-Gb_3 (4.6)

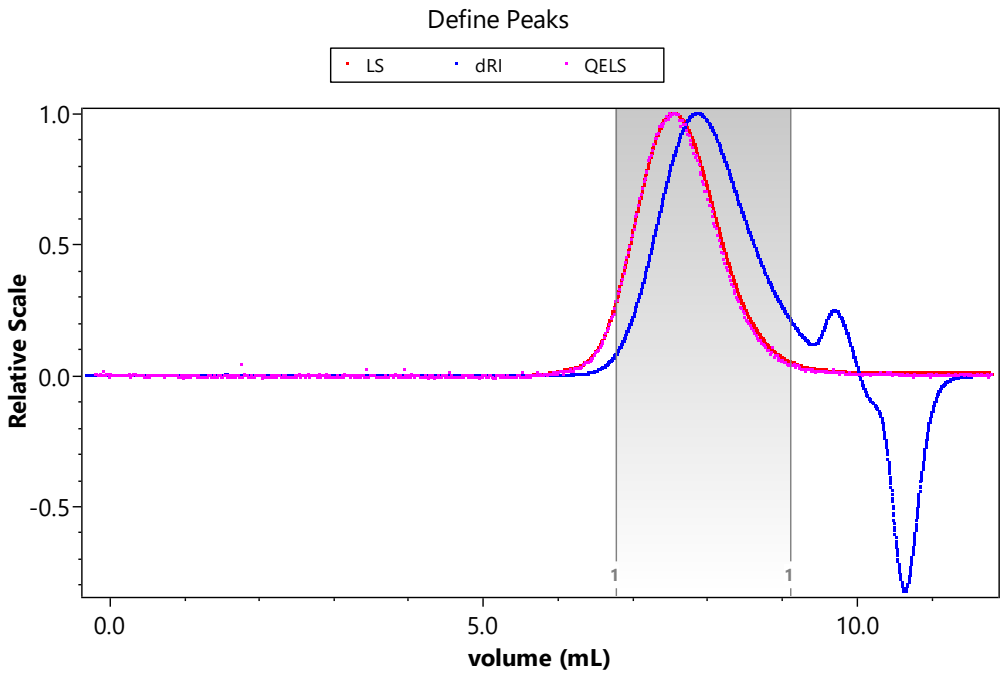

Figure 9.33: Chromatogram of the Size Exclusion Column following by the Multi-Angle Light Scattering detector data. Red and pink dots represent the data regarding the light scattering measurement and the quasi-elastic light scattering respectively while blue dots represent the refractive index of the sample. The blue region represents the surface of the peak.

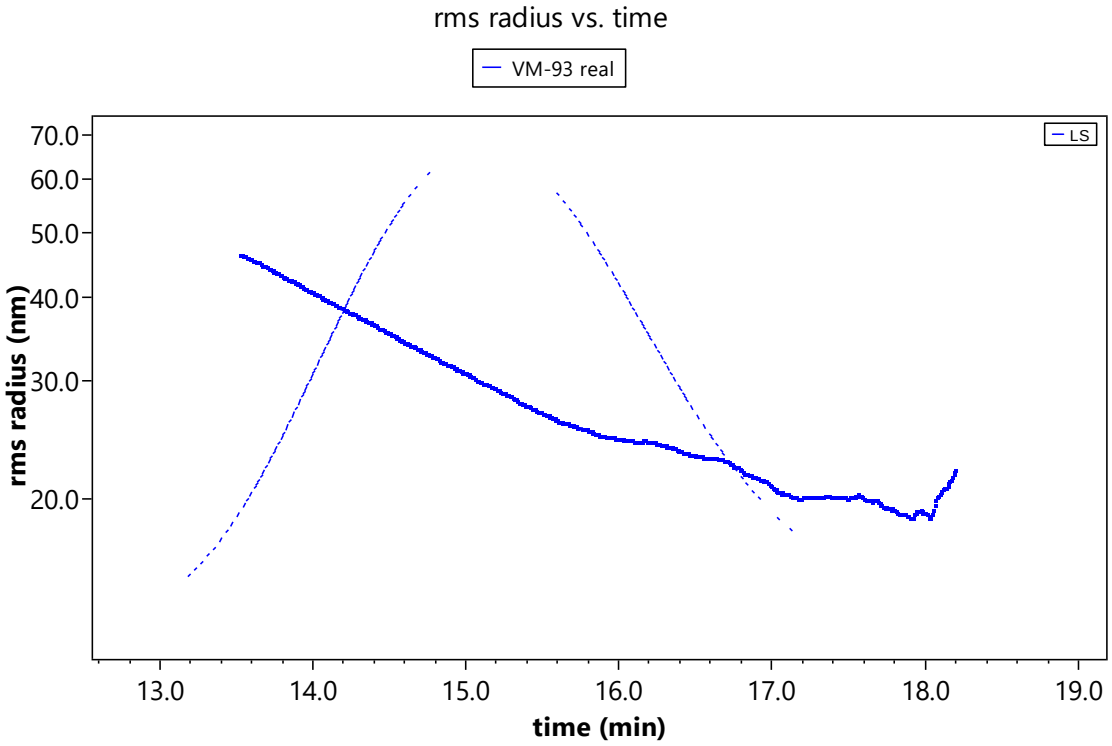

Figure 9.34: Representation of the radius of gyration (rms radius in nm) versus the time according the peak selected in the SEC chromatogram.

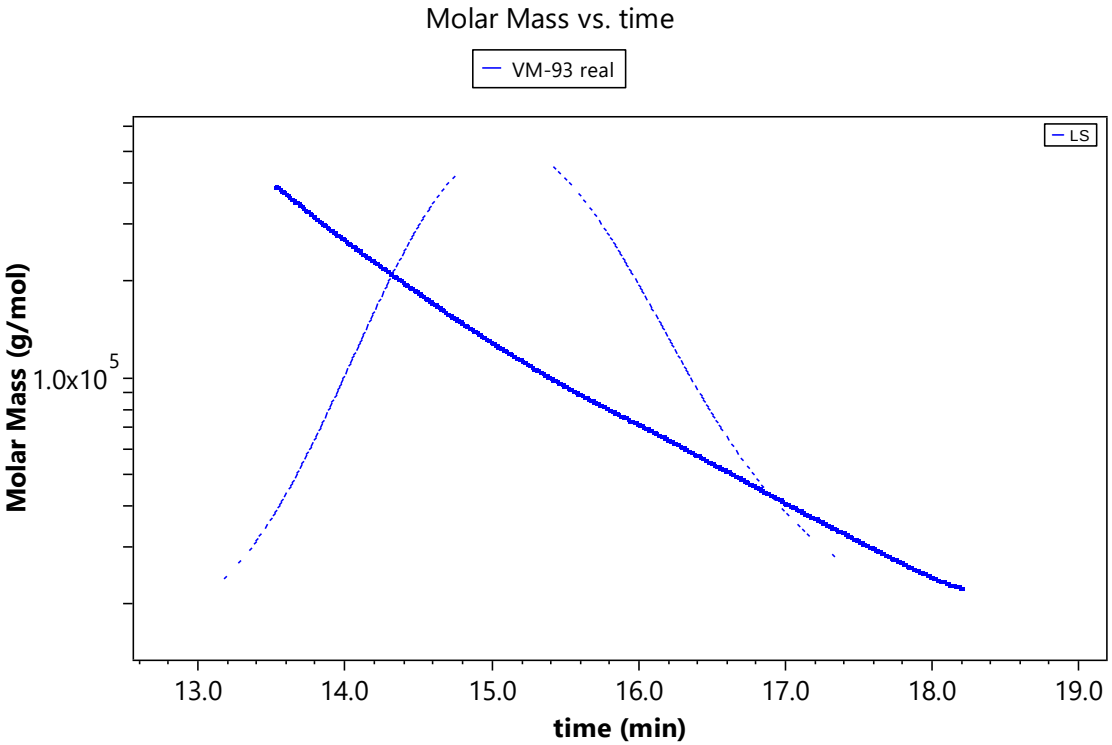

Figure 9.35: Representation of the molar mass (in g/mol) versus the time according the peak selected in the SEC chromatogram.

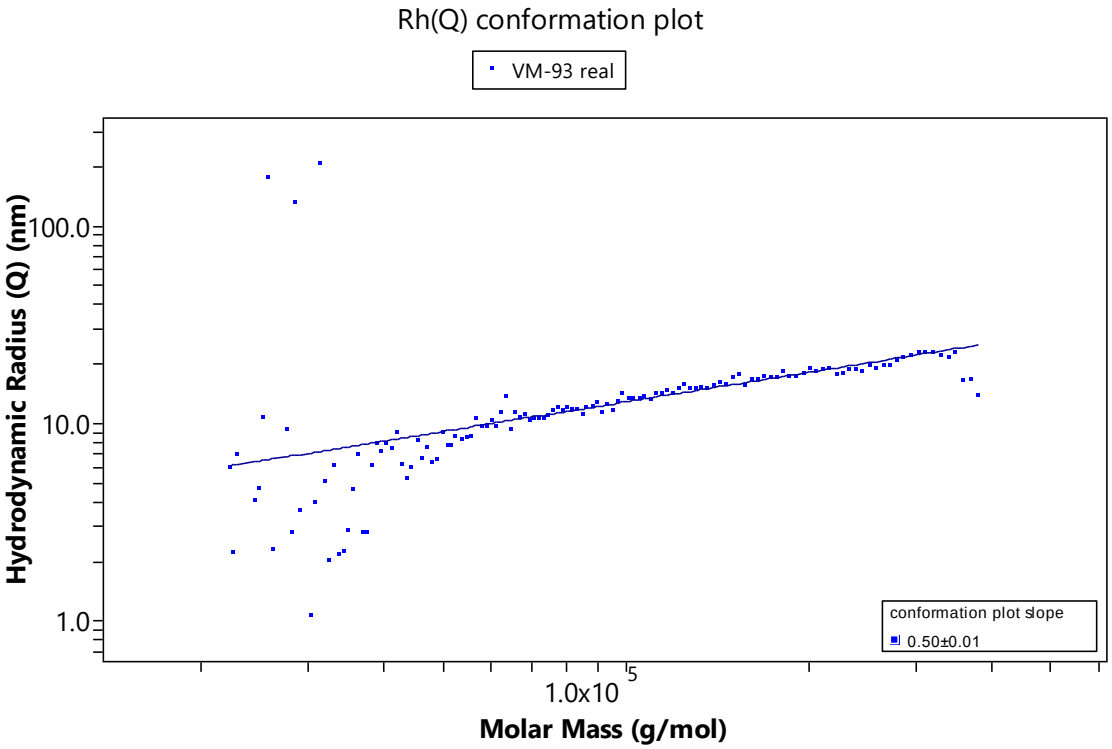

Figure 9.36: Plot of the hydrodynamic radius (Q in nm) versus the molar mass (in g/mol) of the peak selected in the SEC chromatogram.

9.2 QCM-D results

9.2.1 Control experiment for HA-*g*-Le^x

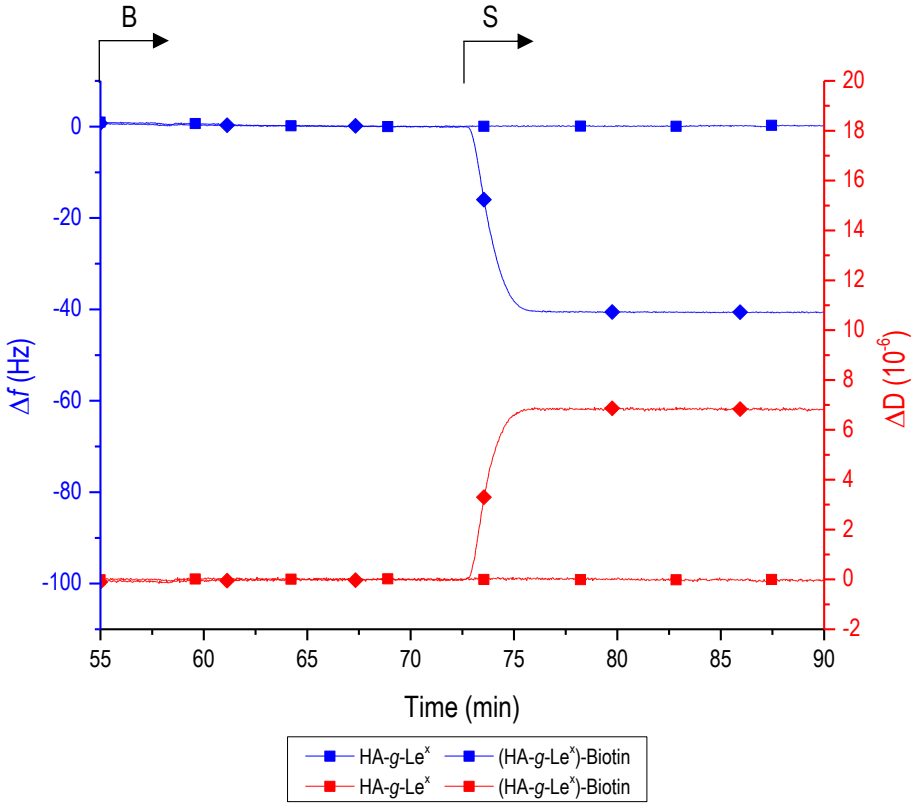

Graph 9.1: Quartz crystal microbalance with dissipation monitoring (QCM-D) data demonstrating successful anchorage of (HA-*g*-Le^x)-Biotin on a SAv-on-SLB surface. Shown are data for the formation of a supported lipid bilayer (from SUVS containing 5 mol-% biotinylated lipids), subsequent binding of streptavidin to monolayer coverage, and ultimately the addition of HA-*g*-Le^x (as a control) or (HA-*g*-Le^x)-Biotin. Abbreviations: B - working buffer (HBS; HEPES 10 mM, NaCl 150 mM, pH 7.4), S – sample: HA-*g*-Le^x or (HA-*g*-Le^x)-biotin. Arrows atop the graph indicate the start of incubation with each –samples as indicated. Incubation conditions: S – 20 µg/mL. All solutions were prepared in working buffer (HBS; HEPES 10 mM, NaCl 150 mM, pH 7.4)

9.2.2 Control experiment for HA-*g*-Gb_3

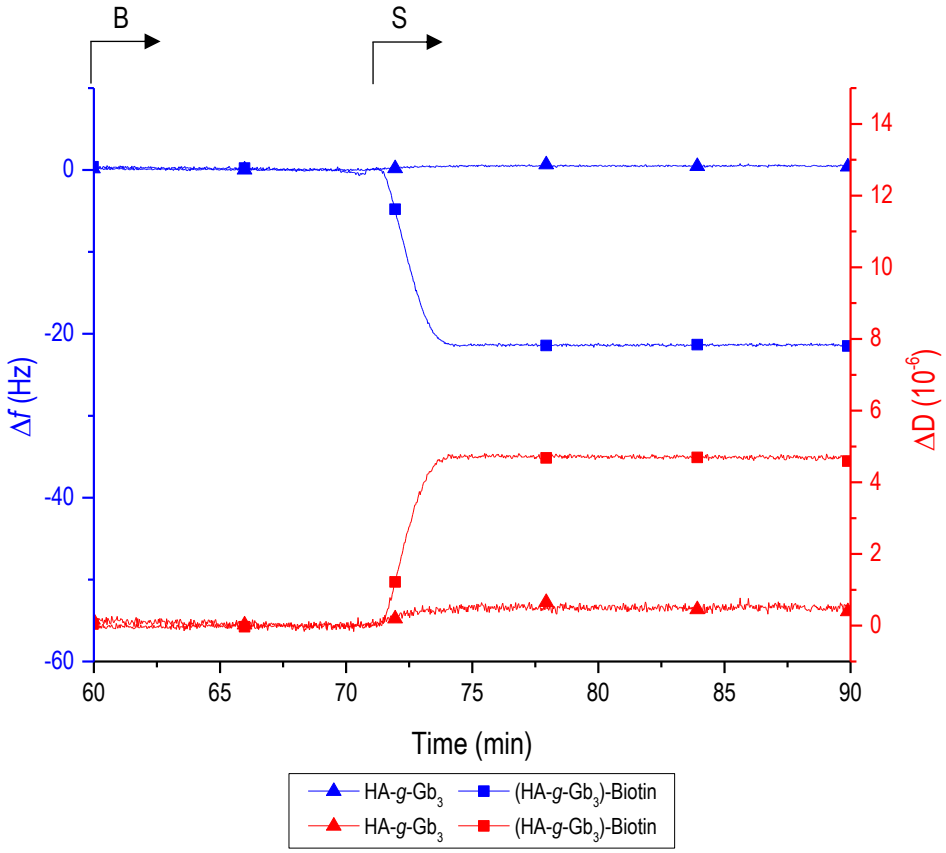

Graph 9.2: Quartz crystal microbalance with dissipation monitoring (QCM-D) data demonstrating successful anchorage of (HA-*g*-Gb_3)-Biotin on a SAv-on-SLB surface. Shown are data for the formation of a supported lipid bilayer (from SUVS containing 5 mol-% biotinylated lipids), subsequent binding of streptavidin to monolayer coverage, and ultimately the addition of HA-*g*-Gb_3 (as a control) or (HA-*g*-Gb_3)-Biotin. Abbreviations: B - working buffer (HBS; HEPES 10 mM, NaCl 150 mM, pH 7.4), S – sample: HA-*g*- Gb_3 or (HA-*g*- Gb_3)-biotin. Arrows atop the graph indicate the start of incubation with each –samples as indicated. Incubation conditions: S – 20 µg/mL. All solutions were prepared in working buffer (HBS; HEPES 10 mM, NaCl 150 mM, pH 7.4)

9.2.3 Experiment for HA-Biotin (40-50 kDa)

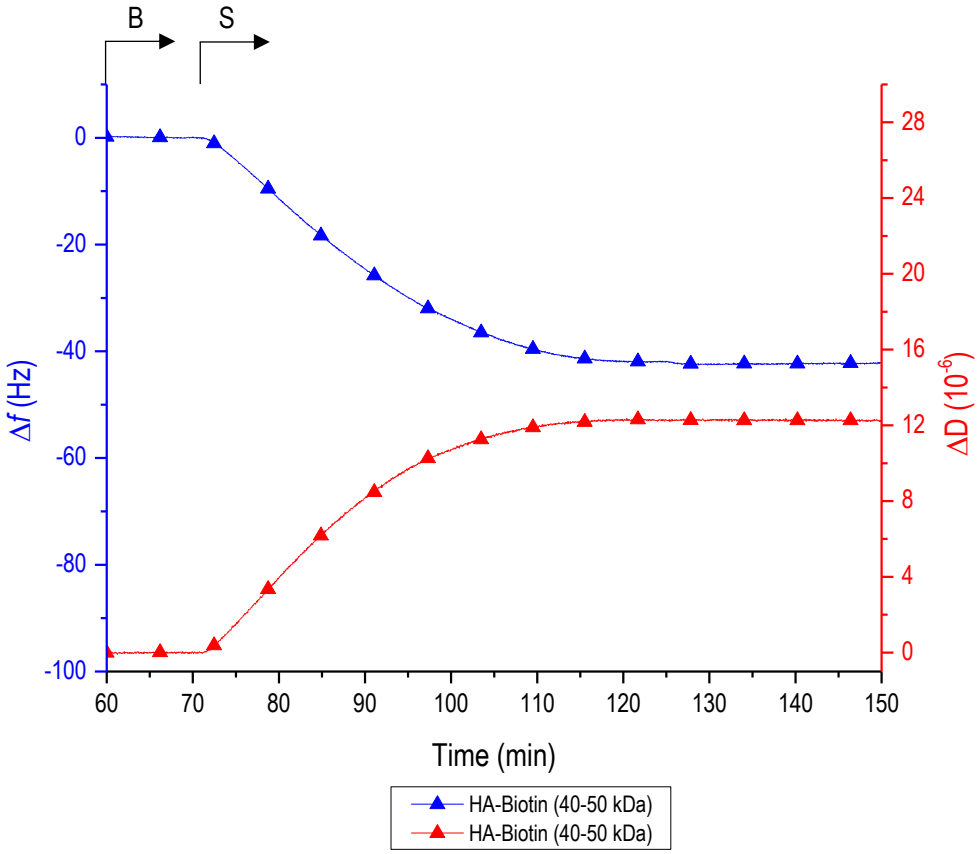

Graph 9.3: Quartz crystal microbalance with dissipation monitoring (QCM-D) data demonstrating successful anchorage of (HA-*g*-Gb_3)-Biotin on a SAv-on-SLB surface. Shown are data for the formation of a supported lipid bilayer (from SUVS containing 5 mol-% biotinylated lipids), subsequent binding of streptavidin to monolayer coverage with HA-Biotin (40-50 kDa). Abbreviations: B - working buffer (HBS; HEPES 10 mM, NaCl 150 mM, pH 7.4), S – sample: HA-Biotin. Arrows atop the graph indicate the start of incubation with each –samples as indicated. Incubation conditions: S – 20 µg/mL. All solutions were prepared in working buffer (HBS; HEPES 10 mM, NaCl 150 mM, pH 7.4)